

Probes of tocopherol biochemistry: fluorophores, imaging agents, and fake antioxidants

by

Mikel Ghelfi

A thesis submitted to the Department of Chemistry
In partial fulfillment of the requirements for the
degree of Doctorate of Philosophy

Supervised by
Professor Jeffrey K. Atkinson

Brock University
St. Catharines, Ontario
2017

© Mikel D. Ghelfi 2017

Abstract

Abstract

The body has many defence systems against reactive radical species, but none are as crucial in the protection of lipid membranes as vitamin E. As a result of a selection process mediated by the α -tocopherol transfer protein (α -TTP), α -tocopherol is the only form of vitamin E retained in the body. This chaperon protein has been well studied because of its role in vitamin E transport. Furthermore, malfunctions of α -TTP cause vitamin E deficiency leading to ataxia and other neurodegenerative disease. Protection of neuronal tissue is critical and is reflected in the high retention of α -tocopherol in the central nervous system. Neuronal tissues receive α -tocopherol from astrocytes, cells that are linked to hepatic tissue and able to express α -TTP, however the exact path of delivery between these cells is still unclear.

A technique called fluorescent microscopy allows the tracking of fluorescent molecules in cells to find their location and interactions with other parts of the cell. The focus of this study is the synthesis of a fluorescent tocopherol analogue with a long absorption wavelength, high photostability, and that binds selectively to α -TTP with high affinity.

Most health benefits associated with vitamin E consumption are based on its capability to inhibit lipid peroxidation in cell membranes by scavenging reactive oxygen species (ROS). Oxidative damage in membranes puts cells in a “stressful” state, activating signalling events that trigger apoptosis. Vitamin E down-regulates apoptotic functions like inflammation, macrophage activation and cell arrest in a stressed state, returning the cell back to normal functioning. At the same time, vitamin E has a preventive effect for atherosclerosis, Alzheimer’s and cancer.

With the deeper understanding of cell signalling processes associated with vitamin E the question arose whether protein interactions or the ROS scavenging is responsible for cell survival. To test this hypothesis, a non-antioxidant but α -TTP binding tocopherol analogue was synthesized and administered into oxidatively stressed, α -TTP deficient cells. If the cells were unable to restore homeostasis and stop apoptosis with the new molecule, this would suggest that the antioxidant function of α -tocopherol is the reason for survival.

Cancer is regarded as one of the most detrimental diseases with a high mortality rate. One key aspect in medical research is the increased drug specificity towards targeting cancer.

Chemotherapy applies cytotoxic compounds, which weaken the immune system because both malignant and healthy cells are destroyed. The specificity of the anti-cancer drugs are enhanced when encapsulated into liposomes that bear target-directing molecules such as antibodies which recognize cancer cell specific antigens on the cell membrane. The question remains if the encapsulated drug reaches the cancer or not.

Magnetic resonance imaging (MRI) and computed tomography (CT) are used to find malignant tissue in the body. CT imaging uses highly charged X-ray particles to scan the patient, possibly having damaging cytotoxic effects. Obtaining MRI results require the use of contrast agents to enhance the quality of images. These agents are based on transition metals, which potentially have chronic toxicity when retained in the body. Alternatively short-lived radiotracers that emit a γ -photon upon positron decay are used through a process called positron emission tomography (PET). Rapid decay times make the use of PET a less toxic alternative, however the decay products might be toxic to the cell.

For this reason a vitamin E based PET agent was created, which produces naturally safe decay products based on known metabolites of vitamin E, useful to track liposomal delivery of chemotherapeutic agents. This work describes the non-radioactive synthetic procedures towards

a variety of vitamin E PET analogues. The cytotoxicity of the most promising vitamin E PET tracer was evaluated along with its synthetic byproducts.

Acknowledgements

I would like to thank my supervisor Dr. Jeffrey Akinson for allowing me to pursue my graduate studies in his laboratory. I am grateful for his unmeasurable support and guidance from the beginning of my journey towards my degree. Dr. Akinson truly inspired my passion for science with his knowledge and enthusiasm, something I value deeply and will carry on for the rest of my life.

I further extend my gratitude to my thesis committee members Dr. Tony Yan and Dr. Melanie Pilkington for all their great input into my work. I thank you for always being helpful throughout all these years.

I am thankful for the tremendous contributions towards this work from our collaborators. Mr. Lucas Maddalena and Dr. Jeff Stuart for the help in the toxicological analysis and fluorescence microscopy work on the imaging agents. My thanks are extended to Dr. Drew Marquardt and Dr. Thad Harroun for their insight in the creation of the imaging agents.

I thank Dr. Theocharis Stamatatos for referring me to his colleague, Dr. Kyriakos Bourikas, helping me to solve a crucial part of my work.

I would like to thank Mr. Razvan Simionescu, Mr. Tim Jones and Mrs. Liquin Qiu for all their help and assistance in the analysis of spectra.

I especially thank our collaborators at Case Western University, Dr. Danny Manor and Dr. Lynn Ulatowski, for their contributions on the study towards a fluorescent tocopherol and fake-antioxidant.

My sincere gratitude goes towards all my past and present group members and co-workers who contributed towards this work with all their help in the lab and the fruitful discussions. Special

thanks to: Candace Panagabko, Matilda Baptist, Parthajit Mukherjee, Andrew Hildering, Nick Kruger, Venkata Krishna Garapati Roa, Ryan West, Stephan Ohnmacht.

Finally, I would like to thank both NSERC and Hoffmann-La Roche, whose funding made this work possible.

Table of contents

Fluorescent Tocopherol 1-4

| | | |
|----------|---|------------|
| 1 | Introduction..... | 29 |
| 1.1 | Discovery and Structure | 29 |
| 1.2 | Natural sources and tocopherol synthesis | 30 |
| 1.3 | Tocopherol chemical synthesis..... | 32 |
| 1.4 | Biosynthesis..... | 35 |
| 1.4.1 | Shikimate pathway | 35 |
| 1.4.2 | Non-mevalonate pathway | 37 |
| 1.5 | Biological absorption & transport | 38 |
| 1.5.1 | Tocopherol metabolism | 41 |
| 1.6 | Structure of the α -Tocopherol transfer protein..... | 43 |
| 1.6.1 | AVED..... | 49 |
| 1.6.2 | Vitamin E and neurological health | 51 |
| 1.7 | Biological tracing | 60 |
| 1.7.1 | Principles of fluorescence | 63 |
| 1.7.2 | Light scattering..... | 65 |
| 1.7.3 | Vitamin E labeling: Advantages of fluorophores..... | 71 |
| 1.7.4 | Fluorescent labeling: Fluorophores..... | 71 |
| 1.7.5 | Tocopherol labeled fluorophores | 74 |
| 2 | Project overview | 75 |
| 2.1 | Structure design | 75 |
| 2.2 | Synthesis plan | 81 |
| 3 | Results and Discussion | 85 |
| 3.1 | Synthesis..... | 85 |
| 3.2 | Photophysical studies | 104 |
| 3.2.1 | Absorption spectra..... | 104 |
| 3.2.2 | Quantum yield..... | 105 |
| 3.3 | Binding Studies..... | 106 |
| 3.3.1 | α -TTP expression & purification..... | 106 |
| 3.3.2 | Binding study to α -TTP in SET-Buffer | 107 |
| 3.3.3 | Binding study to α -TTP in TKE-Buffer | 118 |
| 3.4 | Cell studies | 130 |
| 3.4.1 | Cell assay | 130 |
| 4 | Conclusion | 135 |

Design and synthesis of a biomimetic non-antioxidant tocopherol 5-8

| | | |
|----------|--|------------|
| 5 | Introduction..... | 136 |
| 5.1 | Antioxidant function..... | 136 |
| 5.1.1 | Lipid peroxidation..... | 136 |
| 5.1.2 | Kinetics of hydroperoxyl radical quenching by tocopherol | 138 |
| 5.1.3 | Quenching of vitamin E | 143 |
| 5.1.4 | Hydrophobic antioxidants; carotene and ubiquinol..... | 145 |

| | | |
|-------------|--|------------|
| 5.1.5 | Vitamin E function and movement in membranes..... | 146 |
| 5.1.6 | Position and dynamics of vitamin E in membranes | 147 |
| 5.1.7 | Vitamin E membrane curvature and flip-flop | 149 |
| 5.2 | Cellular role of vitamin E..... | 150 |
| 5.2.1 | Protein kinase C and Phospholipase A ₂ | 150 |
| 5.2.2 | Atherosclerosis | 151 |
| 6 | Project overview | 153 |
| 6.1 | Structural design..... | 154 |
| 6.1.1 | Halogen tocopherol..... | 154 |
| 6.1.2 | Hydroxymethyl tocopherol | 158 |
| 6.2 | Synthesis | 161 |
| 7 | Results and Discussion | 163 |
| 7.1 | Synthesis | 163 |
| 7.2 | Spectroscopic and chemical properties of HM-Toc..... | 165 |
| 7.3 | Binding studies | 166 |
| 7.4 | Oxidation assay | 170 |
| 7.4.1 | Cyclic voltammetry studies | 171 |
| 7.4.2 | Lipid peroxidation..... | 173 |
| 7.4.3 | Cellular oxidation studies..... | 174 |
| 7.5 | Cell studies and Animal trials..... | 175 |
| 8 | Conclusion | 176 |
| | PET-tocopherol 9-12 | |
| 9 | Introduction..... | 177 |
| 9.1 | Positron emission tomography (PET) | 179 |
| 9.1.1 | Clinical PET Tracer..... | 183 |
| 9.1.2 | Single-photon emission computed tomography SPECT | 185 |
| 9.1.3 | ¹⁸ F radio-nuclide synthesis..... | 187 |
| 9.1.4 | ¹⁸ F nuclide synthesis | 189 |
| 9.2 | ¹⁸F-Fluorination..... | 190 |
| 9.2.1 | Nucleophilic fluorination..... | 190 |
| 9.2.2 | Aromatic ¹⁸ F-fluorination..... | 193 |
| 9.2.3 | Electrophilic / radical fluorination | 199 |
| 10 | Project overview | 203 |
| 10.1 | Structure design | 204 |
| 10.1.1 | Tocopherol based PET tracer | 204 |
| 10.1.2 | Tocopherol dual label: PET tracer and fluorophore | 206 |
| 11 | Results and Discussion | 207 |
| 11.1 | 6-F-Tocopherol synthesis..... | 207 |
| 11.2 | Synthesis | 209 |
| 11.2.1 | Nucleophilic F-Toc synthesis: | 209 |
| 11.2.2 | Synthesis of 6-F-tocopherol by electrophilic fluorination: | 235 |
| 11.2.3 | γ-Tocopherol fluorination to 5-fluoro-γ-tocopherol | 245 |
| 11.2.4 | 5-F-methyl-α-tocopherol synthesis | 251 |
| 11.2.5 | 6-F-methyl-α-tocopherol synthesis..... | 261 |
| 11.2.6 | 13-HO-α-tocopherol fluorination to 13-F-α-tocopherol | 266 |
| 11.3 | BODIPY fluorination..... | 269 |
| 11.4 | Cell cytotoxicity of 6-F-α-tocopherol, thienyl-ene-BODIPY and hydroxymethyl tocopherol..... | 277 |

| | | |
|---------|--|-----|
| 11.4.1 | Cell cytotoxicity of the liposomal delivery 6-F- α -tocopherol..... | 282 |
| 11.5 | Cellular uptake of in liposome incorporated thienyl-ene-BODIPY | 284 |
| 12 | Conclusion | 288 |
| 13 | General procedures | 291 |
| 13.1 | Reagents | 291 |
| 13.2 | Ligand binding and competitive binding assays with α -TTP | 291 |
| 13.3 | Cyclic voltammetry | 292 |
| 13.4 | AMVN lipid peroxidation | 292 |
| 13.5 | HM-Toc stability..... | 293 |
| 13.6 | Cytotoxicity study..... | 293 |
| 13.7 | Lipid-BODIPY extrusion | 295 |
| 13.8 | Imaging of cellular uptake of thienyl-ene-BODIPY liposomes..... | 296 |
| 14 | Synthetic procedures and NMR & MS | 296 |
| 14.1 | Fluorescent Tocopherol..... | 297 |
| 14.1.1 | Synthesis of (<i>S</i>)-methyl 6-((<i>tert</i> -butyldimethylsilyl)oxy)-2,5,7,8-tetramethylchroman-2-carboxylate (5) | 298 |
| 14.1.2 | Synthesis of (<i>S</i>)-6-((<i>tert</i> -butyldimethylsilyl)oxy)-2,5,7,8-tetramethylchroman-2-carbaldehyde (6) | 298 |
| 14.1.3 | Synthesis of (3-hydroxypropyl)triphenylphosphonium bromide (7) | 299 |
| 14.1.4 | Synthesis of (<i>S,Z</i>)-4-(6-((<i>tert</i> -butyldimethylsilyl)oxy)-2,5,7,8-tetramethylchroman-2-yl)but-3-en-1-ol (8)..... | 300 |
| 14.1.5 | Synthesis of (<i>R</i>)-4-(6-((<i>tert</i> -butyldimethylsilyl)oxy)-2,5,7,8-tetramethylchroman-2-yl)butan-1-ol (9)..... | 300 |
| 14.1.6 | Synthesis of (<i>R</i>)-4-(6-((<i>tert</i> -butyldimethylsilyl)oxy)-2,5,7,8-tetramethylchroman-2-yl)butanal (10) | 301 |
| 14.1.7 | Byproduct (<i>R</i>)- <i>tert</i> -butyl((2-butyl-2,5,7,8-tetramethylchroman-6-yl)oxy)dimethylsilane (9.2) | 302 |
| 14.1.8 | Synthesis of 1-(1-benzyl-1 <i>H</i> -pyrrol-2-yl)- <i>N,N</i> -dimethylmethanamine (11x)..... | 302 |
| 14.1.9 | Synthesis of <i>N,N</i> -dimethyl-1-(1 <i>H</i> -pyrrol-2-yl)methanamine (10x)..... | 303 |
| 14.1.10 | Synthesis of <i>N,N</i> -dimethyl-1-(1 <i>H</i> -pyrrol-2-yl)methanamine (11) | 303 |
| 14.1.11 | Synthesis of ((1 <i>H</i> -pyrrol-2-yl)methyl)triphenylphosphonium iodide (10) | 304 |
| 14.1.12 | Synthesis of (3-bromopropyl)triphenylphosphonium bromide (14) | 305 |
| 14.1.13 | Synthesis of (<i>R</i>)-4-(6-((<i>tert</i> -butyldimethylsilyl)oxy)-2,5,7,8-tetramethylchroman-2-yl)butyl methanesulfonate (9-OMs) | 305 |
| 14.1.14 | Synthesis of (<i>R</i>)-((2-(4-bromobutyl)-2,5,7,8-tetramethylchroman-6-yl)oxy)(<i>tert</i> -butyl)dimethylsilane (16) | 306 |
| 14.1.15 | Synthesis of (<i>R</i>)-4-(6-((<i>tert</i> -butyldimethylsilyl)oxy)-2,5,7,8-tetramethylchroman-2-yl)butyltriphenylphosphonium bromide (18) | 307 |
| 14.1.16 | Synthesis of (<i>R</i>)- <i>tert</i> -butyl((2-(4-iodobutyl)-2,5,7,8-tetramethylchroman-6-yl)oxy)dimethylsilane (17) | 307 |
| 14.1.17 | Synthesis of (<i>R</i>)-4-(6-((<i>tert</i> -butyldimethylsilyl)oxy)-2,5,7,8-tetramethylchroman-2-yl)butyltriphenylphosphonium iodide (19)..... | 308 |
| 14.1.18 | Synthesis of 4-(1-benzyl-1 <i>H</i> -pyrrol-2-yl)but-3-en-1-ol (20)..... | 310 |
| 14.1.19 | Synthesis of (6-((<i>tert</i> -butyldimethylsilyl)oxy)-2,5,7,8-tetramethylchroman-2-yl)methyl methanesulfonate (22-OMs)..... | 312 |
| 14.1.20 | Synthesis of ((2-(bromomethyl)-2,5,7,8-tetramethylchroman-6-yl)oxy)(<i>tert</i> -butyl)dimethylsilane (23) | 313 |
| 14.1.21 | Synthesis of (<i>R</i>)-(5-bromothiophen-2-yl)((<i>S</i>)-6-((<i>tert</i> -butyldimethylsilyl)oxy)-2,5,7,8-tetramethylchroman-2-yl)methanol (25)..... | 314 |
| 14.1.22 | Synthesis of (<i>S</i>)-((2-((5-bromothiophen-2-yl)methyl)-2,5,7,8-tetramethylchroman-6-yl)oxy)(<i>tert</i> -butyl)dimethylsilane (26) | 315 |

| | | |
|-------------|---|------------|
| 14.1.23 | Synthesis of (<i>S</i>)-methyl 6-(benzyloxy)-2,5,7,8-tetramethylchroman-2-carboxylate (27) | 315 |
| 14.1.24 | Synthesis of (<i>S</i>)-6-(benzyloxy)-2,5,7,8-tetramethylchroman-2-carbaldehyde (21) | 316 |
| 14.1.25 | Synthesis of (<i>R</i>)-((<i>S</i>)-6-(benzyloxy)-2,5,7,8-tetramethylchroman-2-yl)(5-bromothiophen-2-yl)methanol (28) | 317 |
| 14.1.26 | Synthesis of (<i>S</i>)-6-(benzyloxy)-2-((5-bromothiophen-2-yl)methyl)-2,5,7,8-tetramethylchroman (29) | 318 |
| 14.1.27 | Synthesis of (<i>S</i>)-2-(5-((6-((<i>tert</i> -butyldimethylsilyl)oxy)-2,5,7,8-tetramethylchroman-2-yl)methyl)thiophen-2-yl)-1 <i>H</i> -pyrrole (30) | 319 |
| 14.1.28 | Synthesis of (<i>S</i>)-2-(5-((6-(benzyloxy)-2,5,7,8-tetramethylchroman-2-yl)methyl)thiophen-2-yl)-1 <i>H</i> -pyrrole (32) | 321 |
| 14.1.29 | Synthesis of (<i>S</i>)-7-(5-((6-(benzyloxy)-2,5,7,8-tetramethylchroman-2-yl)methyl)thiophen-2-yl)-5,5-difluoro-1,3-dimethyl-5 <i>H</i> -dipyrrolo[1,2- <i>c</i> :2',1'- <i>f</i>][1,3,2]diazaborinin-4-ium-5-uide (33) | 322 |
| 14.1.30 | Synthesis of (<i>S</i>)-5-((6-((<i>tert</i> -butyldimethylsilyl)oxy)-2,5,7,8-tetramethylchroman-2-yl)methyl)thiophene-2-carbaldehyde (34) | 323 |
| 14.1.31 | Synthesis of byproduct (<i>S</i>)-2,5,7,8-tetramethyl-2-(thiophen-2-ylmethyl)chroman-6-yl formate (36) | 324 |
| 14.1.32 | Synthesis of 5,5-difluoro-7,9-dimethyl-5 <i>H</i> -dipyrrolo[1,2- <i>c</i> :2',1'- <i>f</i>][1,3,2]diazaborinin-4-ium-5-uide (37) | 325 |
| 14.1.33 | Synthesis of (<i>S,E</i>)-7-(2-(5-((6-((<i>tert</i> -butyldimethylsilyl)oxy)-2,5,7,8-tetramethylchroman-2-yl)methyl)thiophen-2-yl)vinyl)-5,5-difluoro-9-methyl-5 <i>H</i> -dipyrrolo[1,2- <i>c</i> :2',1'- <i>f</i>][1,3,2]diazaborinin-4-ium-5-uide (39) | 327 |
| 14.1.34 | Synthesis of (<i>S,E</i>)-5,5-difluoro-7-(2-(5-((6-hydroxy-2,5,7,8-tetramethylchroman-2-yl)methyl)thiophen-2-yl)vinyl)-9-methyl-5 <i>H</i> -dipyrrolo[1,2- <i>c</i> :2',1'- <i>f</i>][1,3,2]diazaborinin-4-ium-5-uide (3) | 328 |
| 14.1.35 | Synthesis of (<i>S,E</i>)-5,5-difluoro-7-(2-(5-((6-methoxy-2,5,7,8-tetramethylchroman-2-yl)methyl)thiophen-2-yl)vinyl)-9-methyl-5 <i>H</i> -dipyrrolo[1,2- <i>c</i> :2',1'- <i>f</i>][1,3,2]diazaborinin-4-ium-5-uide (40) | 332 |
| 14.2 | Non-antioxidant-Tocopherol | 333 |
| 14.2.1 | Synthesis of (2 <i>R</i>)-2,5,7,8-tetramethyl-2-(4,8,12-trimethyltridecyl)chroman-6-yl trifluoromethanesulfonate (41) | 333 |
| 14.2.2 | Synthesis of (2 <i>R</i>)-2,5,7,8-tetramethyl-2-(4,8,12-trimethyltridecyl)chroman (42) | 333 |
| 14.2.3 | Synthesis of (2 <i>R</i>)-6-chloro-2,5,7,8-tetramethyl-2-(4,8,12-trimethyltridecyl)chroman (43) | 334 |
| 14.2.4 | Synthesis of (2 <i>R</i>)-2,5,7,8-tetramethyl-2-(4,8,12-trimethyltridecyl)chroman-6-carbaldehyde (46) | 335 |
| 14.2.5 | Synthesis of ((2 <i>R</i>)-2,5,7,8-tetramethyl-2-(4,8,12-trimethyltridecyl)chroman-6-yl)methanol (44) | 335 |
| 14.3 | PET-Tocopherol | 338 |
| 14.3.1 | Synthesis of (2 <i>R</i>)-6-fluoro-2,5,7,8-tetramethyl-2-(4,8,12-trimethyltridecyl)chroman (47) | 338 |
| 14.3.2 | Synthesis of 2,2,5,7,8-pentamethylchroman-6-yl 4-methylbenzenesulfonate (52) | 341 |
| 14.3.3 | Synthesis of naphthalen-2-yl 4-methylbenzenesulfonate (54) | 341 |
| 14.3.4 | Synthesis of 4,4,5,5-tetramethyl-2-((2 <i>R</i>)-2,5,7,8-tetramethyl-2-(4,8,12-trimethyltridecyl)chroman-6-yl)-1,3,2-dioxaborolane (56) | 342 |
| 14.3.5 | Synthesis of 1-iodopyridin-1-ium chloride (71) | 343 |
| 14.3.6 | Synthesis of (2 <i>R</i>)-6-iodo-2,5,7,8-tetramethyl-2-(4,8,12-trimethyltridecyl)chroman (70) | 344 |
| 14.3.7 | Synthesis of phenyl((2 <i>R</i>)-2,5,7,8-tetramethyl-2-(4,8,12-trimethyltridecyl)chroman-6-yl)iodonium 4-methylbenzenesulfonate (69) | 345 |
| 14.3.8 | Synthesis of (2 <i>R</i>)-5-bromo-2,7,8-trimethyl-2-(4,8,12-trimethyltridecyl)chroman-6-ol (76) | 346 |

| | | |
|---------|---|-----|
| 14.3.9 | Synthesis of (2 <i>R</i>)-5-fluoro-2,7,8-trimethyl-2-(4,8,12-trimethyltridecyl)chroman-6-ol (48) | 346 |
| 14.3.10 | Synthesis of (2,5-dihydroxy-3,6-dioxocyclohexa-1,4-diene-1,4-diyl)bis(dimethylsulfonium) acetate (<i>S</i> -Ylide) | 348 |
| 14.3.11 | Synthesis of (2 <i>R</i>)-5-(fluoromethyl)-2,7,8-trimethyl-2-(4,8,12-trimethyltridecyl)chroman-6-yl acetate (78) | 349 |

References

List of Figures

| | |
|--|----|
| Figure 1 Conditions used in the industrial synthesis of α -tocopherol by condensation of TMHQ and isophytol. ^{36,37,42,43} | 33 |
| Figure 2. Structure of Tocomonoenol & marine derived Tocopherol (MDT). ⁵⁶ | 34 |
| Figure 3. Shikimate pathway. Synthesis of Chlorismate from D-erythrose-4-phosphate (E4P) and phosphoenolpyruvate (PEP). ^{63,64} | 36 |
| Figure 4. Biosynthetic conversion of chorismate to 4-HPPA. ⁶⁶ | 36 |
| Figure 5. Tocopherol biosynthesis. ⁶⁹ | 38 |
| Figure 6. Tocopherol intestinal absorption & distribution. | 40 |
| Figure 7. Vitamin E metabolites. | 42 |
| Figure 8. Protein interactions of the α -TTP active side with α -tocopherol. | 45 |
| Figure 9. Open and closed lid crystal structure. | 47 |
| Figure 10. Calculated interactions between the lipid-binding domains of α -TTP with the hydrocarbon core of the lipid bilayer: (A) α -TTP in “open” (1OIZ) and (B) “closed” (1R5L) conformations. | 48 |
| Figure 11. α -TTP structure highlighting the amino acid residues in the PI(4,5)P2 binding cavity and lid helix 9-11 α -TTP structure enclosing α -Toc. | 49 |
| Figure 12. α -TTP mutations across the ttpa gene. | 50 |
| Figure 13. Structural differences in Purkinje neurons between <i>ttpa</i> ^{+/+} and <i>ttpa</i> ^{-/-} VE (vitamin E) mice. ¹¹¹ | 52 |
| Figure 14. Inhibition of lipid peroxidation with α -tocopherol and NMDA. | 54 |
| Figure 15. Localization of vitamin E in neurons by TOF-MS. | 58 |
| Figure 16. Localization of α -TTP expression in neuronal tissue. | 59 |
| Figure 17. Proposed model of vitamin E delivery from astrocytes to neurons. ¹¹¹ | 60 |
| Figure 18. Fluorescent stained actin filaments of gastrula-stage <i>Drosophila</i> embryo. | 62 |
| Figure 19. Jablonski diagram. | 63 |
| Figure 20. Quantum yield (Φ) and fluorescent lifetime (τ) of Eosin & Erythrosin B. ¹⁶¹ | 65 |
| Figure 21. Interaction of visible light with particles. | 67 |
| Figure 22. Extinction coefficient (k) of water for the 200 – 1000nm spectral region as a summary from CJ: Clark and Jelly, LSG: Lenoble, Saint-Guilly and TSW: Tyler. ^{171,172,173} | 68 |
| Figure 23. Total absorption coefficient μ_a (cm ⁻¹), as water is added (volume fraction $f_{v,water}$ = 0.1 by 0.1 to 0.9), blood at 75 oxygen saturation is added (average $f_{v,blood}$ = 10 ⁻⁴ by 10 ⁻⁴ to 2 \times 10 ⁻³), bilirubin is added (1 by 1 to 20 mg dL ⁻¹ , where 20 mg dL ⁻¹ = 342 μ M is a bilirubin concentration in the blood of a jaundiced neonate), fat is added ($f_{v,fat}$ = 0.3 by 0.3 to 0.9), and melanin is added ($f_{v,melanosome}$ = 0.01 by 0.01 to 0.10). ¹⁷⁶ | 69 |
| Figure 24. Reduced scattering coefficient for different tissues based on literature values for the seven groups of tissues (red circles, data found in reference). | 70 |
| Figure 25. Structures of frequently applied fluorescent microscopy dyes. ¹⁹⁰⁻¹⁹⁷ | 73 |
| Figure 26. Nummering system of the BODIPY core structure and example structures of differently substituted BODIPYs. ²¹⁷⁻²²⁰ | 77 |
| Figure 27. X-ray diffraction analysis of AO- α -toc (1a & 1b) and α -tocopherol (2a & 2b) bond to α -TTP. | 79 |

| | |
|--|----|
| Figure 28. Novel designed fluorescent α -Toc ligands compared to BODIPY-Toc and α -tocopherol..... | 81 |
| Figure 29. (a) BODIPY formation from oct-7-ene-pyrrole and 2,4-dimethylpyrrole aldehyde. Formation of byproduct 1,3,5,7-tetramethyl-BODIPY. (b) Olefin metathesis reaction between vinyl TBSO-Trolox-ene and oct-7-ene-BODIPY. Formation of dimer bis-oct-7-ene-BODIPY. ²⁰⁶ | 83 |
| Figure 30. Synthetic strategy towards product 1..... | 84 |
| Figure 31. Synthetic strategy towards product 2..... | 84 |
| Figure 32. Synthetic strategy towards product 3..... | 85 |
| Figure 33. Synthesis of TBSO trolox aldehyde from Trolox® by esterification, TBS protection of the chroman phenol and reduction of the methylester to the aldehyde. | 86 |
| Figure 34. Synthesis of phosphonium salt, 7, from 3-bromopropan-1-ol ²³⁵ and Wittig reaction of 7 with TBSO Trolox aldehyde to create product 8. ²⁰⁶ | 86 |
| Figure 35. Synthesis of product 9 by hydrogenation of 8 with 10% palladium on carbon. | 87 |
| Figure 36. (a) Double bond hydrogenation of compound 8. | 88 |
| Figure 37. Griffin's proposed alcohol oxidation mechanism with water and palladium / platinum metal [M]. | 89 |
| Figure 38. Synthesis of product 10 by Dess-Martin oxidation of 9. ²⁴⁶ | 89 |
| Figure 39. Synthesis of product 13 by Wittig reaction of aldehyde 10 with phosphonium salt 11 and 12. | 90 |
| Figure 40. Synthesis of product 20 by Wittig reaction of aldehyde 16 with phosphonium salt 7 and lithium hexamethyldisilazide as a base. ²⁵⁰ | 90 |
| Figure 41. Conversion of alcohol 9 to the bromine 16 and iodine 17 by mesylation, followed by nucleophilic bromide and iodide substitution of the mesylate with lithium bromide (LiBr) and potassium iodide (KI). ²⁵⁴ | 91 |
| Figure 42. Synthesis of phosphonium salts 18 and 19 by reaction of 16 and 17 with triphenylphosphine (PPh ₃) in a microwave oven (MV). ²⁵⁵ | 91 |
| Figure 43. Synthesis of product 20 by Wittig reaction of <i>N</i> -benzylpyrrole-2-carboxaldehyde with phosphonium salt 7 and lithium hexamethyldisilazide as a base. ²⁰¹ | 92 |
| Figure 44. Synthesis of product 13 by Wittig reaction of <i>N</i> -benzylpyrrole-2-carboxaldehyde with phosphonium salt 18 and 19 and lithium hexamethyldisilazide as a base. ^{201,249} | 92 |
| Figure 45. Decrease in chain length from target product 1 to 2. | 93 |
| Figure 46. 2-Bromothiophene addition to Trolox by displacement of an electrophile on position 1..... | 93 |
| Figure 47. Synthetic routes chosen to synthesize 26 from TBS trolox aldehyde 6..... | 94 |
| Figure 48. (a) Synthesis of product 23 by mesylation of TBS trolox alcohol 22, followed by nucleophilic bromide displacement of the mesyl group with lithium bromide. ²⁵⁴ (b) Appel reaction of 22 yielded TBS deprotected product 24. ²⁵⁹ | 95 |
| Figure 49. Synthesis of product 26 by reaction of 23 with 2-bromothiophene. ^{261,262} | 95 |
| Figure 50. Synthesis of product 25 by reaction of 6 with 2-bromothiophene. ²⁶² | 96 |
| Figure 51. Synthesis of benzyl protected trolox aldehyde 21..... | 96 |
| Figure 52. Synthesis of product 28 by reaction of 21 with 2-bromothiophene. ²⁶² | 97 |
| Figure 53. Reduction of 28 to product 29 and 25 to product 26 with triethylsilane and borontrifluoride. ²⁷⁴ | 98 |
| Figure 54. Negishi coupling of 26 with pyrrole to create product 30. Synthesis of dimer byproduct, 31. ²⁷⁵ | 98 |

| | |
|--|-----|
| Figure 55. Negishi coupling of 29 with pyrrole to create product 32 and trace amounts of 29-H. ²⁷⁵ | 99 |
| Figure 56. Synthesis of 33 by condensation of 32 with 3,5-dimethylpyrrole-2-carbaldehyde. ²⁰⁶ | 99 |
| Figure 57. Attempts to debenzylate 33 to form product 2. | 100 |
| Figure 58. Synthesis of product 34 by formylation of 26 by lithium halogen exchanged and quenching with DMF. ²⁹¹ | 101 |
| Figure 59. (a) Synthesis of 36 from 35 by Vilsmeier-Haack formylation. (b) Proposed reaction mechanism of the aryl O-formate protection of TBSO protected 2-thiophenemethyl α -chromane. | 102 |
| Figure 60. Synthesis of dimethyl-BODIPY building block, 37, by condensation of 2,4-dimethyl pyrrole and 2-pyrrole carboxaldehyde. ^{206,295} | 103 |
| Figure 61. Synthesis of 39 by Knoevenagel condensation of 34 with dimethyl BODIPY 37. ²⁹⁶ | 103 |
| Figure 62. Synthesis of target product 3 by acetic phenol TBSO-deprotection of 39 with 8% HCl MeOH. ²⁰⁶ | 104 |
| Figure 63. Thienyl-ene-BODIPY absorption and emission curve. | 104 |
| Figure 64. Fluorescein and thienyl-ene-BODIPY gradients for quantum yield determination. | 106 |
| Figure 65. Direct binding of [ligand] BODIPY- α -Toc C6, C7 and C8 to 0.2 μ M α -TTP in SET buffer. | 108 |
| Figure 66. BODIPY- α -Toc in EtOH direct binding to 0.2 μ M α -TTP in SET buffer repeated with freshly expressed protein. | 109 |
| Figure 67. Direct binding of thienyl-ene-BODIPY (3) in EtOH to 0.5 μ M α -TTP in SET buffer using West's et al. conditions. | 110 |
| Figure 68. Competition assay of 0.2 μ M α -TTP, saturated with 1.0 μ M BODIPY- α -Toc in SET buffer, with [competitor] α -Toc & cholesterol in EtOH. | 111 |
| Figure 69. Competition assay of 0.2 μ M α -TTP, saturated with 0.25 μ M thienyl-ene-BODIPY (3) in SET buffer, with α -tocopherol (α -toc) in EtOH. | 112 |
| Figure 70. Direct binding of C9-NBD- α -Toc in EtOH to 0.2 μ M α -TTP in SET buffer. λ_{ex} = 495nm λ_{em} = 535nm. | 112 |
| Figure 71. Competition assay of 0.2 μ M α -TTP, saturated with 1.0 μ M NBD-Toc in SET buffer and 100 μ M TX100, with [competitor] α -Toc & cholesterol in EtOH. | 113 |
| Figure 72. Competition assay of 0.5 μ M α -TTP, saturated with 1.0 μ M thienyl-ene-BODIPY (3) in SET buffer, with α -Toc & 100 μ M TritonX100. | 114 |
| Figure 73. Direct binding of thienyl-ene-BODIPY (3) in EtOH to 0.2 μ M α -TTP in SET buffer with 100 μ M TX100. | 114 |
| Figure 74. Direct binding of thienyl-ene-BODIPY (3) in EtOH to 0.2 μ M α -TTP in SET buffer with 10 μ M TX100. | 115 |
| Figure 75. Titration of 0.5 μ M α -TTP, saturated with 1.0 μ M thienyl-ene-BODIPY (3) in SET buffer, test with increasing TX100 amounts by 10 μ M. | 116 |
| Figure 76. Direct binding of thienyl-ene-BODIPY (3) in EtOH to 0.5 μ M α -TTP & BSA. | 117 |
| Figure 77. Thienyl-ene-BODIPY (3) solubility test with DMSO in TKE buffer. | 118 |
| Figure 78. Direct binding of thienyl-ene-BODIPY (3) in EtOH to 0.2 μ M α -TTP in TKE buffer. | 119 |
| Figure 79. Direct binding of thienyl-ene-BODIPY (3) in EtOH to 0.5 μ M α -TTP in TKE buffer. | 119 |

| | |
|---|-----|
| Figure 80. Direct binding of thienyl-ene-BODIPY (3) in EtOH to 0.5 μ M α -TTP & BSA in TKE buffer..... | 120 |
| Figure 81. Test of ligand over addition. Direct binding of thienyl-ene-BODIPY (3) in EtOH to 0.4 μ M α -TTP in TKE buffer..... | 121 |
| Figure 82. Competition assay of 0.1 μ M α -TTP, saturated with 0.2 μ M thienyl-ene-BODIPY (3) in TKE buffer, with α -Toc in EtOH. | 122 |
| Figure 83. Competition assay of 0.1 μ M α -TTP, saturated with 0.5 μ M thienyl-ene-BODIPY (3) in EtOH in TKE buffer, with cholesterol. | 122 |
| Figure 84. Thienyl-ene-BODIPY (3) test competition assay of 0.4 μ M α -TTP, saturated with 0.8 μ M (black), 0.4 μ M (red and pink) thienyl-ene-BODIPY (3) in TKE buffer, with cholesterol (as EtOH solutions, red & black) and EtOH only (pink)..... | 123 |
| Figure 85. Direct binding of thienyl-ene-BODIPY (3) in DMF to 0.4 μ M α -TTP in TKE buffer..... | 124 |
| Figure 86. Competition assay of 0.4 μ M α -TTP, saturated with 0.4 μ M thienyl-ene-BODIPY (3) in TKE buffer, with α -Toc solution in DMF and DMF alone..... | 124 |
| Figure 87. Competition assay of 0.4 μ M α -TTP, saturated with 0.4 μ M thienyl-ene-BODIPY (3) in TKE buffer, with cholesterol (in DMF) and DMF..... | 125 |
| Figure 88. Competition assay of 0.4 μ M α -TTP, saturated with 0.4 μ M thienyl-ene-BODIPY (3) in TKE buffer, with α Toc (DMF), EtOH and DMF..... | 126 |
| Figure 89. Synthesis of MeO-thienyl-ene-BODIPY (40)..... | 126 |
| Figure 90. Direct binding of MeO-Thienyl-ene-BODIPY (40) in DMF to 0.4 μ M α -TTP in TKE buffer..... | 127 |
| Figure 91. Direct binding of thienyl-ene-BODIPY (3) in dioxane 0.4 μ M to α -TTP in TKE buffer..... | 128 |
| Figure 92. Competition assay of 0.4 μ M α -TTP, saturated with 0.4 μ M thienyl-ene-BODIPY (3) in TKE buffer, with α -Toc (in dioxane) and dioxane. | 128 |
| Figure 93. Competition assay of 0.4 μ M α -TTP, saturated with 0.4 μ M thienyl-ene-BODIPY (3) in TKE buffer, with cholesterol (in dioxane) and dioxane..... | 129 |
| Figure 94. α -TTP facilitated secretion of thienyl-ene-BODIPY 3, from cultured hepatocytes. | 131 |
| Figure 95. Averages and standard deviations of 5 images from three independent experiments. | 132 |
| Figure 96. α -TTP-induced α -tocopherol secretion in HepG2-TetOn-TTP cells. | 133 |
| Figure 97. Quantification of intracellular NBD- α -tocopherol fluorescence over time in cells that do (white bars) or do not (black bars) express TTP..... | 134 |
| Figure 98. PUFA oxidation: Initiation, propagation and termination. ³¹⁹ | 137 |
| Figure 99. Product distribution for the peroxidation of methyl linolenate peroxide product. ³²² | 138 |
| Figure 100. Radical reactions in lipids..... | 139 |
| Figure 101. Oxidation products of methyl linolate and α -tocopherol. ³²⁷ | 140 |
| Figure 102. The decay of 5,7-diisopropyl-tocopheroxyl radical reacted with ethyl stearate, linoleate, linolenate and arachidonate observed at 417 nm in benzene at 25.0°C [Toc: 0.17 mM and [LH] _{t=0} 75.0 mM]. ³³³ | 142 |
| Figure 103. Orbital alignments in chroman and benzofurane. ³³⁴ | 143 |
| Figure 104. Disappearance of vitamin E and vitamin C in the oxidation of methyl linoleate at 37°C in <i>tert</i> -butyl alcohol/methanol (3:1 by volume)..... | 144 |
| Figure 105. β -carotene reaction with singlet oxygen (¹ O ₂) and RO*, ROO*. ³⁴⁷ | 145 |

| | |
|--|-----|
| Figure 106. Effect of oxygen concentration in peroxyradical formation in methyl linolate 18:3 (200mM) initiated by AMVN (1mM) at 37°C. | 146 |
| Figure 107. Position of tocopherol to the phospholipid head group. ^{363,364} | 148 |
| Figure 108. Location of tocopherol in membranes. ³⁶³ | 149 |
| Figure 109. Vitamin E inhibition of LDL and oxLDL receptor mediated atherosclerosis. ³⁹⁰ | 152 |
| Figure 110. Basic principle of halogen and hydrogen bonding to a Lewis base. | 155 |
| Figure 111. Calculated charge distribution of alkyl halides (top) and halogenated nucleobases (bottom). ⁴⁰³ | 156 |
| Figure 112. Halogen bonding interaction of a substituted indomethacin ethanolamide analogue to COX-1. ⁴⁰⁵ | 157 |
| Figure 113. Cartoon representation of possible halogen bonding of a halo- α -tocopherol interaction in α -TTP. | 158 |
| Figure 114. Radical abstractions bond dissociation energies of HM-Toc & α -Toc. ⁴⁰⁹ | 159 |
| Figure 115. Calculated hydrophilic interaction of α -tocopherol (A, top) and γ -tocopherol (B, bottom) in the wild-type α -TTP binding pocket. | 160 |
| Figure 116. Cartoon representation of possible HM-Toc position in α -TTP. | 161 |
| Figure 117 Synthetic strategies to Cl-Toc, 43, and HM-Toc, 44, from α -tocopherol. ^{423,428,429} | 162 |
| Figure 118. Synthetic strategies to racemic Cl-Toc, 43, and racemic HM-Toc, 44, from 2,3,5-trimethylphenol and 45. ^{423,428} | 163 |
| Figure 119. AcO- α -Toc deprotection to α -tocopherol. | 163 |
| Figure 120. α -Toc conversion to α -tocopherol triflate 41, followed by reduction to H-Toc, 42. ⁴²³ | 164 |
| Figure 121. Chlorination of H-Toc 42 to Cl-Toc 43. ⁴²⁹ | 164 |
| Figure 122. Hydroxymethylation of H-Toc 42 to HM-Toc 44. | 164 |
| Figure 123. Rieche formylation of H-Toc 42 to product 46. ⁴²⁸ | 165 |
| Figure 124. Reduction of 46 to HM-Toc 44. | 165 |
| Figure 125. Absorption spectra HM-Toc in EtOH. | 166 |
| Figure 126. Competition assay of 0.4 μ M α -TTP, saturated with 1.6 μ M NBD-C9-Toc in SET buffer, with α -Toc and Cl-Toc in EtOH. | 167 |
| Figure 127. Competition assay of 0.4 μ M α -TTP, saturated with 1.6 μ M NBD-C9-Toc in SET buffer, with α -Toc and HM-Toc in EtOH. | 168 |
| Figure 128. Micelle test 1.6 μ M NBD-C9-Toc with HM-Toc and α -Toc in SET buffer. | 169 |
| Figure 129. Competition assay of 0.4 μ M α -TTP, saturated with 1.6 μ M NBD-C9-Toc in SET buffer, with α -Toc and HM-Toc in EtOH adjusted with micelle data (Figure 137). | 169 |
| Figure 130. Expected UV absorption (230nm) of the non-antioxidant tocopherol. | 170 |
| Figure 131. Radical initiators and peroxidation systems used to oxidize PC. ⁴³²⁻⁴³⁴ | 171 |
| Figure 132. CV (BASi-Epsilon) oxidation of α -tocopherol (2.5 mM in dry dichloromethane) at 200 mV/s with 80 mM tetrabutylammonium hexafluorophosphate. | 171 |
| Figure 133. CV (BASi-Epsilon) oxidation of HM-Toc (2.5 mM in dry dichloromethane) at 200 mV/s with 80 mM tetrabutylammonium hexafluorophosphate. | 172 |
| Figure 134. CV (BASi-Epsilon) oxidation of H-Toc (2.5 mM in dry dichloromethane) at 200 mV/s with 80 mM tetrabutylammonium hexafluorophosphate. | 172 |
| Figure 135. AMVN initiated oxidation of multilamellar SoyPC vesicle with HM-Toc & α -Toc. | 173 |
| Figure 136. Products observed during the assessment of HM-Toc stability in acetic media. | 175 |

| | |
|--|-----|
| Figure 137. Relative survival of cancer over a 5-year span in the USA..... | 178 |
| Figure 138. Positron emission (β^+) and electron capture via x-ray fluorescence or Auger electron emission. ⁴⁴⁴ | 180 |
| Figure 139. Positron annihilation, formation of two γ -photons each having an energy of 511keV. ⁴⁴⁹ | 181 |
| Figure 140. 18-F Radiotracers of biological importance towards the study of cancer (Fluodeoxyglucose, Fluciclovine, fluoroethyltyrosine), neurodegenerative diseases (Flutemetamol, Fluoro- <i>L</i> -DOPA, Florbetair) and addictions (Cyclofoxy). ^{449,453,456} | 185 |
| Figure 141. SPECT imaging agents based on ¹²³ I (Ibenguane, Ioflupane) and ^{99m} Tc (Sestamibi, Ceretec) and the nuclei decay times and emitted particle energies..... | 186 |
| Figure 142. Particle acceleration in a cyclotron..... | 187 |
| Figure 143. Halex reaction, formation of a Meisenheimer complex (MHC). ⁴⁷⁴ | 193 |
| Figure 144. Halex fluorination of electron deficient aromatics. | 194 |
| Figure 145. (a) Balz-Schiemann reaction of benzene, ⁴⁸² (b) 5- ¹⁸ F- <i>L</i> -DOPA ⁴⁸³ and (c) ¹⁸ F-Haloperidol synthesis. ⁴⁸⁴ | 195 |
| Figure 146. Wallach reaction of benzene. ⁴⁸⁶ | 195 |
| Figure 147. Radio-fluorination of diaryliodonium- and triarylsulfonium salts. ^{487,488} | 196 |
| Figure 148. Formation of diaryliodonium salts by reaction of aromatics with aromatic hypervalent iodines. ⁴⁸⁸ | 196 |
| Figure 149. (a) Dependence of diaryliodonium salt fluorination on the electronic nature of the aromatics involved. | 197 |
| Figure 150. (a) Transition metal mediated radio fluorination with (a) nickel ⁴⁹⁴ (b) copper ⁴⁹⁵ and (c) palladium. ⁴⁹³ | 198 |
| Figure 151. Nucleophilic fluorination of aromatic sulfonates. | 199 |
| Figure 152. (a) Palladium mediated fluorination of aryl triflates. ⁴⁹⁶ (b) Deoxyfluorination with Phenofluor®. ⁴⁹⁸ | 199 |
| Figure 153. Electrophilic fluorinating agents. ⁴⁹⁹⁻⁵⁰¹ | 201 |
| Figure 154. Electrophilic aromatic radiofluorination (¹⁸ F ₂) with of aryl stannanes and electron rich phenols. | 202 |
| Figure 155. Electrophilic aromatic fluorination reaction mechanisms. | 202 |
| Figure 156. (a) Hunsdieker reaction of benzoic acid with xenondifluoride. ⁵⁰⁰ Silvermediated fluorination of (b) arylstannane ⁵⁰⁷ and (c) arylboronic acids. ⁵⁰⁸ | 203 |
| Figure 157. ¹⁸ F-containing α -tocopherol radiotracers as a tool to follow cancer-targeting liposomes. | 204 |
| Figure 158. Designed ¹⁸ F-tocopherol tracers, 47-51, and their products formed after radioactive decay..... | 206 |
| Figure 159. Designed dual-lable ¹⁸ F-thienyl-ene-BODIPY ¹⁸ F-3..... | 207 |
| Figure 160. Problems associated with electrophilic- and nucleophilic fluorination. | 208 |
| Figure 161. Synthetic strategies towards 6'-F- α -tocopherol by nucleophilic and electrophilic fluorination ^{514, 515} | 209 |
| Figure 162. Synthetic scheme for TiO ₂ mediated fluorination of aryl tosylates. ⁵¹⁸ | 210 |
| Figure 163. Tosylation of pentamethylchromanol. | 210 |
| Figure 164. Change of TiO ₂ anatase percentage dependend on the calcination time at 600°C..... | 211 |
| Figure 165. (a) Copper mediated fluorination of boronic esters and synthesis of ¹⁸ F-FPEB. ⁴⁹⁵ (b) 2- ¹⁸ F-fluoro- <i>L</i> -tyrosine synthesis via Fluoro-destannylation and silver mediated fluorination of stannyl- δ -tocopherol. ^{527,507} | 216 |
| Figure 166 δ -Tocopherol triflate stannylation by Ritter ⁵⁰⁷ and Miller ⁵²⁸ and stannylation attempts of α -Tocopherol. | 217 |

| | |
|---|-----|
| Figure 167. Synthesis of α -tocopherolpinacolboronic ester 56, δ -6'- tocopherolpinacolboronic ester from α -tocopherol triflate. ⁵²⁸ | 218 |
| Figure 168. (a) Mazzini's α -tocopherol amine synthesis. ⁵²⁹ (b) α -Tocopherol triflate borylation with Mazzini's conditions. (c) α -Tocopherol triflate borylation with PdCl ₂ (dppf). ⁵³⁰ | 219 |
| Figure 169 Palladium catalyzed borylation of sterically demanding, electron-rich aromatics. | 219 |
| Figure 170. Tetrakispyridine copper(II)triflate catalyzed fluorination of 56. ⁵³³ | 220 |
| Figure 171. Synthesis of Phenofluor® precursor Cl-NHC. ⁵³⁴ | 220 |
| Figure 172. Attempted Phenofluor® fluorination of α -tocopherol. ⁵³⁴ | 221 |
| Figure 173 Phenofluor® intermediate 59 formation with phenols. | 222 |
| Figure 174. ¹⁸ F-fluorination of NHC-bound phenols. ⁵¹⁷ | 223 |
| Figure 175. Ruthenium catalysed Phenofluor® fluorination of δ -tocopherol. ⁵³⁷ | 223 |
| Figure 176. Nucleophilic fluorination of diaryliodonium salts. | 224 |
| Figure 177. Designed electron rich 6- α -tocopherol iodonium salts with different auxiliaries: Thiophene 60 ·OTs, 61 ·OTf, 62 ·BF ₄ and <i>p</i> -methoxybenzene 63 ·OTs, 64 · OTf, 65 ·BF ₄ . | 224 |
| Figure 178. Synthesis of iodonium salts via insitu oxidation of aryl iodides with aromatics (Y) (top), with pre-oxidized hypervalent iodines / aromatics (middle) and boronic acids / esters or stannylates (bottom). ^{540,541,489} | 225 |
| Figure 179. Fluorination of Meldrum's acid iodonium ylides. ⁵⁴² | 225 |
| Figure 180. (Aryl)- α -tocopherol iodonium salt synthesis from H-Toc or 6-I- α -Toc. | 226 |
| Figure 181. Synthesis of (thiophene)- α -tocopherol iodonium trifluoroacetate, 61. ⁵⁴⁴ | 226 |
| Figure 182. 2-(Diacetoxy)thiophene synthesis by Wu ⁵⁴⁵ , followed by addition to H-Toc. | 227 |
| Figure 183. Synthesis of (<i>R</i>)-(2-hexadecyl-2,5,7,8-tetramethylchroman-6- yl)(phenyl)iodonium bromide 67 from H-Toc. ⁵³⁸ | 227 |
| Figure 184. Synthesis of (<i>R</i>)-(2-hexadecyl-2,5,7,8-tetramethylchroman-6- yl)(phenyl)iodonium trifluoroacetate 68 from H-Toc. ⁵⁴⁴ | 228 |
| Figure 185. Synthesis of (<i>R</i>)-(2-hexadecyl-2,5,7,8-tetramethylchroman-6- yl)(phenyl)iodonium tosylate 69 from H-Toc. ⁵⁴⁶ | 228 |
| Figure 186. Carboxylation of 6-I- α -Toc via lithium-halogen and Grignard reaction. | 231 |
| Figure. 187 Carboxylation of 6-I- α -Toc 71 with magnesium (top), ⁵⁵³ lithium-halogen exchange (middle) and palladium dichloride catalyzed carbonylation (bottom). ⁵⁵⁴ | 232 |
| Figure 188. Photoborylation of aryl iodides with B ₂ OH ₂ by Chen. ⁵⁵⁵ | 232 |
| Figure 189. Fluorination of spirocyclic Meldrum's acid iodonium ylides. ⁵⁵⁶ | 233 |
| Figure 190. Meldrum's acid- α -tocopherol iodonium ylide synthesis 73 from 6-I- α -Toc. ⁵⁴² | 234 |
| Figure 191. Synthesis of (diacetoxy)iodo- α -tocopherol 74 from 70. ⁵⁴⁰ | 234 |
| Figure 192. Iodination of H-Toc. (a) with ICl, ⁵⁵⁸ (b) ICl, DDQ, ⁵⁵⁸ (c) I ₂ , AgOTf ⁵⁵⁹ and (d) 1- iodopyridinium chloride 71. ⁵⁶⁰ | 236 |
| Figure 193. Synthesis of F-Toc from H-Toc with electrophilic fluorinating reagents F-Py BF ₄ , Selectfluor® and NFSI. ^{567,505} | 238 |
| Figure 194. HPLC separation of α -toc, F-Toc, H-Toc, 6-I- α -toc, 6-Cl- α -toc. | 241 |
| Figure 195. HPLC separation of F-Toc and H-Toc. | 243 |
| Figure 196. HPLC separation of 6-I- α -Toc, 6-Cl- α -Toc and H-Toc. | 244 |
| Figure 197. Separation of benzenes with increasing fluorine substitution. | 245 |
| Figure 198. Synthetic strategies towards 5-F- γ -tocopherol by electrophilic fluorination. | 246 |

| | |
|--|-----|
| Figure 199. Electrophilic ^{18}F -fluorination of phenols..... | 247 |
| Figure 200. Phenol fluorination with electrophilic fluorinating reagents (a) NFSI, (b) Selectfluor and (c) 1-Fluoropyridinium triflate. ^{584,586,587} | 248 |
| Figure 201. Byproducts 76 formed during the fluorination of γ -tocopherol sodium phenolate with NFSI. | 249 |
| Figure 202 Byproduct 76 formation from γ -tocopherol sodium phenolate fluorination with NFSI. ⁵⁶¹ | 250 |
| Figure 203 Poon's 5,5' - δ -telluro- <i>bis</i> -tocopherol synthesis. ⁵⁷⁷ | 250 |
| Figure 204. Bromination of γ -tocopherol with TBAB. ⁵⁷⁷ | 250 |
| Figure 205 Fluorination of 5-Br- γ -tocopherol via lithium-halogen exchange reaction..... | 251 |
| Figure 206 γ -Tocopherol fluorination with acetylhypofluorite. | 251 |
| Figure 207 Synthetic strategies towards 5-F-Me- α -tocopherol by nucleophilic fluorination. | 252 |
| Figure 208 Benzylically ^{18}F -labeled biologically active compounds. ⁵⁹¹ | 252 |
| Figure 209 Manganese(salen) catalyzed fluorination of δ -tocopherol. ⁵⁹¹ | 253 |
| Figure 210. Benzylic ^{18}F -fluorination by nucleophilic substitution. ^{592,593,594} | 253 |
| Figure 211 Substitution of 5-Br-Me- α -toc with nucleophiles. ⁵⁹⁵ <i>N</i> -protection of aminoacids with α -tocopherol ⁵⁹⁶ | 254 |
| Figure 212 Thermally induced formation of α -tocopherol spiro-dimer formation from 5-Br-Me- α -toc. ⁵⁸⁸ | 254 |
| Figure 213 AcO-5'Br-Me- α -toc 77 synthesis from α -tocopherol. ⁵⁸⁸ | 255 |
| Figure 214. Fluorination of 78 with CsF and <i>t</i> -BuOH. Formation of product 78 and byproduct 79. ⁵⁹⁷ | 256 |
| Figure 215 Deprotection of 78 in basic media with KOH in EtOH. Formation of ethoxyether 80. ²⁷⁹ | 256 |
| Figure 216. Attempted deprotection of AcO-5-F-Me- α -toc 78 in acetic media with TFA and formation of byproduct 5-trifluoroacetyl α -tocopherol acetate 81..... | 257 |
| Figure 217. α -Tocopherol <i>ortho</i> -quinone methide (oQM) dimerization to the α -tocopherol-spirodimer and stabilization of the α -tocopherol oQM by NMMO and <i>S</i> -ylide. ^{599,600,601} | 258 |
| Figure 218. Synthesis of (<i>O</i> -acetylsalicyl)saligenin from <i>o</i> -cresol. ⁶⁰¹ | 258 |
| Figure 219. Synthetic strategies towards 6'-F-Me- α -tocopherol 50..... | 261 |
| Figure 220. Synthesis of benzylic- ^{18}F -fluoromethyl-spiperone and 1-phenylpiperazine. ⁶⁰⁵ | 261 |
| Figure 221. ^{18}F -Fluorination of methyl 4-(bromomethyl)-2-chlorobenzoate. ⁶⁰⁶ | 262 |
| Figure 222. Deoxyfluorination of benzylic alcohols with DAST, Xtalfluor-E® and Xtalfluor-M®. ⁶⁰⁷⁻⁶⁰⁸ | 262 |
| Figure 223. HM-Toc fluorination with CsF and <i>t</i> -BuOH. Synthesis of byproduct 46 and 81. ⁵⁹⁷ | 264 |
| Figure 224. Synthesis of sulfonate esters, 82 and 83, from HM-Toc, formation of dimer 46. ^{603,610} | 265 |
| Figure 225. Iodination of HM-Toc with I_2 , PPh_3 and DMAP to product 84..... | 265 |
| Figure 226. Alternative benzylic iodination / bromination of HM-Toc. ^{613,616,617} | 266 |
| Figure 227. Synthesis of 13-F- α -Toc, 51, from α -tocotrienol. | 267 |
| Figure 228. Taylor's synthesis of 13-HO- α -Toc, 86, from α -tocotrienol..... | 268 |
| Figure 229. Synthesis of 13-HO- α -Toc, 86, from garcinoic acid. ⁶¹⁹ | 269 |
| Figure 230. BOIDPY ^{19}F - ^{18}F exchange with (a) TMSOTf ⁶²¹ and (b) Lewis acid ⁶²² | 270 |

| | |
|--|-----|
| Figure 231. 1,3-Dimethyl BODIPY fluoride exchange via mono-OTf BODIPY intermediate 87. ⁶²¹ | 270 |
| Figure 232. Direct TBAF addition to 1,3-Dimethyl BODIPY. | 271 |
| Figure 233. Direct TBAF addition to 2,8-diethyl-1,3,5,7,9-pentamethyl BODIPY..... | 272 |
| Figure 234. Fluorine exchange of 1,3-dimethyl-BODIPY, 37, followed by UV / VIS..... | 273 |
| Figure 235. 1,3-Dimethyl-BODIPY. Left: standard reference 0.32 μ M. Right cuvette: 0.32 μ M. Blue line in Figure 234..... | 273 |
| Figure 236. 1,3-Dimethyl-BODIPY. Left cuvette: standard reference 0.32 μ M. Right cuvette: Tf ₂ O addition. Red line in Figure 234..... | 274 |
| Figure 237. 1,3-Dimethyl-BODIPY. Left cuvette: standard reference 0.32 μ M. Right cuvette: 1) <i>t</i> -BuOH 2) Lutidine 3) TBAF addition. Green line in Figure 234. | 274 |
| Figure 238. Fluorine exchange of thienyl-ene-BODIPY, 3, followed by UV/ Vis..... | 275 |
| Figure 239. Thienyl-ene-BODIPY. Left cuvette: standard reference 0.16 μ M. Right cuvette: 0.32 μ M. Blue line in Figure 238. | 276 |
| Figure 240. Thienyl-ene-BODIPY. Left cuvette: standard reference 0.16 μ M. Right cuvette: Tf ₂ O addition. Red line in Figure 238..... | 276 |
| Figure 241. Thienyl-ene-BODIPY. Left cuvette: standard reference 0.16 μ M. Right cuvette: 1) <i>t</i> -BuOH 2) Lutidine 3) TBAF addition. Green line in Figure 238. | 277 |
| Figure 251. Viability of mouse cells cultured in the presence of α -, F-, and HM-tocopherol derivatives at concentrations ranging from 1 nM to 1 mM..... | 279 |
| Figure 252. Viability of mouse cells cultured in the presence of BODIPY-tocopherol at concentrations ranging from 1 nM to 0.1 mM..... | 280 |
| Figure 253. Viability of mouse cells cultured in the presence of H-tocopherol (H-toc) at concentrations ranging from 1 nM to 1 mM. | 281 |
| Figure 254. Viability of mouse cells cultured in the presence of I-tocopherol (I-toc) at concentrations ranging from 1 nM to 1 mM. | 282 |
| Figure 255. Viability of mouse cells cultured in the presence of varying concentrations of large unilamellar vesicles (LUVs)..... | 283 |
| Figure 256. Viability of mouse cells cultured in the presence of varying concentrations of large unilamellar vesicles (LUVs)..... | 284 |
| Figure 257. C2C12 cell uptake of thienyl-ene-BODIPY-tocopherol (BODIPY-tocopherol) delivered in LUVs..... | 285 |
| Figure 258. Uptake of thienyl-ene-BODIPY-tocopherol (BODIPY-tocopherol) in C2C12 cells at 30 min after delivery via DMSO or LUVs..... | 286 |
| Figure 259. Mouse embryonic fibroblast uptake of thienyl-ene-BODIPY-tocopherol (BODIPY-tocopherol) delivered in LUVs..... | 287 |
| Figure 260. Mouse embryonic fibroblast uptake of BODIPY-tocopherol delivered in DMSO. | 288 |
| Figure 261. Fluorine exchange (F _a -F _b) on thienyl-ene-BODIPY..... | 290 |

List of tables

| | |
|---|-----|
| Table 1. Tocopherol and tocotrienol structures. ¹⁰ | 30 |
| Table 2. Vitamin E amount in unsaponifiable palm oil. ^{Error! Bookmark not defined.} | 31 |
| Table 3. Ligand binding to CRAL-domain proteins; Comparison of dissociation constants of α -TTP, <i>S. cerevisiae</i> Sec14p, SPF, and CRALBP for various hydrophobic ligands. | 46 |
| Table 4. Antioxidant inhibition of α -tocopherol, melatonin & <i>N</i> -acetyl-serotonin in mitochondria and microsomes as IC ₅₀ values based on 50% inhibition of light emission. ¹²⁴ | 56 |
| Table 5. Maximum wavelength, absorption and fluorescence of aromatic amino acid. ¹⁷⁴ | 68 |
| Table 6. Excitation and emission wavelength of commercial dyes for fluorescent microscopy. ¹⁸¹⁻¹⁸⁷ | 72 |
| Table 7. Comparison of BODIPY-Toc to α -Toc-C9-NBD. ^{200,205} | 74 |
| Table 8. Influence of chain length linker on the α -TTP dissociation constants (K_d) of NBD- α -Toc and BODIPY (BDP)- α -Toc. ²⁰⁵ | 78 |
| Table 9. Conjugation effects to BODIPY. | 80 |
| Table 10. Inhibition rates (k_{inh}) of vitamin E by different techniques. ³²⁷ | 140 |
| Table 11. Content of α -tocopherol (mmol/mol lipid) in subcellular membranes of rats fed a standard laboratory diet. ³⁵² | 147 |
| Table 12. Halogen bond and the influence of bonding angle α on bond length and strength. ^{397,398} | 155 |
| Table 13. Stability assessment of HM-Toc. | 174 |
| Table 14. Radiation weight factor (W_r) of different radiation types. ⁴⁴⁴ | 182 |
| Table 15. Tissue weight factor (W_T). | 183 |
| Table 16. Nucleophilic and electrophilic ¹⁸ F radio nucleotide synthesis. ⁴⁵⁸⁻⁴⁶¹ | 190 |
| Table 17. Solubility of alkali halides in methanol. | 191 |
| Table 18. Solubility of sodium-, potassium- and caesium fluoride in acetonitrile and dimethylformamide with and without 18-Crown-6. ⁴⁶⁸ | 193 |
| Table 19. Anatase percentage (%A) in Degussa P25 TiO ₂ at increasing temperature, after 24 h. | 212 |
| Table 20. TiO ₂ mediated fluorination of TsO-PMC. | 213 |
| Table 21. TiO ₂ mediated fluorination of TsO-Naphthol. | 214 |
| Table 22. TiO ₂ mediated fluorination of with EPRUI® 200 nm TiO ₂ NP. | 215 |
| Table 23 Fluorination of (<i>R</i>)-(2-hexadecyl-2,5,7,8-tetramethylchroman-6-yl)(phenyl)iodonium tosylate 69. | 229 |
| Table 24. Photoborylation of 6-I- α -Toc to form 72. | 233 |
| Table 25. Fluorination of 6-I- α -toc with BuLi and NFSI. | 237 |
| Table 26. Fluorination of H-Toc with electrophilic fluorinating reagents. | 239 |
| Table 27. Fluorination of γ -tocopherol with electrophilic fluorinating reagents. | 249 |
| Table 28. Fluorination of AcO-5-Br-Me- α -toc. ⁷⁷ | 255 |
| Table 29. 78 was stirred in a μ -wave oven or for 10-20 min. | 257 |
| Table 30 α -Tocopherol fluorination with Ag ₂ O. | 259 |
| Table 31. α -Tocopherol fluorination with Ag ₂ O and stabilizing agents. | 260 |
| Table 32. Deoxyfluorination of HM-Toc. | 263 |
| Table 33. Nucleophilic fluorination of HM-Toc. | 264 |
| Table 38. Contents for 10 mg/mL of 7:3:4-POPC:POPG:Cholesterol. | 295 |

| | |
|--|-----|
| Table 39. Contents for 2 mg/mL of 7:3:4:0.1-POPC:POPG:Cholesterol:BODIPY. | 295 |
|--|-----|

List of Abbreviations

| | |
|---------------------|---|
| -CH ₂ - | Methylene (-CH ₂ -) bridge |
| 4-HPPA | 4-Hydroxypyruvate |
| 5-LOX | 5-Lipoxygenase |
| 9-CDMOHC | 9-Carboxymethyloctylhydroxychromanol |
| 11-CDMDHC | 11-Carboxydimethyldecylhydroxychromanol |
| 17-β-E ₂ | 17-β-estradiol |
| [³ T] | Tritium |
| α | Alpha |
| β | Beta |
| γ | Gamma |
| δ | Delta |
| ω | Omega |
| ε | Extinction coefficient |
| Φ _F | Fluorescence quantum yield |
| τ | Fluorescence lifetime |
| λ | Wavelength |
| α-CEHC | Alpha-carboxyethylhydroxychroman |
| α-TL | Alpha-tocopheronelactoneα-tocopheronelactone |
| α-Toc | Alpha-tocopherol |
| α-TocO [•] | Alpha-tocopherol radical |
| α-TTP | Alpha-tocopherol transfer protein |
| γ-NGT | 5'-NO ₂ Tocopherol |
| Å | Ångström |
| AA | Arachidonic acid |
| ABCA1 | ATP-binding cascade A1 transporters |
| Aβ | β-amyloid protein |
| AMPA | α-amino-3-hydroxy-5-methyl-4-isoxazolepropionic acid receptor |
| AO-α-Toc | ω-anthroyloxy-α-tocopherol |

| | |
|-------------------------------------|--|
| Apo | Apolipoprotein |
| APP | Amyloid precursor protein |
| ATP | Adenosine triphosphate |
| AVED | Ataxia with Vitamin E Deficiency |
| BHT | Butylated hydroxyl toluene / 2,6-di- <i>tert</i> -butyl-4-methylphenol |
| BODIPY | 4,4-Difluoro-4-bora-3a,4a-diaza-s-indacene |
| Bq | Bequerel |
| BSA | Bovine serum albumin |
| BuLi | Butyllithium |
| CCl ₄ | Carbon tetrachloride |
| CEHC | Carboxyethyl hydroxychromans |
| CLSM | Confocal light scanning microscope |
| CNS | Central nervous system |
| CoQ(10) | Coenzyme Q 10 / Ubiquinone |
| CoQH ₂ | Ubiquinol |
| COX-2 | Cyclooxygenase-2 |
| CRALBP | Cellular retinaldehyde binding protein 1 |
| DABCO / TEDA | 1,4-Diazabicyclo[2.2.2]octan / Triethylendiamin |
| DAG | Diacylglycerol |
| DAHP | 3-Dehydroxy-D-arbino-heptalose-7-phosphate |
| DCM | Dichloromethane |
| DFOA | Desferrioxaamine |
| DHQ | 3-Dehydroquinone |
| DHQD | Dehydroquinase dehydratase |
| Di- <i>i</i> -pro-TocO [•] | Di- <i>i</i> -propyl tocopheroxy radicals |
| DIBAL | Diisobutylaluminium hydride |
| DLPC | 1,2-Dilauroyl-sn-glycero-3-phosphorylcholine |
| DMAPP | Dimethylallyl pyrophosphate |
| DMF | Dimethylformamide |
| DMSO | Dimethylsulfoxide |
| DOPE | Dioleoylphosphatidylethanolamine |
| DOPS | 1,2-Dioleoyl-sn-glycero-3-phospho-L-serine |
| DPPH | 2,2-Diphenyl-1-picrylhydrazyl |
| DSSC | Dye sensitized solar cell |

| | |
|-------------------------------|--|
| E4P | D-erythrose-4-phosphate |
| EAATS | Excitatory amino acid transporters |
| EDTA | Ethylenediamine tetraacetic acid |
| EPR | Electron spin resonance |
| EPSP | 5-Enolpyruvylshikimate-3-phosphate |
| ER | Endoplasmic reticulum |
| FA | Fatty acid |
| Fluorazophore-L | 2,3-Diazabicyclo[2.2.2]-2-octene palmate (DBO-palmate) |
| FRET | Förster resonance energy transfer |
| GGDP | Geranylgeranyldiphosphate |
| GGPP | Geranylgeranylpyrophosphate |
| GGR | Geranylgeranyl reductase |
| GOLD | Golgi dynamics |
| GPCR | G-protein coupled receptors |
| GPP | Geranyl pyrophosphate |
| GS | Glutamine synthase |
| GSSG | Glutathione disulfide |
| H ₂ O ₂ | Hydrogen peroxide |
| Hc | Hectare |
| HCl | Hydrogen chloride |
| HDL | High-dense lipoproteins |
| HGA | Homogentistic acid |
| HO [•] | Hydroxyl radical |
| HOMO | Highest occupied molecular orbital |
| IAS | Inhibitory auto-oxidation assay with the styrene |
| IC ₅₀ | Inhibitory concentration 50% |
| ICAM-1 | Intracellular adhesion molecule-1 |
| ICM | Intermediate chain metabolites |
| IP ₃ | Inositol trisphosphate |
| IPP | Isopentenyl pyrophosphate |
| IRS-1 | Insuline receptor substrate 1 |
| k_d | Dissociation constant |
| k_{inh} | Inhibition rate |
| k_p | Propagation rate |

| | |
|------------------------------|---|
| k_q | Antioxidant efficiency |
| kDa | Kilo dalton |
| KIE | Kinetic isotope effect |
| LCM | Long chain metabolites |
| LDL | Low density lipoprotein |
| LHMDS | Lithium hexamethyldisilazide |
| LOO [•] | Lipid peroxy radical |
| LPA | Lysophosphatic acid |
| LPL | Lipoprotein lipase |
| LRP | Low-density receptor related protein receptors |
| LUMO | Lowest unoccupied molecular orbital |
| MAO-B | Monoamine oxidase B |
| MAP | Mitogen-activated protein |
| MD | Molecular dynamic |
| MDA | Malondialdehyde |
| MDT | Marine-derived tocopherol |
| mGluR | Metabotropic glutamate receptor |
| MMT | <i>L</i> -Methionine <i>S</i> -methyl transferase |
| MPP ⁺ | 1-Methyl-4-phenylpyridinium |
| MPTP | 1-Methyl-4-phenyl-1,2,3,6-tetrahydropyridin |
| mtNOS | Mitochondrial nitric oxide synthase |
| NAS | <i>N</i> -acetyl-serotonin |
| NBD | Nitrobenzoxadiazole |
| NF- κ B | Nuclear factor- κ B |
| NMDA | <i>N</i> -Methyl- <i>D</i> -aspartate |
| NMR | Nuclear magnetic resonance |
| NO | Nitric oxide |
| NOS | Nitric oxide synthase |
| NPC1L1 | Niemann-Pick C1-like protein 1 receptors |
| O ₂ ^{•-} | Superoxide |
| O ₂ ¹ | Singlet oxygen |
| PA | Phosphatidic acid |
| PC | Phosphatidylcholine |

| | |
|-------------------------|---|
| Pd/C | Palladium on carbon |
| PDP | Phytyldiphosphate |
| PEP | Phosphoenolpyruvate |
| PE | Phosphatidylethanolamine |
| PI | Phosphatidylinositol |
| PI(4,5)P ₂ | Phosphatidylinositol(4,5)bisphosphate |
| PI(3,4,5)P ₃ | Phosphatidylinositol(3,4,5)triphosphate |
| PKC | Protein kinase C |
| PLA ₂ | Phospholipase A ₂ |
| PLC | Phospholipase C |
| PMC | Pentamethylchromanol |
| POPC | 1-Palmitoyl-2-oleoyl- <i>sn</i> -glycero-3-phosphocholine |
| PP ₂ A | Protein phosphatase 2A |
| PPh ₃ | Triphenylphospine |
| PTP | Protein tyrosine phosphate |
| PUFA | Polyunsaturated fatty acid |
| RAF | Rapidly accelerated fibrosarcoma protein kinase |
| R _i | Initiation rate |
| RKIP | RAF-1 kinase inhibitor protein |
| ROS | Reactive oxygen species |
| SCM | Short-chain metabolites |
| SDS | Sodium dodecyl sulfate |
| Sec14p | <i>Saccharomyces cerevisiae</i> phosphatidylinositol transfer protein |
| SEM | Standard error of mean |
| SOD | Superoxide dismutase |
| SPF | Supernatant protein factor |
| SR-B1 | Class B type 1 scavenger receptor |
| STED | Stimulated emission depletion microscopy |
| Sv | Sievert |
| TAP | Tocopherol associated protein |
| TBARS | Thiobarbituric acid reactive substances |
| TBS | <i>t</i> -Butyldimethylsilane |
| TAP/SPF | Tocopherol alike protein / Supernatant protein factor |
| TH | Tyrosine hydroxylase |

| | |
|---------------------|--|
| THF | Tetrahydrofuran |
| TMHQ | 2,3,6-Trimethylhydroquinone |
| TBARS | Thiobarbituric acid reactive substance |
| Tocored | 2,2,7,8-tetramethyl-5,6-chromanquinone |
| TOF-MS | Time-of-flight mass spectrometry |
| TRIO | TRIO guanine exchange factor |
| Trolox [®] | 6-hydroxy-2,5,7,8-tetramethylchroman-2-carboxylic acid |
| TS | Tocopherol synthase |
| tta | Total tocopherol amount |
| ttc | Total tocopherol content |
| VCAM-1 | Vascular cell adhesion molecule-1 |
| VE | Vitamin E |
| VE-RBA | Vitamin E relative biological activity |
| VLDL | Very-low-density lipoprotein |
| Vitamin C | Ascorbate |

Fluorescent Tocopherol

1 Introduction

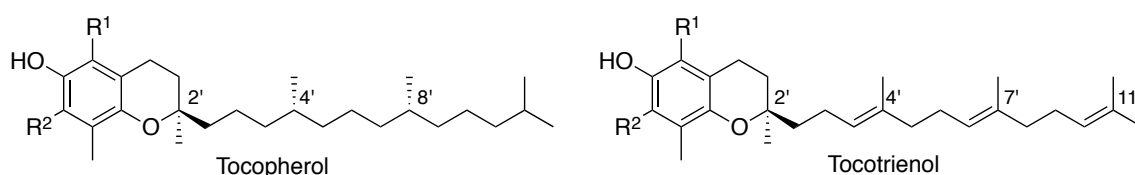
1.1 Discovery and Structure

The discovery of Vitamin E started in 1920 when Henry A. Mattill investigated the effect of a milk diet on the reproductive success of female rats. The female rats, given a strict diet of only fresh milk, were healthy and grew normally but were not able to reproduce.¹ Later tests with other diets, containing different amounts of dried milk and various additives like starch, lard and salts, also could not complete live births. Mattill proposed that the female rats did not reproduce because they lacked a compound found in their normal diet.² He based this idea on the paper “*Oestrous cycle in the Rat*” published by Evans in 1922 and the associative effects on health seen by the recently discovered vitamins A, B and C.³ In the same year Evans and Bishop provided evidence that the assumption of Mattill was correct, that female rats did not reproduce on a purified diet of casein, cornstarch, lard, butterfat, salts and Vitamin A, B and C. Successful reproduction was recovered when rats were fed lettuce leaves.⁴

Barnett Sure named the missing substrate Vitamin E however the actual structure and biochemical mechanism were unknown until Evans isolated and characterised Vitamin E in 1936 from concentrated wheat germ oil.^{5,6,7} The isolated compounds were named “*tocopherol*”, derived by the Greek words “*tocos*”, which means childbirth and “*phero*”, meaning to bring. The ending “*ol*” refers to the hydroxyl group in the molecule.⁸

Vitamin E represents a collective of eight molecules (vitamers) split into two groups called tocopherols and tocotrienols, both with a chromanol “head” substituted with a 16-carbon “tail” on the 2' position as a basic skeleton.

Tocopherols have a saturated carbon tail, based on the structure of phytyldiphosphate (PDP), whereas tocotrienols have an unsaturated tail with unsaturation on the 3', 7', and 11' positions, and which is derived from geranylgeranyl diphosphate (GGDP). Tocopherols and tocotrienols are further differentiated by their methyl substitution pattern on the aromatic side of the chroman ring (α -, β -, γ , and δ).^{9,10} All Vitamin E molecules have a chiral centre at the 2' position, the tocopherols have two additional ones at the 4' and 8' position. The main natural form is the (RRR) isomer (Table 1).¹¹



| Tocopherol | Tocotrienol | R ₁ | R ₂ |
|----------------------|-----------------------|----------------|----------------|
| α -Tocopherol | α -Tocotrienol | Me | Me |
| β -Tocopherol | β -Tocotrienol | Me | H |
| γ -Tocopherol | γ -Tocotrienol | H | Me |
| δ -Tocopherol | δ -Tocotrienol | H | H |

Table 1. Tocopherol and tocotrienol structures.¹⁰

1.2 Natural sources and tocopherol synthesis

All eight commonly known vitamin E vitamers are synthesized primarily in plants and are distributed throughout the plant organs in different amounts. The largest amounts are found in seeds, where most plants store predominantly α - or γ -tocopherol. In humans, dietary differences across populations change intake of the different forms. The American diet uses predominantly corn oil ($\sim 70\%$ γ -, $\sim 20\%$ α - in 1000 $\mu\text{g/g}$ total tocopherol amount (tta))¹⁰ and soybean oil ($\sim 70\%$ γ -, $\sim 7\%$ α - in 1200 $\mu\text{g tta}$)¹⁰ and partially sesame seed oil ($\sim 98\%$ γ -, $\sim 2\%$ α in 530 μg

tta), all containing mainly γ -tocopherol. European diets, on the other hand, contain mostly α -tocopherol enriched oils. High amounts of α -tocopherol are found in sunflower seed oil ($\sim 96\%$ α -, $\sim 3\%$ γ - in 700 μg tta)¹⁰, safflower seed oil ($\sim 94\%$ α -, $\sim 3\%$ γ - in 609 μg tta) and olive oil ($\sim 94\%$ α -, $\sim 1\%$ γ - in 191 μg tta). Rape seed (canola oil) ($\sim 45\%$ α -, $\sim 55\%$ γ - in μg tta) contains both tocopherols in equal amounts.¹²

Oil palm fruits are known as rich sources of hydrophobic natural products and are therefore annually harvested in extraordinary amounts (4-5t per Hc per year). Other oils mentioned yield around 0.2-1.0t per Hc per year.¹³ Despite being a major plant oil source the overall vitamin E content is low (500-800 $\mu\text{g/g}$ tta, 350-630 $\mu\text{g/g}$ when refined) (Table 3).^{14,15}

The highest overall amount in vitamin E content is found in wheat germ oil (2.15 mg/g).¹⁶

| Component | % | Mg/kg (in palm oil) |
|----------------------------|------|---------------------|
| Carotenoids | | |
| <i>α-carotene</i> | 36.2 | 500 - 700 |
| <i>β-carotene</i> | 54.4 | |
| <i>γ-carotene</i> | 3.3 | |
| <i>Lycopene</i> | 3.8 | |
| <i>Xanthophylls</i> | 2.2 | |
| Vitamin E | | |
| <i>α-tocopherol</i> | 28 | 500 - 800 |
| <i>α-tocotrienol</i> | 29 | |
| <i>γ-tocotrienol</i> | 28 | |
| <i>δ-tocotrienol</i> | 14 | |
| Sterols | | |
| <i>Cholesterol</i> | 4 | ~300 |
| <i>Campesterol</i> | 21 | |
| <i>Stigmasterols</i> | 21 | |
| <i>β-sitosterol</i> | 63 | |
| Phosphatides | | 500 - 1000 |
| Total alcohols | | |
| <i>Triterpenic alcohol</i> | 80 | ~800 |
| <i>Alipahitic alcohol</i> | 20 | |

Table 2. Vitamin E amount in unsaponifiable palm oil.¹²

More information on the vitamin E oil composition can be found in DellaPenna (2005)¹⁰, Hess (1993)¹⁷, Schreurs (1985)¹⁸, Taylor and Barnes (1980)¹⁹ & (1981)²⁰ and their amounts in foods²¹.

1.3 Tocopherol chemical synthesis

RRR- α -tocopherol is the most biologically potent antioxidant of all the vitamers.²² Since only low amounts of α -tocopherol are isolated from plants, industrial synthetic processes have been developed to satisfy demand, which was 100,000T/year (synthetic) in 2015 (22,000T/Yr in 2001 with 2,000T from natural sources). Its main use is in animal stock feeds, dietary supplementation, and pharmaceuticals. The current market value for mixed tocopherols lies around \$ 2 B/Yr in 2015 (~100 M/Yr in 1998).²³ The vitamin E business used to be monopolised by F. Hoffmann-La Roche Ltd., but is currently shared by several companies. The main manufacturers are Dutch States Mines “DSM” (who bought the vitamin division from Roche in 2003) (25,000T/Yr, 50% of the world wide demand in 2010),²⁴ BASF, Sanofi-Aventis (ex Rhone-Poulenc Animal Nutrition) and Chinese Chemical and Pharmaceutical Industry association “cpia” (12’000T/Yr, 30% of the worldwide demand in 2010)²⁵.

Synthetic α -tocopherol is industrially produced as a racemate by an acid catalyzed condensation of 2,3,6-trimethylhydroquinone (TMHQ)²⁶ and isophytol.²⁷ Much research effort has been put into the synthetic optimization in production of the two starting materials as outlined by Mercier & Chabardes (1994).²⁸ Oxidative assays have verified the potency of the racemic mixture and shown an antioxidant power of (1 : 1.49) to the *RRR*- α -tocopherol isomer.²⁹

To further increase the yield of α -tocopherol isolation from natural oil sources was a semisynthetic route developed by methylating residual γ - and δ -tocopherol.³⁰

Diverse synthetic strategies towards optically pure tocopherols have been described in literature. The key step in all approaches is a cyclization reaction mimicking the tocopherol cyclase (Figure 1).^{31,32,33,34,35,36,37,38,39,40,41,42,43} Further synthetic effort lies in the synthesis of the phytyl / geranylgeranyl side chain.^{44,45,46,47}

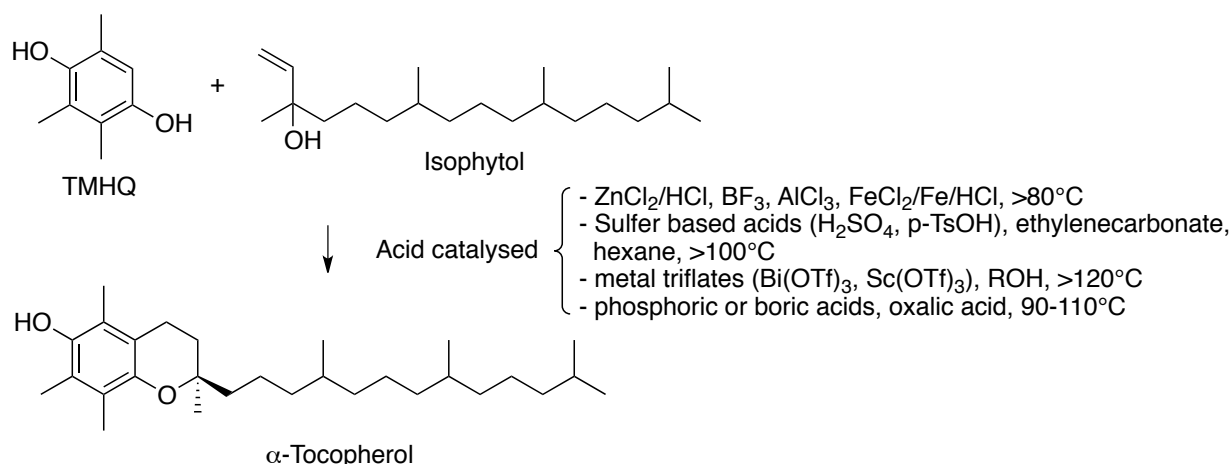


Figure 1 Conditions used in the industrial synthesis of α -tocopherol by condensation of TMHQ and isophytol.^{36,37,42,43}

The vitamin E family has in recent years been extended by new derivatives found in nature. Studies on different plant and vegetable oil extracts in 1995-1996 discovered partially reduced form of α -tocotrienol, tocomonoenol.^{48,49} Palm oil fibre is a rich source of tocotrienols with high concentrations of α -tocomonoenol (430 ± 6 ppm, α -tocopherol; 1810 ± 10 $\mu\text{g/g}$).⁵⁰ Higher quantities of γ -tocomonoenol (118.7 ± 1.0 $\mu\text{g/g}$) and γ -tocopherol; 586.0 ± 4.6 $\mu\text{g/g}$) were found alongside α -tocomonoenol (17.6 ± 0.6 $\mu\text{g/g}$) in pumpkin parts of *Slovenska golica*.⁵¹

δ -Tocomonoenol (23.0 ± 0.1 $\mu\text{g/g}$, δ -tocopherol; 30.7 ± 0.1 $\mu\text{g/g}$) was successfully isolated from kiwi fruits, *Actinidia chinensis*, by Fiorentino.⁵² His group further assessed δ -tocomonoenol antioxidant properties by a thiobarbituric acid reactive substance (TBARS) assay⁵³ and its radical scavenging activity against DPPH⁵⁴ and superoxide.⁵⁵ The results showed lower activities compared to natural α -tocopherol, but higher activities than its δ -tocopherol brethren.

In 2001, Yamamoto isolated from chum salmon eggs a new α -tocomonoenol, dubbed as marine derived tocopherol (MDT).⁵⁶ The vitamin E concentrations of diverse salmon, cod, and herring fish tissues were determined⁵⁷ and it was concluded that MDTs are common among cold water fish. MDT is not a fish metabolite but are obtained from the fish's diet. Cold water phyto- and

zooplankton keep 10-20% MDT in their vitamin E stock. Interestingly, no tocotrienols were found in any of the samples (Figure 2).

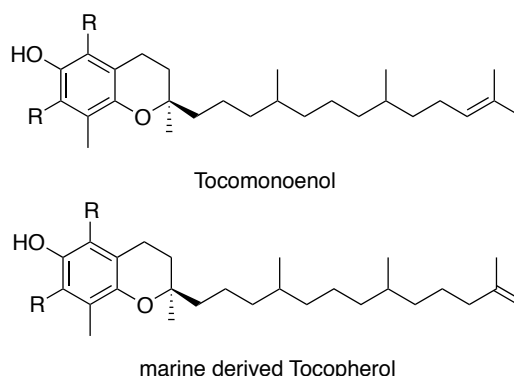


Figure 2. Structure of Tocomonoenol & marine derived Tocopherol (MDT).⁵⁶

MDTs have similar antioxidant values to tocomonoenols. When equimolar cholesterol amounts were added to enhance the liposomal membrane microviscosity showed MDT superior antioxidant activity to α tocopherol at 0°C.⁵⁸ The increase antioxidant ability is based on the increased unsaturation in the phytyl chain, which leads to enhanced membrane permeability at lower temperature, as Serbinova showed for tocotrienols.⁵⁹ The vitamin E relative biological activity (VE-RBA) of both mono-unsaturated derivatives showed a higher bioavailability than β - & γ -tocopherol when fed to mice over a 28-day period.⁶⁰ The majority of MDT and tocomonoenol VE-RBA were found in the liver, none in the lungs & spleen. The brain, known for its long lasting vitamin E stock⁶¹, only accumulated minimal amounts of monounsaturated-tocopherols. This is explained by having already residual α -tocopherol stockpiled. Between marine derived tocopherol (MDTs) and tocomonoenols have MDTs a higher VE-RBA. The small difference of olefin position on the phytyl-chain influences the biophysical nature of the cell membrane. Furthermore, both monoenols have different lateral diffusion coefficients in membranes, affecting the capability to reach sites of oxidative stress. The anti-oxidant function does not change since it is conserved in the chroman ring portion.

1.4 Biosynthesis

All vitamin E vitamers are produced in photosynthetic plants by the combination of the shikimic acid^{62,63} and non-mevalonate pathway.

1.4.1 Shikimate pathway

The shikimic acid pathway starts by combining phosphoenolpyruvate (PEP) with D-erythrose-4-phosphate (E4P). 3-Dehydroxy-D-arabino-heptalose-7-phosphate (DAHP) is the product of the two starting synthons. DAHP is rearranged to form a cyclohexanone in 3-dehydroquinate (DHQ). In the third and fourth step dehydroquinase dehydratase (DHQD) and shikimate dehydrogenase DHQ catalyze the formation of shikimate. After phosphorylation of the third hydroxyl group, pyruvate is added to the C-5 position by PEP. Dehydration of the obtained 5-enolpyruvylshikimate-3-phosphate (EPSP) yields the final intermediate of the pathway, chorismate. Chorismate is a key precursor for aromatic compounds in plant biosynthesis (Figure 3).^{64,63}

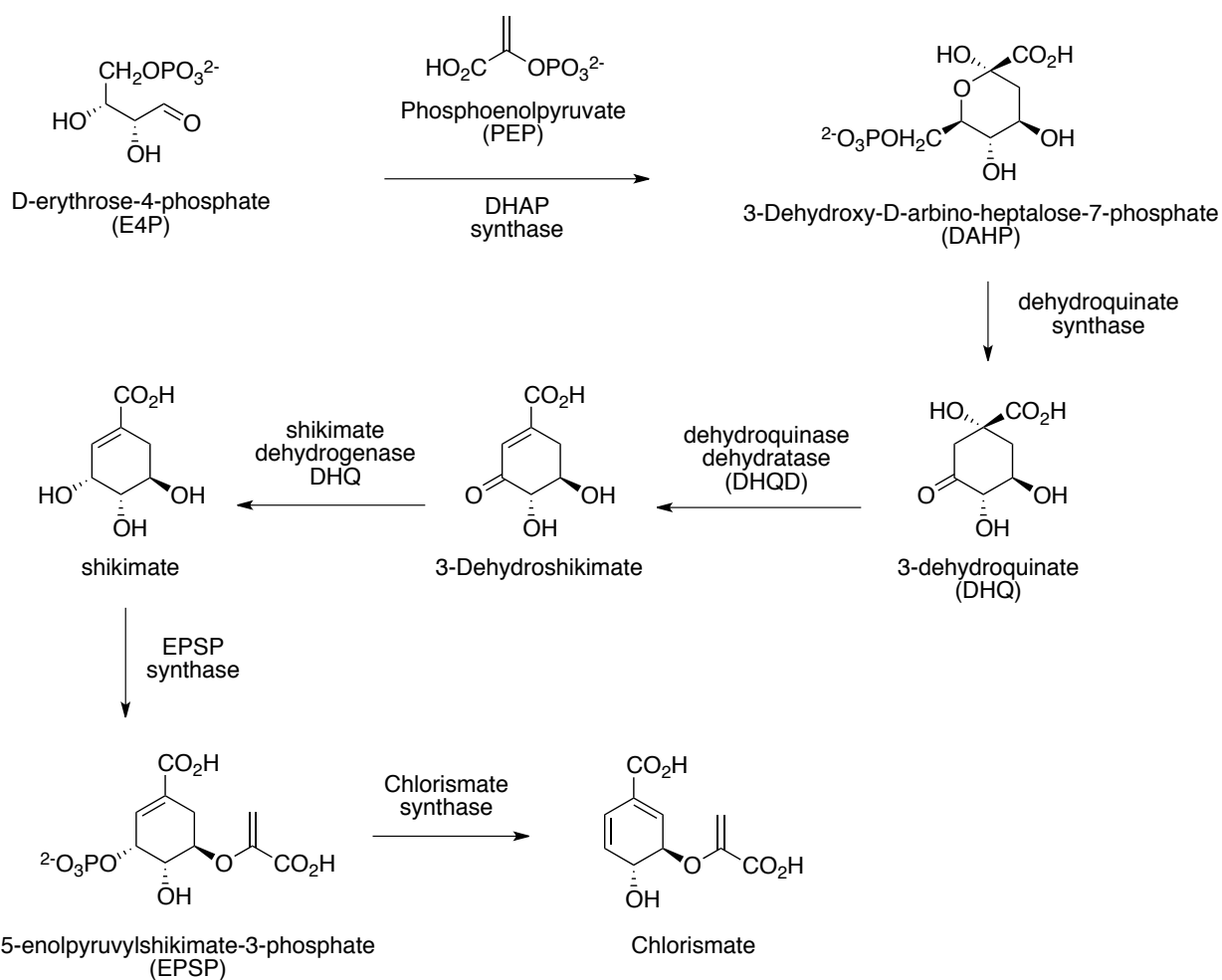


Figure 3. Shikimate pathway. Synthesis of Chlorismate from D-erythrose-4-phosphate (E4P) and phosphoenolpyruvate (PEP).^{63,64}

For tocopherol biosynthesis, chorismate is turned into 4-HPPA by a two-step process; first, a Claisen rearrangement produces prephenate, which is aromatized by NAD^+ mediated decarboxylation to the 4-hydroxypyruvate (4-HPPA) (Figure 4).^{65,66}

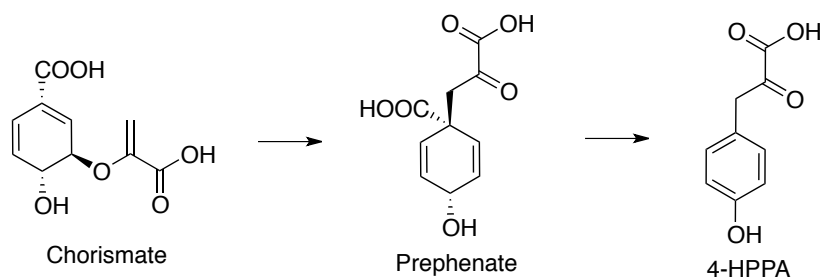


Figure 4. Biosynthetic conversion of chorismate to 4-HPPA.⁶⁶

The next part of the biosynthesis is a rearrangement of 4-HPPA by 4-HPPA-dioxygenase. In one conserved step 4-HPPA is oxidized, undergoes a rearrangement and is decarboxylated to form Homogentistic acid (HGA). The CH₂ of 4-HPPA is now in the meta-position with respect to 4-hydroxy phenol and resembles the 8'-methyl group in vitamin E.

1.4.2 Non-mevalonate pathway

The second part of the tocopherol biosynthesis prepares the phytyl/geranyl sidechain. The chains are synthesised from the isopentenyl pyrophosphate (IPP) and dimethylallyl pyrophosphate (DMAPP) monomers, the final products from the non-mevalonate pathway (MEP/DOXP pathway).⁶⁷⁻⁶⁸

IPP and DMAPP are combined to form geranyl pyrophosphate (GPP), which is driven by the loss of diphosphate. Two more IPP units are attached to form geranylgeranyl pyrophosphate (GGPP). GGPP is reduced by geranylgeranyl reductase (GGR) to phytylpyrophosphate (PPP) and combined with HGA.

The resulting 2-methyl-6-phytyl-1,4-benzoquinol is directly cyclized by tocopherol synthase (TS) to δ -tocopherol or methylated by a *L*-methionine *s*-methyl transferase (MMT) to access the γ -quinol. β -Tocopherol is obtained by methylation of δ -tocopherol, α -tocopherol by cyclization of γ -tocopherol followed by a methylation. The same methylation / cyclization pathway is used when GGPP is cyclized with HGA to obtain the tocotrienols (Figure 5).⁶⁹

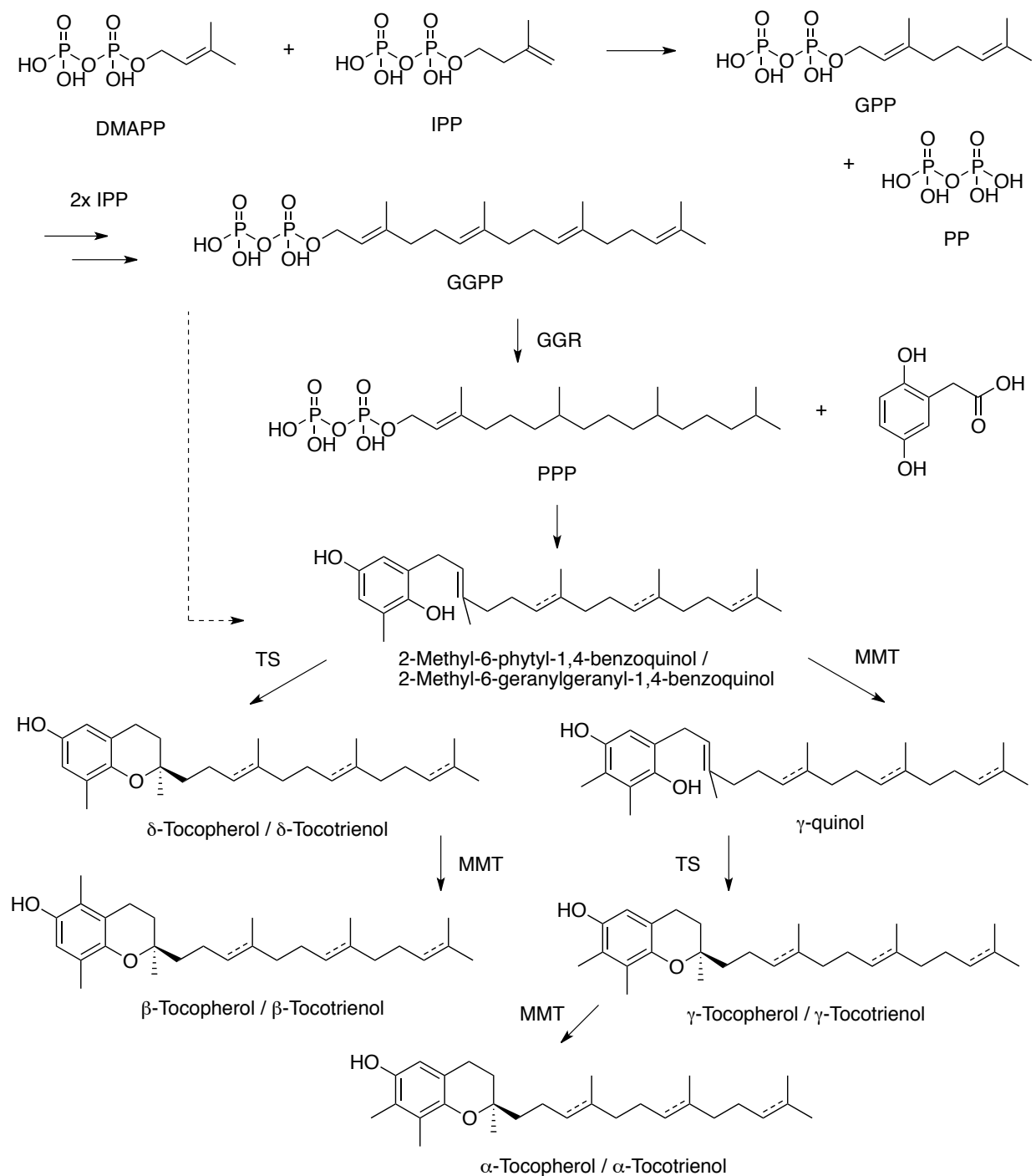


Figure 5. Tocopherol biosynthesis.⁶⁹

1.5 Biological absorption & transport

The human body is not able to synthesize vitamin E and therefore there is a requirement in our diet; 15-30 milligrams daily intake is suggested.¹¹ Of the consumed vitamin, 20-40% passes through the intestinal membrane. Tocopherol is absorbed across the intestinal membrane as micelles

with fatty acid esters and cholesterol (and bile salts) by passive diffusion or via class B type 1 scavenger receptor (SR-B1) and Niemann-Pick C1-like protein 1 receptors (NPC1L1) on the gut lumen wall. Once transported across the luminal site all vitamins are packed into chylomicrons at the ER. Chylomicrons are 75-600 nm in size and composed of ~90% triglycerides, ~10% phospholipids, ~2% cholesterol. Chylomicrons bind the intestinal apolipoprotein ApoB-48 (non-HDL) and ATP-binding cassette A1 transporters (ABCA1) at the apical side of the lumen, which sends the remnants into the lymphatic system and eventually to the bloodstream.^{70,71,72}

High-density lipoproteins (HDL) place ApoE and ApoC2 onto the now mature chylomicron remnants. The chylomicron ApoC-2 activates lipoprotein lipase (LPL) which turns chylomicrons into smaller vesicles called chylomicron remnants (30-50 nm). Extra hepatic cells absorb the released fatty acids and triglycerides (and some tocopherol) as part of muscle stimulation and fat storage in adipose cells. The Apo proteins attached on the LPL are transferred back to free flowing HDLs. Remnant specific low-density receptor related protein receptors (remnant-LRP) on the liver cell endocytose these small packages. The resulting endosomes contain all possible vitamins, which at this stage are not distinguished from each other (Figure 6).⁷³

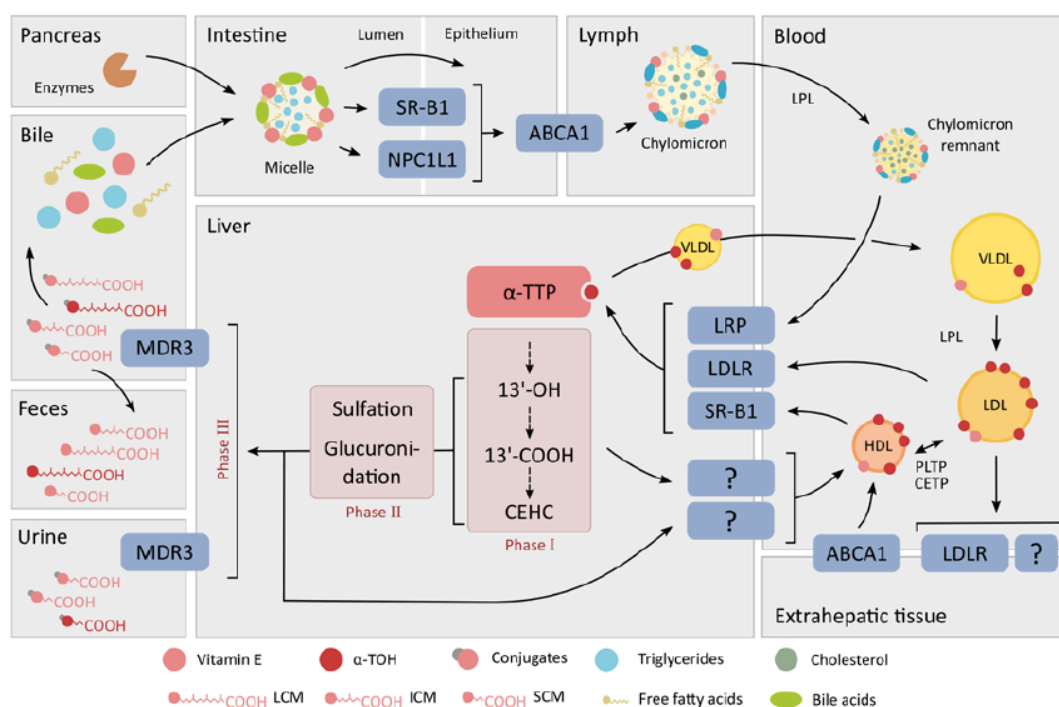


Figure 6. Tocopherol intestinal absorption & distribution.

Acronyms are explained in the text.⁷³

Most of the β -, γ -, and δ -tocopherols /trienols are degraded to carboxyethylhydroxychromans (CEHC), which are excreted via the urine.⁷⁴ Patients that obtained deuterium labeled vitamin E mixtures have shown higher blood plasma concentrations of the *RRR*- α -tocopherol after 24h over any other form.⁷⁵ The liver contains one third of all the α -tocopherol in the body, making it the largest storage pool of α -tocopherol.⁷⁶ Endosomal α -tocopherol is bound and transported to the cell membrane by the α -tocopherol transfer protein (α -TTP). α -TTP is expressed from the *tta* gene and has a calculated mass of 31.7kD and consists of 278 amino acids and is expressed by the *tta* gene.

Recent studies describe that α -TTP is transported to the hepatocyte membrane in recycling endosomes, bearing the GTPase Rab8, transferrin and the transferrin receptor CD71.⁷⁷ α -TTP is transferred from the endosome to the hepatocyte cell membrane, where α -tocopherol release is mediated by PI(4,5)P₂ binding to α -TTP.⁷⁸ On the membrane, ABCA1 participates in the secretion of very-low-density lipoproteins (VLDLs) as a transport system for α -tocopherol in

the blood. VLDL binds ApoE and ApoC, and interacts during the transport in the blood with LPLs, creating low-density lipoproteins (LDL), which are transformed to HDLs. LDL or HDL-receptors (LDLR/SR-BI) on extrahepatic cells incorporate the α -tocopherol by endocytosis. Excess tocopherol is reintegrated into the liver by SR-BI mediated uptake of HDL particles and is either recycled or metabolized.^{79,80}

1.5.1 Tocopherol metabolism

Two groups of tocol metabolites can be extracted from urine. The first group consists of three metabolites called Simon products, α -tocopheronic acid, α -tocopheronolactone (α -TL), and α -tocopheryl quinone. Ring opening of tocopheryl quinone creates Simon products. The second group are chain-shortened products, ultimately resulting in α -carboxyethylhydroxychroman (α -CEHC). It is still questioned whether Simon products are oxidized prior to or during the chain breakdown. The metabolites still bearing the chroman ring are excreted as sulfonated and glycosylated adducts.^{81,82}

Tocopherol breakdown starts in the ER, where the cytochrome P450 enzymes CYP4F2 and 3A4 hydroxylates tocopherol at the ω -position of the phytyl chain. CYP4F2 and 3A4 oxidation is the rate-limiting step of tocol metabolism (blue colored part, top panel, in Figure 7).⁸³

Dehydrogenases oxidize α -tocopherol-13-OH to the carboxylic acid and afterwards undergo rounds of β -oxidation (β -scission) producing 3-carbon products, forming first carboxydimethyldecylhydroxychromanol (11-CDMDHC, green colored part, middle panel, Figure 7). The chain shortens by one more β -scission cleaving to carboxymethyloctylhydroxychromanol (9-CDMOHC). All oxidized tocopherol products to this point are termed long-chain metabolites (LCM) and are not found in urine. Two more β -oxidations in the peroxisome form the 5 and 7-COOH tocopherol metabolites. Both belong to the category of intermediate-chain metabolites (ICM), and are found in small percentages in

$\mu\text{mol/L}$. The plasma level amounts of α -, γ -, δ -CEHC levels after the same 24h were 0.02, 0.35, 0.09 $\mu\text{mol/L}$.⁸⁴ Analysis of the metabolic profile of tocopherol, specifically the α -CEHC metabolite, is suggested to be an adequate way to monitor the daily α -tocopherol intake.⁸⁵ Concentrations of tocopherol metabolites were found to be an indication of cellular levels of oxidative stress. Deuterated α -CEHC was used as a biomarker to detect oxidative stress of smokers. After supplementation with deuterated α -tocopherol for 6 days, concentrations of deuterated α -CEHC found in urinal and serum samples of smokers showed a lower concentration of α -tocopherol, suggesting an increased use of α -tocopherol in protection against oxidative damage associated with smoking.⁸⁶ Increased oxidative stress is also seen in early onsets of type I and II diabetes in children. An increase in all tocopherol metabolites was observed in the test group. The most significant difference found was the high ratio ($\sim 14:1$) between α -tocopheronolactone and its conjugates to the control group.⁸⁷

1.6 Structure of the α -Tocopherol transfer protein

In early studies, incubation of [^3H]- α -tocopherol with rat liver cytoplasm allowed the purification and identification a ~ 30 kDa protein.⁸⁸ Studies with α -, β -, γ -, δ -tocopherols showed a high specificity for protein binding to α -tocopherol and the ability to catalyze tocopherol transfer between membranes, resulting in the protein being called the α -tocopherol transfer protein.⁸⁹

α -TTP is most abundant in liver tissue,⁹⁰ but α -TTP mRNA expression has also been found in kidney heart, spleen, and brain tissue.⁹¹ The tocopherol transfer protein genes have high sequence homology among other mammals, as seen between human and rat α -TTP (94%).^{92,93} α -TTP gene expression is increased upon tocopherol depletion, which is caused by oxidative stress, liver diseases and neurological pathologies like Alzheimer's disease.

TPP belongs to the SEC14 lipid binding protein family. The Sec14 domain (Smart entry: smart00516 binds small hydrophobic molecules and is named based on the archetypal protein from Sec14 from *Saccharomyces cerevisiae* (Sec14p). Almost all of these transporters contain another set of domains named after their similarity to cellular retinaldehyde binding protein 1 (CRALBP) and a TRIO guanine exchange factor (TRIO) binding domain (CRAL_TRIO Pfam entry: PF00650) in the active side.⁹⁴

Sec14 domains differ in their ligand specificity. Yeast Sec14p was found to bind both phosphatidylinositol and phosphatidylcholine. Additional domains like Golgi dynamics (GOLD), are found in SEC14L1 – SEC14L5. The GOLD domain on the C-terminus of SEC14L consisted of eight β -sheets (jelly-roll) and are thought to interact with other protein domains in the Golgi such as Fab1p/YotB/Vac1p/ EEA1 (FYVE domain), regulating cell signalling and lipid transport. Tocopherol associated protein (TAP), also known as supernatant protein factor (SPF) by its original discoverers, bears a SEC14L like lipid binding domain. Five TAP (1-5) proteins have been found so far. TAP1 (also known as SEC14L2) was found to bind squalene, all tocopherols, α -tocopheryl quinone, PI and PC. The binding site of TAP1 has a similar folding to SEC14p and α -TTP, but is slightly larger. TAP2 (SEC14L-3) differs from TAP1 by having a more preferred binding to PI(3,4,5)P₃, despite being 86% identical to TAP1.⁹⁵

The structure of the active side of α -TTP explains the preferential binding to *RRR*- α -tocopherol. Crystal structures of the TTP active site describe a predominantly hydrophobic environment. Ser136, Ser140 and three water molecules form a hydrophilic pocket deep in the active site where they and Tyr 117 form H-bonds to the 6-hydroxyl of the chroman ring. One water molecule is H-bonded to Val182 and Leu189 for further stabilisation of the bound substrate (Figure 8).^{94,96}

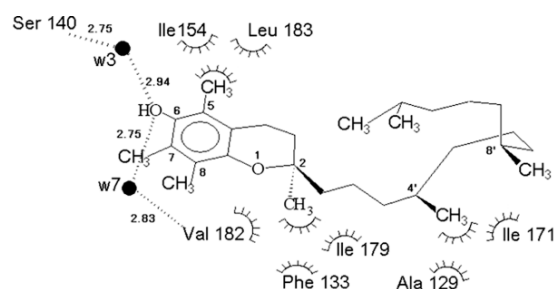


Figure 8. Protein interactions of the α -TTP active side with α -tocopherol.

W3 and W7 are water molecules.⁹⁴

The specific binding of α -TTP to α -tocopherol comes from the additional interaction of the 5-methyl group with Leu183 Ile154 and Ile194. Binding studies by Hosomi *et al.* showed the binding preference of α -TTP to the *RRR*-forms of tocopherols have the order $\alpha > \beta > \gamma > \delta$ tocopherol.⁹⁷ *RRR*- α -Toc has a stronger affinity than the *SRR* form. Leth & Sondergraad determined biological activity of the tocopherols in a rat resorption gestation assays (relative to *D,L*-tocopheryl acetate = 100%). α -TTP binding *in vivo* follows the same trend of protein affinity as direct enzyme titration with the $\alpha > \beta > \gamma > \delta$ tocopherols.⁹⁸ More recent values by Panagabko *et al.* compared the tocopherols against other binding and transfer proteins containing the CRAL-TRIO motif. α -TTP was found to have a higher affinity to α -tocopherol than Sec14p, SPF/TAP, or CRALBP (Table 3).⁹⁹

| ligand | dissociation constant (nM) ^a | | | | relative affinity of TTP for α -tocopherol ^b | rat-resorption gestation assays ^c |
|--|---|----------------|----------------|-----------------|---|---|
| | α -TTP | Sec14p | SPF | CRALBP | | |
| α -tocopherol | 25.0 \pm 2.8 | 373 \pm 89 | 615 \pm 15 | 528 \pm 9 | 100 | 80 |
| β -tocopherol | 124 \pm 4.7 | 3914 \pm 286 | 393 \pm 32 | nd ^d | 38.1 \pm 9.3 | 45 |
| γ -tocopherol | 266 \pm 9 | 3990 \pm 420 | 268 \pm 13 | nd | 8.9 \pm 0.6 | 13 |
| δ -tocopherol | 586 \pm 75 | 3908 \pm 900 | 731 \pm 82 | nd | 1.6 \pm 0.3 | <0.4 |
| SRR- α -tocopherol | 545 \pm 62 | nd | nd | nd | 10.5 \pm 0.4 | 59 (d/l) |
| Trolox | 1004 \pm 126 | ic | nd | nd | 9.1 \pm 1.2 | |
| α -tocopheryl acetate | 1639 \pm 89 | 5559 \pm 900 | nd | nd | 1.7 \pm 0.1 | 136 |
| α -tocopheryl succinate | 526 \pm 54 | nd | nd | nd | | |
| 6- <i>O</i> -carboxymethyl- α -tocopherol | 879 \pm 65 | nd | nd | nd | | |
| α -tocotrienol | 214 \pm 13 | 4726 \pm 884 | nd | nd | 12.4 \pm 2.3 | 13 |
| α -tocopheryl quinone | 814 \pm 86 | 5701 \pm 395 | 441 \pm 4 | nd | | |
| cholesterol | ic | ic | nd | nd | | |
| oleic acid | 7200 \pm 1030 | ic | ic | nd | | |
| squalene | ic | ic | 879 \pm 123 | nd | | |
| <i>n</i> - β -octyl glucopyranoside | ic | ic | nd | nd | | |
| phosphatidylinositol | 1415 \pm 106 | 381 \pm 43 | 216 \pm 31 | nd | | |
| phosphatidylcholine | nd | 6123 \pm 234 | 1183 \pm 178 | nd | | |
| 9- <i>cis</i> -retinal | 786 \pm 67 | nd | nd | 67.5 \pm 1.9 | | |
| <i>trans</i> -retinol | ic | ic | nd | nd | | |
| retinoic acid | ic | ic | nd | nd | | |

Table 3. Ligand binding to CRAL-domain proteins; Comparison of dissociation constants of α -TTP, *S. cerevisiae* Sec14p, SPF, and CRALBP for various hydrophobic ligands.

(a) All data are expressed as the average \pm SEM. (b) Ref 102 (Hosomi *et al.*) (c) Ref 103 (Leth & Sondergaard) (d) nd: not determined. ic: incomplete competition; competition was not achieved at 20 μ M [ligand].⁹⁹

The phytyl tail interacts with hydrophobic residues in the binding pocket, but the effect is stronger for *RRR*- α -tocopherol form due to interactions with Phe133, Val182, and Ile179. The tail bends into a U form to fill the cavity.⁹⁴

X-ray crystal structures of α -TTP with and without bound ligand show that the sequence 198-211 (helix A10) is a mobile lipid-exchange loop or “lid”, that is used to close the active side. The lid side facing inside the cavity has a hydrophobic nature, interacting with the phytyl chain of bound ligand through Ile202, Phe203, Val206, Ile210, Leu214. The other side of the lid has a more polar surface. The lid undergoes conformational changes that include an 80° rotation from the open to the closed form.^{94,96} The lid closes towards the hydrophobic phenylalanine residues of the helix A8 (F165, F169), which resides at the lower end of residues 165-185 (A9) (Figure 9). [Protein Data Bank (PDB) ID: 1OIP open, 1R5L closed state. 1OIZ, with bound Triton-X-100 open lid]

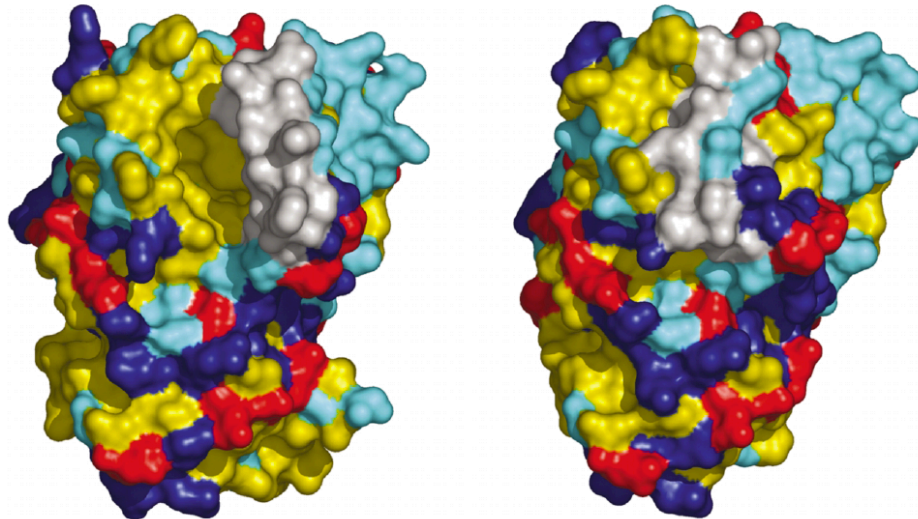


Figure 9. Open and closed lid crystal structure.

Yellow: hydrophobic residues (Ala, Val, Cys, Leu, Ile, Phe, Tyr, Trp, Pro), blue: basic residues (Arg and Lys), red: acidic amino acids (Glu and Asp), cyan: polar residues (Asn, Gln, Ser, Thr, Gly). Light gray: “lid” (residues 198–221).⁹⁴

Helices A8 and A10 are the key motifs for α -TTP binding to the plasma membrane, transferring α -Toc into the membrane upon contact. Zhang *et al.* found that the hydrophobic lid binds to the membrane and opens upon binding to the membrane.¹⁰⁰ The A8 helix (Phe F165 & F169) is thereby anchored at a fixed position in the membrane in the apo (open, $7.9 \pm 0.1 \text{ \AA}$) and holo (closed, $4.5 \pm 0.1 \text{ \AA}$) form.

A205, V206, M209, I210, P212, F213 of helix A10 reside in the membrane during the tocopherol transfer as the second, movable anchor (purple, Figure 10). The importance of this residue was tested by mutation of F165 & F169 to aspartate (F165D, F169D) which lead to a large decrease in the rate of tocopherol transfer, 90% & 88% respectively. Mutation of residues I202D & M209D in A10 affected the transfer rates less (78% & 63% reduction). More conserved mutations of hydrophobic residues to alanines rather than charged aspartates such as F165A (71%) and F169A (47%) reduced the rate of transfer only partially. Exchange of the basic K211 and K217 residues on the A10 lid to alanine had no impact on α -TPP binding, proving that hydrophobic and not electrostatic interactions are the major driving force of α -

TPP binding to the membrane.¹⁰⁰

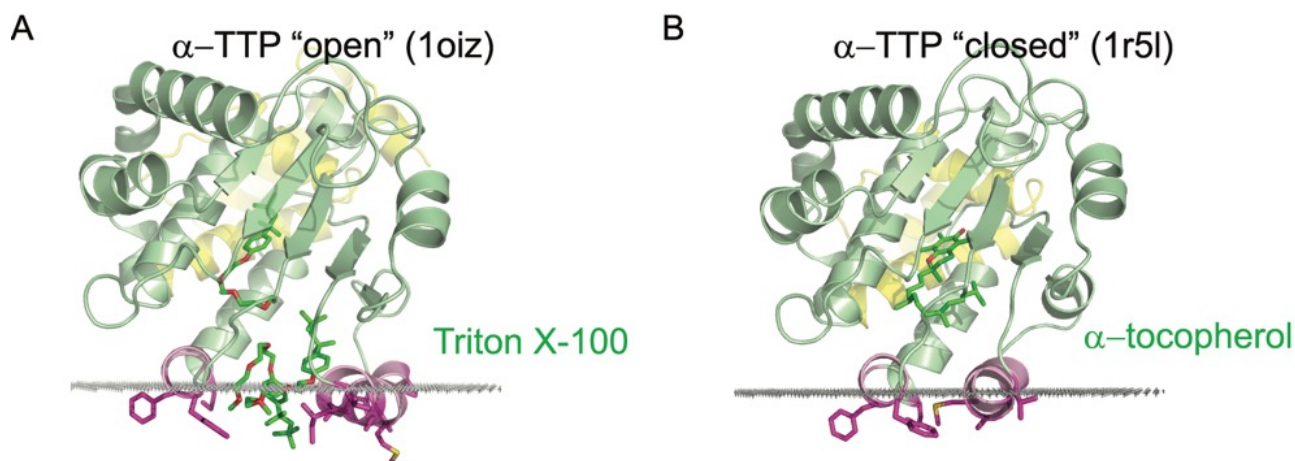


Figure 10. Calculated interactions between the lipid-binding domains of α -TTP with the hydrocarbon core of the lipid bilayer: (A) α -TTP in "open" (1OIZ) and (B) "closed" (1R5L) conformations.

Protein backbone is shown in a cartoon representation with helices colored in green, N-terminal α -helical domain is colored in yellow, and lid helices (fixed and mobile) enclosing the binding cavity are colored in pink. Residues that penetrate into the acyl chain region of the lipid bilayer are colored purple. Molecules of detergents bound to "open" conformations (Triton X-100 in 1oiz, located in protein binding pocket and in lipid bilayer in dark green), hydrophobic ligands bound to "closed" conformations (α -tocopherol in 1r5l, located in protein binding pocket in dark green).¹⁰⁰

Binding of phosphatidylinositolbisphosphate (PI(4,5)P₂ and PI(3,4)P₂) may initiate opening of the lid by electrostatic interactions to a positively charged groove of lysine (K190, K217) and arginine (R59, R68, R192, R221) residing on the sequence 184-192. The lysine K190 and arginine R192 are part of sequence connecting helices A9-A11. Helix A11 contains residues K217, R221 and helix A2 R59, R68) (Figure 11).¹⁰¹ PIP(4,5)₂ was found bind more favourably to α -TTP than other phosphatidylinositol diphosphates.¹⁰⁰

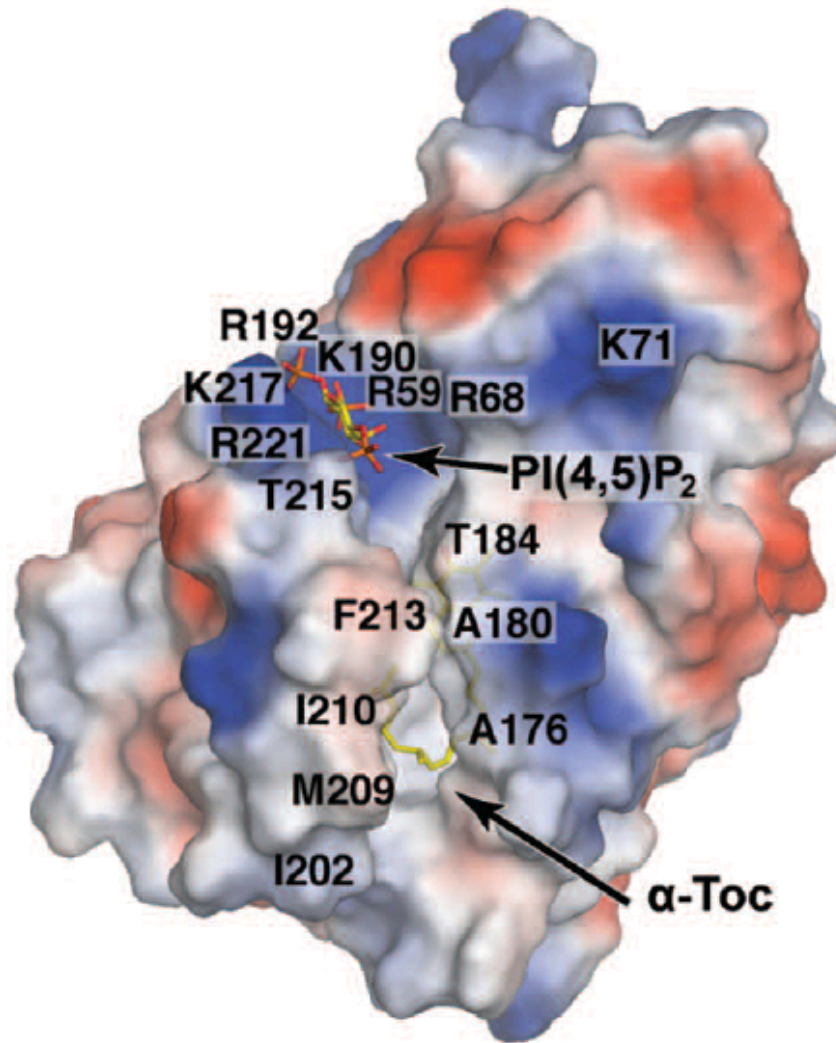


Figure 11. α -TTP structure highlighting the amino acid residues in the PI(4,5)P₂ binding cavity and lid helix 9-11 α -TTP structure enclosing α -Toc.

Electrostatic potential surfaces: blue area represents electropositive sites, red electronegative.⁷⁸

Other proteins besides α -TTP have been found to act as transporters of tocopherols. Afamin is a human plasma protein encoded from the AFM-gene, which binds α - and γ -tocopherol with low affinity ($K_d = 18\mu\text{M}$). Afamin may transport tocopherols between cells through human plasma and follicular fluids. The intercellular transportation by afamin is suggested to be more predominant when tocopherol transport by lipoproteins is impaired.^{102,103}

1.6.1 AVED

Low cellular plasma vitamin E concentrations ($3 \leq \mu\text{M}$) are associated with certain pathologies especially neurodegeneration causing ataxia and other symptoms like dysarthria hyporeflexia and vibratory sensation. Ataxia based on vitamin E deficiency (AVED, Friedrich's ataxia) is caused by an inherited mutation of the *ttpa* gene. The defect lowers the incorporation of tocopherol into VLDLs and thus vitamin E is not retained in the plasma. Over 20 different mutations have been characterized so far that results in varying degrees of neuropathology. Cavalier, Schuelke, Mariotti, Hentati, Arai & more (see full list in Manor & Morley¹⁰⁴) analysed the key amino acid residues affected and studied the effects of the mutated proteins.^{78,105,106,107,108}

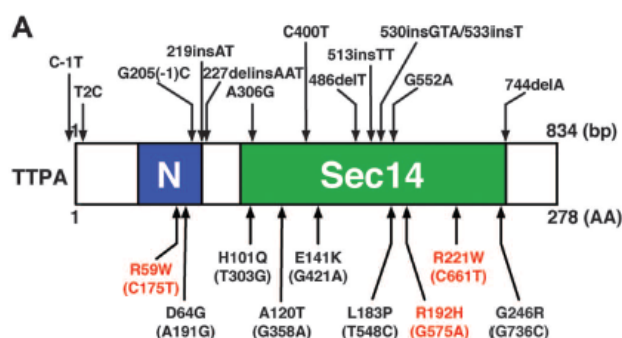


Figure 12. α -TTP mutations across the *ttpa* gene.

Blue box: CRAL_TRIO_N domain and green box Sec14 domain. On top: insertions, deletions, and splicing mutations. Below: Missense mutations.⁷⁸

Insertion, deletion, and splicing errors raise problems during gene transcription and protein expression. Premature terminations, disrupted initiations and frame shifts create shortened and mis-folded protein structures. Missense mutations of single amino acid affected tocopherol / PIP_2 binding and overall stability of the protein.

Arai studied the missense mutations of arginine residues R59W, R192H, and R221W (orange in Figure 12) in the PIP_2 binding region. R59W and R221W have a severe effect on the structure, incapacitating the ability to differentiate between RRS and RRR isomers. A ~20% decrease in tocopherol secretion was shown in assays using McA-RH7777 hepatic cells having the R59W

mutation in the TTP gene. Usuki and Maruyama described another missense mutation on the CRAL-TRIO part on α -TTP where Asp64 turned to glycine (D64G).¹⁰⁹

Current regulations on healthy dietary intake generally suggest a regular uptake of the necessary $\approx 15 \text{ mg} \leq$ of vitamin E per day.¹¹ In the case of AVED, excess amounts of vitamin E need to be ingested to combat the low uptake

1.6.2 Vitamin E and neurological health

The poor physiological outcomes of AVED make it clear that vitamin E plays an important role in the protection of neurological tissue. The brain and nervous system have a high potential for oxidative damage. Increased oxygen use, increased number of mitochondria, higher amounts of polyunsaturated acids, and lower amounts of antioxidants present an increased risk for generation of reactive oxygen species (ROS). Several studies on neurological damage induced by oxidative stress indicated vitamin E as the main source of protection against ROS. The study of the neurological protection by vitamin E is of special interest, as a better understanding benefits the treatment of neurological diseases.

Vitamin E depleted rats (around 50% of normal values) that were subjected to a 100% oxygen atmosphere over 48h had changes in synaptic morphology such as decreased membrane fluidity, swollen astrocytes, mitochondria, nerve terminals and nuclei deformation. Vitamin E addition to normal rats 48h prior to the assay (1.3x to normal values) protected synaptic tissue. In both cases vitamin E was depleted in the hyperoxic environment by 60% of the starting value. Endothelial cells didn't show these symptoms, confirming that neurological tissue is more susceptible to this form of oxidative stress.¹¹⁰ Ulatowski studied the structural integrity and motor coordination function of Purkinje neurons in vitamin E deficient *ttpa*^{-/-} mice,

mimicking AVED conditions. *Ttpa*^{-/-} mice had shorter dendrites (70 μ m compared to 130 μ m) and 30% less connections than wild type *ttpa*^{+/+} mice (Figure 13). Oxidative stress monitored by increased 3-nitrotyrosine concentrations was 3x higher in *ttpa*^{-/-} mice, but was reduced upon vitamin E supplementation and seen by partially regained cognitive functions and motor coordination.¹¹¹ Vitamin E is therefore crucial in maintaining structural integrity and function of neuronal tissue.

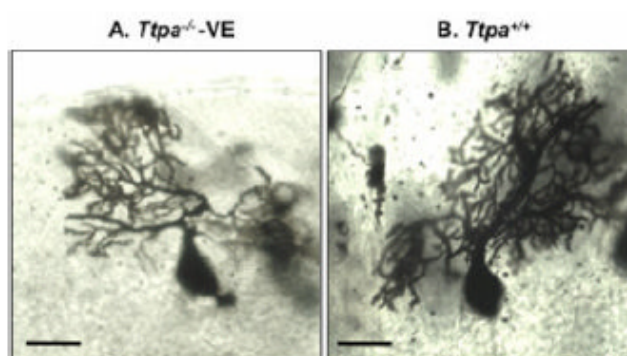


Figure 13. Structural differences in Purkinje neurons between *ttpa*^{+/+} and *ttpa*^{-/-}VE (vitamin E) mice.¹¹¹

1.6.2.1 Vitamin E, Parkinson's and Alzheimer's disease: influence of metal ions on ROS production, inhibition of glutamin synthase

Diseases like Parkinson's and Alzheimer's affect millions of people worldwide and are associated with increased ROS levels. An accumulation of iron as a part of aging was observed in rat brains as a consequence of leakage in ferritin iron storage or degradation of iron-dependent proteins like haemoglobin, cytochrome oxidase, aconitase and proline hydroxylase. Ferric iron (Fe^{3+}) is reduced to ferrous (Fe^{2+}) by ascorbate or superoxide (Fenton reaction). The *ferrous* species then acts as a reducing agent with hydrogen peroxide (H_2O_2) to form a hydroxyl radical (HO^\bullet). Hydrogen peroxide is produced by SOD dismutation of superoxide. The overall conversion of $\text{O}_2^{\bullet -}$ to HO^\bullet is known as the Haber-Weiss reaction.¹¹² Hydroxyl radicals can react with virtually anything, including polyunsaturated lipids, DNA bases and ribose.¹¹³ Direct

injection of iron(III) chloride into rat brains showed increased malonedialdehyde (MDA) and decreased superoxide dismutase levels (SOD) in younger rats.¹¹⁴

ROS generation by reaction of 6-hydroxydopamine with oxygen in neonatal rat pups has been shown to inhibit glutamine synthase (GS). Glutamate is a neuronal transmitter synthesized in the brain and assists in the initiation of an action potential by interacting with ionotropic receptors *N*-methyl-*D*-aspartate (NMDA, Ca^{2+}), α -amino-3-hydroxy-5-methyl-4-isoxazolepropionic acid receptor (AMPA, Na^+ , K^+), or kainate (Na^+ , K^+) receptor, and the regulatory metabotropic glutamate receptor (mGluR). After the ion release, glutamate is rapidly transported from the synaptic cleft to astrocytes by excitatory amino acid transporters (EAATS). Glutamine synthase in the astrocytes turn glutamate to glutamine by using ammonia and ATP. Glutamine is then redistributed into neurons, where it is converted back to glutamate. This process is known as the glutamate-glutamine cycle, that protects neurons from excitotoxicity by metabolizing excess glutamate and ammonia. The oxidative species damaging glutamine synthase is not known. A test reaction with hydroxy radical quencher DMSO didn't stop the inhibition.¹¹⁵ Vitamin E injection has been found to inhibit damage to astrocyte GS by ROS, preventing excess Ca^{2+} initiated cellular necrosis that forms oxidized lipids upon membrane degradation. FeCl_2 was used to initiate oxidative stress. FeCl_2 + vitamin E reduced malonedialdehyde (MDA) levels back to the normal (control) state (Figure 14). Increasing Ca^{2+} levels by adding NMDA was cancelled by increased GS activity.¹¹⁶

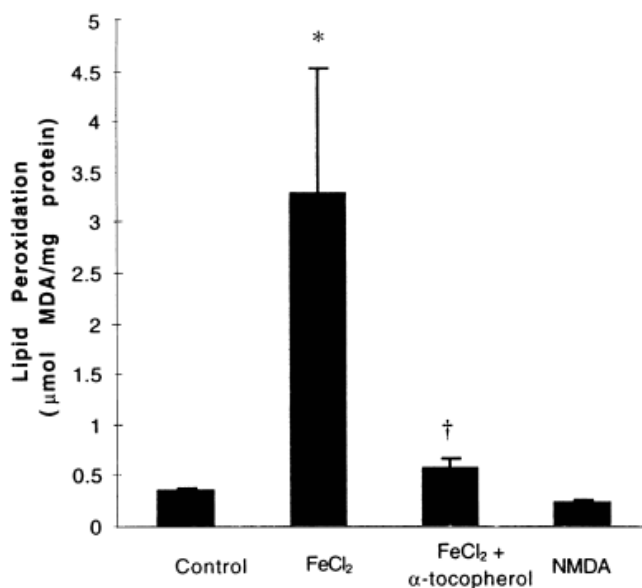


Figure 14. Inhibition of lipid peroxidation with α -tocopherol and NMDA.

Decrease of MDA levels with α -tocopherol + iron(II)chloride and NMDA. The effect of NMDA (320 mM) on lipid peroxidation as expressed by the concentration of malondialdehyde (MDA)/mg protein. Data are the mean \pm SEM for more than three experiments. * $P < 0.05$ compared with controls; † $P < 0.05$ as compared with FeCl₂ alone (Student *t*-test).¹¹⁶

1.6.2.2 Vitamin E and Alzheimer's disease: β -amyloid aggregation as an result of increased ROS levels

Besides impaired motor systems in Parkinson's disease, iron- or copper catalyzed oxidative products are partially responsible for the memory loss and neuro-degradation in Alzheimer's disease.

Alzheimer's disease is linked to β -amyloid protein ($A\beta$) aggregation with consequent increase of H₂O₂. $A\beta$ is formed upon degradation of the neuronal membrane stabilizer amyloid precursor protein (APP) by β - and γ -secretases (β -secreatase cleaves APP outside the membrane, γ -secretase inside the membrane).¹¹⁷ The reduction of ROS by vitamin E has been recognized as a beneficial nutritional supplement in efforts to treat $A\beta$ associated diseases.¹¹⁸

1.6.2.3 Vitamin E in neuronal mitochondria protection

ROS damage in the electron transport chain of mitochondria has been found to be associated with Parkinson's disease. NADH-dehydrogenase (or ubiquinone oxidoreductase, complex I) oxidizes NADH to NAD⁺, thereby reducing ubiquinone (CoQ10) to ubiquinol. This is the first step in the mitochondrial electron transport and, when inhibited, reduces or halts ATP production potentially leading to apoptosis. Neurons have a high demand for ATP and thus severe pathological issues can result upon mitochondrial damage.

The neurotoxin 1-methyl-4-phenyl-1,2,3,6-tetrahydropyridin (MPTP) is used to induce oxidative stress in mitochondria of dopaminergic neurons in the substantia nigra of the brain. MPTP easily passes the blood brain barrier where it is oxidized by monoamine oxidase B (MAO-B) to MPP⁺, which incorporates into complex I to inhibit CoQ10 reduction. MPP⁺ further reduces dopamine synthesis by inhibiting tyrosine hydroxylase (TH), which catalyzes the oxidation of tyrosine to L-dopamine with O₂. Mitochondria and TH use oxygen in their catalytic processes, making them susceptible to oxidative damage. A study by Lan and Jiang looked at iron and MPP⁺ damage to dopaminergic neurons with regards to vitamin E and the iron chelator desferrioxamine (DFO(A)). The assay showed increased glutathione disulfide (GSSG) and MDA production as oxidative stress increased. Increased free iron levels were found to accumulate in all tissues from aged Parkinson's patients.¹¹⁹ The importance of the studies of Lan and Jiang was that dopamine synthesis was reduced as a result of oxidative damage, and returned to normal when treated with vitamin E.¹²⁰

Studies of oxidative damage in hippocampal mitochondria were followed by monitoring complex I activity. Complex I activity decreased during ageing 53% (hippocampus) and 35% (frontal cortex) over an 8-month period. Supplementation with vitamin E restored enzymatic

activity back to 95% (hippocampus) and 92% (frontal cortex). Similar results were observed in cytochrome oxidase (complex IV) and mitochondrial nitric oxide synthase (mtNOS).¹²¹

1.6.2.4 Vitamin E antioxidant efficiency compared to other neuro-protective antioxidants: melatonin, N-acetyl-serotonin (NAS) and 17- β -estradiol

Neuro-protective antioxidants like melatonin, *N*-acetyl-serotonin (NAS) and 17- β -estradiol were found to decrease oxidative stress and reduced apoptosis initiated by ROS-sensitive nuclear factor- κ B (NF- κ B).¹²² Addition of vitamin E to bovine retinal homogenates revealed that copper(I) ion-promoted lipid peroxidation was 29% more effectively quenched by α -tocopherol than *N*-acetyl-serotonin (NAS).¹²³ Inhibition of ascorbate/ Fe^{2+} -induced lipid peroxidation in rat testicular microsomes and mitochondria were tested with melatonin, NAS and vitamin E. Chemiluminescence increased following ascorbate- Fe^{2+} addition as a direct response to oxidative stress in the form of malondialdehyde formation.¹²⁴ Equimolar amounts of each antioxidant were tested and revealed better protection by α -tocopherol over the other antioxidants tested (Table 4).¹²⁵

| Antioxidant | Mitochondria IC ₅₀ | Microsomes IC ₅₀ |
|----------------------------|----------------------------------|--------------------------------|
| α -Tocopherol | 0.078 | 0.144 |
| Melatonin | 0.67 | 4.98 |
| <i>N</i> -acetyl-serotonin | 0.25 | 4.50 |

Table 4. Antioxidant inhibition of α -tocopherol, melatonin & *N*-acetyl-serotonin in mitochondria and microsomes as IC₅₀ valius based on 50% inhibition of light emission.¹²⁵

Neuronal protection by 17- β -estradiol (17- β -E₂) by ROS reduction and glutamate reduction by NMDA inhibition, has been described for spinal motor neurons¹²⁶ and dopaminic neurons.¹²⁷ Other steroids like testosterone, corticosterone, and cholesterol did not show these effects. Protection of ROS by estrogen was compared to tocopherol in cerebellular rat neurons as an effect of β -amyloid protein induced H₂O₂ and glutamate increase. The results included a

maximum of 20% increased cell survival with preincubated natural (65% α -tocopherol in soybean oil) and synthetic α -tocopherol upon peroxide addition, which was matched by 17- β -E₂ at higher concentrations (10⁻⁶M). Cell survival tests with increased glutamate concentration showed a 90-100% survival at the lowest concentration tested with both tocopherols. 17- β -E₂ on the other hand was able reach 80% at increased concentrations (10⁻⁶M). An increase in NF- κ B induced apoptosis was also observed by matching luciferase activity increase with higher amounts of tocopherols.¹²⁸

1.6.2.5 Vitamin E localization in neuronal tissue

Vitamin E distribution in a single neuron was analyzed by TOF-MS. Lipid abundance was visualized using choline (Panel **a** in Figure 15) and acetyl (Panel **b**) fragments from PC and sphingolipids. Tocopherol fragmented on both sides of the chroman 2'-position (165 m/z, 205 m/z) (Panel **c**). The relative intensity of vitamin E (Panel **d**) revealed high vitamin E presence in the junction (between soma and axon) > soma > neurite (= axon with myelin-sheets).¹²⁹ The lack of tocopherol in axons explains why axonal swelling is one of the first issues observed in AVED patients.¹³⁰

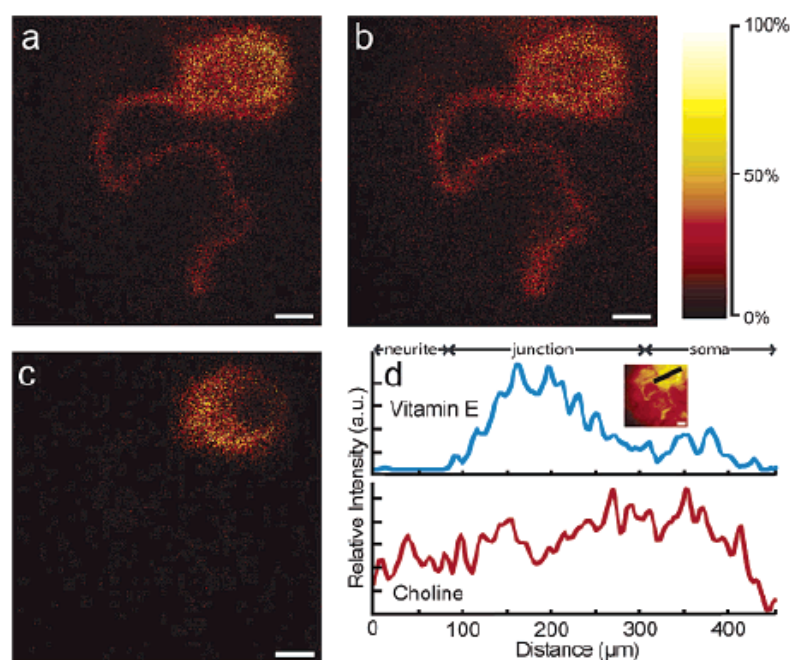


Figure 15. Localization of vitamin E in neurons by TOF-MS.

Lipid abundance visualization by MS fragments (a) choline, (b) acetyl from sphingolipids. (c) Visualization of tocopherol fragments. (d) Relative intensity of vitamin E and choline in neurite, junction and soma.¹²⁹

Vitamin E / α -tocopherol has a crucial role in neuronal protection and is therefore one to two orders of magnitude better retained in the CNS than in any other tissue.¹³¹ The *ttpa* gene expression was localized in rat brains and CNS when oxidative stress was applied.^{91,132}

Antibody staining of cerebellar astrocytes with glial fibrillary acidic protein (GFAP) and β -tubulin-III marked neurons localized α -TTP in GFAP-stained astrocytes (yellow, Figure 16).¹¹¹

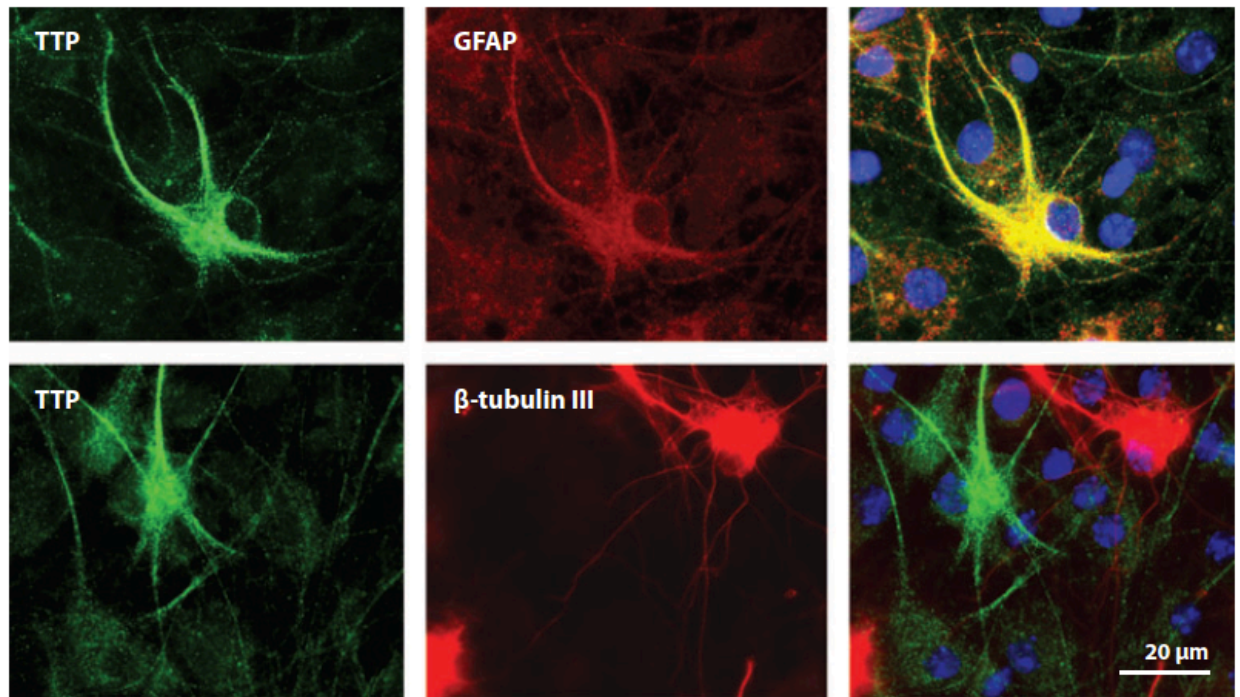


Figure 16. Localization of α -TTP expression in neuronal tissue.

Top pictures: detection of α -TTP in astrocytes (green), astrocyte visualized with GFAP (red) and α -TTP - GFAP overlay (yellow). Bottom pictures: α -TTP in astrocytes, neurons visualized with β -tubulin III (red) and α -TTP - β -tubulin III overlay (bottom right picture).¹¹¹

Neurons normally receive other lipophilic molecules from astrocytes and this seems to be also the case for vitamin E.¹³³ This finding led to the model proposed by Manor and Ulatowski, that HDL-loaded vitamin E is shuttled across the blood brain barrier (BBB) by SR-BI receptors, where ApoE lipoproteins guide the particles to the astrocytes (Figure 17).¹³⁴ Oxidative stress stimulates *tppa* gene expression and stored vitamin E is transported by α -TTP to the cell membrane, packaged into ApoE liposome constructs by ABCA-1 and delivered through the cerebrospinal fluid to neurons.¹³⁵ The proposed model raises the question of how oxidative stress activates *tppa* and how neurons receive the vitamin E packages from astrocytes.

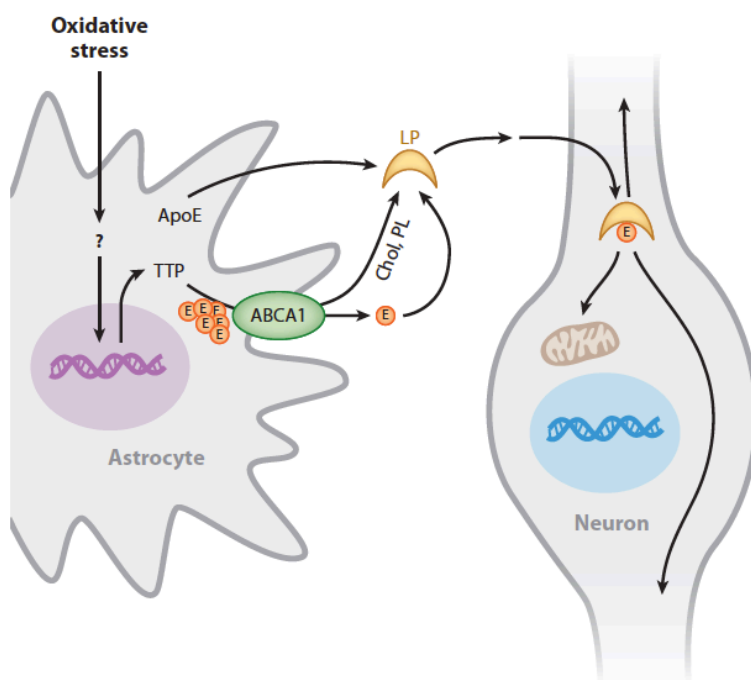


Figure 17. Proposed model of vitamin E delivery from astrocytes to neurons.¹¹¹

1.7 Biological tracing

How do molecules move and interact in living organisms? Distinguishing single molecules from each other without any specific label in real time in a living system is not yet possible. Larger molecular structures or networks in the cell are visible by microscopy. Optical microscopy has been used for biological research since the late 17th century.¹³⁶ Despite major improvements over the last centuries optical microscopy (bright field microscopy) cannot overcome certain physical limits. The technique depends on a difference in contrast on the surface observed. The high permeability of cells lets conventional optical microscopy only visualize larger, stronger absorbing or reflecting structures like nuclei or cell membranes.¹³⁷

The diffraction limit (d) for light microscopy is around 200 nm according to Abbe $d = \frac{\lambda}{2NA}$ and Rayleigh resolution $d = \frac{0.61\lambda}{NA}$ (NA stands for the numerical aperture and is defined by the refractive index, n , times $\sin\theta$. λ stands for the wavelength).¹³⁸⁻¹³⁹ More powerful microscopy techniques use x-ray radiation. X-rays penetrate tissue better and diffract with all tissue

allowing resolution down to 10-100 nm.¹⁴⁰ Since this radiation is high in energy the samples are often destroyed during the experiment.¹⁴¹

To increase the visibility of specific structures, cells are stained with light sensitive compounds.¹³⁶ However, addition of external stains often changes the cell physiologies, inhibits cellular processes, or are cytotoxic.¹⁴² Staining of larger areas normally requires fixed cells and is commonly used in histology to visualize diseased or damaged tissue.¹⁴³ Such staining techniques are sufficient to create static pictures of organelles, but are impractical when biological processes are to be followed over time. Instead of light, electron beams can be used to enhance the resolution. Scanning electron microscopy and transmission electron microscopy allow a 200,000x – 500,000x magnification down to 1nm to observe organelles like mitochondria. The samples used are fixed since the sample is in a vacuum environment, then bombarded with high energetic radiation.¹⁴⁴ Currently the technique with the highest resolution / selectivity and that is non-invasive¹⁴⁵ uses optical microscopy and fluorescent reporter molecules.

The main difference between fluorescence microscopy and light microscopy is the use of monochromatic light to illuminate the incorporated fluorophore in the cells.¹³⁷ The light source used to create monochromatic light are Xe-arc lamps / Hg-vapour arc lamps and lasers more recently light emitting diodes LED. Most microscopes use noble gas lasers (Xe, Ne).^{146,147}

Lasers are more intense and allow deeper penetration into tissues. Point scanning microscopy techniques like confocal laser scanning microscopy (CLSM) need high powered energy light sources to create better, more resolved pictures and videos.¹⁴⁸ CLSM revolutionized the field of microscopy as a technique able to overcome background fluorescence interference of deeper layers. To differentiate the axial depth of labelled structures unwanted reflected light is discarded by filters and resolved to create three-dimensional pictures. A newer type of

microscopy called 4π microscopy has superior axial differentiation over CLSM and has 6-7 times stronger resolution down to ~ 100 nm.^{149,150,151}

4π microscopy is used for new fluorescence techniques like RESOLFT based on stimulated emission depletion microscopy (STED). In STED is a secondary light beam used to eliminate a section of stimulated light, thereby enhancing the resolution of the residual stimulated section. STED pushed the boundaries of diffraction limit for live imaging down to 20 nm, giving clear images of small particles like vesicles or proteins (Figure 18).^{152,150}

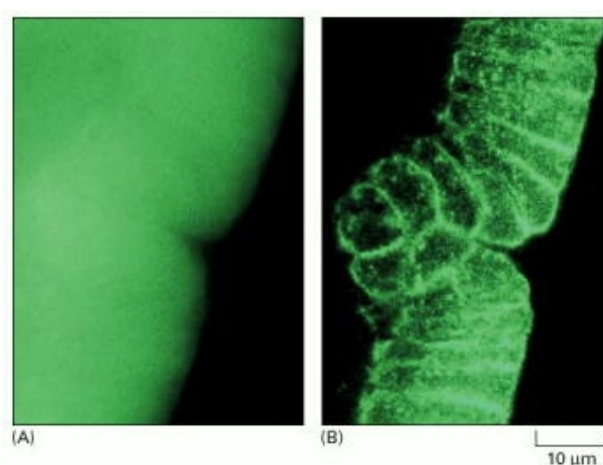


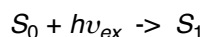
Figure 18. Fluorescent stained actin filaments of gastrula-stage *Drosophila* embryo.

Conventional (A) to confocal (B) microscopy.¹³⁶

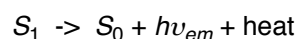
Live cell imaging captures fluorophore emission as transient light (bright field microscopy), scattered light (dark field microscopy) and interference pattern of two different combining light waves (differential interference microscopy).¹⁴⁵ The short lifetime of fluorescence (usually nanoseconds) requires a constant flux of light onto the fluorophore for prolonged observation. These so called steady-state conditions are great to observe particle movement in cells.¹⁵³ Unfortunately, the lifetime of the fluorophores under such intense light can be brief, as photobleaching and destructive radical formation increases. Hence, the fluorophores should have high photochemical and chemical stability.

1.7.1 Principles of fluorescence

The principle of fluorescence describes the absorption of a photon ($h\nu_{ex}$) by the ground state of the fluorophore (S_0) and release of a lower energetic photon ($h\nu_{em}$) after relaxation from the first singlet excited state (S_1) to the ground state by loss in vibrational energy (heat). A bathochromic (red-shift) shift in the wavelength is consequently observed (1).¹⁵⁴



1



The process is explained by the Frank-Condon principle, stating that the energy states of the excited state after internal conversion (IC) from higher excited state S_2 to $S_{1vib(x)}$ favours the same vibrational energy state in the ground state ($S_{0vib(x)}$) before reaching $S_{1vib(0)}$.¹⁵⁵ Other energy transitions compete with fluorescence; energy transfer into nearby located orbitals (spin coupling / crossover), IC of the singlet excited state S_1 to the triplet excited state T_1 (intersystem crossing, ISC) and release of the energy as phosphorescence, and other IC by complete nonradiative decay via heat release or chemical reactions. The Jablonski diagram is used to portray these different types of energy relaxation (Figure 19).^{156-157,158}

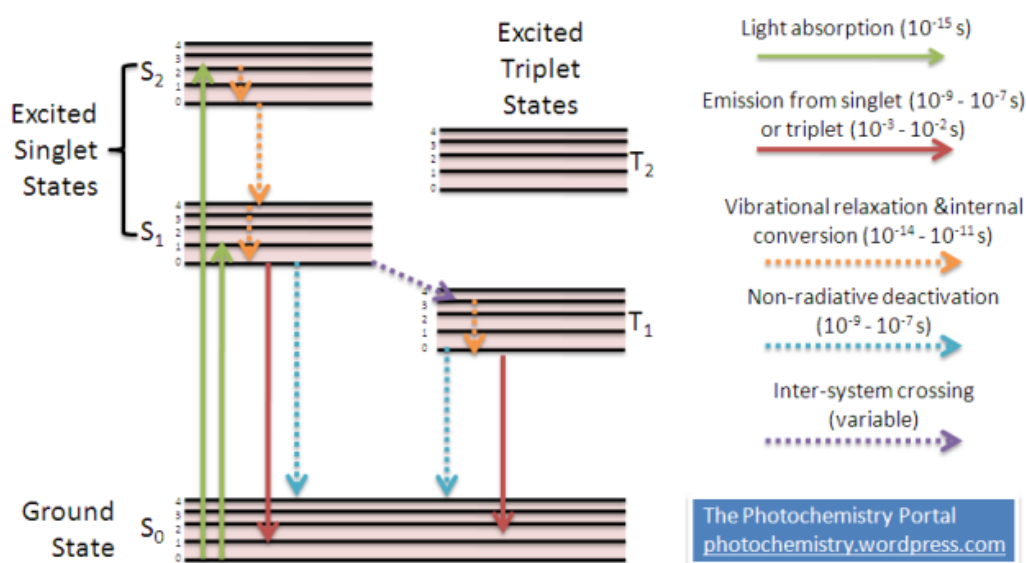


Figure 19. Jablonski diagram.¹⁵⁹

The fluorescence efficiency of an atom or molecule is described by the fluorescence quantum yield (Φ_F), which is the ratio of how much of the total excitation energy is converted to fluorescence, divided by how many of the absorbed photons are emitted back as photons. Φ_F is calculated from the emission rate of the fluorophore (Γ) minus the rate of all other nonradiative pathways combined (k_{nr}) (2). Has a molecule a quantum yield of $0.1 \leq 1.0$ is seen as being fluorescent.¹⁵⁴

$$2 \quad \Phi_F = \frac{\Gamma}{\Gamma + k_{nr}}$$

The rates of these processes vary. Fluorescence lifetimes are around 10^{-9} - 10^{-7} s. Light absorption is extremely fast 10^{-15} s, as is internal conversion 10^{-14} - 10^{-12} s.¹⁵⁴ Phosphorescence on the other hand is several orders of magnitude slower ($\sim 10^{-3}$ s or longer). The time spent in the S_1 excited state before decay to S_0 ground state is known as the fluorescence lifetime (τ) and depends on the nonradiative decay rate k_{nr} (3).

$$3 \quad \tau = \frac{1}{\Gamma + k_{nr}}$$

The natural fluorescence lifetime (τ_n) excludes nonradiative decay, giving the actual time of fluorescence and is on average ~ 1 - 10 ns (4).

$$4 \quad \tau_n = \frac{1}{\Gamma}$$

To calculate τ_n , τ is divided by the quantum yield Φ_F (5).^{154,160}

$$5 \quad \tau_n = \frac{\tau}{\Phi_F}$$

The addition of nitro groups and heavy heteroaromatic groups like halogens reduces the lifetime and quantum yield. Eosin (bromine) and Erythrosine B (iodine) have the same structure, but differ between their halogen substitutions. Despite similar extinction coefficients and radiative

moment upon light absorption. The interaction is more prone with blue light (400nm) as higher frequency light results in more collisions in the same distance traveled as red light (700nm).¹⁵⁴ Hence, the smaller the propensity the molecule is to the wavelength (λ), the stronger the scattering. Different types of scattering are possible with visible light. Rayleigh, Mie and optical scattering,^{168,169,170}

Rayleigh described the scattering by particles below one-tenth the size of the photons wavelength. The scattering coefficient (α) is determined by the particle size (d) and the wavelength of the incident light (λ) ($\alpha = >1:10$ for Rayleigh scattering) (6).

$$6 \quad \alpha = \frac{\pi d}{\lambda}$$

For visible light (400-700nm) the particles are around 0.1 - ~70nm. The intensity of the scattered light (I) depends on the amount of photons (N) and its distance to the spherical (8π) particle (R), scattering angle (θ), the polarizability of the molecule (α) and the photon influx intensity (I_0) (7).

$$7 \quad I = I_0 \frac{8\pi^4 N \alpha^2}{\lambda^4 R^2} (1 + \cos^2 \theta)$$

Mie scattering describes the interaction for particles between $\alpha = 1/10 < \lambda$ to the size of λ . Assuming a wavelength of 500nm, particles of the size of 50-500nm would experience Mie scattering, ranging from larger protein structures to viruses.

Optical (geometrical) scattering occurs on particles the same size or bigger than the wavelength of the photons ($\alpha = \text{particle} > \lambda$). It starts around 1-50 μm for wavelengths in the visible region. Particles of such size always scatter light in any direction with regards to its surface pattern (Figure 21).^{168,169}

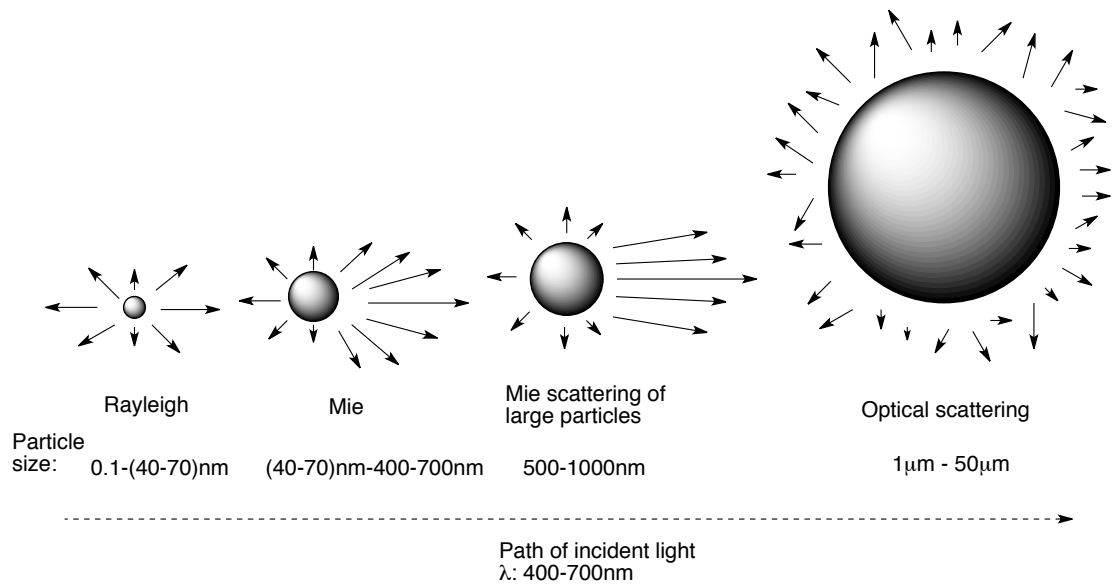


Figure 21. Interaction of visible light with particles.

Increasing particle size (0.1nm<1µm) favors scattering of visible light into the direction of the incident light. Larger particles (1µm<) scatter light into all directions.^{168,169}

The bigger the particle, the less scattering depends on the wavelength.

The cross section of the particle, referring to the amount of back-scattering (reflection) of the particle (σ), is the same or bigger ($1 \leq$) to the size of the particle (**8**).

8

$$1 \leq \frac{\sigma}{\pi r^2}$$

Tissue and blood have a broad range of UV / VIS absorbance, with most biological molecules having absorptions between 200-400nm. Water as the most abundant molecule in the body absorbs light most efficiently shorter than 180nm and longer than 1000nm. Extinction coefficients (k) of water was measured by several groups in the past and summarized by Hale and Querry (Figure 22).^{171,172,173,174}

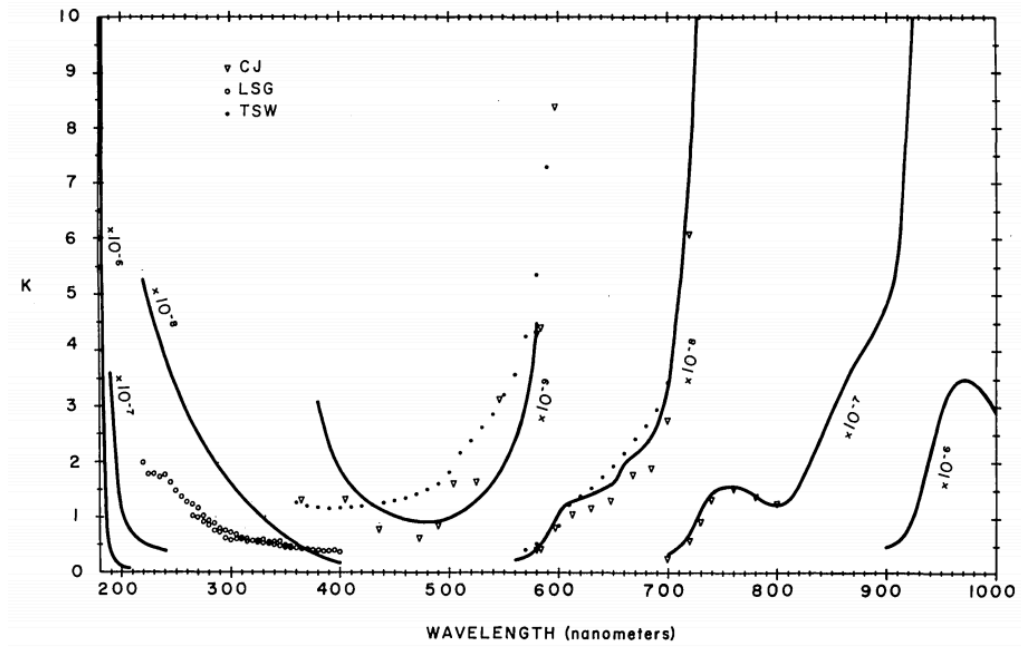


Figure 22. Extinction coefficient (k) of water for the 200 – 1000nm spectral region as a summary from CJ: Clark and Jelly, LSG: Lenoble, Saint-Guilly and TSW: Tyler.^{171,172,173}

Besides water, tissues consist of fats and other absorbing / scattering molecules. Proteins, for example, have aromatic amino acids like tryptophan, tyrosine, and phenylalanine, absorbing in the UV light (Table 5).¹⁷⁵

| Amino acid | Absorption | | Fluorescence | |
|---------------|-----------------|--------------|-----------------|---------------|
| | Wavelength (nm) | Absorptivity | Wavelength (nm) | Quantum yield |
| Tryptophan | 280 | 5,600 | 348 | 0.20 |
| Tyrosine | 274 | 1,400 | 303 | 0.14 |
| Phenylalanine | 257 | 200 | 282 | 0.04 |

Table 5. Maximum wavelength, absorption and fluorescence of aromatic amino acid.¹⁷⁵

To reproduce the visible light absorption of tissue, water (W), fat (F), melanin (M), bilirubin (C_{bili}), β -carotene ($C_{\beta C}$), haemoglobin oxygen saturated mixed with arterio-venous vasculature (BS) and deoxygenated blood as an average blood volume fraction (B) were combined (Figure 23). Total absorbance coefficient (μ_a) measurement by Rayleigh and Mie scattering is given by the transmission of the residual scattered light (T) and the path length traveled in cm (L) (9).¹⁷⁶

$$9 \quad \mu_a = -\frac{1}{L} \frac{\partial T}{\partial L}$$

Transmission of all components was measured from 300-1200nm, with decreasing μ_a from 10^2 - 10^0 . This trend is based on an experimentally made tissue with the chosen concentrations. In the same review article by Jacques is a reference list of 47 different tissues listed with their B, S, W, F, and M concentrations to calculate their individual absorptivity profile (10).¹⁷⁶

$$10 \quad \mu_a = BS\mu_{a.oxy} + B(1 - S)\mu_{a.deoxy} + W\mu_{a.water} + F\mu_{a.fat} + M\mu_{a.melanosome} + 2.3C_{bili}\epsilon_{bili} + 2.3C_{\beta C}\epsilon_{\beta C}.$$

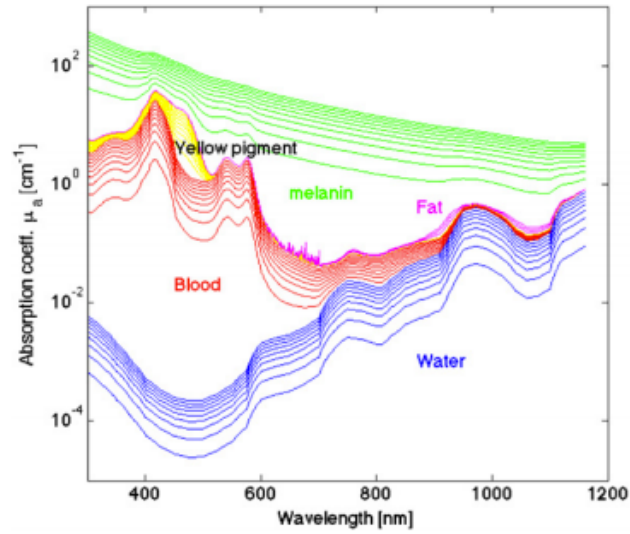


Figure 23. Total absorption coefficient μ_a (cm^{-1}), as water is added (volume fraction $f_{v.water} = 0.1$ by 0.1 to 0.9), blood at 75 oxygen saturation is added (average $f_{v.blood} = 10^{-4}$ by 10^{-4} to 2×10^{-3}), bilirubin is added (1 by 1 to 20 mg dL^{-1} , where $20 \text{ mg dL}^{-1} = 342 \mu\text{M}$ is a bilirubin concentration in the blood of a jaundiced neonate), fat is added ($f_{v.fat} = 0.3$ by 0.3 to 0.9), and melanin is added ($f_{v.melanosome} = 0.01$ by 0.01 to 0.10).¹⁷⁶

The decrease in scattering with increasing wavelength is found among all tissue. The review compared the scattering coefficient (u'_s) of skin, brain, breast, bone, soft tissues (liver, muscle, heart, stomach wall *etc.*), fibrous tissues (tumor, prostate *etc.*) and fatty tissues (red dots) (Figure 24). The experimental values were plotted as a function to the wavelength. Two functions were used: **11** determines (u'_s) by normalizing the wavelength (λ) with a reference wavelength of 500nm. The normalized value is then raised by the “scattering power” b , which shows the dependents to the wavelength used in u'_s . The term is scaled by the factor a , which represents the value $u'_s(\lambda = 500\text{nm})$. Equation **12** takes in count the separate fractions for

Rayleigh ($f_{\text{Ray}} (\lambda / 500\text{nm})^{-4}$) and Mie scattering $(1-f_{\text{Ray}})(\lambda / 500\text{nm})^{-b_{\text{Mie}}}$, seen as the dashed black lines in the graphs. Scaling factor a' is the same as $a (u'_s (\lambda = 500\text{nm}))$ in equation 11.¹⁷⁶

$$11 \quad \mu'_s = a \left(\frac{\lambda}{500(\text{nm})} \right)^{-b}$$

$$12 \quad \mu'_s(\lambda) = a' \left(f_{\text{Ray}} \left(\frac{\lambda}{500(\text{nm})} \right)^{-4} + (1 - f_{\text{Ray}}) \left(\frac{\lambda}{500(\text{nm})} \right)^{-b_{\text{Mie}}} \right)$$

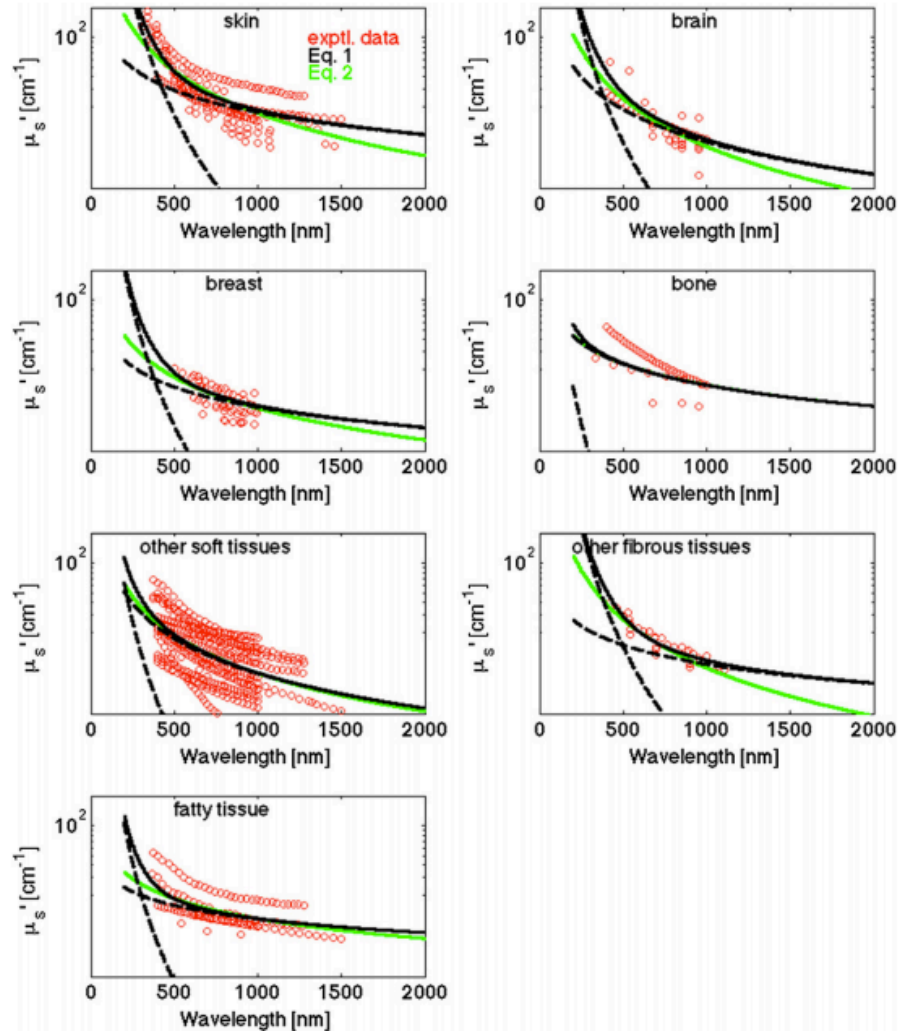


Figure 24. Reduced scattering coefficient for different tissues based on literature values for the seven groups of tissues (red circles, data found in reference).

The green line is the fit using equation (11). The black solid line is the fit using equation (12), with the black dashed lines showing the Rayleigh and Mie components of the fit.¹⁷⁶

When measuring scattering coefficients, it is best to have tissues samples at a thickness of 100μm or less to avoid loss of the signal by multiple scattering. Mie scattering is more prone in

all tissues than Rayleigh scattering. In average have tissues with higher overall lipid composition like fibrous, skin and brain tissue a high scattering coefficient.^{168,176}

As a general trend does tissue scatter and absorb light with lower wavelength much better. In fluorescent microscopy, therefore, fluorophores with higher absorption wavelengths are more visible.

1.7.3 Vitamin E labeling: Advantages of fluorophores

The transport of α -tocopherol has been studied previously with radio labeled [³T] and fluorescent derivatives.⁷⁰ Radio labeled molecules expose the organism to radiation, which lowers the overall radiation tolerance per year (20 Bq/L, 0.0003 mSv in Canadian drinking water) and can cause cell damage.¹⁷⁷ Fluorescence labeling offers a non-invasive way to track the cellular pathway of α -tocopherol. Fluorescence microscopy has been used to observe the transport of the vitamin by following intensity changes of the fluorescence emission in cultured cells, or Förster resonance energy transfer (FRET) in assays to study in vitro the interactions with proteins or and phospholipid membranes.⁷⁷ Fluorescence bleaching is commonly used to determine diffusion rates in phospholipid membranes.¹⁷⁸

1.7.4 Fluorescent labeling: Fluorophores

When talking about fluorophores in fluorescent microscopy imaging, a line has to be drawn between staining of organelles and labled molecules / proteins. Stains as discussed earlier are for specific organelles.^{144,154} They are based on chemical interactions to specific sites as in the case of Hoechst stains or 4',6-diamidino-2-phenylindole (DAPI), that specifically bind to A-T, A-U regions in the minor groove of the DNA / RNA and thus easily visualize nuclei.^{179,180}

Others are based on polarity like Nile red that selectively stains non-polar regions of cells such as lipid bodies.¹⁸¹ Immunofluorescence describes the use of fluorescent anti-bodies to targeted

to antigen expressing cells, or expression of fluorescent proteins in the targeted cells. The reactive fluorescent linkers in antibody staining are often isothiocyanates (FITC), which create stable thiourea linkages. The chosen dye should not interfere with protein function.

Staining multiple cellular compartments requires different excitation / emission wavelengths for each dye. For this purpose new dyes have been developed and sold by various manufacturers (Table 6).^{182,183,184,185,186,187,188}

| Name | Target organelle | Excitation λ | Emission λ |
|---|------------------------------|------------------------|------------------------|
| Höchst stains, DAPI ^{179,180} | DNA-minor groove, mycoplasma | 455nm | 510-540nm |
| Nile red | Lipid membranes | 450-500nm | 500-600nm |
| 3,3-dihexyloxacarbocyanine iodide (DIOC ₆) ^{182,185} | Endoplasmatic reticulum | | |
| Rhodamine dyes | Antibodies | | |
| Acridine orange ¹⁸² | RNA / DNA differentiation | 460nm RNA 502nm DNA | 650nm RNA 525nm DNA |
| Propidium iodide ¹⁸⁷ | Perforated cells | 488nm | 535-610nm |

Table 6. Excitation and emission wavelength of commercial dyes for fluorescent microscopy.¹⁸²⁻¹⁸⁸

The most prominent dyes in microscopy are based on coumarin, xanthine and cyanine structures.¹⁸⁹ Coumarin commonly emits in the blue-green region between 440-520 nm, but can reach 560 nm in some derivatives. They offer a high Stokes shift of 50-100 nm, making them useful in microscopy with energy transfer like FRET.^{182,190}

Dyes based on xanthenes include fluorescein and rhodamine.¹⁹¹ They are known to have high absorption coefficients, high absorption / emission wavelength, quantum yields and chemical stability. At the same time these properties are easily modified by substitution on the aromatic rings and change of the phenol / ketone to amines / imines or sulfonates as in the Alexa Fluor[®] series of dyes. Fluorescein and rhodamine have attached at the 9'-position an aromatic group, red-shifting the wavelength of the dyes more into the yellow-red region. When exchanging the 9'-carbon with a nitrogen atom an oxazine is created, which also exhibits a red shift in absorption / emission.¹⁹¹

Cyanine dyes are based on alkyl / aryl nitrogen capped polymethines. Increasing the size of the aromatic group or the number of double bonds in the polyene chain increases the wavelength into the near to far IR region.¹⁹²

Other dyes in the visible region used in microscopy are naphthalimides like brilliant sulfaflavin¹⁹³, phenyl-conjugated dyes like PQP¹⁹⁴ or anthracenes (PMAA),^{195,196,197} BODIPYs (Figure 25).

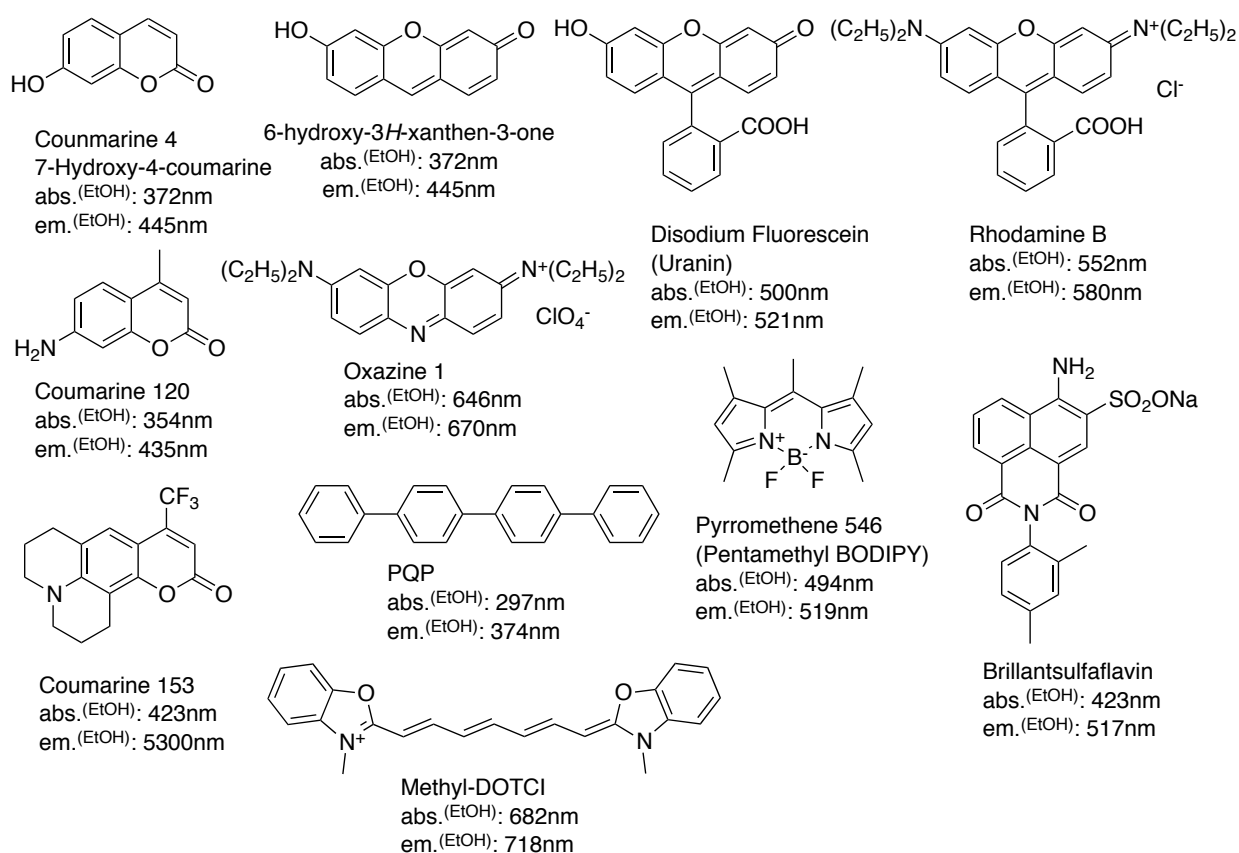


Figure 25. Structures of frequently applied fluorescent microscopy dyes.¹⁹⁰⁻¹⁹⁷

Instead of synthetic fluorescent small molecules, one can use naturally fluorescent proteins expressed as a fusion with a targeted protein. The green fluorescent protein (GFP) from *Aequorea victoria* jellyfish was the first such naturally fluorescent protein to be discovered and used as a tool in cell biology. This protein converts blue light (395 nm) to green light (509 nm).¹⁹⁸ The GFP sequence can easily be expressed in *C. elegans* and *E. coli* and several similar proteins have been engineered with a variety of emission wavelengths.^{199,200}

1.7.5 Tocopherol labeled fluorophores

Over the last decade our lab has synthesised several fluorescent α -tocopherol tracers. Most successful were the tocopherol analogues that incorporated nitrobenzoxadiazole (NBD) and dipyrrometheneborono difluoride (BODIPY) dyes.^{201,202,203,204} Both dyes are have a small molecular size and are non-polar enough, which benefits the binding affinity to the α -TTP. However, the NBD dye is linked to the vitamin E skeleton through a nitrogen atom that increases the polarity and consequently shows a lowered binding to α -TTP compared to α -tocopherol.²⁰⁵ The chain terminal tocopherol-BODIPY analogues are connected by a carbon-carbon bond to the C2-position and good mimics of the non-polar tocopherol tail. Other advantages of the BODIPY structure are a three times higher quantum yield than NBD, a five times higher extinction coefficient (ϵ), longer chemical stability in-vivo / in-vitro and, most importantly, longer wavelengths of absorption and emission (Table 7).²⁰⁶

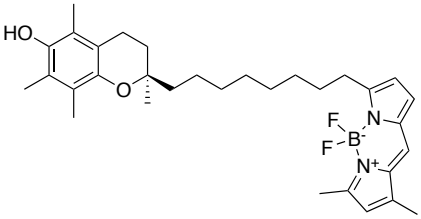
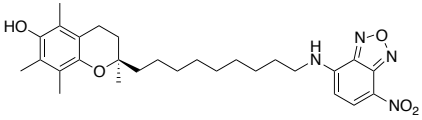
| Fluorophore | BODIPY-Toc | α -Toc-C9-NBD |
|--------------------------------------|---|---|
| Structure |  |  |
| Quantum yield Φ_F | 0.9 | 0.3 |
| ϵ ($M^{-1}cm^{-1}$) | 90'000 $M^{-1}cm^{-1}$ | 20'000 $M^{-1}cm^{-1}$ |
| Wavelength (abs.-em. λ max.) | 507-511nm | 460-480nm |
| Photostability | High | Low (<5min) |
| Use | Microscopy | Microscopy & FRET |
| K_d (α -TTP) (nM) | 94nM | 54nM |

Table 7. Comparison of BODIPY-Toc to α -Toc-C9-NBD.^{201,206}

One drawback of BODIPY is the small Stokes shift of only ~ 4 nm, which does not allow easy FRET-based assays. The overlap of the maximum absorption and emission band wavelength

causes self-quenching and decreases the fluorescence intensity, however, the high extinction coefficient compensates this problem.^{205,201} When looking at the binding to α -TTP, NBD-tocopherol has slightly higher affinity.

Both molecules have been successfully used in several biological studies.^{77,101,207,208,209,210,211,212,213,214,215}

2 Project overview

The goal of this research project is the synthesis of a new BODIPY fluorophore containing α -tocopherol analogue with a longer excitation wavelength than previous molecules, potentially a larger Stokes shift, and with a similar or higher affinity to α -TTP.²⁰⁶ Such a molecule would make the tracking of intracellular tocopherol transport easier and lead to a better understanding of the biological role of Vitamin E.

Fluorescent conjugates for biomolecular research should have absorption and emission wavelengths that allow for efficient cell and tissue penetration of both the incident and fluorescent light. Better penetration of light through tissues occurs at a wavelength around 500-700 nm, and can yield brighter and more detailed images in fluorescence microscopy. To achieve this goal for a fluorescent tocopherol, we envisioned an additional aromatic functional group added to the BODIPY to increase the absorption and emission maximum up to 550-580 nm. Additionally, this structural change must not alter the molecule's ability to bind with high affinity to the tocopherol transport protein.

2.1 Structure design

Two key aspects need to be considered in the structural design. First, the molecule needs to have a longer excitation wavelength than our previously synthesized molecule.²⁰⁶ Second, the molecule needs to bind to α -TTP with high affinity.

One way to increase the wavelength of the BODIPY fluorophore is additional conjugation of aromatic functional groups. The overlap of the π -orbitals lowers the HOMO, decreases the overall energy of absorptive electronic transition, thus shifting light absorption to less energetic light. Several examples in the literature describe BODIPYs with increased wavelengths into the red and even the near-IR region as potential sensitizers for solar cell applications. Conjugation of aromatic groups to the 1, 2, 3, 5, 6, 7 and 8 (meso) position have proven to increase the wavelength.²¹⁶ For instance, fusing BODIPY with other ring systems like benzothienophene increase the absorption maximum to 670nm.^{217,218} Substitution of the boron with alkyl (C-BODIPY) or ethynyl (E-BODIPY) also increases the Stokes shift (Figure 26).^{219,220}

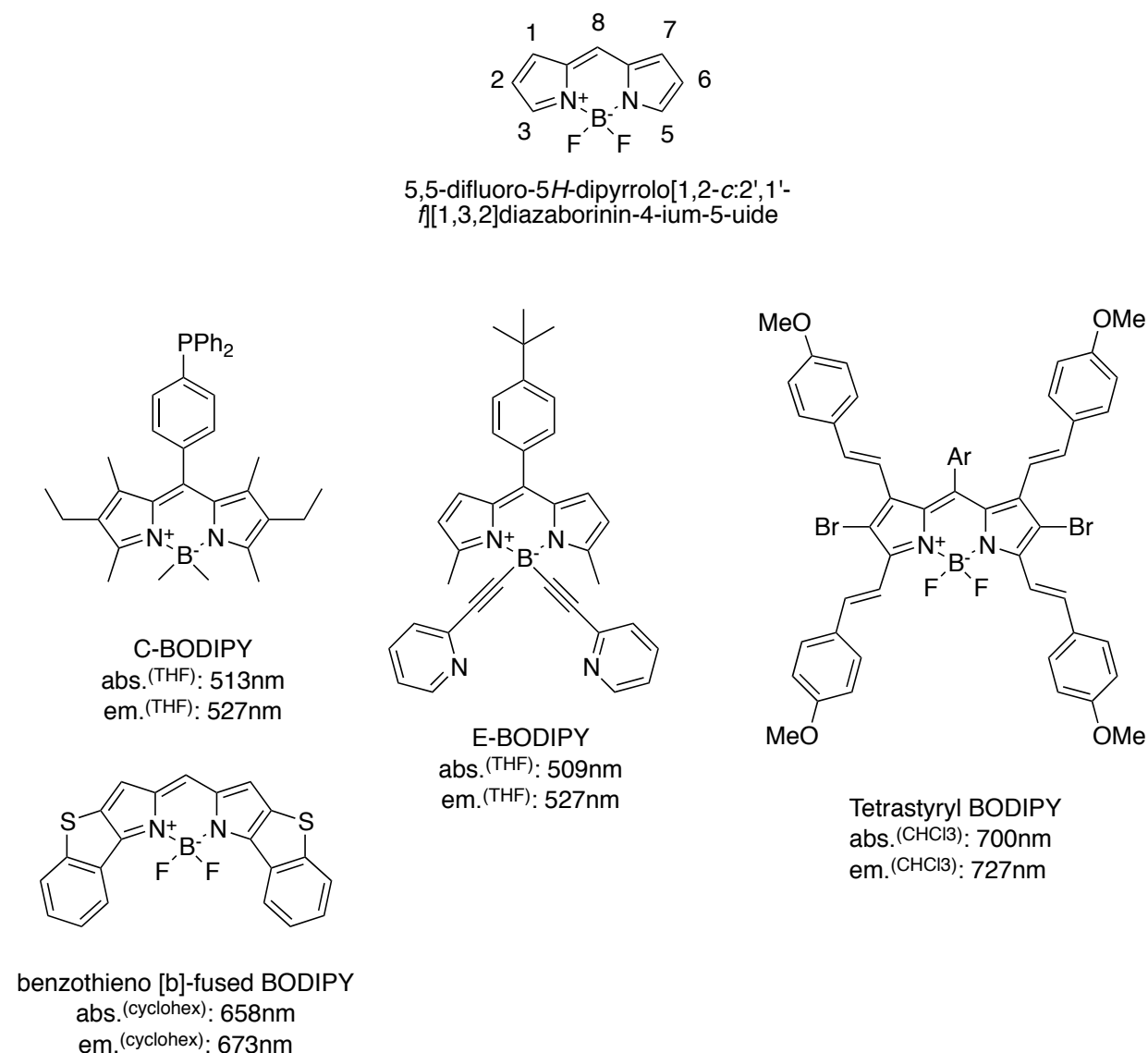


Figure 26. Nummering system of the BODIPY core structure and example structures of differently substituted BODIPYs.²¹⁷⁻²²⁰

The second issue of ligand design is the binding to the hydrophobic pocket of α -TTP. To ensure specific binding the chroman ring should remain intact. This means that changes can only be made to the phytyl chain. Natural tocopherol has a chain length of thirteen carbons. Our previously prepared BODIPY- α -tocopherol ligands revealed that binding affinities differed significantly with chain lengths (Table 8). The best results were obtained with an eight-carbon linker ($K_d = 94 \pm 3$ nM).²⁰⁶ Similarly, NBD-tocopherols with a nine-carbon spacer (C9) had the highest affinity ($K_d = 56 \pm 15$ nM).²⁰¹ Longer chains than C9 decreased the binding affinity. A

higher K_d for the BODIPY can be rationalized by having a larger size than NBD, interfering with protein binding.

| NBD- α -Toc | K_d (nM) | BDP- α -Toc | K_d (nM) |
|--------------------|--------------|--------------------|--------------|
| C6 | 299 ± 37 | C6 | 232 ± 10 |
| C7 | 106 ± 21 | C7 | 130 ± 4 |
| C8 | 142 ± 35 | C8 | 94 ± 3 |
| C9 | 56 ± 15 | | |

Table 8. Influence of chain length linker on the α -TTP dissociation constants (K_d) of NBD- α -Toc and BODIPY (BDP)- α -Toc.²⁰⁶

The smallest groups that can be added to the BODIPY to extend conjugation are a simple double bond, or the aromatic thiophene and benzene groups. Arroyo described the synthesis and optical properties when functional groups are conjugated at the 8-positions. Double bond conjugation followed, to a certain extent, the Woodward-Fieser rules, increasing the absorption maxima by 5-20 nm.^{221,222} In addition, an increase of the Stokes shift upon double bond conjugation occurs, in some cases up to 40 nm, which would be useful for FRET studies. However, the quantum yields (Φ_F) reported were 15-110 fold lower. Alkyl groups on C8 have a slight inductive effect into the BODIPY conjugate, decreasing the wavelength by < 5 nm.²²³ Substitution of the BODIPY meso position by alkyl groups stabilizes the BODIPY structure when treated in acetic conditions and during fluorine ligand exchange. A close resemblance is seen when comparing our anthroyloxy- α -tocopherol (AO- α -Toc) to a BODIPY linked at the meso position. Computational studies of the AO- α -Toc - α -TTP complex suggested that the large fluorophore fits into the hydrophobic binding pocket. Tocopherols phytyl chain and AO- α -Toc are slightly curved in α -TTP (Figure 27). Experimental results however revealed that the 9-position linked anthracene created too much steric bulk in the hydrophobic binding pocket ($K_d = 279 \pm 124$ nM for the C9-chain- α -Toc).²⁰¹

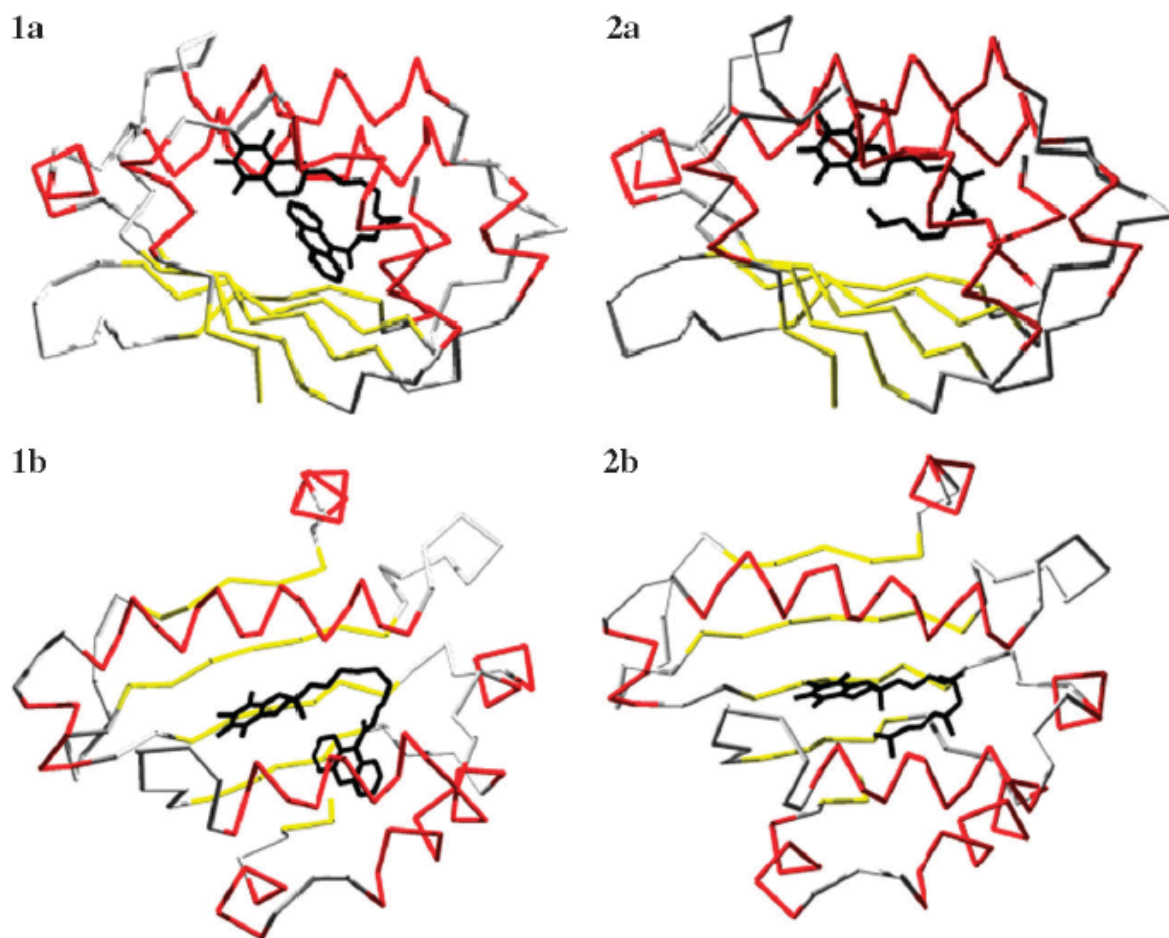
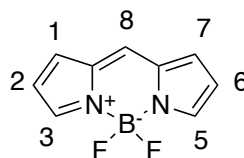


Figure 27. X-ray diffraction analysis of AO- α -toc (1a & 1b) and α -tocopherol (2a & 2b) bound to α -TTP.

Only amino acid residues 99-225, resembling the mayor part of the active side, are shown in two ways: 1a and 2a projected for looking down the long axis of the binding site. 1b and 2b from above.²⁰¹

Previous BODIPY- α -Tocs had the fluorophore attached at the 3 position, which proved to be superior in binding to α -TTP ($K_d = 94 \pm 3$ nM). Wavelength extension by an aromatic group must therefore be at the 3- or 5-position of the BODIPY. A BODIPY conjugated at the 3-, 5-, and 8-position have been reported in the literature with anisole, *para*-toluene, and thienyl groups providing increased wavelengths of absorption and emission for all compounds (Table 9).^{223,224,225,226,227,228,229}



| Functional group | Absorption (λ max) | Emission (λ max) | ϵ (M ⁻¹ cm ⁻¹) | Φ_F (%) | Solvent | Ref. |
|---|--------------------------------|------------------------------|--|--|------------------|-------------|
| No substitution | 500nm | 516nm | dnr | 77% ^a | THF | 223 |
| 8-Isopropyl | 496nm | 511nm | dnr | 78% ^a | THF | 223 |
| 8- <i>Trans</i> -methylmethylene | 507nm | 554nm | dnr | 5% ^a | THF | 223 |
| 8-Phenyl, 2- <i>para</i> -alkoxy- | 540nm | 568nm | dnr | dnr | EtOH | 224 |
| 8-Phenyl, 2- <i>para</i> -toluene- | 525nm | 549nm | dnr | 0.04 ^b | MeOH | 225 |
| 8-Phenyl, 2-Styrene- | 564nm | 579nm | dnr | 0.55 ^b | MeOH | 225 |
| 2-Styrene-ene- | 581nm | 591nm | 139,444 | dnr | ACN | 226, 227 |
| 8-Phenyl, 2-Phenylethynyl- | 556nm | 569nm | dnr | 0.98 ^b | MeOH | 225 |
| 8- <i>p</i> -Br-phenyl, 2-Thienyl, 5-Chloro | 570nm | 587nm | 71,500 | 0.40 | EtOH | 228 |
| 2,5-Di-thienyl- / | 606nm | 649nm | 58,000 | 0.81 | Tol. | 229 |
| 8- <i>p</i> -Br-Phenyl, 2,5-di-Thienyl- | 622nm | 643nm | 69,700 | 0.82 | EtOH | 228 |
| 8- <i>p</i> -Br-Phenyl, 2-Thienyl-ene- | 580nm | 593nm | 98,400 | 0.82 | EtOH | 228 |
| 8-Phenyl, 2-3 fused Mono- Benzothieno[b]- Fused ^c | 562nm | 584nm | dnr | 0.24% 0.025% for 8- phenyl ^d | Cyclo- hexane | 217 |

Table 9. Conjugation effects to BODIPY.

a: In paper (Φ_F compared to fluorescein (Φ_F 79% in 0.1M NaOH) **b:** Φ_F Standards; rhodamine 6G in water (Φ_F = 0.78) or cresyl violet acetate in methanol (Φ_F = 0.55) **c:** sulfur is connected to the 3 position (β , 2 position = α) **d:** "Absolute quantum yields determined by a calibrated integrating sphere system" ref 217. Data not recorded in publication (dnr).

Thienyl- and thienyl-ene- structures were chosen since they are somewhat smaller in size than phenyl groups.

Target **1** has the thienyl-group at the 5'-position, with a five-carbon chain. Compound **2** has the thienyl-group as a part of the carbon chain and is directly linked to the BODIPY core.

Compound **3** uses the thienyl-ene extension with the design of **2** (Figure 28). Rohand found during his cross-coupling studies that phenyl groups directly attached to the 2-position have a low quantum yield.²²⁵ This is not the case with thienyl or thienyl-ene- groups as seen in Rihn's paper.²²⁸ The only decrease in Φ_F was observed with chlorine substituted in the 5-position.

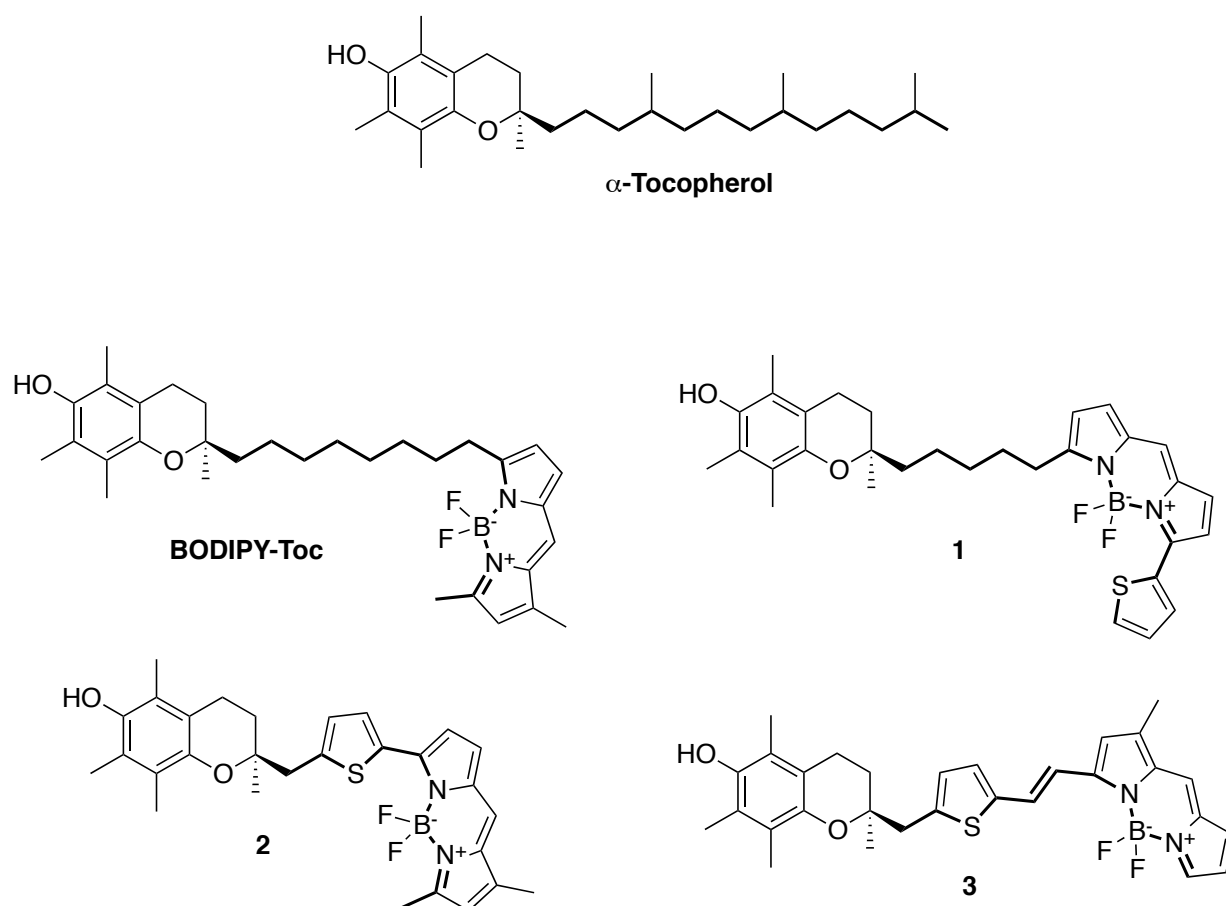


Figure 28. Novel designed fluorescent α -Toc ligands compared to BODIPY-Toc and α -tocopherol.

Target **1** and **2** have a thiophene group directly linked at the 2-position to the 5-position of the BODIPY. Target **3** resembles target **2**, but has an ethylene bridge between the thiophene and the BODIPY.^{206,216}

2.2 Synthesis plan

Target **1** resembles the structure of previously prepared BODIPY- α -Tocs, having an additional terminal thienyl-group on the BODIPY. The synthesis had certain issues, which have to be considered in the design of the targeted BODIPY tocopherols. The formation of the BODIPY

framework from condensation of 2,4-dimethylpyrrole aldehyde and oct-7-ene-2-pyrrole produced the self-condensed 1,3,5,7-tetramethyl-BODIPY as a side product, tricky to isolate and purify (**a**, Figure 29). In the next step, the oct-7-ene-BODIPY was reacted in a cross metathesis reaction with (*S*)-*tert*-butyldimethyl((2,5,7,8-tetramethyl-2-vinylchroman-6-yl)oxy)silane (TBSO-Trolox-ene). Hoveyda-Grubbs second generation catalysts produced only moderate yields and might form small amounts smaller chain length isomers as byproducts that require separation by preparative HPLC. Further, the oct-7-ene-BODIPY favoured self-condensation over cross metathesis (**b**, Figure 29). Therefore, another scheme was devised that followed synthetic plans similar to long chain *N*-heterocyclic tocopherols²³² and NBD-tocopherols.²⁰¹

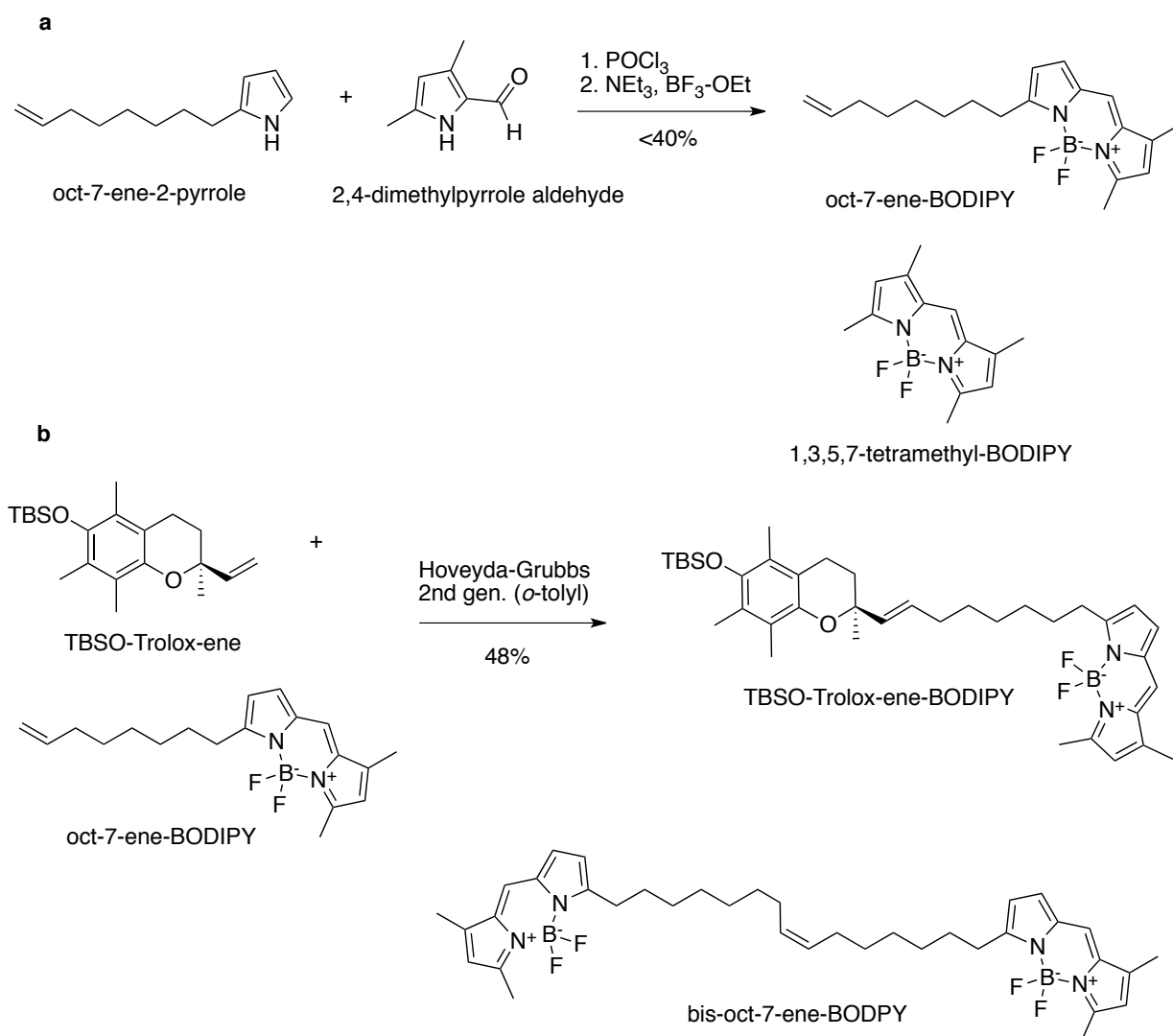


Figure 29. (a) BODIPY formation from oct-7-ene-pyrrole and 2,4-dimethylpyrrole aldehyde. Formation of byproduct 1,3,5,7-tetramethyl-BODIPY. (b) Olefin metathesis reaction between vinyl TBSO-Trolox-ene and oct-7-ene-BODIPY. Formation of dimer bis-oct-7-ene-BODIPY.²⁰⁶

Trolox® is a chroman acid commonly used as an antioxidant reference to measure the total antioxidant capacity of fruits and vegetables.²³⁰ Successful use in prior projects made Trolox® the choice of starting material for the new BODIPY-tocopherols as well. Trolox® is converted over three steps to **6** by methyl ester formation, TBS-protection of the phenol and reduction of the ester to an aldehyde (Trolox aldehyde). A Wittig reaction with 4-hydroxypropyltriphenylphosphonium bromide produced **8**, which was converted to the aldehyde **10**. Pyrrole was added by a Wittig reaction with 2-methylpyrrolephosphonium

bromide to **13** and condensation to the BODIPY core with thiophenepyrrole aldehyde followed by deprotection yielded target **1** (Figure 30).

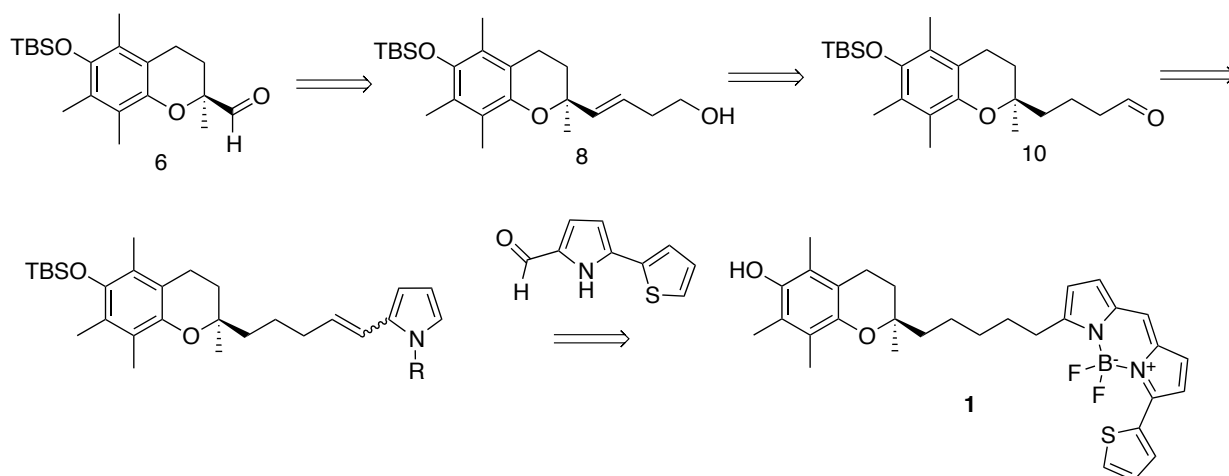


Figure 30. Synthetic strategy towards product 1.

TBSO trolox aldehyde, **6**, is converted to product **8** by a Wittig reaction. Reduction of the olefin and oxidation of the terminal hydroxide creates product **10**, which is turned into product **10** by a second Wittig reaction. BODIPY product **1** is formed by reacting **13** with 5-(thiophen-2-yl)-1H-pyrrole-2-carbaldehyde.

For target **2**, Trolox aldehyde was reacted with thiophene bromide. The resulting product **26** was cross-coupled with pyrrole to product **30** and condensation with pyrrole aldehyde forms product **2** (Figure 31).

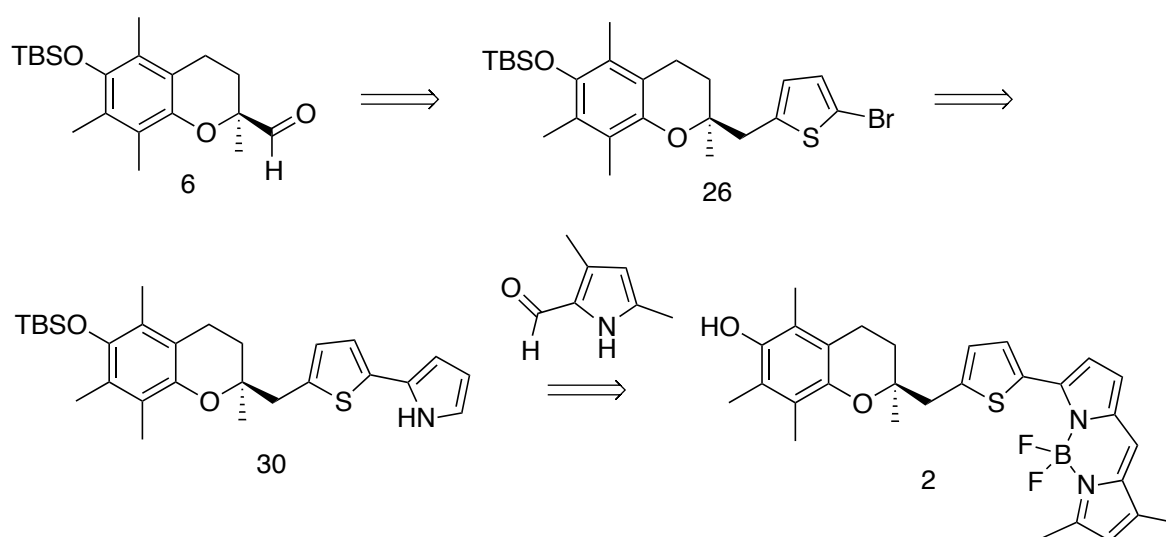


Figure 31. Synthetic strategy towards product 2.

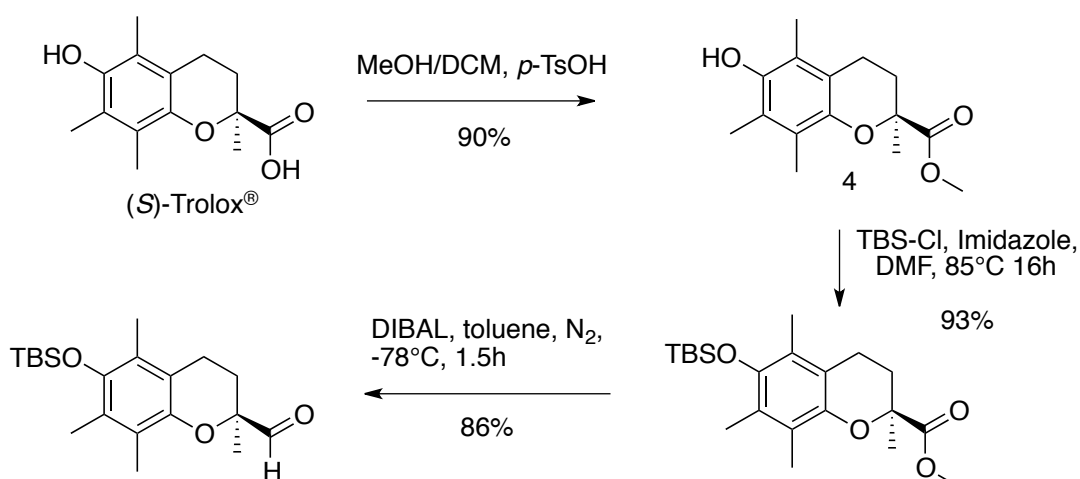


Figure 33. Synthesis of TBSO trolox aldehyde from Trolox® by esterification, TBS protection of the chroman phenol and reduction of the methylester to the aldehyde.

A saturated three-carbon linker was added using hydroxy phosphonium salt **7**, itself synthesized from 3-bromo-1-propanol.^{235,236,237} Two equivalents of lithium hexamethyldisilazide (LHMDS) were used to create the active ylide at room temperature. Addition of **6** in dry THF yielded 76% of product **8** (Figure 34).

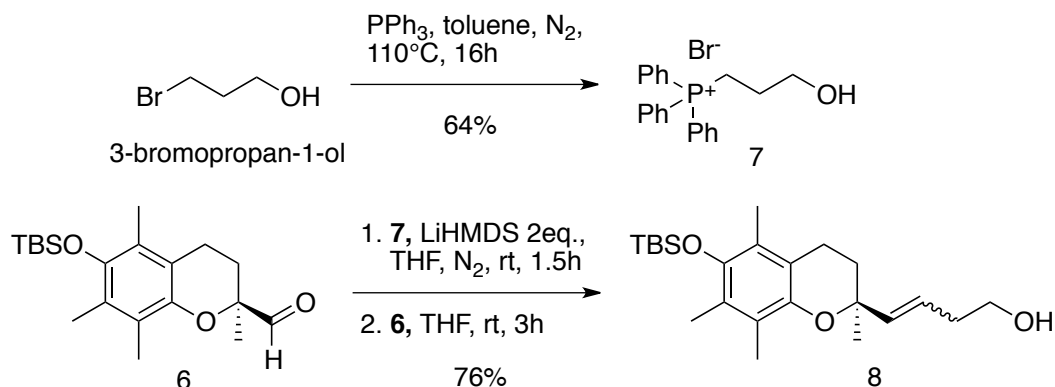


Figure 34. Synthesis of phosphonium salt, **7, from 3-bromopropan-1-ol²³⁵ and Wittig reaction of **7** with TBSO Trolox aldehyde to create product **8**.²⁰⁶**

Following the Wittig condensation the olefin **8** was reduced with H₂ over Pd/C 10%. This reaction, however, gave a mixture of products upon hydrogenation. Ethyl acetate was chosen as a solvent based on a report by Sajiki, which mentioned desilylation in EtOH, MeOH, water, hexane, DMF and THF.²³⁸ Besides the expected product **9** (40%) also obtained were the saturated aldehyde **10** (31%) and the fully reduced C4 alkyl product **9.2** (8.6%). Reduction of **8**

to the **9** was accomplished specifically and completely when the solvent was thoroughly dried prior before use (Figure 35).

Figure 35. Synthesis of product 9 by hydrogenation of 8 with 10% palladium on carbon.

Such side reactions have not been reported in prior Wittig reactions with the Trolox aldehyde. Linkers had a minimum length of five carbons following the efforts of Lei *et al.*²³¹ After the discovery of these side-reactions the same results were observed with the Trolox allylic alcohol (12) in Hilderling's attempts to synthesize tocopentaenol.²³⁴ Using new palladium catalyst did not change the outcome. It is known that primary alcohols can oxidize to the corresponding aldehyde in the presence of palladium as a catalyst.²³⁹ To understand this phenomenon the unsaturated C4 alcohol **8** was reacted with palladium acetate and 10% Pd/C in ethyl acetate with air as an atmosphere for several days at elevated temperature.²⁴⁰ No product aldehyde was formed in both cases. Migrations of double bonds by metal complexes have been described in the literature. Isomerization of allyl ethers to aldehydes by platinum(II)hydrido complexes was reported by Clark in 1972.²⁴¹ Metal mediated isomerization with 10% Pd/C is more prone with allylic alcohols and allylic ethers and less with more distant double bonds. However, no reaction occurred without any hydrogen gas present.^{242,243,244}

Most likely two separate reactions were taking place when water was present. The hydrogenation of the double bond occurs with and without water (**a**, Figure 36), as it is missing in all isolated products, **9**, **9.1**, **10**. Any water present in the reaction is turned into an active nucleophile by the hydrogen present on the palladium surface (**b**, Figure 36).

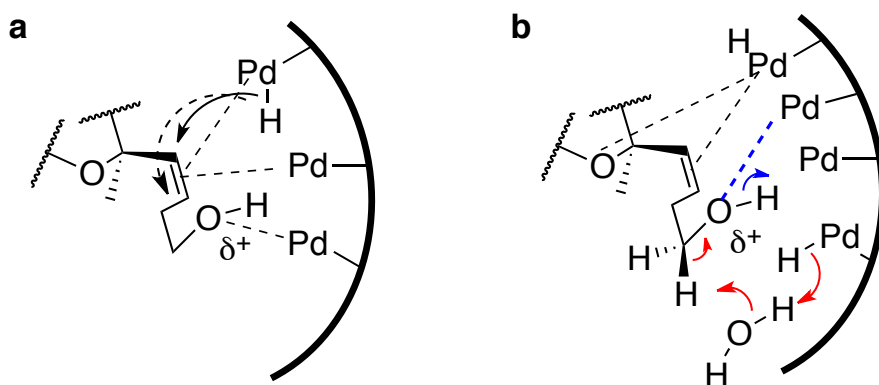


Figure 36. (a) Double bond hydrogenation of compound 8.

The cartoon represents the addition of the palladium-hydride from the catalyst surface to the double bond. (b) Model of hydroxide oxidation under reductive conditions. The hydroxide is interacting with the metal surface, making the hydroxide more delta-positive, and thereby weakens the carbon-hydrogen bond (blue dashed line and arrow). The water acts as a nucleophile and abstracts the alcohol carbon-hydrogen. The newly formed hydronium ion is instantly quenched on the metal surface by metal-hydrides (Pd-H), reforming the metal catalyst and water. The abstraction of the alcohol carbon-hydrogen and hydronium quenching are in this picture combined in one step (red arrows).

Griffin described the oxidation of 1-, 2- and 3-pentanol to the corresponding aldehyde and acid (Figure 37). He used 1-5% water and water / base mixtures on palladium and platinum catalysts in his study. Full conversion of geraniol to citral was seen after 6h. The metal catalyst is in this case solely acting as a Lewis acid. Pentanol binds to the metal surface and water acts as a base by abstracting the hydrogen on the alcohol carbon, releasing the aldehyde / ketone and a metal hydride species (M-H), which reacts with water to reform the metal catalyst. Strong basic conditions increased the reaction rate. Oxidation of to the carboxylic acid occurs in the presents oxygen in the solvent.²⁴⁵

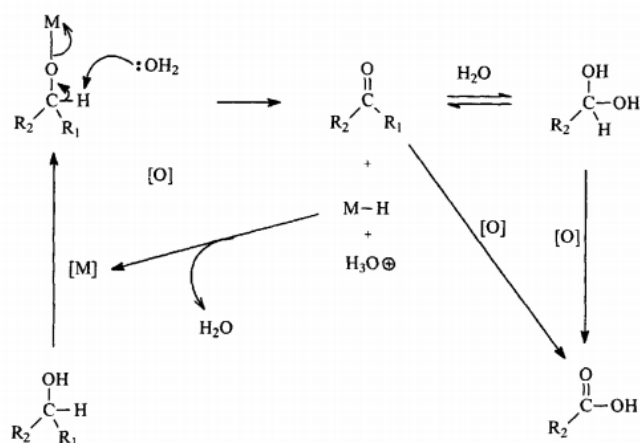


Figure 37. Griffin's proposed alcohol oxidation mechanism with water and palladium / platinum metal [M].

Pentanol is activated by binding to the metal, allowing C-H hydrogen abstraction by water to occur to form the aldehyde (ketone if 2-, 3-pentanol). The metal hydride (M-H) formed in the process reacts with water to reform the metal catalyst. Oxidation of the aldehyde to the carboxylic acid was observed when oxygen was present in the solvent.²⁴⁵

The reaction of **8** has not been tested with catalytic amounts of hydroxide. The proximity of the Trolox ring system may have influenced the reactivity of longer carbon chain linkers as the latter did not show any aldehyde sideproducts. The details of palladium involvement is unknown.

The oxidation of **8** under Swern conditions (Oxalylchloride, DMSO, TEA in dry DCM) gave a complex mixture of inseparable products, but ¹H-NMR indicated the absence of the TBS group.²⁴⁶ The TBS-C4 aldehyde **10** was successfully synthesised in a 22% yield with Dess-Martin periodinate (DMP) as the oxidizing reagent. The yield was improved to 67% by stirring the reaction for 16 h instead of 2 h (Figure 38).

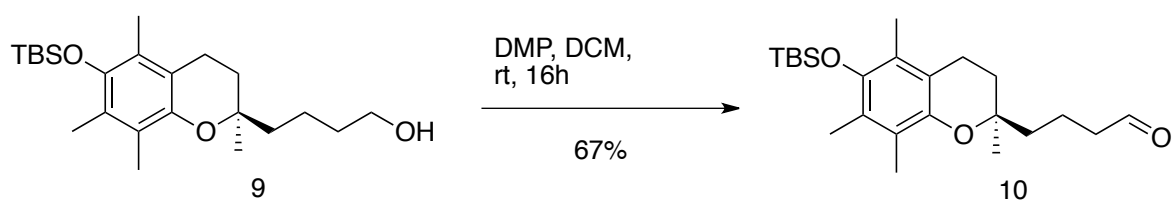


Figure 38. Synthesis of product 10 by Dess-Martin oxidation of 9.²⁴⁶

Wittig reaction of **10** with 2-methyl pyrrole triphenylphosphonium bromide **11** did not work as described in the literature.²⁴⁷ To increase reactivity the pyrrole was protected at nitrogen with a benzyl group²⁴⁸ despite this adding one more step in the synthesis.²⁴⁹ An acid labile group like *t*-butyloxycarbonyl (Boc) cannot be used since the phenol TBS would be simultaneously cleaved under such conditions. *N*-Benzyl protection **12** was chosen because of inert deprotection conditions by catalytic hydrogenation. Unfortunately, reaction of **10** with 2-methyl pyrrole triphenylphosphonium bromide did not yield any of product **13**, only starting material was recovered (Figure 39). Testing different bases like sodium hydride (NaH), *n*-butyl lithium (*n*-BuLi), or potassium *tert*-butoxide (*t*-BuOK) to deprotonate the phosphonium salt followed by stirring the ylide with the aldehyde for over 16h did not work either.

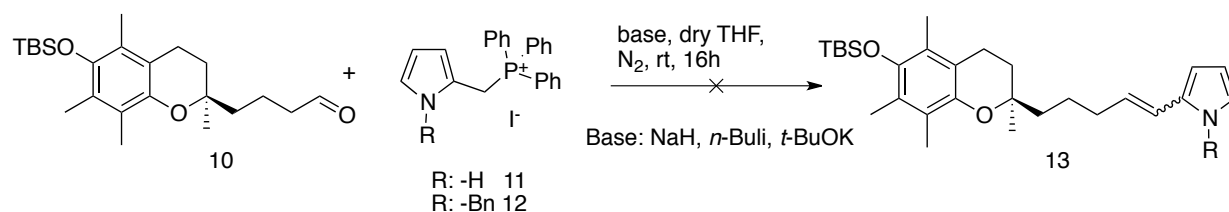


Figure 39. Synthesis of product **13** by Wittig reaction of aldehyde **10** with phosphonium salt **11** and **12**.

The reaction was run with sodium hydride (NaH), *n*-BuLi, *t*-BuOK as a base.^{247,249}

To solve this problem the functional groups were reversed on the pyrrole and chroman.

Synthesis of the chroman phosphonium bromide was achieved by converting alcohol **9** to the bromide **16** via the mesylate. A more direct path was tried following reports in the literature using Trolox aldehyde and a 3-bromopropyl phosphonium bromide **14** to access the bromide **15** directly (Figure 40).^{250,251}

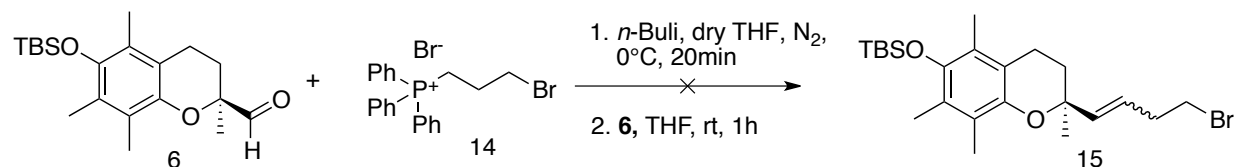


Figure 40. Synthesis of product **20** by Wittig reaction of aldehyde **16** with phosphonium salt **7** and lithium hexamethyldisilazide as a base.²⁵⁰

The reaction did not yield any product **15**, but mixtures of cyclopropane based byproducts along with starting material were suspected in the crude $^1\text{H-NMR}$, could not be isolated.

Cyclopropane formation by internal ylide cyclization is known in the literature.^{252,253} The conversion of alcohol **9** to the bromide **16** and iodide **17** was achieved in 57% / 54% yield via formation of the intermediate mesylate of **9** (Figure 41).²⁵⁴

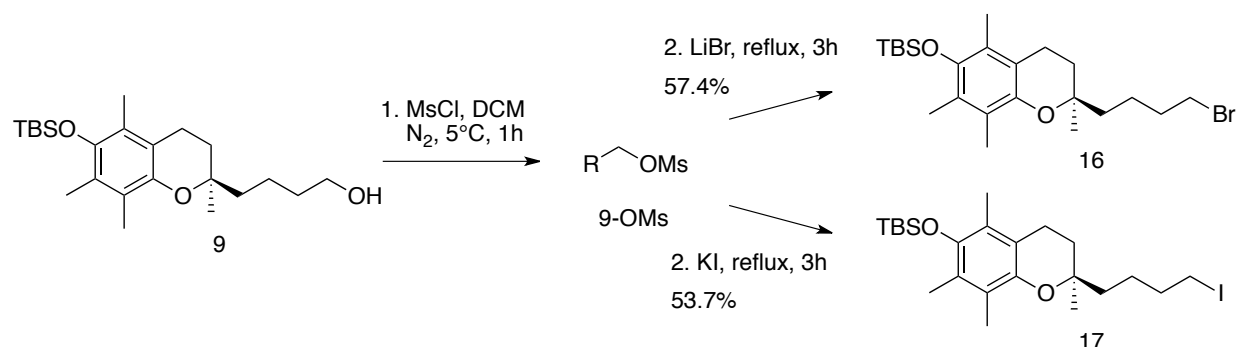


Figure 41. Conversion of alcohol **9 to the bromide **16** and iodide **17** by mesylation, followed by nucleophilic bromide and iodide substitution of the mesylate with lithium bromide (LiBr) and potassium iodide (KI).**²⁵⁴

Both halides were converted to the triphenylphosphonium salts **18** (bromide) and **19** (iodide) (Figure 42).²⁵⁵

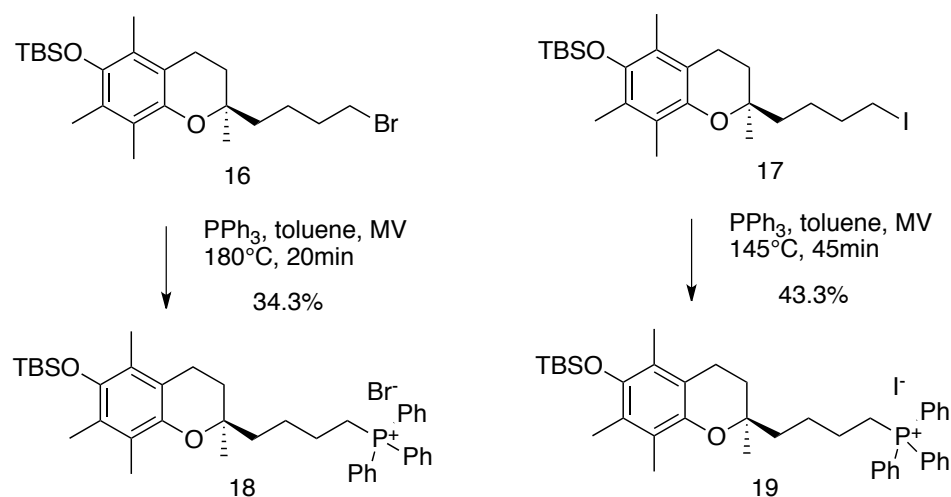


Figure 42. Synthesis of phosphonium salts **18 and **19** by reaction of **16** and **17** with triphenylphosphine (PPh_3) in a microwave oven (MV).**²⁵⁵

Deprotonation of the phosphonium salts to the ylides was achieved at -10 to 0°C with LiHMDS and NaH in THF, leading to a colour change to orange/red.

Before these Trolox linked phosphonium ylides were reacted with the protected pyrrole **6**, the C3 hydroxy phosphonium salt **7** was tested with *N*-benzylpyrrole aldehyde, using the same conditions when forming **8** (Figure 43).²⁰¹ A yield of 14-19% was obtained for product **20**.

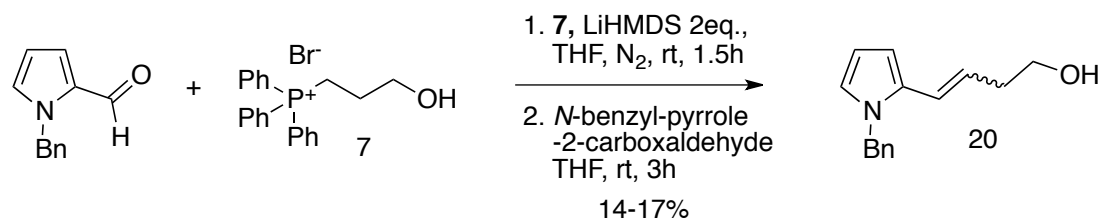


Figure 43. Synthesis of product **20** by Wittig reaction of *N*-benzylpyrrole-2-carboxaldehyde with phosphonium salt **7** and lithium hexamethyldisilazide as a base.²⁰¹

Similar reactions reported by Soares with methyl or ethyl triphenylphosphonium bromide on *N*-benzylpyrrole aldehyde.^{249,256} Unfortunately, the reaction was unsuccessful with ylides **18** and **19**. This was peculiar, given the success of the other Wittig reaction to form product **20**. (Figure 44) At this point in the project, the synthesis of **2** was started. The Wittig reaction was re-attempted in dry conditions with *n*-BuLi as a base at 0°C, but still didn't yield any product.

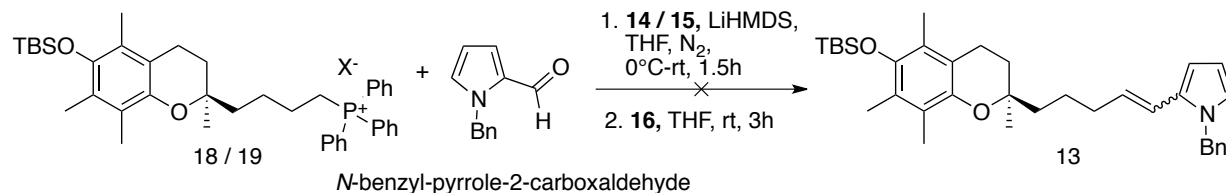


Figure 44. Synthesis of product **13** by Wittig reaction of *N*-benzylpyrrole-2-carboxaldehyde with phosphonium salt **18** and **19** and lithium hexamethyldisilazide as a base.^{201,249}

During the work to synthesis compound **1**, we considered putting the thiophene extension between the chroman and the BODIPY group. This new target, **2**, design has a shorter carbon chain length than target α -tocopherol and **1** (Figure 45). The curvature of the phytol chain in the active site seen in model studies suggests that there is enough space to accommodate the thiophene. Evidence for ligands with shortened chainlengths being better as α -TTP ligands is seen with NBD-Toc, which is shorter in overall length and less bulky than BODIPY- α -Toc.

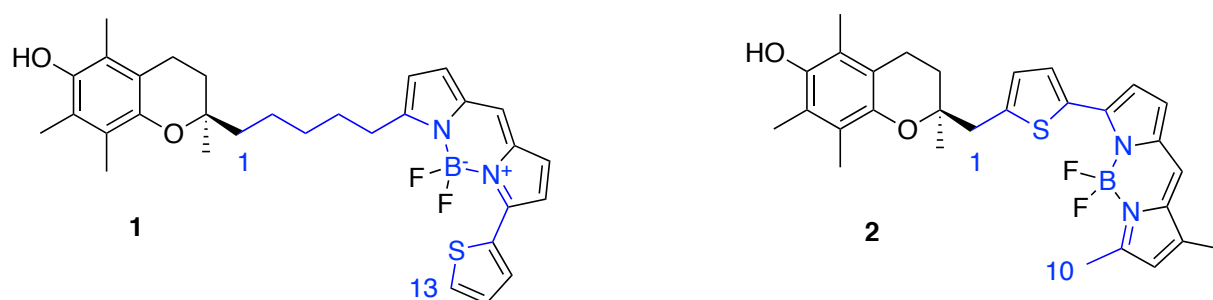


Figure 45. Decrease in chain length from target product 1 to 2.

The innermost chain was used to compare the overall chainlength. The blue numbers represent the first and last atom of the chain.

Placing the thiophene group closer to the chroman ring has certain synthetic advantages.

Thiophenes are known to have a higher reactivity than benzene and react regioselectively with electrophiles under mild conditions.²⁵⁷ Addition of the thiophene to the chroman can be performed by nucleophilic addition to the electrophilic center connected to the 1'-position on the chroman ring (Figure 46).

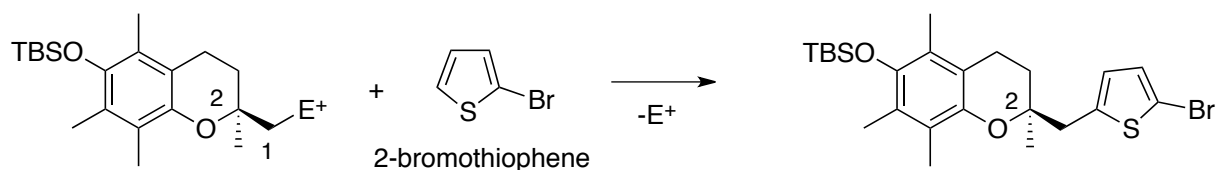


Figure 46. 2-Bromothiophene addition to Trolox by displacement of an electrophile on position 1.

Synthesis of compound **2** started with the TBS-protected aldehyde **6** or benzyl-protected **21**.

The benzyl group was chosen because of its high stability to most reaction conditions and the low yields observed during the TBS-deprotection with HCl / MeOH and TBAF in our prior BODIPY synthesis by West.²⁰⁶ Deprotection of the chroman by hydrogenation was expected to be high yielding and gentle on the final structure.

Two ways were chosen to attach the thiophene group: reduction to the Trolox alcohol **22**, followed by conversion to alkylbromide **23** and displacement of the halogen by thiophene, or by thiophene addition to the aldehyde followed by reduction of the alcohol **25** to the alkane **26** (Figure 47).

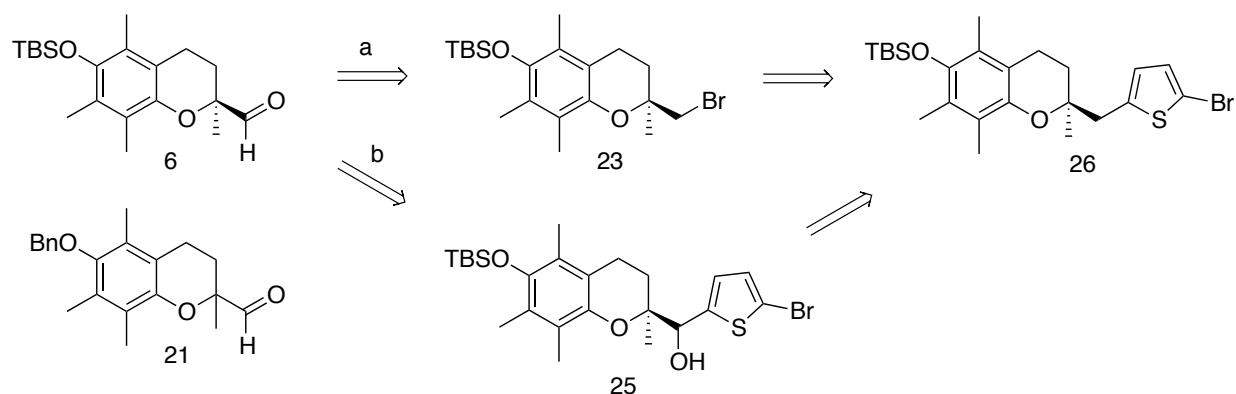


Figure 47. Synthetic routes chosen to synthesize 26 from TBS trolox aldehyde 6.

(a) Reduction of the aldehyde and bromination of the hydroxide created TBS Trolox bromide 23. Displacement of the bromine with 2-bromothiophene created product 26. (b) Nucleophilic addition of 2-bromothiophene to 6 creates 25, which by reduction of the secondary alcohol is turned into product 26. Racemic benzyl protected Trolox aldehyde was used because of higher stability towards most reaction conditions and the low yields observed during TBS deprotection.²⁰⁶

Wang described the protected Trolox alcohol **22** by reduction of the methyl ester or acid with lithium aluminium hydride.^{254,258} It can also be obtained as an over-reduced byproduct during the DIBAL reduction to the Trolox aldehyde **6**, more so when the reaction is run at 0°C.²³³ Swern oxidation of alcohol **22** can be used to regain the aldehyde.²⁴⁶ Conversion of **22** to the bromide **23** was successful by synthesis of the mesylate **22-OMs** (73%) followed by addition of excess lithium bromide (42%).²⁵⁴ Appel reaction conditions (CBr₄, PPh₃ in toluene) were tested as described in the literature, but this deprotected the phenol TBS group (**24**) (Figure 48).²⁵⁹

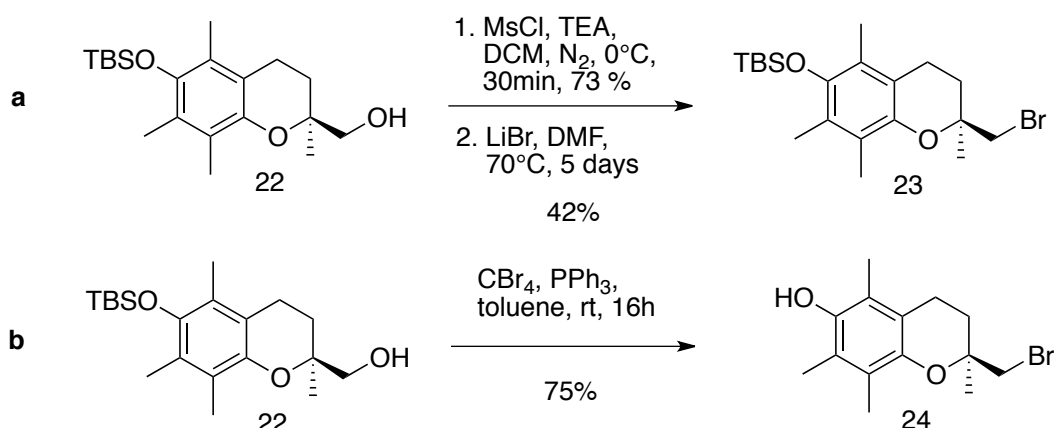


Figure 48. (a) Synthesis of product 23 by mesylation of TBS trolox alcohol 22, followed by nucleophilic bromide displacement of the mesyl group with lithium bromide.²⁵⁴ (b) Appel reaction of 22 yielded TBS deprotected product 24.²⁵⁹

Hoye described a thiophene addition to a bromo alkene in the presence of an alkyl chloride. The reaction was conducted at 0°C to room temperature, with prior formation of the 2-lithiothiophene from 2-bromothiophene.²⁶⁰ Unfortunately, the arylbromide functional group is lost in the product, which would then have to be re-installed in the next step for the Negishi cross coupling to pyrrole. Rebromination on the 5-position has been described, but would involve an additional synthetic step.²⁶¹ Lithiation of 2-bromothiophene at -78°C produces the anion opposite to the bromine at the 5-position. The reaction of 5-bromo-2-lithiothiophene with **23** at low temperature was attempted, but did not yield any product (Figure 49).

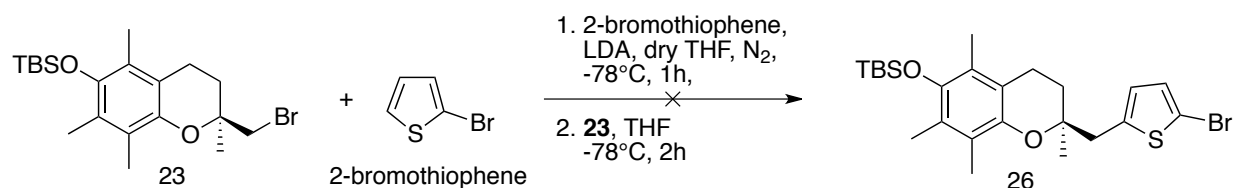


Figure 49. Synthesis of product 26 by reaction of 23 with 2-bromothiophene.^{261,262}

Peyron described this reaction with alkyl aldehydes as electrophiles.²⁶² Alternatively, β -(5-bromo)-2-thienyl nucleotides have been synthesized by Friedel-Crafts type reaction from Lewis acid activated C-methyl glycosides.²⁶³ Following Peyron's reaction protocol **6** was reacted with 2-bromothiophene, providing a stereochemical mixture of secondary alcohols **25** (75:25) with a 53-87% yield (Figure 50).

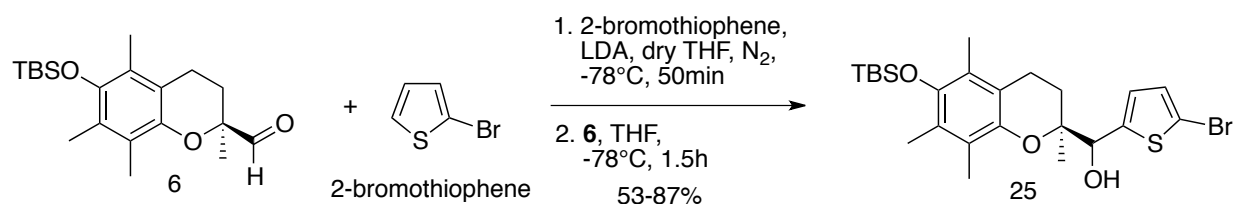


Figure 50. Synthesis of product 25 by reaction of 6 with 2-bromothiophene.²⁶²

Based on these reasonable yields and the previously known chemistry to synthesise the Trolox aldehyde **6** in high yield, the alkyl bromide pathway (Figure 47, a) was abandoned. To maintain high yields and not waste the expensive enantiomerically pure *R*-TBS protected product **25** for the dehydroxylation step a racemic chroman was synthesised. The protecting group on the phenol changed to a benzyl group (Bn), since acidic conditions might be used to assist the reduction of the secondary alcohol.²⁶⁴

The racemic chroman building block for the trial benzyl protection was synthesized by an improved oxa-Diels-Alder reaction of 2-methylmethacrylate and trimethylhydroquinone described by Hilderling.²³⁴ Product yields were in the high 90% range and obtained in a short amount of time. The racemic product was benzyl protected **27** and reduced to the aldehyde (**21**) in very good yields. Trace amounts of over reduced alcohol **21.2** were observed (Figure 51).²⁶⁵

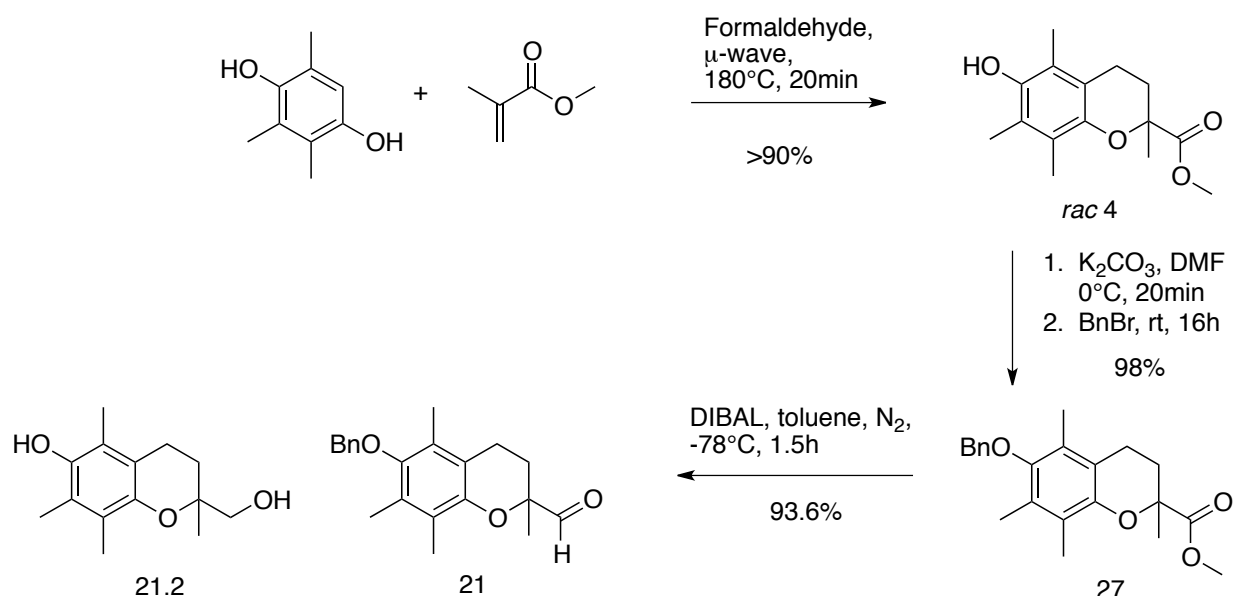


Figure 51. Synthesis of benzyl protected trolox aldehyde 21.

Oxa-Diels Alder reaction of trimethylhydroquinone with methylmethacrylate to racemic (*rac*) product **4**. Benzyl protection of **4** created **27**, which was reduced to aldehyde **21**. Overreduced product, **21.2**, was isolated in trace amounts.^{234,232}

A chemoenzymatic synthesis was described by Chenevert using *Candida antarctica* lipase B lipase catalyzed esterification to obtain the benzylated chroman aldehyde.²⁶⁶ A choice was made to use the racemic material to test the next steps in the reaction scheme, despite not being the pure *R*-enantiomer. Synthesis of the benzylated thiophene alcohol **28** followed the same procedure as described in Figure 50 (Figure 52).

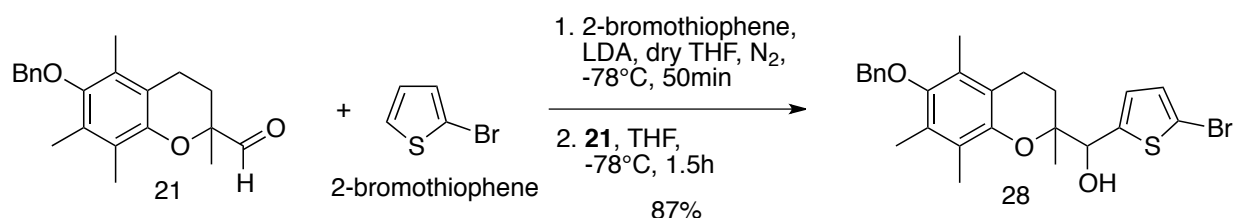


Figure 52. Synthesis of product **28 by reaction of **21** with 2-bromothiophene.**²⁶²

To dehydroxylate **28** different hydrides were added with acids and Lewis acids for activation of the benzylic alcohols.^{267,268} Protonation of the alcohol with trifluoroacetic acid, followed by addition of triethylsilane (TES) as a hydride source did not yield product.²⁶⁴ Zinc chloride or iodide with sodium cyanoborohydride yielded <1%-11% of product.²⁶⁹ LiAlH₄ with AlCl₃ did not react at all.^{270,271} Activation of the alcohol using mesyl or tosyl groups followed by reduction have been described in the literature.^{272,273} The mesyl group was successfully synthesized, but the crude product did not yield any of the reduced deoxygenated product when treated with excess LiAlH₄.

Finally, the product **29** was successfully synthesized in a short reaction time and high yield by reduction with TES, but instead of TFA using BF₃ as a Lewis acid catalyst. A similar system, using perfluorotriphenylborane with TES has been used to fully reduce carboxylic acids, esters and aldehydes to the alkanes.²⁷⁴ Similar yields (80-90%) were observed with the TBS protected alcohol **25** to product **26** (Figure 53).

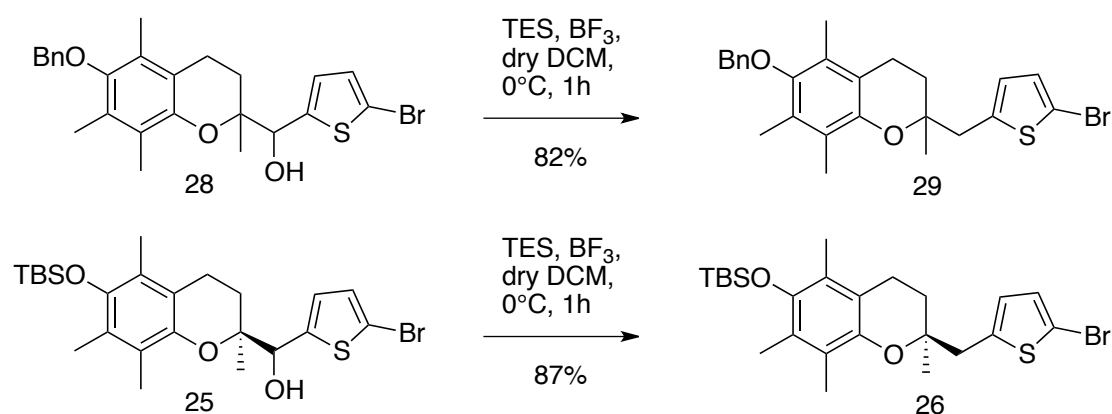


Figure 53. Reduction of 28 to product 29 and 25 to product 26 with triethylsilane and borontrifluoride.²⁷⁴

To attach the pyrrole moiety that is needed for the BODIPY formation the TBSO-thiophene bromide **26** was reacted with a pyrrole zincate in a Negishi coupling.²⁷⁵ Two fractions were isolated, one as an oil and the other as a solid, together yielding 10.8% of products (Figure 54). Product **30** was formed in traces along with the dimer (**31**). NMR spectroscopy of the oil showed noise peaks in the aromatic region whereas the solid showed clear peaks indicating a mixture of two products. This seemed to be the effect of π -stacking between the molecules. To verify the products an EI⁺ mass spectrum was recorded, but unfortunately did not give any molecular ion. The dimer was confirmed by MALDI mass spectroscopy.²⁷⁶

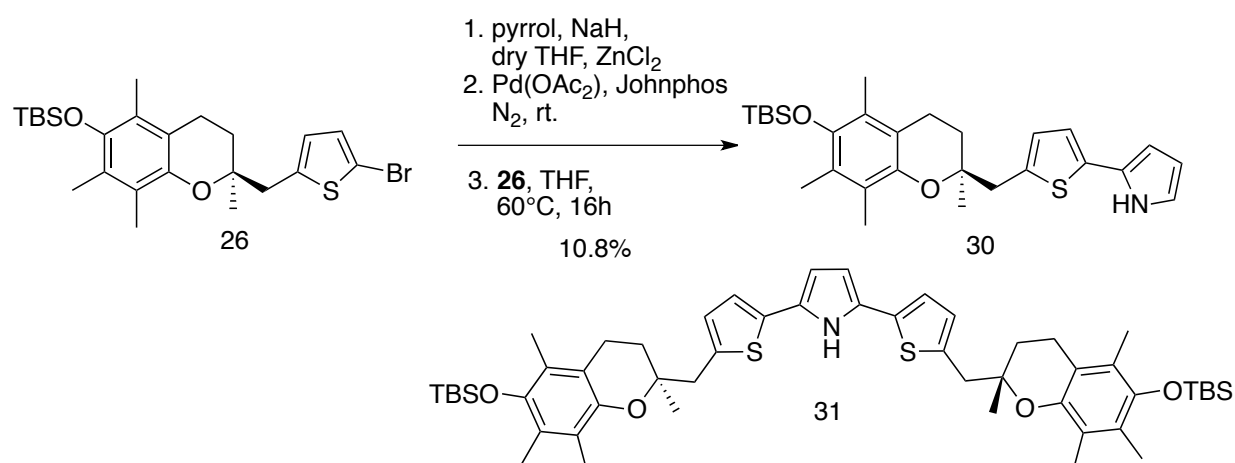


Figure 54. Negishi coupling of 26 with pyrrole to create product 30. Synthesis of dimer byproduct, 31.²⁷⁵

Separation of the dimer and **31** was not possible by column chromatography and was used as a 1:1 mixture in the next step. The Negishi chemistry was tried with the BnO-protected bromothiophene **29**. Product was isolated in similar yield (10.3% **32** only) as a mixture of products. Purification by chromatography afforded the debrominated byproduct (**29-H**, 1%), but the dimer was inseparable. **32** was used as a 1:1 mixture in the next step (Figure 55).

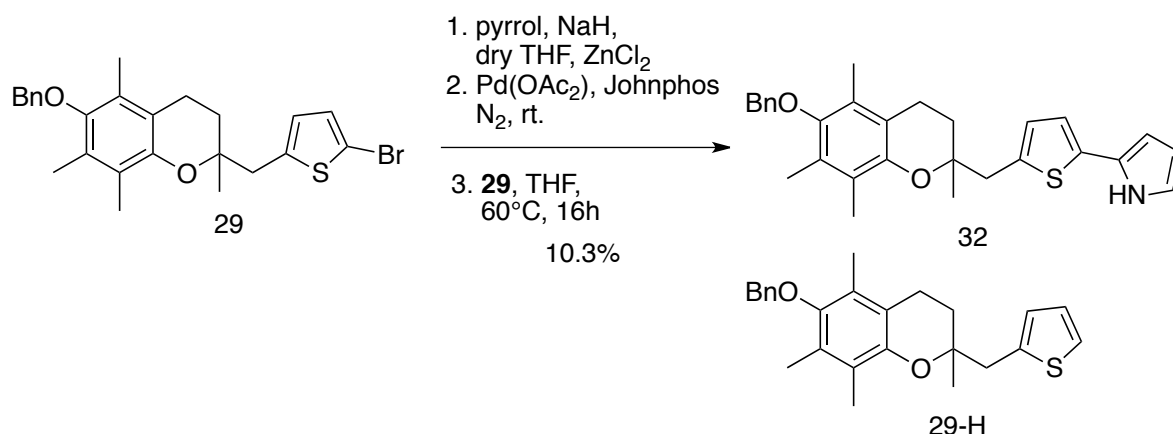


Figure 55. Negishi coupling of **29** with pyrrole to create product **32** and trace amounts of **29-H**.²⁷⁵

BODIPY formation was carried out with 3,5-dimethylpyrrole-2-carboxaldehyde, following the conditions used for the synthesis of BODIPY- α -Toc.²⁰⁶ Product **33** was isolated in 13% yield (Figure 56).

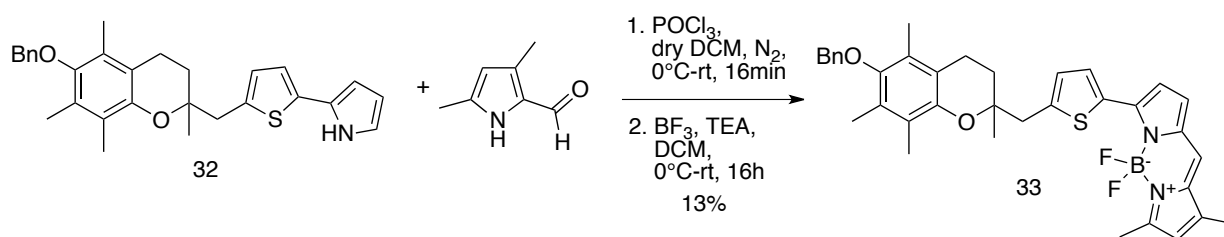


Figure 56. Synthesis of **33** by condensation of **32** with 3,5-dimethylpyrrole-2-carbaldehyde.²⁰⁶

At this point there were 23 mg of **33** available for the deprotection of the chroman ring to product **2**. Hydrolysis with Wilkinson's catalyst in EtOH was chosen from our experience with BODIPY- α -Toc synthesis, but did not yield product.²⁰⁶ The reaction was rerun in EtOAc for the same time, but no product was found. The starting material was then reacted with Pd/C 10% on carbon in dry EtOAc overnight.²⁷⁷ A new fluorescent spot was seen by TLC and

isolated, giving 1 mg of seemingly de-benzylated product by NMR, but had too much contaminating grease to be verified and used further. Hydrogenation with H₂ under prolonged stirring with Pd/C 10% at elevated pressure can decompose BODIPYs.²⁰⁶ To increase hydrogen absorption a transfer hydrogenation with excess trimethylsilane and Pd/C 10% was attempted at room temperature, but also did not yield any product.²⁷⁸ Birch reduction conditions are known to de-benzylate alpha-tocopherol²⁶⁶ thus, 5 mg of **33** were treated with Li metal and ethylamine/ether at -78°C, but no product was observed after 1h (Figure 57).

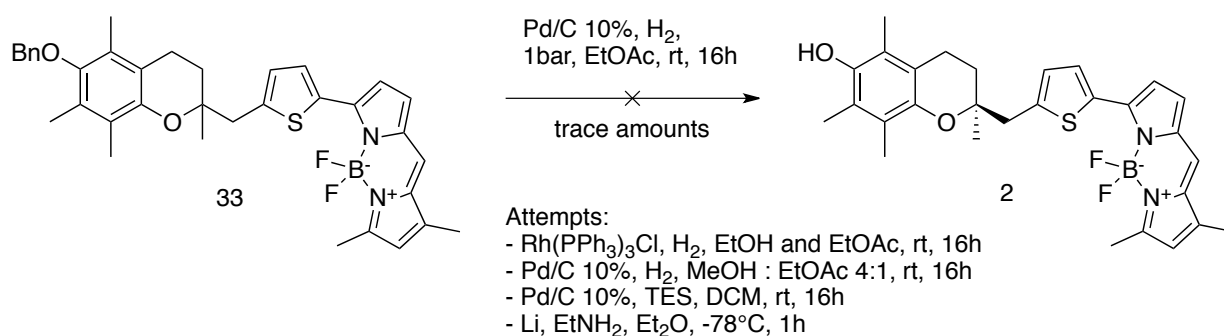


Figure 57. Attempts to debenzylate 33 to form product 2.

Conditions tried were hydrogenation with H₂, using 10% palladium on carbon (Pd/C 10%) as a catalyst with ethyl acetate and methanol as a solvent²⁷⁷, and with Wilkinson's catalyst (Rh(PPh₃)₃Cl) in EtOH.²⁰⁶ Pd/C 10% was further used in a transfer hydrogenation with triethylsilane (TES) in DCM.²⁷⁸ Alternatively was lithium metal with ethylamine applied as a reductive condition.²⁶⁶

The recovered benzylated chroman BODIPY was stored as a reference. The remaining quantity, even with a successful debenzylation, was not enough material to conduct binding studies with α-TTP or trials in hepatic cell culture.

With more material in hand, different oxidative and reductive debenzylations would be tested. Transfer hydrogenation with different hydrogen sources like formamide, cyclohexadiene and palladium catalyst.^{279,280} Lewis acids like BX₃, TiCl₄ have also shown promising results as debenzylation additives in the literature, but might be problematic because BODIPY B-F bonds are activated by the same molecules with subsequent halogen exchange or addition of any nucleophile present in solution.^{281,282,283}

With the pyrrole coupling and BODIPY formation reaction not yielding enough product an alternative approach was necessary to reach **2**. To avoid the Negishi pyrrole coupling a cross coupling with bromothiophene **29** and a *N*-protected pyrrole with a boronic acid / pinacol ester or alkylstannylate at the 2-position is required. The leaving groups on thiophene and *N*-protected pyrrole can be reversed in case of low reactivity.^{284,285,286,287,288}

While searching through the literature on how to connect the pyrrole to the thiophene bromide an alternative route was considered to link the BODIPY framework to the thiophene. Cross coupling reactions of aryl groups with BODIPY halides have been described in the literature.²⁸⁹

A common way to C-C couple BODIPYs to aryl groups is by Knoevenagel reaction of aryl carbonyls with a methyl group at the 2'-position on the BODIPY.²⁹⁰ As mentioned earlier, target **2** has a shorter length than the phytyl chain in tocopherol. The Knoevenagel reaction bridges a *trans*-double bond of the aryl aldehyde and BODIPY, which brings the overall sidechain length back to the length of the tocopherol phytyl chain. Furthermore, the wavelength would be extended by an additional ~10-20 nm. Therefore, we shifted focus to target **3**.

Formylation of thiophenes are well described in literature.^{290,291} Lithium halogen exchange at -78°C followed by DMF addition formed aldehyde **34** in 88% yield (Figure 58).

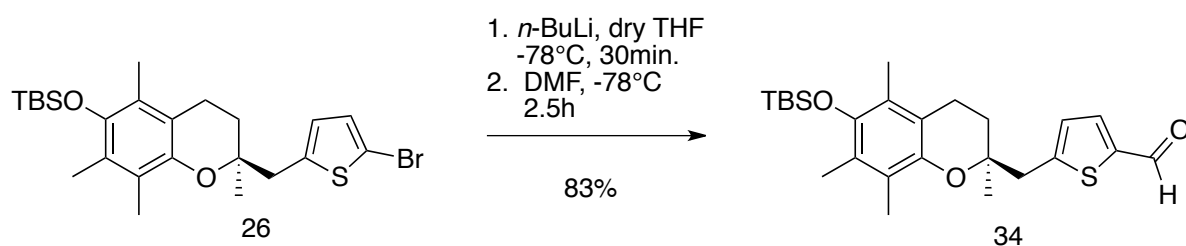


Figure 58. Synthesis of product 34 by formylation of 26 by lithium halogen exchanged and quenching with DMF.²⁹¹

A debrominated byproduct **35** was formed due to residual water in the reaction mixture.

Attempts to recycle the byproduct by Vilsmeier-Haack conditions with DMF and POCl₃ did not work, as the TBSO protection group was cleaved, followed by *in situ* protection of the phenol to the aryl formate **36** (37%) (Figure 59).^{292,293,294,295} The formate protection was a rather unexpected result. It is most likely that in the increasingly acidic environment the TBS-group was cleaved to the phenol, which then reacted with the chloroiminium ion reagent.

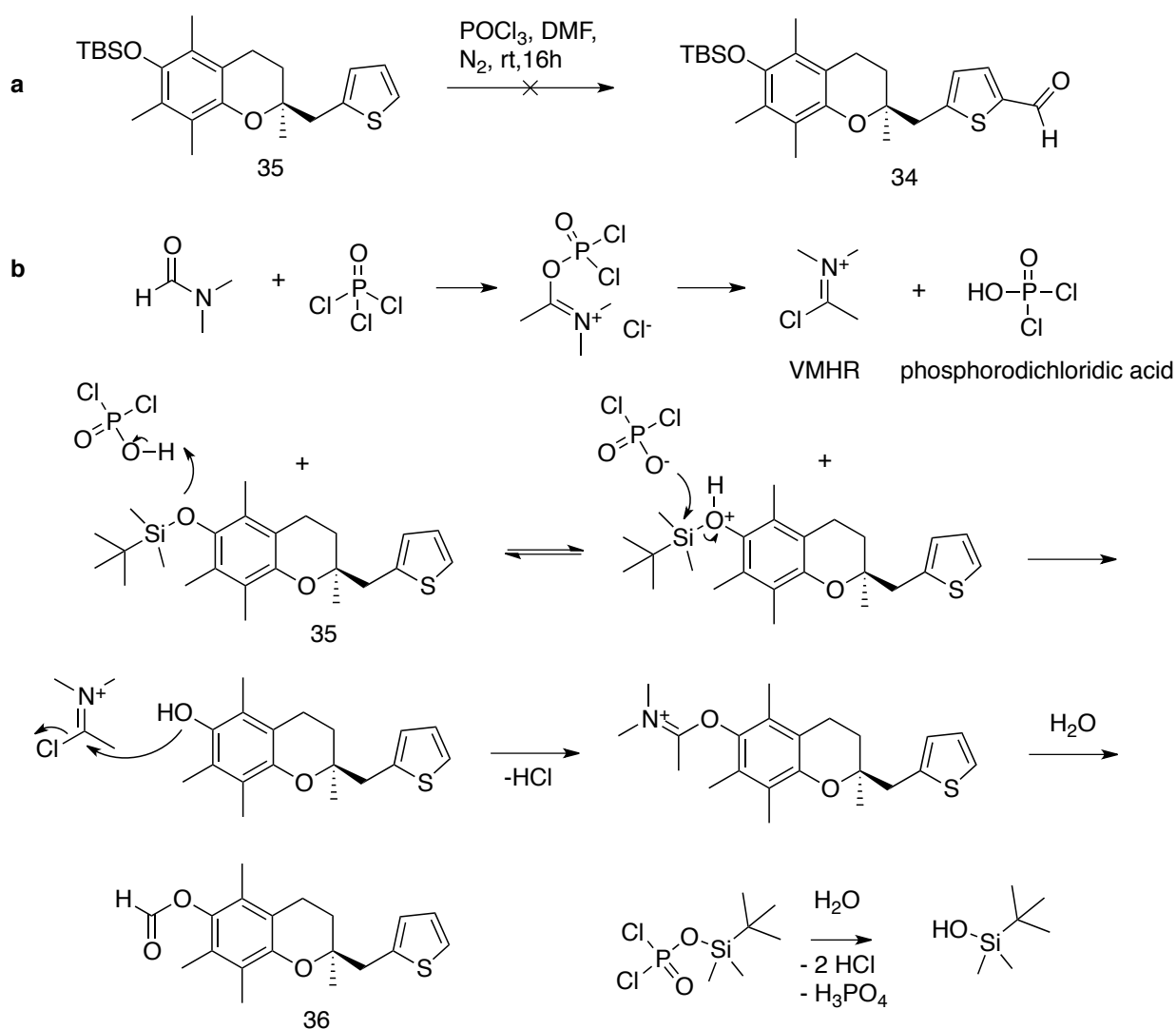


Figure 59. (a) Synthesis of 36 from 35 by Vilsmeier-Haack formylation. (b) Proposed reaction mechanism of the aryl O-formate protection of TBSO protected 2-thiophenemethyl α -chromane.

In acetic environment is the TBSO protonated and deprotected by phosphorodichlorate. DMF is turned into the Vilsmeier-Haack reagent (VMHR), which reacts with the phenol to form product **36**.²⁹⁵

BODIPY building block **37** was synthesized by using 2,4-dimethyl pyrrole and 2-pyrrole carboxaldehyde (Figure 60). Pyrrole was first reacted with 3,5-dimethyl pyrrole carboxaldehyde, however this reaction yielded more of the tetramethyl-BODIPY byproduct (**38**).²⁰⁶

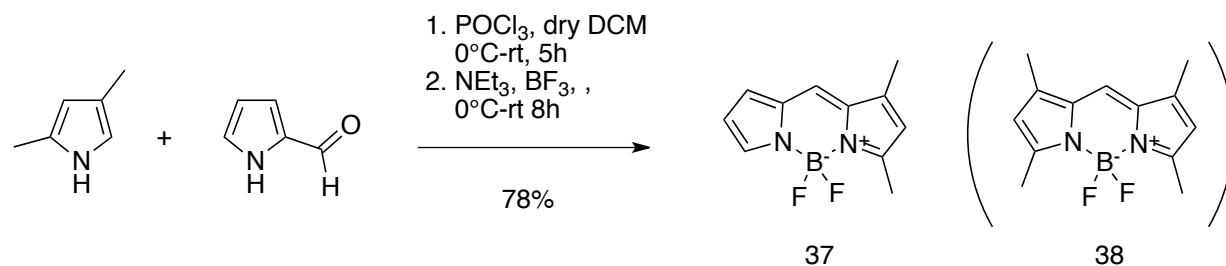


Figure 60. Synthesis of dimethyl-BODIPY building block, **37**, by condensation of 2,4-dimethyl pyrrole and 2-pyrrole carboxaldehyde.^{206,295}

Knovenagel reaction yielded BODIPY **39** in rather low yield (24%) (Figure 61).²⁹⁶ Such aryl carbonyl condensations with methylated BODIPYs often vary in yield, and usually do not exceed a median yield of 50%.^{297,290,298}

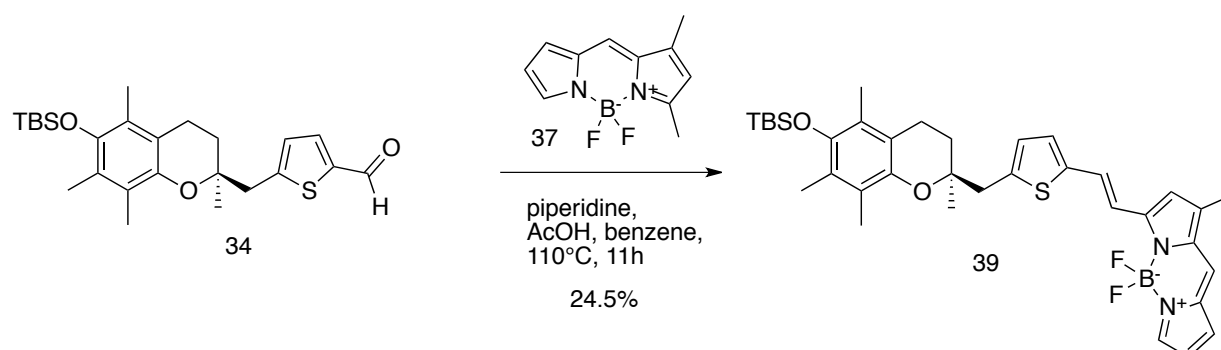


Figure 61. Synthesis of **39** by Knoevenagel condensation of **34** with dimethyl BODIPY **37**.²⁹⁶

Yields seem to drop with prolonged stirring, a condition that would have to be investigated in future scale up reactions. Deprotection to compound **39** followed by West's protocol yielded product **3** in moderate yield (Figure 62).²⁰⁶

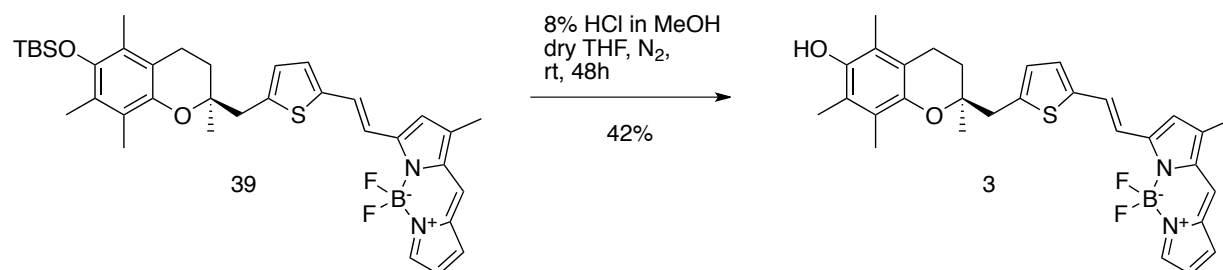


Figure 62. Synthesis of target product **3** by acetic phenol TBSO-deprotection of **39** with 8% HCl MeOH.²⁰⁶

3.2 Photophysical studies

3.2.1 Absorption spectra

The UV absorption maximum (λ_{abs}) of product **3** was determined to be 571 nm in absolute EtOH, with a secondary absorption maximum at 536 nm (Figure 63). The emission maxima (λ_{em}) was at 583 nm, giving a Stokes shift of 12 nm.

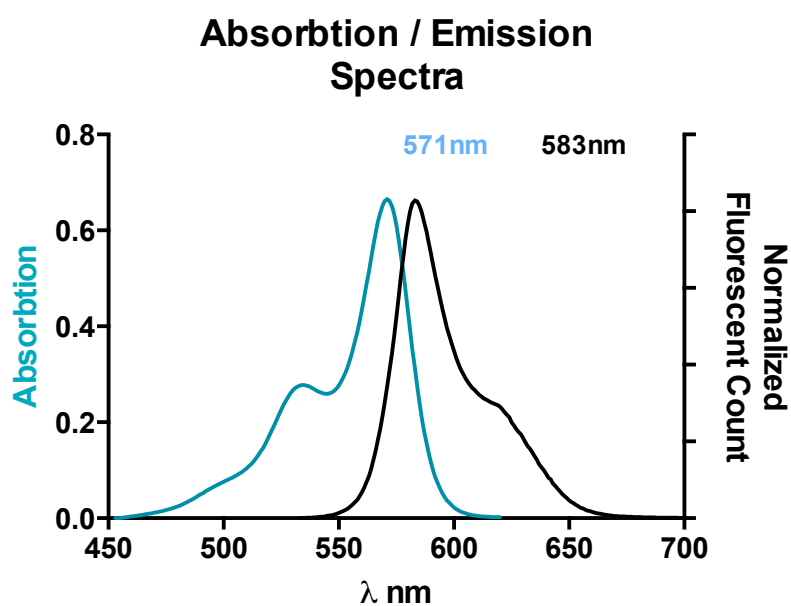


Figure 63. Thienyl-ene-BODIPY absorption and emission curve.

The molar extinction coefficient (ϵ) was determined, being $125\,000\text{ M}^{-1}\text{ cm}^{-1}$ at 571nm (abs. EtOH, diam. 1cm).

3.2.2 Quantum yield

The quantum yield was determined by using Williams method,²⁹⁹ comparing the fluorescence intensity to standard fluorescein (0.1M NaOH). Fluorescein is used as a standard to compounds with emission maximas from 500-600 nm.

Plotting UV/VIS absorbance (A) vs fluorescence intensity (FI) at a set concentration created a gradient for the standard and compound **3** (**3-BODIPY**). The determined gradient from the plotted line **3** ($Grad_3$) is divided by the gradient of the standard ($Grad_{\text{Fluorescein}}$), multiplied by the ratio of the refractive index ($\eta^2_3 / \eta^2_{\text{Fluorescein}}$) of the solvents (EtOH $\eta = 1.33$, 0.1M NaOH $\eta = 1.33$)^{300,301} used and multiplied by the relative quantum yield of fluorescein ($\Phi_{\text{Fluorescein}} = 0.79$).

$$\Phi_3 = \Phi_{\text{fluorescein}} \left(\frac{FI_{3-\text{BODIPY}}}{FI_{\text{fluorescein}}} \right) \left(\frac{A_{\text{fluorescein}}}{A_{3-\text{BODIPY}}} \right) \left(\frac{\eta^2_{3-\text{BODIPY}}}{\eta^2_{\text{fluorescein}}} \right)$$

$$\Phi_3 = \Phi_{\text{fluorescein}} \left(\frac{Grad_{3-\text{BODIPY}}}{Grad_{\text{fluorescein}}} \right) \left(\frac{\eta^2_{3-\text{BODIPY}}}{\eta^2_{\text{fluorescein}}} \right)$$

The relative quantum yield was determined to be 0.98.

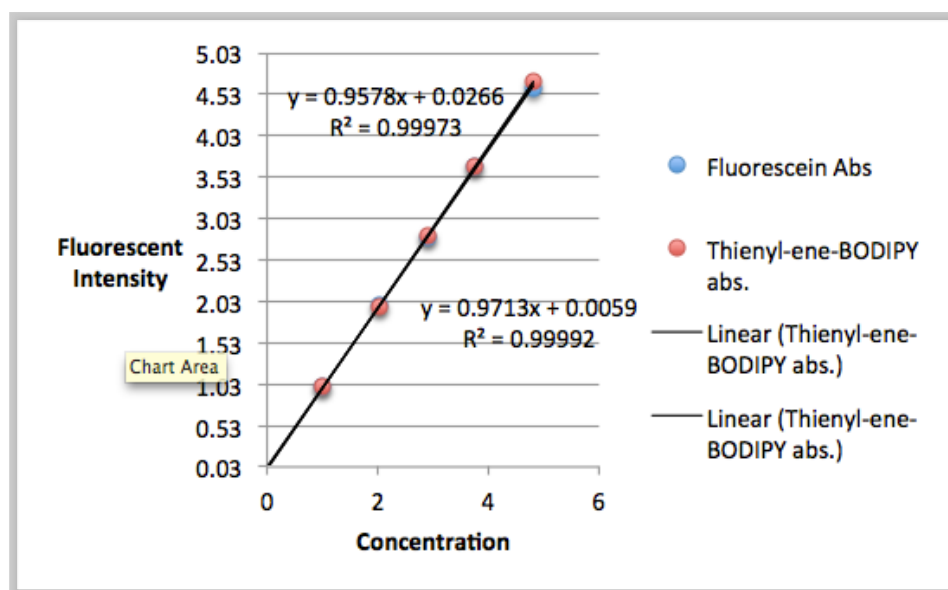


Figure 64. Fluorescein and thienyl-ene-BODIPY gradients for quantum yield determination.

Conc.: 90nM, 180nM, 270nM, 360nM, 450nM. $\eta = 1.33$ (for EtOH and 0.1M NaOH). ($\Phi_{\text{Fluorescein}}$) = 0.95.

3.3 Binding Studies

Binding affinities will be determined by direct binding towards α -TTP. The ligand will be tested as a competitive inhibitor against natural tocopherol and cholesterol. Cholesterol does not bind to α -TTP, and therefore shouldn't decrease the bound ligand. To access binding specificity towards the α -TTP protein the ligand will be tested with bovine serum albumin (BSA).

3.3.1 α -TTP expression & purification

Human α -TTP was expressed following a protocol we have described previously.²⁰⁷ Frozen cultures of BL21(DE3) *E. coli* cells containing a pGEX 4T-3/ α -TTP construct were induced with ampicillin at 37°C overnight. The preculture was then inoculated in 1 L of lysogeny broth (LB) (1 : 100 LB broth). After an optical density (OD₆₀₀) of 0.4-0.6 was achieved, the culture was treated with isopropyl- β -D-thiogalactopyranosid (IPTG) overnight, after which centrifugation yielded the TTP cells.

The cells were treated with lysozyme for 30 min at 0°C. The solution was then treated with MgCl₂, Triton-X-100, DNase, RNase and incubated for 30 min at 0°C. After sonication (3x for 15 s at 500 W) cell debris was removed by centrifugation (17500 rpm for 25 min at 4°C). The supernatant was purified by affinity chromatography over a pre-washed glutathione-Sepharose column. After flow through of supernatant, column was washed again and incubated with thrombin and stored at 4°C overnight. The protein was collected the next day.

The purified protein concentration was quantified by using the Bradford assay. A standard curve was prepared, plotting absorbance at 595 nm against bovine serum albumin (BSA) concentration from 0-1 mg/ml. The concentration of the purified protein stock solution used for the binding assays was 130 µM.

3.3.2 Binding study to α-TTP in SET-Buffer

We tested how well the new ligand, **3**, would bind to the apo-form of α-TTP by performing a fluorescence titration. The increase in fluorescence intensity was measured as increasing amounts of ligand were titrated into a buffered solution containing α-TTP. The dissociation constant (K_d) is measured by fitting the data points to a one site specific binding model using Prism. Equation **1** was used to calculate the K_d .

$$\mathbf{1} \quad Y = \frac{B_{max}X}{(K_d + X)}$$

To obtain the dissociation constant (K_d) of **3** the methods reported by West *et al.* were repeated.²⁰⁶ In the event, to 0.2 µM α-TTP in SET buffer (50 mM Tris-HCl, 100 mM KCl, 1 mM EDTA, 150 mM sucrose pH 7.4), was added 0-5 µM ligand (final concentration 3.5µM) in small aliquots of absolute EtOH. The total amount of EtOH did not exceed 0.1% of the final solution. The sample was stirred for 25-40 min at room temperature for equilibrium to be

established and fluorescence measured at 514 nm at an excitation wavelength of 506 nm and 5 nm slit widths (Figure 65).

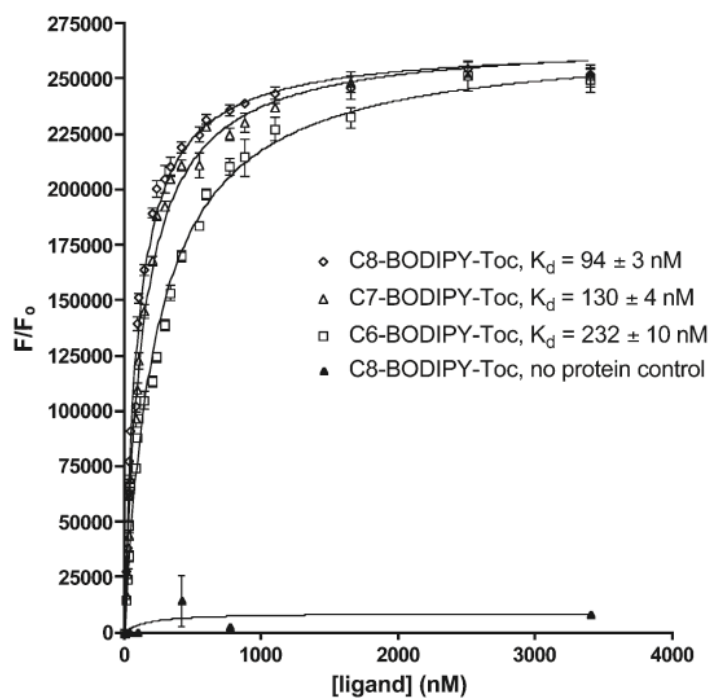


Figure 65. Direct binding of [ligand] BODIPY- α -Toc C6, C7 and C8 to 0.2 μ M α -TTP in SET buffer.

Final concentration reached was 3.5 μ M. Data was measured and triplicate and error bars represent standard deviations from the mean. Data from literature.²⁰⁶

The excitation wavelength was adjusted to $\lambda = 492$ nm, with an emission from 512 - 528 nm, to not reach the fluorometers maximum fluorescent count (FC) of 4×10^6 (Figure 66). Titration with C8-BODIPY-Toc was repeated with fresh α -TTP. The fluorescent counts were half as recorded prior. The obtained K_d of 90 nM is in the close range of the recorded literature value (94 ± 3 nM).²⁰⁶

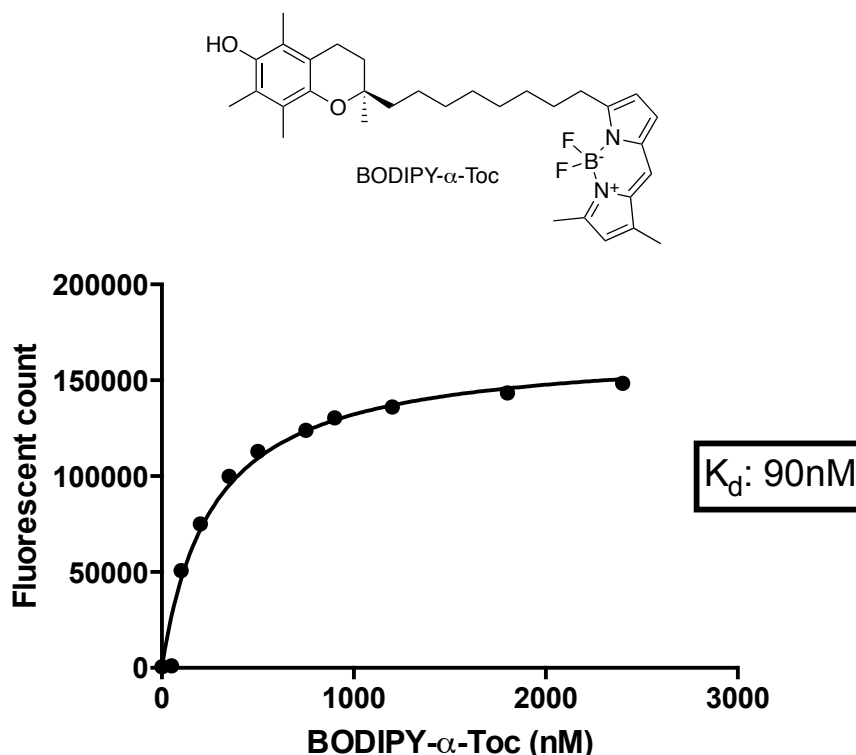


Figure 66. BODIPY- α -Toc in EtOH direct binding to $0.2 \mu\text{M}$ α -TTP in SET buffer repeated with freshly expressed protein.

Data was measured as a singular titration. A K_d of 90 nM was determined, which matches literature values 94 ± 3 nM.

Ligand **3** was also tested in triplicate under these same conditions. A blank sample, containing no protein, was also measured to see how the fluorescence intensity increased due to free ligand in buffer. The excitation wavelength was 564 nm, and the emission was measured from 584 - 588 nm at a slit width of 5 nm (Figure 67).

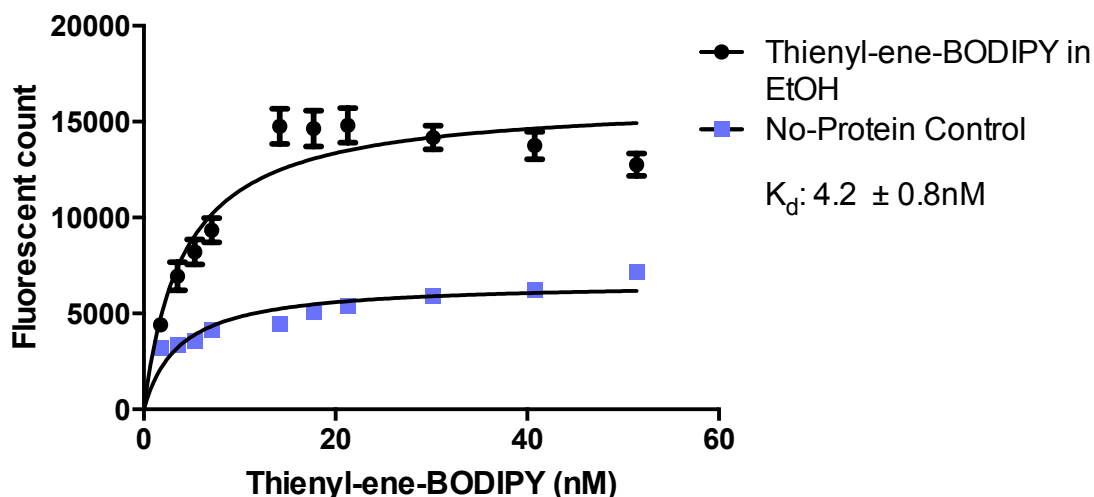


Figure 67. Direct binding of thienyl-ene-BODIPY (**3**) in EtOH to 0.5 μ M α -TTP in SET buffer using West's et al. conditions.

The data was collected in triplicate and error bars represent standard deviations from the mean.²⁰⁶

The K_d of 4.2 ± 0.8 nM obtained from these tests was surprisingly low compared to C8-BODIPY- α -Toc. However, the fluorescent counts (FC) were also ten times lower.

This phenomenon most likely is due to the interaction of **3** with the binding site of α -TTP being different than for C8-BODIPY- α -Toc. It would appear the fluorophore of **3** is more solvent exposed and thus has its fluorescence intensity suppressed.

The difference between the no-protein control and the ligand **3** is rather small, about 10000 fluorescence counts at 15 μ M of ligand. The increasing amounts of EtOH added to the SET buffer increases the solvent hydrophobicity, likely explaining the increase in fluorescence intensity in the blank.

Ligand **3** was also tested in a competition assay with α -tocopherol and cholesterol, following previous protocols. To assure full ligand saturation, α -TTP was preincubated with 5x more **3** prior to addition of tocopherol or cholesterol. In case of C8-BODIPY- α -Toc, 0.2 μ M protein was mixed with 1.0 μ M ligand, however, for the thienyl-ene-BODIPY **3** only 1.25-times excess ligand was used for 0.25 μ M protein since the K_d was so much lower (Figure 68).

Addition of the natural α -tocopherol to a sample of α -TTP saturated with **3** will lower the starting fluorescence should the added ligand compete with the **3** for access to the binding site. α -Tocopherol nearly completely reduced the original fluorescence intensity from bound C8-BODIPY- α -Toc, but cholesterol had almost no effect.

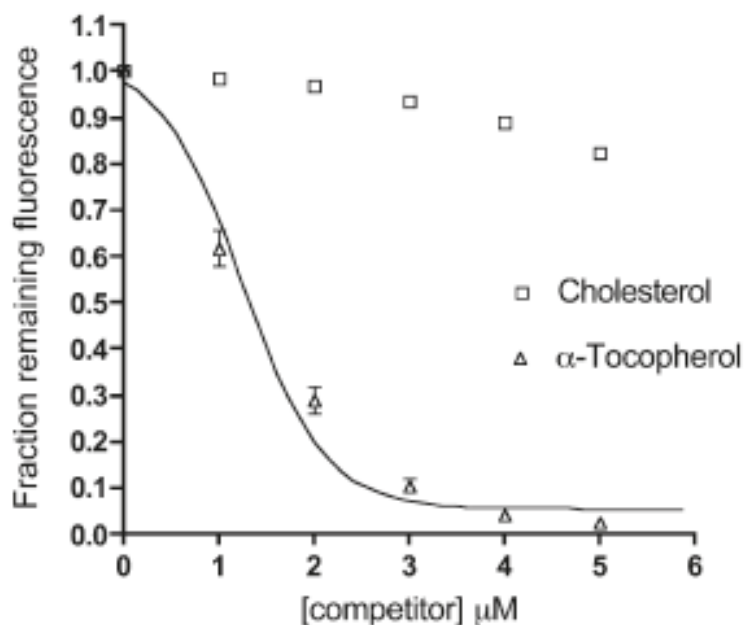


Figure 68. Competition assay of 0.2 μM α -TTP, saturated with 1.0 μM BODIPY- α -Toc in SET buffer, with [competitor] α -Toc & cholesterol in EtOH.

In the graph were the collected data points normalized to 1.0. Data was measured and triplicate and error bars represent standard deviations from the mean. Data from literature.²⁰⁶

The fluorescence intensity of α -TTP bound **3** decreased, but not as much as with C8-BODIPY- α -Toc. The addition of tocopherol was ~30% successful in competing the ligand off the protein (Figure 69). A control titration was used to obtain a value of fully out-competed ligand **3**. To a solution of thienyl-ene-BODIPY without α -TTP was tocopherol added. No change in absorption was observed. After 0.6 μM α -tocopherol was added to the solution with α -TTP was a plateau reached.

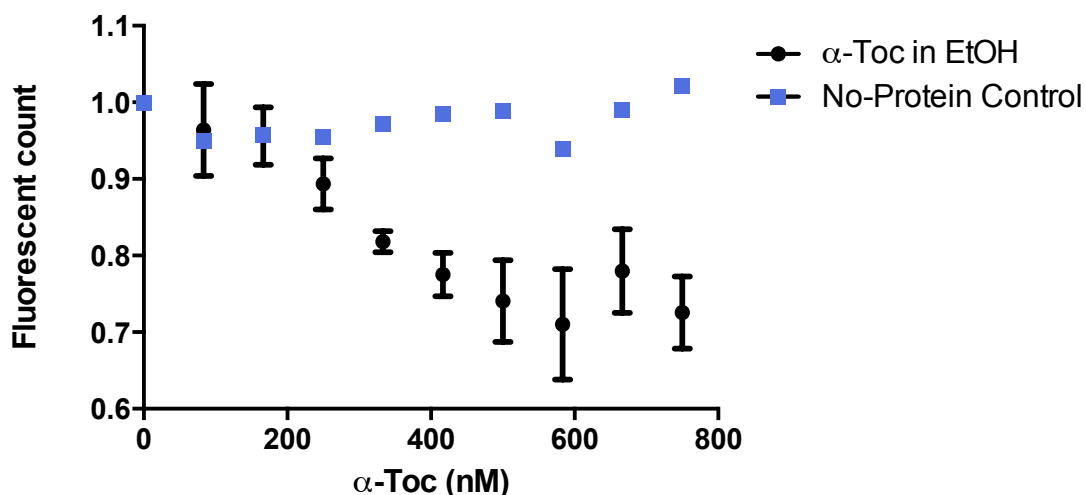


Figure 69. Competition assay of 0.2 μ M α -TTP, saturated with 0.25 μ M thienyl-ene-BODIPY (3) in SET buffer, with α -tocopherol (α -toc) in EtOH.

In the graph were the collected data points normalized to 1.0. Data was measured and triplicate and error bars represent standard deviations from the mean.

To get higher fluorescence intensities with a larger differentiation to the no-protein control, the competitive assay was run in the presence of detergent, as had been used in the assessment of NBD-Toc binding (Figure 70).²⁰¹ Detergents are used to make it more thermodynamically favourable for poorly soluble hydrophobic ligands to leave the active site during a competition experiment.

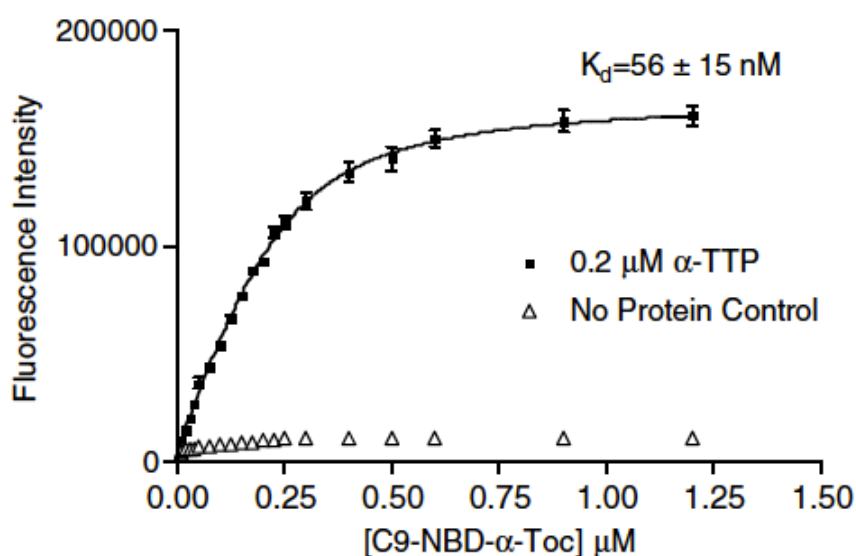


Figure 70. Direct binding of C9-NBD- α -Toc in EtOH to 0.2 μ M α -TTP in SET buffer. $\lambda_{\text{ex}} = 495\text{nm}$ $\lambda_{\text{em}} = 535\text{nm}$.

Data was measured and triplicate and error bars represent standard deviations from the mean. Data from literature.²⁰¹

Competition assay with NBD-Toc (Figure 71): 0.2 μM α -TTP in 3 ml SET buffer and 100 μM Triton-X-100 (TX100), adding 1 μM NBD-Toc (5x excess). After each ligand addition the cuvette was equilibrated for 15 min.²⁰¹ The same time was applied for the thienyl-ene-BODIPY **3** ligand.

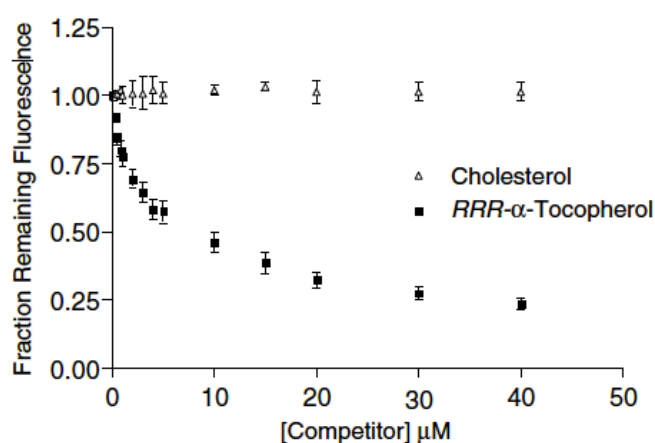


Figure 71. Competition assay of 0.2 μM α -TTP, saturated with 1.0 μM NBD-Toc in SET buffer and 100 μM TX100, with [competitor] α -Toc & cholesterol in EtOH.

In the graph were the collected data points normalized to 1.0. Data was measured and triplicate and error bars represent standard deviations from the mean. Data from literature.²⁰¹

0.5 μM α -TTP, 1.0 μM thienyl-ene-BODIPY, **3**, with 100 μM TX100 were titrated with α -tocopherol (Figure 72). Adding a detergent makes the media more hydrophobic, which makes the ligand less likely to bind to α -TTP. Therefore, in the competition experiment with TX100 was twice the amount of thienyl-ene-BODIPY to α -TTP used to have more ligand-bound protein. Increasing hydrophobicity raised the background fluorescent to 67000 FC in the no-protein control. The gap between no protein control and ligand was increased from 1500 FC to 20000 FC, which would suffice to measure the competition qualitatively. Unfortunately, the background fluorescence was too high to accurately detect any changes in the competition experiment.

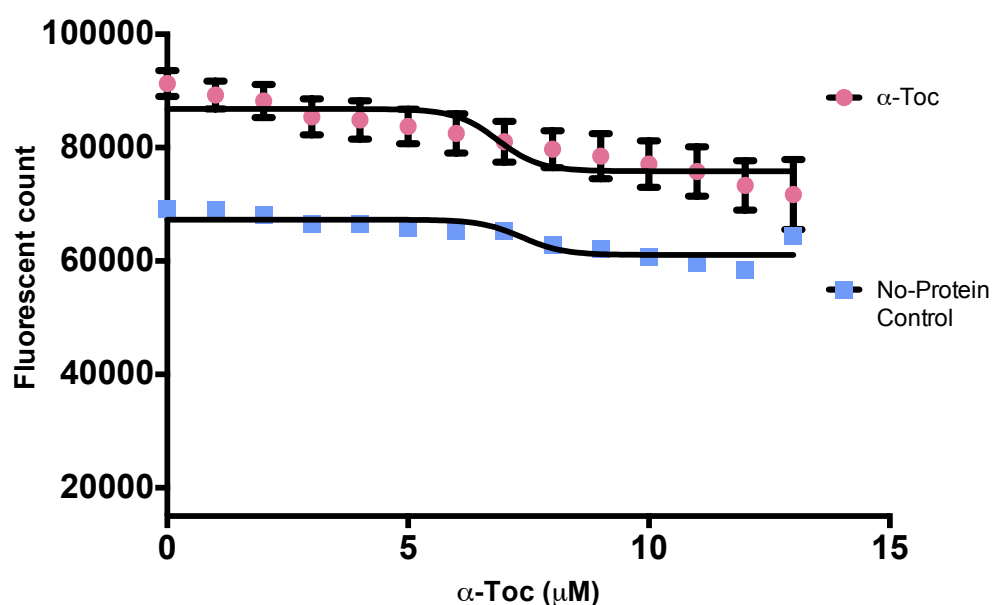


Figure 72. Competition assay of 0.5 μM $\alpha\text{-TTP}$, saturated with 1.0 μM thienyl-ene-BODIPY (3) in SET buffer, with $\alpha\text{-Toc}$ & 100 μM TritonX100.

Data was measured and triplicate and error bars represent standard deviations from the mean.

A direct binding assay with 100 μM detergent gave no difference to the no-protein control (Figure 73).

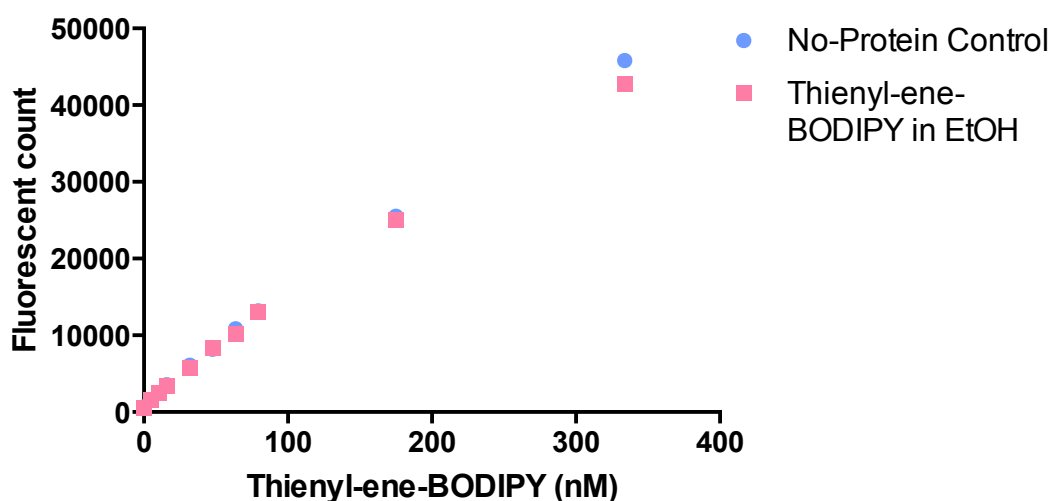


Figure 73. Direct binding of thienyl-ene-BODIPY (3) in EtOH to 0.2 μM $\alpha\text{-TTP}$ in SET buffer with 100 μM TX100.

The same test was repeated with 10 μM detergent, which showed an increase of about 1000 fluorescence counts to the direct binding curve having no detergent present (Figure 74).

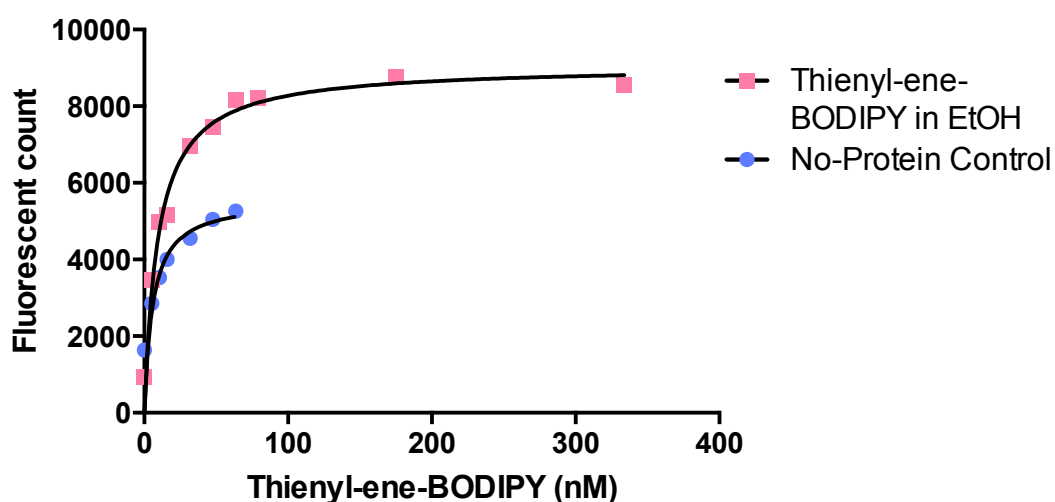


Figure 74. Direct binding of thienyl-ene-BODIPY (3) in EtOH to 0.2 μM α -TTP in SET buffer with 10 μM TX100.

To find the optimal amount of detergent a competition assay with saturated protein (0.5 μM α -TTP, 1.0 μM thienyl-ene-BODIPY) and a no-protein control were treated with increasing increments of TX100 (10 μM) (Figure 75).

The difference between the control and protein sample at 100 μM TX100 was again of 20000 FC. At 10 μM a value of 15000 FC was observed. Compared to the first binding assay (Figure 67) without TX100 and using the same amount of protein (0.5 μM), is an increase of 5000 FC was observed. The direct binding with TX100 (Figure 74) used less protein (0.2 μM) and has therefore a smaller difference of 3000 FC.

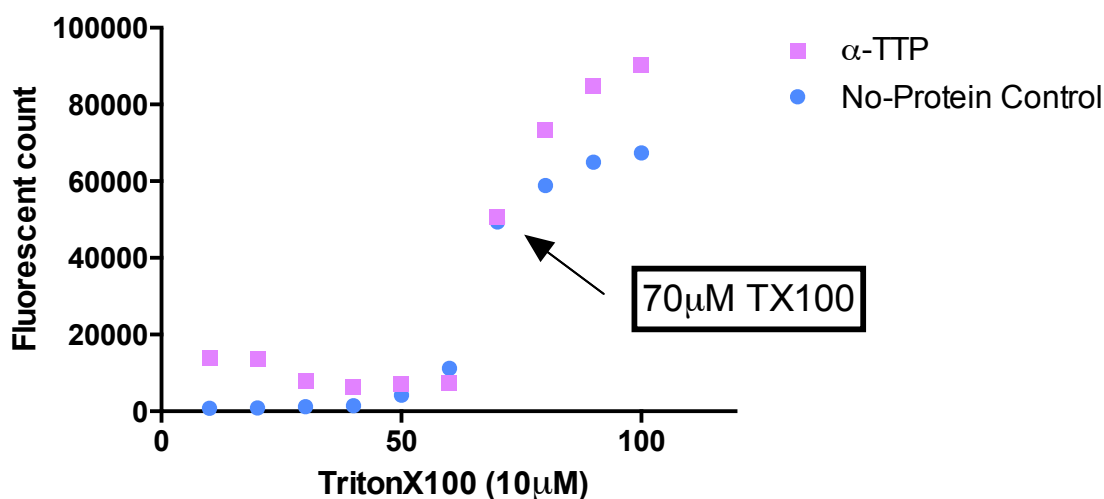


Figure 75. Titration of 0.5 μM α -TTP, saturated with 1.0 μM thienyl-ene-BODIPY (**3**) in SET buffer, test with increasing TX100 amounts by 10 μM .

The difference in fluorescence between a no-protein control and α -TTP with 100 μM TX100 diverges somewhere between 70 and 100 μM . Since a larger observable window with low fluorescence background (30% <) is needed to make a qualitative judgement, we concluded that TX100 not beneficial for the study of thienyl-ene-BODIPY **3**.

As a further control, titration of **3** to BSA solutions verified ligand specificity to α -TTP. BSA is known to be a lipid carrier and does bind tocopherol non-specifically with low affinity.³⁰² The shape of the titration curve would suggest that BSA does bind **3**, however the no-protein control shows higher fluorescence than the BSA curve, so the signal for a BSA titration may not reflect real protein-ligand association (Figure 76).

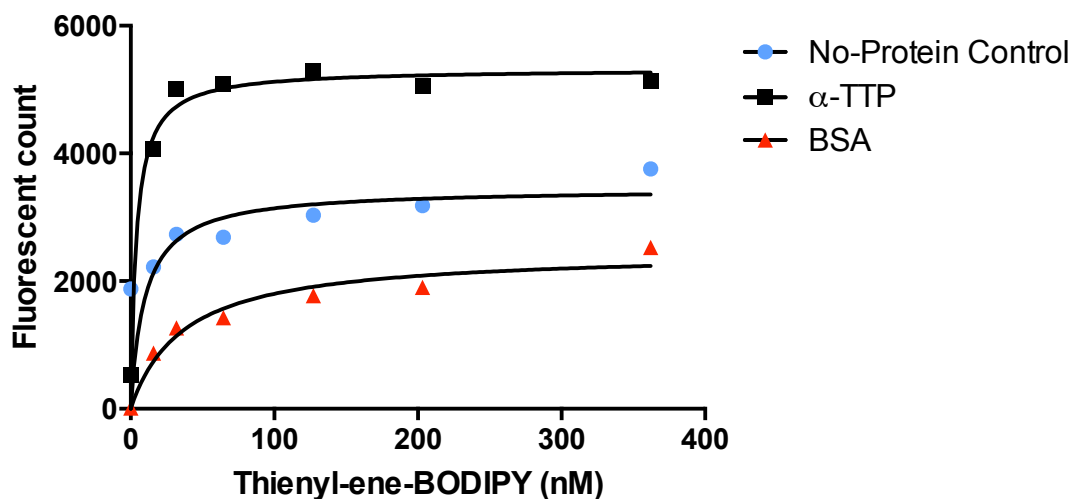


Figure 76. Direct binding of thienyl-ene-BODIPY (**3**) in EtOH to 0.5 μ M α -TTP & BSA.

To further explore the effect of additives in binding assays we tested a new buffer TKE (50 mM Tris-HCl, 100 mM KCl, 1 mM EDTA) and used DMSO as supportive organic solvent.

Fluorimeter slits were set to 6 nm to better observe changes at low fluorescence counts. DMSO is, like EtOH, a standard solvent used in biological assays. This was tested by first adding to 0.2 μ M α -TTP 0.5 μ M solutions of **3** prepared with different percentages of DMSO (0%, 5%, 10% & 15%). After 1 min, 10 min and 15 min of equilibration time fluorescence intensity was measured (Figure 77).

The highest increase in fluorescence intensity was observed at 10 min in the cuvette without any DMSO. **2**. After 15 min another 0.5 μ M of **3** was added to the non-DMSO cuvette to see if there would be any further increase in fluorescent intensity. No increase was observed. The FC plateaued at 30000.

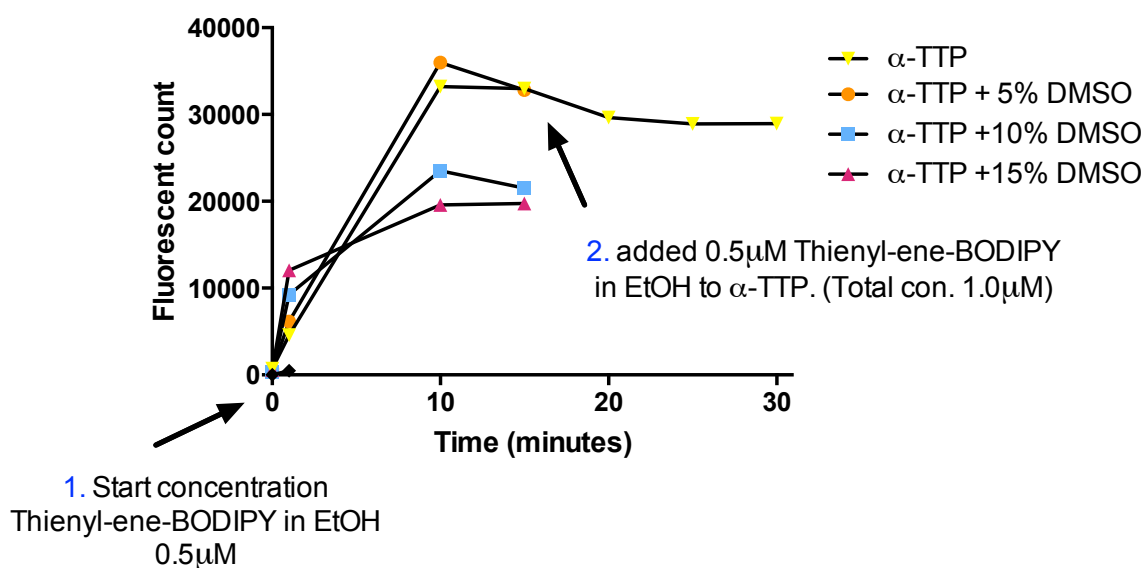


Figure 77. Thienyl-ene-BODIPY (3) solubility test with DMSO in TKE buffer.

To four different 0.2 μM α -TTP solutions in TKE buffer, three of them containing either 5% (orange), 10% (blue) and 15% (pink) DMSO in the overall 3ml volume, was 0.5 μM thienyl-ene-BODIPY 3 in EtOH added. (1.) The fluorescence of all four solutions was measured after 1 min, 10 min and 15 min. To the solution without DMSO (yellow) was after the 15min (2.) scan an additional 0.5 μM thienyl-ene-BODIPY 3 in EtOH added.

3.3.3 Binding study to α -TTP in TKE-Buffer

Thienyl-ene-BODIPY 3 was tested in a direct binding assay against 0.2 μM and 0.5 μM α -TTP in TKE buffer (Figure 78 and 79). The binding curves in both concentrations had a higher fluorescence intensity and a greater difference from the non-protein control than the assay performed in SET buffer.

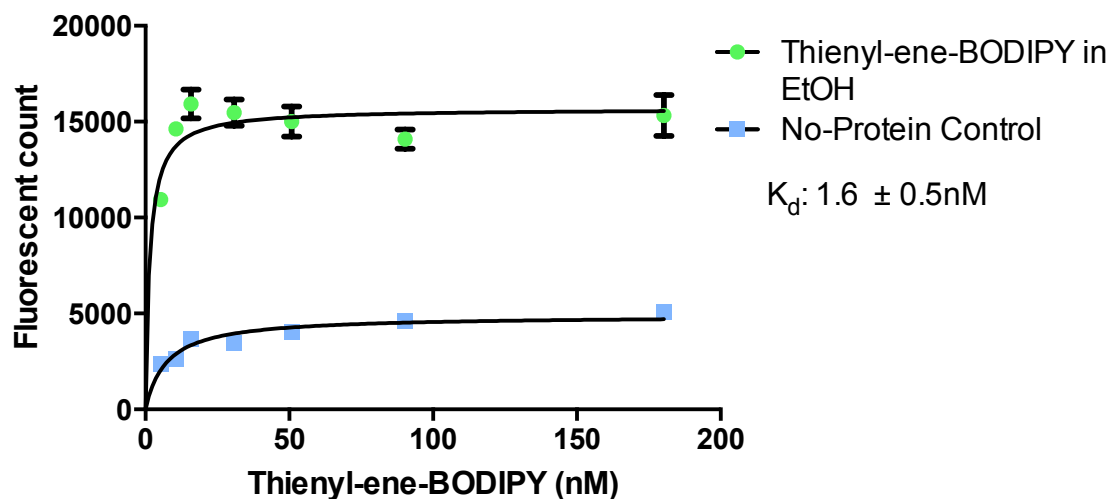


Figure 78. Direct binding of thienyl-ene-BODIPY (3) in EtOH to 0.2 μM α-TTP in TKE buffer.

The data was collected in triplicate and error bars represent standard deviations from the mean.

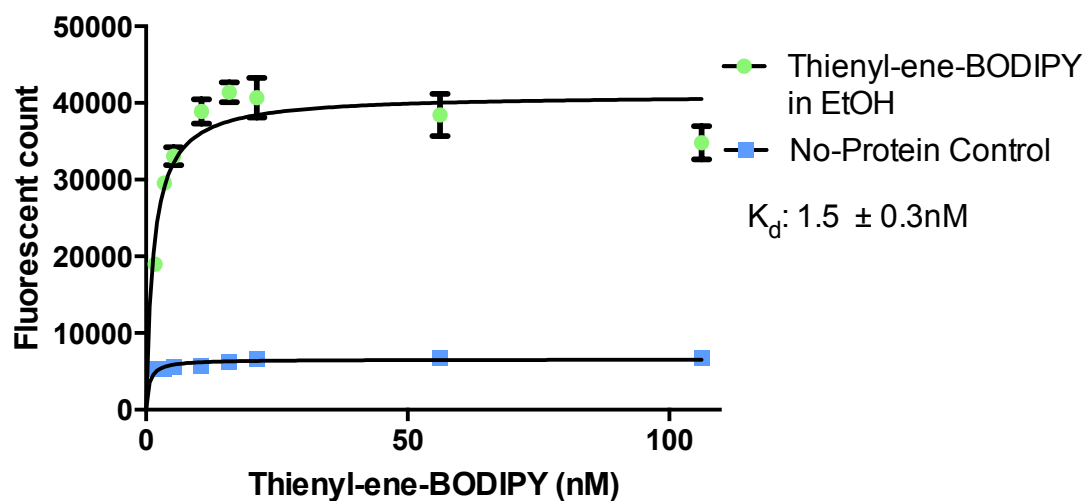


Figure 79. Direct binding of thienyl-ene-BODIPY (3) in EtOH to 0.5 μM α-TTP in TKE buffer.

The data was collected in triplicate and error bars represent standard deviations from the mean.

Direct binding to BSA in TKE was giving the expected result. nPC is lower than the BSA in the TKE buffer (Figure 80).

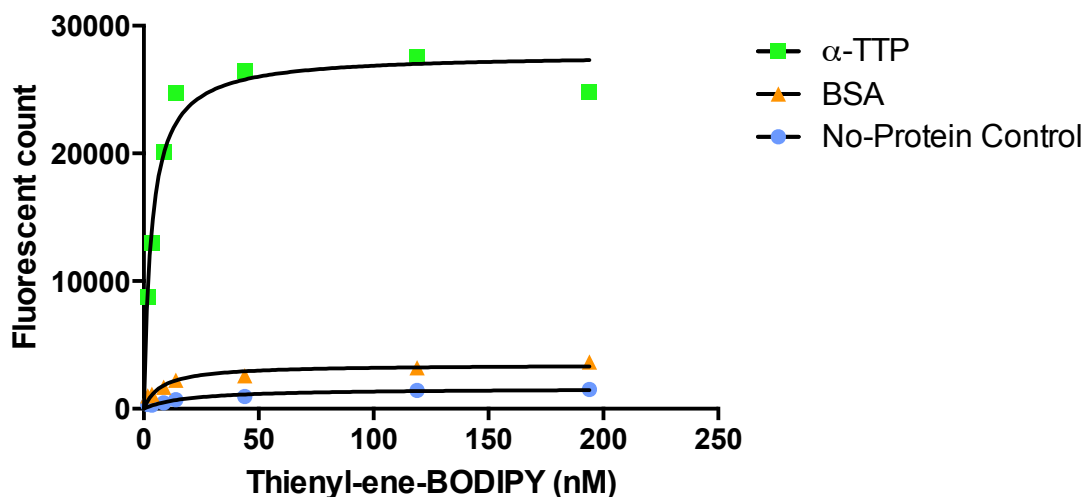


Figure 80. Direct binding of thienyl-ene-BODIPY (**3**) in EtOH to 0.5 μ M α -TTP & BSA in TKE buffer.

In all the direct binding assays with ligand **3** a slight decrease in fluorescence was observed after saturation (around 120 nM). Therefore, we tested if this trend would continue when increasing amounts of **3** were added (Figure 81). After a \sim 120 nM there was a steady decrease in fluorescence signal that plateaued at approximately 10 μ M. Such concentrations are not realistic in terms of measuring the binding affinity and are unlikely to ever be used in cells. However, it indicates that self-quenching occurs (inner filter effect) or aggregation of the fluorophore occurs as the concentration is increased.³⁰³

Future competition assays will take this effect into account by not oversaturating the protein with the ligand. A maximum ratio of 2:1 ligand to protein seems to be still acceptable.

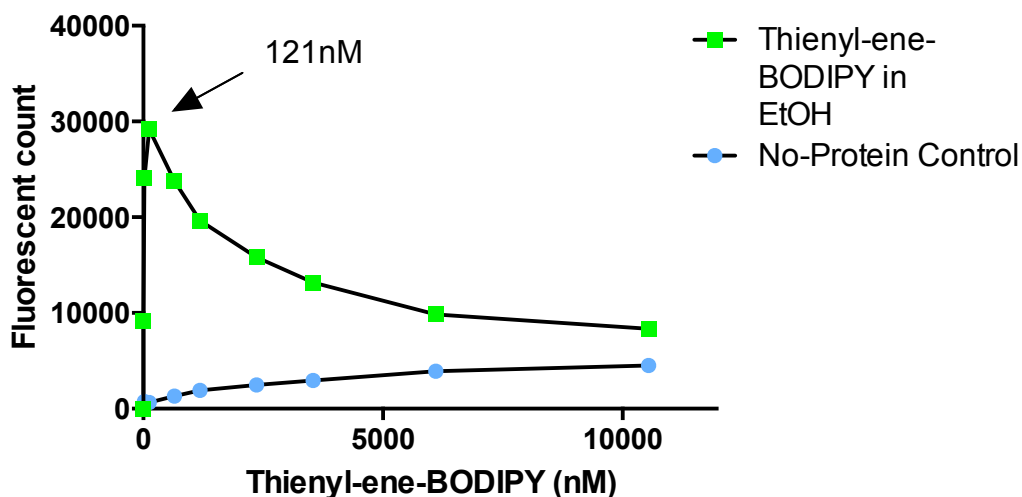


Figure 81. Test of ligand over addition. Direct binding of thienyl-ene-BODIPY (3) in EtOH to 0.4 μ M α -TTP in TKE buffer.

Now that the best conditions have been determined to perform binding assays, a competition assay with α -tocopherol was conducted (Figure 82). Less thienyl-ene-BODIPY was added in this assay since from prior binding assays it was clear that protein saturation under these conditions occurs at \sim 20 nM of 3.

Fluorescence intensity dropped by 50% (16000 fluorescence counts) at a concentration 180 nM of α -tocopherol. The non-protein control increased 50% (4000 FC) at the same concentration. When taking the increased fluorescence intensity in non-protein controls into account, the fluorescence decrease by α -tocopherol addition clearly shows that competition has occurred. After 200 nM the increase in EtOH content increases the fluorescence of both curves in a similar fashion, negating the observation of more complete competition at higher tocopherol concentrations.

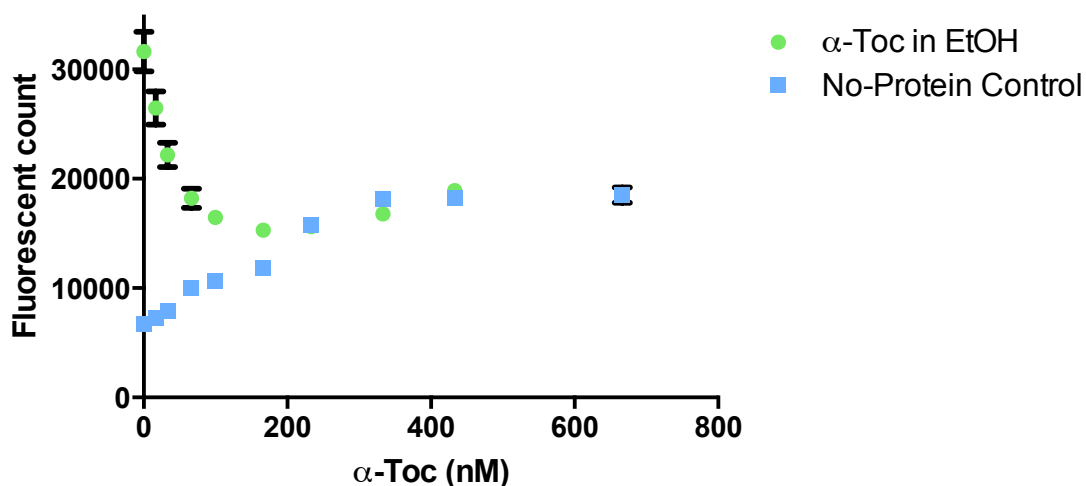


Figure 82. Competition assay of 0.1 μM α -TTP, saturated with 0.2 μM thienyl-ene-BODIPY (3) in TKE buffer, with α -Toc in EtOH.

The data was collected in triplicate and error bars represent standard deviations from the mean.

For the competition assay with cholesterol α -TTP was preincubated with a 5-fold excess of ligand 3. Surprisingly, cholesterol successfully reduced the observed fluorescence by almost 65%. On the other hand the no protein control (but still containing 0.4 μM of 3) had extremely low fluorescent counts that did not increase over the course of cholesterol addition (Figure 83).

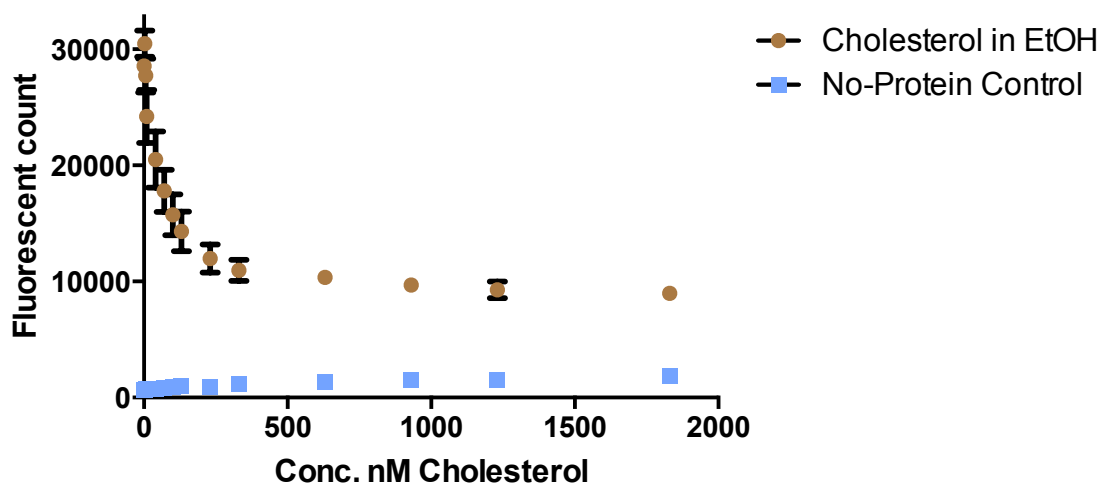


Figure 83. Competition assay of 0.1 μM α -TTP, saturated with 0.5 μM thienyl-ene-BODIPY (3) in EtOH in TKE buffer, with cholesterol.

The data was collected in triplicate and error bars represent standard deviations from the mean.

The experiment was repeated with a 1:1 eq and 2:1 mole ratio of **3** to α -TTP (Figure 84). Both concentrations were titrated with cholesterol, but one additional cuvette with 0.4 μ M **3** was titrated with only EtOH.

The 2:1 eq cuvette (black) was a higher FC, but had the same decrease in fluorescent intensity by 30% at 250 nM (2:1 = 8000 FC 1:1 = 6000 FC). More importantly is the observation that EtOH (square pink points) addition creates the same curve as 1:1 eq cholesterol addition, undoubtedly prove that the solvent is causing the decrease in fluorescents.

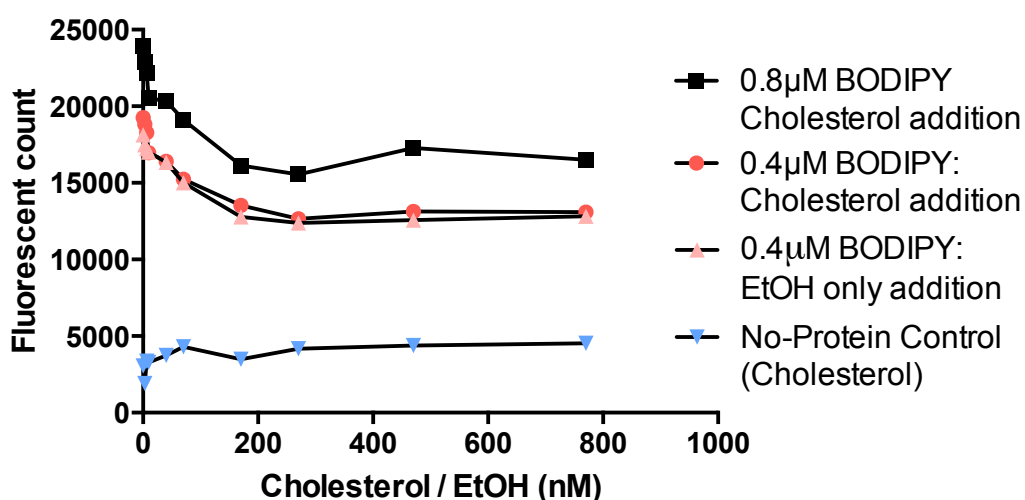


Figure 84. Thienyl-ene-BODIPY (**3**) test competition assay of 0.4 μ M α -TTP, saturated with 0.8 μ M (black), 0.4 μ M (red and pink) thienyl-ene-BODIPY (**3**) in TKE buffer, with cholesterol (as EtOH solutions, red & black) and EtOH only (pink).

To see if the effect of EtOH as the supporting solvent could be avoided we tried DMF as an alternative solvent. The fluorescence titration curve with DMF as the supporting organic solvent (Figure 85) was similar to the experiment with EtOH in TKE buffer (Figure 78 & 79).

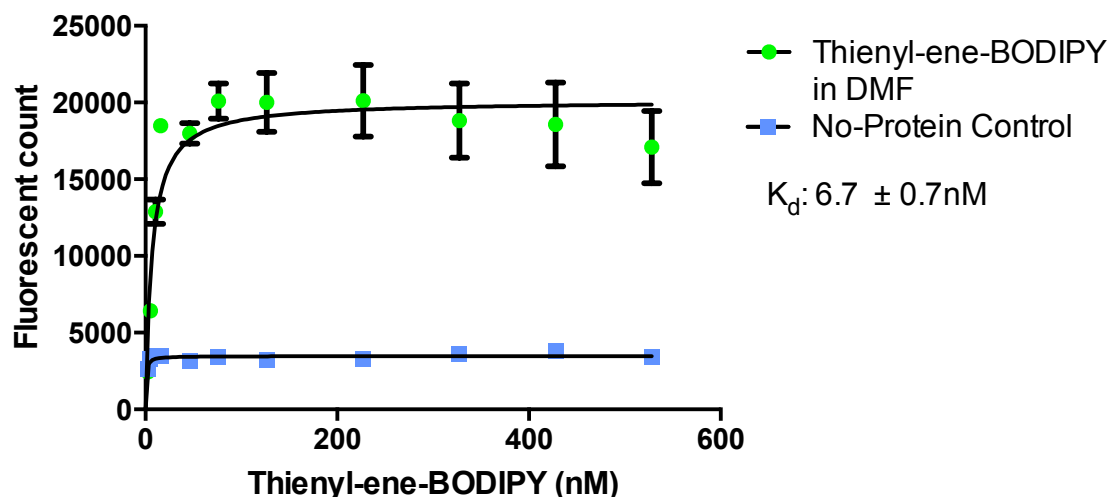


Figure 85. Direct binding of thienyl-ene-BODIPY (3) in DMF to 0.4 μ M α -TTP in TKE buffer.

The data was collected in triplicate and error bars represent standard deviations from the mean.

When competition assays were performed using DMF solutions of α -toc to displace **3** from α -TTP, we observed competition regardless of whether the DMF stock solution contained tocopherol or not (Figure 86). As in the case of cholesterol in EtOH (Figure 86) the solvent was displacing **3** from the protein. In fact, DMF alone was a better competitor than α -tocopherol up to about 200 nM DMF. The solvent may interfere with the protein binding by interfering with interactions of the ligand in the binding site or by partially denaturing the protein causing ligand release.

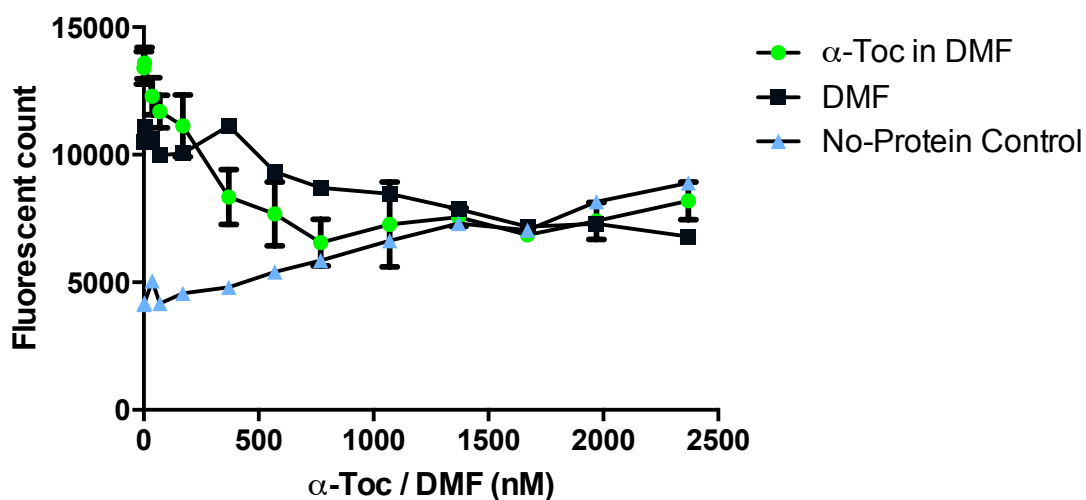


Figure 86. Competition assay of 0.4 μ M α -TTP, saturated with 0.4 μ M thienyl-ene-BODIPY (3) in TKE buffer, with α -Toc solution in DMF and DMF alone.

The data was collected in duplicate (for α -toc in DMF) and error bars represent standard deviations from the mean.

Competitive displacement assays with solutions of cholesterol dissolved in DMF followed the same trend as α -toc (Figure 87).

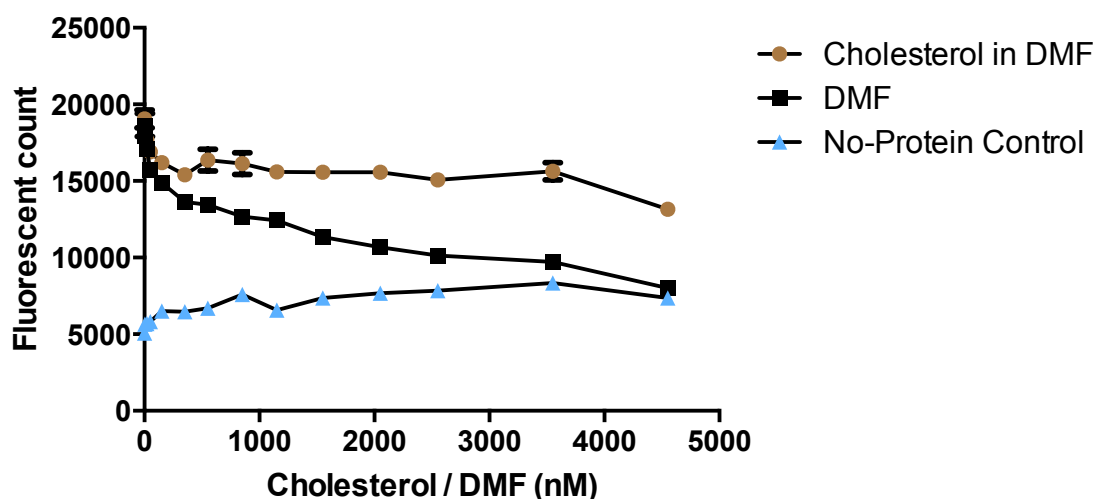


Figure 87. Competition assay of $0.4 \mu\text{M}$ α -TTP, saturated with $0.4 \mu\text{M}$ thienyl-ene-BODIPY (3) in TKE buffer, with cholesterol (in DMF) and DMF.

The data was collected in duplicate (for cholesterol in DMF) and error bars represent standard deviations from the mean.

Comparing EtOH to DMF in a competition assay with tocopherol showed that EtOH initially outcompetes most of the ligand, DMF itself and α -toc in DMF have similar decays up to 200 nM. After 200 nM decreases the fluorescence of α -toc in DMF the most, DMF by itself has the least decrease overall (Figure 88).

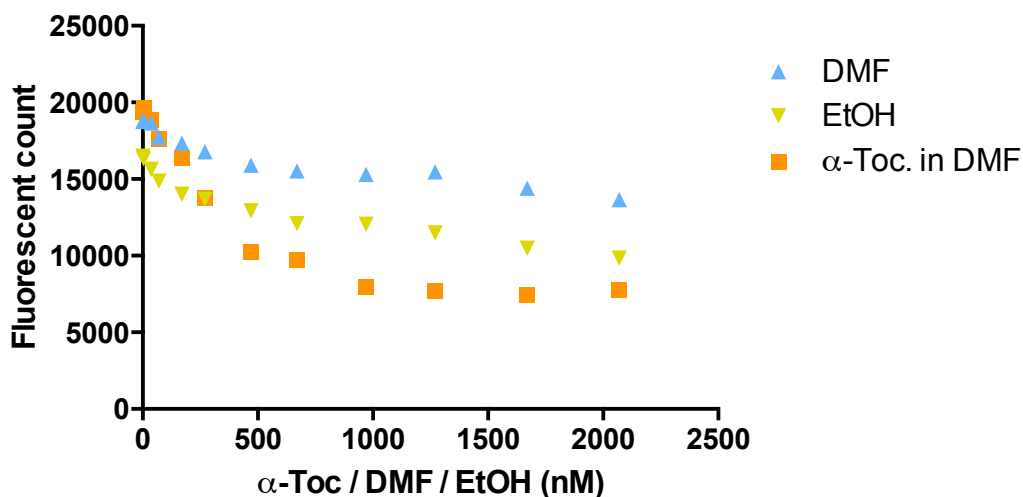


Figure 88. Competition assay of 0.4 μM α -TTP, saturated with 0.4 μM thienyl-ene-BODIPY (**3**) in TKE buffer, with α Toc (DMF), EtOH and DMF.

Thus, we showed that neither DMF nor EtOH are appropriate organic co-solvents for ligand binding and competition assays of **3** with α -TTP. The solvent seems to strongly interact with the protein interfering with ligand binding.³⁰⁴ Concerned that maybe **3** did not actually exhibit specific binding to α -TTP but maybe only bound non-specifically on the protein surface we modified the phenol of the chroman ring with a methyl group, as non-phenolic ligands (such as α -tocopheryl acetate) have much lower affinity to α -TTP (Figure 89).

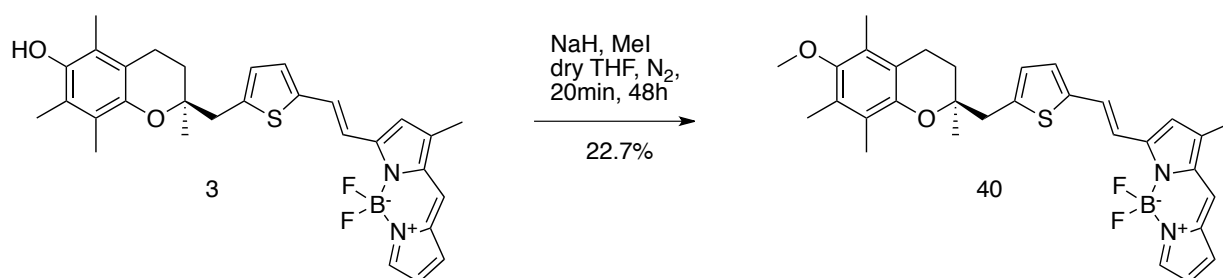


Figure 89. Synthesis of MeO-thienyl-ene-BODIPY (**40**).

The addition of methoxy (MeO) thienyl-ene-BODIPY **40** to solutions of α -TTP showed very small increases of fluorescence intensity, even lower than the non-protein controls. At high added ligand concentrations, **40** increased the fluorescence and plateaued around 500 nM perhaps as a result of ligand self-quenching (Figure 90).

Since the free phenol **3** showed a markedly higher fluorescence intensity than the ether **40**, it is very likely that compound **3** binds specifically in the α -TTP binding site.

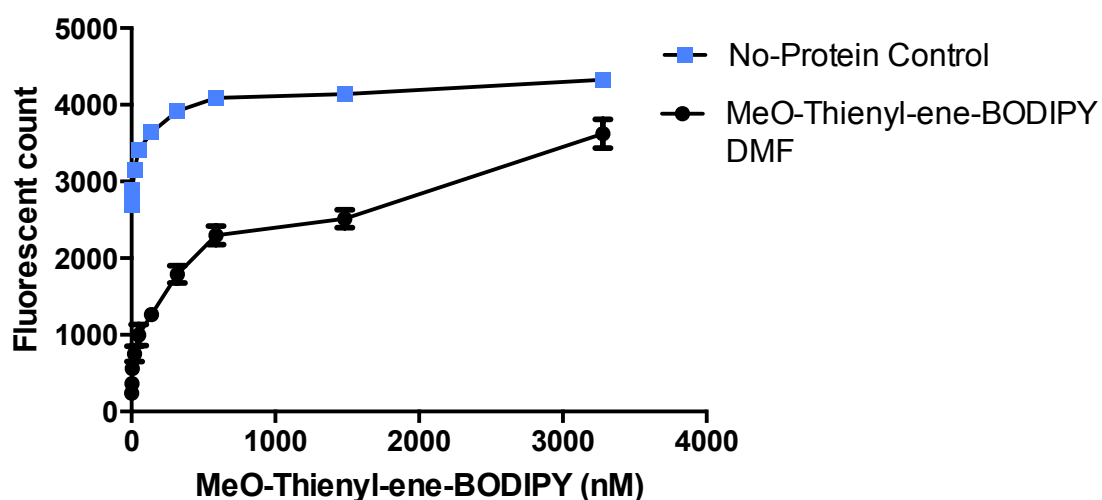


Figure 90. Direct binding of MeO-Thienyl-ene-BODIPY (**40**) in DMF to 0.4 μ M α -TTP in TKE buffer.

The data was collected in triplicate and error bars represent standard deviations from the mean.

Finally, dioxane was chosen as a solvent to solve the competition assay problem. Dioxane has a lower dielectric constant ($\epsilon = 2.25$) than DMF ($\epsilon = 36.7$) and EtOH ($\epsilon = 24.5$), which should lower the solvent interactions with the polar residues on the protein.³⁰⁵⁻³⁰⁶ Fluorescence quenching in buffer has been found to be lower in dioxane compared to DMF and other solvents.³⁰⁷ The fluorescence titration binding curve using dioxane as the supporting organic co-solvent shows the same intensity of fluorescent as in DMF (see Figure 91, Figure 85 describes the binding with DMF).

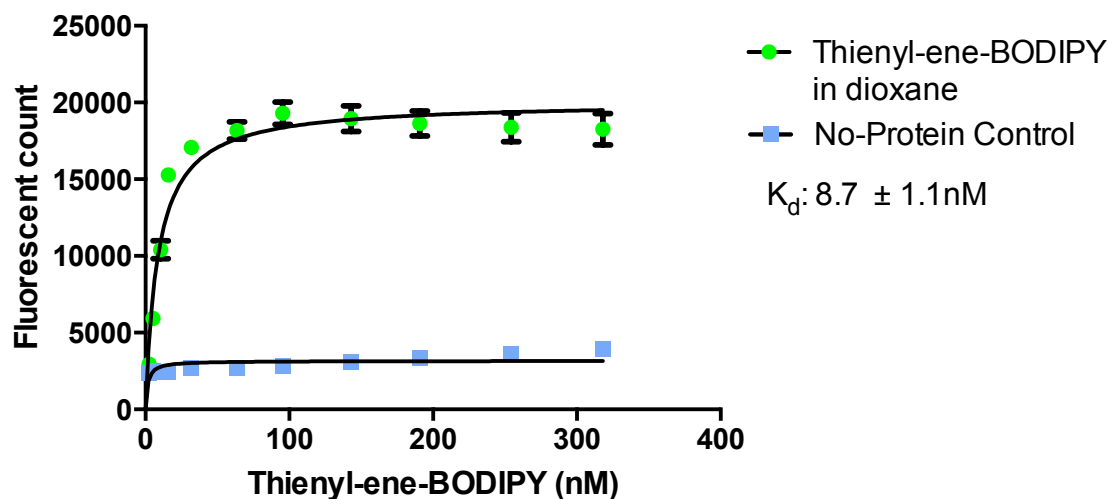


Figure 91. Direct binding of thienyl-ene-BODIPY (3) in dioxane 0.4 μ M to α -TTP in TKE buffer.

The data was collected in triplicate and error bars represent standard deviations from the mean.

Importantly, the use of dioxane allows a distinct difference to be seen between α -tocopherol and dioxane solvent, about 4000-5000 fluorescence counts. A plateau was reached at around 3-4 μ M. Around 57% of the fluorescence of **3** was reduced by competition at 2 μ M concentration of tocopherol (Figure 92).

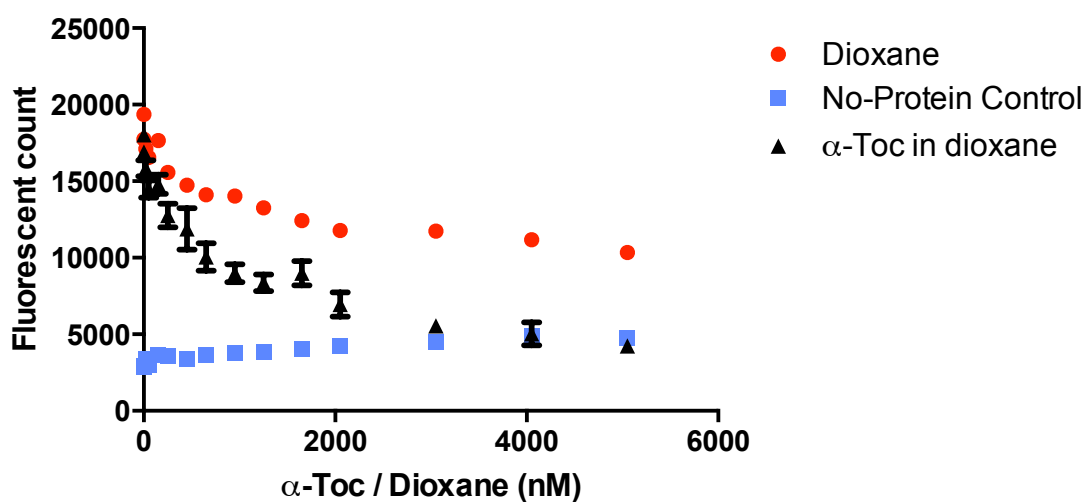


Figure 92. Competition assay of 0.4 μ M α -TTP, saturated with 0.4 μ M thienyl-ene-BODIPY (3) in TKE buffer, with α -Toc (in dioxane) and dioxane.

The data was collected in duplicate (for α -Toc in dioxane) and error bars represent standard deviations from the mean.

No fluorescence change was observed when cholesterol, dissolved in dioxane, was used as a competing ligand (Figure 93). Dioxane alone competed for ligand **3** and reduced the fluorescence by only 8% at 2 nM.

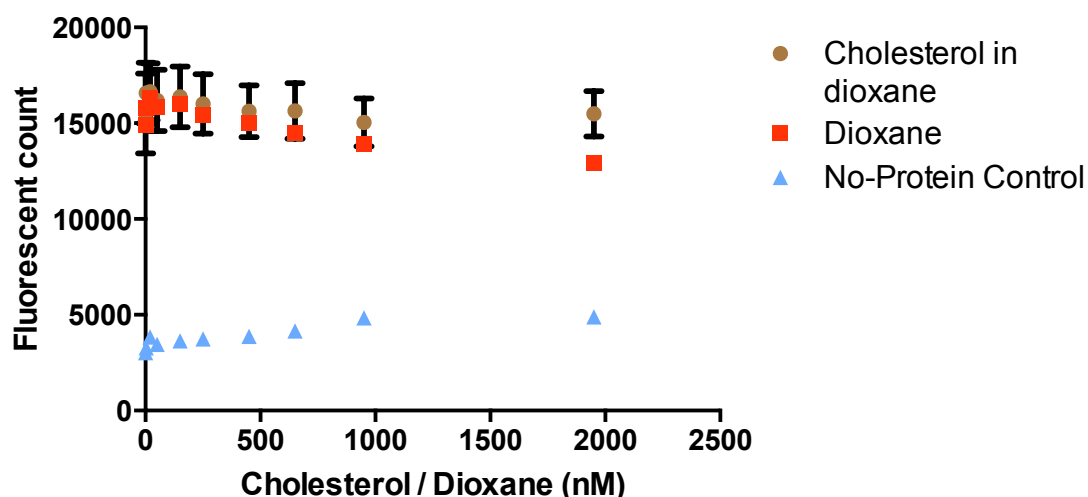


Figure 93. Competition assay of 0.4 μ M α -TTP, saturated with 0.4 μ M thienyl-ene-BODIPY (**3**) in TKE buffer, with cholesterol (in dioxane) and dioxane.

The data was collected in duplicate (for cholesterol in dioxane) and error bars represent standard deviations from the mean.

The titration of α -TTP bound **3** with dioxane solutions of α -tocopherol in TKE buffer showed that thienyl-ene-ligand **3** exhibits specific and reversible binding to α -TTP. Cholesterol, which does not bind to α -TTP, did not displace **3** from α -TTP, emphasizing the specific nature of binding.

Certain points have to be addressed at the end of the binding study. Testing fluorescent ligand affinities to proteins by measuring fluorescence intensity is a valid method, but needs to be well-screened for solvent effects and the affects of additives.

On advise by the comittee was the solubility of ligand **3** tested. The ligands solubility was tested in water and aqueous solutions with EtOH and dioxane (1%, 5% and 10%), but no result was obtained.³⁰⁸

In comparison with C8-BODIPY- α -Toc, **3** has a 5x lower fluorescence intensity at 100 nM ligand concentration in buffer, but has a higher extinction coefficient and similar quantum yield.²⁰⁶ However, binding to α -TTP was confirmed to be of higher affinity for **3**.

In conclusion, **3** binds to α -TTP in high affinity in both buffer systems (SET and TKE) and all solvents tested (EtOH, DMF and dioxane). The calculated dissociation constant of $K_d = 8.7 \pm 1.1$ nM (dioxane, TKE) is lower than that of natural tocopherol $K_d = 25$ nM determined in a radiolabelled binding assay.⁹⁹ Thus, compound **3** binds to α -TTP as well as or better natural α -tocopherol. The specificity of the ligand to α -TTP was verified by competition assay using cholesterol, which failed to compete, and by comparing the binding to BSA. The ligand binding is reversible since α -tocopherol competes for α -TTP binding with the fluorescent ligand. Specific binding requires the free phenol, as seen by the lack of binding of the methoxy analogues **40**.

3.4 Cell studies

The ligand with the highest binding affinity will be accessed in a doxycycline-induced secretion assay in Morris hepatoma 7777 (McA-RH7777) rat hepatoma cells. The decrease in the area of fluorescence will be used to determine the amount of secretion. Our prior fluorophores were tested in the same cell lines.

3.4.1 Cell assay

Thienyl-ene-BODIPY- α -tocopherol was sent to our collaborator at Case Western University, Dr. Danny Manor to test the suitability of the ligand in cell-based assays of intracellular tocopherol transfer and secretion. The transport was followed by observing the location and

duration of fluorescence in cultured cells, in what is known as a secretion assay. It is understood that α -TTP is responsible for the specific retention of α -tocopherol in the liver and its secretion into plasma lipoproteins such as VLDL.⁷⁵ In fact, cultured hepatocytes are shown to transport compound **3** out of the cell as observed by an overall fluorescence decrease. The test was carried out as described in the following section:

For secretion assays, previously described doxycycline-inducible α -TTP-expressing McA-RH7777 rat hepatoma cells were used.^{210,309} Forty-eight hours after treating cells with 1 μ g/ml doxycycline or vehicle control, all cells were loaded with 15 μ M of fetal bovine serum complexed thienyl-ene-BODIPY **3**, for 18 h. Media was removed and the cells were washed four times prior to a four-hour secretion / incubation into serum-containing normal growth media. Following α -TTP-facilitated secretion, cells were washed three times in PBS and live cell imaging was performed using a Leica DM 4000B inverted fluorescence microscope. For each experiment the accumulated fluorescence of **3** was captured from 10 equally confluent microscopic fields at 20x magnification (Figure 94). Fluorescence intensities were quantitated and normalized using Image J software (<http://rsbweb.nih.gov/ij/index.html>) as previously described.^{310,311}

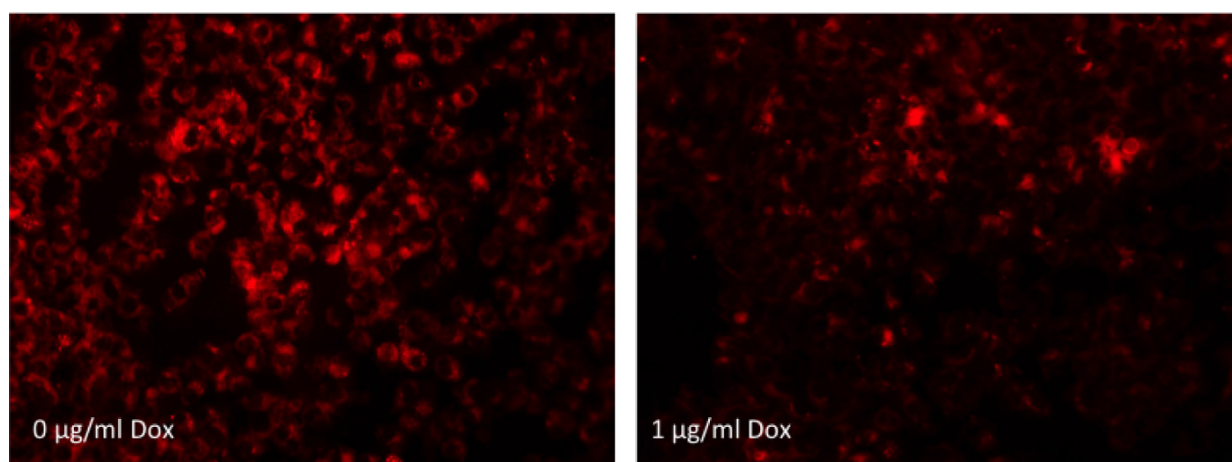


Figure 94. α -TTP facilitated secretion of thienyl-ene-BODIPY **3**, from cultured hepatocytes.

(A) McA-RH7777-TetOn-TTP cells^{210,212} were cultured as described. Where indicated, expression of α -TTP was induced by addition of doxycycline (1 mg/ml). Doxycycline activates the Tet-On gene, starting the transcription of *tppa*.³¹² Twenty-four hours post induction, serum-complexed 3 was added to the culture media (final concentration 15 μ M) for 18 h. The thienyl-ene-BODIPY 3 was then washed with normal media, and after 4 h ('secretion' phase) the cells were imaged by epifluorescence microscopy. Fluorescence in images were quantified in multiple fields and normalized to cell protein content.³¹¹

The decrease in the total area of fluorescence is around 30% after 4 h (Figure 95). The results are not directly relatable to other tocopherol analogues like [¹⁴C]-Toc and NBD-tocopherol because of the difference in structure. However, similar secretion assay have been performed with both ligands.^{309,77}

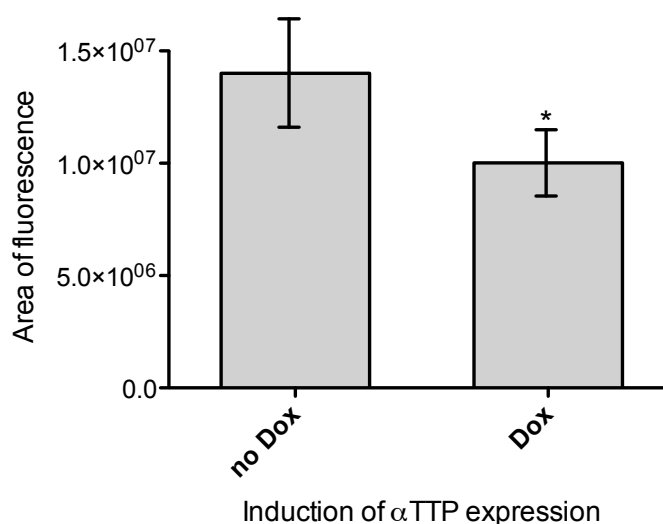


Figure 95. Averages and standard deviations of 5 images from three independent experiments.

Asterisks denote significant difference ($P > 0.05$) between the α -TTP-expressing and nonexpressing cells, as determined by Student's *t*-test.³¹¹

Secretion of [^{14}C]-Toc in HepG2-TetOn-TTP cell lines was around 20% after 48 h when α -TTP was induced with doxycycline (Figure 96). The value was obtained by measuring radioactivity by scintillation counting.³⁰⁹ The authors found that HepG2-TetOn-TTP cell line [^{14}C]-Toc secretion is identical in McA-RH7777-TetOn-TTP cells.

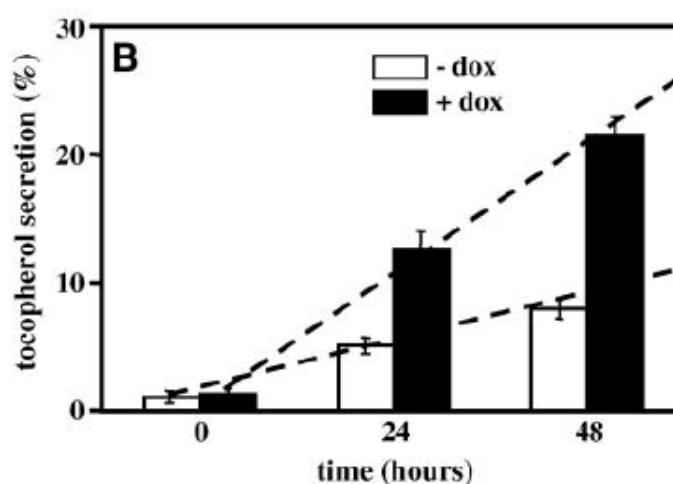


Figure 96. α -TTP-induced α -tocopherol secretion in HepG2-TetOn-TTP cells.

Cells were loaded with [^{14}C]RRR- α -tocopherol for 36 h and washed, and the appearance of radioactivity in the media was assayed at the indicated times by scintillation counting. Shown are averages and standard deviation of quadruplicate wells. Data are representative of 10 independent experiments. When those data are fitted to linear functions (dashed lines), their slopes differ by 3.3-fold.³⁰⁹

NBD-Tocopherol was used to study the intracellular trafficking in liver cells and the influence of PIP₂. Fluorescence decrease after α -TTP expression (TTP +) decreased by 50% after 1h, 60% after 2h respectively (Figure 97).⁷⁷ The concentration of NBD-Toc in these cells was 10 μM . The higher decrease of fluorescence is partly caused by photobleaching of the NBD-tocopherol.

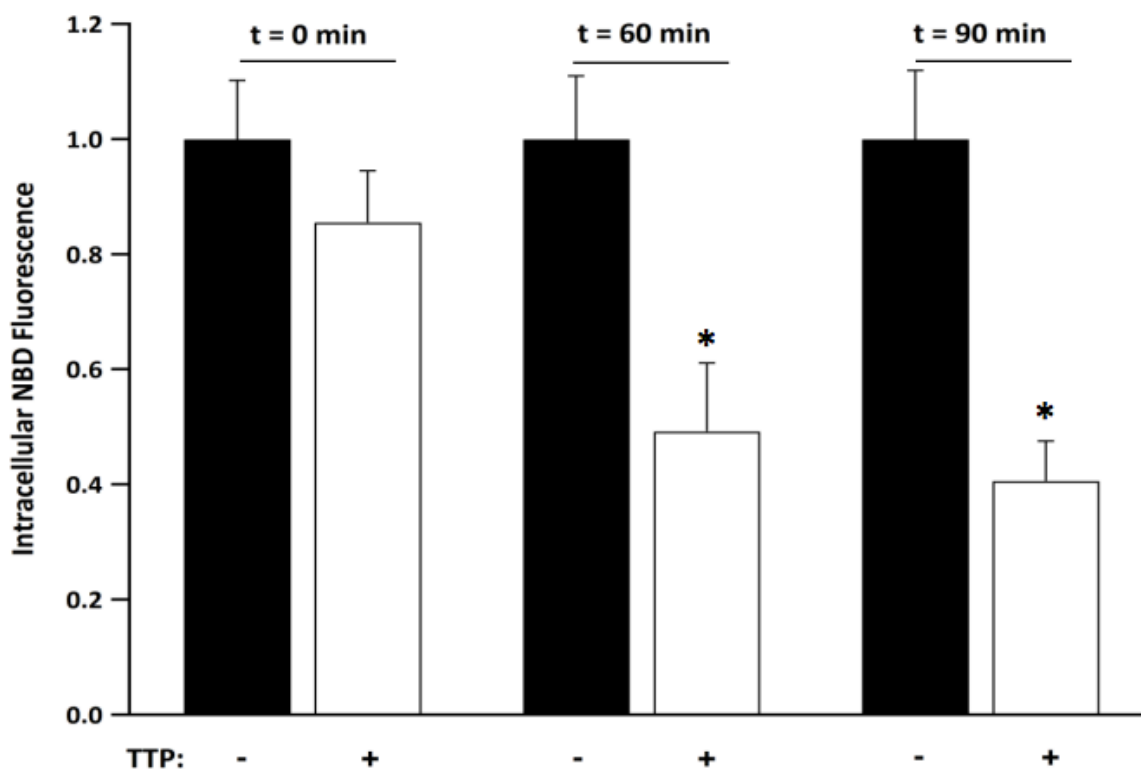


Figure 97. Quantification of intracellular NBD- α -tocopherol fluorescence over time in cells that do (white bars) or do not (black bars) express TTP.

Shown are averages and standard errors of NBD- α -tocopherol fluorescence quantified in confocal images of ~50 cells of each group from 3 independent experiments. Asterisks denote statistical significance with $p < 0.01$, calculated by Student's *t*-test. Fluorescence intensities were normalized to the values of non-TTP expressing cells.⁷⁷

NBD-tocopherol loses around 50% of its fluorescence intensity after 20 minutes of observation due to photobleaching by the excitation laser light. No fluorescent decay was observed with thienyl-ene-BODIPY in the same time span.

Our collaborators mentioned that while testing label **3** an overall similar loss of fluorescence was observed as in NBD-tocopherol secretion. It was stated that the use of higher wavelengths allowed the capturing of microscopic pictures much more easily with smaller quantities of ligand than used before.

4 Conclusion

The fluorescent tocopherol **3** has shown similar results in cell assays as the previously prepared NBD-tocopherol. No photobleaching was observed with **3** and the high quantum yield, extinction coefficient and longer absorption wavelength produced qualitatively better fluorescence micrographs, which can be seen in even low amounts of applied ligand. The synthesis of **3** was successful with a 14% overall yield from Trolox[®]. Currently the compound is being used for studies of tocopherol location and transport in neuronal cells and brain tissue slices, and to visualize lipid bodies in a study that uses tocopherol to treat fatty liver disease.

Design and synthesis of a biomimetic non-antioxidant-tocopherol

5 Introduction

5.1 Antioxidant function

The most studied and understood action of vitamin E is its function as an antioxidant to protect the cell membrane from oxidation, which would lead to the death of the cell. The components protected in the cell membrane are lipids that are susceptible to attack from highly reactive species such as radicals.

5.1.1 Lipid peroxidation

Molecules bearing unpaired electrons, or free radicals, are generated in the body by metabolic processes in the mitochondria or by external sources such as X-rays, pesticides (DDT), smoke, and ozone.³¹³ When any type of electron rich non-radical species donates an electron to oxygen (O_2), superoxide ($O_2^{\cdot-}$) is formed. The $O_2^{\cdot-}$ is a short lived species and can abstract hydrogen atoms from labile sites like bis-allylic C-H bonds to form a hydrogen peroxide anion.³¹⁴

Superoxide is one of the so-called reactive oxygen species (ROS). Superoxide is technically able to oxidize lipids, but is too polar to enter the hydrophobic membrane environment unless protonated to form HOO^{\cdot} ($pK_a \sim 4.7$). The reduced polarity of HOO^{\cdot} allows diffusion into the hydrophobic parts of the membrane.^{315,316} Cell membranes consist of different types of lipids, of which the majority are made up of glycerophospholipids. The phospholipid structure comprises a glycerol esterified to two hydrophobic fatty acids and a negatively charged, polar, phosphate-containing head group. The mono-esterified phospholipid structure is doubly negatively charged and referred to as phosphatidic acid (PA). Other diacylglycerol phosphates are found substituted with ethanolamine, choline, serine, or inositol. The acyl chains may be either saturated or unsaturated. HOO^{\cdot} radicals can react with polyunsaturated fatty acids (PUFAs),

containing varying numbers of *cis*-double bonds with a methylene (-CH₂-) bridges.³¹⁷

Hydroperoxyl radicals are reactive enough to abstract the hydrogen at the methylene bridge (pK_a: 4-5, bond-dissociation energy bis-allylic hydrogen: ~73 kcal/mol) and form a carbon centred radical, which rearranges to a stable conjugated dienyl radical (Figure 98).³¹⁸ The remaining allylic radical reacts extremely quickly with oxygen ($k = 10^9 \text{ M}^{-1} \text{ s}^{-1}$) to form a peroxy radical on the lipid chain (LOO[•]).³¹⁹ Several reactions occur after the formation of the diene peroxy radical.^{320,321} Propagation of the radical chain occurs by lipid peroxy radical abstracting a neighbouring -CH₂- bridge hydrogen atom. The LOOH rearranges after β -scission to form alkenals, hydroxyalkenals and malondialdehyde (MDA). Two dienyl radicals terminate, forming a dimer.

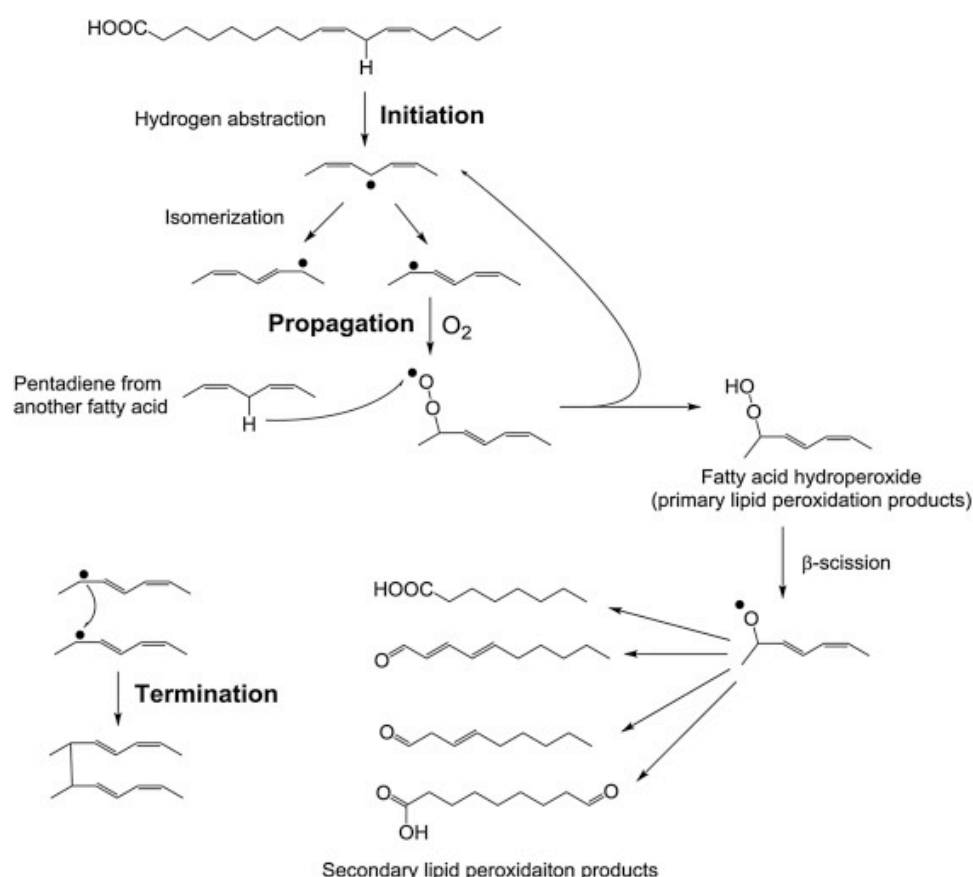


Figure 98. PUFA oxidation: Initiation, propagation and termination.³²⁰

Cells contain a wide variety of unsaturated lipids. The unsaturated FA varies based on the chain length, the position, and degree of unsaturation.

PUFAs can have up to six double bonds, and the greater the degree of unsaturation the more prone the lipid is to hydrogen atom abstraction. As shown with methyl linoleate (Figure 99) several peroxide products are obtained upon autooxidation which can rearrange to different metabolites. The 9-*cis*, *trans* and 16-*cis*, *trans* isomers are the favoured products. When 5 mole % α -tocopherol was present, an almost equal distribution of all products was observed.^{322,323}

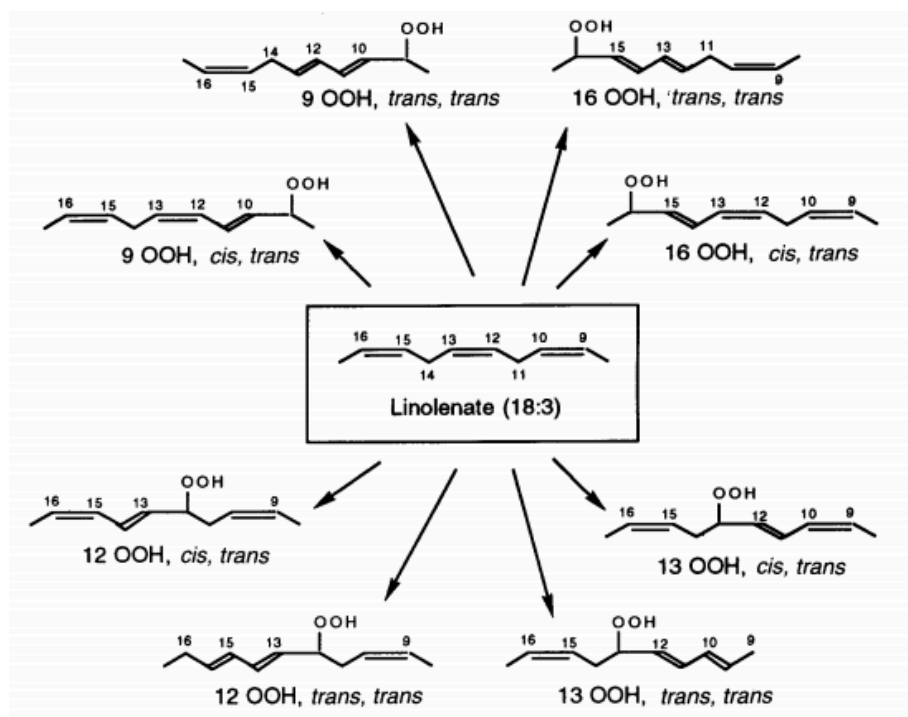


Figure 99. Product distribution for the peroxidation of methyl linolenate peroxide product.³²³

Vitamin E is a chain-breaking antioxidant and prevents membrane peroxidation by donating the hydrogen atom from the chroman ring phenol to the lipid peroxy radical, forming a stable tocopheroxyl radical.

5.1.2 Kinetics of hydroperoxyl radical quenching by tocopherol

The activity of tocopherol as an antioxidant is dependent on its ability to neutralize lipid peroxy radicals.

Antioxidant strength is often given as an inhibition constant by measurement of oxygen ($d[O_2]$) consumption during the peroxidation reaction of lipids in the presence of tocopherol, thereby

taking into account initiation, propagation and termination rates (1).³²⁴ The equation to determine the inhibition constant k_{inh} is represented by n , the number of radical chains inhibited by antioxidant, R_i the initiation and k_p the propagation rate constant of the radical in a certain time (t).

$$1 \quad \frac{d[O_2]}{dt} = \frac{k_p[RH]R_i}{(n[AH]k_{inh})}$$

Electron spin resonance (ESR) has been used to follow the different types of radicals formed during auto-oxidation of lipids.³²⁵ A more lab friendly method measures the UV absorption of conjugated dienes (233-235 nm) to follow reaction progress.³²⁶ The essential steps of tocopherol inhibition of lipid peroxidation are shown in Figure 100. The rate constant k_1 describes the H-atom donation (quenching) from tocopherol to the peroxy radical. The deuterium kinetic isotope effect in an inhibitory auto-oxidation assay (KIE α -toc: k_1^H / k_1^D 5.4 ± 0.4) indicated that this was the rate-determining step.³²⁴

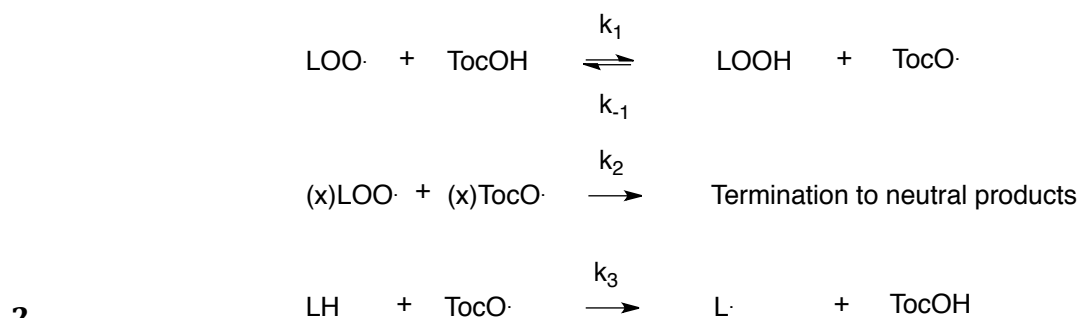


Figure 100. Radical reactions in lipids.

k_1 describes the quenching of lipid peroxy radicals with tocopherol, k_{-1} the reverse reaction, k_2 the termination reaction of lipid peroxy- and tocopheroyl radicals and k_3 the radical abstraction of a lipid *bis*-allyl hydrogen.³²⁴

The reverse reaction k_{-1} and initiation of a new lipid radical k_3 were studied to determine the oxidative power of tocopherol. Radical terminations in k_2 are often neglected since they do not contribute to any pro-antioxidant activity (2). Various products are formed depending on which

radicals react with each other. $\text{LOO}^\bullet / \text{LO}^\bullet$ radicals (L = methyl linolate) terminate with α -tocopheroxyl radicals (TocO^\bullet) at the C-8 position of tocopherol to a lipid-peroxy / lipid oxy tocopherol ($\alpha\text{-Toc-8a-OOL} / \alpha\text{-Toc-8a-OL}$). Also observed were a phenol ether with L^\bullet . $\alpha\text{-Toc-8a-OOL} / \alpha\text{-Toc-8a-OL}$ react further to form the $\alpha\text{-Toc-para-quinone}$, which can even further oxidize with O_2 to epoxy tocopherols (Figure 101).^{327,328}

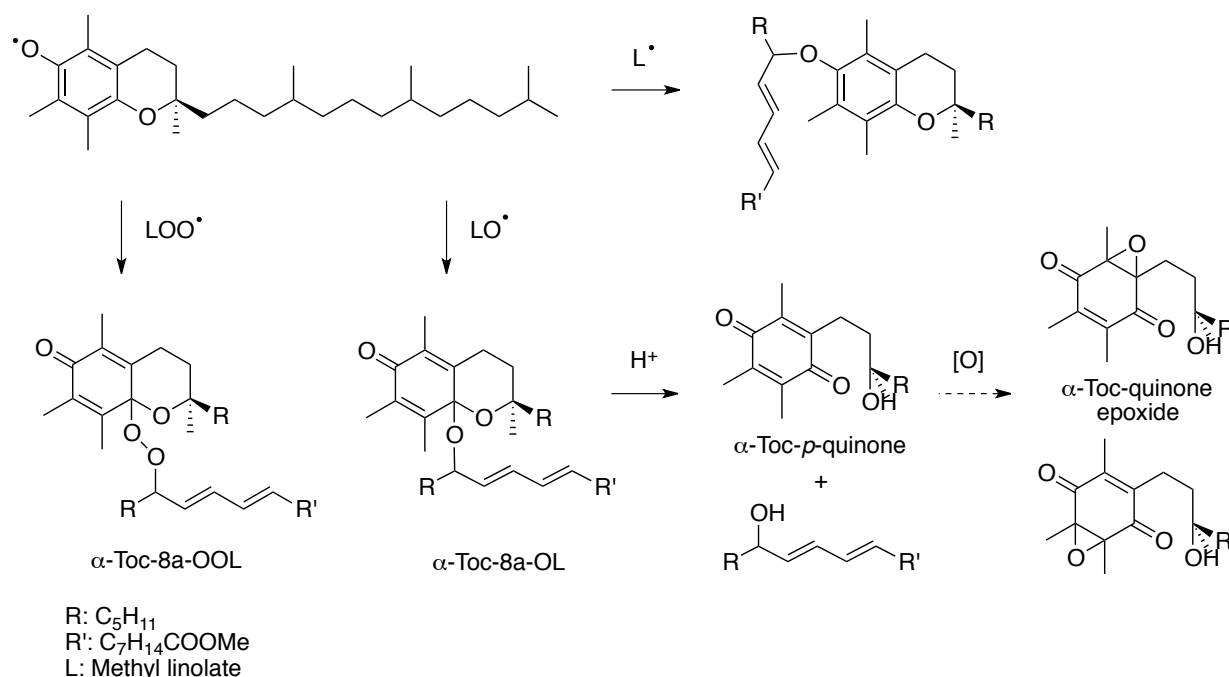


Figure 101. Oxidation products of methyl linolate and α -tocopherol.³²⁸

Many researchers in the 1980s determined k_1 of tocopherol in various medias, using pulse radiolysis, chemoluminescence, or oxygen consumption assays (Table 10).³²⁹ Results depend heavily on the concentration, reaction media, pH, temperature and technique applied.^{323,324}

| Peroxy radical | Technique | Temperature °C | k_{inh} $\text{M}^{-1} \text{s}^{-1}$ |
|--|---------------------------------------|-------------------|---|
| Cl_3COO | Pulse radiolysis | | 5.0×10^8 |
| cyclo- $\text{C}_8\text{H}_{11}\text{OO}$ | Pulse radiolysis | | 2.3×10^7 |
| $\text{C}_6\text{H}_5\text{CH}(\text{CH}_3)\text{OO}$ | Chemiluminescence | 60 | 3.3×10^6 |
| $\text{X}-(\text{CH}_2\text{CH}(\text{C}_6\text{H}_5)\text{OO})_n$ | Oxygen consumption | 30 | 2.35×10^6 |
| $\text{C}_6\text{H}_5\text{CH}(\text{CH}_3)\text{OO}$ | Chemiluminescence | 37 | 1.8×10^6 |
| Methyl linoleoylperoxy | R_{inh} and t_{inh} | 37 | 5.1×10^5 |
| $\text{C}_6\text{H}_5\text{C}(\text{CH}_3)_2\text{OO}$ | Oxygen consumption | 60 | 2.0×10^5 |
| $\text{C}_6\text{H}_5\text{CH}(\text{CH}_3)\text{OO}$ | Chemiluminescence | 25 | 1.5×10^5 |
| Methyl linoleoylperoxy | Pulse radiolysis | | 8×10^4 |

Table 10. Inhibition rates (k_{inh}) of vitamin E by different techniques.³²⁹

A reliable k_1 ($2.35 \times 10^6 \text{ M}^{-1}\text{s}^{-1}$) for α -tocopherol was determined by Burton et al. using an inhibitory auto-oxidation assay with styrene (IAS) (3.95 M styrene in chlorobenzene at 1 atm O_2 , AIBN as initiator).³³⁰ Styrene is not effected by k_3 or k_{-1} because there is no hydrogen abstraction taking place to form a LOO^\bullet , but instead polyperoxy styrene products (LOO-styrene). The insignificance of k_3 / k_{-1} was determined when $\alpha\text{TocO}^\bullet$ was reacted with the same styrene concentration, yielding a rate eight orders of magnitude lower than k_1 ($5.04 \times 10^{-4} \text{ M}^{-1}\text{s}^{-1}$ to $k_1 2.35 \times 10^6 \text{ M}^{-1}\text{s}^{-1}$).

Tocopherol can act as a pro-oxidant when TocO^\bullet reacts with LH, assisting the overall oxidative damage of the lipid. This prooxidant activity occurs under mild oxidative conditions and when co-antioxidants vitamin C or ubiquinone are lacking.³³¹

To determine an accurate k_1 of α -tocopherol the k_{-1} and k_3 values are necessary.

Mukai determined with 5,7-diisopropyl-tocopherol the k_{-1} and k_3 on PC-OO^\bullet and linoleate peroxy radicals. Di-*i*-propyltocopheroxyl radicals do not as easily decompose (natural decay k_0 $3.2 \times 10^{-5} \text{ M}^{-1}\text{s}^{-1}$ in benzene at 25°C) as α -tocopheroxyl radicals and allow a more accurate rate determination (1st order). The k_{-1} was determined with alkyl hydroperoxides (*n*-, *s*-, *t*-butyl) against di-*i*-propyl- TocO^\bullet ($1.34, 2.42, 3.65 \times 10^{-1} \text{ M}^{-1}\text{s}^{-1}$)³³²

Methyl linoleate peroxide inhibition gave a 2nd order rate constant for α -toc k_{-1} of $5.0 \times 10^{-1} \text{ M}^{-1}\text{s}^{-1}$. This value is a decrease in seven orders of magnitude from Burton's result (Burton's k_1 $3.2 \times 10^{-1} \text{ M}^{-1}\text{s}^{-1}$). Di-*i*-pro- TocO^\bullet is not quite as reactive (k_{-1} $1.34 \times 10^{-1} \text{ M}^{-1}\text{s}^{-1}$), but still in the same order of magnitude as α -tocopherol³³³ The second order abstraction rate k_3 of ethyl stearate, oleate ($1.04 \times 10^{-5} \text{ M}^{-1}\text{s}^{-1}$), linoleate ($1.82 \times 10^{-2} \text{ M}^{-1}\text{s}^{-1}$), linolenate ($3.84 \times 10^{-2} \text{ M}^{-1}\text{s}^{-1}$) and arachidonate ($4.84 \times 10^{-2} \text{ M}^{-1}\text{s}^{-1}$) was calculated with the diisopropyl substituted radical (Figure 105). Di-*i*-propyl- TocO^\bullet decay measurements showed faster reactions with increased unsaturation of the substrate (Figure 102). Increased fatty acid concentration (LH: 25 mM, 50 mM, 75 mM 100 mM) verified a pseudo-first order dependence (k_{obsd}).³³⁴

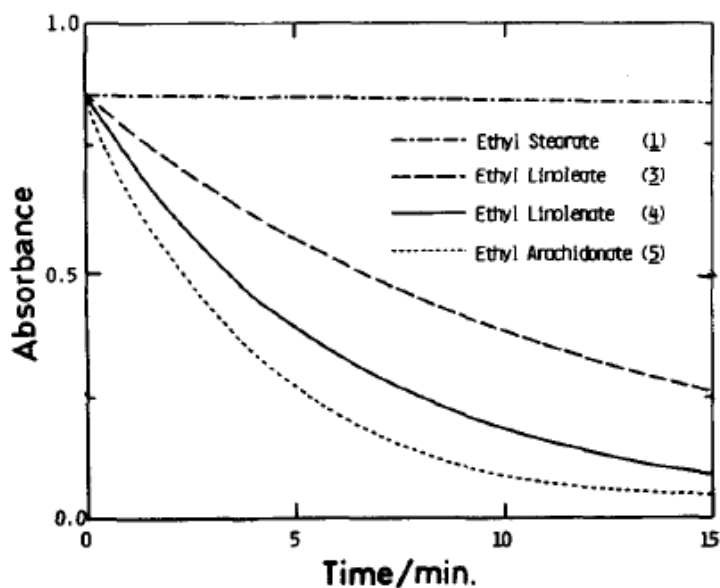


Figure 102. The decay of 5,7-diisopropyl-tocopheroxyl radical reacted with ethyl stearate, linoleate, linolenate and arachidonate observed at 417 nm in benzene at 25.0°C [Toc: 0.17 mM and $[LH]_{t=0}$ 75.0 mM].³³⁴

Tocopherol is a much better antioxidant than other phenols. Butylated hydroxy toluene (2,6-di-*tert*-butyl-4-methylphenol, BHT), a commercially available phenol used as a preservative in foods, cosmetics, and fuels, is often used as a lipophilic standard to compare antioxidant properties. BHT is 250-times less reactive than tocopherol and 300-times more reactive than PMC in a styrene auto-peroxidation assay.³³⁵ However, tetramethyl-*p*-methoxyphenol is only 30-times more active than BHT. The presence of a substituted *para*-oxygen atom greatly stabilizes the phenoxy radical.³³⁶ The fused ring system helps by favouring the overlap of the *p*-orbitals of both oxygen atoms with each other through the π -system of the ring.³³⁵ Geometrical analysis by X-ray diffraction revealed a 16° offset of the *para*-oxygen *p*-orbitals (Figure 103). An almost perfect alignment was achieved by reducing the ring size to a benzofuran. 2,2,4,6,7-pentamethyl-2,3-dihydrobenzofuran-5-ol (B) is 445-times more potent than BHT.^{323,337}

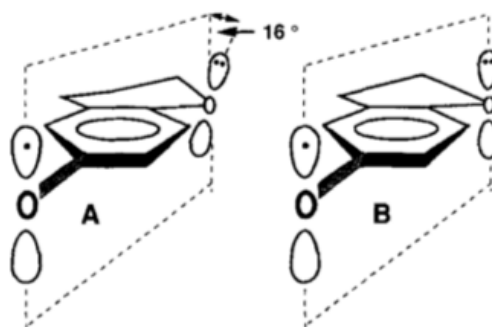


Figure 103. Orbital alignments in chroman and benzofurane.³³⁵

Hydrogen abstraction measurements in various media showed that α -tocopherol has the highest rate of all tocopherols.³³⁸ Decreasing the methyl substitution on the chroman ring lowers the radical stability. Reduction potentials of α -, β -, γ - and δ -tocopherol measured by Wacks indicated the higher reduction potential of α -tocopherol: ($< \alpha$) +0.273, +0.343, +0.348, and +0.405 volts.³³⁹ Burton's styrene auto-oxidation assay showed a similar trend (23.5, 16.6, 15.9, and $6.5 \times 10^5 \text{ M}^{-1} \text{ s}^{-1}$).³³⁰ Membrane ratios of tocopherol to phospholipid are relatively low (1:500-3000), which makes ROS lipid peroxidation more likely than direct quenching of ROS by tocopherol. In terms of lipid oxidation, HOO^\bullet is the only species found to damage the membrane substantially.³⁴⁰

5.1.3 Quenching of vitamin E

Water-soluble reductants like vitamin C (ascorbic acid) reduce the tocopheroxyl radical back to tocopherol once it reaches the membrane surface.¹¹

Peroxyl radical quenching rates for each form of tocopherol were tested against methyl linoleate in protic solvent (Figure 104). The inhibition rate determined for α -tocopherol was $5.1 \times 10^5 \text{ M}^{-1} \text{ s}^{-1}$.³⁴¹ Vitamin C alone showed antioxidant properties in the same assay one order of magnitude slower than vitamin E $3.2 \times 10^4 \text{ M}^{-1} \text{ s}^{-1}$. Both antioxidants combined had a rate of lipid peroxide inhibition of $4.0 \times 10^5 \text{ M}^{-1} \text{ s}^{-1}$, meaning that vitamin E abstracts the peroxyl radical and vitamin C works synergistically to reduce the tocopheroxy radical. In the case of in vivo cytosolic

radicals, other antioxidants are involved in radical scavenging, enhancing the antioxidant effect of tocopherols.³⁴¹

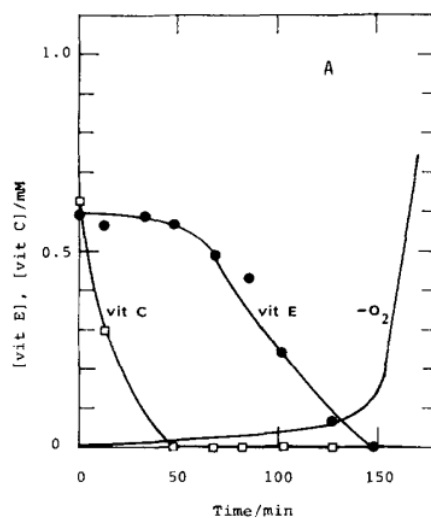


Figure 104. Disappearance of vitamin E and vitamin C in the oxidation of methyl linoleate at 37°C in *tert*-butyl alcohol/methanol (3:1 by volume).

[LH] = 0.60 M, [AMVN] = 0.010 M, [vitamin E] = 0.595 mM, [vitamin C] = 0.620 mM (A) (Niki et al.).³⁴¹

Ascorbate quenches the tocopheroxy radical relatively fast $1.55 \pm 0.2 \text{ M}^{-1} \text{ s}^{-1}$.³⁴²

5.1.4 Hydrophobic antioxidants; carotene and ubiquinol

Other antioxidants like carotenes and ubiquinol are also present in membranes and have important synergistic effects with vitamin E and ascorbic acid.³⁴³ Carotene is a tremendous quencher of singlet oxygen (O_2^1)³⁴⁴, a ROS detected as products from oxygen-consuming enzymes like myeloperoxidase³⁴⁵ and xanthine oxidase.^{346,347} O_2^1 -based lipid oxidation and its inhibition by carotene follows a 4+2 cycloaddition. Alkoxy and peroxy radicals are quenched by free radical reactions (Figure 105).³⁴⁸

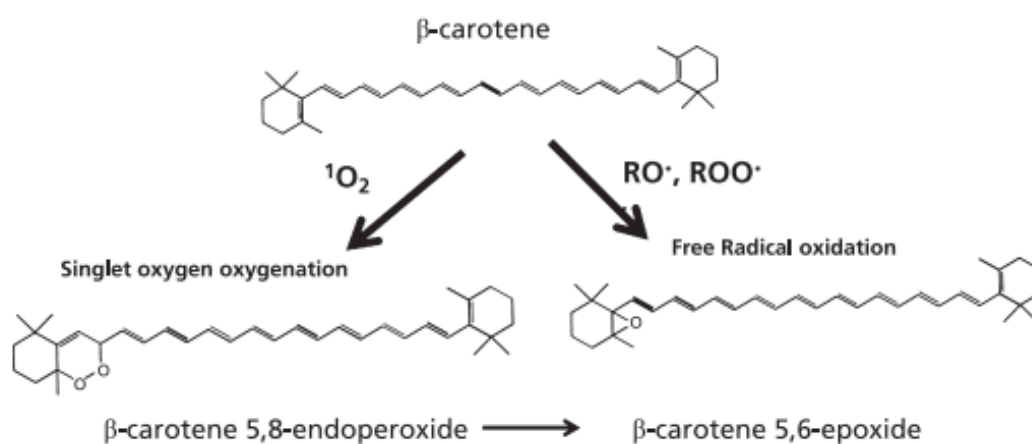


Figure 105. β -carotene reaction with singlet oxygen (1O_2) and RO^\bullet, ROO^\bullet .³⁴⁸

Comparison of chain-breaking antioxidant functions between vitamin E and carotenes show the dependence on partial oxygen pressure (Figure 106). Carotene only exhibits similar inhibitory results at lower partial oxygen pressure (at 2% oxygen concentration; 20% as standard).^{349,343}

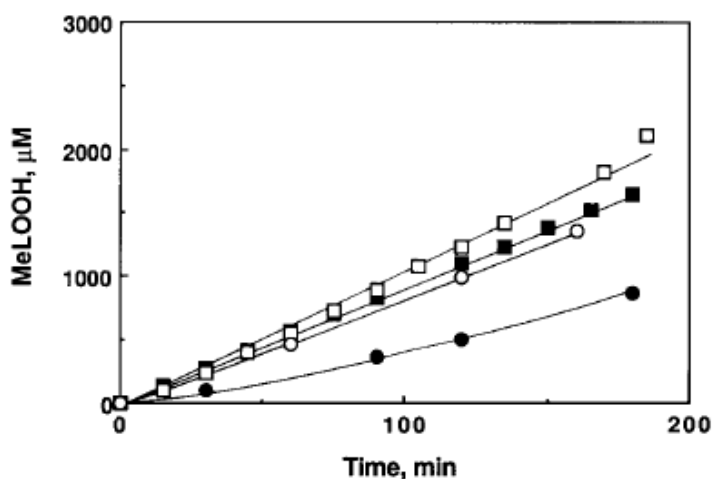


Figure 106. Effect of oxygen concentration in peroxyl radical formation in methyl linolate 18:3 (200mM) initiated by AMVN (1mM) at 37°C.

Clear symbols represent absence of β -carotene, full with ($5.36\mu\text{M}$ β -carotene). Squares represent the reaction in air (20% O_2), circles 2% O_2 .³⁴³

Mitochondrial ubiquinol (CoQH_2) and ubiquinone (CoQ) transport electrons from complex I and II to III as part of the respiratory chain.³⁵⁰ Ubiquinone is the only hydrophobic antioxidant produced in mammalian cells.^{351,352} To assure a continuous electron flow in mitochondria protection from ROS, CoQ is reduced by NADPH to reform CoQH_2 . The Constantinescu group proved that CoQH_2 reforms vitamin E by quenching tocopheryoxyl radicals in cells. Experimental evidence by Villalba shows that ubiquinyl radicals are quenched by ascorbic acid.^{353,354} The combination of vitamin E, ascorbate and CoQ assure a maximal protection against ROS, especially in oxygen rich environments like the mitochondria.

5.1.5 Vitamin E function and movement in membranes

The membrane protection capability of vitamin E in living cells is heavily dependent on the membrane composition. Membranes with a low vitamin E : phospholipid ratio of 1:1000-3000 need higher recycling rate of vitamin E (Table 11).³⁵⁵

| Subcellular fraction | α -Tocopherol (mmol/mol lipid P) |
|----------------------|---|
| Nuclear fraction | 0.72 ± 0.16 |
| Mitochondria | 1.07 ± 0.27 |
| Inner membrane | 1.27 ± 0.32 |
| Outer membrane | 1.14 ± 0.35 |
| Lysosomes | 14.60 ± 2.33 |
| Microsomes | 0.52 ± 0.08 |

Table 11. Content of α -tocopherol (mmol/mol lipid) in subcellular membranes of rats fed a standard laboratory diet.³⁵⁵

Vitamin E stabilizes lipid bilayers via Van der Waals interactions with phospholipids.³⁵⁶

Comparison between the known phospholipids showed that vitamin E has a strong association towards phosphatidylethanolamine (PE).

After phospholipids, cholesterol is the major lipid component of cell membranes (around 20-30% in plasma membranes, less in intracellular membranes) and helps to maintain its stiffness.

Membrane proteins are fixed in specific places by cholesterol and moved via lipid rafts to induce protein-protein interactions and initiate cell signaling processes.^{357,358,359} Higher cholesterol content in membranes makes them more viscous / stiffer by ordering the crystalline phase, which decreases lateral diffusion and membrane permeability of electrolytes and small molecules like acetate or propionate by disordering the gel phase.³⁶⁰ Nau showed that vitamin E diffusion and mobility is affected by temperature and cholesterol percentage by monitoring fluorescence quenching in POPC membranes.^{361,362}

5.1.6 Position and dynamics of vitamin E in membranes

The efficiency of tocopherol quenching of free radicals depends on the location of each molecule in the membrane. Quenching is less prone the deeper the radical lies in the interior of the membrane, and more prone on the cell surface.³⁶³ Solid state NMR, neutron scattering, spin

labeling, and MD-simulation experiments provide strong evidence of the location and movement of vitamin E in cell membranes. The chromanol portion lies between the hydrophilic - hydrophobic interphase around 5-10 Å deep into the membrane. This is approximately at the position of the first few methylenes from the acyl chain carboxyl end. Neutron diffraction, NMR, and UV spectroscopy experiments with all types of PUFA have concluded that in this interphase all LOO[•] chain length types with an unsaturated position between carbons 5-15, and fast diffusing cytosolic HOO[•] radicals are quenched.³⁶⁴ Hydrogen bonding between the chromanol phenol and the phospholipid head groups dictates the depth, and can vary by around 5Å. This ~5Å difference is based on the three different possibilities of how the chromanol phenol hydrogen bonds to the phosphate headgroup; closer to the membrane surface by bonding only to the phospholipid oxygens (A, Figure 107), deeper when H-bonds are shared between phospholipid oxygen and ester carbonyl (B, Figure 107) and buried deepest into the bilayer when only bonding to the ester (C, Figure 107).³⁶⁵

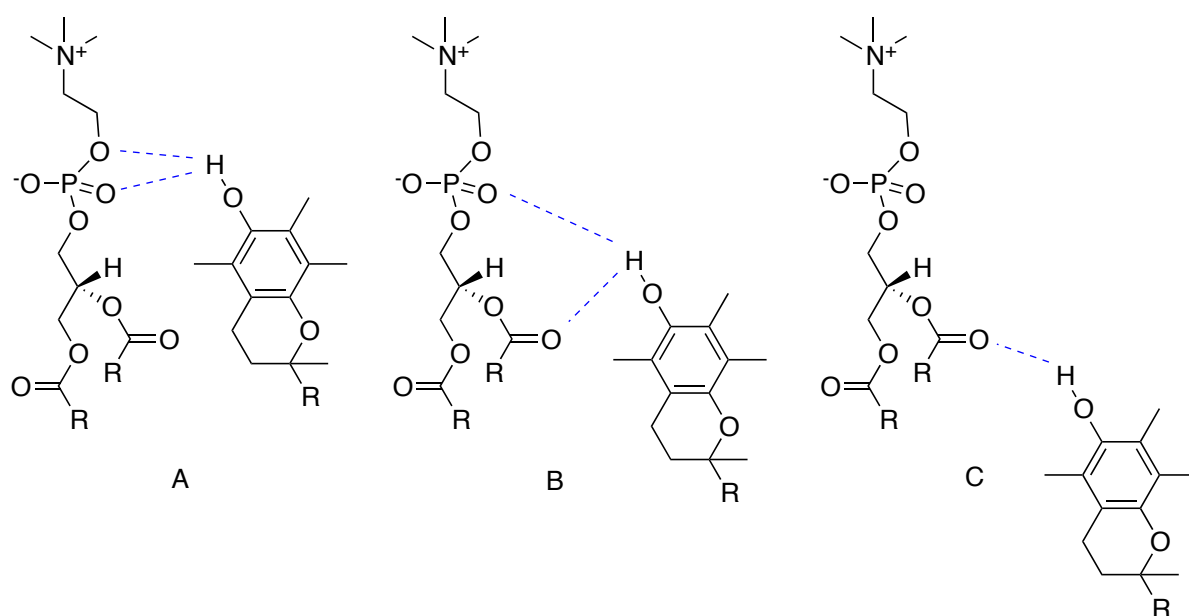


Figure 107. Position of tocopherol to the phospholipid head group.^{364,365}

The transverse motion (bobbing) is affected by the degree of unsaturation of the fatty acid chains. Increased unsaturation on the phospholipid fatty acids puts vitamin E deeper into the

membrane. Headgroups in membranes are rather static, whereas the carbon chains are bending in all directions. Hence, interactions between the double bonds of polyunsaturated lipids and the chroman occur, dragging the head group deeper into the membrane to the active zone where peroxy radical quenching can occur (Figure 108). Oxidized lipids increase in polarity and move their tails towards the bilayer surface into the active zone.³⁶⁴

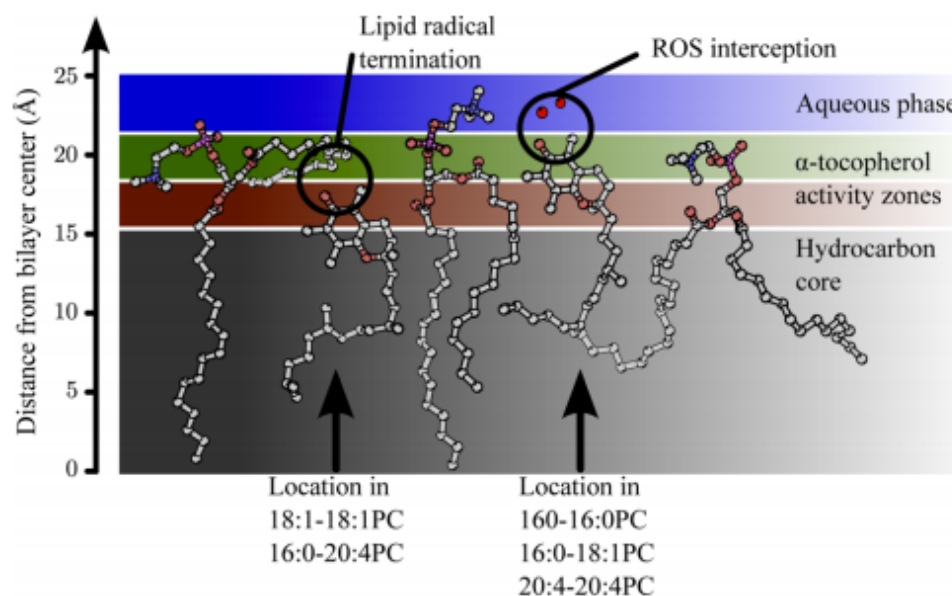


Figure 108. Location of tocopherol in membranes.³⁶⁴

5.1.7 Vitamin E membrane curvature and flip-flop

Membrane curvature describes the geometrical stresses and shape of the membrane and is a function of the chemical composition of the membrane and associated proteins. A biological membrane consists of many distinct regions acting out specific functions, like protein anchoring. In addition, some lipids take part in signal cascades and are therefore enriched in certain cell regions. An example of the importance of membrane curvature is the BAR (Bin, Amphiphysin, Rvs) domain, binding only onto highly curved membrane parts and changing the membranes curvature.^{207,366} A more closely related example was the finding that α -TTP transports NBD-tocopherol much faster to vesicles with more curvature like small unilamellar vesicles (SUV).²⁰⁷

Distribution of lipids across the whole membrane is important for maintenance of a constant ratio of lipids on each side of the bilayer.³⁶⁷ Lipid movement across membranes in a so-called flip-flop motion is generally extremely slow and restricted in the case of phospholipids.³⁶⁸ Enzymes called flippases (inside to outside) and floppases (outside to inside) are membrane proteins responsible for a faster distribution of phospholipids.^{369,370} However, α -tocopherol flip-flops in 50-75 ns intervals, therefore, it easily reaches any radical on either side of the membrane (membrane thickness = $\sim 60\text{\AA}$). Fast inter-leaflet transfer is necessary as oxidized membranes disturb the membrane surface, ultimately leading to perforation that allows biomolecules to leak from the cell. Research on lipid membrane restoration has shown that tocopherol is capable of assisting the repair of damaged membranes. The antioxidant action was found to be crucial for membrane restoration.^{371,372}

5.2 Cellular role of vitamin E

Tocopherols and tocotrienols have been found to participate several biological functions that effect cell proliferation. α -Tocopherol has been the focus of most studies because of its preferential retention in the body. Most cellular effects are traced back to the radical scavenging, but not all functions have been fully determined yet.

5.2.1 Protein kinase C and Phospholipase A₂

α -Tocopherol interacts with certain isoforms of protein kinase C (PKC). cPKCs are part of a signal transduction pathway that regulates cell growth and proliferation by phosphorylating serine and threonine residues of several proteins like rapidly accelerated fibrosarcoma protein kinase (RAF) in the RAF / RAF-1 kinase inhibitor protein (RKIP) complex (part of the mitogen-activated protein (MAP)), insulin receptor substrate 1 (IRS-1) tyrosine³⁰⁸ and nuclear factor- κ B (NF- κ B) (part of B-cell immune response).³⁷³

Vitamin E was found to have a stimulatory effect on protein phosphatase 2A (PP₂A) in endothelial cells, which leads to higher dephosphorylation of PKC and therefore inhibits growth in vascular muscle cells.^{374,375} PKC inhibition was confirmed in several varieties of cell types, such as monocytes³⁷⁶, fibroblasts³⁷⁷, neurophils³⁷⁸, and mesangial cells.^{379,380} Tocopherol stimulation of PP₂A is not based on ligand-protein binding. Inhibitory effects of vitamin E are largely based on secondary interaction / stimulatory effects as in the case of PP₂A / PKC inhibition.³⁸¹

5.2.2 Atherosclerosis

Vitamin E has been shown to prevent atherosclerosis in early stages. In early stages of the disease, oxidized low-density lipoproteins (LDLs) are removed by macrophages, which turn into lipid-laden foam cells that accumulate within the cell wall. Studies have revealed that Vitamin E acts as an inhibitor / regulator of several post-transcriptional processes to prevent the early stages of atherosclerosis.^{382,383}

1) Monocyte (macrophage) adhesion to arterial walls is prevented by downregulation of intracellular adhesion molecule-1 (ICAM-1) and vascular cell adhesion molecule-1 (VCAM-1). These two molecules regulate the amount of monocytes produced in the body.^{384,385}

2) Platelet adhesion and aggregation was reduced with vitamin E in a clinical trial and the findings were that γ -tocopherol is more potent than α -tocopherol.³⁸⁶ Further studies have shown that the reduction is an effect of PKC inhibition rather than its anti-oxidant function towards LDLs³⁸⁷

3) Cyclooxygenase-2 (COX-2) and 5-lipoxygenase (5-LOX) are inflammatory mediators and when inhibited by tocopherols showed less monocyte activation.³⁸⁸

4) Inhibition of scavenger receptor SR-BI and cluster of differentiation 36 (CD36) scavenger receptors on monocytes stops the uptake of oxidized low-density lipoproteins (oxLDL), hindering the formation of foam cells. Inhibition occurs in two ways: decrease of oxLDL levels by radical scavenging ROS that create oxLDL from LDLs and inhibition of oxLDL activated protein kinase B (PKB) / peroxisome proliferator-activated receptor gamma (PPAR γ) stops the upregulation of SR-BI, SR-AI and CD36 (Figure 109).^{389,390}

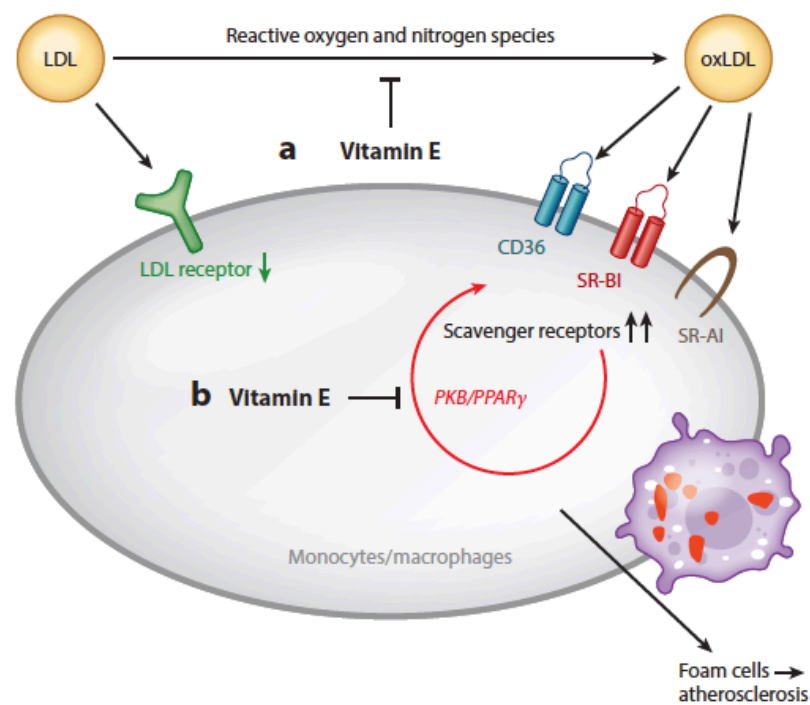


Figure 109. Vitamin E inhibition of LDL and oxLDL receptor mediated atherosclerosis.³⁹¹

A detailed update on the effects of vitamin E on signal transduction is found in Zingg's review.³⁹¹

6 Project overview

Over the last 60 years, vitamin E research has been primarily devoted to its antioxidant properties and corresponding biological functions. Vitamin E is the most potent chain breaking antioxidant that protects membrane structure, and is involved in the inhibition of inflammation, cell proliferation, and prevention of atherosclerosis.

A question has arisen in recent years whether tocopherol might protect cells through other mechanisms unrelated to its antioxidant capability. A role has been suggested for α -tocopherol affecting the transcription of genes responsible for cellular survival when under stress.^{392,393}

Such ideas were based on research where tocopherol was linked to elevated or inhibited enzyme functions, as in the case of PKC, PP₂A and COX-2.³⁹¹

The idea that vitamin E has biological activities independent of antioxidant action gained more attention as the other tocopherols (β , γ , δ) and antioxidants like *N*-acetyl cysteine (NAC) were shown to lack the activity of α -tocopherol, despite being similar radical scavengers. Preliminary results from our collaborators have shown that transcription of the TTPA gene is upregulated by α -tocopherol but not by NAC in astrocytes under oxidative stress. Tocopherol analogues like tocopherol succinate³⁹⁴, tocopheryloxy acetic acid³⁹⁵ and tocopheryloxybutyric acid (TOB)^{396,397}, which are not capable of acting as antioxidants, can induce apoptosis in cancer cells.

Furthermore, these tocopherol analogues cannot bind to α -TTP, meaning they are not reliable substrates to study the function of α -tocopherol in gene activation and enzyme upregulation. To shine light on this additional function we designed a tocopherol that maintains most of its

structure and interaction to α -TTP, but lacks antioxidant properties. Ultimately, this molecule will be studied in dietary trials with normal and TTP-knockout mice. Knockout mice lacking TTP have chronically low concentrations of plasma and tissue vitamin E, so they eventually develop the neurological symptoms of deficiency. However, they can be recovered by large dietary doses of vitamin E. A recovery in deficient mice with a “fake” non-antioxidant form of tocopherol would mean that tocopherol’s activation of other ROS scavenging mechanisms is an important function for cell survival, even more than its antioxidant function towards lipidperoxyl radicals.³⁹⁸

6.1 Structural design

The tocopherol structure has two parts, the chromanol and the phytyl chain. The antioxidant chemistry is associated with the chromanol by H-atom donation to a lipid peroxyl radical to form the kinetically more stable tocopheroxyl radical. Any analogue that is to be a non-functional antioxidant must remove the phenol but leave the phytyl chain untouched. However, certain properties must be maintained besides the lack of radical abstraction. The new molecule must be transported to cell membranes by α -TTP. The molecule should also be able to mimic the position of tocopherol in a membrane. The chosen functional group cannot be too big in size, as it would not bind to α -TTP. The easiest way would be to turn the phenol into the methyl ether, but binding studies with **40** (MeO-thienyl-ene-BODIPY, See Figure 90) have shown no affinity for TTP. An alternative would be a functional group with similar high polarity and hydrogen bonding ability.

6.1.1 Halogen tocopherol

One possibility is to substitute the phenol oxygen with a halogen atom. A halogen would maintain a single bond to the aromatic ring, and a similar electronegativity as an oxygen atom (Figure 110).

Halogens can act as Lewis acids (and make H-bonds) by accepting a lone pair of electrons into an electron deficient region opposite to the covalent bond of halogen, called a sigma hole.

Halogen bonding distance and strength is similar to weaker H-O bonding.³⁹⁹

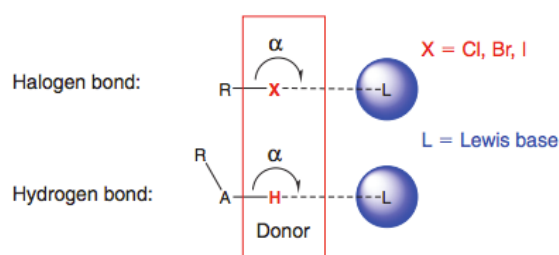


Figure 110. Basic principle of halogen and hydrogen bonding to a Lewis base.

Indication of the optimal bonding angle α .⁴⁰⁰

However, steric hindrance and binding angle (α) have a larger influence on the bonding strength.⁴⁰⁰ A perfect angle ($C-X\cdots O$) for a halogen bond is 180° . Calculations have shown a decrease in bond length the further the $C-X\cdots O$ angle is away from 180° (Table 12).⁴⁰¹

| Halogen – Oxygen (X-OH) | Mean: $C-X\cdots O$ angle α ($^\circ$) / Distance $X\cdots O$ (\AA) | Degrees away to 180° = % decrease in bond strength |
|-------------------------|---|---|
| Halogen | 180° / \AA | 0° |
| Chlorine | 157.4° / 3.08\AA | 20° - 20-30% |
| Bromine | 159.9° / 3.13\AA | 30° - 45-60% |
| Iodine | 160.4° / 3.27\AA | |
| $O-H\cdots O(H)-C$ | 160.4° / $2.2-3.2\text{\AA}$ | |

Table 12. Halogen bond and the influence of bonding angle α on bond length and strength.^{400,401}

In recent years, researchers have recognized that halogen bonding plays an important role in ligand-protein interaction and drug design.⁴⁰² Amino acids having an oxygen (serine, threonine, tyrosine), sulfur (cysteine), amine (lysine) or aromatic groups (phenylalanine, tryptophan) act

as Lewis bases.⁴⁰³ Iodine has the largest sigma hole of all halogens because it has the least electron density distributed over the largest volume (Figure 111).⁴⁰⁴

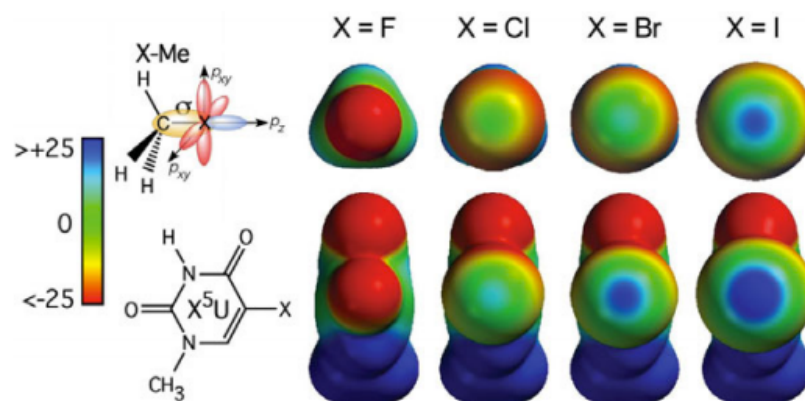


Figure 111. Calculated charge distribution of alkyl halides (top) and halogenated nucleobases (bottom).⁴⁰⁴

The sigma hole is diminishingly small in alkyl chlorides (i.e. CH₃Cl) and is non-existent in the case of alkyl or aryl fluorides. However, when electrons are pulled from the halogen atom as in CF₃Cl, both chlorides and fluorides are able to create significant electropositive σ -holes.^{405,403}

In biological systems, a halogen bonding interaction with aryl chlorides was found while studying the active site of *S*- α -substituted indomethacin ethanolamides to COX-1. The inhibitors place the aryl chloride close to the Ser530, partially helping to stabilize the drug in the active side. The calculated bond distance was 3.23-3.18Å with C-Cl \cdots O bond angles of 147.5°-140.7° (Figure 112).⁴⁰⁶

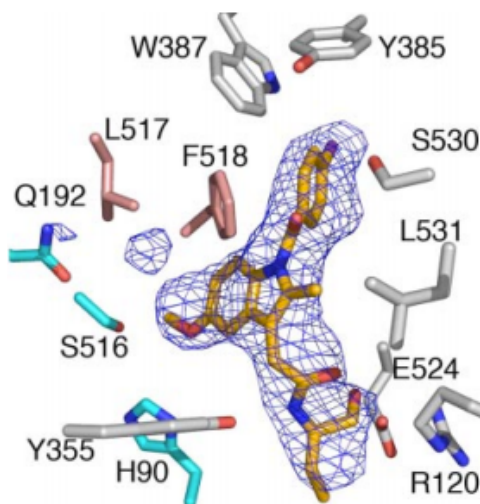


Figure 112. Halogen bonding interaction of a substituted indomethacin ethanolamide analogue to COX-1.⁴⁰⁶

6.1.1.1 Halogen tocopherol in α -TTP

All halide derivative of α -tocopherol would be able to fit into the active site of α -TTP, based on the covalent radius of the halides; however, a rearrangement of the static water molecules and the decreased distance to serine with increased covalent diameter will lower the overall binding (Figure 113). Hydrophobic interactions of the phytol chain with the hydrophobic pocket might add additional stability, but generally does not contribute much to the overall binding strength. Chlorine seems to be the best choice of all halogens, since it balances the steric repulsion in the binding area with a moderate halogen bonding acceptor and donor capability. Furthermore, chlorine is less prone to oxidation by cellular ROS or iron-porphyrins.^{407,408,409}

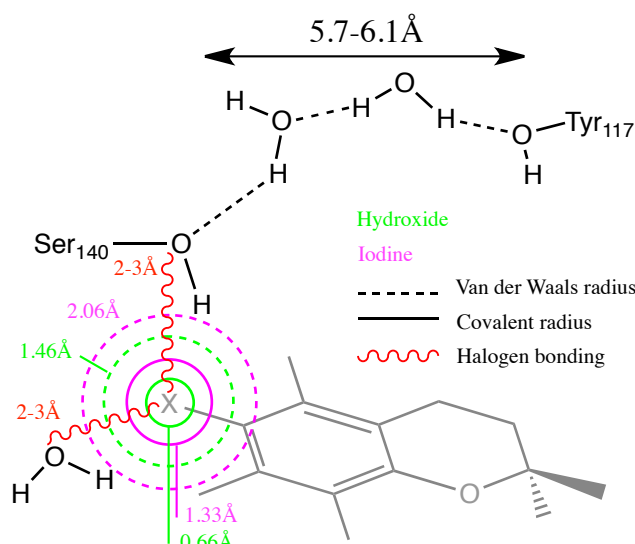


Figure 113. Cartoon representation of possible halogen bonding of a halo- α -tocopherol interaction in α -TTP.

6.1.2 Hydroxymethyl tocopherol

Since α -tocopherol is the major lipid-soluble antioxidant in mammals, the analogue will need to maintain the same three methyl groups on the chroman ring. Maintaining a hydroxyl group would be the best solution to keep the hydrogen bonding interactions. Placing a one-carbon spacer between the oxygen and the aromatic structure forms a hydroxymethyl (HM), small in size and no longer overlapping with the π -system of the aromatic group. If H-atom donation were to occur in a manner similar to α -tocopherol, then an H-atom could be removed from either the OH of the hydroxyl group or either of the two benzylic methylenes. Hydroxyl H-O bond dissociation energies (BDE) for benzylic hydroxides are ~ 107.0 kcal/mol. Lipid peroxide radical abstraction by tocopherol is much lower in energy (~ 78.23 kcal/mol as measured for pentamethylhydroxychroman (PMHC)).^{410,411} The BDE of the benzylic C-H bonds are stabilized by resonance stabilization, but were calculated to be less prone to H-atom abstraction than tocopherol (~ 90.3 kcal/mol) (Figure 114).⁴¹²

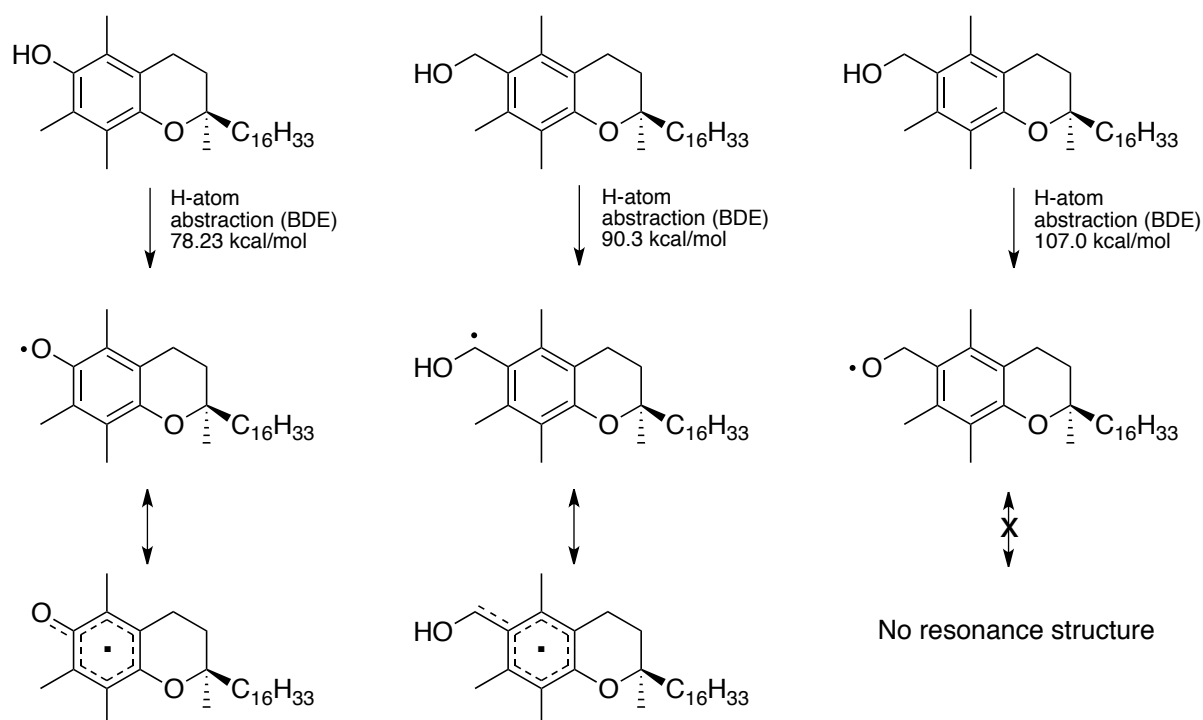


Figure 114. Radical abstractions bond dissociation energies of HM-Toc & α-Toc.⁴¹⁰

Helbling's studies of α- and γ-tocopherol binding in wild type human α-TTP showed changes in the hydrogen-bonding network between Tyr117 and Ser140 surrounding the phenol (Figure 115). A small change, such as the missing methyl group in γ-tocopherol shortens the distance between Tyr117 and Ser140 from 6.1 Å to 5.1 Å, allowing only one water molecule to bridge the two amino acid residues. The change in conformation leads to a 10-fold decrease in binding affinity from 25 nM (α-toc) to 266 nM (γ-toc).⁴¹³

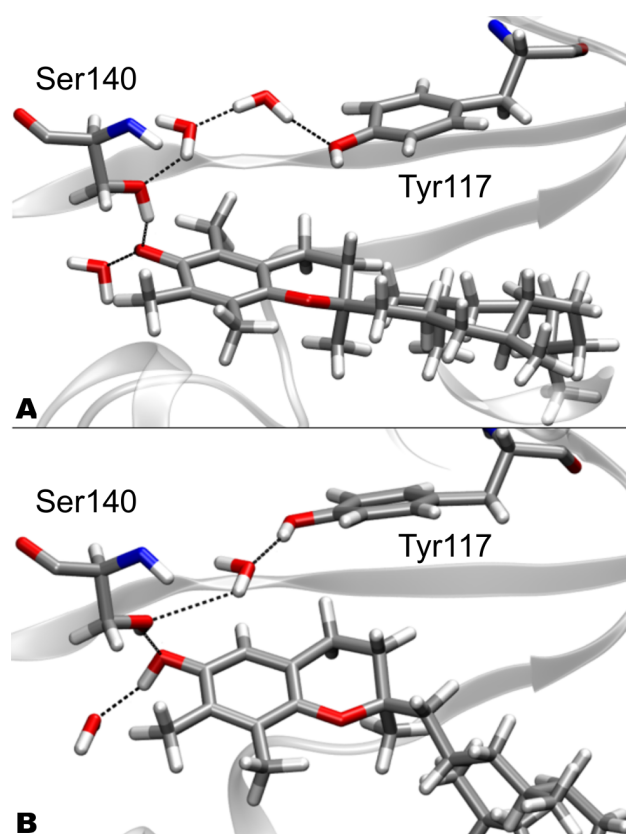


Figure 115. Calculated hydrophilic interaction of α -tocopherol (A, top) and γ -tocopherol (B, bottom) in the wild-type α -TTP binding pocket.

The residues involved in the H-bond network (Ser140 and Tyr117) are shown as licorice representation.⁴¹³

The hydroxymethyl group will most likely have the same or a slightly decreased binding affinity. This assumption is based on the shifted chroman framework, which is around 1.3-1.5Å away from the original position (Figure 116).

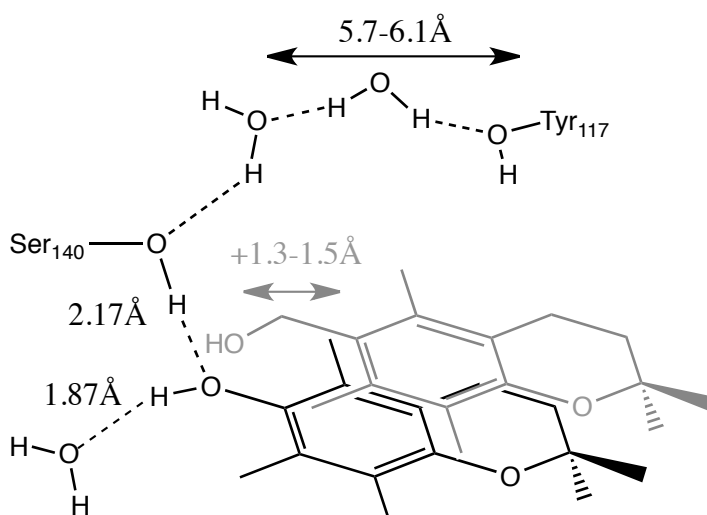


Figure 116. Cartoon representation of possible HM-Toc position in α -TTP.

6.2 Synthesis

The main structural difference between α -tocopherol and the targeted 6-hydroxymethyl analogue is the oxygen at the 6-position on the chroman ring. These 6H-chromanes are commonly synthesized by cyclization reactions of phenols.^{414,415} Tocopherol is industrially synthesised by a cyclization reaction between iso-phytol and hydroquinones.³⁶ Natural *RRR*- α -tocopherol would be a compelling starting material, since the phytyl chain is already present with the correct *R*-stereochemistry at the 2'-position on the chroman. Direct nucleophilic substitution at the ipso-position with chloride or a carbon nucleophile is possible when the phenol is turned into a leaving group.⁴¹⁶ To enhance the reactivity phenols are bonded to an oxophyllic functional group with a strong electron withdrawing effect.⁴¹⁷ Bay has chlorinated diverse phenols with phenylphosphorus tetrachloride at 160°C.⁴¹⁸ Schnabel turned phenols into the chloroformate esters and reacted them at 100-200°C with PPh₃ in an autoclave to obtain the chlorobenzenes.⁴¹⁹ Carbon-carbon bond formation to the hydroxymethyl product is not possible with the free phenol. Turning the phenol into the aryl triflate allows metal mediated cross-coupling reactions with carbonyl functional groups.^{420,421}

The best way to introduce the chlorine and HM at C6 of tocopherol is by electrophilic aromatic substitution from (*R*)-2,5,7,8-tetramethyl-2-((4*R*,8*R*)-4,8,12-trimethyltridecyl)chroman (6H-tocopherol or H-Toc) **42**.^{422,423} To do so, the phenol of α -tocopherol must first be deoxygenated. Mahdavian described this exact transformation of α -tocopherol H-Toc by converting the phenol to the triflate **41** followed by reduction by hydrogenation with Pd/C.⁴²⁴ Wang⁴²⁵, Sajiki⁴²⁶ and Mori⁴²⁷ described similar chemistry, with different sulfonates and hydride sources. After the deoxygenation chemistry H-Toc may be directly hydroxymethylated with formaldehyde or formylated by methods of Gattermann, Vielsmeyer-Hack, or Rieche reactions with subsequent reduction.^{428,292,429} Chlorination of H-Toc to **43** could then be achieved with a number of diverse electrophilic chlorinating agents (Figure 117).⁴³⁰

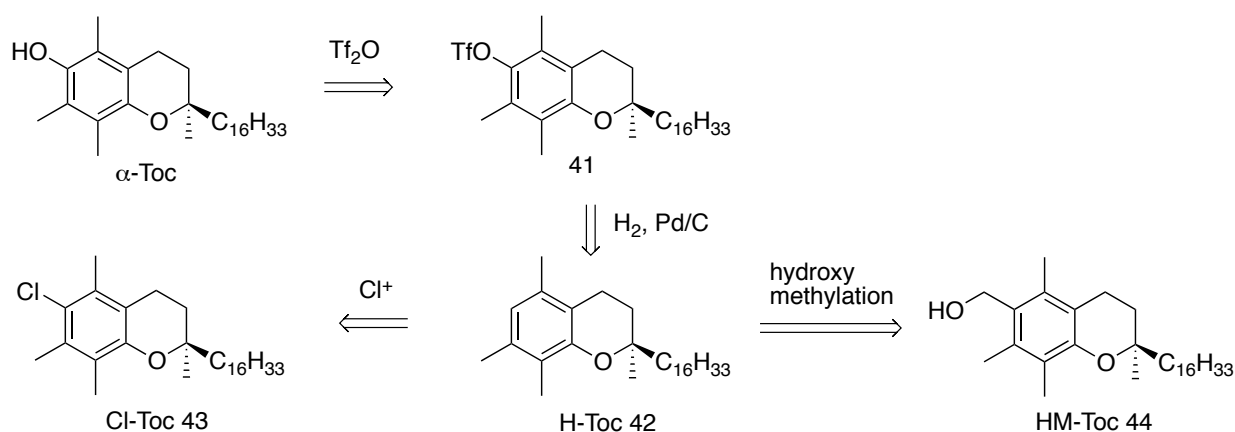


Figure 117 Synthetic strategies to Cl-Toc, **43, and HM-Toc, **44**, from α -tocopherol.**^{424,429,430}

An alternative design uses an oxa-Diels-Alder reaction of 4-hydroxymethyl-2,3,5-trimethylphenol **45** with isophytol to obtain HM-Toc. Isophytol is commercially available and the aryl co-reactant can be synthesized from 2,3,5-trimethylphenol using the same formylation chemistry as described for H-Toc. The cyclization with isophytol has been described several times in the literature with 2,3,5-trimethylhydroquinone.³⁷ Both reactions described would, however, form racemic products (Figure 118).

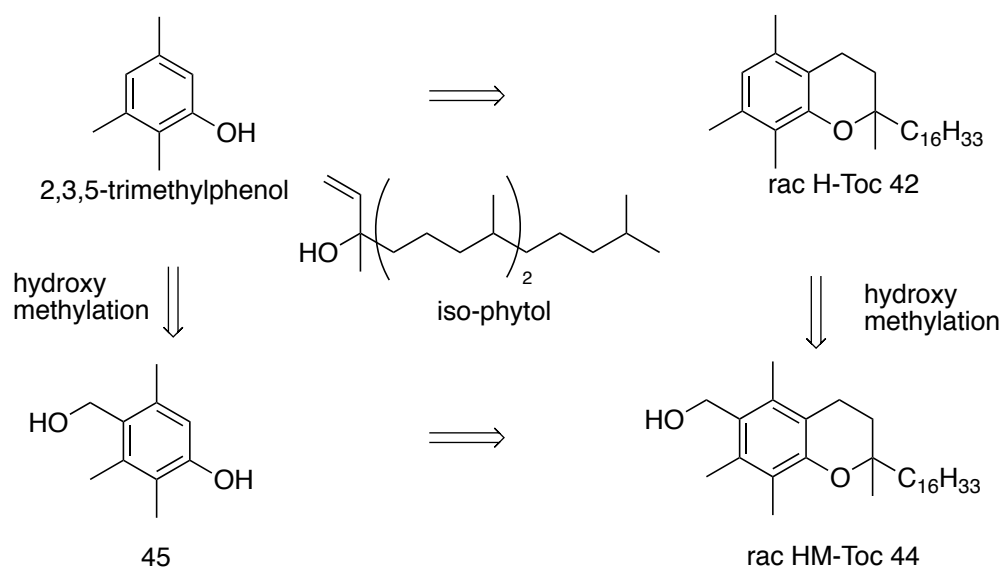


Figure 118. Synthetic strategies to racemic Cl-Toc, 43, and racemic HM-Toc, 44, from 2,3,5-trimethylphenol and 45.^{424,429}

In the case that either of these two routes did not work, **41** could be turned into **44** by transition metal mediated carbonylation or esterification followed by reduction with LiAlH_4 .^{431,421}

7 Results and Discussion

7.1 Synthesis

The first goal was the synthesis of H-Toc **42** by following Mahdavian's route. The Diels-Alder cyclization between isophytol and 2,3,5-trimethylphenol would create H-Toc in one step, but does not maintain the *R* stereochemistry at the 2'-position, which would decrease specific binding to α -TTP. Therefore, the synthesis started with deprotection of acetylated α -tocopherol (AcO-Toc) under basic conditions (Figure 119). AcO-Toc is an inexpensive, stable, non-oxidizable source of tocopherol, which can be stored long-term in a cool environment.

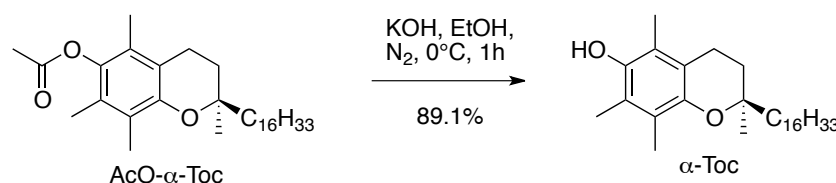


Figure 119. AcO- α -Toc deprotection to α -tocopherol.

α -Tocopherol was then reacted with trifluoromethanesulfonic anhydride to generate the triflate **41**.⁴²⁴ Hydrogenation of **41** with Pd/C 10% and H₂ was conducted in a Paar-shaker (15 psi). A faster reaction time is achieved when a pressurized autoclave system (Paar/Ashcroft) was used, which is capable of reaching pressures up to (60-70 psi). Running the reaction for 2-5 days ensured a high product yield (Figure 120).

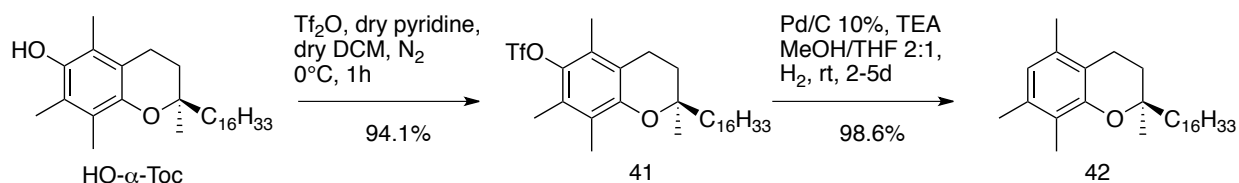


Figure 120. α -Toc conversion to α -tocopherol triflate **41, followed by reduction to H-Toc, **42**.**⁴²⁴

Chlorination of **42** with N-chlorosuccinimide (NCS) generated product **43** in 56% yield (Figure 121).⁴³⁰

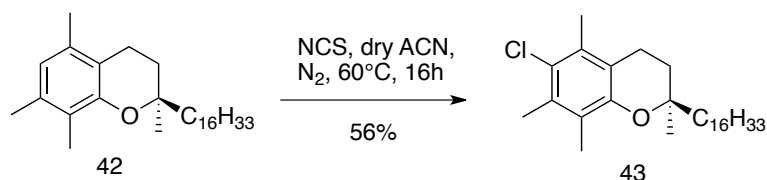


Figure 121. Chlorination of H-Toc **42 to Cl-Toc **43**.**⁴³⁰

Hydroxymethylation of **42** was first attempted with two equivalents of paraformaldehyde and *p*-TsOH in EtOH. Some small new spots were observed on TLC, but even after addition of an extra nine equivalents of paraformaldehyde and refluxing at 70° for several hours, the starting material was still the major component of the reaction. Dioxane was then chosen as the solvent to increase the solubility of the starting material. After refluxing for 30 h there several new polar spots were observed on TLC. The new spots were isolated, giving product **44** in a 14% yield (Figure 122).

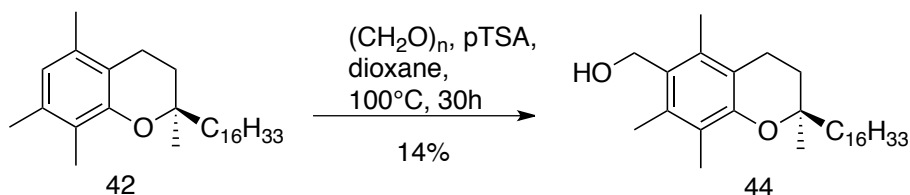


Figure 122. Hydroxymethylation of H-Toc **42 to HM-Toc **44**.**

An alternative method was attempted by first formylating at the 6-position, followed by reduction. Rieche's procedure was used, reacting H-Toc **42** with α,α' -dichloromethylmethylether (α,α' -Cl₂OMe) and titanium tetrachloride (TiCl₄), which produced **46** in a 95% yield.⁴²⁹ Scaling up the reaction (5× to a mass of 8g) lowered the yield slightly to 77% (Figure 123).

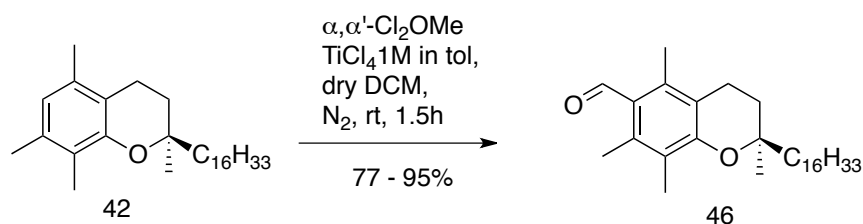


Figure 123. Rieche formylation of H-Toc 42 to product 46.⁴²⁹

Reduction of aldehyde **46** was successful with NaBH₄, creating product **43** in a 52% yield.

Reduction with LiAlH₄ increased the yield to 74-98% (Figure 124).

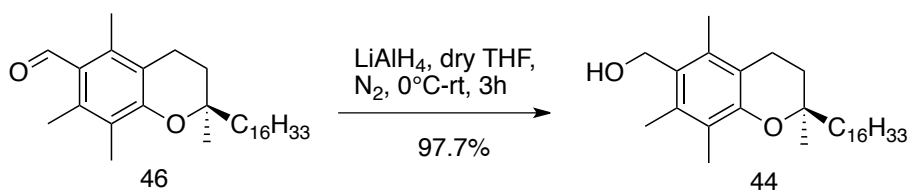


Figure 124. Reduction of 46 to HM-Toc 44.

7.2 Spectroscopic and chemical properties of HM-Toc

The maximum absorption of HM-Toc **44** measured by UV spectroscopy was at 278 nm & 287 nm (in EtOH), with a calculated extinction coefficient (ϵ) of 1080 cm⁻¹M⁻¹, significantly less than that for α -tocopherol 3056 cm⁻¹M⁻¹ (Figure 125).⁴³²

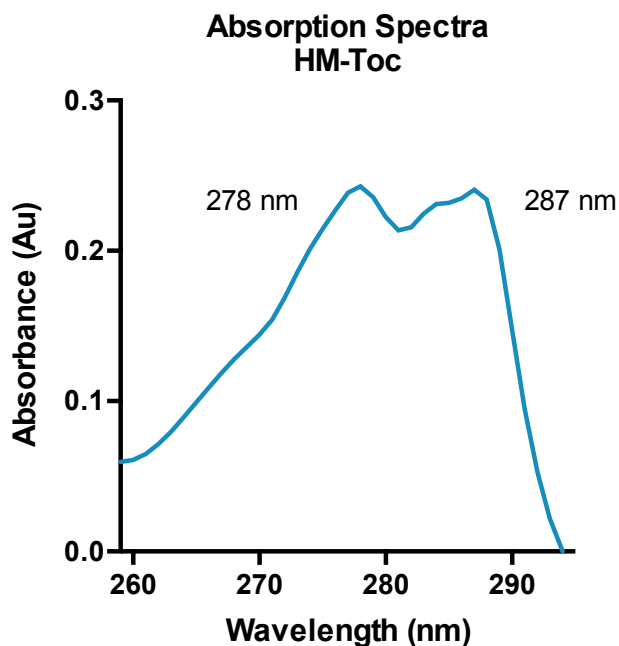


Figure 125. Absorbtion spectra HM-Toc in EtOH.

7.3 Binding studies

The new molecules were tested to see if they were capable of binding to α -TTP. A competitive binding assay against NBD-tocopherol was used to evaluate binding strength.²⁰¹

α -TTP was expressed the same way as described in previously (Section 1, Binding studies to α -TTP).

In a first assay, Cl-Toc **43** was titrated to TTP following Nava's protocol.²⁰¹ To determine the ability of chlorochroman **43** to bind to α -TTP, it was tested in a competitive assay with the well-characterized NBD-Toc. In the assay, 0.4 μ M α -TTP was saturated with 1.6 μ M NBD-C9-Toc in SET buffer and compound **43** was added in increments as a solution in EtOH (Figure 126). No decay in fluorescence (λ_{em} 535 nm) was observed even when 2 mM of **43** was added. α -Tocopherol addition to NBD-C9-Toc loaded α -TTP was used as a control experiment, which showed about 30% competition of the fluorophore after addition of 2 mM α -tocopherol. The

same extent of competition was seen in Nava's α -tocopherol competitive assay, which used 0.2 μ M α -TTP saturated with 1.0 μ M NBD-C9-Toc.²⁰¹

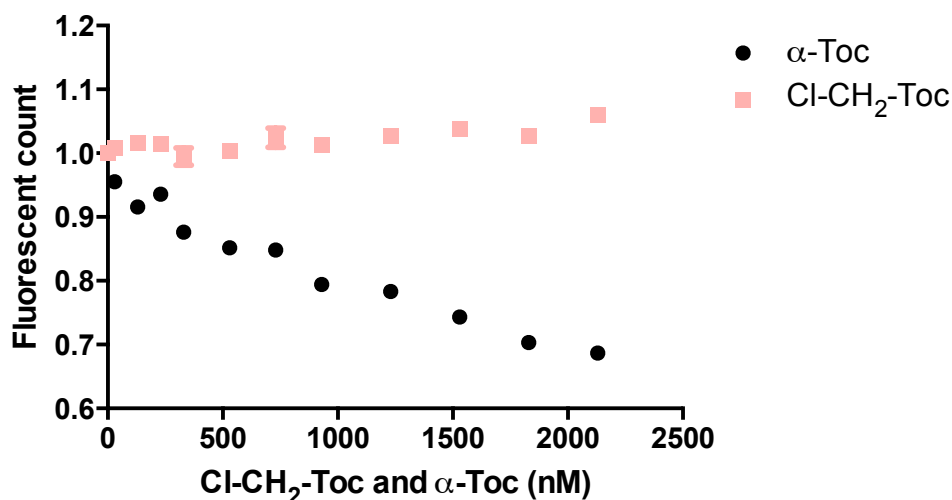


Figure 126. Competition assay of 0.4 μ M α -TTP, saturated with 1.6 μ M NBD-C9-Toc in SET buffer, with α -Toc and Cl-Toc in EtOH.

The graph was normalized to 1.0. The data was collected in triplicate (Cl-Toc) and error bars represent standard deviations from the mean.

This result proved that Cl-Toc (**43**) does not bind to α -TTP, even at high concentrations.

Therefore, no further tests were conducted with Cl-Toc.

Titration with HM-Toc **44** showed a positive result, seemingly competing for bound NBD-Toc with a similar efficiency to α -toc. HM-Toc plateaued at 1.5 mM and started to increase at higher concentration while the residual fluorescence following addition of tocopherol continued to drop (Figure 127).

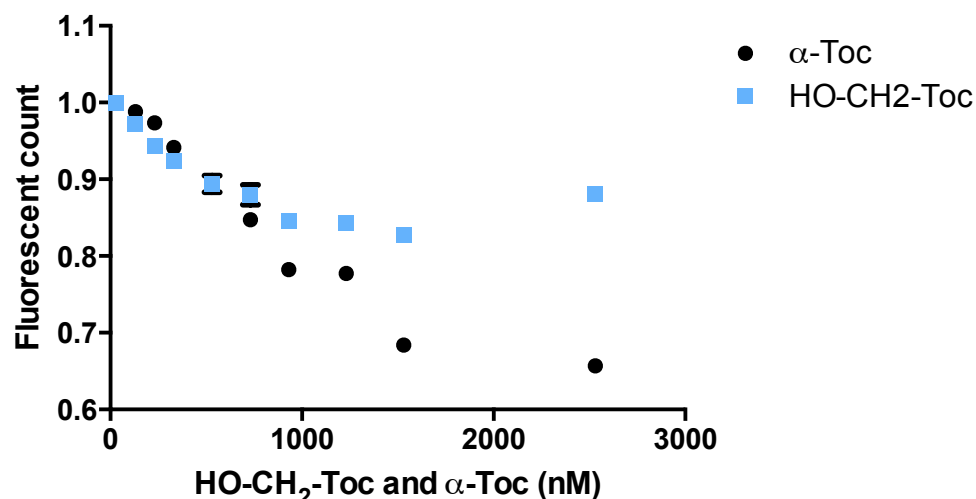


Figure 127. Competition assay of 0.4 μM α -TTP, saturated with 1.6 μM NBD-C9-Toc in SET buffer, with α -Toc and HM-Toc in EtOH.

The graph was normalized to 1.0. The data was collected in triplicate (CI-Toc) and error bars represent standard deviations from the mean.

To understand why fluorescence increase for 6-HM-Toc trials at higher concentration α -Toc was added to a solution of NBD-C9-Toc in SET buffer that lacked the α -TTP protein (Figure 128). HM-Toc increased the observed fluorescence by almost 50% at 1mM, whereas α -Toc had no such effect over the course of the titration. The increase observed is likely based on the formation of micellar structures between displaced NBD-C9-Toc and 6-HM-Toc. These structures provide a more hydrophobic environment which enhances the fluorescence of the NBD-fluorophore in aqueous media.

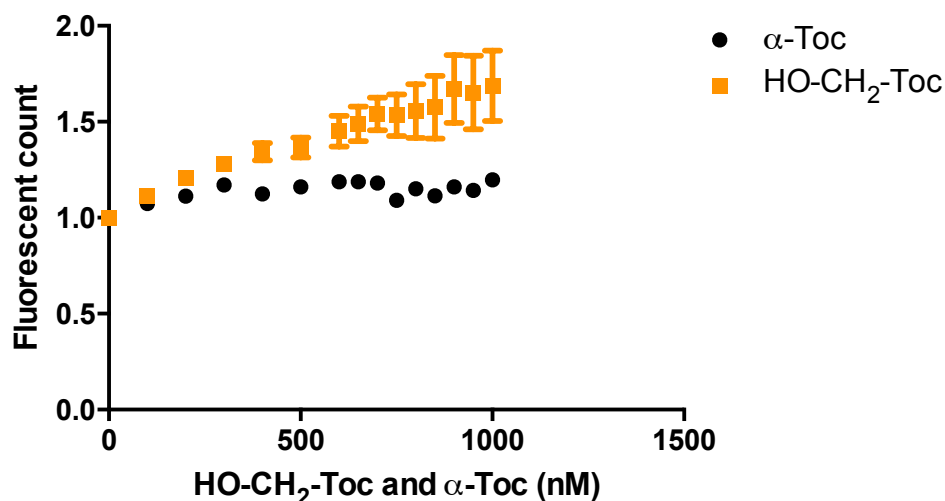


Figure 128. Micelle test 1.6 μM NBD-C9-Toc with HM-Toc and α -Toc in SET buffer.

The graph was normalized to 1.0. The data was collected in triplicate and error bars represent standard deviations from the mean.

A more reliable competition curve was obtained by subtracting the micellar data from the competition assay. α -Tocopherol follows the same decay trend as seen before in the Cl-Toc 43 titration (Figure 126). HM-Toc 44 thus appears to be an equal or marginally better competitor for α -TTP bound NBD-C9-Toc than natural α -tocopherol when the micelle data is removed from to the graph (Figure 129).

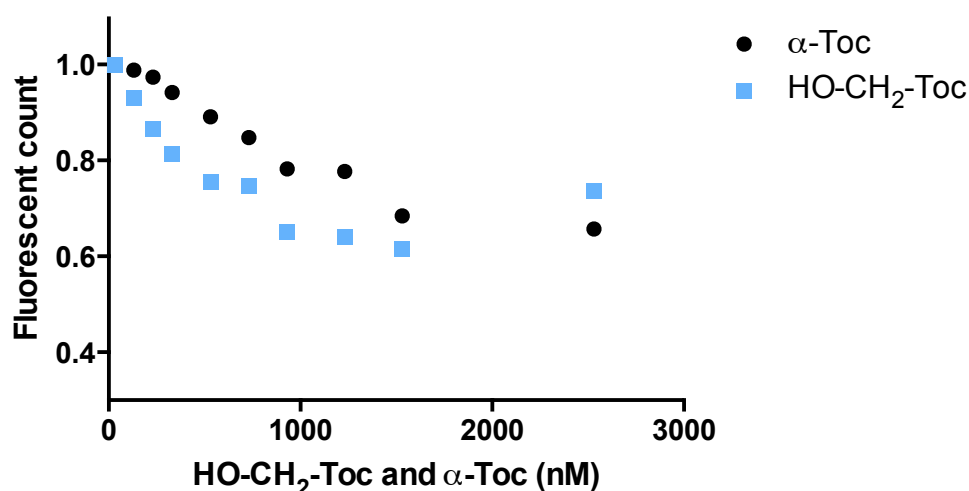


Figure 129. Competition assay of 0.4 μM α -TTP, saturated with 1.6 μM NBD-C9-Toc in SET buffer, with α -Toc and HM-Toc in EtOH adjusted with micelle data (Figure 137).

The graph was normalized to 1.0.

This result assures that the new HM-Toc binds to α -TTP.

7.4 Oxidation assay

Lipid peroxidation inhibition is tested by measuring the formation of conjugated dienes in liposomes in the presence of a postulated inhibitor. An immediate response is expected as seen by an increase of diene absorption in a UV/VIS spectrometer, observable at 230 nm. With α -tocopherol, there is a several minute delay, before the absorption at 230 nm increases (Figure 130).

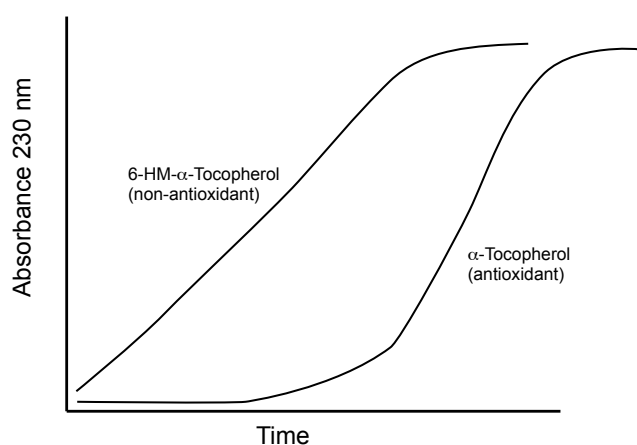
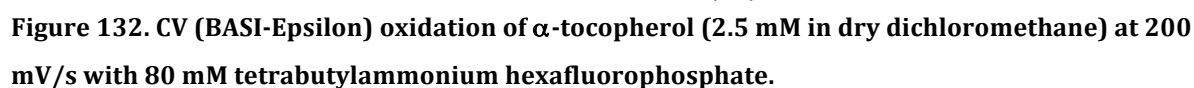


Figure 130. Expected UV absorption (230nm) of the non-antioxidant tocopherol.

Different conditions can be used to start the peroxidation. The hydrophilic radical initiator 2,2'-azobis(2-amidinopropane) dihydrochloride (AAPH) and the hydrophobic initiators azobis(isobutylnitrile) (AIBN), and 2'-azobis(2,4-dimethylvaleronitrile) (AMVN), and iron(II)chloride with H_2O_2 or copper(II)chloride with or without ascorbate.^{433,434,435} The lipids chosen were soyPC (Figure 131) that contains a rich supply of PUFA.



Cyclic voltammetry (CV) measurements on HM-Toc **44** were compared to the oxidation potential of α -tocopherol and H-Toc. Tocopherol showed two electron oxidation potentials around 1100 mV (Figure 132). The reversible wave has two potentials at 800 mV and 550 mV.



For HM-tocopherol the oxidation potential shifts to 1300 mV (Figure 143 HM-Toc). Similarly, the oxidation potential of H-Toc shows maxima at 1300 mV and 1700 mV (Figure 134 H-Toc).

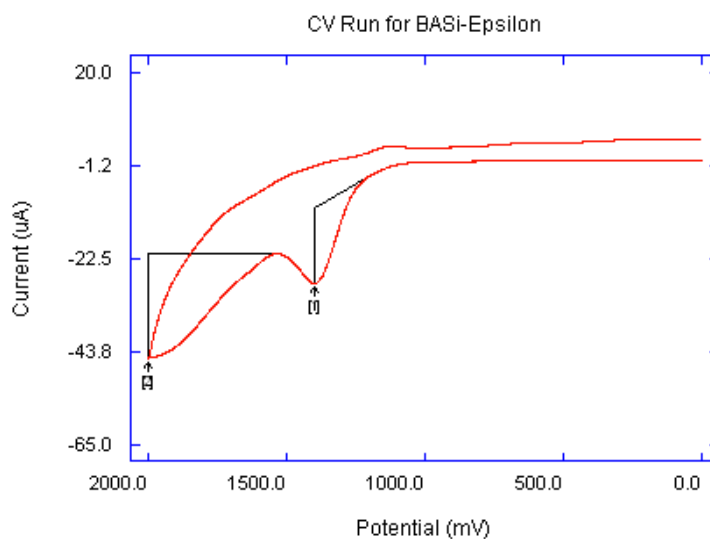


Figure 133. CV (BASI-Epsilon) oxidation of HM-Toc (2.5 mM in dry dichloromethane) at 200 mV/s with 80 mM tetrabutylammonium hexafluorophosphate.

Ag wire was used as a reference electrode.

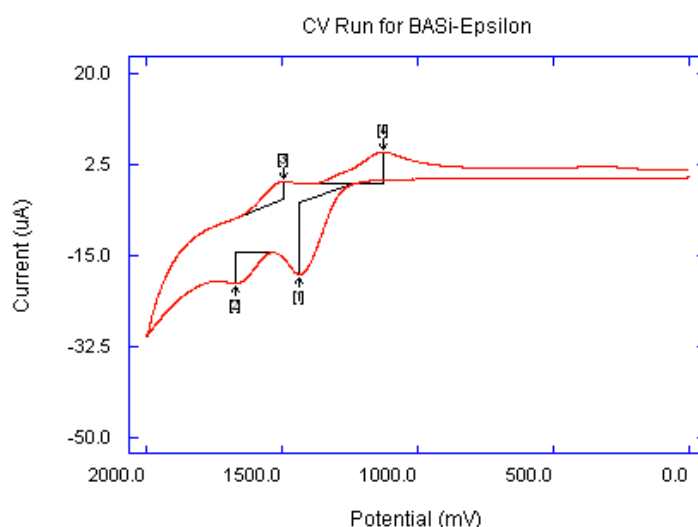


Figure 134. CV (BASI-Epsilon) oxidation of H-Toc (2.5 mM in dry dichloromethane) at 200 mV/s with 80 mM tetrabutylammonium hexafluorophosphate.

Ag wire was used as a reference electrode

These results indicate that, not surprisingly, the more electron rich phenols are more readily oxidized than the hydroxymethyl and unsubstituted analogues. CV studies on γ -, δ -tocopherols and α -, γ -, δ -tocotrienols by Kruger¹ showed a similar oxidation potential for α -tocopherol around 1100-1200 mV. Since the oxidation is conducted solely in dichloromethane, no direct

¹ Data by Nick Nick Krueger, MSc thesis, 2017

connection can be drawn to its antioxidant capability in cells, as the lipid environment influences the oxidation potential and rate. The antioxidant ability is based on the capability of donating a hydrogen atom to reactive radicals, and so the phenol should be a far better antioxidant than HM-Toc and H-Toc.⁴³⁶

The higher oxidation potential for HM-toc, was expected to lower the overall antioxidant capability in a cellular environment.

7.4.2 Lipid peroxidation

Oxidation of soy PC lipids with the radical initiator 2,2'-azobis(2,4-dimethylvaleronitrile), AMVN, indicated that the HM-Toc **44** is not capable of inhibiting lipid peroxidation (Figure 145). α -Tocopherol efficiently inhibits the formation of conjugated dienes as observed by an increase in UV absorption at 234 nm for about the first 75 minutes of the assay, at which point it has been fully consumed and a steady increase in absorbance was observed with a slope similar to both the assay with no antioxidant and that containing 6-HM- α -Toc. The data clearly indicates that HM-Toc cannot act as an antioxidant in a simple lipid peroxidation assay.

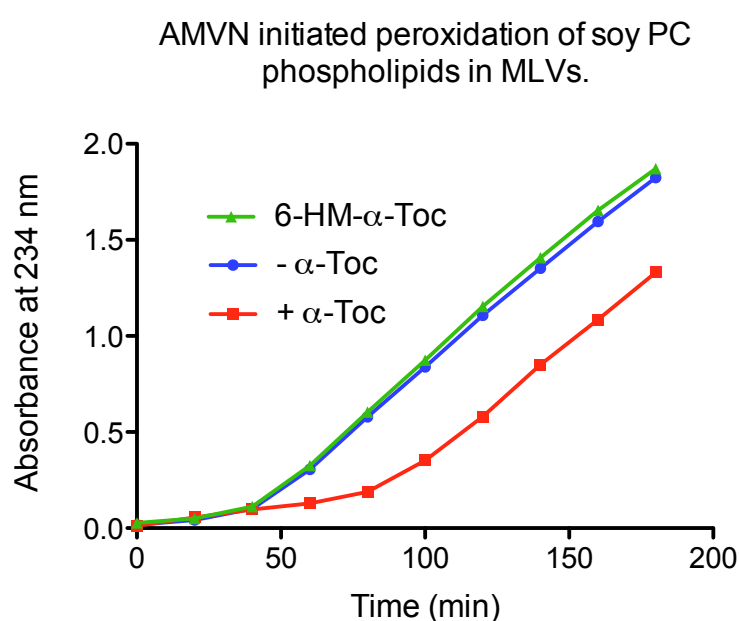


Figure 135. AMVN initiated oxidation of multilamellar SoyPC vesicle with HM-Toc & α -Toc.

7.4.3 Cellular oxidation studies

Knowing that HM-Toc can bind to α -TTP and that it is not an effective antioxidant in vitro, the compound was sent to our collaborators at Case Western Reserve University to study whether HM-Toc could rescue cells and animals (mice) that were subjected to oxidative stress. Six grams of HM-Toc were produced for this purpose. The overall yield was 50% over five steps starting from AcO-Toc.

The stability of the product was assessed, after our collaborators observed impurities in ethanol stock solutions. The compound was tested in biologically relevant solvents and the effect of different pH conditions for certain periods of time. Acidic conditions were mimicked by addition of hydrochloric acid, basic conditions with potassium carbonate (Table 13). ^1H -NMR spectroscopy was used to follow the decay.

| Solubility | Acidic | Neutral | Basic | Time |
|-------------------|--------|---------|-------|---------|
| EtOH | 1.2% | - | - | 1h |
| EtOH | 20% | - | - | 30h |
| EtOH | 25% | - | - | 40h |
| Dioxane | - | - | - | 9 days |
| DMSO | - | - | - | 10 days |
| EtOH + TKE 1:1 | | - | | 30h |

Table 13. Stability assessment of HM-Toc.

Aqueous HCl or potassium carbonate was added to the HM solutions and stored for the described time. The solvents were evaporated and extracted with water and hexane, the organic phase was then dried over sodium sulphate. ^1H -NMR in CDCl_3 was used to monitor the decay. Green (-): No change was observed by ^1H -NMR. Yellow: low quantities of byproduct (% of 47 and 48 combined) were detected. Red: large amounts of byproduct (% of 47 and 48 combined) were detected. White: conditions not tested.

Decomposition under acidic conditions was first recognized during the analysis of the synthetic HM-Toc. After reduction of aldehyde **45** with LiAlH_4 , analysis by ^1H -NMR spectroscopy

indicated impurities in the product. It was discovered that the older CDCl_3 solvent used for NMR sample preparation was the problem. When the CDCl_3 was washed through a small pad of basic alumina, no byproduct was observed. An experiment was conducted whereby the HM-Toc was monitored over time. The new compound formed was the self-condensed HM-Toc ether **47**. Benzylic ethyl ether **48** was formed using protic solvents like EtOH from under slightly acetic condition (Figure 136). No decay was observed when the compound was stored in basic or neutral environment.

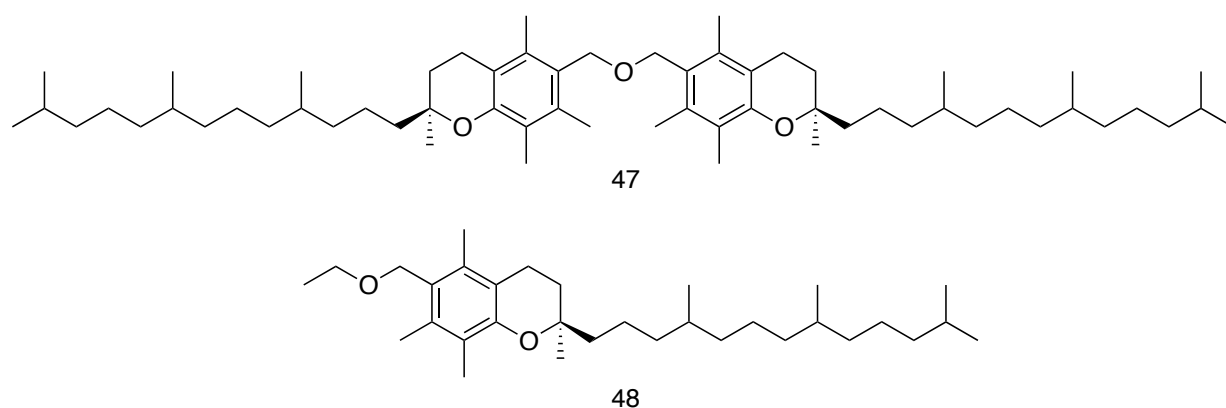


Figure 136. Products observed during the assessment of HM-Toc stability in acetic media.

Dimer 47 in old CDCl_3 and 48 in EtOH.

7.5 Cell studies and Animal trials

As mentioned, the new ligand will be tested for their ability to rescue α -TTP knockout mice.¹¹¹ A concentration dependent cytotoxicity screen of the new ligand will be conducted in cell lines that have not been previously stressed. Any possible toxic effects by the new molecule would have to be considered in the study with deficient mice. The ligand's ability to reinstate normal conditions will be tested first in oxidatively stressed astrocytes. In these stressed cells it will also be determined if the *ttpa* gene has been upregulated.

α -TTP knockout mice will be used to mimic the vitamin-deficient state. These mice show the first signs of ataxia after 10-12 days after birth. Three groups of α -TTP knockout mice will be tested: with the new ligand in the diet (800mg ligand / kg diet), with α -tocopherol (800mg α -

tocopherol / kg diet) and with a α -tocopherol depleted diet. The hypothesis is that tocopherol supplementation will prevent the development of ataxia, whereas supplementation with 6-HM-Toc will not.

Preliminary work in cells has been finished, but the study is currently ongoing.

8 Conclusion

The designed non-antioxidant tocopherols Cl- and HM-Toc were successfully synthesized without major issues in moderate to high yields in each step. HM-Toc showed a similar affinity to α -TTP as natural α -tocopherol, but Cl-Toc did not bind at all to α -TTP. Cl-Toc would have been better in terms of oxidative resistance, but the binding affinity had to be maintained. Despite this, a high oxidation potential was observed for HM-Toc by cyclic voltammetry. Lipid peroxidation assays with AMVN showed that HM-Toc is not an antioxidant. Cell and animal studies are ongoing. With the result of the current biological studies on HM-Toc activity as an antioxidant will the ongoing debate about the importance of the antioxidant function of tocopherols to protect membranes be solved.

9 Introduction

Medical research scientists have had great success in treating or even curing most life threatening diseases, most often without inducing additional harm to the patient. But despite this tremendous costly research effort, no broad applicable cure been found for the king of all diseases, cancer. Cancer is described as a malfunctioning of cells associated with uncontrolled cell reproduction that spreads through the vascular and lymph system, leading potentially to organ and system failure, and death.^{437,438}

The causes of cancer are diverse and challenging to uncover, and equally more so to prevent. The disease is frequently traced back to a chronic exposure to low levels of a toxin over a prolonged time. External sources like intense radiation (α , β , γ rays) or chemicals used in cigarettes (formaldehyde) or produced during combustion, pesticides (dioxines), industrial solvents (benzene) and mining (heavy metals like chromium) have all been shown in many studies to induce cancer. DNA and RNA viruses, specifically Epstein-Baar, hepatitis B, human papilloma viruses (DNA) and hepatitis C, human T lymphotropic virus type 1 (RNA), have been shown to induce cancer.⁴³⁹ Lowering the possible exposure to harmful sources can reduce the risk, but nobody is guaranteed a cancer-free life. Life with cancer is like a game of roulette. You can be lucky by having a non-malignant tumor, which is operable or is diagnosed early enough to be treatable without major side effects. People with prostate cancer can live up to several decades without any returned symptoms (in the USA) after successful treatment. And yet other cancers guarantee a $> 90\%$ mortality, as it is for pancreatic cancer (Table 137).^{438,440}

| Cancer site | 5-y relative survival (95% CI) | | Change over time (95% CI) | |
|----------------------------------|--------------------------------|---------------------|---------------------------|------------------------|
| | 1975–1977 | 2006–2012 | Absolute, % | Proportional, % |
| All sites (case-mix adjusted) | 50.3 (50.1 to 50.6) | 66.4 (66.2 to 66.5) | 16.0 (15.7 to 16.3) | 31.9 (31.1 to 32.6) |
| Lung and bronchus | 12.2 (11.8 to 12.6) | 18.7 (18.4 to 19.1) | 6.5 (6.0 to 7.1) | 53.6 (47.5 to 59.7) |
| Colon and rectum | 49.8 (49.1 to 50.6) | 66.2 (65.7 to 66.7) | 16.4 (15.5 to 17.3) | 32.9 (30.7 to 35.1) |
| Breast (female) | 74.8 (74.2 to 75.5) | 90.8 (90.5 to 91.1) | 16.0 (15.3 to 16.7) | 21.4 (20.3 to 22.5) |
| Prostate | 67.8 (66.7 to 68.9) | 99.3 (99.1 to 99.5) | 31.5 (30.4 to 32.6) | 46.5 (44.2 to 48.9) |
| Oral cavity and pharynx | 52.5 (51.1 to 54.0) | 67.0 (66.1 to 67.9) | 14.4 (12.7 to 16.1) | 27.4 (23.5 to 31.4) |
| Esophagus | 5.0 (4.0 to 6.2) | 20.5 (19.4 to 21.7) | 15.5 (13.9 to 17.1) | 308.1 (217.6 to 398.6) |
| Stomach | 15.2 (14.1 to 16.3) | 31.1 (30.1 to 32.2) | 15.9 (14.4 to 17.4) | 104.7 (88.2 to 121.1) |
| Pancreas | 2.5 (2.0 to 3.0) | 8.5 (8.0 to 9.0) | 6.0 (5.3 to 6.7) | 244.7 (175.9 to 313.5) |
| Liver and intrahepatic bile duct | 3.4 (2.4 to 4.7) | 18.1 (17.3 to 18.9) | 14.6 (13.3 to 16.0) | 427.6 (251.4 to 603.9) |
| Urinary bladder | 72.3 (70.9 to 73.6) | 78.5 (77.7 to 79.2) | 6.2 (4.6 to 7.7) | 8.5 (6.3 to 10.8) |
| Kidney and renal pelvis | 50.1 (48.1 to 52.0) | 74.7 (73.9 to 75.4) | 24.6 (22.6 to 26.7) | 49.2 (43.3 to 55.1) |
| Melanoma of the skin | 81.9 (80.4 to 83.3) | 93.2 (92.6 to 93.6) | 11.3 (9.8 to 12.8) | 13.8 (11.7 to 15.8) |
| Cervix uteri | 69.1 (67.4 to 70.7) | 68.8 (67.4 to 70.2) | −0.3 (−2.4 to 1.8) | −0.4 (−3.5 to 2.7) |
| Corpus and uterus, NOS | 86.9 (86.0 to 87.7) | 83.4 (82.7 to 84.0) | −3.5 (−4.6 to −2.4) | −4.0 (−5.3 to −2.8) |
| Ovary | 36.0 (34.5 to 37.6) | 46.4 (45.3 to 47.6) | 10.4 (8.5 to 12.3) | 28.9 (22.5 to 35.3) |
| Non-Hodgkin lymphoma | 46.5 (45.0 to 48.0) | 72.6 (71.9 to 73.2) | 26.1 (24.4 to 27.7) | 56.1 (50.8 to 61.3) |
| Myeloma | 24.6 (22.6 to 26.6) | 50.2 (48.9 to 51.6) | 25.7 (23.3 to 28.1) | 104.5 (87.0 to 122.0) |
| Leukemia | 34.2 (32.8 to 35.5) | 62.7 (61.8 to 63.5) | 28.5 (26.9 to 30.1) | 83.6 (75.9 to 91.2) |
| Brain and other nervous system | 22.4 (21.0 to 23.9) | 35.0 (34.0 to 36.0) | 12.5 (10.8 to 14.3) | 55.9 (44.6 to 67.1) |
| Thyroid | 92.1 (90.7 to 93.3) | 98.3 (97.9 to 98.6) | 6.1 (4.8 to 7.4) | 6.6 (5.1 to 8.2) |

Figure 137. Relative survival of cancer over a 5-year span in the USA.

Comparison between data collected from 1975-1977 to 2006-2012 with a high confidence interval. The change over time between the collected data is given as an absolute and proportional percentage. NOS: not otherwise specified. ⁴⁴⁰

In cancer your own cells start to work against you. The close similarity of cancerous cells to normal cells in the early stages of the disease lowers the chance of detection. Further, cancer cells differ from patient to patient, as the cause of uncontrolled growth varies.⁴⁴¹

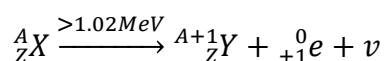
To kill malignant cells cytotoxic drugs or radiation are frequently used and almost all cancer types have shown susceptibility to a certain degree. The drawback with these treatments is the uniform damage across all tissue, especially in the near environment around the cancer. It is often the case that the patient suffers worse health effects as a direct effect to the treatment. Side effects include weakness, fatigue, loss of appetite, loss of hair and a weakened immune system that leaves the patient vulnerable to infection.⁴⁴² A guaranteed cure is rarely possible. Even if the cancerous solid tumour has been reduced in size, or blood-borne tumours reduced to undetectable levels, there remains the possibility that surviving cancer cells will continue to grow. It is often the case that such relapsed cases show a higher resistance to the chemotherapeutic agent used in the first round of treatment.⁴⁴³ More indepth research to

increase cancer cell specific treatment is crucial to patient survival and well-being.⁴⁴⁴ Treatment of malignant tissue is first and foremost dependent on its localization in the body.

9.1 Positron emission tomography (PET)

Nuclear magnetic imaging techniques are used to monitor and visualize the physiological functioning of tissues and cells with low risk to the patient. Positron emission tomography (PET) is a nuclear imaging technique which relies on the decay of radionuclides. The decay of the nuclei chosen results in the emission of a positively charged electron (e^+ , β^+), called positron, and a neutrino (ν), which both are produced during the conversion of a proton into a neutron (1).⁴⁴⁵ Energy of at least 1.02 MeV between parent and daughter nuclei is necessary for a nucleus to undergo β^+ decay. If the energy is below 1.02 MeV, β^+ decay is forbidden and an electron of the inner shells (k or l_I shell) reacting with the excess proton in a process called electron capture (2). Thereby an electron-hole is formed in the $k(l_I)$ shell after neutron formation. Two specific types of electronic transitions can occur to fill the empty electron-hole (Figure 138). An electron from an outer shell fills the electron-hole of the inner shell (l_I to k transition), with emission of an x-ray photon, leaving a positively charged atom behind. The x-ray emitted has a distinct wavelength, depending on which shell the electron has transitioned from. This process is better known as x-ray fluorescence. Alternatively the transition energy is transferred to an electron in a higher shell (l_x, m, n etc.), which is then ejected from an atom. This specific decay process is also known as Auger-Meitner effect and the particles emitted are so-called Auger electrons. An example of 100% electron capture is the decay of ^{83}Rb to ^{83}Kr , emitting an energy of 0.9MeV.⁴⁴⁵

1



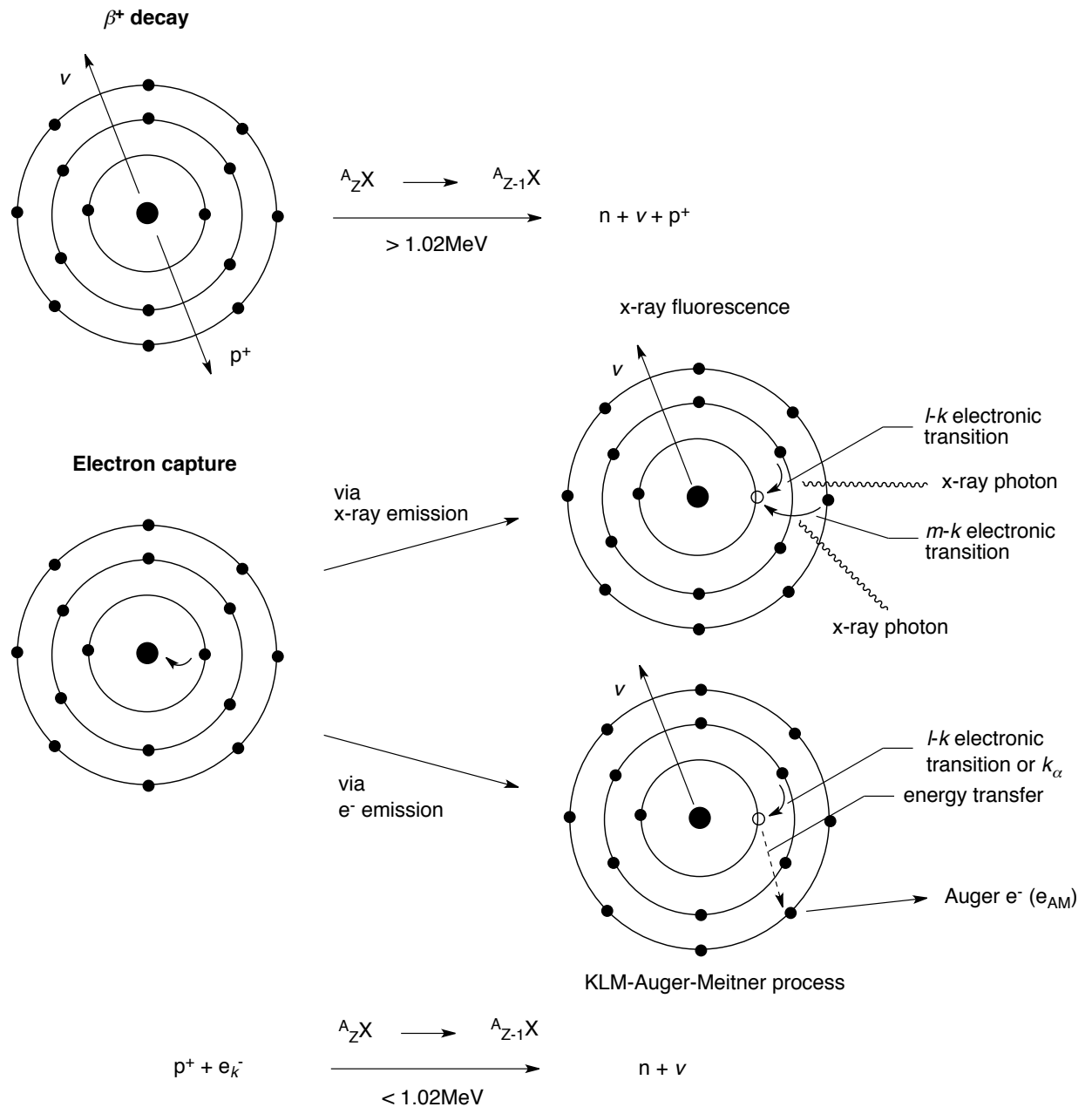
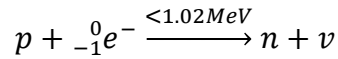


Figure 138. Positron emission (β^+) and electron capture via x-ray fluorescence or Auger electron emission.⁴⁴⁵

A positron (e^+) travels some millimeters in tissue losing most of its energy before reacting with an electron (e^-) in an event called electron–positron annihilation, which results in the perpendicular emission of two gamma ray photons. These two photons travel with an energy of 511 keV ($1.02\text{ MeV} : 2 = 511\text{ keV}$) and are recognized by a circular detector around the patient (Figure 139). This type of data collection is defined as coincidence counting and allows for an

emitted pair of γ -photons to record the position of positron annihilation. Because the annihilation radiation is high in energy are most of the photons are detected. Despite the small offset in electron–positron annihilation from the original decay, scattering effects of photons and photon annihilation on tissue provides on average a resolution of 3-7 mm with PET.⁴⁴⁵

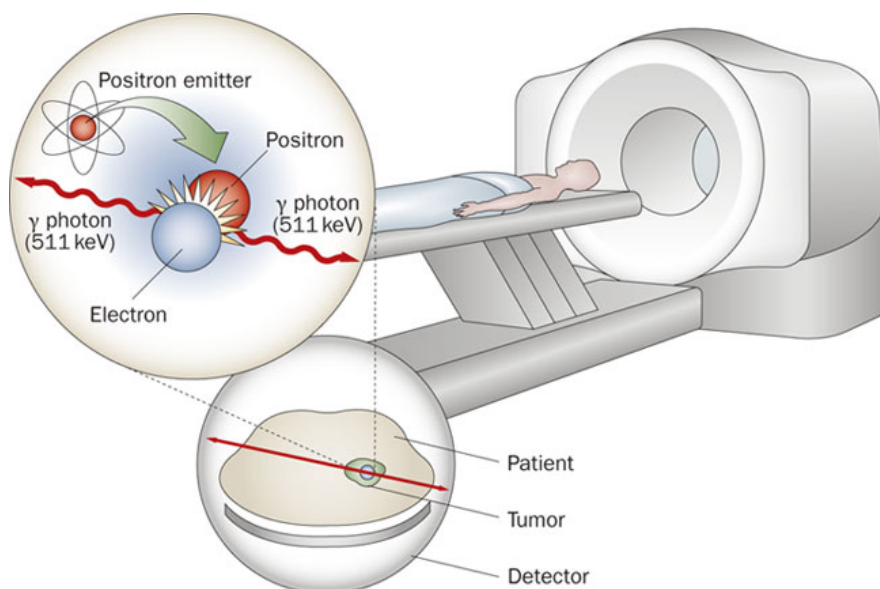
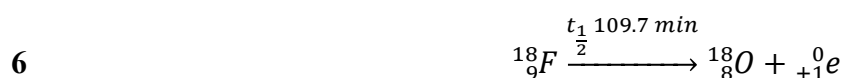


Figure 139. Positron annihilation, formation of two γ -photons each having an energy of 511keV.⁴⁵⁰

The PET marker can be an analog of a molecule of interest bearing within its structure radionuclides such as ^{15}O , ^{13}N , ^{11}C and ^{18}F , suitable for acquiring in vivo biochemical and physiological information about a tissue or an organ.⁴⁴⁵ The nuclei vary in their half lives ($t_{\frac{1}{2}}$), from 2 min up to 109 min (3-6). These PET agents have a high β^+ transition probability all above 97% (C, O and N have a 100% probability).⁴⁴⁵



The half-life states describes the loss of half a radionuclides initial activity in a certain time and creates for each radionuclei its own decay constant (λ) (7).⁴⁴⁵

$$7 \quad \lambda = \frac{0.693}{t_{\frac{1}{2}}}$$

The rate of decay, called activity (A), is needed to calculate the nummers of nuclei (N) left after the initial time (8). The Si-unit is the Bequerel (Bq) and describes the number of decays per second.

$$8 \quad A = \lambda N$$

To determine the amounts of radionuclei and radioactivity the activity after a certain time (A_t) is calculated by plotting the initial activity (A_0) against time (t) (9).⁴⁴⁵

$$9 \quad A_t = A_0 e^{-\lambda t}$$

Radioactive exposure has to be kept to a minimum in a patient to minimize radiation damage in cells. When looking at living organisms radiation is measured as a response to a biological effect. The SI-unit gray (Gy) describes the deposition of a joule of radiation in a kilogram (1 J/kg) of matter (tissue).⁴⁴⁵ When an imminent response to large amounts of radiation occurs the gray unit is used to describe the health effects from the absorbed dose. In cases of small amounts of radiation, as it is with PET scans, a so-called radiation weighting factor (W_r) is used to scale the different radiation (α -, β -, γ -, p-, n-particles) in terms of their impact on the biological tissue and is described by the SI-unit Sievert (Table 14).^{446 447}

| Type of radiation | W_r |
|--|-------|
| X-rays, γ rays, β particles | 1.0 |
| Neutrons and protons | 10.0 |
| α particles | 20.0 |
| Heavy ions | 20.0 |

Table 14. Radiation weight factor (W_r) of different radiation types.⁴⁴⁷

Sieverts describes the equivalent dose absorbed by a tissue (H_T in Sv) and therefore depends on the type of the radiation weighting factor W_R and the amounts of a specific radiation a certain tissue can absorb ($D_{T,r}$ in grays) (10).^{446,447}

10
$$H_T = \sum_R W_R D_{T,r}$$

Since PET scans are directly injected into the body the long-term exposure of the effective dose per organ / body is calculated (H_E), as certain organs cover a larger area in the body. The tissue weigh factor (W_T) determines the biological susceptibility of the tissue to a certain type of radiation (Table 15).^{446,447}

11
$$H_E = \sum_T W_T H_T$$

| Tissue | W_T^a |
|-----------------|---------|
| Gonads | 0.25 |
| Breast | 0.15 |
| Red bone marrow | 0.12 |
| Lungs | 0.12 |
| Thyroid | 0.03 |
| Bone surfaces | 0.03 |
| Remainder | 0.30 |
| Total body | 1.00 |

Table 15. Tissue weigh factor (W_T).

(a) 10th Code of federal regulation page 20.⁴⁴⁷

Radiation exposure is tightly regulated, as high doses induce chronic health problems like cancer. In the US each person receives a dose of 3.1 mSv as background radiation, from radioactive gases like radon (^{222}Ra) and cosmic / terrestrial radiation. Doses of > 500 mSv are known to induce cancer.⁴⁴⁸

9.1.1 Clinical PET Tracer

Most PET markers have ^{18}F incorporated in their structure because it has the longest half-life of all relevant second period β^+ emitters. In a recent computer tomography (CT)/PET scan study the effective dose of ^{18}F -FDG and ^{18}F -*L*-DOPA were tested.⁴⁴⁹ CT scans are run with PET scans to create a background image of the patient, which is overlayed with the PET image to identify metabolic hotspots with higher percision. ^{18}F -FDG is a glucose analog containing a ^{18}F at the C-2 position and is used as a standard metabolic tracker to detect cancer.^{450,451} ^{18}F *L*-DOPA is used to study neurological diseases like Parkinson's disease.⁴⁵²

The study focused on the dose in the whole body (60kg) and the brain in 300 patients. PET scans apply around 1.6 MBq/kg body weight, 2x for CT/PET. An ^{18}F -FDG dose of 370 MBq was the effective dose 6.5-18 mSv (PET only, tube current 100-350 mA). CT scans add around 50% of mSv to the PET imaging. The overall exposure was around 12-36 mSv per scan and 4-12 times the natural dose exposed per year. However, the fast clearance of the PET agents form the body lowers the risk of cancer development to a minimum.⁴⁵³

Many different ^{18}F based PET agents like ^{18}F -Fluciclovine and ^{18}F -Fluoroethyltyrosine are used to detect various cancer types. ^{18}F -containing molecules like ^{18}F -Flutemetamol or ^{18}F -Cyclofoxy have clinical significance in the study of neurological diseases like addictions and Alzheimer's and Parkinson's disease (Figure 140).^{454,455,456,457}

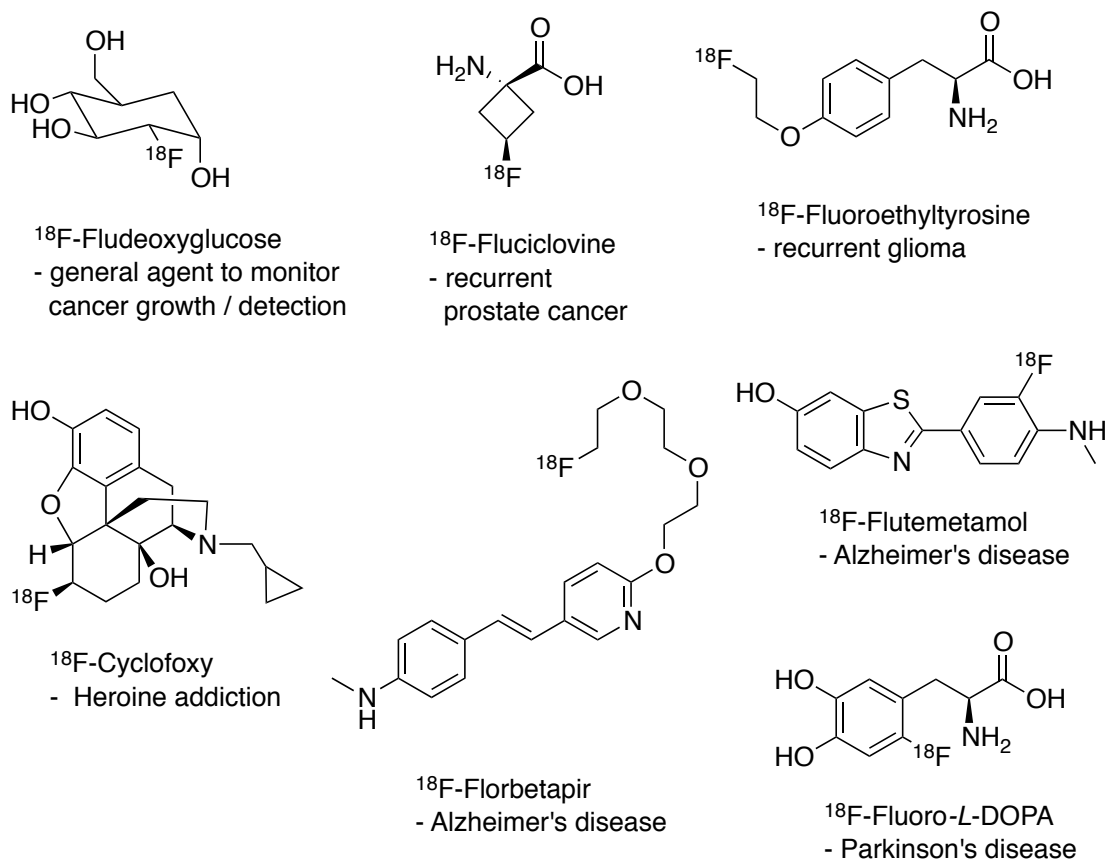


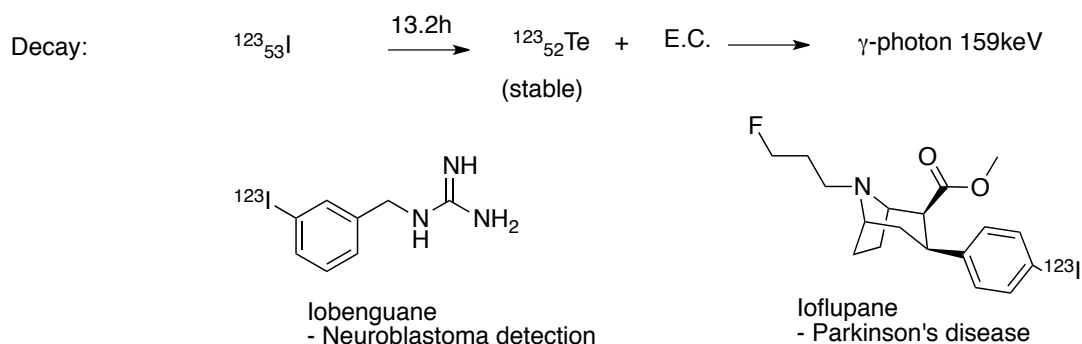
Figure 140. ¹⁸F Radiotracers of biological importance towards the study of cancer (Fludeoxyglucose, Fluciclovine, fluoroethyltyrosine), neurodegenerative diseases (Flutemetamol, Fluoro-L-DOPA, Florbetair) and addictions (Cyclofoxy).⁴⁵⁰⁴⁵⁴⁴⁵⁷

9.1.2 Single-photon emission computed tomography SPECT

The closely related technique called single-photon emission computed tomography (SPECT) has in comparison to PET a lower resolution of 7-12 mm. SPECT's disadvantage is the annihilation of only one, weaker photon upon nucleide decay. To detect the photon one or several large scintillation cameras (0.5 m-0.5 m diameter) are moved 180° around the patient in an orbital or body-contour orbit around the patient.⁴⁵⁸ Movement of the detector is often restricted to 180° as 360° lowers the resolution, which compared to PET offers less sides of detection. The main problem is the use of collimators in the scintillation cameras, lowering the total amount of radiation detected to a minimum.⁴⁴⁵

The nuclei commonly used in SPECT are ^{123}I and $^{99\text{m}}\text{Tc}$ for myocardial perfusion, brain or bone scans (Figure 141). Both nuclei have energetically lower γ -photons emitted, which leads to increased small-angle photon scattering and therefore a smaller signal to noise ratio (^{123}I = 159 keV, $^{99\text{m}}\text{Tc}$ = 98.6% 140.5 keV, 1.4% 142.6 keV). A larger amount of SPECT agent is required to obtain a qualitatively good image. Patients with thyroid cancer obtain doses of 5.5-7.4 GBq of ^{123}I -imaging agents and up to 29.5 GBq in repeated treatments. SPECT imaging is more often used to study longer lasting events in the brain and heart.⁴⁴⁵

^{123}I -iodine



$^{99\text{m}}\text{Tc}$ -technecium

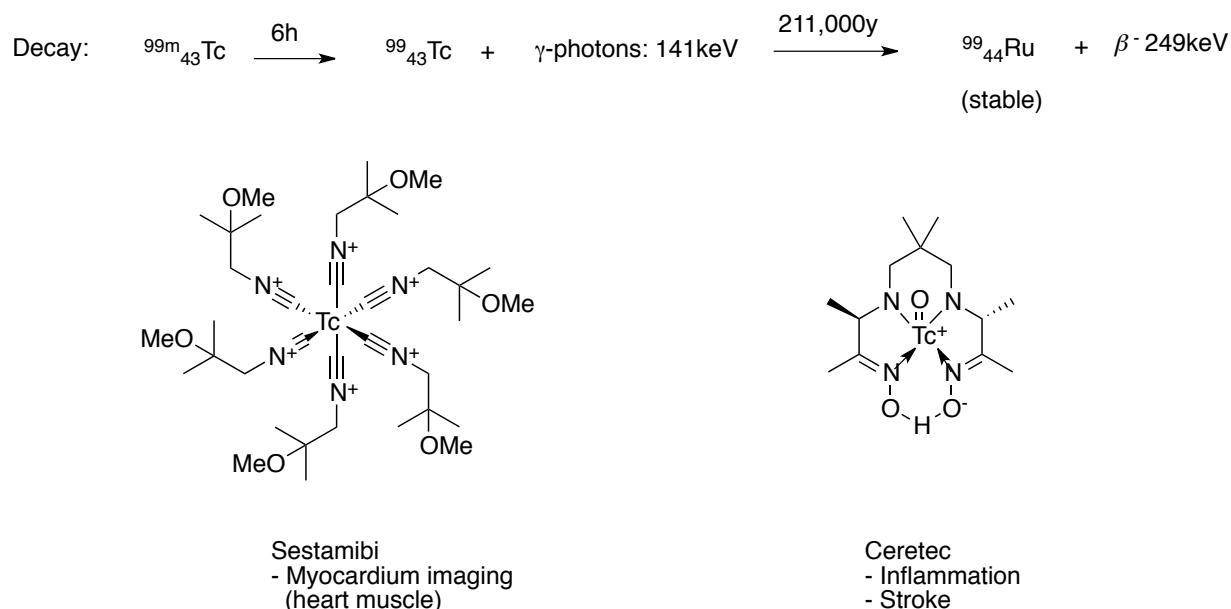


Figure 141. SPECT imaging agents based on ^{123}I (Iobenguane, Ioflupane) and $^{99\text{m}}\text{Tc}$ (Sestamibi, Ceretec) and the nuclei decay times and emitted particle energies.

9.1.3 ^{18}F radio-nuclide synthesis

Radionucleotides for positron emission tomography are synthesized in cyclotrons. Cyclotrons accelerate charged particles like protons, deuterons and alpha-particles in an outwards spiralling trajectory. Two circular electromagnets create a perpendicular magnetic field holding the particles in a planar space. The charged particles are added in the middle of a metal vacuum chamber and the magnetic field induces circular motion perpendicular to the magnetic field. To accelerate the particles two semi-circular, hollow, D-shaped, oscillating high-frequency generating electrodes (dees) are used, which surround the particles. In between the semi-circles is a small gap, which is needed for particles to break the circular motion in an outwards spiralling motion (acceleration gap). In each turn passing the acceleration gap the electrodes are switched to the same pole as the particle, creating static repulsion. By increasing the frequency of the electrode, each passing turn the charged particle is accelerated. At the furthest point of the circle the particle has the necessary energy to induce a nuclear reaction and is ejected into a reaction chamber (Figure 142).⁴⁴⁷

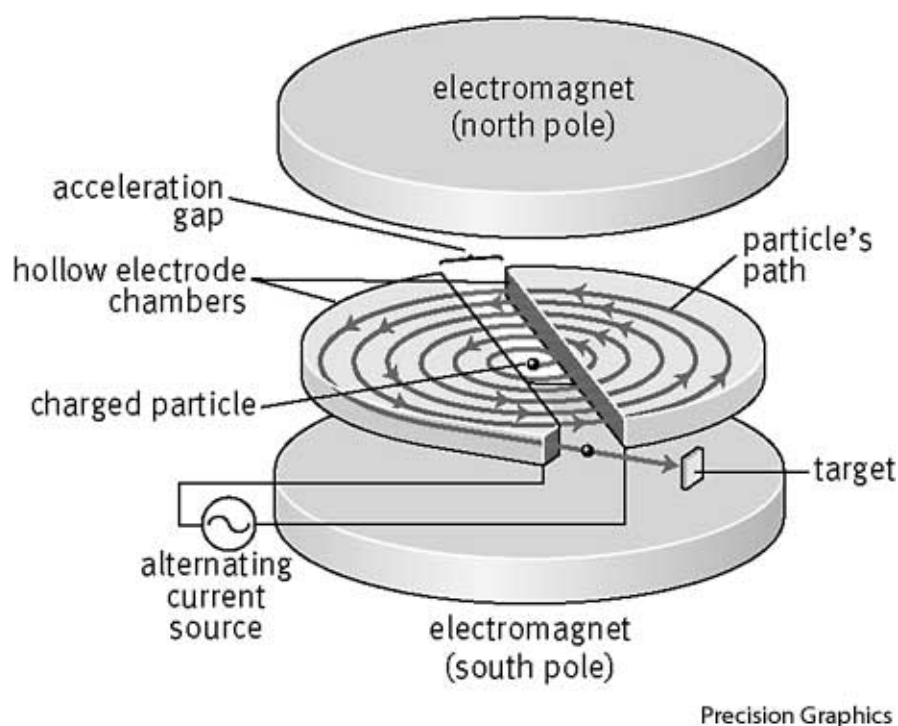


Figure 142. Particle acceleration in a cyclotron.

Particles increase in velocity in a spiral motion perpendicular to an electromagnetic field with the use of static repulsion induced by oscillation of two D-shaped electrodes.⁴⁵⁹

The centipetall force (F_C) required to maintain a particle in the spiral path depends on the mass of the particle (m), its velocity (v) and the radius (r) from the center of the chamber (12).^{445,447}

$$12 \quad F_C = \frac{mv^2}{r}$$

The magnetic field strength (F_B) sets the limit for the maximum possible energy reached. The Lorenze force describes the force of a moving (v) charged particle (q) in a magnetic field (B) (13).

$$13 \quad F_B = qvB$$

The energy of the particle depends on the mass (m) and charge (q) of the particle, the particles velocity (v) upon exit of the circle, the radius (R) of the circle before exiting the acceleration chamber and the magnetic field (B) (14).^{445,447}

$$14 \quad E = \frac{1}{2}mv^2 = \frac{q^2B^2R^2}{2m}$$

A median energy difference of > 1.02 MeV is necessary for a nuclei to undergo (β^+) decay. The more energy is inserted into the nucleus the more likely is positron decay. In the case of ^{18}F the maximum energy possible in the nuclei is 1.655 MeV, resulting in an energy loss upon β^+ transition of 0.634 MeV. On average the β^+ particle has an energy of 250 keV.⁴⁶⁰ The activity (A) of a daughter nuclei can be increased by longer bombardment or increasing the energy of the charged particle and the intensity (I) of irradiation (15). A quantitative calculation can be used to figure out the activity achieved, by knowing the intensity (I) of the particle beam (nr of particles/cm² s), the number of targeted nuclei (n), formation cross section in cm² (σ , given in barn, were 1 barn = 10⁻¹²cm²), decay constant (λ) and the bombardment time (t). The unit of

activity is given in MBq/mAh, where mAh describes the intensity used of the beam (1 Ampere (A) = 1 Coulomb (C/s). 1 C = 6.25×10^{18} protons).⁴⁴⁷

15

$$A = \lambda N (1 - e^{-\lambda t})$$

The activity is more commonly expressed as the specific activity (SA), which describes the radioactivity per mass (m) of a radioactive nucleotide (MBq/mg) (16). Often the unit is expressed as MBq/mole or mCi/ μ mol.

16

$$SA = \frac{A}{m} = \frac{\lambda N}{m}$$

9.1.4 ^{18}F nuclide synthesis

Different ways are used to produce radioactive fluorine, either as fluoride ions $^{18}\text{F}^-$ or as fluorine gas $^{18}\text{F}_2$. $^{18}\text{F}^-$ is either synthesized by bombardment of H_2^{18}O with a proton (p) or alternatively by H_2^{16}O reaction with helium-3 ion (^3He) (Table 16).⁴⁴⁷

Of all these reactions is the synthesis of $^{18}\text{F}^-$ fluoride ions by ^{18}O bombardment with protons yielding the highest activity. Cyclotrons fire protons with energies of 11-20 MeV with a current of 20-60 mA, yielding in 1-2 h of 37-370 GBq (1-10 Ci) of $^{18}\text{F}^-$. The reaction with $^{16}\text{H}_2\text{O}$ yields around 70 mCi in 30 min (25 μ A) when irradiated with 22 MeV ^3He ions.⁴⁶¹ Synthesized aqueous fluoride ions are bound to metal ions like caesium (CsF) or potassium (KF) present in the reactor for nucleophilic fluorinations in non-aqueous media.^{447,462}

Fluorine gas is produced by bombardment of neon-20 with a deuteron, splitting off a ^3He or reaction of $^{18}\text{O}_2$ with a proton.^{445,447} Synthetic protocols for $^{18}\text{F}_2$ production by ^{20}Ne bombardment with deuterons (60 MeV) yield after 2.5 h an activity of 0.125 GBq (3.4 mCi), around half the dose normally applied for PET scans.⁴⁶³ Synthesis from $^{18}\text{O}_2$ (10 MeV, 30 mA)

yields 0.117 GBq (0.7 Ci) of F₂ gas.⁴⁶⁴ The isolated ¹⁸F gas is used further as a 1% gas mixture in neon or krypton, having a 0.1-1% of ¹⁸F₂ to ¹⁹F₂ present.

| | Nucleophilic fluoride (F⁻) | | Electrophilic fluorine (F₂) | |
|----------|--|---|--|--------------------------------------|
| Reaction | ¹⁸ O(p,n) ¹⁸ F | ¹⁶ O(³ He,p) ¹⁸ F | ²⁰ Ne(d, ³ He) ¹⁸ F | ¹⁸ O(p,n) ¹⁸ F |
| Target | ¹⁸ H ₂ O | ¹⁶ H ₂ O | ²⁰ Ne | ¹⁸ O ₂ |
| Products | ¹⁸ F ⁻ _{aq} (CsF, KF) | | [¹⁸ F]F ₂ | |
| Activity | 1-10Ci | 70mCi (6mCi/μAh) ⁴⁶¹ | 3.4mCi | 0.7Ci |

Table 16. Nucleophilic and electrophilic ¹⁸F radio nucleotide synthesis.⁴⁶¹⁻⁴⁶⁴

Production of PET imaging agents like ¹⁸F is a so-called carrier free process, which means that the newly synthesized daughter nuclei (¹⁸F) differs chemically from the parent nuclei (¹⁸O).^{445,465}

9.2 ¹⁸F-Fluorination

Introduction of ¹⁸F fluorine into a molecule is possible in three ways; nucleophilic, electrophilic, and radical fluorination.

9.2.1 Nucleophilic fluorination

9.2.1.1 Fluoride properties in organic reactions

Fluoride is found naturally in minerals, the most important source being calciumfluoride (CaF₂). In terms of a fluorination chemistry alkali metal fluorides are the preferred fluoride salts because of their increased reactivity due to a lower lattice energy than CaF₂ (CsF>RbF>KF>>NaF>>LiF). Caesium and rubidium fluoride are the most reactive of these alkali metal salts, but because of their lower abundance are more expensive. Sodium fluoride is the cheapest of all, but barely reactive as a nucleophile. On an industrial scale potassium fluoride is the most suitable salt, as it balances reactivity with expense in the best way.⁴⁶⁶ A large difference is seen between sodium and potassium fluoride reactivity in fluorination

reactions.⁴⁶⁶ Sodium fluoride has a higher lattice energy and lower solvation energy.⁴⁶⁷

Consequently, sodium fluoride has a lower solubility. Compared to the other halogens the lattice energies of alkali fluorides are much higher. The solubility of fluoride salts increases with increasing atomic radius of the alkali metal, because of higher solvation energy. The other halogens (chloride, bromide, iodide) differ in terms of solubility as no linear increase is seen with increasing atomic size of the alkali metal (Table 17).⁴⁶⁷

| Solubility in MeOH (g/100ml) | Fluoride | Chloride | Bromide | Iodine |
|-------------------------------------|-----------------|-----------------|----------------|---------------|
| Lithium | 0.0024 | 41.8 | 120 | 298 |
| Sodium | 0.020 | 1.38 | 16.8 | 79.4 |
| Potassium | 10.3 | 0.54 | 2.15 | 16 |
| Rubidium | 69.7 | 1.36 | 2.48 | 10.8 |
| Caesium | 152 | 3.26 | 2.12 | 3.45 |

Table 17. Solubility of alkali halides in methanol.

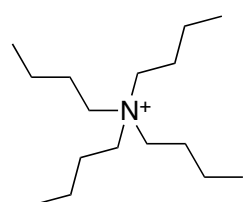
The solvation of fluoride salts decreases the more hydrophobic the solvent. Reaction with organic substrates are generally run in polar aprotic solvents like acetonitrile, dimethylformamide and dimethylsulfoxide to balance the solubility between reactant and salt. Fluorides have a high tendency to react as a base, which has been applied in aldol-, alkylation-, elimination-, cyclization- and oxidation reactions.⁴⁶⁶

9.2.1.2 Phase transfer catalysts

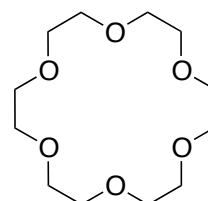
To increase the nucleophilicity of fluorides, phase transfer catalysts are used to break the strong ionic fluoride-metal interactions and distribute them better into the organic media.

Tetralkylammonium salts are able to disrupt the metal salts lattice and bind the fluoride ion to the positively charged nitrogen center.⁴⁶⁸ The alkyl chain lengths of these salts vary, but ethyl and butyl have been shown to be the most effective in radiochemical fluorinations. To bind the fluoride to these alkyl ammonium salts another weakly basic ion must first be displaced, commonly bicarbonates are the ion of choice.⁴⁶⁹ The drawback of ammonium salts is their high

hygroscopic nature and low thermal stability ($100^{\circ}\text{C} <$).⁴⁶⁶ Another way to increase fluoride nucleophilicity is the caging of the metal ion in between cyclic polyethers, leaving the fluoride ion “naked” in solution with. Such cyclic polyethers are called crown ethers and are available in different ring sizes.⁴⁷⁰ 18-Crown-6 is the most commonly used crown ether and has a strong affinity for potassium and caesium metal ions. Wynn tested the effect of crown ethers capable of solvating fluoride ions in different organic media. The solubility of KF and CsF increased by at least 10-fold in acetonitrile and dimethylformamide (DMF) (Table 18).⁴⁷¹ Polycyclic diaza polyether analogues of crown ethers, known as cryptands, are better in caging metal ions. The most popular analogue used in radiochemistry is cryptand 2.2.2 (Kryptofix[®] 2.2.2), having a high affinity for potassium over the other ions.⁴⁷² The only drawback of crown ethers and cryptands is their toxicity, as they are able to assist the diffusion of various cations across lipid membranes (ionotropes), disrupting membrane potentials in cells.^{470,473,474}

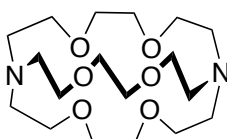


tetrabutylammonium



1,4,7,10,13,16-hexaoxacyclooctadecane

18-Crown-6



4,7,13,16,21,24-hexaoxa-1,10-diazabicyclo[8.8.8]hexacosane

Cryptand 2.2.2

| Salt | Solvent | 18-Crown-6 | Solubility 25°C (mM) |
|--------------------|-------------------|------------|----------------------|
| Sodium fluoride | Acetonitrile | | 0.029 |
| | | yes | 0.026 |
| | Dimethylformamide | | 0.031 |
| | | yes | 0.13 |
| Potassium fluoride | Acetonitrile | | 0.031 |
| | | yes | 0.94 |
| | Dimethylformamide | | 0.12 |

| | | | |
|------------------|------------------|-----|------|
| | | yes | 1.57 |
| Caesium fluoride | Acetonitrile | | 0.25 |
| | | yes | 3.50 |
| | Dimethylfomamide | | 0.60 |
| | | yes | 5.59 |

Table 18. Solubility of sodium-, potassium- and caesium fluoride in acetonitrile and dimethylformamide with and without 18-Crown-6.⁴⁷¹

9.2.2 Aromatic ¹⁸F-fluorination

9.2.2.1 Halex reaction

Historically the fluorination of aromatic compounds was restricted to electron deficient aromatic compounds via nucleophilic aromatic fluorination. The reaction precedes thereby through a Meisenheimer complex (MHC) (Figure 143).⁴⁷⁵

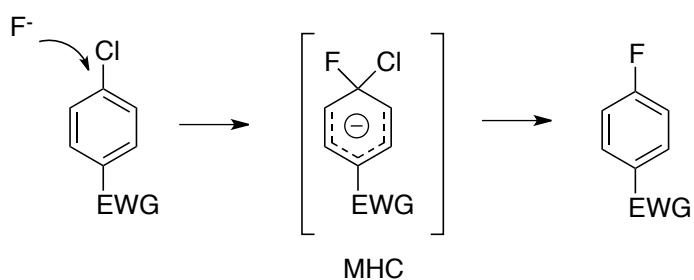


Figure 143. Halex reaction, formation of a Meisenheimer complex (MHC).⁴⁷⁵

This process is better known as the Halex (halogen exchange) reaction, because the main functional groups exchanged were other halides.⁴⁷⁶ However, quarternary ammonium salts,⁴⁷⁷ nitro-⁴⁷⁸ and *t*-butyl groups have been used as leaving groups. Heteroaromatics are fluorinated in good yields, which allows the easy labeling of derivatized nucleotides or natural building blocks like nicotinamide.^{479,480} The Halex process is still used in ¹⁸F chemistry, especially when ¹⁸F is not introduced in late state fluorination, but rather to synthesize aromatic linkers. Synthesis of ¹⁸F-fluoro- aldehydes, esters or nitriles use the Halex process, which are then linked to other molecules like amines or alcohols (Figure 144).^{481,482}

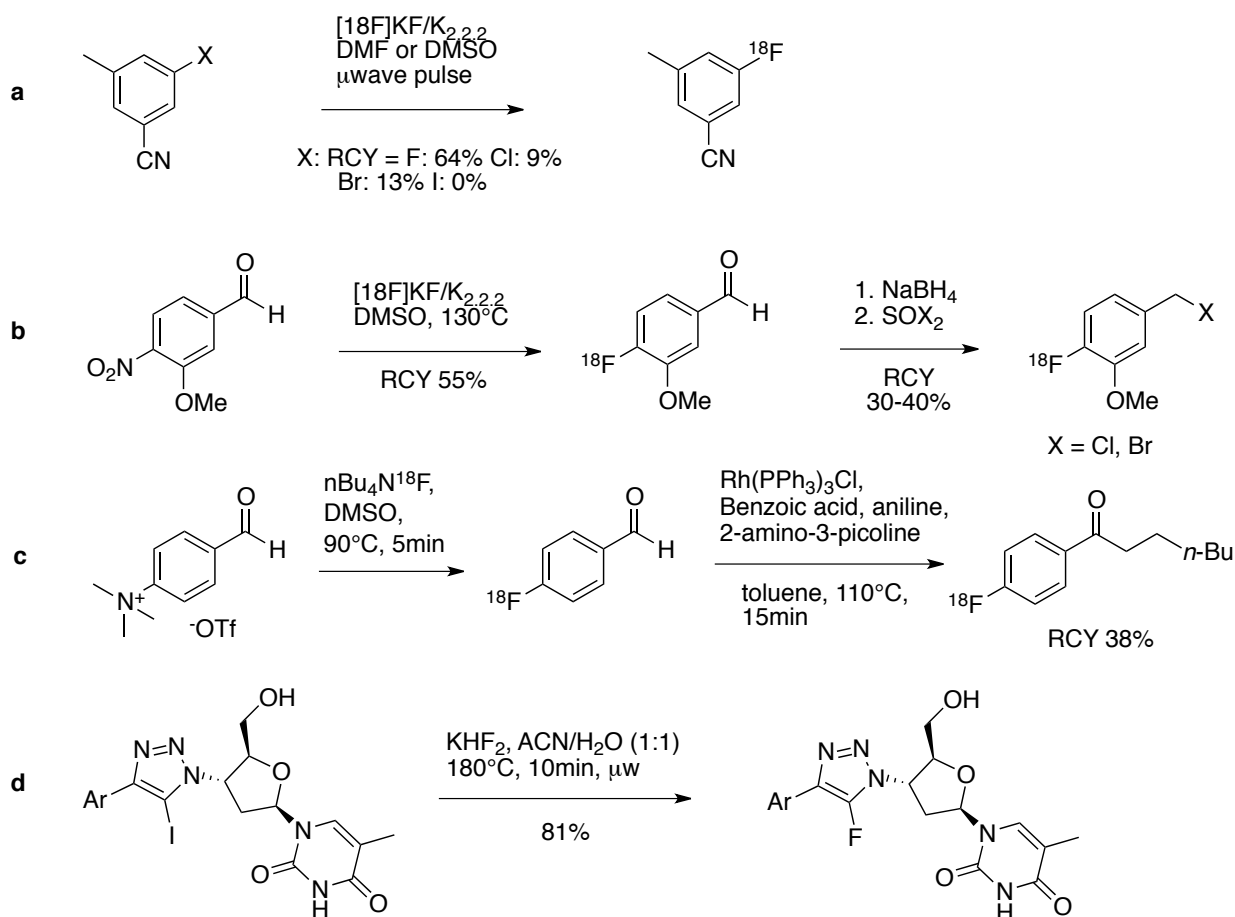


Figure 144. Halex fluorination of electron deficient aromatics.

(a) Halogen exchange on aryl cyanides. (b) Exchange of nitro groups on aromatic aldehydes (c) Exchange of quaternary ammonium salts on aromatic aldehydes.⁴⁷⁷ Halogen exchange on heterocycles: (d) fluorination of 3-iodotriazole-5-methyluridine and (e) methyl-2,6-dichloronicotinate.⁴⁷⁶⁻⁴⁷⁹

9.2.2.2 Balz-Schiemann and Wallach reaction

The earliest nucleophilic fluorinations on electron rich aromatic were possible by using diazonium piperidines (Wallach reaction 1886) and diazonium salts (Balz-Schiemann 1927). Heating induced decomposition of the diazonium species and creates a positive charge on the aromatic ring, which is quenched by a fluoride ion.⁴⁸³

The Balz-Schiemann reaction is a variation of the Sandmeyer reaction, using boron tetrafluoride (BF_4^-) as a counter ion. Only one fluoride of the BF_4^- is added to the aromatic ring, hence the chance of ^{18}F incorporation is a maximum of 25%. Molecules like ^{18}F -L-DOPA, ^{18}F -tryptophan and ^{18}F -peridone, that are used to study dopamine receptors in the brain, were synthesized in

way (Figure 145).^{484,485,486}

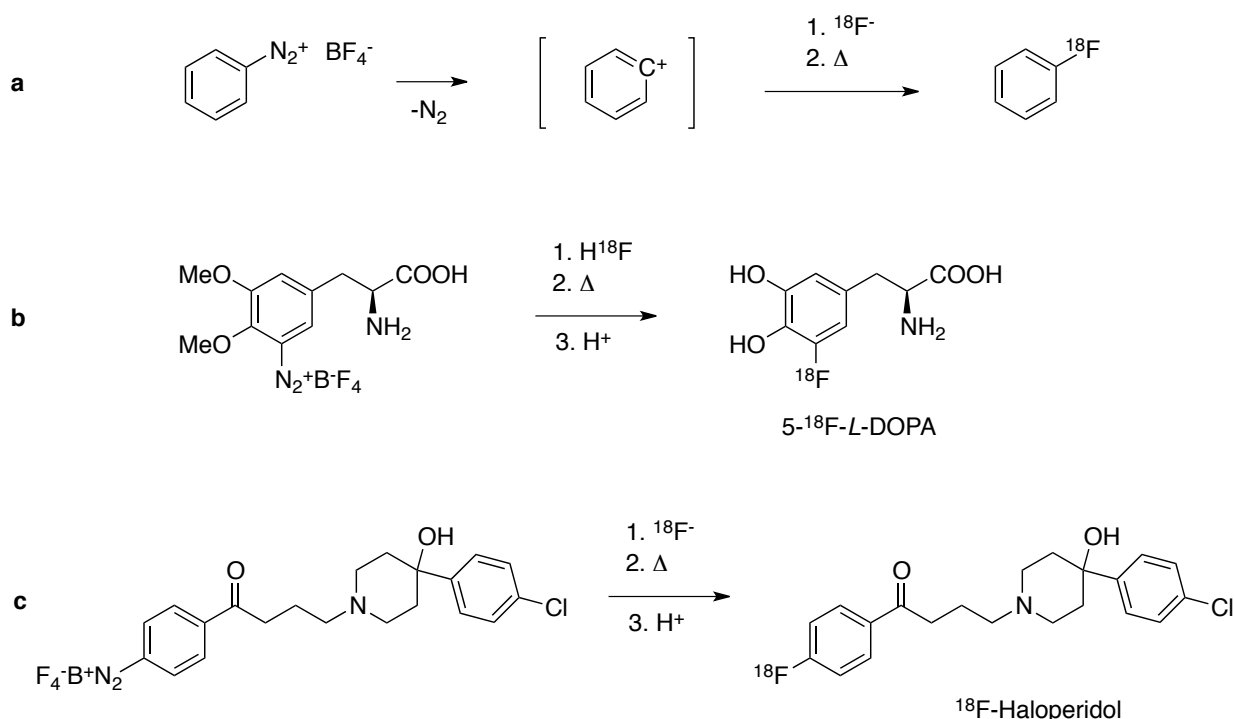


Figure 145. (a) Balz-Schiemann reaction of benzene,⁴⁸³ (b) 5-¹⁸F-L-DOPA⁴⁸⁴ and (c) ¹⁸F-Haloperidol synthesis.⁴⁸⁵

The Wallach reaction uses triazenes with a piperidine as a terminal group and, as with the Balz-Schiemann reaction, is a positive charge formed upon triazene decomposition (Figure 146).

Despite having an equimolar ratio of fluorine to starting material the isolated products of radiochemical Wallach reactions have low radiochemical yields.⁴⁸⁷

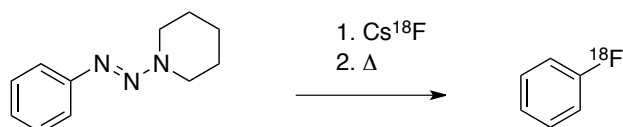


Figure 146. Wallach reaction of benzene.⁴⁸⁷

9.2.2.3 Fluorination of diaryliodonium salts

As PET agents gained more attention in medical imaging there has been an increased demand for new, high yielding radiofluorination methods of electron rich aromatic compounds. A way to lower the electron density on the aromatic ring is by bonding to a positively charged atom.

However, prior work with diazonium salts has shown this approach to be impractical for ^{18}F fluorination, as generally only small amounts of radiochemical product was obtained. Instead, hypervalent iodonium and sulphur salts were used in the form of diaryliodonium salts and sulphur triaryl iodonium salts (Figure 147). Both have been successfully used in radiochemical fluorinations.^{488,489}

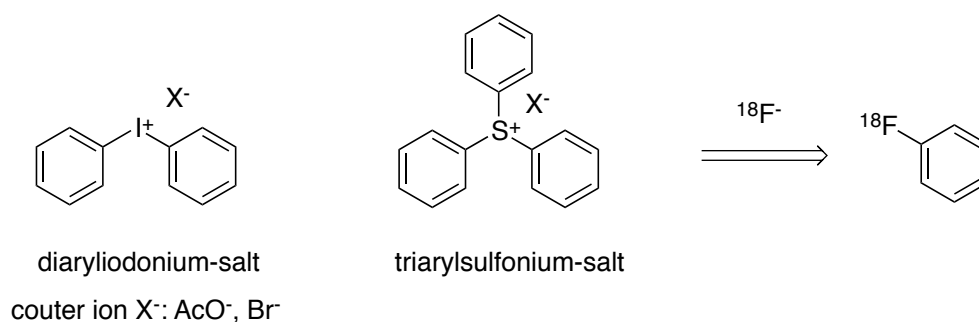


Figure 147. Radio-fluorination of diaryliodonium- and triarylsulfonium salts.^{488,489}

Iodonium salts are synthesized by the reaction of oxygen or halide hypervalent iodine species with aromatics. Reactions are mediated in acetic media, which also provides the counter ion of the iodonium salt formed (Figure 148).⁴⁸⁹

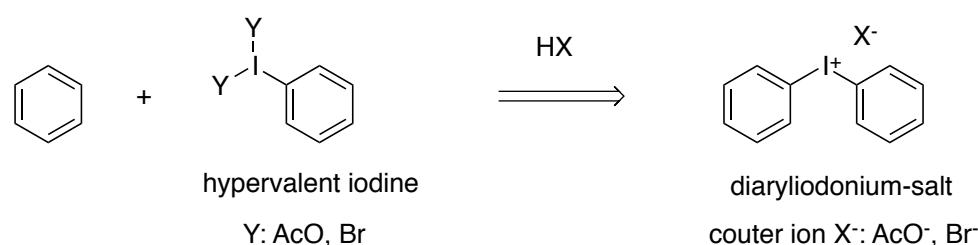


Figure 148. Formation of diaryliodonium salts by reaction of aromatics with aromatic hypervalent iodines.⁴⁸⁹

Fluorination of aryl iodonium salt occurs on both aryl groups. Electron poor aromatics are more prone to be fluorinated over electron rich aromatics. This electronic effect allows even products with a more electron rich nature to be fluorinated, by having a strong electron donating counter aromatic group (auxiliary) also substituted on the ring. Radiotracers like ^{18}F -flumazenil were successfully synthesized by nucleophilic fluorination with this method (Figure 149).^{489,490}

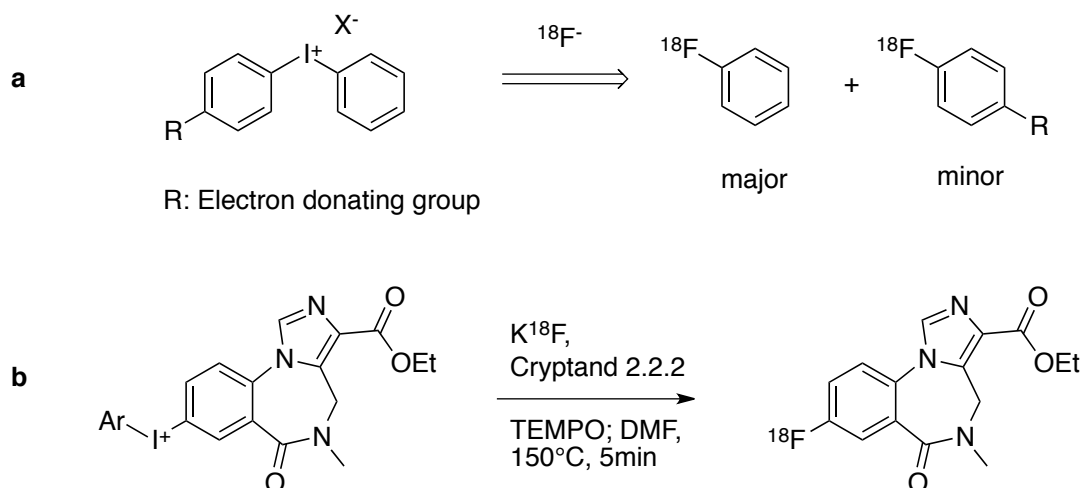


Figure 149. (a) Dependence of diaryliodonium salt fluorination on the electronic nature of the aromatics involved.

Electron rich aromatic groups (auxiliary aromatic) forces the fluorination onto of the other aromatic.⁴⁸⁹

(b) Synthesis of ^{18}F -flumazenil from a diaryliodonium salt.⁴⁹⁰

9.2.2.4 Transition metal mediated ^{18}F fluorination

Transition metal mediated reactions have revolutionized the functionalization of aromatics and allowed the synthesis of many previously inaccessible compounds. Fluorination of aromatics with transition metals has been used to incorporate ^{19}F -fluoride with palladium,⁴⁹¹ ruthenium,⁴⁹² and copper.⁴⁹³ However, the use in radiofluorination with transition metals has been limited because of long reaction times. In recent years, researchers like Ritter^{494,495} and Sanford⁴⁹⁶ have improved the fluorination reactions with palladium, nickel, and copper and demonstrated the use with ^{18}F . The benefit of metal catalyzed ^{18}F -fluorination is the use of simple aryl starting materials compared to diaryliodonium salts (Figure 150).

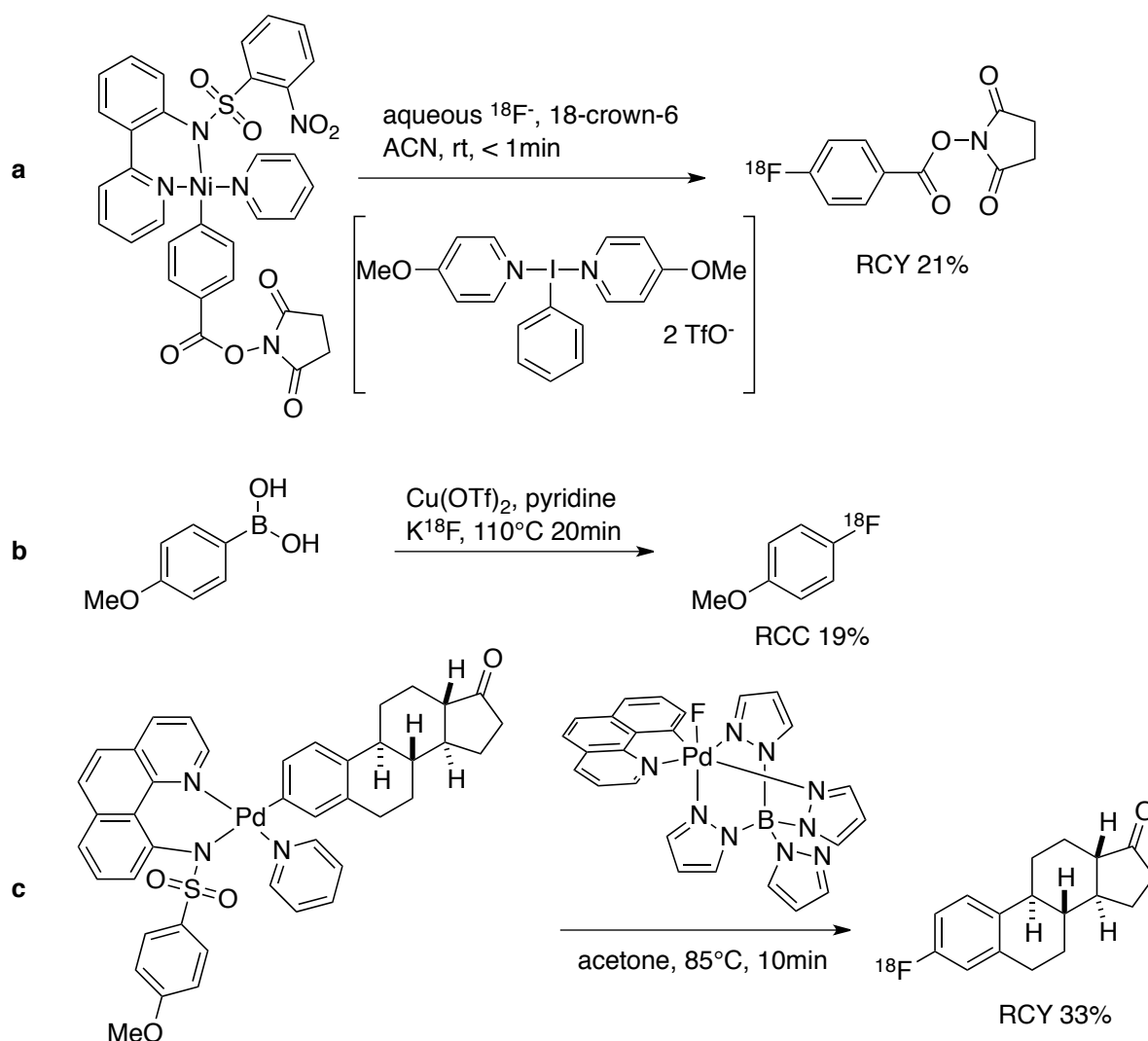


Figure 150. (a) Transition metal mediated radio fluorination with (a) nickel⁴⁹⁵ (b) copper⁴⁹⁶ and (c) palladium.⁴⁹⁴

RCY: radiochemical yield, RCC: radiochemical conversion.

9.2.2.5 Deoxy fluorination of phenols

Functional groups like nitro, halogens, *t*-butyl, ammonium and diazonium salts on electron deficient aromatic rings are exchanged with fluorine by nucleophilic fluorination. However, phenols are often neglected as addition of fluoride creates a non-exchangeable leaving group in the form of a phenolate. Phenols are common starting materials found in high abundance in nature, making them attractive building blocks for many synthetic applications. To enhance leaving group characteristics of phenols electron withdrawing sulfonates have been linked to the

phenol. Heating in the presence of fluoride makes deoxygenative fluorination of aromatic sulfonates possible. This method has so far not been used in radiochemical late-stage fluorinations as they have long reaction times and are low yielding (Figure 151).

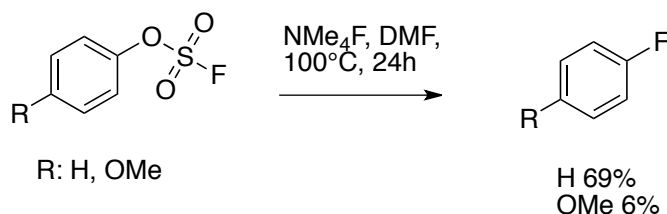


Figure 151. Nucleophilic fluorination of aromatic sulfonates.

In recent years several groups have looked into the deoxygenative fluorination, most notably Buchwalds, and Ritters. Buchwald described a palladium-mediated fluorination of aryl triflates with phosphine ligands, which has been tested with ^{18}F -fluoride.^{497,498} Ritter found that N-heterocyclic carbenes could be used to exchange phenols with fluorines in good yields.⁴⁹⁹ The reagent developed, called Phenofluor®, has proven to be tolerant towards many functional groups, fluorinating electron rich phenols and was found to work well as a radiofluorinating agent (Figure 152).

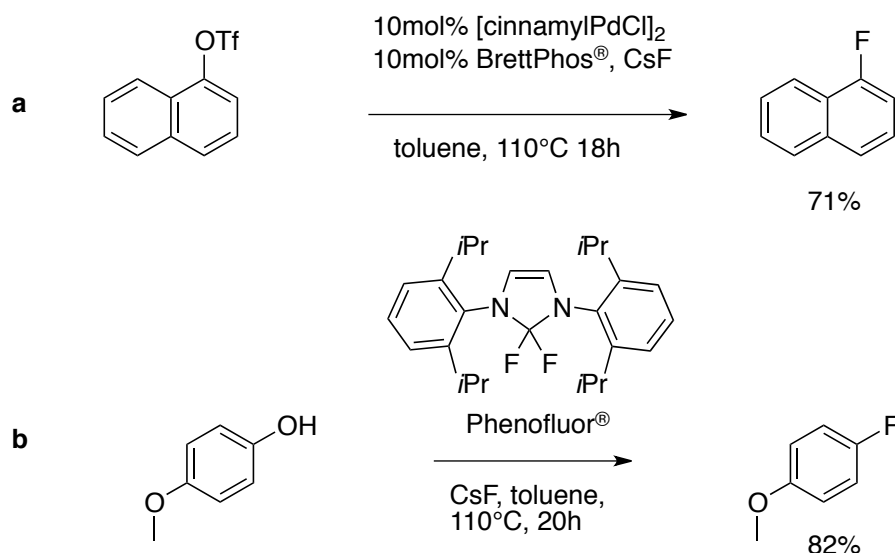


Figure 152. (a) Palladium mediated fluorination of aryl triflates.⁴⁹⁷ (b) Deoxyfluorination with Phenofluor®.⁴⁹⁹

9.2.3 Electrophilic / radical fluorination

9.2.3.1 Electrophilic fluoride reagents

Because of its high electronegativity fluorine is not prone to react as an electrophile and therefore no electrophilic fluorine source is found in nature. Fluorine gas (F_2) was the first chemical used as an electrophilic fluorinating agent, synthesized by electrolysis of potassium bifluoride KHF_2 in HF. However, the applications were limited in organic chemistry since F_2 is a strong oxidizer, tending to oxidize most functional groups. Milder reagents were soon developed by binding fluorine to a strongly electron withdrawing leaving groups. Halogen and oxygen based withdrawing groups were the first reagents produced in the form of peroxychlorides, fluoroxysulfates and hypofluorites.⁵⁰⁰

These reagents were easier to handle, but still strong oxidizers, extremely sensitive to moisture and needed to be used after *in situ* creation. Xenon difluoride was developed as a mild, stable alternative, but is still a strong oxidizer and expensive to create.⁵⁰¹ Binding fluorine to electron withdrawing nitrogen-based leaving groups created bench stable, crystalline electrophilic fluorinating agents (N^+-F). Electrophilic fluorination in current organic chemistry is almost completely based on N^+-F agents, with the most prominent agents being Selectfluor[®], N-fluoropyridines and N-fluoro-N-(phenylsulfonyl)benzenesulfonamide (Figure 153).⁵⁰² These reagents are soluble in most organic solvents and do not need of carrier additives compared to inorganic fluorides.

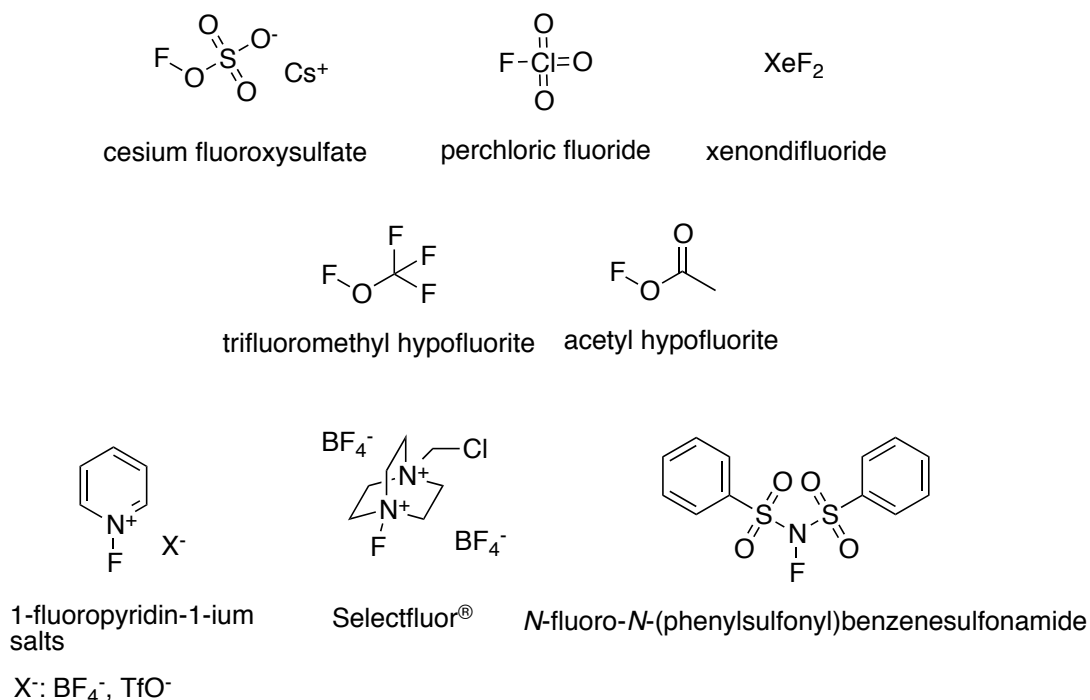


Figure 153. Electrophilic fluorinating agents.⁵⁰⁰⁻⁵⁰²

9.2.3.2 Electrophilic aromatic fluorination

The application of electrophilic radiofluorination is usually avoided when possible because of the low $^{18}\text{F}_2$ activity obtained from the cyclotron synthesis. However, before the use of iodonium ylides as starting materials electrophilic fluorination with F_2 and acetyl hypofluorite was the best option to introduce ^{18}F into electron-rich molecules. Reactions were conducted on electron-rich arenes like phenols and aryl stannanes, synthesizing molecules like ^{18}F -2b-carbomethoxy-3b-(4-fluoro)tropane fluorococaine (CFT) and 2,4,5-trifluororezazurin (2,4,5-TFRA). (Figure 154).^{503,504,505}

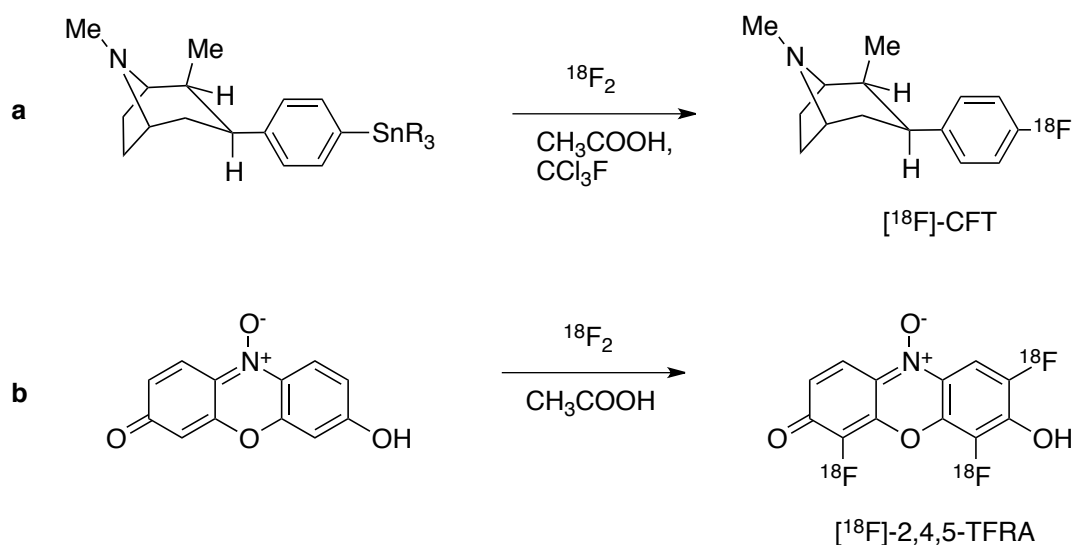


Figure 154. Electrophilic aromatic radiofluorination ($^{18}\text{F}_2$) with of aryl stannanes and electron rich phenols.

(a) Synthesis of ^{18}F -CFT⁵⁰⁴ and (b) ^{18}F -2,4,5-TFRA.⁵⁰⁵

Because of the weak bond strength, two different types of reactivities are possible with N-F reagents. Nucleophiles react by a simple electrophilic aromatic substitution reaction ($\text{S}_{\text{E}}\text{Ar}$) or by a process involving a single-electron transfer (SET) mechanism (Figure 155).⁵⁰⁶

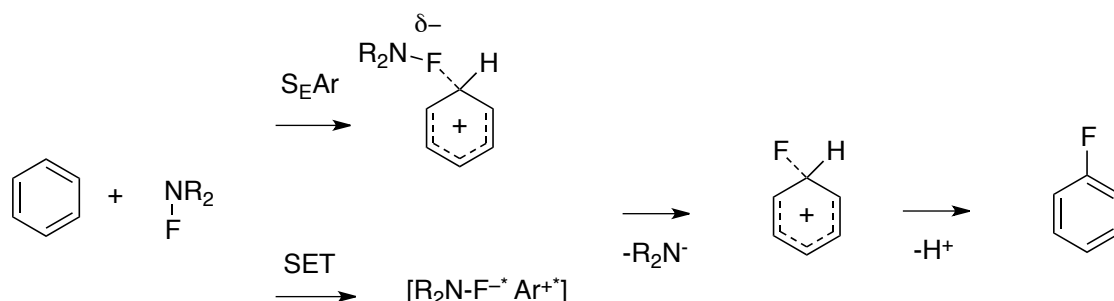


Figure 155. Electrophilic aromatic fluorination reaction mechanisms.

(Top) Electrophilic aromatic substitution $\text{S}_{\text{E}}\text{Ar}$ or (bottom) single electron transfer SET.⁵⁰⁶

9.2.3.3 Radical fluorination

The ability of electrophilic fluorine reagents to react in a single electron transfer mechanism offers the possibility to fluorinate by a strictly radical reaction. The Hunsdieker reaction is based on radical fluorination, whereby an aromatic carboxylic acid acts as a leaving group.⁵⁰¹

Metals like silver and manganese have been used in radical fluorination. Fluorination

generally takes place on the metal and N^+-F reagents are commonly used to act as fluorine transfer agents.⁵⁰⁷ Silver catalyzed fluorinations have been described on aryl stannanes and borylates (Figure 156).^{508,509}

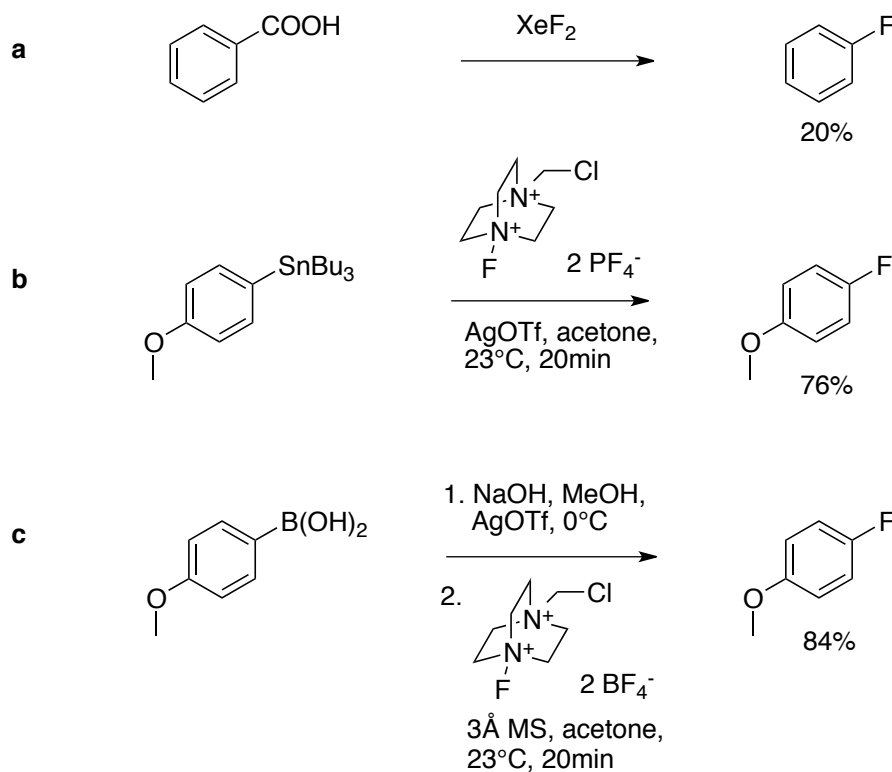


Figure 156. (a) Hunsdieker reaction of benzoic acid with xenondifluoride.⁵⁰¹ Silvermediated fluorination of (b) arylstannane⁵⁰⁸ and (c) arylboronic acids.⁵⁰⁹

10 Project overview

The goal of this project was to create a ^{18}F -containing vitamin E (α -tocopherol) analogue as an *in vivo* tracker of a liposomal drug delivery system. Any decay products of such tracers resemble α -tocopherol and α -tocopherol metabolites and are not toxic to the body, guaranteeing their safe use. Our liposomal constructs in use are sensitive to degradation by radicals. Reformation of tocopherols helps protecting the liposomal constructs from radical based damage on the phospholipid fatty acid chains and maintains at the same time the liposomal integrity better than other liposomal trackers, leading to a longer survival time during admission

and circulation in the blood stream. This new ^{18}F -containing molecule will be incorporated into liposomes targeting cancer cells (Figure 157). The delivery technology is the intellectual property of the company Exact Delivery, Inc.

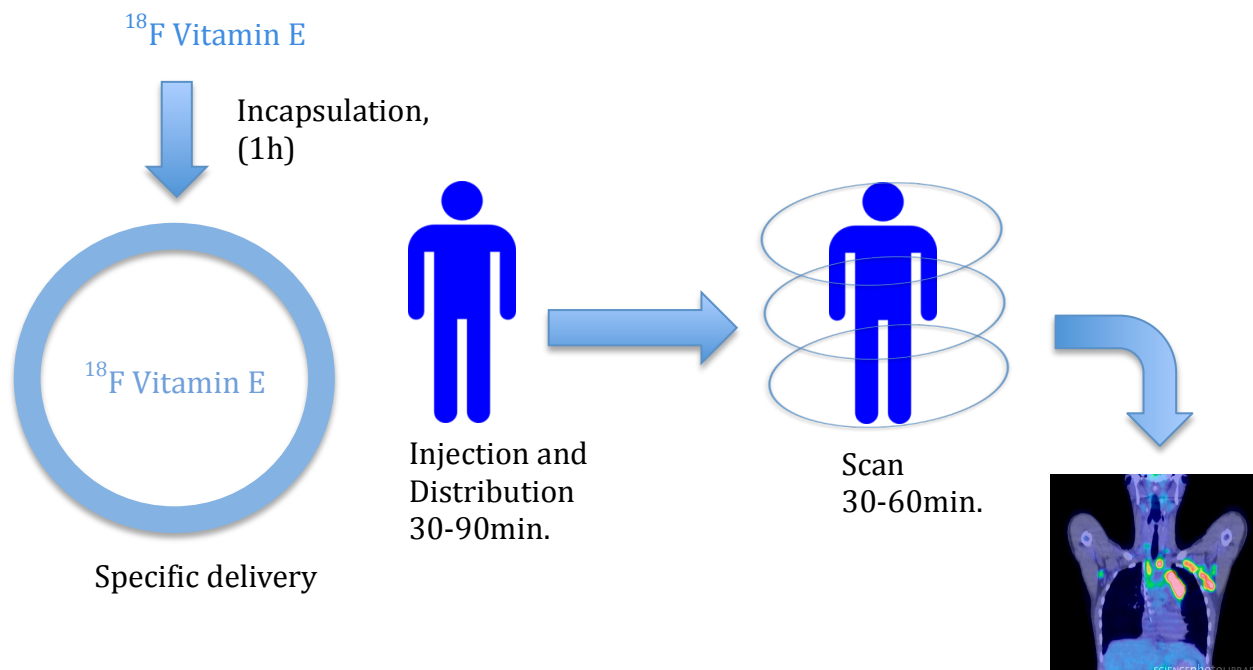


Figure 157. ^{18}F -containing α -tocopherol radiotracers as a tool to follow cancer-targeting liposomes.⁵¹⁰

10.1 Structure design

10.1.1 Tocopherol based PET tracer

The most important aspect of the design of a ^{18}F -containing vitamin E is to maintain the structure of α -tocopherol after the ^{18}F has decayed to ^{18}O . The C6 position of the phenol oxygen is the most suitable place to fluorinate as α -tocopherol is reformed after decay (F-Toc **47**, Figure 158). Tocopherol has been found in some cases to prevent cancer, to lower cancer growth and to reduce side effects occurring in chemotherapy.^{511,512} Hence, the main goal of this project is the establishment of a rapid synthetic process towards F-Toc, **47**. Other positions were considered for fluorination, but would not form natural α -tocopherol after ^{18}F decay.

Insertion of the fluorine at the 5-position of γ -tocopherol (5-F- γ -Toc **48**, Figure 158) will form a 5,6-catechol-tocopherol (5,6-catechol-Toc) decay product, which oxidizes to the metabolite tocored.³²³ A metabolite observed in studies of α -tocopherol is the 5-hydroxymethyl- α -tocopherol (5-HO-Me- α -Toc).³²³ Fluorination of the benzylic positions on the chroman ring may be possible by nucleophilic fluorination, creating the 5-F-Me- α -Toc **49** (Figure 158). Further, HM-Toc was chosen as a substrate for benzylic fluorination (6-F-Me- α -Toc **50**, Figure 158) because of its resemblance to α -tocopherol (see Chapter 2, non-antioxidant-tocopherol). Insertion of ^{18}F into the phytyl chain is possible by nucleophilic fluorination using tocotrienols as starting materials. Fluorination at the terminal methyl position (C13 or C13') creates 13-F- α -Toc **51**. The decay product would in this case be 13-HO- α -Toc, which is the first product of the tocopherol phytyl chain oxidative metabolism.⁷³

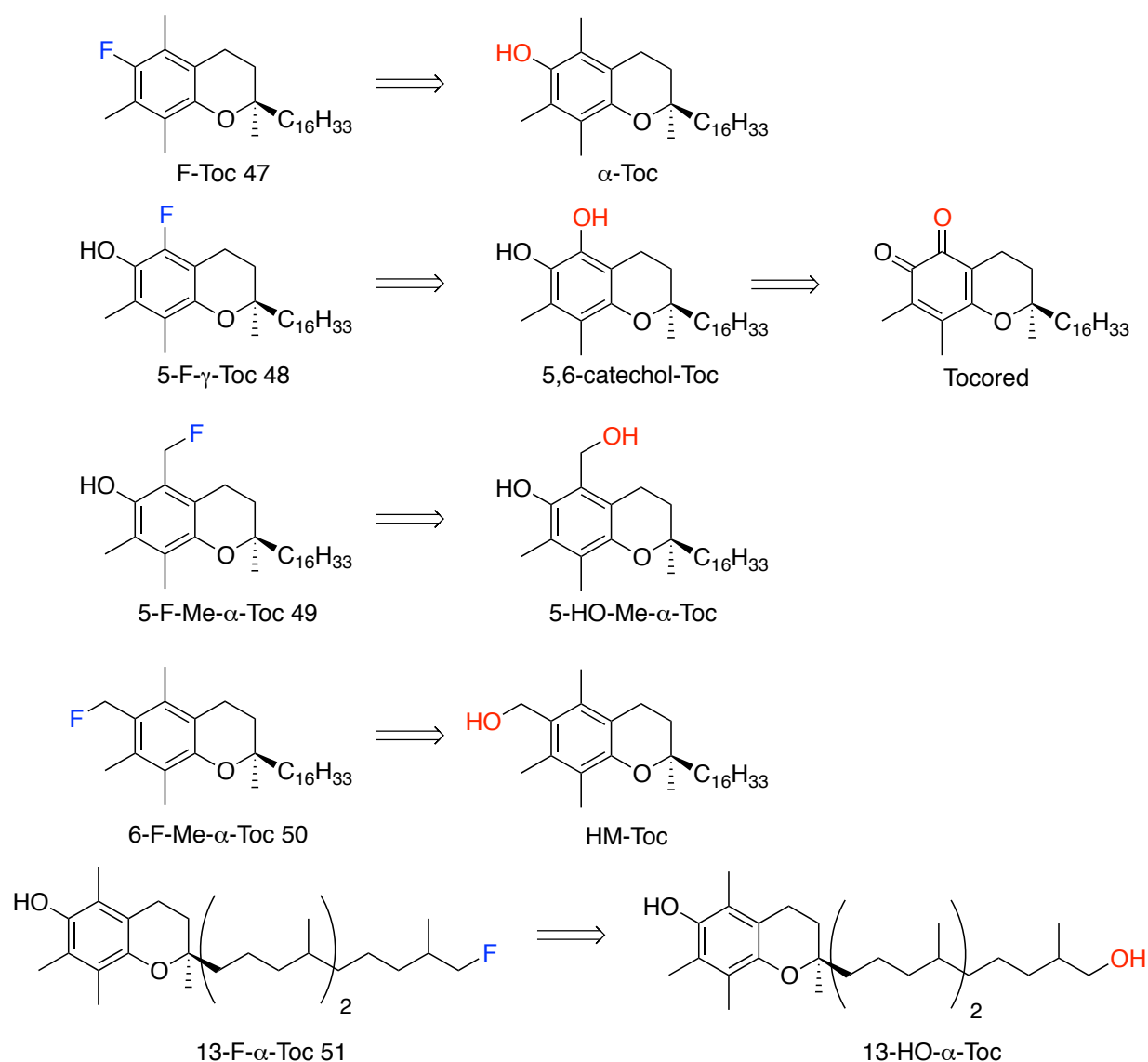


Figure 158. Designed ^{18}F -tocopherol tracers, 47-51, and their products formed after radioactive decay.

10.1.2 Tocopherol dual label: PET tracer and fluorophore

BODIPY groups have two fluorines attached to the boron center. Several fluorine exchange reactions on BODIPYs have been described in the literature.⁵¹³ An exchange of the BODIPY fluorines with ^{18}F in compound **3** would create a PET and fluorescent lable (^{18}F -**3**) that binds to α -TTP (Figure 159). Dual labels have the advantage to act as PET agents to highlight a specific site *in vivo* and as an optical probe, showing the location of the tracer in *in vitro*.⁵¹⁴

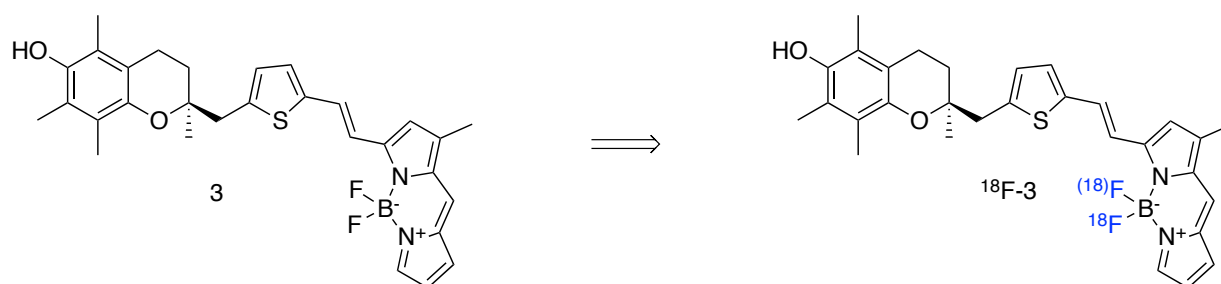


Figure 159. Designed dual-lable ^{18}F -thienyl-ene-BODIPY ^{18}F -3.

Two possible products are formed, mono- or di-substituted $^{18(18)}\text{F}$ -3.

Certain time limits were set for the fluorination chemistry in considering the follow up work that would be required to make liposomes. We decided that a maximum reaction time of 30 min should not be exceeded. Reaction work-up and purification should be rapid and clean with as few by-products as possible. Analysis by HPLC has to be highly reproducible and fast. If possible, the starting material for the fluorination should be stable for a prolonged time before use. Also, hazardous / toxic chemicals like metal catalysts and moisture sensitive reagents should be avoided in the synthetic procedure if possible, to lower the risk for any possible danger to patient and worker.

The creation of a tocopherol PET tracer is part of the intellectual properties of Exact Delivery, Inc. In regards to use of a ^{18}F -tocopherol PET tracer in the future, it would be more convenient if its preparation avoided currently patented methodologies.

11 Results and Discussion

11.1 6-F-Tocopherol synthesis

6-Fluorotocopherol (F-Toc) structurally resembles the previously synthesized molecule Cl-Toc **41**. The radioactive decay of the ^{18}F nuclide is limiting the reaction time of the chemistry and therefore demands a rapid synthesis. Fluorination chemistry could proceed either by electrophilic or nucleophilic fluorination.^{515,516} Similar to Cl-Toc, F-Toc can be synthesized by

electrophilic fluorination, but higher ^{18}F incorporation is possible with nucleophilic radiofluorination. Electrophilic fluorinating agents are synthesized from $^{18}\text{F}_2$ gas and have a maximum ^{18}F incorporation of 50%.⁵¹⁶ Nucleophilic fluorination with fluoride incorporates 100% ^{18}F and is, therefore, the preferred method of radiofluorination. Unfortunately, nucleophilic fluorinations of electron-rich, sterically hindered aromatics like tocopherol are not high yielding (Figure 160).⁵¹⁶

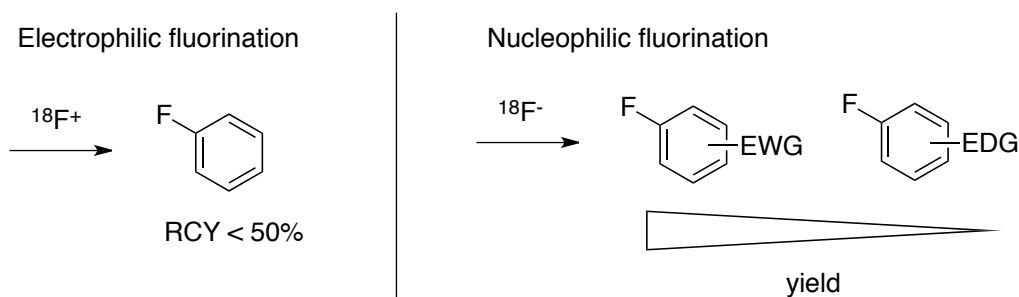


Figure 160. Problems associated with electrophilic- and nucleophilic fluorination.

Electrophilic fluorination uses ^{18}F - F_2 gas as a source of ^{18}F . Only one of the atoms in F_2 is a ^{18}F , which leads to maximum possible radiochemical yield (RCY) of 50%. Direct nucleophilic fluorination with ^{18}F -fluoride favours aromatics with electron withdrawing groups (EWG) like carbonyls or nitro groups and are less effective (or not possible) with aromatic substrates bearing electron donating groups (EDG) like methoxy or amines.⁵¹⁶

α -Tocopherol is a good starting material because of its availability and low cost. Ritter has described the direct fluorination of phenols with the deoxyfluorination reagent Phenofluor[®].⁵¹⁷ Recently, Phenofluor[®] has been used to fluorinate phenols with radioactive ^{18}F .⁵¹⁸ However, the Phenofluor methodology is patented and will only be used here to create a 6-F-Toc reference sample. Figure 161 highlights our chemical approaches: **(a)**. nucleophilic aromatic ^{18}F -fluorination chemistry to obtain 6-F- α -tocopherol: **(b)** titanium dioxide (TiO_2) catalyzed fluorination of aryl tosylates⁵¹⁹ **(c)** reaction with aryl iodonium salts⁴⁸⁹ **(d)** electrophilic fluorination by electrophilic aromatic substitution with H-Toc and **(e)** lithium-halogen exchanged of 6-iodotocopherol.⁵²⁰

Leaving groups like aryl stannanes or borylates are used to incorporate ^{18}F .⁵²¹ δ -Tocopherol has been fluorinated at the 6-position via the stannylated 6- δ -tocopherol. Attempts will be made to fluorinate α -tocopherol with borylates and stannylates as leaving groups (**f**, Figure 161).

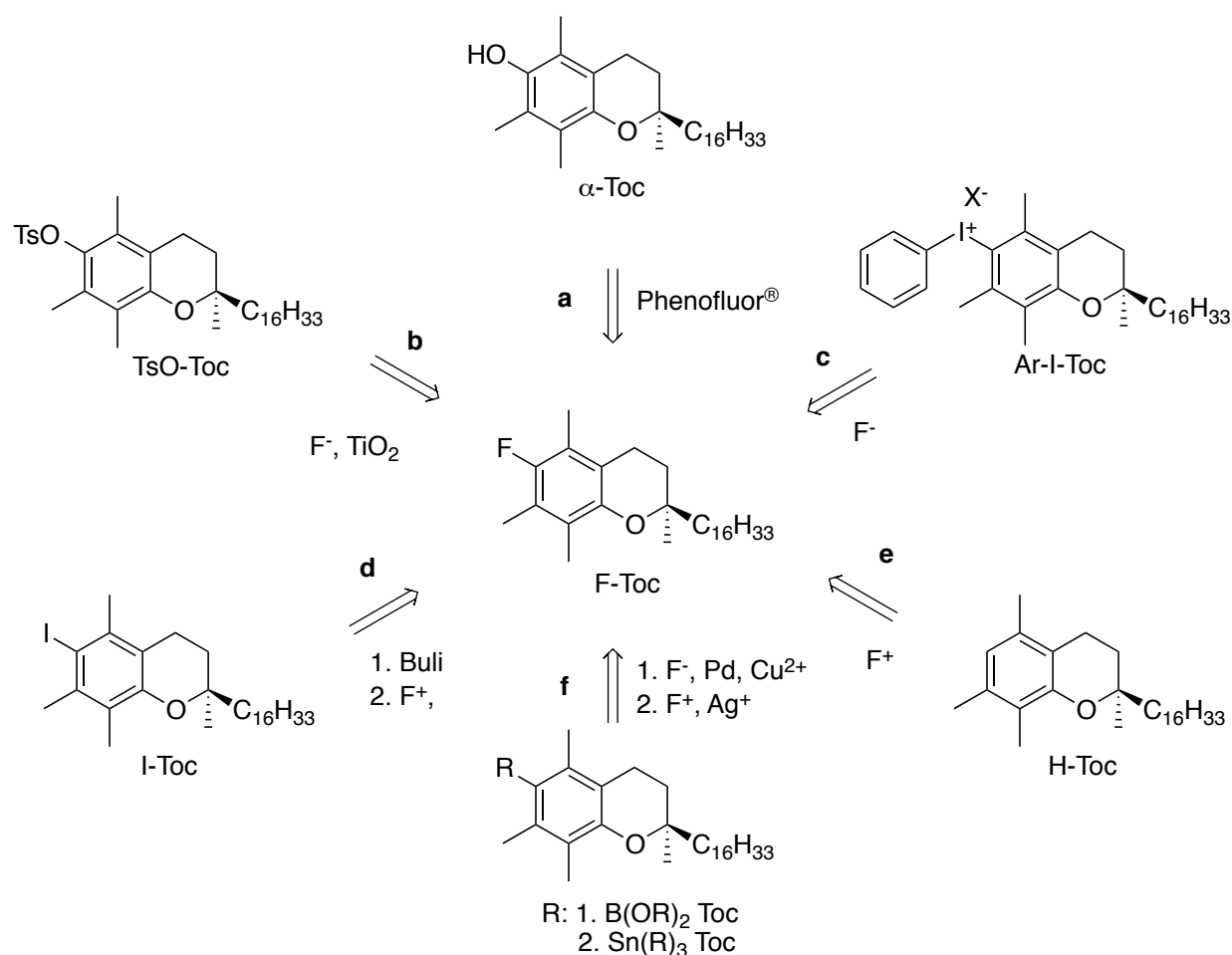


Figure 161. Synthetic strategies towards 6'-F- α -tocopherol by nucleophilic and electrophilic fluorination^{515,516}

11.2 Synthesis

11.2.1 Nucleophilic F-Toc synthesis:

11.2.1.1 TiO_2 catalysed α -tocopherol tosylate fluorination

The chemistry discovered by Sergeev and co-workers describes the fluorination of aryl tosylates with H₂O solvated ¹⁸F fluoride in ACN / thexyl alcohol (Thex-OH 1:1 v/v) with TiO₂ nanoparticles (NP) comprising 55:45 anatase / rutile (<200nm particle size) and tetrabutylammonium bicarbonate (Bu₄N⁺HCO₃⁻) at 110°C for 5-15 min (Figure 162). Benefits of this reaction are; the use of aqueous ¹⁸F fluoride saves time by avoiding the full azeotropic drying of the ¹⁸F with ACN and resuspension in another reaction solvent. Good yields were recorded when the reaction was diluted with organic solvents to the point where water made up 25% of the total reaction volume. Additionally, aryl tosylates are simple starting materials and the *p*-toluenesulfonic acid byproduct is easily separated by extraction.

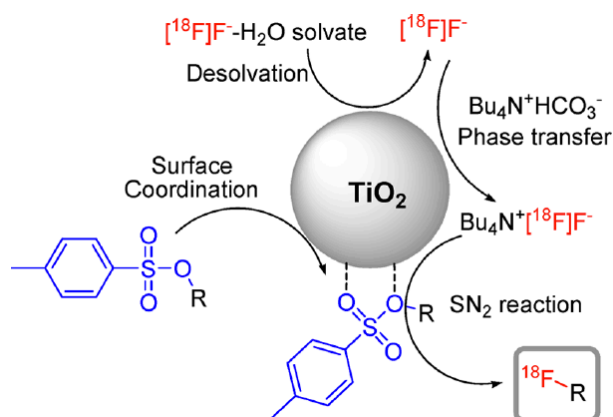


Figure 162. Synthetic scheme for TiO₂ mediated fluorination of aryl tosylates.⁵¹⁹

To test the reaction we used pentamethylchromanol (PMC), which allows a more critical analysis of the products formed by NMR and mass spectroscopy. PMC was tosylated with tosylchloride (TsCl) and pyridine in a 51% yield (Figure 163).

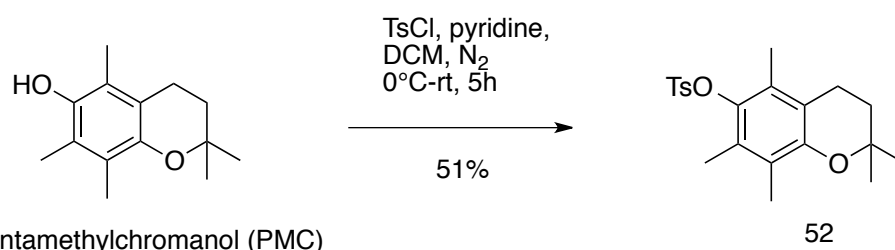


Figure 163. Tosylation of pentamethylchromanol.

No description was given for the synthesis of the TiO₂ NP or which vendor sold them. An 80:20 mixture of anatase / rutile is commercially available, called Degussa P25, having a 150 nm

particle size.⁵²² To obtain a 55:45 anatase / rutile TiO_2 mixture a synthesis was attempted according to a procedure by Xiong.⁵²³ Titanium trichloride (TiCl_3) was oxidized with a specific amount of graphine oxide (GO) (However, the reaction did not yield a 55:45 ratio, only 100% anatase TiO_2 was isolated.

While trying to find a way to synthesize the TiO_2 nanoparticles mentioned above, Brock University chemistry professor Dr. Stamatatos told me that his friend at Hellenic Open University of Patras, Dr. Bourikas, was studying the phase transitions and surface changes of TiO_2 . In Dr Bourikas' study the TiO_2 mixture Degussa P25 anatase/rutile (80:20) was calcinated at different temperatures ranging over 500-800°C for up to 24 h, which increased the amount of rutile phase (Figure 164 and Table 19).^{524,525} Translating Dr. Bourikas' research results to the procedure used by Sergeev would mean that heating the 55:45 mixture of anatase / rutile at 550°C for 12 h will increase the overall percentage of rutile phase. Unsure of the actual TiO_2 phase ratio responsible for the chemistry, it was decided to test the Degussa P25 TiO_2 , each TiO_2 anatase and rutile phase separately, and in the correct 55:45 ratio.

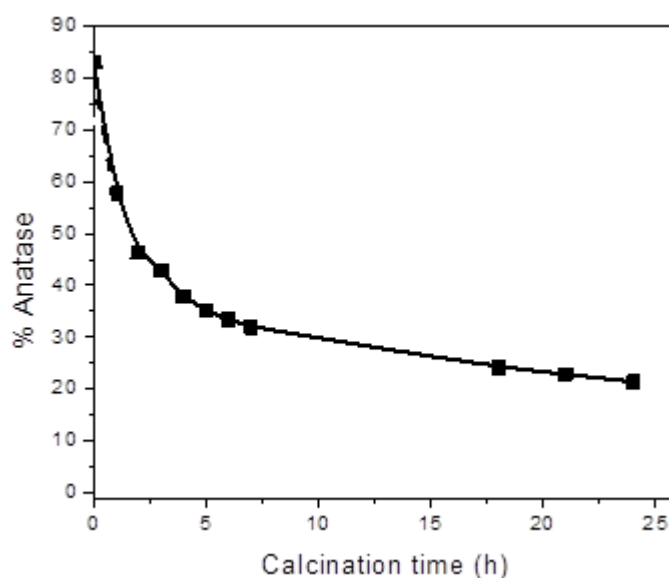


Figure 164. Change of TiO_2 anatase percentage dependend on the calcination time at 600°C.

Preliminary results sent by Dr Bourikas.⁵²⁴

The values of the anatase percentage (%A) in P25 determined by temperature programmed furnace (TP)-XRD analysis.

| Temperature (°C) | %A |
|---------------------|------|
| 500 | 81.5 |
| 550 | 84.1 |
| 600 | 83.3 |
| 650 | 80.4 |
| 700 | 73.1 |
| 750 | 47.8 |
| 800 | 8.3 |

Table 19. Anatase percentage (%A) in Degussa P25 TiO₂ at increasing temperature, after 24 h.

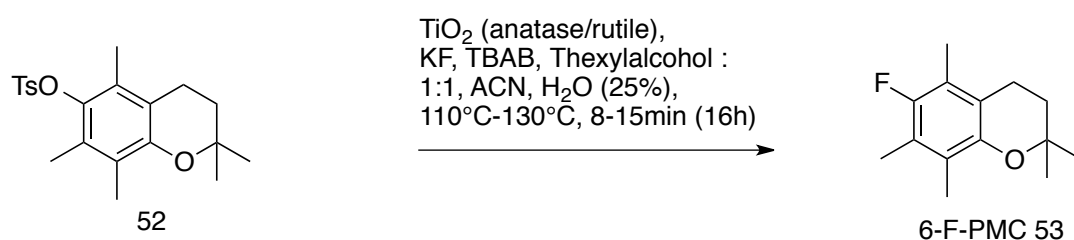
The reaction was conducted in temperature programmed furnace with an X-ray powder diffraction (TP-XRD). Preliminary results sent by Dr Bourikas.⁵²⁴

By calcination at 700°C for 16h, part of the isolated anatase material was converted to the rutile TiO₂.

Fluorination of PMC-OTs, **47**, was conducted according to the optimized procedure found in the supporting information of Sergeev's paper, with adjustments for fluorination with the "cold" ¹⁹F isotope.

At this point it is important to mention the synthetic difference between ¹⁸F and ¹⁹F fluorination in terms of the actual equivalency of reagent used. Synchrotron synthesized ¹⁸F in Sergeev's procedure had an activity of 1.5-4 mCi, what corresponds to 0.3-0.8 nmol (¹⁸F-Fallypride specific activity of 5±2 Ci/μmol⁵¹⁹). TiO₂ was used in a 165000:1 ratio (10 mg / 0.125 mmol of

TiO₂) to the ¹⁸F fluoride. Commonly, the ratio of synchrotron isolated ¹⁸F fluoride to ¹⁹F fluoride is approximately 1:1000, which makes the actual ratio to all fluoride present in the reaction to TiO₂ 1:165. ¹⁹F-fluorination mimicking radioactive fluorination normally uses equimolar amounts of reagents or excess fluorine. To monitor the formation of 6-F-PMC, **53**, ¹⁹F-NMR spectroscopy was used. The test reactions were run with 10-20 mg of TsO-PMC, **52**, to keep the amount of TiO₂ low (130-260 mg) (Table 20).



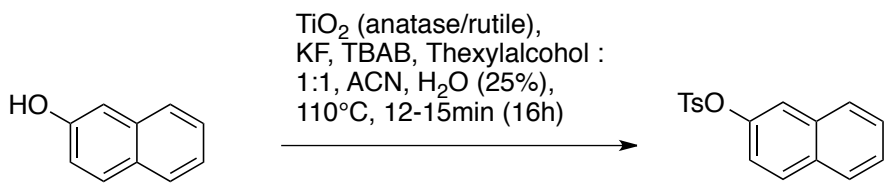
| KF (eq) | TBAB (eq) | Thex-OH : ACN | TiO ₂ phase (eq) | Temperature (°C) | Time | Yield ^a |
|---------|-----------|---------------|---------------------------------|------------------|------------|--------------------|
| 14 | 14 | 1:1 | P25 80:20, 60 eq | 110 | 10min | - |
| 1 | 14 | 1:1 | P25 80:20, 60 eq | 130 | 15min | - |
| 1 | 14 | 1:1 | P25 80:20, 60 eq (dried 3 days) | 110 | 10min | - |
| 1 | 7 | 1:1 | rutile 100%, 60 eq | 130 | 8min, +16h | - |
| 1 | 7 | 1:1 | Anatase 100%, 60 eq | 130 | 8min, +16h | - |
| 1 | 7 | 1:2 | Anatase 55% / rutile 45%, 60 eq | 130°C | 8min, +16h | - |

Table 20. TiO₂ mediated fluorination of TsO-PMC.

TiO₂ was dried in the oven at 500°C for 6-12 h and crushed in a mortar to a fine powder before use. TsO-PMC **47** (20 mg, 67 μM) was added with thexyl alcohol (0.35 ml) and dry ACN (0.35 ml) to the TiO₂ NP (260 mg) in a closable vial under N₂. TBAB (227 mg) was incubated with KF (3.1 mg) in 25% v/v water (0.23 ml) for 1h at 60°C in a separate vial. The KF-TBAB was transferred to the TiO₂ and heated at 110°C for 8-15 min (a) Yield ¹⁹F-NMR.

Only starting material was observed in the spectra of crude products; there was no trace of product in the ¹⁹F-NMR (Table 20). Stirring the reaction for a longer time (16 h) did not change the outcome. To understand the problem with this reaction a reference compound in the original

publication was chosen as a test substrate. Tosylation of 2-naphthol with TsCl, K₂CO₃ in THF/H₂O led to product **54** in a 93.2% yield.⁵²⁶ In the reaction with 2-tosylnaphthol, **54**, the TiO₂ was only dried for 30-60 minutes at 550°C (Table 21).



2-Naphtol

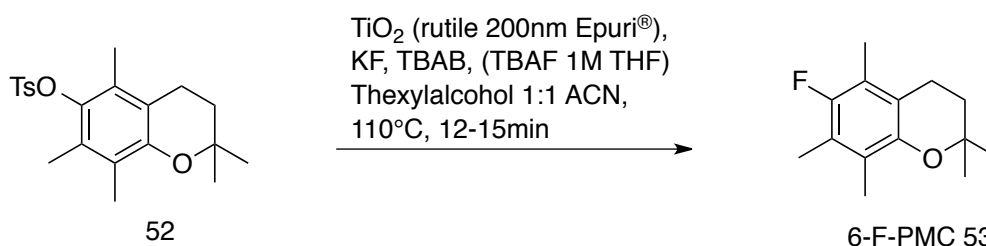
2-TsO-Napthol 54

| KF (eq) | TBAB (eq) | Thex-OH : ACN 1:1(ul) | | TiO ₂ phase (eq) | Temperature (°C) | Time (min) | Yield (%) ^a |
|---------|-----------------|-----------------------|---------------------|---------------------------------|------------------|------------|------------------------|
| 1eq | 7 ^b | 0.476ml | | rutile 100%, 60 eq | 110 | 12min | - |
| 1eq | 7 | 1:1 | | Anatase 55% / rutile 45%, 60 eq | 110 | 12min | - |
| 1eq | 14 | 1:1 | | Anatase 55% / rutile 45%, 60 eq | 110 | 12min | - |
| 1eq | 14 ^c | 1:1 | H ₂ O 0% | Anatase 55% / rutile 45%, 60 eq | 110 | 15min | - |

Table 21. TiO₂ mediated fluorination of TsO-Naphthol.

(a) Yield ¹⁹F-NMR. (b) KF & TBAB incubation for 20 min at rt. (c) A SepPak® cartridge was washed with water and EtOH. KF in water was loaded onto the cartridge (1ml), and washed off with TBAB in ACN (1ml), followed by ACN (3ml). The solution was dried at 80°C and resuspended in ACN.

To enhance the activity of the phase transfer catalyst the water was eliminated from the reaction. The TiO₂ used to this point was produced in our lab, and had an unknown particle size which might have caused the low yield. Anatase and rutile TiO₂ NP with a ~200 nm size were ordered from Eprui® (Table 22). No pre-heating of the TiO₂ was required.



| KF (eq) | TBAB (eq) | Thex-OH : ACN | TiO ₂ phase (eq) | Temperature (°C) | Time | Yield ^a |
|------------------|------------------|------------------|-----------------------------|------------------|-------|--------------------|
| 1eq | 7eq ^b | 1:1 ^c | rutile 100%, 60 eq | 110 | 12min | - |
| 2eq ^d | - | 1:1 | rutile 100%, 60 eq | 110 | 10min | - |

Table 22. TiO₂ mediated fluorination of with EPRUI® 200 nm TiO₂ NP.

(a) Yield ¹⁹F-NMR. (b) SepPak® elution as prior described. (c) TsO-PMC, Thex-OH and ACN preincubated for 1h at rt. (d) 1M TBAF in THF (53 µl) was used instead of KF with TBAB.

Again, even using the commercial TiO₂ sample, no product was observed by ¹⁹F-NMR, and thus we decided to contact the author for advice. The author stated that the TiO₂ catalysed reaction had not been done with ¹⁹F in their laboratory, only with ¹⁸F. In the original paper a reaction was possible in acetonitrile and thexyl alcohol with a 25% v/v water present, but the author's replied that their best results occurred when water was absent. The reaction in table 22 were run without water, but no product was observed. Sergeev mentioned that when they analysed their 55:45 anatase / rutile TiO₂, a composition of anatase / rutile of 97:3 was found. The influence of the TiO₂ phase composition is still unknown, but smaller particle sizes were confirmed in his group to yield more product. It remains possible that TiO₂-mediated fluorination creates only trace amounts of product, not detectable by standard laboratory techniques like NMR. The author mentioned also that their follow up studies with electron rich and bulky halides have shown zero conversion. Thus, tosylated tocopherol is not suitable for this type of chemistry.

11.2.1.2 Aryl borane and stannylated tocopherol fluorination

¹⁸F-fluorination of aromatics by de-stannylation and de-borylation has been used to create biologically relevant molecules.^{521,527} ¹⁸F-3-fluoro-5-[(pyridin-3-yl)ethynyl]benzonitrile (¹⁸F FPEB) is used to quantify metabotropic glutamate receptors 5 (mGluR5) and has been synthesized by copper-catalyzed ¹⁸F-fluorination of boronic acids / esters.⁴⁹⁶ 2-¹⁸F-Fluoro-L-

tyrosine was synthesized by fluoro-destannylation⁵²⁸ and δ -tocopherol has been fluorinated at the 6-position by Ritter via a silver mediated stannyl fluoride exchange reaction (Figure 165).⁵⁰⁸

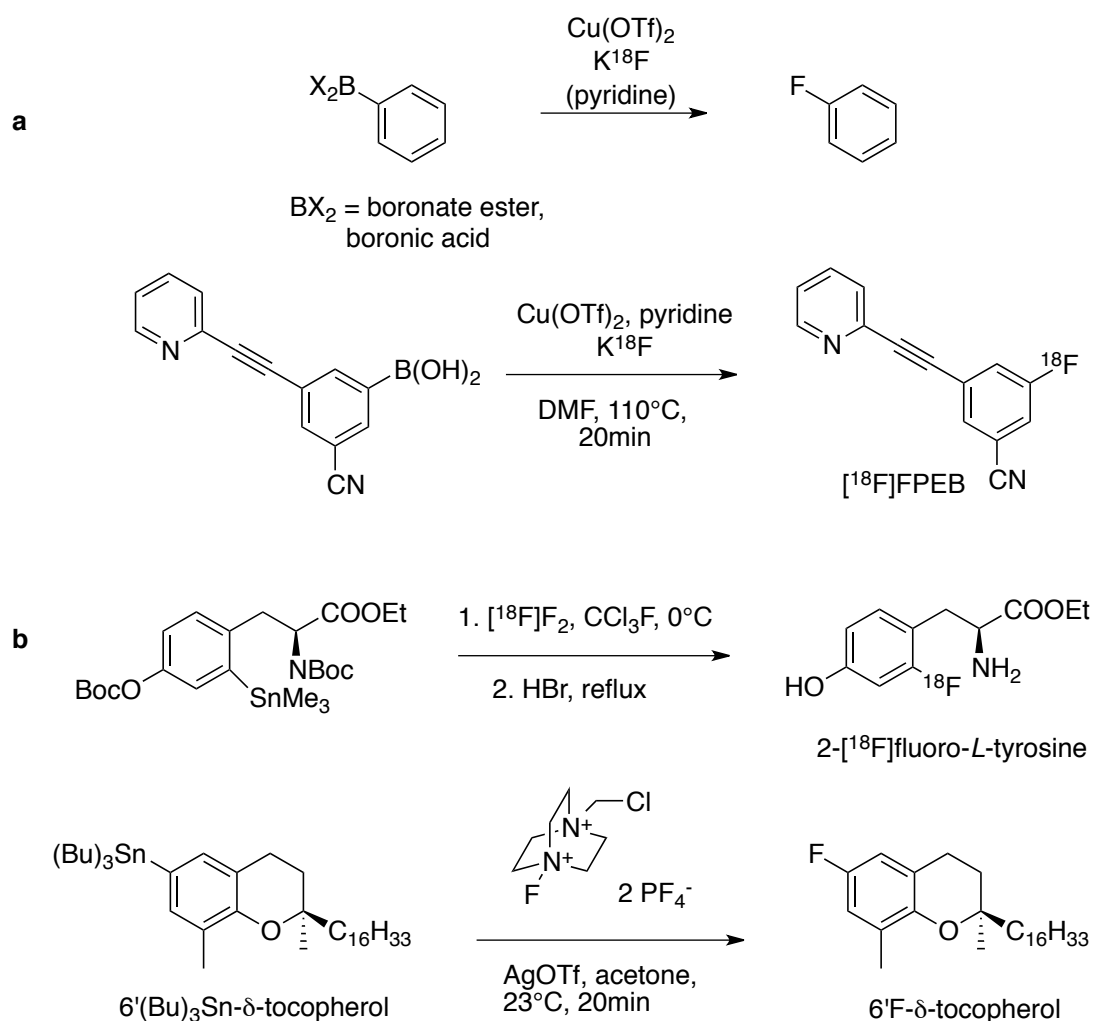


Figure 165. (a) Copper mediated fluorination of boronic esters and synthesis of ^{18}F -FPEB.⁴⁹⁶ (b) 2- ^{18}F -fluoro-*L*-tyrosine synthesis via Fluoro-destannylation and silver mediated fluorination of stannyl- δ -tocopherol.^{528,508}

Tocopherol stannylates and borylates have so far only been synthesized on δ -tocopheryl triflates.⁵²⁹ Stannylation of α -tocopherol triflate to **55** using dibutyltinhydride and (Bu_3Sn_2) and tetrakis(triphenylphosphine)palladium gave no discernible fluorination products despite longer reaction times (5 days) (Figure 166).

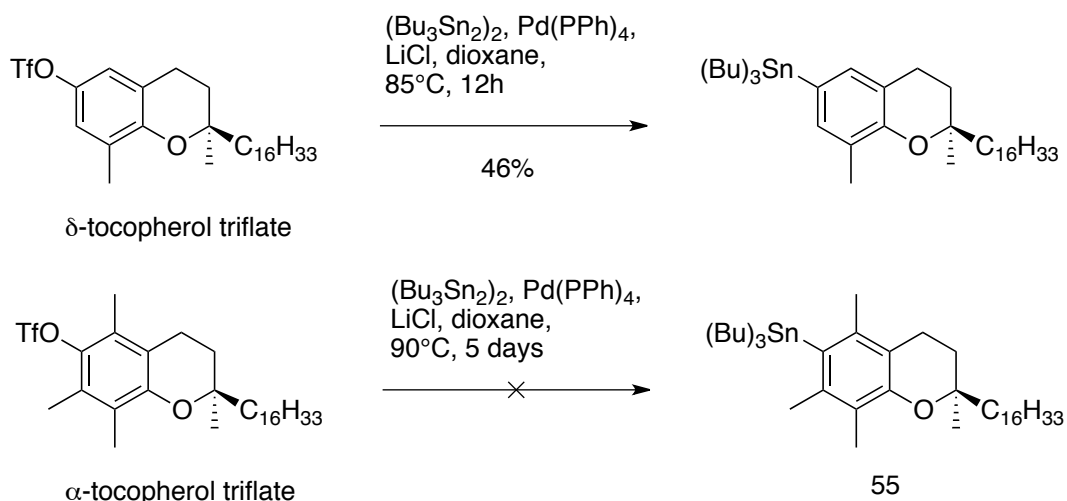


Figure 166 δ -Tocopherol triflate stannylation by Ritter⁵⁰⁸ and Miller⁵²⁹ and stannylation attempts of α -Tocopherol.

The yield of the δ -stannyl tocopherol in Miller's case was moderate, because the purification process by chromatography leads to protodesilylation. In their case the crude stannyl product was directly iodinated in a 93% yield. α -Tocopherol triflate seems to be too sterically hindered to attach the stannylate. It is also expected to have a higher tendency towards protodesilylation with 6-stannyl- α -tocopherol, which would not allow purification and would create further purification problems during the ^{18}F fluorination. Therefore, this idea was discarded.

In the same paper, δ -tocopherol triflate was Myaura-borylated in high yields with $\text{Pd}_2(\text{dba})_3$ and bispinacolborane over 12 h. However, attempted borylation of α -tocopherol triflate to **56** did not occur after 5 days (Figure 167).⁴²⁴

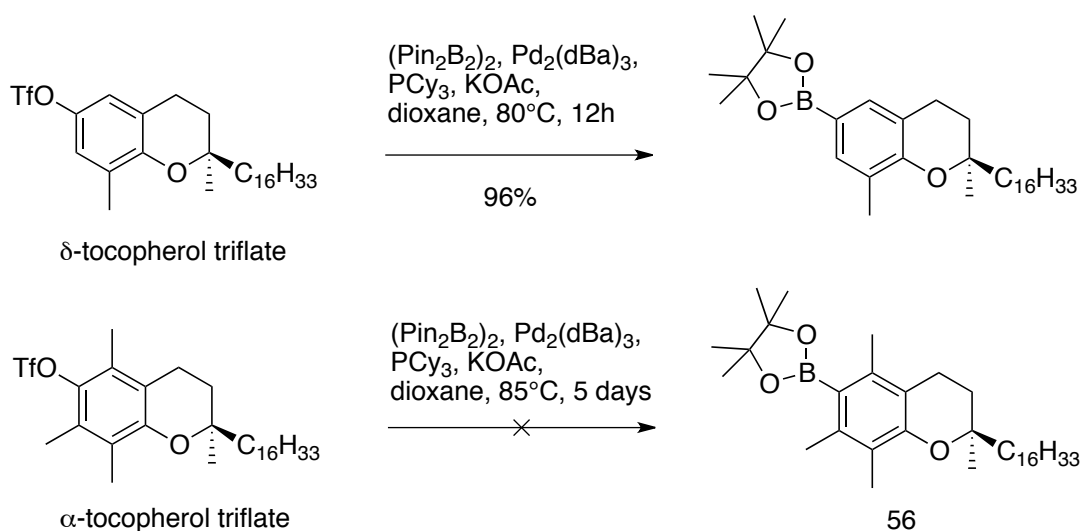


Figure 167. Synthesis of α -tocopherolpinacolboronic ester 56, δ -6'-tocopherolpinacolboronic ester from α -tocopherol triflate.⁵²⁹

Since Miller's stannylation and borylation did not work new reaction conditions were needed to borylate the α -tocopherol triflate. The catalyst was changed to palladium acetate ($\text{Pd}(\text{OAc})_2$) and BINAP, a version that worked for Mazzini in α -tocopherol triflate cross coupling reaction with amines.⁵³⁰ After 5 days the pinacole boronic acid was isolated in 6% yield. Changing the catalyst to 1,1'-bis(diphenylphosphino)ferrocene (dppf) was tested, as it had been reported to lead to high yields with aryl triflates, but it did not provide the expected product after 16 h (Figure 168).⁵³¹

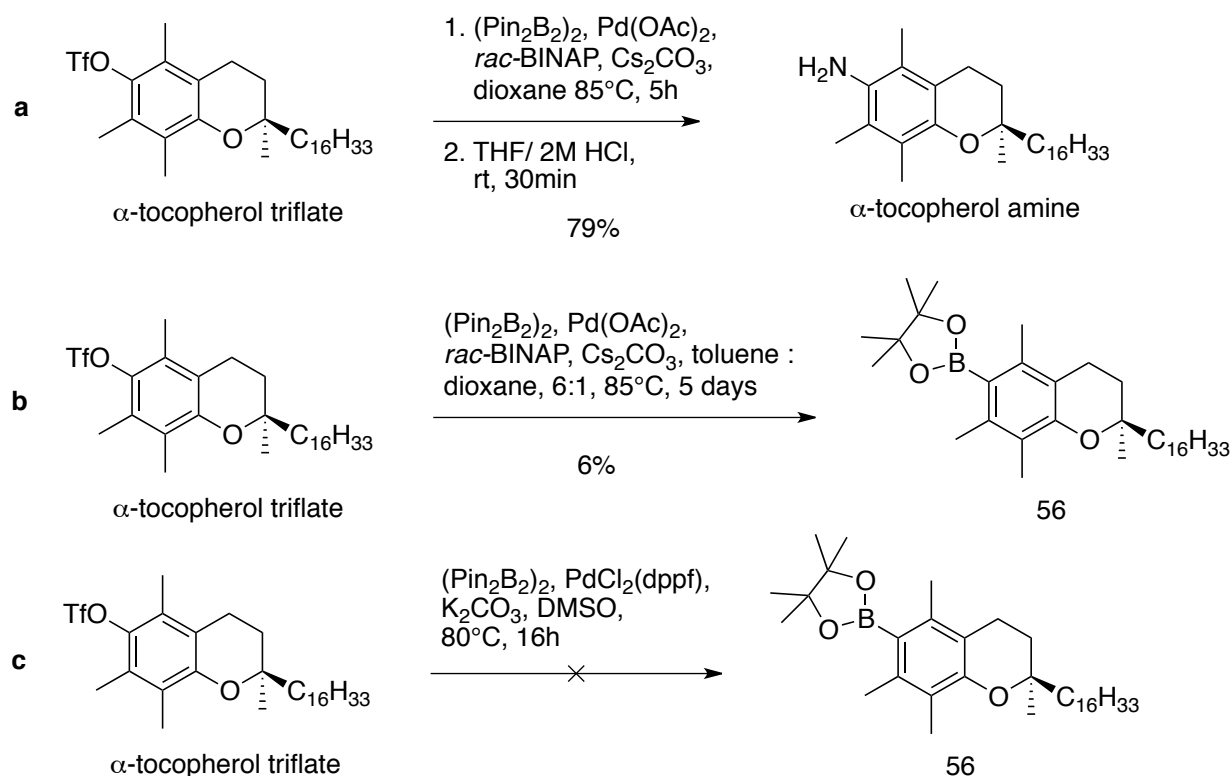


Figure 168. (a) Mazzini's α -tocopherol amine synthesis.⁵³⁰ (b) α -Tocopherol triflate borylation with Mazzini's conditions. (c) α -Tocopherol triflate borylation with $\text{PdCl}_2(\text{dppf})$.⁵³¹

Diemer found that ferrocene based ligands like 1,1'-bis(diphenylphosphino)ferrocene (dppf) are able to borylate sterically demanding, electron-rich iodoarenes. Recently, the reaction with 6-I- α -Toc yielded the α -tocopherol pinacole boryl ester **56** in low yield (Figure 169).^{532,533}

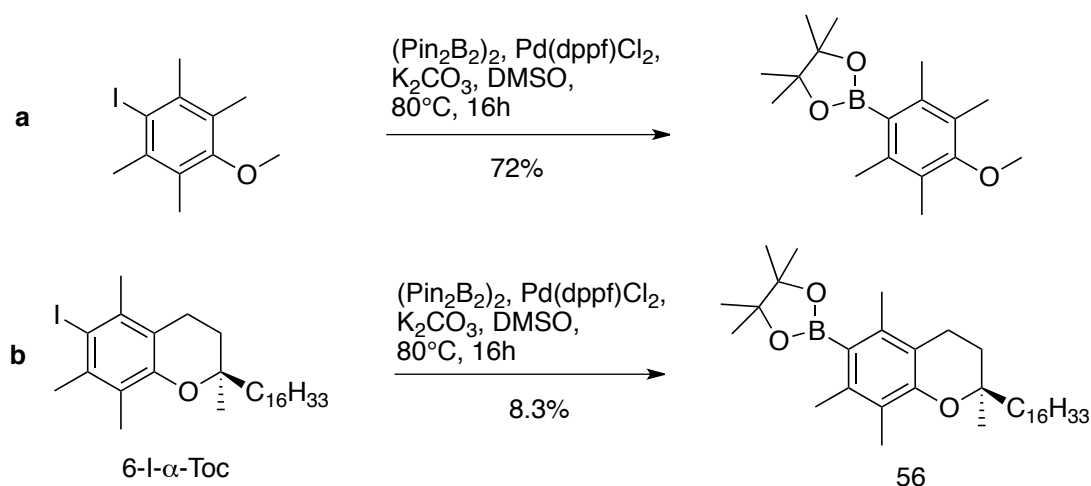


Figure 169 Palladium catalyzed borylation of sterically demanding, electron-rich aromatics.

(a) Diemer's borylation of 2,3,5,6-tetramethyliodoanisole. (b) Borylation of 6-I- α -Toc.⁵³²

Fluorination of **56** with tetrakispyridine copper(II)triflate fully converted the starting material, yielding H-Toc as the main product with trace amounts of **47** (Figure 170).⁵³⁴ Formation of H-Toc was caused by the presence of water in the reaction mixture.

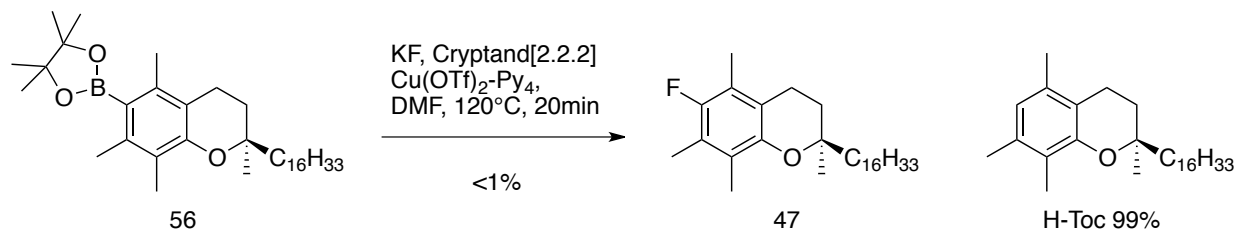


Figure 170. Tetrakispyridine copper(II)triflate catalyzed fluorination of **56.**⁵³⁴

11.2.1.3 Deoxyfluorination

Ritter's deoxyfluorination reaction uses the difluorinated N-heterocyclic carbene (NHC) Phenofluor[®] at elevated temperature in organic solvents to fluorinate phenols. An updated version of the original procedure was used for the fluorination of tocopherol. Instead of using the very hygroscopic phenofluor directly the precursor chloro-NHC salt, **58**, reacted with excess cesium fluoride (CsF) to form the active reagent *in situ*.⁵³⁵ **58** was produced according to the literature by chlorination of **57** with hexachloroethane (Figure 171).

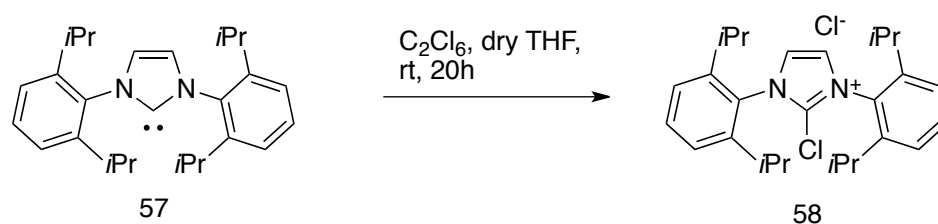


Figure 171. Synthesis of Phenofluor[®] precursor Cl-NHC.⁵³⁵

α -Tocopherol was reacted with **58** and 10 eq of CsF in dry toluene at 110°C for several days, but no fluorination product was observed. Testing the reaction on γ - and δ -tocopherol also did not yield a fluorinated product (Figure 172).

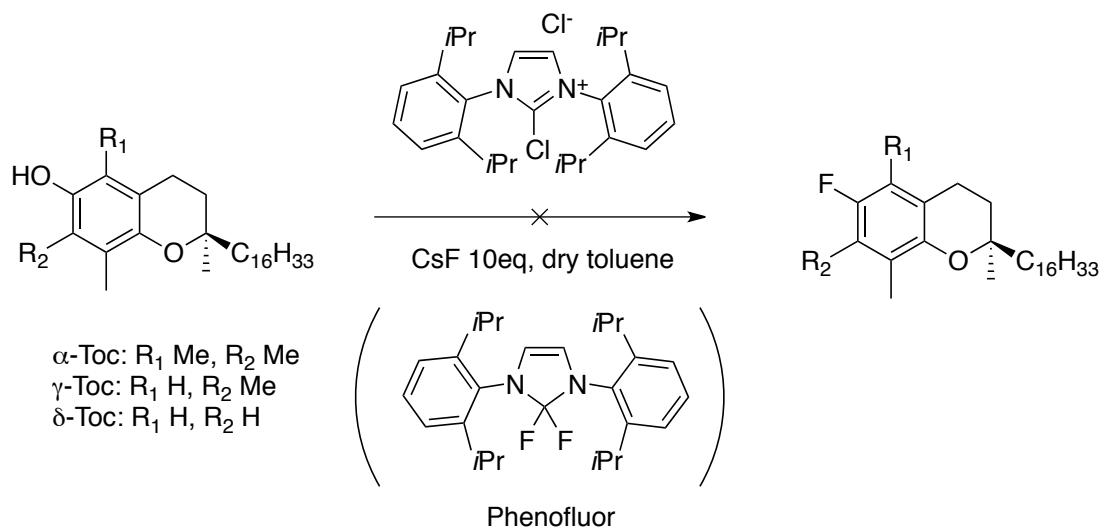


Figure 172. Attempted Phenofluor® fluorination of α -tocopherol.⁵³⁵

The starting material was re-isolated with trace amounts of unidentifiable products of high molecular mass (ESI: 600-1000 m/z). The crude product did not show any ¹⁹F NMR peaks of the expected 6-F- α -Toc at 131.49 ppm. No NHC substituted phenol intermediate **59** was seen by NMR spectroscopy with α -, γ -, or δ -tocopherol, an intermediate isolated with other aromatic phenols when studying the Phenofluor® reactivity (Figure 173).⁵¹⁸

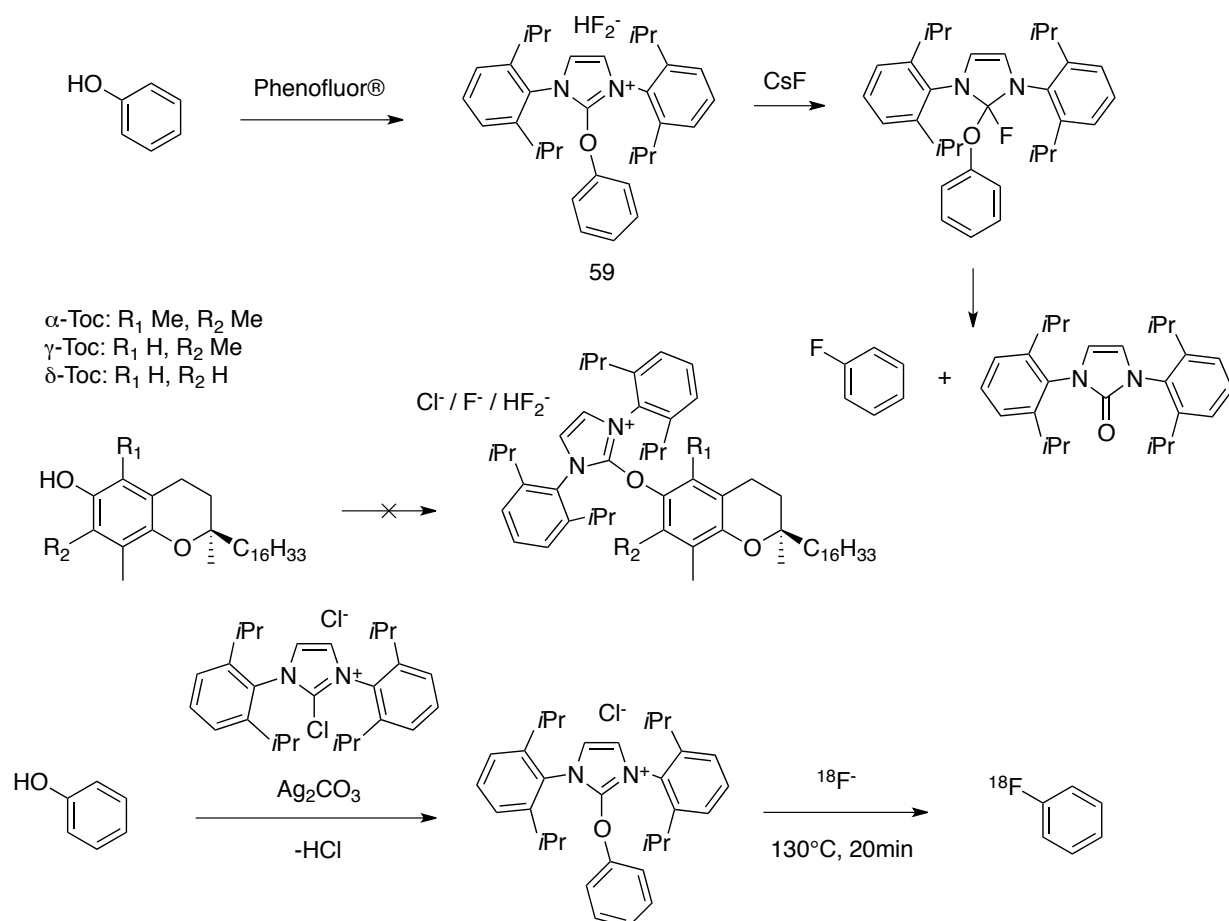


Figure 173 Phenofluor® intermediate 59 formation with phenols.

No NHC-tocopherol intermediate was observed.⁵³⁵

Since Phenofluor has been shown to yield product on a variety of phenols, this result was rather unexpected. However, in almost all literature examples no *ortho*-substituents are present. The two methyl groups *ortho* to the phenol of α -tocopherol seem to provide enough steric repulsion to inhibit the fluorination by Phenofluor®. δ -Tocopherol, on the other hand, has no *ortho*-methyl groups and still did not produce fluorinated product. Phenofluor has been recently used as a way to introduce ¹⁸F fluoride. The method described in Neumann's paper attaches the chloro-NHC salt to the phenol with silver carbonate (Ag₂CO₃), hence assisting fluorination (Figure 174).⁵¹⁸

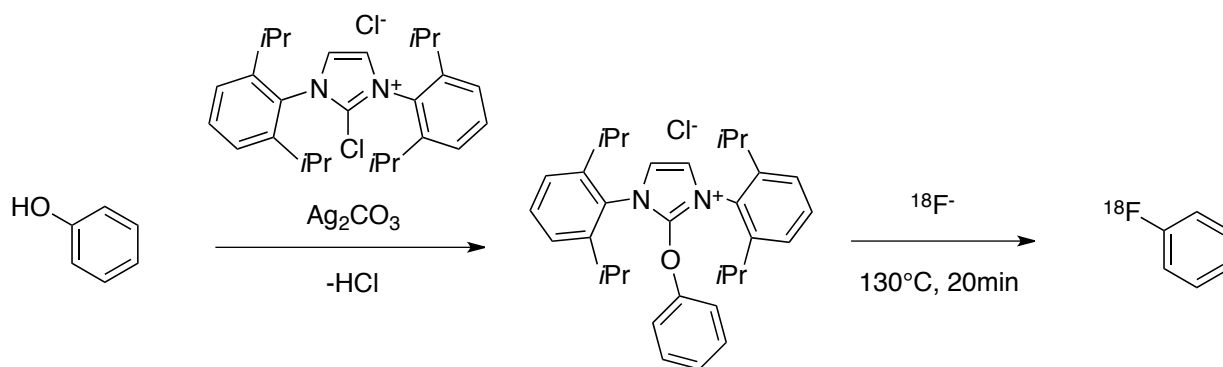


Figure 174. ^{18}F -fluorination of NHC-bound phenols.⁵¹⁸

In the case of tocopherols, silver salts are known to act as oxidizers, possibly forming the quinone or the quinone methide.^{536,537}

Ritter's group published a new way to substitute phenols with fluorine by using Phenofluor[®] with ruthenium complex $\text{CpRu}(\text{COD})\text{Cl}$. The group was able to ^{18}F -label δ -tocopherol with a 62% RCY in a short overall reaction time (Figure 175).⁵³⁸

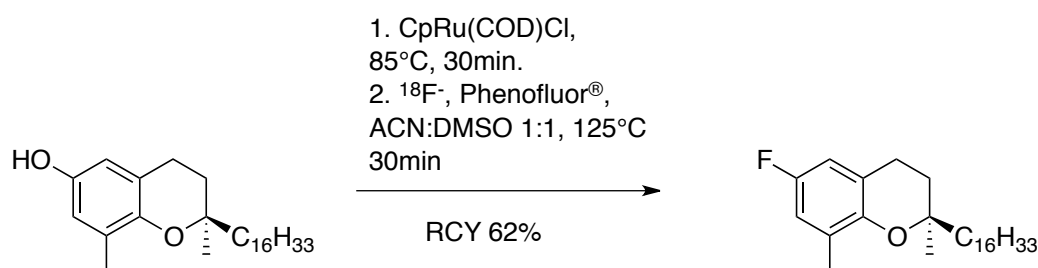


Figure 175. Ruthenium catalysed Phenofluor[®] fluorination of δ -tocopherol.⁵³⁸

11.2.1.4 Fluorination of α -Tocopherol Iodonium Salts

Nucleophilic fluorination of electron rich aromatic substrates has been achieved in high yields with diaryl iodonium salts. Fluorination depends on the electronic nature of the substituents and the aromatic groups involved. Electron-poor aromatics have higher fluoride incorporation.

Substituents on the *ortho*-position have been shown to effect the transition state equilibrium during the fluoride addition, Ts_1 vs Ts_2 , partially favouring the substituted aromatic transition state, Ts_1 . (Figure 176).^{539,540}

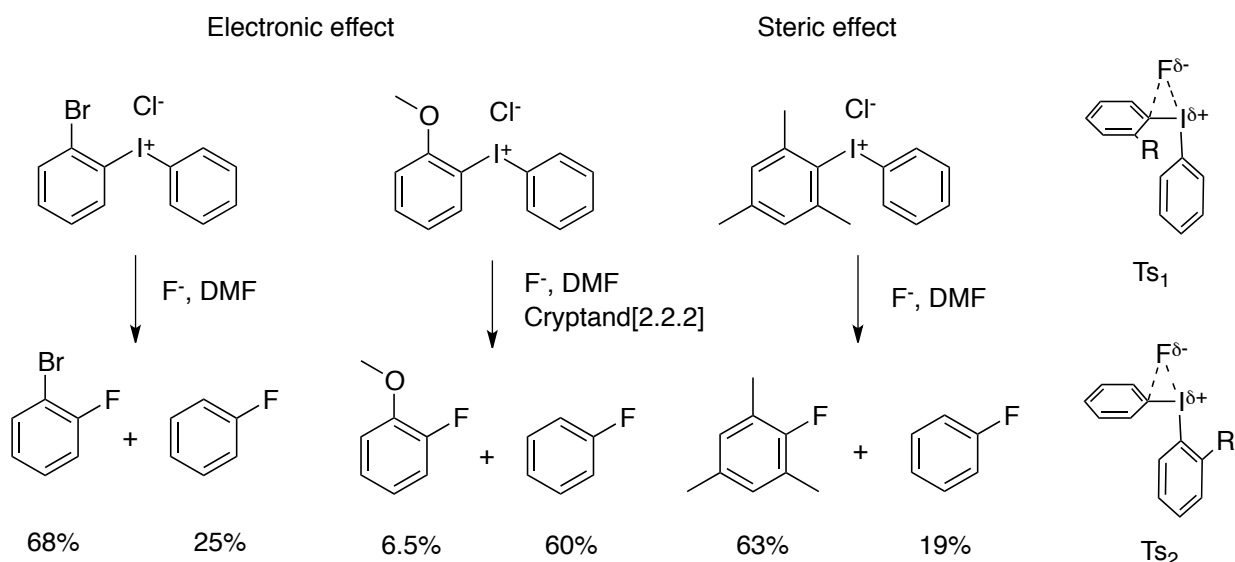


Figure 176. Nucleophilic fluorination of diaryliodonium salts.

Electronic effects of the aromatic ring: electron deficient aromatics are more prone to fluorination.
Steric effects of the aromatic ring: aromatics with *ortho*-substitution are more prone to fluorination, represented in $Ts_1 > Ts_2$. Yields represent observed radiochemical yields (RCY).^{539,540}

Tocopherol has two methyl groups at the *ortho*-position and is electron rich in nature.

Therefore, the aromatic group opposite to tocopherol (auxiliary) should be as electron-rich as possible. Two functional groups suitable for this purpose are *p*-methoxybenzene and thiophene (Figure 177).^{539,540}

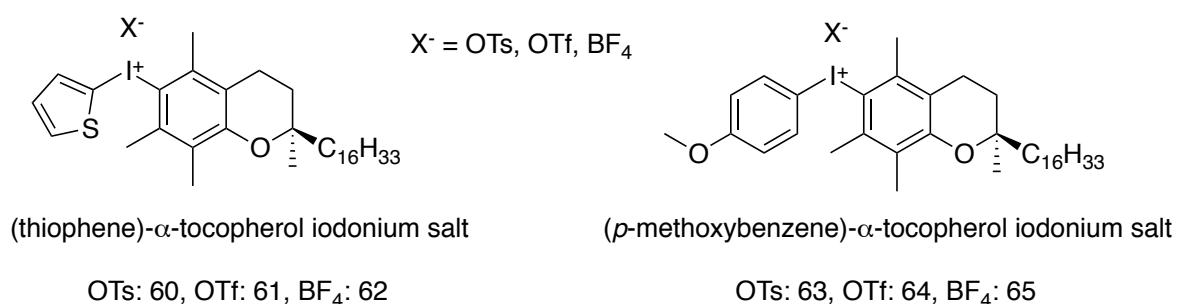


Figure 177. Designed electron rich 6- α -tocopherol iodonium salts with different auxiliaries: Thiophene 60 ·OTs, 61 ·OTf, 62 ·BF₄ and *p*-methoxybenzene 63 ·OTs, 64 ·OTf, 65 ·BF₄.

Diaryliodonium salts are synthesized by coupling hypervalent iodines with an aromatic group.

The hypervalent iodine is thereby either created *in situ* by oxidation of the aryl iodide with the

second aromatic group present or in a prior reaction.⁵⁴¹ Boronic esters⁵⁴² and stannanes⁴⁹⁰ have been used with hypervalent iodines to form the diaryliodonium salts (Figure 178).

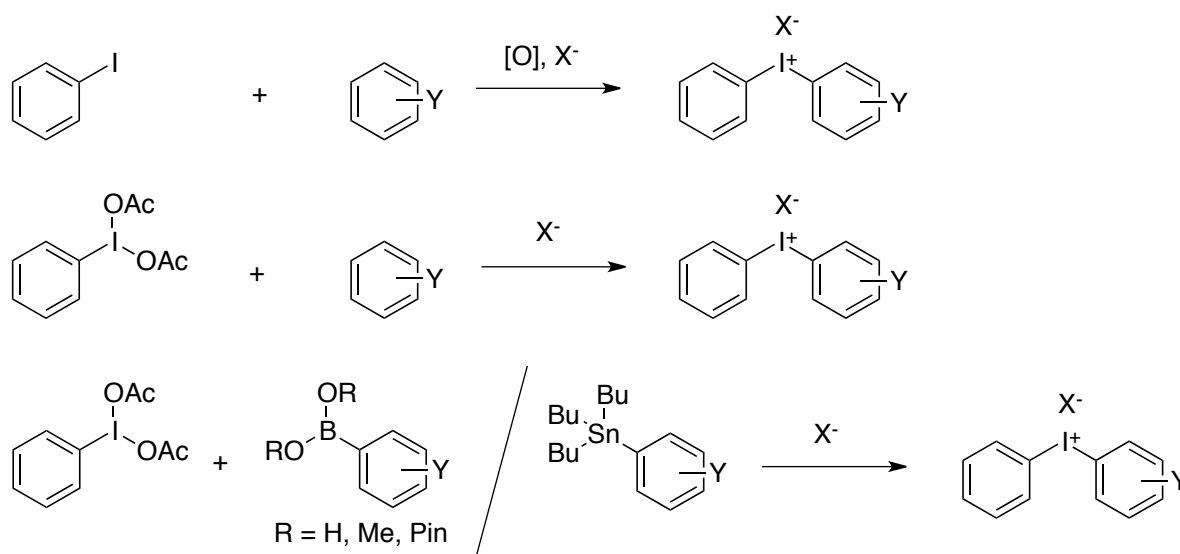


Figure 178. Synthesis of iodonium salts via insitu oxidation of aryl iodides with aromatics (Y) (top), with pre-oxidized hypervalent iodines / aromatics (middle) and boronic acids / esters or stannylates (bottom).^{541,542,490}

Recently, iodonium ylides with Meldrum's acid have been used as the counter auxiliary with good fluoride incorporation (Figure 188).^{543,544}

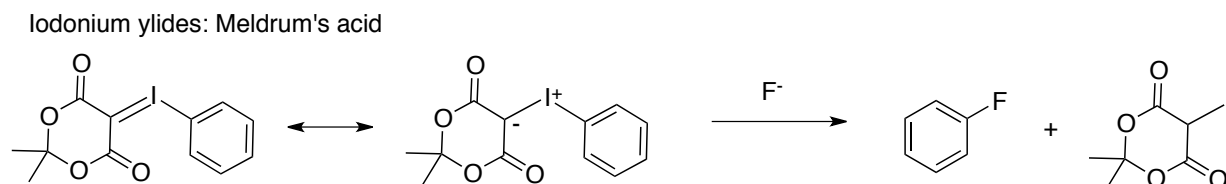


Figure 179. Fluorination of Meldrum's acid iodonium ylides.⁵⁴³

The synthesis of 6-diaryliodonium salts of tocopherol can be achieved by reacting H-Toc with hypervalent iodine or by oxidation of 6-I-Toc in reaction with another aryl group (Figure 180).

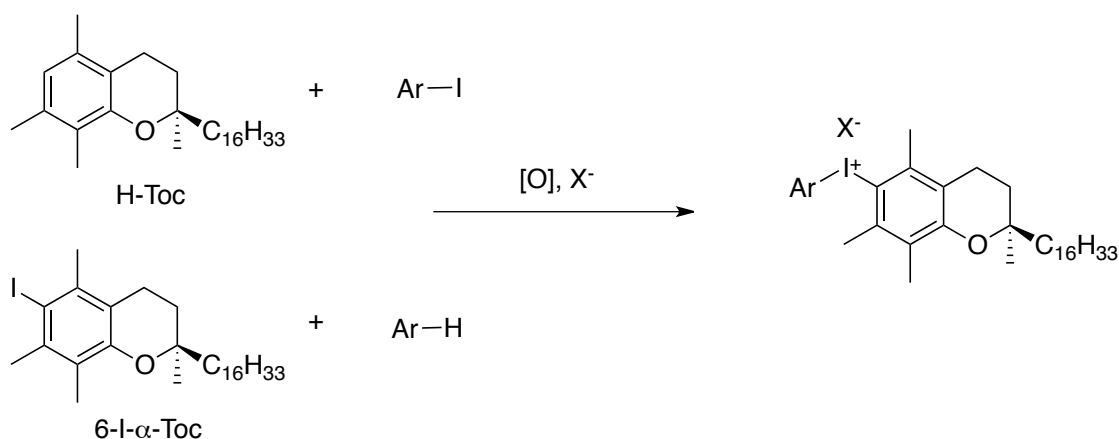


Figure 180. (Aryl)- α -tocopherol iodonium salt synthesis from H-Toc or 6-I- α -Toc.

In a first attempt to create the 6-(thiophene)iodo- α -tocopherol, trifluoroacetate salt, **61**, was prepared by reacting H-Toc with 2-iodothiophene, *meta*-chloroperbenzoic acid (*m*CPBA) and trifluoroacetic acid at -78°C .⁵⁴⁵ The reaction did not yield the desired product, but rather α -tocopheryl quinone and 6,6'-bis-tocopherol, **66**, besides the unreacted starting material (Figure 181).

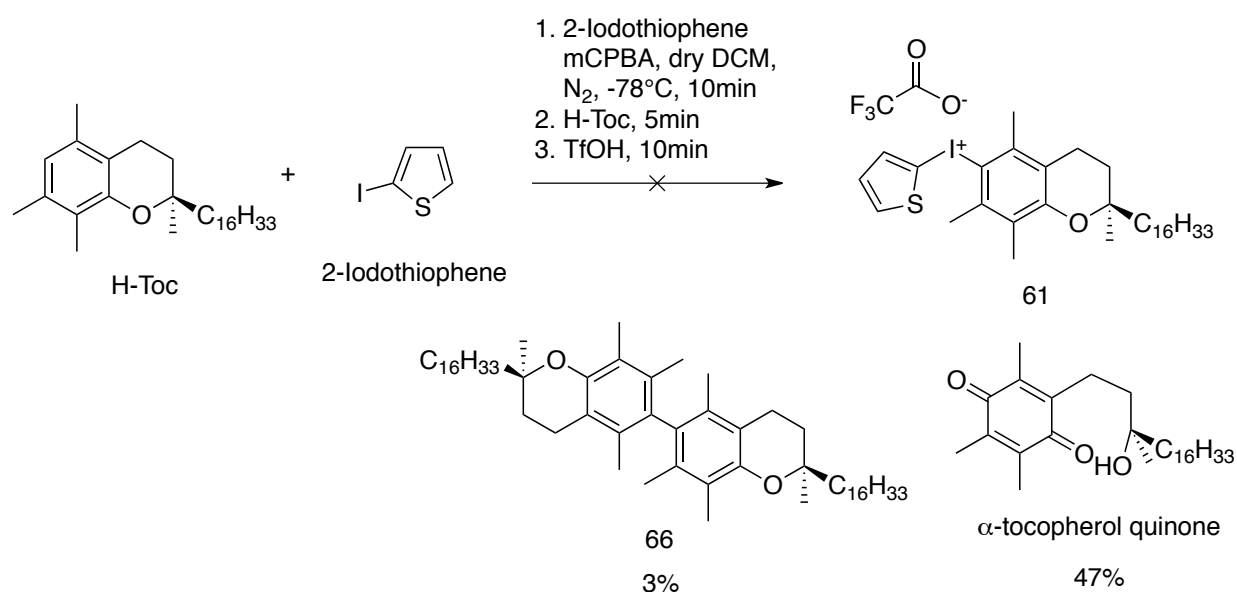


Figure 181. Synthesis of (thiophene)- α -tocopherol iodonium trifluoroacetate, **61.⁵⁴⁵**

Byproducts α -tocopherol quinone and 6,6'-bis- α -tocopherol **66 were formed as products.**

Oxidizing agents like *m*-CPBA react with H-Toc to form oxidized tocopherol products after prolonged stirring. To avoid this problem the auxiliary ligand was created in a prior reaction is created before being mixed with H-Toc (Figure 182).⁵⁴⁶

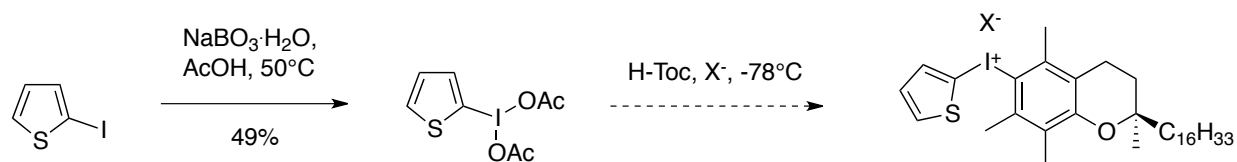


Figure 182. 2-(Diacetoxy)thiophene synthesis by Wu⁵⁴⁶, followed by addition to H-Toc.

Before trying the reaction with (diacetoxy)iodothiophene the (phenyl)tocopherol iodonium salt was created with (diacetoxy)iodobenzene. Electron rich aromatics like (diacetoxy)iodothiophenes are more reactive when forming the diaryliodonium salt and form less stable diaryliodonium salts that are prone to faster decomposition. The (phenyl)tocopherol iodonium salt offers a more stable, easier to synthesize alternative to study the fluorination reaction. The reaction of H-Toc with (diacetoxy)iodobenzene and acetic acid with potassium bromide should yield **67** or with trifluoroacetic acid **68**, but neither product was obtained, only dimer **66** (Figure 183 and 184).⁵³⁹

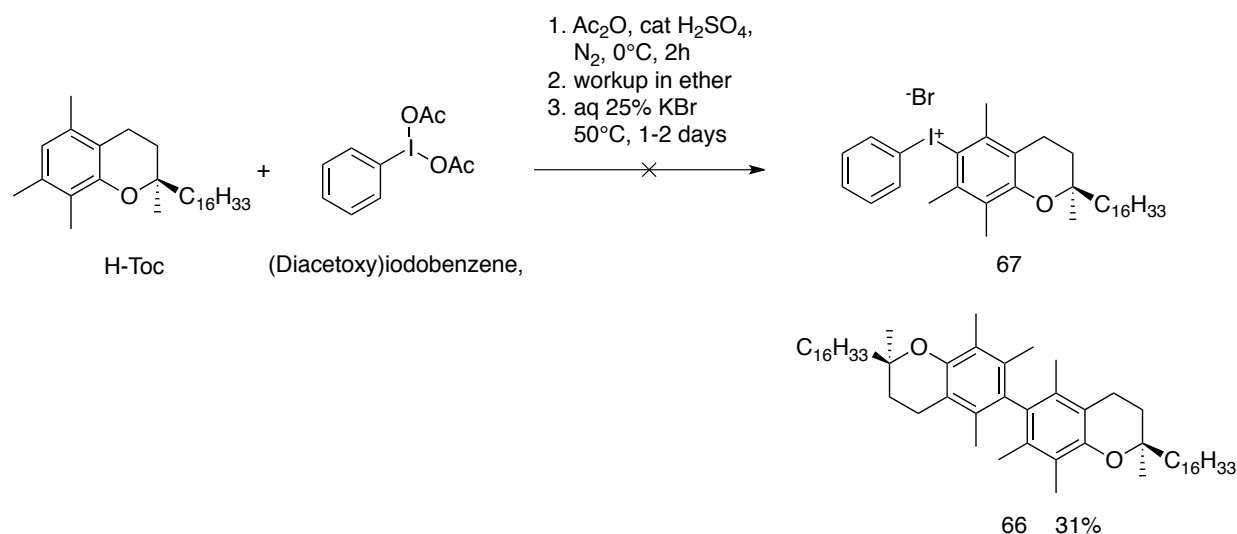


Figure 183. Synthesis of (R)-(2-hexadecyl-2,5,7,8-tetramethylchroman-6-yl)(phenyl)iodonium bromide **67** from H-Toc.⁵³⁹

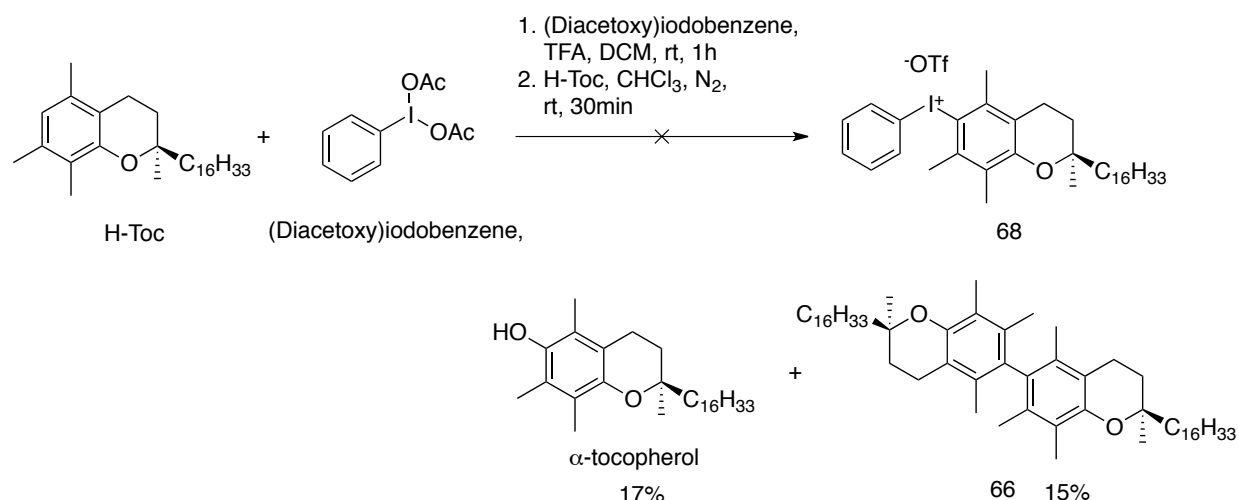


Figure 184. Synthesis of (*R*)-(2-hexadecyl-2,5,7,8-tetramethylchroman-6-yl)(phenyl)iodonium trifluoroacetate **68 from H-Toc.⁵⁴⁵**

By using a procedure described by Chun (diacetoxy)iodobenzene was reacted with H-Toc in the presence of *p*-toluenesulfonic acid, yielding product **69** in low yield (Figure 185).⁵⁴⁷

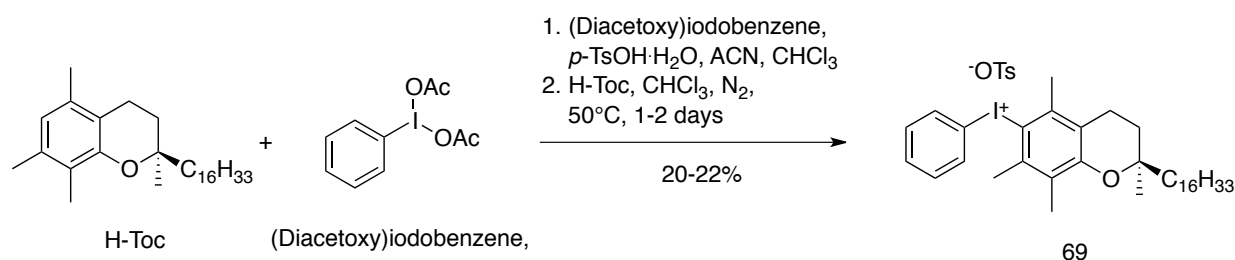
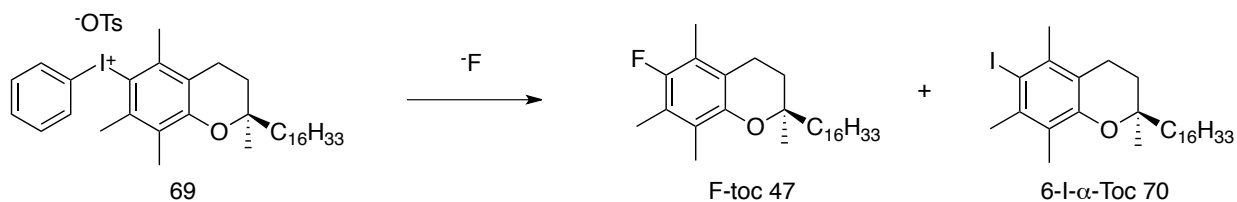


Figure 185. Synthesis of (*R*)-(2-hexadecyl-2,5,7,8-tetramethylchroman-6-yl)(phenyl)iodonium tosylate **69 from H-Toc.⁵⁴⁷**

In a first attempt, **69** was fluorinated using cesium fluoride (CsF) without any fluoride carrier additives like cryptand[2.2.2] or 18-crown-6 (non-carrier additive, NCA) in acetonitrile, which yielded **47** in low yields after 1-2 days. Fluorination was then conducted in the presence of 18-crown-6, cryptand[2.2.2] as carrier additive (CA) and potassium fluoride (KF), and CsF as fluoride sources at 80°C. Reactions were run for a maximum of 30 min and one third isolated after 5 min and 10 min. Acetonitrile was chosen as the solvent of choice because it is easier to remove from the reaction mixture. Fluorination with CA tetrabutylammonium fluoride (TBAF) was conducted in THF and DMF to see the how different solvents effect the outcome of the fluorination (Table 23).



| F ⁻ -source | Fluoride carrier additive | | Solvent ⁵⁴⁸ | Temp (°C) | Time | Yield F-Toc ^a |
|------------------------|---------------------------|---------------|------------------------|-----------|-------------------------------------|--------------------------|
| CsF (2eq) | - | | Dry ACN 2.5mM | rt | 2days | 9.1% |
| CsF (2eq) | - | | Dry ACN 2.5mM | 80 | 1day | 3.6% |
| CsF (1eq) | 18-Crown-6 (1eq) | | Dry ACN 5mM | 80 | 5min ^b 15min 30min | - - 2.7% |
| CsF (5eq) | 18-Crown-6 (5eq) | | Dry ACN 5mM | 80 | 5min ^b 15min 30min | - - - |
| KF (1eq) | Cryptand[2.2.2] (1eq) | | Dry ACN 5mM | 80 | 5min ^b 15min 30min | - - 11.3% |
| KF (5eq) | Cryptand[2.2.2] (5eq) | | Dry ACN 5mM | 80 | 5min ^b 15min 30min | - - - |
| KF (1eq) | 18-Crown-6 (1eq) | | Dry ACN 5mM | 80 | 30min | 6.6% |
| TBAF 1M in THF (1eq) | | | Dry ACN 5mM | 80 | 30min | 5.7% |
| TBAF 1M in THF (1eq) | | | Dry THF 5mM | 80 | 30min | 2.3% |
| TBAF 1M in THF (1eq) | | | Dry DMF 5mM | 80 | 30min | 10.1% |
| KF (1eq) | Cryptant[2.2.2] (1eq) | | Dry DMF 5mM | 150 | 15min | 25.6% |
| KF (1eq) | Cryptant[2.2.2] (1eq) | TEMPO (0.2eq) | Dry DMF 5mM | 150 | 15min | 23.4% |
| TBAF 1M in THF (1eq) | | | Dry DMF 5mM | 150 | 15min | 24.4% |
| TBAF 1M in THF (1eq) | TEMPO (0.2eq) | | Dry DMF 5mM | 150 | 15min | 22.3% |

Table 23 Fluorination of (R)-(2-hexadecyl-2,5,7,8-tetramethylchroman-6-yl)(phenyl)iodonium tosylate 69.

69 (20 mg, 25.3 μmol) was dissolved in ACN, THF or DMF. Fluoride was added with an additive and stirred for 5-30 min. The solvent was evaporated and the residual mixture partitioned between with hexane and water. The organic phase was dried with Na_2SO_4 , filtrated and purified over a small SiO_2 column with hexane. (a) Yield by $^1\text{H-NMR}$ (b) After 5 min was 1/3 of the reaction mixture worked up. The reaction yield is calculated to 1/3 of the starting material.

It was expected that the (phenyl)tocopherol iodonium salt, **69**, would lead to low fluorine incorporation into the tocopherol. NCA fluorination without carrier additives like 18-crown-6, cryptand[2.2.2] and tetraalkylammonium in ACN does not yield product in a short time period. A reaction time of at least 30 minutes is needed to obtain product in a 10% yield without CA.⁵⁴⁹ 6-Iodotocopherol was the major by-product obtained. DMF was the best solvent for the fluorination with TBAF when the temperature was kept at 80°C. Running the reaction at 150°C in DMF for 20 min increased the yield to 22-25%.⁵⁴¹ The best reaction conditions discovered so far (1eq KF/Cryptand[2.2.2] and TBAF in DMF, 150°C) need to be tested in the future with different counter ions.⁵⁵⁰ Reports by Ross and Hamnett showed a higher reactivity with boron tetrafluoride⁵⁵¹ and trifluoroacetic acid⁵⁵² as counter ions. Radical scavengers like TEMPO and BHT have been found to increase the yield, but showed no effect when run with KF/Cryptand[2.2.2] or TBAF in DMF.⁵⁵³

The reaction also forms the 6-iodo- α -tocopherol (6-I- α -Toc, **70**) as a by-product. Purification of the F-Toc by column chromatography is possible, but the retention time of the 6-I- α -Toc is quite similar and this makes the purification less efficient. A better separation is achieved when the 6-I- α -Toc is converted to a more polar functional group, as the retention time difference on the SiO_2 column is increased. Two possibilities were the conversion of 6-I- α -Toc into a carboxylic acid **71** by quenching the respective Grignard species or organolithium from lithium-

halogen exchange of 6-I- α -Toc, with CO₂ (Figure 186).

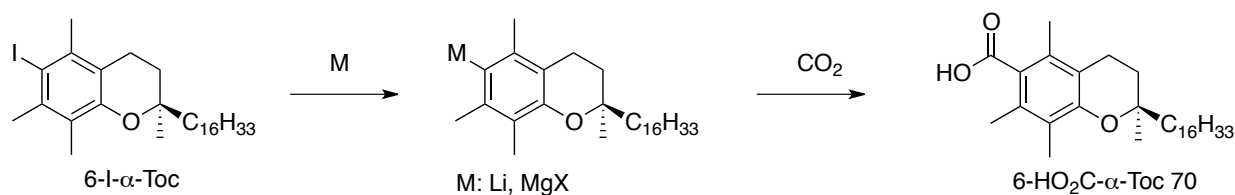


Figure 186. Carboxylation of 6-I- α -Toc via lithium-halogen and Grignard reaction.

Formation of the Grignard species with 6-I- α -Toc in short reaction times did not work with excess magnesium or methylmagnesium chloride (MgMeCl).⁵⁵⁴ Lithium-halogen exchange was conducted at room temperature for an immediate reaction to reduce the reaction time to 1-5 min. However, rapid bubbling with dried CO₂ gas did not yield any carboxylic acid. Fast carbonylation chemistry was used by Al-Qahtani to create ¹¹C-acetophenone adducts.⁵⁵⁵ When the reaction was conducted in water instead, a carboxylic acid formed as the main product. Using catalytic amounts of palladium chloride (PdCl₂) did not yield any product with CO gas. Using equimolar amounts of PdCl₂ to simulate one catalytic turnover did not yield product either (Figure 187).

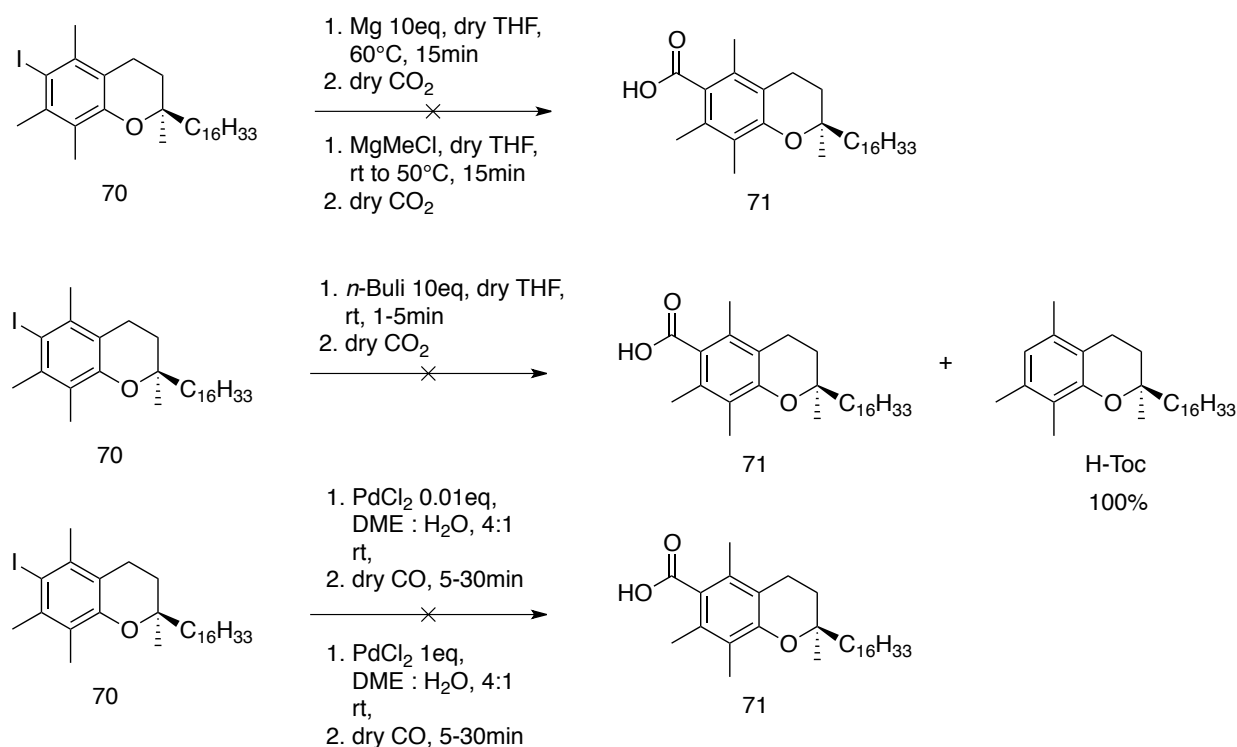


Figure. 187 Carboxylation of 6-I- α -Toc 71 with magnesium (top),⁵⁵⁴ lithium-halogen exchange (middle) and palladium dichloride catalyzed carbonylation (bottom).⁵⁵⁵

Changing the functional group from a carboxylate to a boronic acid would have the same effect of enhancing the retention time difference to ease purification. Chen published a procedure for a fast photoborylation of aryl halides in continuous flow conditions. Bispinacol borane and tetrahydroxydiborane (B₂OH₄) were used as the borylating agent.⁵⁵⁶ Reaction times were in the range of 15 min to obtain products in yields around 90% (Figure 188).

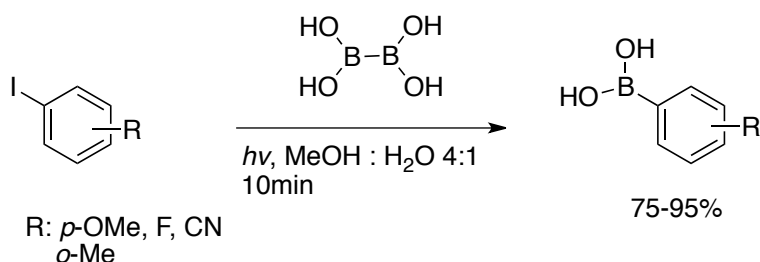


Figure 188. Photoborylation of aryl iodides with B₂OH₂ by Chen.⁵⁵⁶

6-I- α -Toc **70** and B₂OH₄ were passed in different solvent mixtures through a photoreactor with a 300W Hg lamp having an emission maximum around 350 nm (Luzchem, UVA lamp). Initial problems with starting material solubility were overcome by dilution and the use of more non-polar solvents such as acetonitrile and THF. Increasing the reaction time led to almost full

consumption of the starting material, however only H-Toc was isolated, and ^{11}B -NMR has shown no signs of any aryl borylate or boronic acid (around +30 ppm) (Table 24).

| Borylating agent (eq) | Solvent | Time | Yield (HO) ₂ B-Toc (%) ^a | Yield H-Toc (%) | Yield I-Toc recovered (%) |
|------------------------------------|--|-------|--|-----------------|---------------------------|
| B ₂ OH ₄ 2eq | MeOH:H ₂ O 4:1 92mM | 10min | -% | 40% | 60% |
| B ₂ OH ₄ 2eq | ACN:THF 1:1 + H ₂ O 5% 25mM | 3h | -% | 65% | 3% |

Table 24. Photoborylation of 6-I- α -Toc to form 72.

6-I- α -Toc was mixed with B₂OH₂ in the solvents and pressed through a 70 cm, diameter fluorinated ethylene propylene (FEP) tubing by an injection pump. The solvent was evaporated and the crude mixture columned over a SiO₂ column. (a) Verified by ^{11}B -NMR.⁵⁵⁶

Spirocyclic Meldrum's acid iodonium ylides were reported to be stable precursors and good for the incorporation of non-reactive, sterically demanding aromatics (Figure 189).⁵⁵⁷

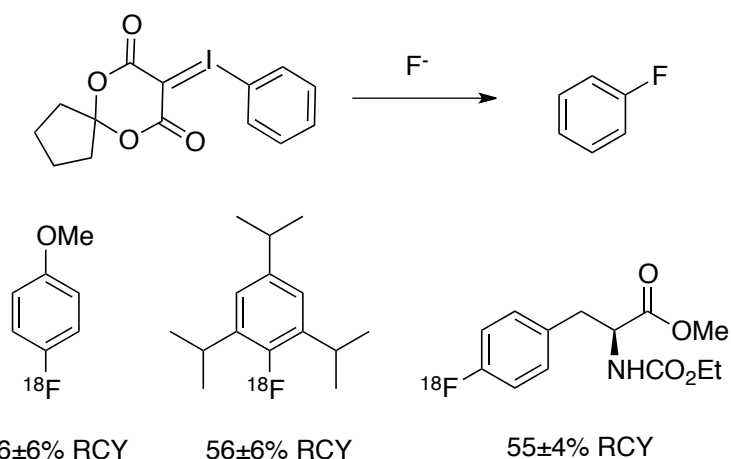


Figure 189. Fluorination of spirocyclic Meldrum's acid iodonium ylides.⁵⁵⁷

An attempt was made to create the 6'-(Meldrum's acid)- α -tocopherol iodonium ylide **73**, following the synthesis of Cardinale.⁵⁴³ Compound **70** (for the synthesis of 6-I- α -Toc **70**, see section 16.2.2 fluorination of 6-iodo- α -tocopherol) was treated first with *m*-CPBA, followed by

addition of Meldrum's acid and excess KOH (7eq). No reaction occurred after the time suggested in the literature. When the reaction was stirred for a longer time after the addition of *m*CPBA and Meldrum's acid, α -tocopherol quinone was formed (Figure 190).

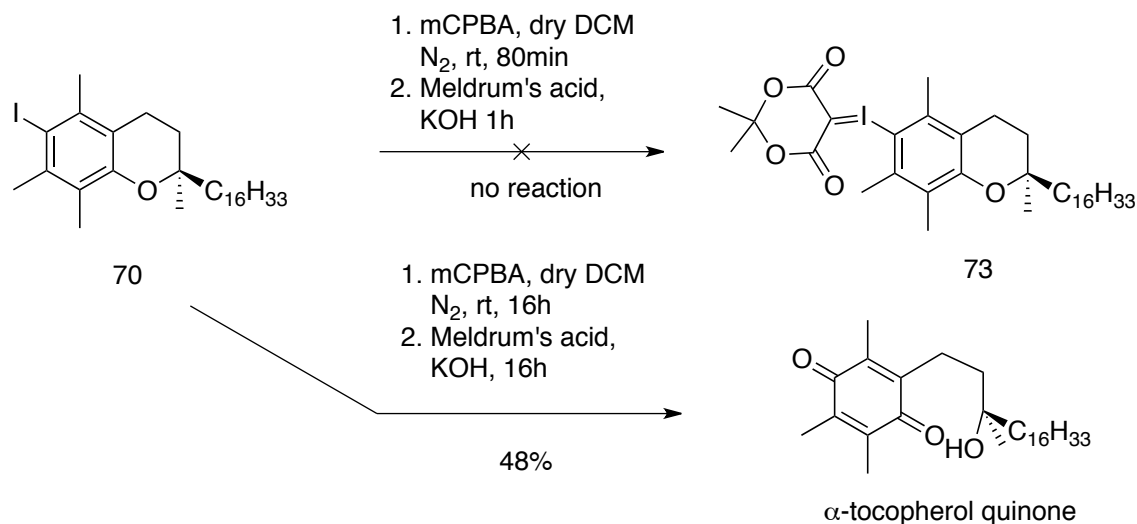


Figure 190. Meldrum's acid- α -tocopherol iodonium ylide synthesis **73** from **6-I- α -Toc**.⁵⁴³

The oxidation of iodotocopherol was tried with peracetic acid in acetic acid with the hope of forming the (diacetoxy)iodo- α -tocopherol, **74**.⁵⁴¹ After 8h reaction time no product could be isolated, and only starting material and α -tocopherol quinone were obtained (Figure 191).

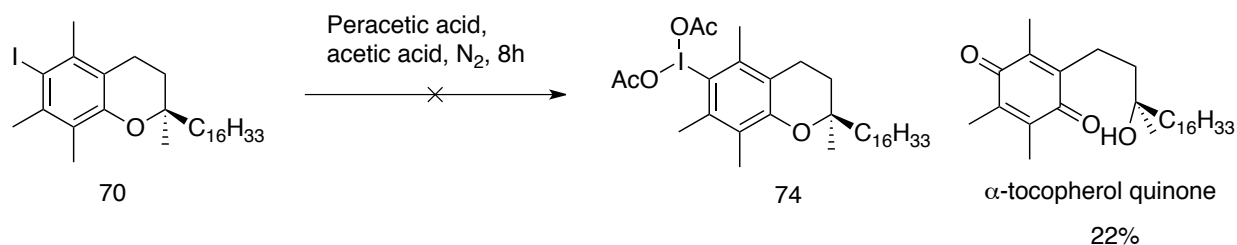


Figure 191. Synthesis of (diacetoxy)iodo- α -tocopherol **74** from **70**.⁵⁴¹

Fluorination of iodonium salts or ylides are a promising methods to synthesize F-Toc. Future work with more electron donating auxiliaries like thiophenes will be necessary to improve the reaction yield. So far, no conditions have been found to oxidize iodotocopherol into a hypervalent iodine species, which makes the addition of more electron rich auxiliaries like thiophene and *p*-methoxybenzene more difficult and prohibits the synthesis of Meldrum's acid derivatives.

11.2.2 Synthesis of 6-F-tocopherol by electrophilic fluorination:

11.2.2.1 Fluorination of 6-Iodo- α -tocopherol

Miller described the synthesis of 6-iodo- δ -tocopherol from the δ -tocopherol triflate via the 6-stannane- δ -tocopherol.⁵⁵⁸ But as described previously, attempts to obtain these compounds were not successful with α -tocopherol (see section stannylation of aryl stannane tocopherol fluorination). Hence, the same strategy was used when synthesizing Cl-Toc, **43**, by iodination of H-Toc. The starting material H-Toc, **42**, was synthesized from α -tocopherol by reduction of its triflate **41**.⁴²⁴

Synthesis of **70** with iodine monochloride (ICl) in DCM did not yield any product **42**. In the same literature DDQ was used to quench radical intermediates, but no product were observed when the reaction was run with DDQ.⁵⁵⁹ Iodination with iodine (I₂) and silvertriflate (AgOTf) did not produce the iodinated product, but the dimerized product **66**.⁵⁶⁰ I-Toc **70** was synthesized with 1-iodopyridinium chloride **71** in a 71% yield (Figure 192).⁵⁶¹

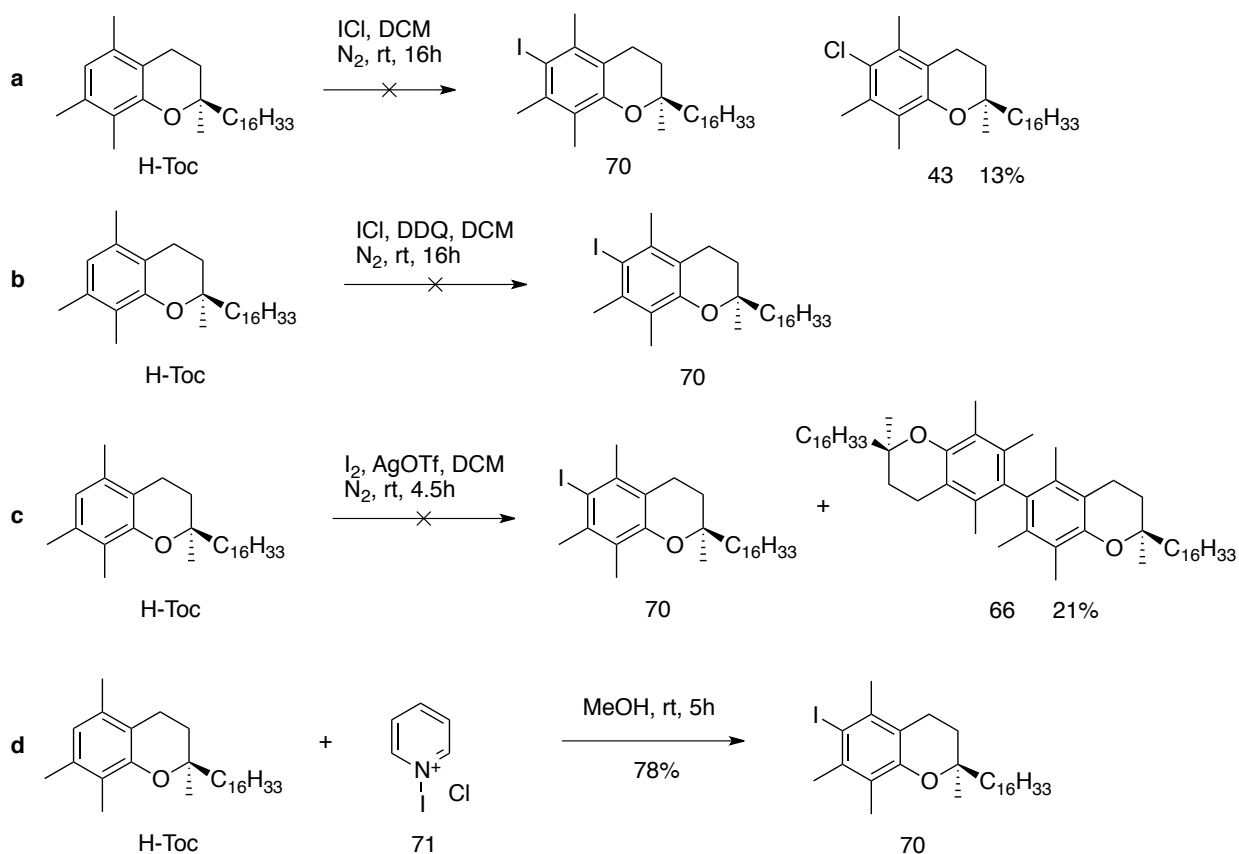
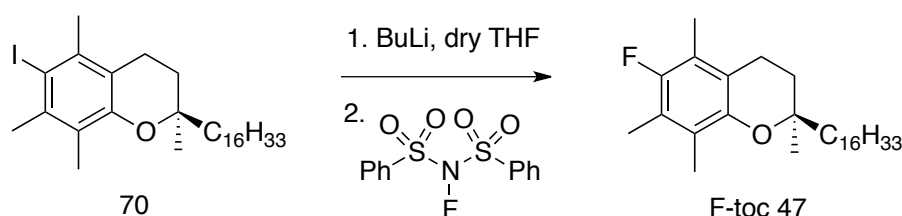


Figure 192. Iodination of H-Toc. (a) with ICl,⁵⁵⁹ (b) ICl, DDQ,⁵⁵⁹ (c) I₂, AgOTf⁵⁶⁰ and (d) 1-iodopyridinium chloride **71.⁵⁶¹**

Nagaki developed an aryl fluorination of lithiated electron-rich and poor aromatic halides (Br, I) in a microreactor flow system.⁵²⁰ Fluorination occurred at temperatures from -40°C to 0°C with N-fluorobenzenesulfonimide (NFSI) and N-fluorosulfam yielding fluoroaryls in 30-85% yields. Reaction times from the injection to the isolation of the product were 15 s.

The electrophilic fluorinating reagent chosen for the fluorination of 6-I- α -Toc was N-fluorobenzenesulfonimide (NFSI), based on reports by Barnette, Satyamurthy and Teare.^{562,563,564} **70** (80-150 mg) was lithiated and fluorinated in batch reactions, first with 1eq of NFSI at 0°C and *n*-BuLi as a test reaction (Table 25). The reaction time of *n*-BuLi was kept short (5 min), which led to a 5.3% yield of F-Toc and 49% of H-Toc. Deprotonation (lithium halogen exchange) of aryl halides are normally done with 2eq of *t*-BuLi, the first for lithium - halogen exchange, the second to quench the *t*-butyl halide to isoprene and lithium iodide.^{565,566} NFSI was dried azeotropically with ACN prior to the next reaction and 2eq of NFSI were used to

achieve a higher yield. A one minute reaction time after *t*-BuLi addition yielded 15% F-Toc (19% H-Toc). Decreasing the reaction time to 30s for each step was attempted with excess *n*- and *t*-BuLi (fresh *t*-BuLi was used) and excess NFSI. Short reaction times with excess base resemble the flow conditions used by Nagaki. In the same paper it was mentioned that the reaction temperature does not influence the reaction yield and so the temperature was changed to room temperature to ease the addition conditions. However, the decreased reaction time did not improve the yield, and even when an 8eq excess of NFSI was used only a small amount of F-Toc was produced. Increasing the lithiation time of 6-I- α -Toc to 50 min at -78°C yielded 8% product after isolation. Lithium-exchange up to 2.75 h did not increase the yield of F-Toc.



| Reagent (eq) | NFSI | Solvent | Temperature | Stirring time BuLi | Stirring time rxn | Yield F-Toc | Yield H-Toc |
|------------------------|-------|---------|-------------|--------------------|-------------------|-------------|-------------|
| <i>n</i> -BuLi (1.3eq) | 1.3eq | THF | 0°C | 5min | 30min | 5.3% | 49% |
| <i>t</i> -BuLi (2eq) | 2eq | THF | 0°C | 1min | 1min | 15% | 19% |
| <i>n</i> -BuLi (2eq) | 4eq | THF | rt | 30s | 30s | 1.1% | 4.6% |
| <i>t</i> -BuLi (2eq) | 4eq | THF | rt | 30s | 30s | 3.1% | 30% |
| <i>t</i> -BuLi (4eq) | 8eq | THF | rt | 30s | 30s | 4.2% | 21% |
| <i>t</i> -BuLi (2eq) | 2eq | THF | -78°C | 50min | 30min | 8.3% | 16.4% |
| <i>t</i> -BuLi (2eq) | 2eq | THF | -78°C | 2.5h | 15min | 9.6% | 53.0% |

Table 25. Fluorination of 6-I- α -toc with BuLi and NFSI.

Reactions were run on a 0.16-0.27 mmol scale as 0.85 M solutions.

All the conditions tried were not as successful as expected. F-Toc was synthesized in a 15% yield in a 2 min reaction time. This is a promising result for this chemistry, but optimization is necessary. Running the reaction in a flow microreactor should be the next step in future attempts. Automated processes based on flow chemistry are already used in hospitals to produce radioactive tracers like ^{18}F -FDG. Advantages of the flow microreactor are the fast reaction times, superior control of the addition speed and better mixing.⁵⁶⁷

11.2.2.2 H-Toc fluorination to 6-F-Toc

Tocopherol analogue H-Toc was fluorinated with nitrogen based fluorinating agents like N-fluorobenzenesulfimide (NFSI), Selectfluor[®] and 1-fluoropyridinium tetrafluoroborate (F-Py BF₄) (Figure 193).^{568, 506}

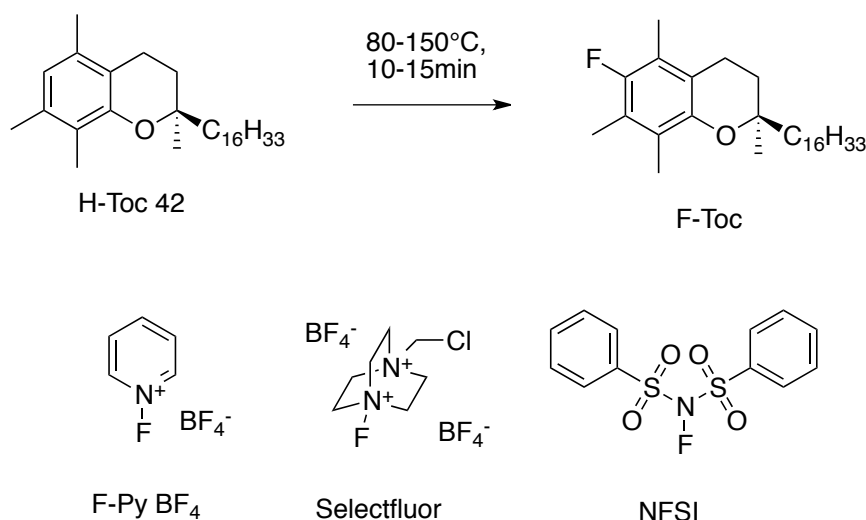


Figure 193. Synthesis of F-Toc from H-Toc with electrophilic fluorinating reagents F-Py BF₄, Selectfluor[®] and NFSI.^{568,506}

Reaction of H-Toc, **42**, with Selectfluor[®] did not yield any product in 0.25 M acetonitrile or THF. NFSI yielded product after several days of stirring in THF. NFSI fluorination has been done in neat conditions with mono- to pentamethylated benzene, yielding fluorinated polysubstituted benzenes with yields up to 70%.⁵⁶⁹ H-Toc reaction with neat NFSI yielded with H-Toc in 10-15 min reaction time up to 34% product (Table 26). Increasing the temperature to 150°C slightly increased the yield with NFSI and additionally gave product with neat Selectfluor[®]. To increase reactivity, the reaction was tested as a concentrated solution (1M solutions) in different solvents. The solvent should help to increase contact between the electrophilic fluorinating reagents and H-Toc. When THF was the solvent product was recovered with NFSI, and DMSO did not yield any product in any case. Fortunately, when the solvent was DMF all fluorinating reagents gave product. The highest yields were obtained with

acetonitrile and NFSI. Using excess (4 eq) NFSI or radical scavenger (2,2,6,6-tetramethylpiperidin-1-oxyl (TEMPO)) did decrease product yield. The addition of TEMPO was thought to lower radical byproduct formation and increase the yield by an electrophilic aromatic fluorination mechanism.⁵⁷⁰ However, the decreased yield with TEMPO verifies that reaction mechanism is based on a single-electron transfer (SET).^{571,572}

| F ⁺ -Source | | Solvent ^a | Temp (°C) | Time | Yield ^b 6-F-Toc (%) | Re-isolated 6-H-Toc (%) |
|------------------------|--------|----------------------|-----------|------------|-----------------------------------|----------------------------|
| Select F | 1eq | 0.25M ACN | 120 | 20min-days | 0% | 0% |
| Select F | 1eq | 0.25M THF | 80 | 20min | 0% | 0% |
| NFSI | 2eq | 0.12M THF | 40 | 4days | 25% | 26% |
| NFSI | 2eq | 0.12M THF | 60 | 4days | 20% | 0% |
| NFSI | 1eq. | Neat | 100 | 13min | 34% | 26% |
| Select F | 1eq | Neat | 100 | 13min | 0% | 100% |
| Py-F BF ₄ | 1eq | Neat | 100 | 13min | 0% | 100% |
| NFSI | 1eq | Neat | 150 | 13min | 38% | 11% |
| Select F | 1eq | Neat | 150 | 13min | 11% | 89% |
| Py-F BF ₄ | 1eq | Neat | 150 | 13min | 0% | 100% |
| NFSI | 1eq. | 1.0M THF | 80 | 13min | 37% | 60% |
| Select F | 1eq | 1.0M THF | 80 | 13min | 0% | 100% |
| Py-F BF ₄ | 1eq | 1.0M THF | 80 | 13min | 0% | 100% |
| NFSI | 1eq | 1.0M ACN | 80 | 13min | 43% | 34% |
| Select F | 1eq | 1.0M ACN | 80 | 13min | 33% | 67% |
| Py-F BF ₄ | 1eq | 1.0M ACN | 80 | 13min | 0% | 100% |
| NFSI | 1eq | 1.0M DMSO | 150 | 13min | 0% | 100% |
| Select F | 1eq | 1.0M DMSO | 150 | 13min | 0% | 100% |
| Py-F BF ₄ | 1eq | 1.0M DMSO | 150 | 13min | 0% | 100% |
| NFSI | 1eq | 1.0M DMF | 150 | 13min | 15% | 30% |
| Select F | 1eq | 1.0M DMF | 150 | 13min | 12% | 43% |
| Py-F BF ₄ | 1eq | 1.0M DMF | 150 | 13min | 2.3% | 97% |
| NFSI | 4eq. | Neat | 100 | 13min | 0% | 0% |
| NFSI | 0.5eq. | Neat | 100 | 13min | 12% | 52% |
| NFSI ^c | 1eq. | Neat | 100 | 13min | 3.3% | 38% |

Table 26. Fluorination of H-Toc with electrophilic fluorinating reagents.

General procedure: In an open vial, 6H-Toc (20-60 mg, 0.480-1.45 mmol) was stirred with the chosen fluorinating agent for 10-15 min at elevated temperature neat or in a solvent. The reaction mixture was extracted with DCM and water, and the organic phase evaporated. The crude mixture was washed over a small SiO₂ column with hexane and was analysed by ¹H and ¹⁹F NMR. (a) dry solvents were used. (b) ¹H NMR yields (c) 1 eq TEMPO added.

11.2.2.3 HPLC profile of 6-F-tocopherol

In PET imaging facilities the radioactive product is analysed by HPLC. A radioactive detector is used to see if the radionuclide has been incorporated into the molecule and if any radioactive by-products have been produced. Radionuclide detection by HPLC is also needed to verify the specific activity of the ^{18}F -product prior to injection into the patient. A chromatographic method has to be created with “cold” ^{19}F -product to have a reference for the PET imaging facilities. A short-time method is preferred to save time in the overall process of producing and analysing the imaging agent.⁵⁷³

Halogenated tocopherols and H-Toc are not soluble in water, and barely in acetonitrile and methanol (< 1mg/ml). Thus, dichloromethane was chosen as a solvent to solubilize the product for injection into the HPLC.

HPLC separation on a standard reverse phase C18 column with polar solvents turned out to be not applicable here, as no chromatographic separation was seen between H-Toc and F-Toc at retention times up to 40-50 minutes, with ACN : water (60:40). In the hope of a better separation, the mobile phase was changed to non-polar solvents. Non-polar reverse phase (NARP) chromatography has been used in the past to separate non-polar molecules like carotenes with great success.⁵⁷⁴ Using a Zorbax ODS column, as in the examples with carotenes, however, did not enhance the separation of H-Toc and F-Toc. A polystyrene based XDB-phenyl column was then chosen, since it promises a better separation of differently substituted aromatic compounds.⁵⁷⁵ The NARP was tested first with a DCM : MeOH or DCM : ACN (95:5 - 80:20). In short elution times of 2-5 minutes separation of the halogenated tocopherols was achieved, but no separation of F-Toc and H-Toc was observed (Figure 194).

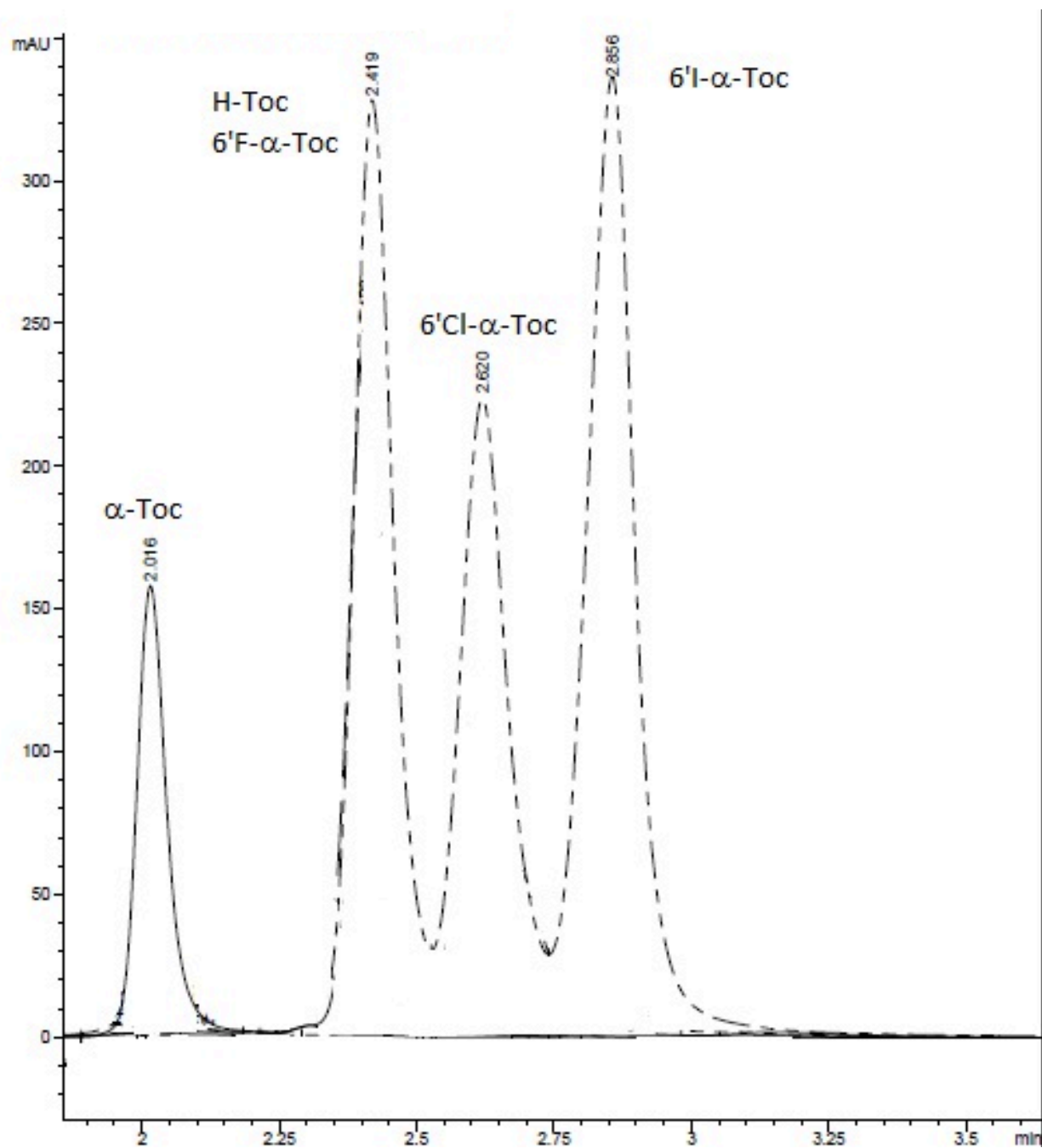
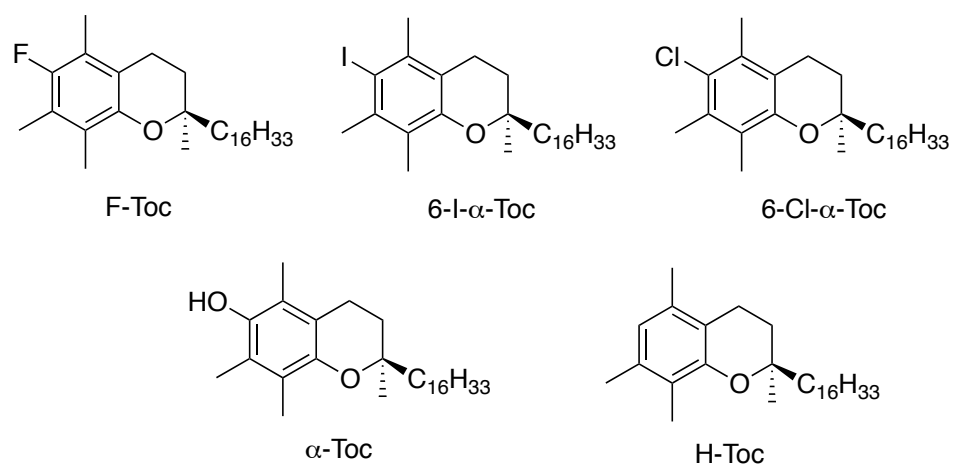
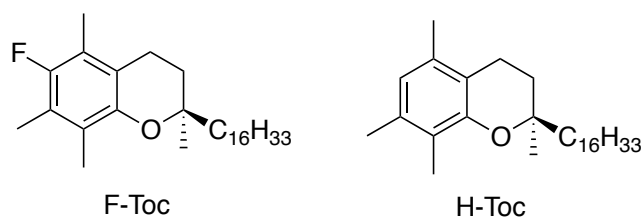


Figure 194. HPLC separation of α -toc, F-Toc, H-Toc, 6-I- α -toc, 6-Cl- α -toc.

Mobile phase gradient ACN:DCM 80:20, Flow rate: 1.0 ml/min. Stationary phase Zorbax XBD Phenyl 30 cm. The sample was dissolved in 10 μ l DCM and 40 μ l MeOH, injection volume 2 μ l. 25°C oven temperature, UV detection at 280 nm.

Switching the mobile phase back to MeOH : H₂O led to the separation of H-Toc (26.21 min) and F-Toc (26.52 min) (Figure 195). Separation between H-Toc (26.46 min), Cl-Toc (28.80 min) and I-Toc (31.65 min) using the same mobile phase was effective to the point where no overlap occurs between the peaks (Figure 196).



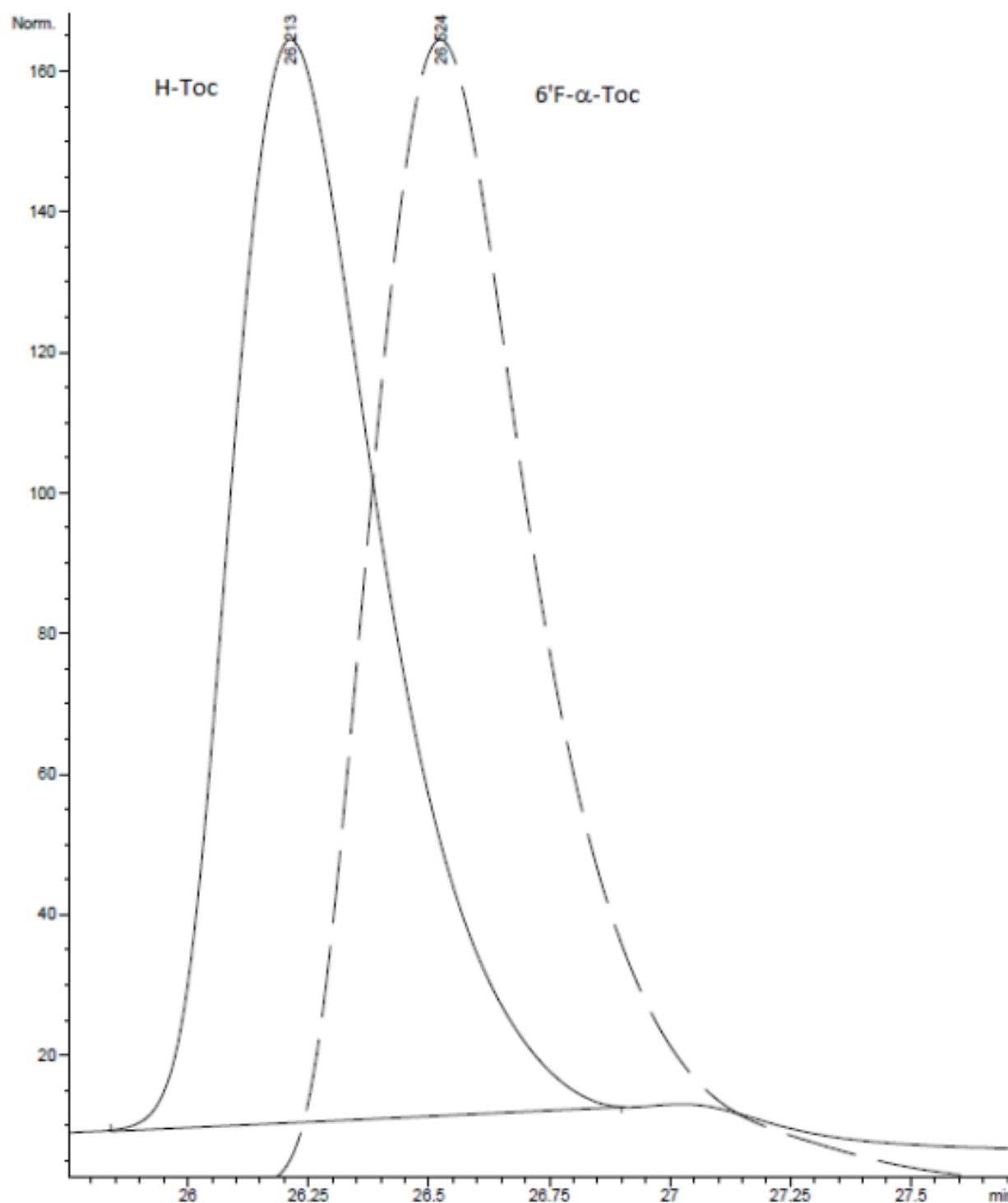


Figure 195. HPLC separation of F-Toc and H-Toc.

Overlay of two separate 6'F-Toc and 6'H-Toc injections to show the spectral overlap. Mobile phase gradient MeOH:H₂O 80:20, 10 min 85:15, 15 min 90:10, 20 min 95:5, Flow rate: 1.0 ml/min. Stationary phase Zorbax XBD Phenyl 30cm. The sample was dissolved in 10 μ l DCM and 40 μ l MeOH, injection volume 2 μ l. 25°C oven temperature, UV detection at 280nm. Y-axis shows a normalized mAU.

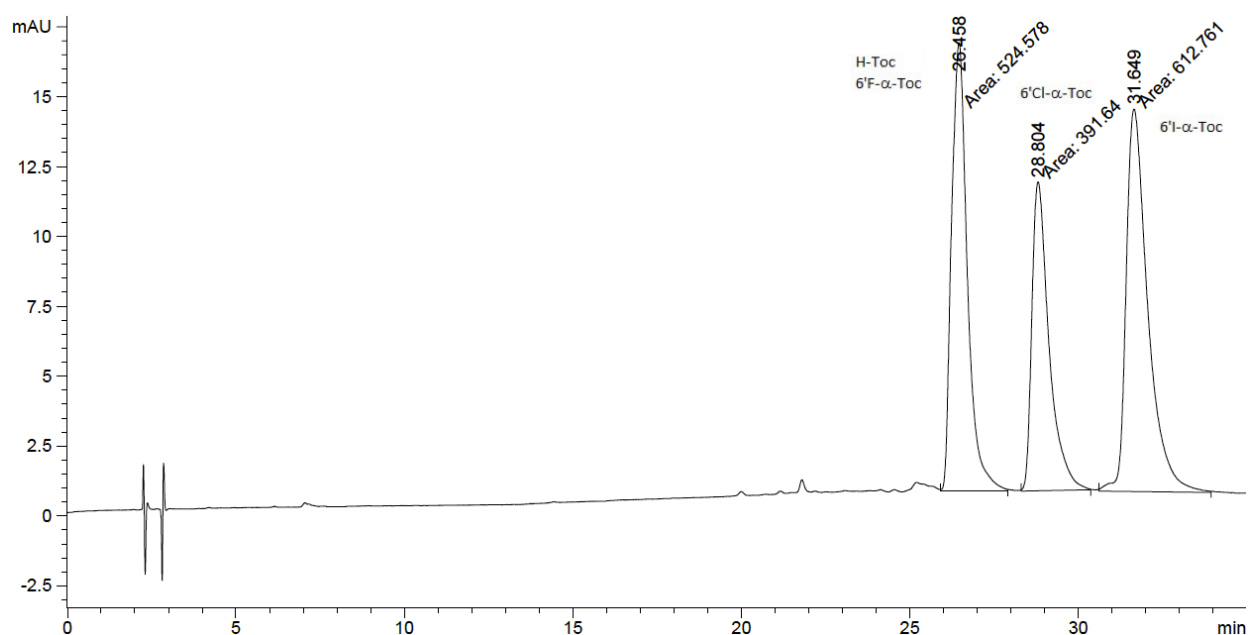


Figure 196. HPLC separation of 6-I-α-Toc, 6-Cl-α-Toc and H-Toc.

Mobile phase gradient MeOH:H₂O 80:20, 10 min 85:15, 15 min 90:10, 20 min 95:5, Flow rate: 1.0 ml/min. Stationary phase Zorbax XBD Phenyl 30 cm. The sample was dissolved in 10 μl DCM and 40 μl MeOH, injection volume 2 μl. 25°C oven temperature, UV detection at 280 nm. Y-axis shows a normalized mAU.

To obtain a faster and better separation, a polyfluorinated C8 silica column will be used in the future. Differentially fluorinated benzenes have been separated on this stationary phase in less than 10 min (Figure 197).⁵⁷⁶

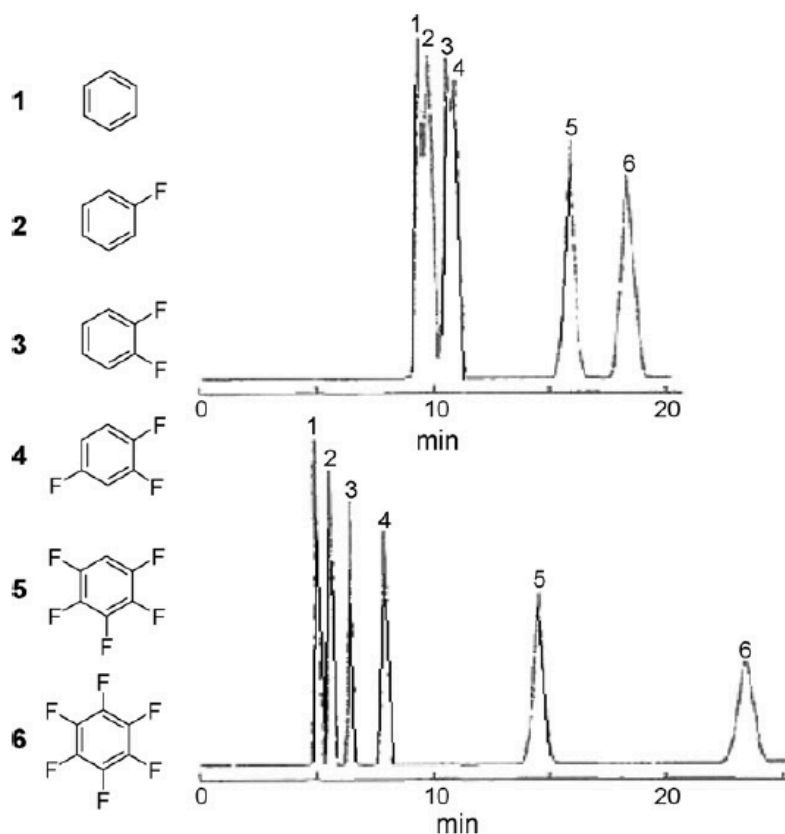


Figure 197. Separation of benzenes with increasing fluorine substitution.

Top spectra: 18C-column, bottom spectra: C₈F₁₇-column.⁵⁷⁶

11.2.3 γ -Tocopherol fluorination to 5-fluoro- γ -tocopherol

Electrophilic fluorination of γ -tocopherol was attempted using similar reagents as for F-Toc.⁵⁷⁷

In a recent paper by Poon *et al.* γ -tocopherol was lithiated at the 5-position and reacted with tellurium tetrachloride (TeCl₄) to create a telluro-*bis*-tocopherol antioxidant.⁵⁷⁸ Instead of tellurium we used fluorinating reagents to quench the lithiated γ -tocopherol (Figure 198).

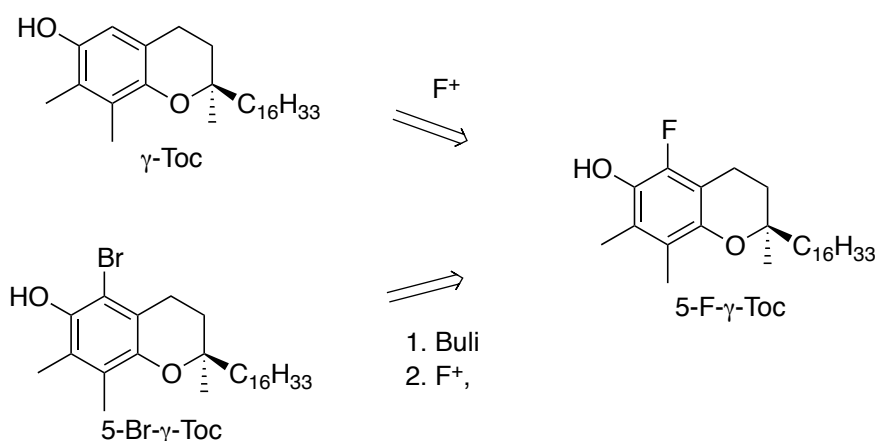


Figure 198. Synthetic strategies towards 5-F- γ -tocopherol by electrophilic fluorination.

Electrophilic ^{18}F -fluorination of phenols has been used to create ^{18}F -labeled *L*-DOPA / tyrosine for neurological studies or ^{18}F -phenolphthalein as *in situ* pH sensors.^{579,580,581,582} Fluorine gas and AcOF have been used to fluorinate phenols, but the high reactivity of these reagents does require careful handling and tends to produce unwanted oxidized or polyfluorinated sideproducts (Figure 199).⁵⁸³

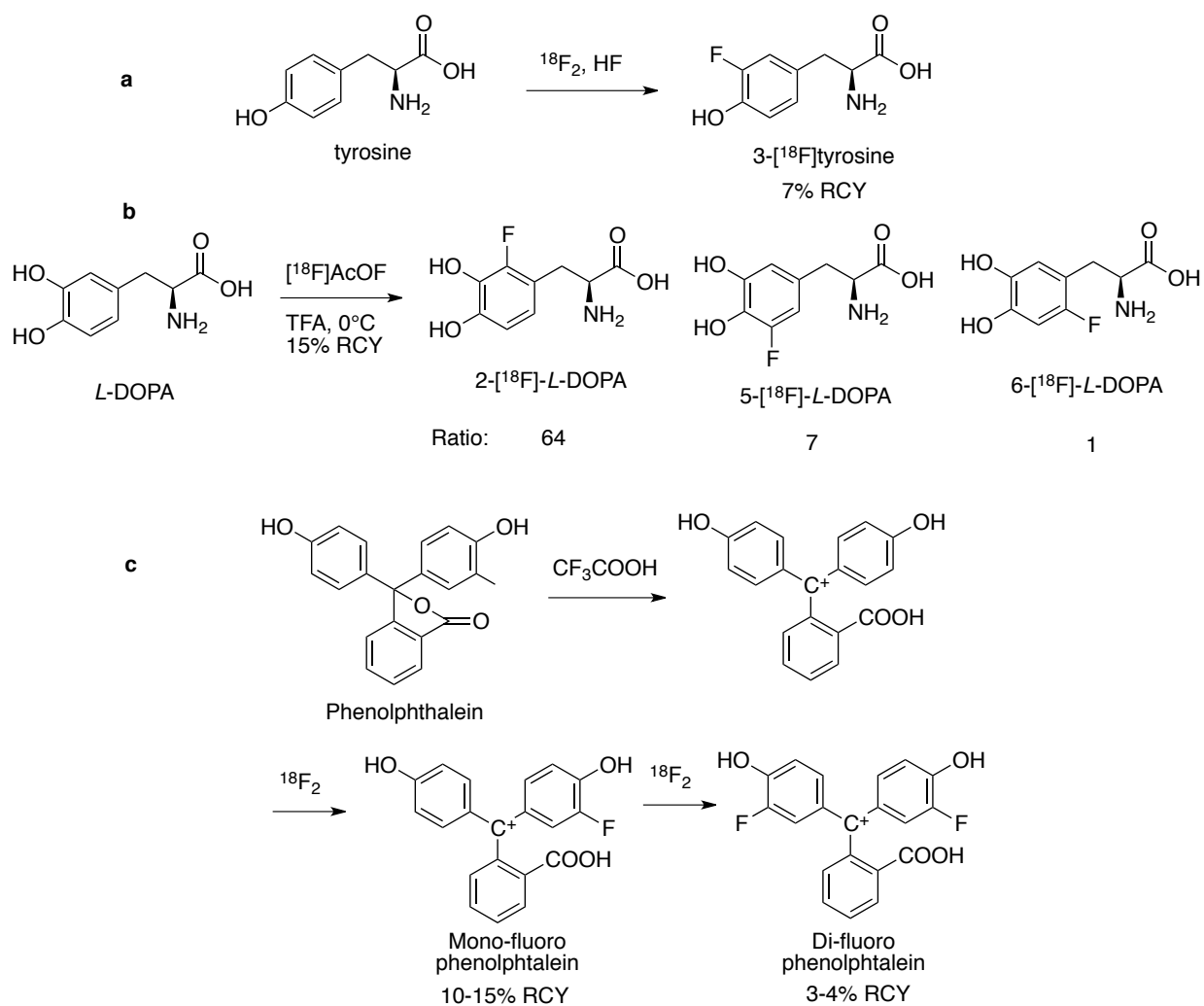


Figure 199. Electrophilic ^{18}F -fluorination of phenols.

(a) 3- L - ^{18}F -tyrosine, (b) L - ^{18}F -DOPA and (c) ^{18}F -phenolphthalein.⁵⁷⁹⁻⁵⁸²

Alternatively, nitrogen based electrophilic fluorinating reagents have been used because they are easier to handle and bench stable (Figure 200).^{584,516}

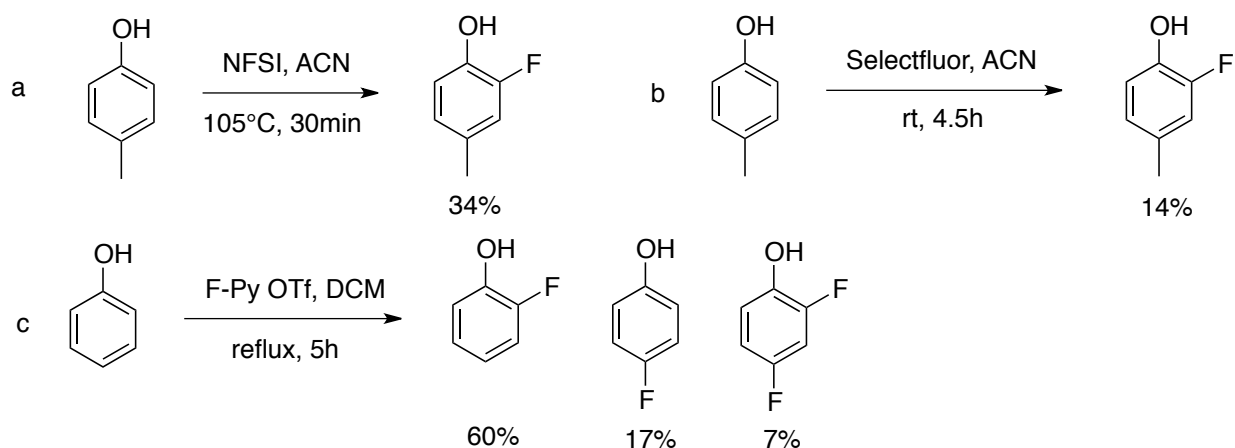
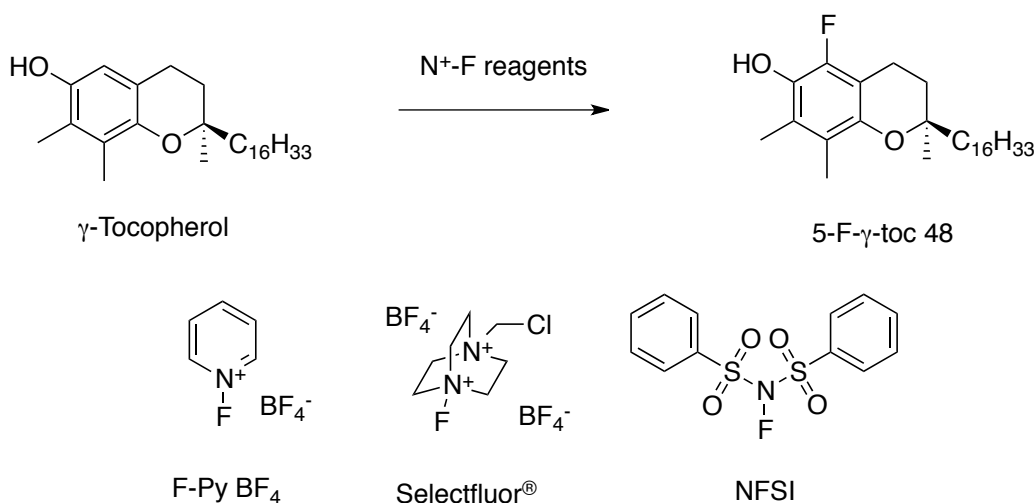


Figure 200. Phenol fluorination with electrophilic fluorinating reagents (a) NFSI, (b) Selectfluor and (c) 1-Fluoropyridinium triflate.^{585,587,588}

Bench stable, commercially available nitrogen-based fluorinating reagents N-fluorobenzenesulfonimide (NFSI)⁵⁸⁵, 1-fluoropyridinium tetrafluoroborate (F-Py BF₄ or 1-Fluoropyridinium triflate F-Py OTf)^{586,587} and Selectfluor^{®588} have been used to fluorinate phenols (Figure 200) and were chosen for the fluorination of γ -tocopherol (Table 27).⁵¹⁶



| F ⁺ -Source | Equiv. | Solvent ^a | Temp (°C) | Time |
|------------------------|--------|--------------------------------------|-----------|----------|
| F-Py BF ₄ | 1eq | 0.06M THF | rt, 80 | 15min-2h |
| F-Py BF ₄ | 1eq | 0.06M toluene | rt, 80 | 15min-2h |
| F-Py BF ₄ | 1eq | 0.06M THF ^b | rt, 80 | 15min-2h |
| F-Py BF ₄ | 1eq | 0.06M CHCl ₃ ^b | rt, 80 | 15min-2h |

| | | | | |
|--------------------------|-----|-----------|-----|----------|
| Selectfluor [®] | 1eq | 0.25M ACN | 80 | 15min-2h |
| Selectfluor [®] | 1eq | 0.25M ACN | rt | 80min |
| NFSI | 1eq | 0.25M THF | rt | 1h |
| NFSI | 3eq | 0.25M THF | 0°C | 1h |

Table 27. Fluorination of γ -tocopherol with electrophilic fluorinating reagents.

To a solution of γ -tocopherol was added the fluorinating reagent added under N₂ atmosphere. Reactions with Py BF₄ and Selectfluor[®] were conducted at room temperature and 80°C. NFSI was reacted at room temperature and at lower temperature with increased amounts of NFSI. The solvent was evaporated and the residual mixture was extracted with water and DCM. NFSI reactions were purified by SiO₂ chromatography. (a) dry solvents (b) added 1 eq of NEt₃.

None of the reactions with F-Py-BF₄ produced any product, **48**, even at elevated temperature and extended reaction time. Selectfluor[®] produced traces of unidentifiable byproducts. None of these byproducts showed any signal in the ¹⁹F-NMR. Reaction with NFSI created byproducts 5-NFSI-tocopherol, **74**, bis-5,5'-tocopherol, **75**, and γ -tocopherol quinone (Figure 201).

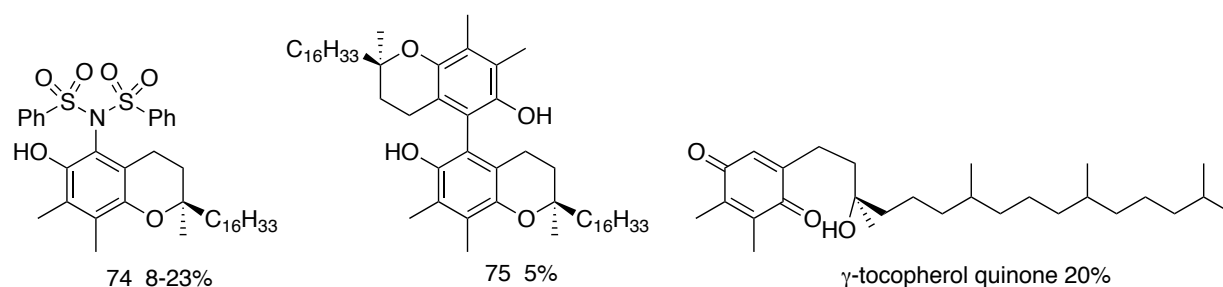


Figure 201. Byproducts 76 formed during the fluorination of γ -tocopherol sodium phenolate with NFSI.

Radical reactions are common with electrophilic fluorinating agents. To counteract the radical reaction the nucleophilicity of the phenol was increased by turning it into the sodium phenoxide, described by Barnette with 2-naphthol.⁵⁶² However, no fluorination occurred, but the phenol was turned into the benzenesulfonate **75** (Figure 202).

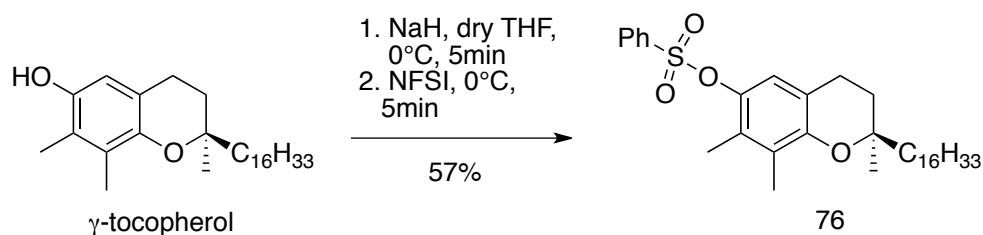


Figure 202 Byproduct 76 formation from γ -tocopherol sodium phenolate fluorination with NFSI.⁵⁶²

Fluorination was then attempted via lithium-halogen exchange of 5-bromo- δ -tocopherol. Poon was able to create a 5,5'- δ -telluro-*bis*-bistocopherol this way.⁵⁷⁸ Stirring the reaction at -78°C overnight was necessary to install the tellurium (Figure 203).

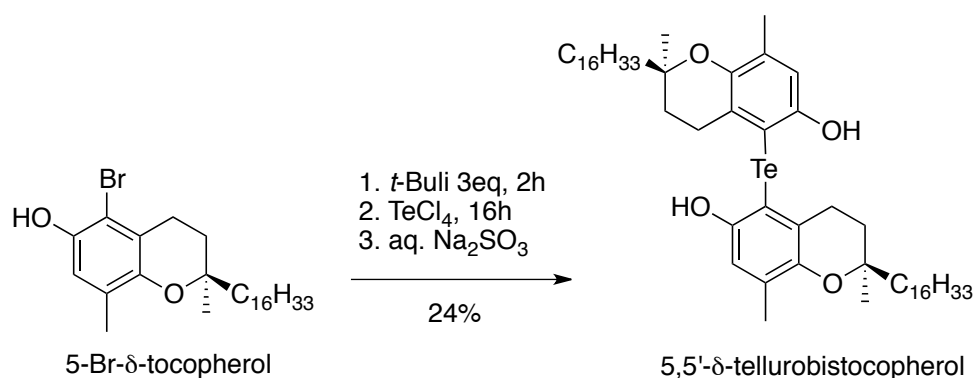


Figure 203 Poon's 5,5'- δ -telluro-*bis*-tocopherol synthesis.⁵⁷⁸

To obtain 5-Br- α -tocopherol **76** γ -tocopherol was reacted with tetrabutylammonium bromide (TBAB) (Figure 204).⁵⁷⁸

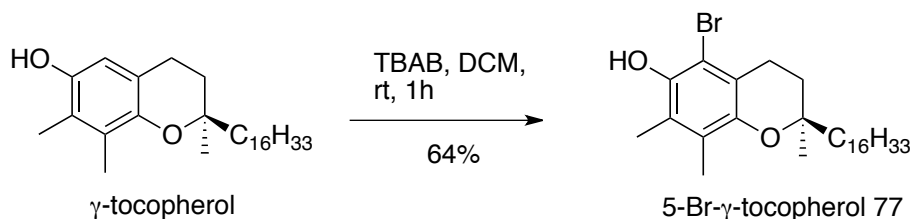


Figure 204. Bromination of γ -tocopherol with TBAB.⁵⁷⁸

To rapidly fluorinate γ -tocopherol, after the lithium-bromide exchange at -78°C for 2 h, the fluorinating agent was added and warmed to room temperature. Despite increasing the temperature to 50°C the reaction only yielded γ -tocopherol with F-Py BF₄ and Selectfluor[®]. After 5 minutes reaction time with NFSI, **77** yielded only the benzosulfonate byproduct **76** (Figure 205).

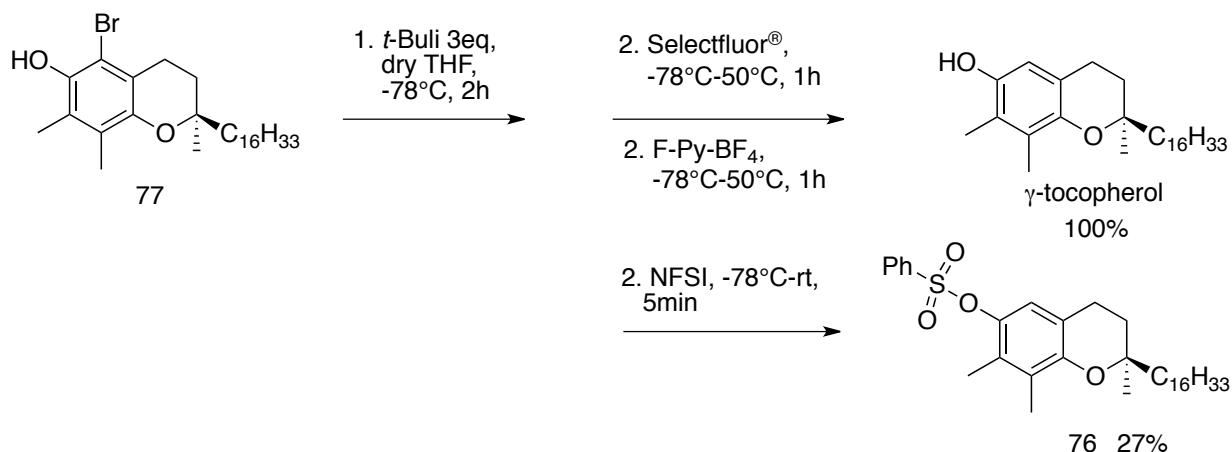


Figure 205 Fluorination of 5-Br- γ -tocopherol via lithium-halogen exchange reaction.

Formation of byproduct 76 with NFSI.⁵⁷⁸

Attempts to fluorinate γ -tocopherol by electrophilic fluorination did not work with any of the chosen fluorinating reagents. In the future, instead of nitrogen-based reagents, acetylhypofluorite in acidic media will be used to fluorinate γ -tocopherol (Figure 206).



Figure 206 γ -Tocopherol fluorination with acetylhypofluorite.

11.2.4 5-F-methyl- α -tocopherol synthesis

Benzylic fluorination at the 5-methyl was tested on the acetyl protected α -tocopherol 5-bromomethyl (AcO-5-Br-Me- α -toc) as a precursor, with nucleophilic fluorinating agents like TBAF, KF-cryptand[2.2.2] and CsF. After deprotection of the acetyl group the targeted 5-F-methyl- α -tocopherol was formed. Oxidation of α -tocopherol with silver oxide in non-polar solvents forms the highly reactive *ortho*-quinone methide (oQM), which is susceptible to nucleophilic addition at the 5-position. Formation of 5-Br-Me- α -toc goes through the same oQM mechanism when brominated with bromine. One part of the bromine is used to abstract

the benzylic hydrogen at the 5-position, the second bromine atom acts as a nucleophile at the electrophilic benzylic position. Thus, fluoride addition might occur in the same manner as in the second step of the bromination (Figure 207).⁵⁸⁹ Since the oQM is such a reactive intermediate additives like N-methylmorpholine-N-oxide (NMMO) and sulfur-ylids (*S*-ylide) can be used to stabilize the intermediate oQM.^{590,591}

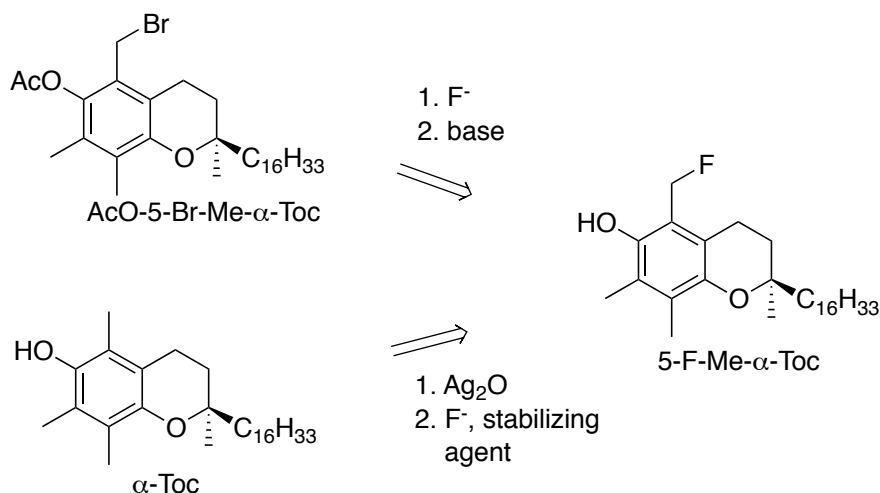


Figure 207 Synthetic strategies towards 5-F-Me- α -tocopherol by nucleophilic fluorination.

Fluorination at the benzylic position of an aromatic group has been used to create ^{18}F -labeled biologically active compounds like nabumetone, celestolide or papaverine (Figure 208).⁵⁹²

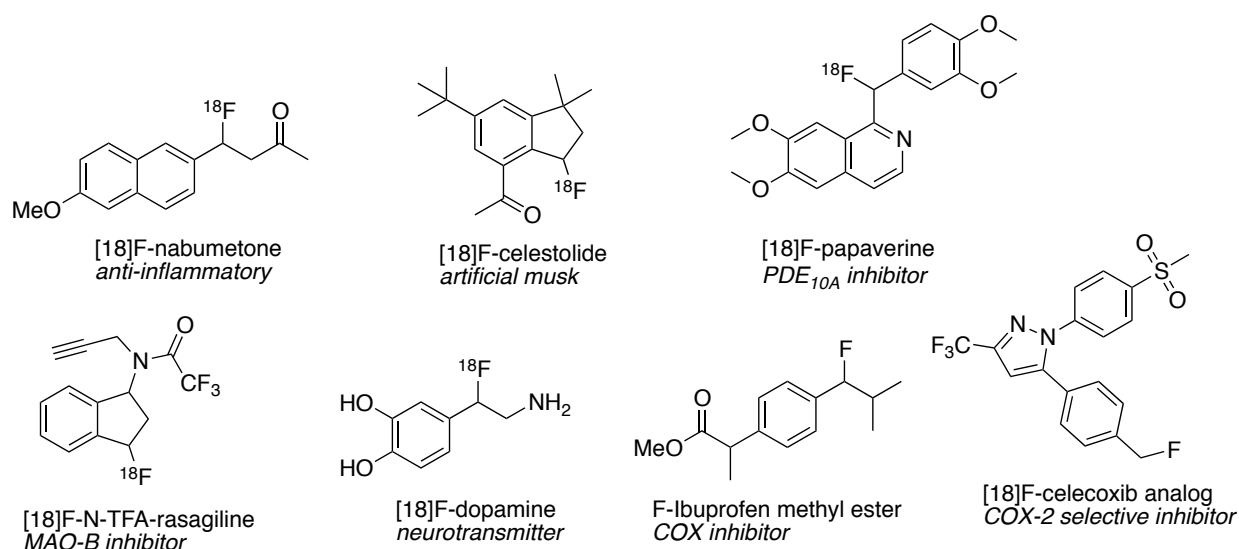


Figure 208 Benzylically ^{18}F -labeled biologically active compounds.⁵⁹²

Synthetically, benzylic fluorinations are much easier than aromatic fluorinations, because nucleophilic substitution reactions can be used. More recently, metal catalyzed benzylic C-H

fluorinations have been used for PET ligand chemistry with great success. δ -Tocopherol was fluorinated by C-H activation with a manganese(salen) catalyst (Figure 209).⁵⁹²

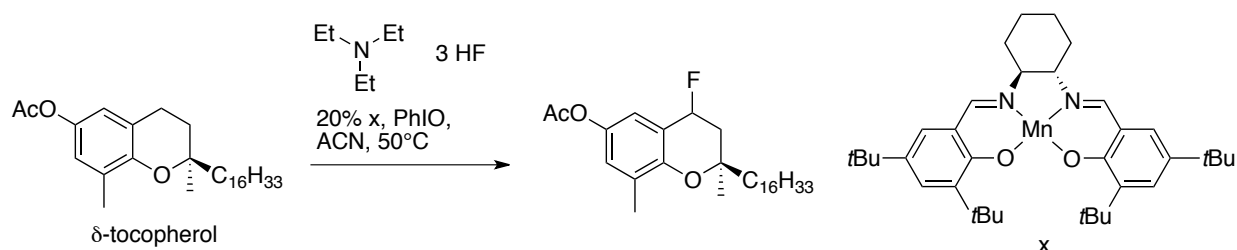


Figure 209 Manganese(salen) catalyzed fluorination of δ -tocopherol.⁵⁹²

11.2.4.1 Synthesis of 5'-F-methyl- α -tocopherol by nucleophilic substitution:

Nucleophilic substitution with fluoride is done by replacing leaving groups like bromine, iodine or tosylates. Substitution at benzylic positions is seen in late stage fluorination to create ^{18}F -trifluoromethyl groups and in the creation of ^{18}F -precursors used in a multistep synthesis (Figure 210).^{593,594,595}

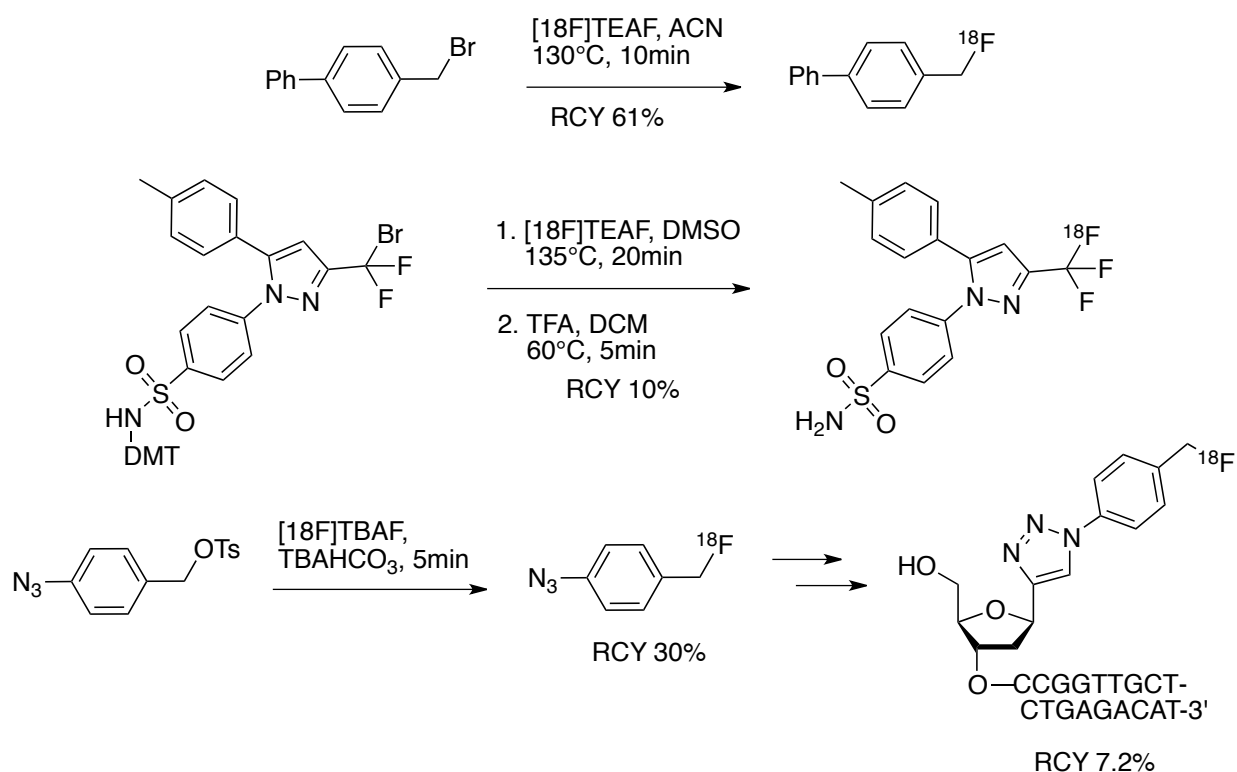


Figure 210. Benzylic ^{18}F -fluorination by nucleophilic substitution.^{593,594,595}

To fluorinate α -tocopherol at the 5-methyl position *O*-acetyl protected 5-bromomethyl- α -tocopherol, **77**, was chosen. The bromine has been replaced previously with other nucleophiles like alcohols, acids, phosphines, and amines.⁵⁹⁶ The 5'-methyl position of tocopherol was used as a benzylic protecting group of the nitrogen in amino acids (Figure 211).⁵⁹⁷

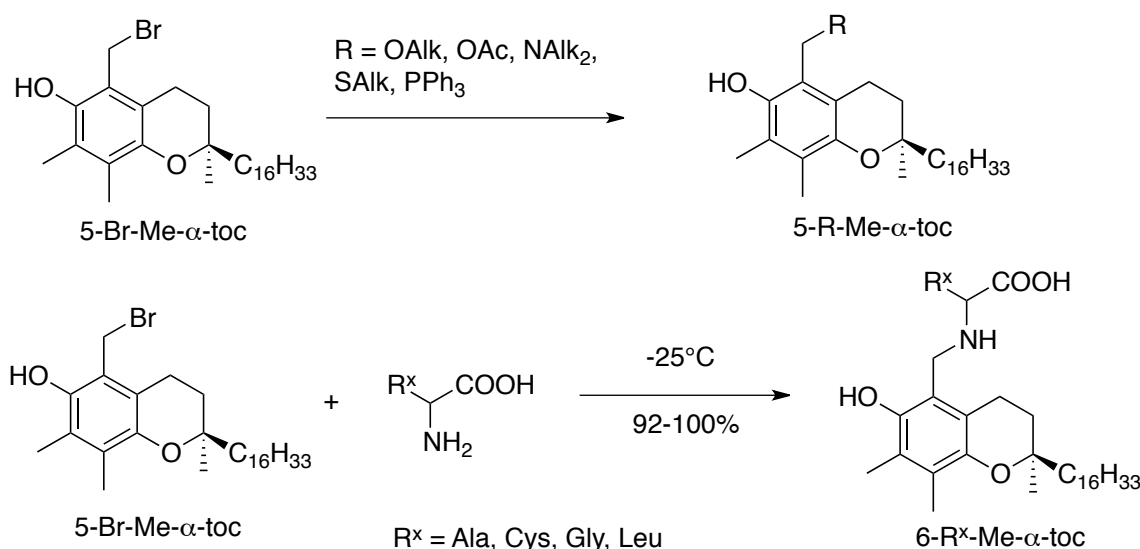


Figure 211 Substitution of 5-Br-Me- α -toc with nucleophiles.⁵⁹⁶ N-protection of aminoacids with α -tocopherol⁵⁹⁷

Because ^{18}F -fluorination reactions are run at elevated temperature (80-250°C) protection of the tocopherol phenol is necessary. At temperatures above > 40°C the 5-Br- α -tocopherol spontaneously turns into the spiro-dimer (Figure 212).⁵⁸⁹

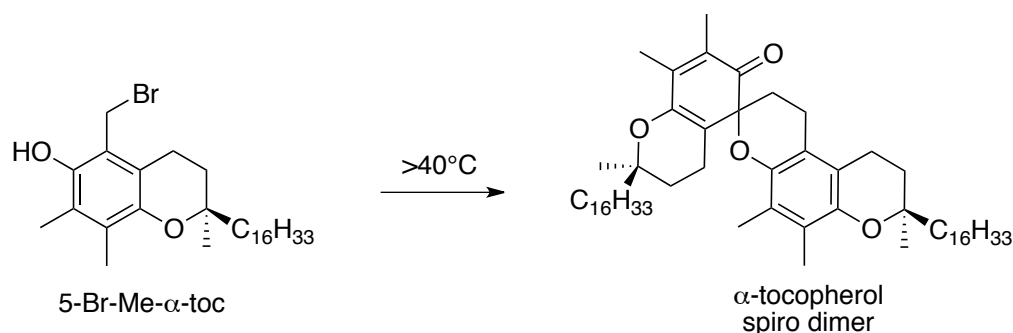


Figure 212 Thermally induced formation of α -tocopherol spiro-dimer formation from 5-Br-Me- α -toc.⁵⁸⁹

AcO-5-Br- α -tocopherol **77** is obtained by bromination of α -tocopherol, followed by reaction with acetic anhydride (Figure 213).⁵⁸⁹

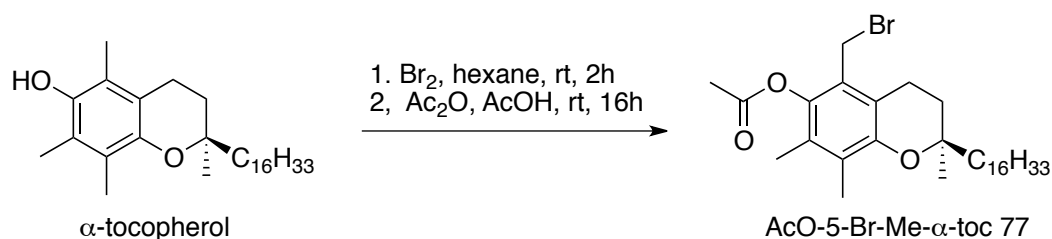
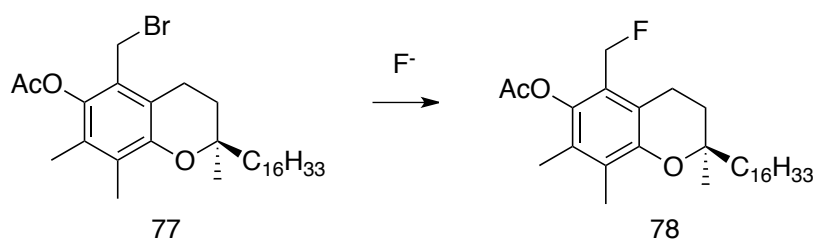


Figure 213 AcO-5-Br-Me- α -toc 77 synthesis from α -tocopherol.⁵⁸⁹

Compound **77** was exposed to potential fluorination conditions using potassium fluoride in acetonitrile or DMF and carrier additives 18-crown-6, cryptand[2.2.2], or tetrabutylammonium (Table 28).



| F ⁻ -Source | Equiv | Carrier | Solvent ^a | Temp (°C) | Time | Prod 5-F | Prod 5-H |
|--------------------------|------------------|----------------|----------------------|-----------|------------|----------|----------|
| KF | 1eq ^b | - | 50mM ACN | 70 | 16h | - | - |
| KF | 1eq ^b | 18-Crown-6 | 50mM ACN | 70 | 16h | - | - |
| KF ^c | 1eq | Cryptand 2.2.2 | 50mM ACN | 100 | 5min (16h) | - | - |
| KF | 1eq | - | 50mM DMF | 70 | 16h | - | 23% |
| KF | 2eq | - | 250mM DMF | 100 | 1h | 6% | 13% |
| KF ^c | 2eq | - | 160mM DMF | 100 | 1h | - | 16% |
| KF | 2eq | - | 100mM DMF | 100 | 16h | 6% | 11% |
| TBAF 1M THF ^c | 3eq | | 40mM THF | 60 | 20min | - | - |

Table 28. Fluorination of AcO-5-Br-Me- α -toc.⁷⁷

All reactants were stirred for 20 min and analysed. (a) dry solvent (b) No product was observed in 20 min-1 h. Continued the reaction up to 16 h. (c) Microwave reactor 200 W.

Conducting the reaction in acetonitrile did not yield any product, even with carrier addition.

Only small amounts of product, **78**, were observed with DMF as the solvent with 2 eq of KF along with the hydro-debrominated product (α -tocopherol acetate) as a byproduct. Heating the

reaction with microwave irradiation was not successful, but decreasing the amount of solvent (250 mM) yield some product in 1h.

A higher yield of product **78** was obtained when the reaction was run in *t*-butanol and cesium fluoride (CsF).⁵⁹⁸ Along with product, **78**, 5'-*t*-butoxyl substituted byproduct, **79**, was also formed (Figure 214).

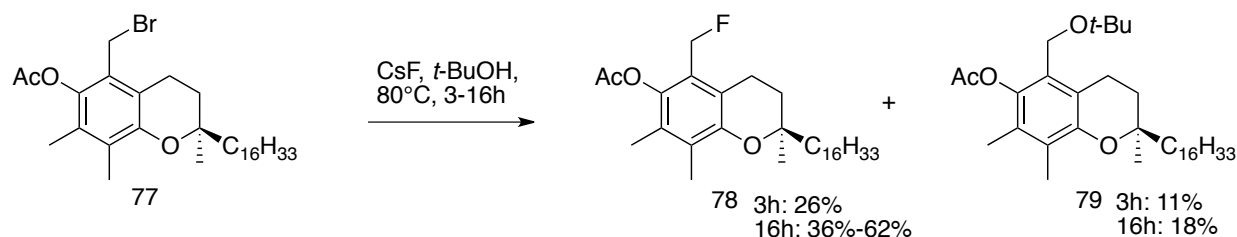


Figure 214. Fluorination of 78 with CsF and *t*-BuOH. Formation of product 78 and byproduct 79.⁵⁹⁸

The CsF / *t*-BuOH methods has an advantage over the KF / DMF fluorination because the *t*-BuO-containing byproduct, **79**, is more easily removed by chromatographic purification than the α -tocopheryl acetate.

Acetyl protecting groups of phenols are normally removed in basic media.²⁷⁹ Deprotection with KOH in EtOH did cleave the acetoxy group, but also substituted the fluorine to create the ethoxyether, **80** (Figure 215).

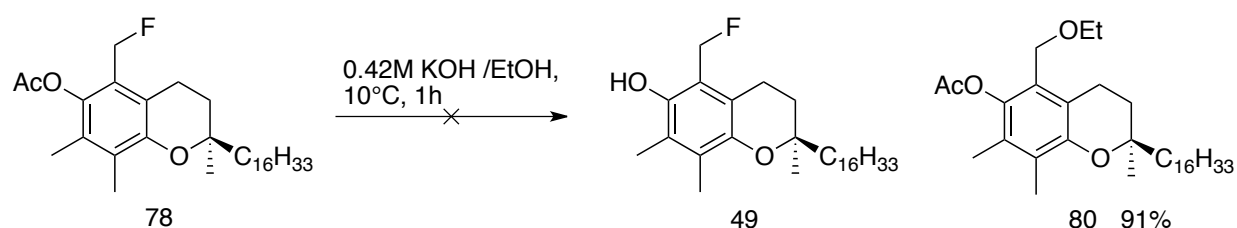


Figure 215 Deprotection of 78 in basic media with KOH in EtOH. Formation of ethoxyether 80.²⁷⁹

Substitution was not expected, since fluorine-carbon bonds are stronger than bromine-carbon bonds ($\text{BDE } \Delta H^\circ_{298} = \text{CH}_3\text{F}: (95.9 \text{ kcal/mol}) - \text{CH}_3\text{Br}: (56.2 \text{ kcal/mol})$).⁵⁹⁹ Instead of basic deprotection we tried the hydrolysis with water and catalytic amounts of trifluoroacetic acid (TFA) in acetonitrile. Deprotection did not work and instead the TFA ester, **81**, was formed by TFA anion substitution of the 5-fluoromethyl of **78** (Figure 216).

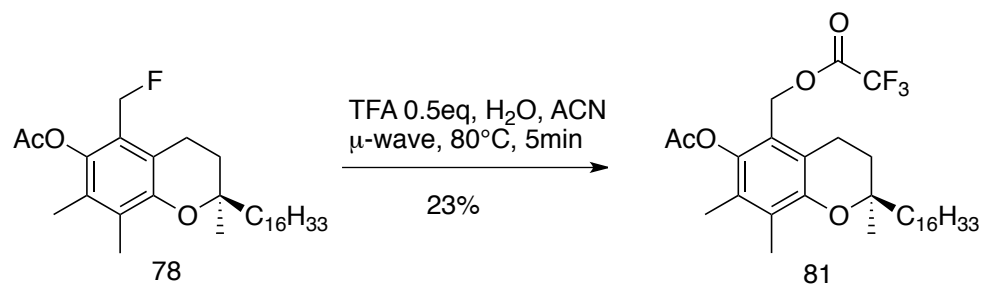
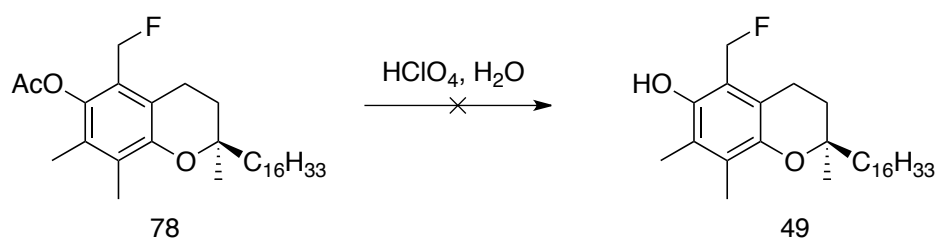


Figure 216. Attempted deprotection of AcO-5-F-Me- α -toc 78 in acetic media with TFA and formation of byproduct 5-trifluoroacetyl α -tocopherol acetate 81.

Perchloric acid (HClO_4) was chosen as an acid, because the perchlorate (ClO_4) counter ion is less nucleophilic than the trifluoroacetate (Table 29).



| Acid | HClO_4 | H_2O | Solvent | Temp ($^\circ\text{C}$) | Time | Prod 20min | Prod 16h |
|----------------------------|-----------------|----------------------|--------------|---------------------------|--------------------|------------|----------|
| HClO_4 | 2eq | 1eq | 125mM ACN | rt | 20min | - | - |
| HClO_4 | 2eq | 1eq | 50mM ACN | 40 | 20min ^a | - | decomp |
| HClO_4 | 2eq | 1eq | 50mM ACN | 80 | 10min ^a | - | decomp |
| HClO_4 | 2eq | 1eq | 100mM ACN | 100 | 10min ^a | - | decomp |
| HClO_4 | 2eq | 1eq | 125mM hexane | 40 | 16h ^a | - | - |
| HClO_4^{b} | 2eq | 1eq | 50mM ACN | 60 | 16h ^a | - | decomp |

Table 29. 78 was stirred in a μ -wave oven or for 10-20 min.

(a) When no product was observed was the reaction continued stirring for 16 h with conventional heating. (b) AcO- α -tocopherol.

None of the applied conditions yielded any de-acetylated product, 49. Stirring the reaction overnight formed a unidentifiable spot on TLC, which did not contain any fluorine peak in the ^{19}F -NMR. The same unidentifiable spot was observed when acetyl protected- α -tocopherol (last entry (b)) was stirred over night.

11.2.4.2 5-F-methyl- α -tocopherol synthesis by orthoquinone methide formation:

Silveroxide (Ag_2O) is used in non-polar solvent to form the α -tocopherol *ortho*-quinone methide (oQM) from α -tocopherol. Without stabilization of the oQM the tocopherol-spirodimer is formed instantly at any temperature. Rosenau reported the stabilization of the oQM with NMMO at -78°C .^{600,601} A later paper by the same author described the used of 2,5-bis(dimethylsulfonio)-3,6-dioxocyclohexa-1,4-diene-1,4-bis(olate) (*S*-ylide) to stabilize the oQM intermediate (Figure 217). The *S*-ylide stabilizes oQM for a longer time at temperatures up to 40°C .⁶⁰²

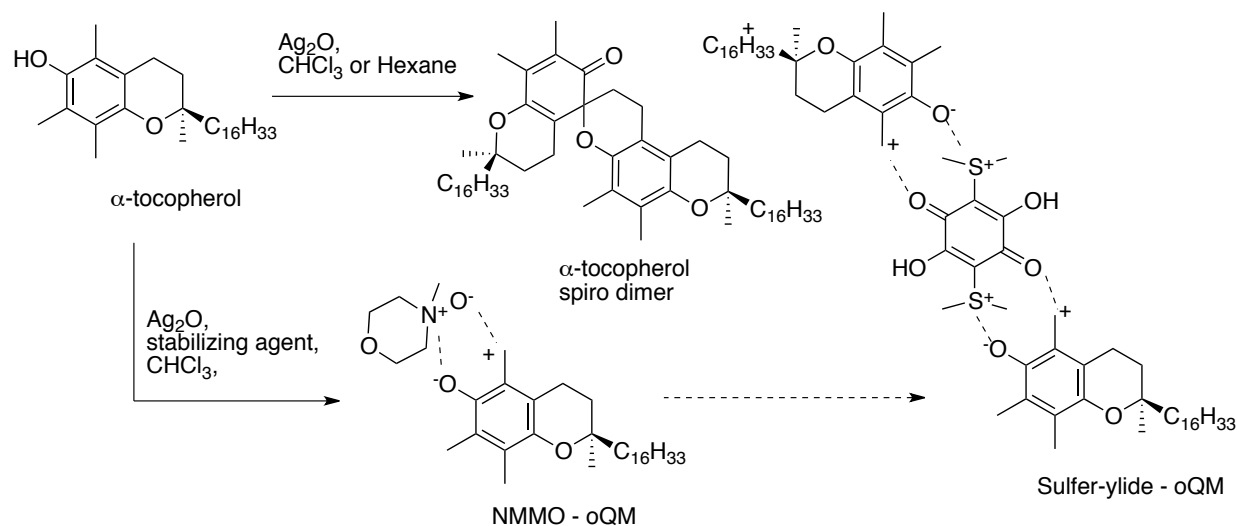


Figure 217. α -Tocopherol *ortho*-quinone methide (oQM) dimerization to the α -tocopherol-spirodimer and stabilization of the α -tocopherol oQM by NMMO and *S*-ylide.^{600,601,602}

The sulfur-ylide has been applied to stabilize the *ortho*-quinone methide of *ortho*-cresol, which was quenched with acetylsalicylic acid to form (*O*-acetylsalicyl)saligenin (Figure 218).⁶⁰²

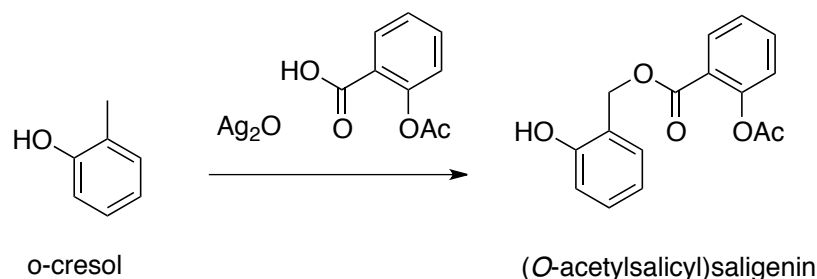


Figure 218. Synthesis of (*O*-acetylsalicyl)saligenin from *o*-cresol.⁶⁰²

The reaction was first tested without any stabilizing agent with excess cesium fluoride in CHCl_3 and DMSO at -78°C and room temperature, but no product was obtained. Tetrabutylammonium fluoride was chosen as the carrier additive in hexane and THF, without success (Table 30).

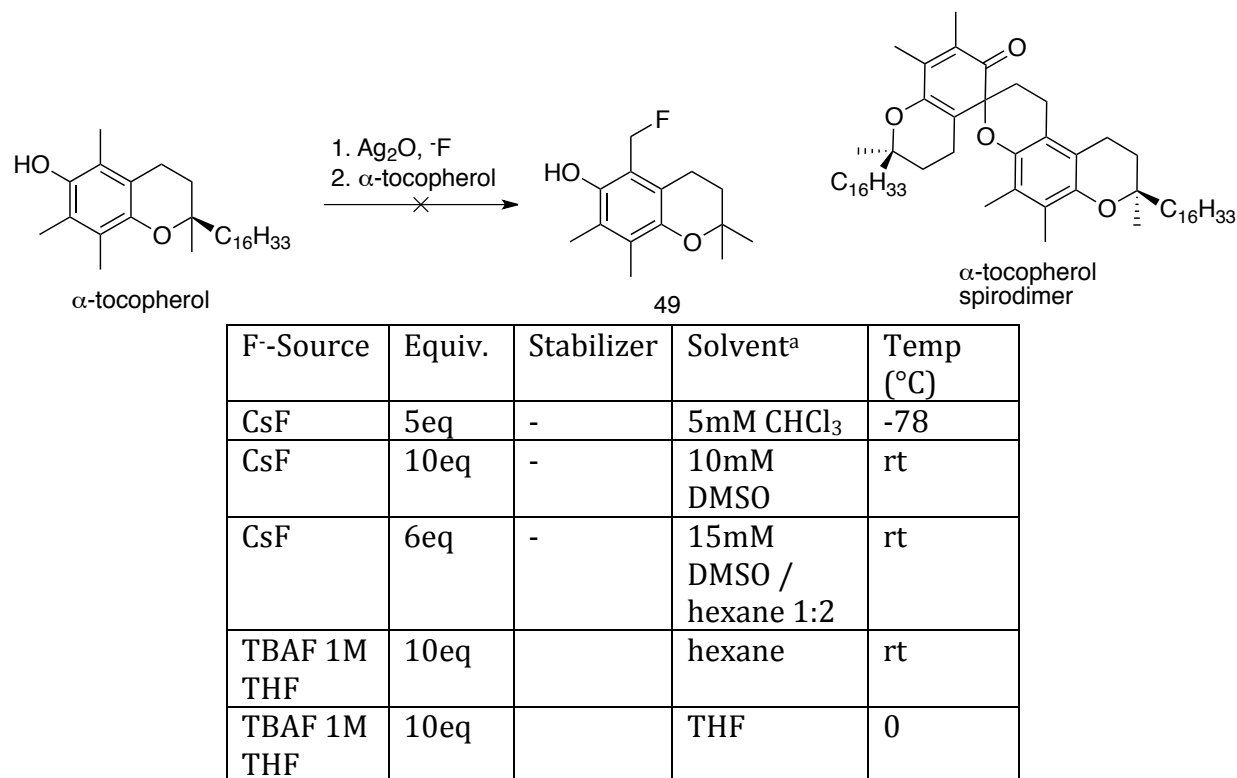
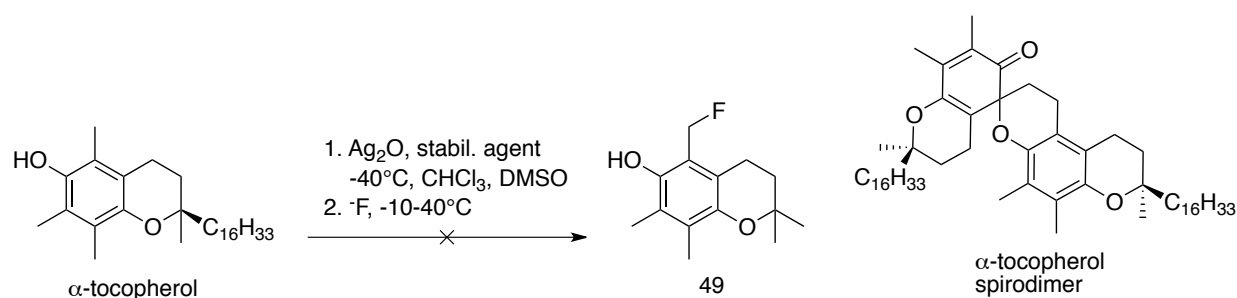


Table 30 α -Tocopherol fluorination with Ag_2O .

To silver oxide (Ag_2O) and fluoride (CsF or TBAF) in the chosen solvent was α -tocopherol added at the given temperature. (a) dry solvent.

All attempts to quench α -tocopherol oQM with fluoride did not result in fluorination but rather formed the spirodimer byproduct. Stabilizing the reaction with NMMO in CHCl_3 was reported to occur at -78°C , however CHCl_3 solidifies at this temperature, preventing any reaction. Having the temperature above -78°C to melt the solvent initiated spirodimer formation. The solvent was therefore changed to hexane, but did not yield any product. The reaction with the *S*-ylide was followed according to procedure, but did not yield any product either. No fluorine incorporation was observed by ^{19}F -NMR in any attempt and the only products observed were the α -tocopherol-spirodimer and α -tocopherol-quinone after prolonged stirring (Table 31).



| F ⁻ -Source | Equiv. | Stabilizer | Stirring time ylide | Solvent ^a | Temp F ⁻ addition(°C) | Stirring time |
|------------------------|--------|------------|------------------------|-------------------------------|----------------------------------|---------------|
| TBAF | 2eq | NMMO | 1min | 10mM CHCl ₃ | -78 | 5min (rt) |
| TBAF | 2eq | NMMO | 1min | 10mM hexane | -78 | 5min (rt) |
| CsF / cryptant 2.2.2 | 2eq | NMMO | 1min | 10mM hexane | -78 | 5min (rt) |
| TBAF | 1eq | S-ylide | | 160mM CHCl ₃ /DMSO | -10 | 15min |
| TBAF | 2eq | S-ylide | 20min | 160mM CHCl ₃ /DMSO | 40 | 1h |
| CsF / cryptant 2.2.2 | 2eq | S-ylide | 30min | 160mM CHCl ₃ /DMSO | rt | 2h |
| TBAF | 1eq | S-ylide | 30min | 1M CHCl ₃ /DMSO | rt | 16h |

Table 31. α -Tocopherol fluorination with Ag₂O and stabilizing agents.

Procedure NMMO: Silver oxide in CHCl₃ or hexane was cooled to -78°C. NMMO was added, followed by addition of NMMO. α -Tocopherol was added directly followed by F⁻. **Procedure S-ylide:** Silver oxide (5 eq) was cooled in dry CHCl₃ (70 ml) to -40°C and α -tocopherol (100 mg) added. S-ylide (0.55 eq) was added with DMSO (2 ml). After 30 min was F⁻ added to the α -tocopherol mixture and the reaction warmed up to -10-40°C in 5 min. **Work up:** After the given time both reactions were quenched with water and the organic phase separated and washed several times with water. **Note:** The silver oxide reactivity was tested by adding silver oxide directly into a solution of α -tocopherol in CHCl₃, which directly formed the spiro-dimer.

α -Tocopherol fluorination at the γ -methyl position was successful by nucleophilic substitution of the acetyl protected 5-bromomethyl- α -tocopherol, but deprotection of the phenol ester was not possible without defluorination. Nucleophilic fluorination on α -tocopherol *ortho*-quinone methide did not produce any product, despite the use of stabilizing agents.

11.2.5 6-F-methyl- α -tocopherol synthesis

HM-toc **44** was used as the starting material to create **50** by displacement of the benzyl hydroxyl group with sulfur based deoxyfluorination reagents diethylaminosulphurtrifluoride (DAST) and Xtalfluor E & M⁶⁰³, and by nucleophilic fluorination of hydroxyl activated sulfonates⁶⁰⁴ or activation by protic / Lewis acids (Figure 219).⁶⁰⁵

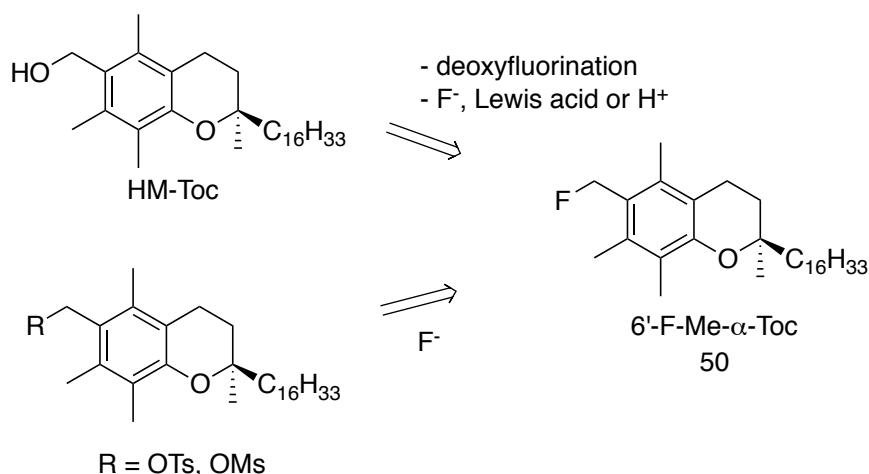


Figure 219. Synthetic strategies towards 6'-F-Me- α -tocopherol **50**.

Fluorination of HM-Toc with deoxyfluorination reagents and by Lewis acid / H⁺ activation.⁶⁰³

Alternatively by fluorination of the benzylic sulfonates.^{604,605}

Radiofluorination of benzylic hydroxides has been described by Chen to create a ¹⁸F-fluoromethyl linker, which was used to attach to spiperone and 1-phenylpiperazine (Figure 220).⁶⁰⁶

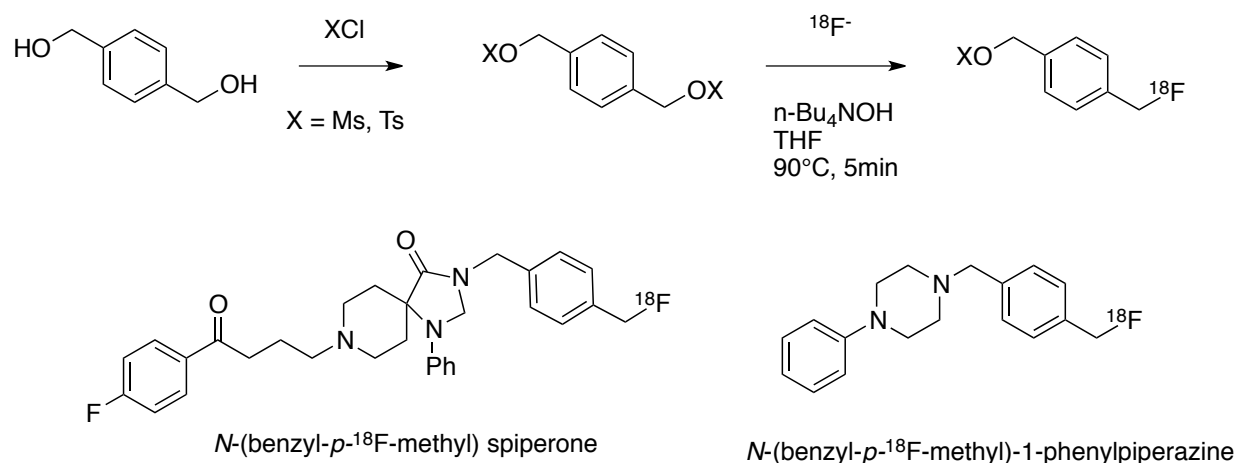


Figure 220. Synthesis of benzylic-¹⁸F-fluoromethyl-spiperone and 1-phenylpiperazine.⁶⁰⁶

Instead of having sulfonates as leaving groups halides like bromine and iodine have been successfully used, as seen in the example of the fluorination ^{18}F -fluorination of methyl 4-(bromomethyl)-2-chlorobenzoate (Figure 221).⁶⁰⁷

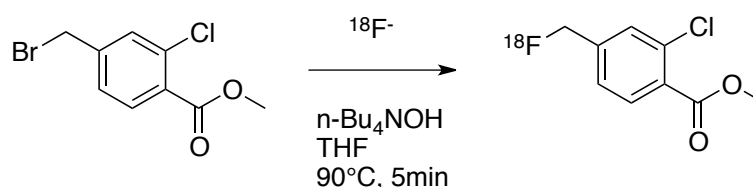


Figure 221. ^{18}F -Fluorination of methyl 4-(bromomethyl)-2-chlorobenzoate.⁶⁰⁷

Xtal-fluor M[®], Xtalfluor E[®] and DAST are reagents used to displace hydroxyl groups by forming a reactive sulfonate intermediate, which is quenched in situ with a fluorine from the reagent.^{608,609} A ^{18}F version of DAST has been synthesized, but has not yet been used in any relevant synthetic procedure (Figure 222).⁶¹⁰

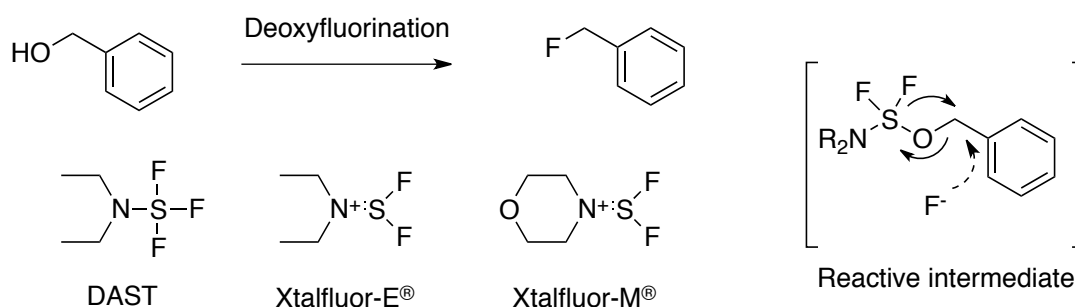
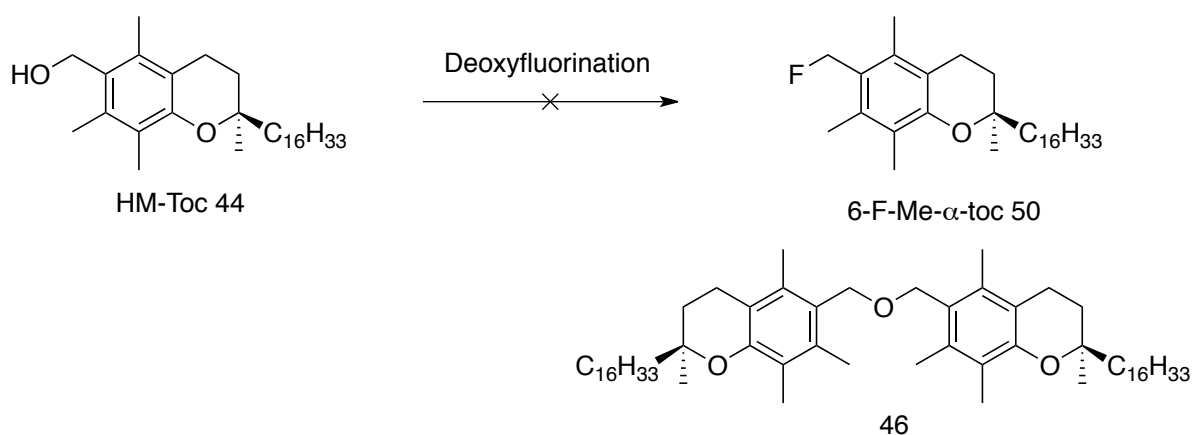


Figure 222. Deoxyfluorination of benzylic alcohols with DAST, Xtalfluor-E[®] and Xtalfluor-M[®].⁶⁰⁸⁻⁶⁰⁹

Reaction with of Xtalfluor M, E and DAST with hydroxymethyl-tocopherol (HM-Toc) instantaneously formed ether **46**, as the only isolated product in all attempts (Table 32).⁶⁰⁸



| F ⁺ -Source | Reaction time: N ⁺ -F | Base | Reaction time: base | Solvent | Temp (°C) | Byproduct |
|----------------------------------|----------------------------------|--------------------|---------------------|------------------------|-----------|-----------|
| Xtalfluor E (1.5eq) | 2min | DBU (1.5eq) | 5min | DCM (130 μ M) | -78 | 20% |
| Xtalfluor M (1.5eq) | 5min | DBU (1.5eq) | 5min | DCM (75 μ M) | 0 | 80% |
| Xtalfluor M (1.0eq) | 1min | DBU (1.0eq) | 2min | DCM (75 μ M) | 0 | 88% |
| DAST (1.0eq) | | Morpholine (0.1eq) | 15min | DCM (75 μ M) | 0 | 94% |
| Xtalfluor M (1.0eq) | 2min | DBU (1.0eq) | 2min | DCM (37 μ M) | -78 | 35% |
| Xtalfluor M (1.0eq) | 2min | DBU (1.0eq) | 5min | DCM 15ml (7.6 μ M) | -78 | 22% |
| Xtalfluor E (1.0eq) ^a | | DBU | 3h | DCM (38 μ M) | -78 | 6% |
| DAST (1.0eq) ^a | | - | 3h | DCM (18 μ M) | -78 | 43% |

Table 32. Deoxyfluorination of HM-Toc.

To a solution of HM-Toc in dry DCM was Xtal fluor E, -M or DAST added at the given temperature under N₂. After 1-5 min was the chosen base added and stirred for a given time. The reaction mixture was concentrated and directly purified over a SiO₂ column. (a) Reverse addition: HM-Toc was added to the deoxyfluorinating agent and DBU at -78°C temperature.

Nucleophilic substitution with activated F⁻ in the form of CsF in *t*-BuOH has worked to replace the 5'-bromomethyl- α -tocopherol to form the 5-fluoromethyl- α -tocopherol (see section 5-F-

methyl- α -tocopherol synthesis). Repeating the same reaction with HM-Toc, using catalytic amounts of hydrogen iodide (HI) to activate the benzylic hydroxide yielded instead the byproduct 6'-*t*-BuO- α -Toc, **81**, alongside dimer, **46**, as a crude mixture. Acidic activation in the presents of excess TBAF did not yield any product (Figure 223).

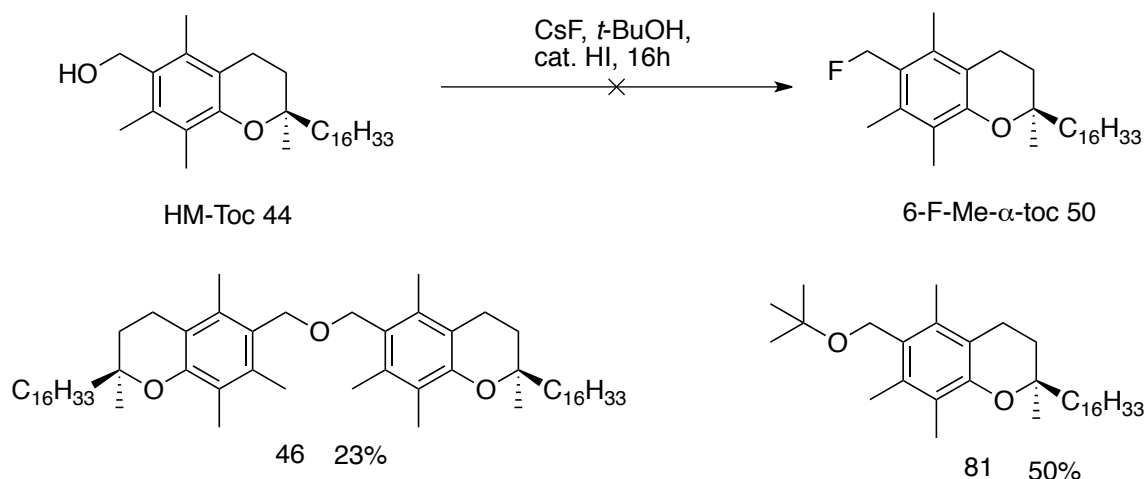


Figure 223. HM-Toc fluorination with CsF and *t*-BuOH. Synthesis of byproduct **46** and **81**.⁵⁹⁸

Makino described a way to directly fluorinate benzyl alcohols using KF activated with a phase transfer catalyst like 18-crown-6 and tosyl fluoride (TsF) as a Lewis acid. Attempts to fluorinate HM-Toc with KF-16-crown-6 and CsF-cryptand[2.2.2] with TsF did not produce any product (Table 33).⁶⁰⁵

HM-Toc 44 - KF, 18-Crown-6, TsF, 4Å MS
or
- CsF, cryptand[2.2.2], TsF, 4Å MS 50

| F ⁺ -Source | Carrier additive | Lewis acid | Solvent ^a | Time | Temp (°C) |
|------------------------|-----------------------|------------|----------------------|------|-----------|
| KF (4eq) ^b | [2.2.2] cyptant (1eq) | TsF (2eq) | THF (80mM) | 3h | rt |
| CsF (4eq) ^a | 18-crown-6 (1eq) | TsF (2eq) | THF (80mM) | 3h | rt |

Table 33. Nucleophilic fluorination of HM-Toc.

44, nucleophilic fluoride reagent, carrier additive, TsF and 4Å molecular sieves (MS) were stirred in THF for up to 3 h. Extracted with water. (a) dry solvents (b) 4Å Molecular sieves 4.5 mg per 1 mg HM-Toc.⁶⁰⁵

Trying to convert the HM-Toc to the tosylate **82** with triethylamine and tosylchloride only formed small amounts of dimer **46** and starting material HM-Toc. Reports by Kochi mentioned the instability of electron rich tosylates and the difficulty to synthesize them.⁶⁰⁴ Trying instead to mesylate **83** HM-tocopherol produced only dimer **46** (Figure 224).⁶¹¹

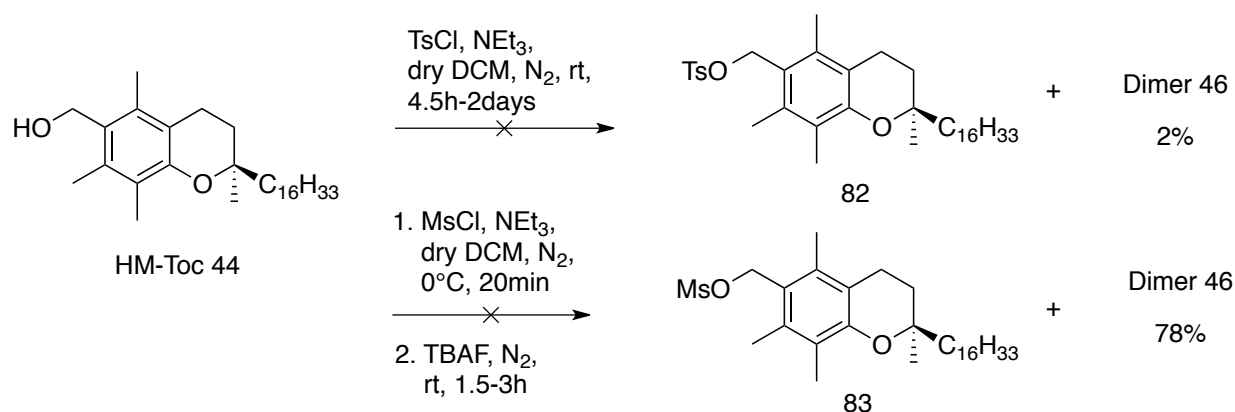


Figure 224. Synthesis of sulfonate esters, **82 and **83**, from HM-Toc, formation of dimer **46**.**^{604,611}

Since HM-Toc is more nucleophilic than activated fluoride the plan was to convert the hydroxyl group into the benzyl iodide, **84**. Iodides are good leaving groups and weak nucleophiles in their ionic form.⁶¹² However, the reaction of HM-Toc with iodine (I_2), triphenylphosphine (PPh_3) and 4-dimethylaminopyridine (DMAP) did only yield dimer **46** (Figure 225).⁶¹³

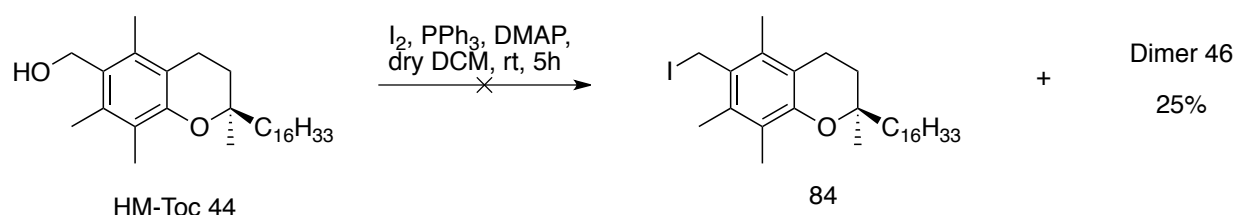


Figure 225. Iodination of HM-Toc with I_2 , PPh_3 and DMAP to product **84.**

Formation of byproduct **46.**⁶¹³

All the attempts to fluorinate HM-Toc did not work and formed dimer **46** as the main product. Future work will therefore be focusing on converting the benzylic alcohol into the halide leaving group. Attempts to convert HM-Toc in the tosylate / mesitylate failed so far, but

different reagents will be used to convert the benzylic hydroxide to the benzylic iodide

84^{614,615,616} or benzylic bromide **85** (Figure 226).^{617,618,614}

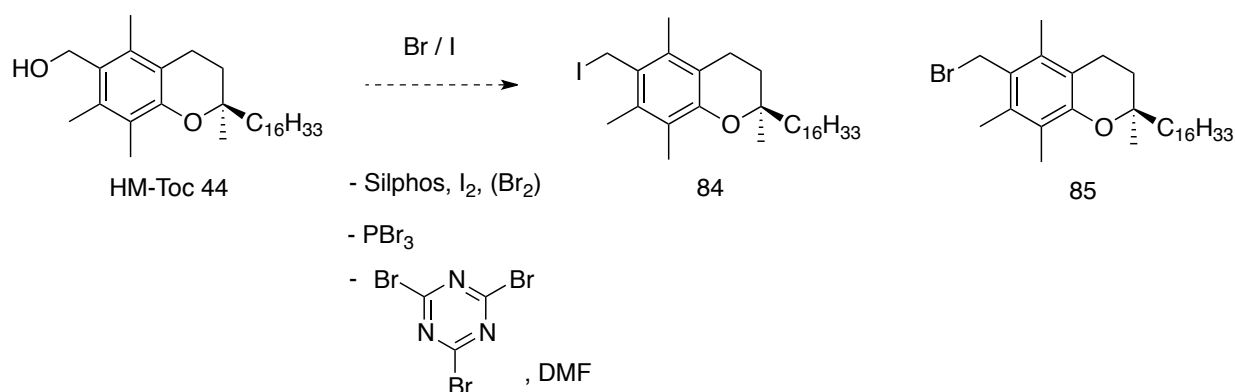


Figure 226. Alternative benzylic iodination / bromination of HM-Toc.^{614,617,618}

11.2.6 13-HO- α -tocopherol fluorination to 13-F- α -tocopherol

Synthesis of the 13-F- α -tocopherol requires the installment of a functional group at the terminal end (13th carbon) of the phytyl chain. α -Tocotrienol has three double bonds and serves as the starting material for the synthesis. Allylic oxidation of the terminal double bond of acetyl-protected tocotrienol with seleniumdioxide (SeO₂) produces 13-hydroxy- α -tocotrienol. Reduction of the olefins turns the hydroxylated trienol into the acetyl protected 13-hydroxy- α -tocopherol. Deoxyfluorination or nucleophilic fluorination with subsequent deprotection of the phenol would produce the 13-F- α -tocopherol (Figure 227).

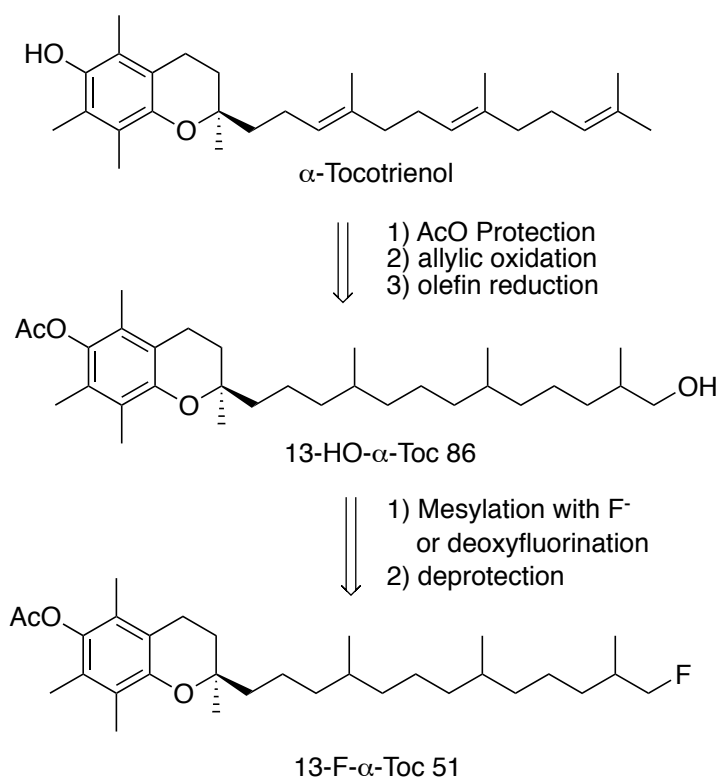


Figure 227. Synthesis of 13-F- α -Toc, 51, from α -tocotrienol.

During the synthesis of the other targeted compounds (47-50) BSc Honours student Luke Taylor was working on a project which had the 13-HO- α -tocopherol as an intermediate. He succeeded in synthesizing the 13-HO- α -tocopherol over a three-step synthesis from α -tocotrienol however, the allylic hydroxylation with selenium dioxide, *tert*-butylhydroperoxide (TBHP) and salycilic acid turned out to be not selective to the terminal olefin, decreasing the overall yield drastically. Despite several attempts was AcO-13'-HO- α -tocotrienol, **86**, produced in maximum 10% yield (Figure 228).

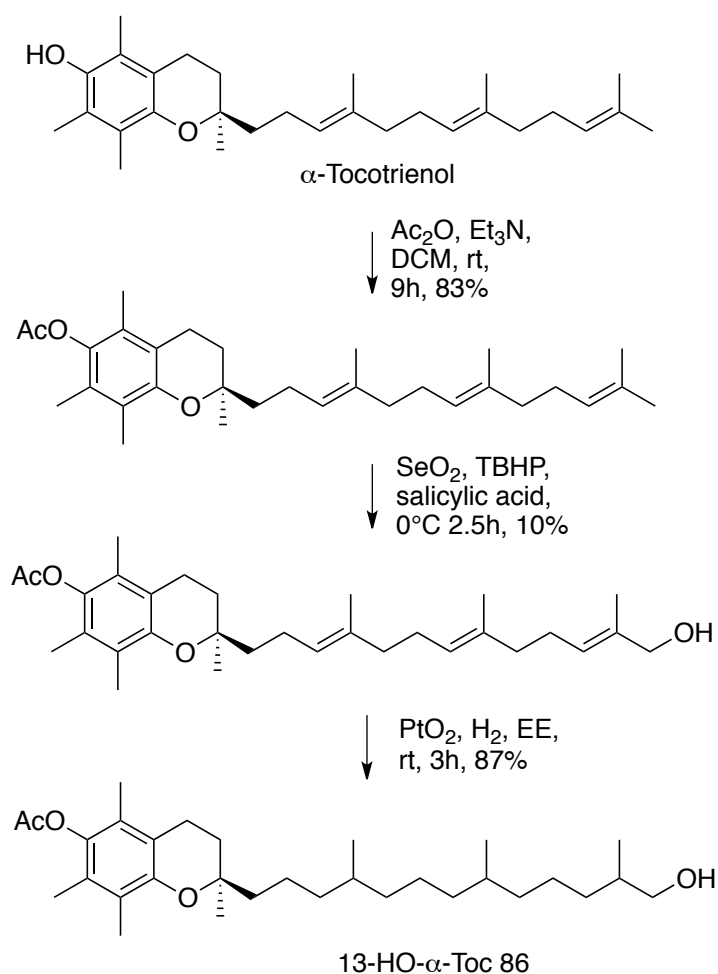


Figure 228. Taylor's synthesis of 13-HO- α -Toc, 86, from α -tocotrienol.

High yielding reactions are required to compensate for the high cost of pure α -tocotrienol (100 mg = \$1,260 CAD Sigma Alderich). Isolation of α -tocotrienol from oil mixtures called Tocomin®50 is cheaper, yielding around 100 mg per 1 g mixture (1 g mixture = \$3.8 CAD).⁶¹⁹ However, a tedious isolation by chromatography is required using large amounts of solvent.

As an alternative starting material the antioxidant garcinoic acid can be used, which is advantageous because of the already installed carboxylic acid at the 13-position. However, the high price of garcinoic acid (90% pure garcinoic acid, 1 mg = \$256 CAD Sigma Alderich) and a necessary three step synthesis to form 13-HO- α -Toc, 86, would not be profitable (Figure 229).^{620,621}

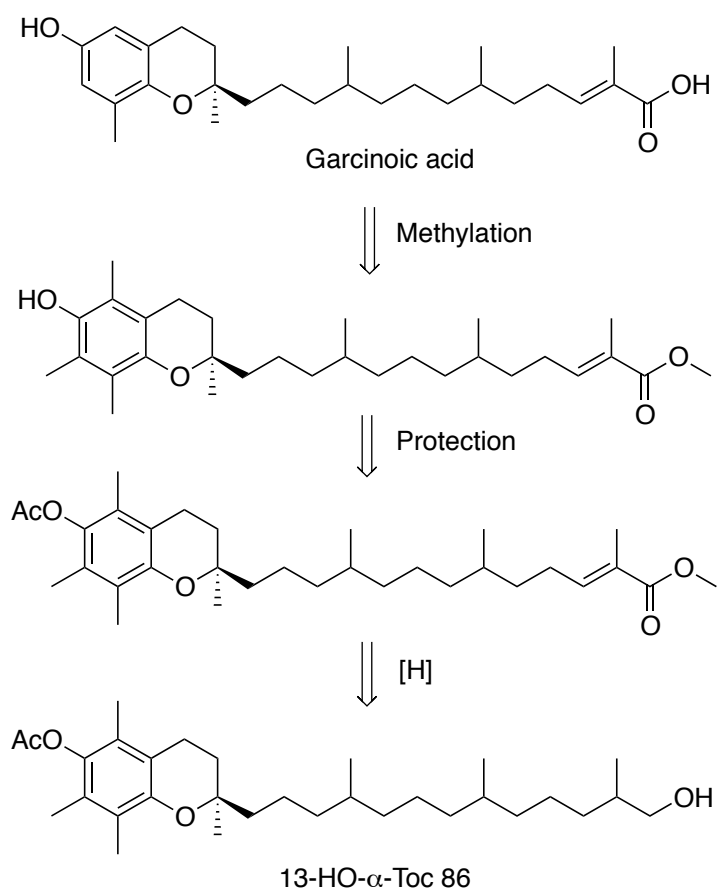


Figure 229. Synthesis of 13-HO- α -Toc, 86, from garcinoic acid.⁶²⁰

11.3 BODIPY fluorination

Hendricks and Liu have described the fluorine exchange reaction of a BODIPY boron-fluorine with a radioactive ^{18}F -fluoride.^{622,623} Hendricks' approach used in the first step trimethylsilyltrifluoroacetic acid (TMSOTf) to exchange the BODIPY boron-fluorine with a triflate group (OTf), followed by ^{18}F -fluoride addition to replace the OTf with ^{18}F .⁶²² Liu instead activated the boron-fluorine bond with Lewis acids like AlCl_3 , TiCl_4 , SnCl_4 and ZnCl_2 to achieve fluorine exchange.⁶²³ Radiochemical yields up to 95% were described with equimolar amounts of SnCl_4 (Figure 230).

dimethyl-BODIPY **37**, had no substituent on the *meso*-position. The wavelength of BODIPY **37** had a higher wavelength when tested in the fluorimeter with the maximum at 542 nm when excited at 480 nm. A first test reaction in the fluorimeter showed that addition of solid TBAF hydrate to TfO-exchanged dimethyl-BODIPY (586 nm) induces rapid decomposition, seen by a colour change to dark brown and by having no remaining fluorescence at 542 nm. When TBAF was added directly to **37**, the sample decomposed the sample in 5 min (Figure 232).

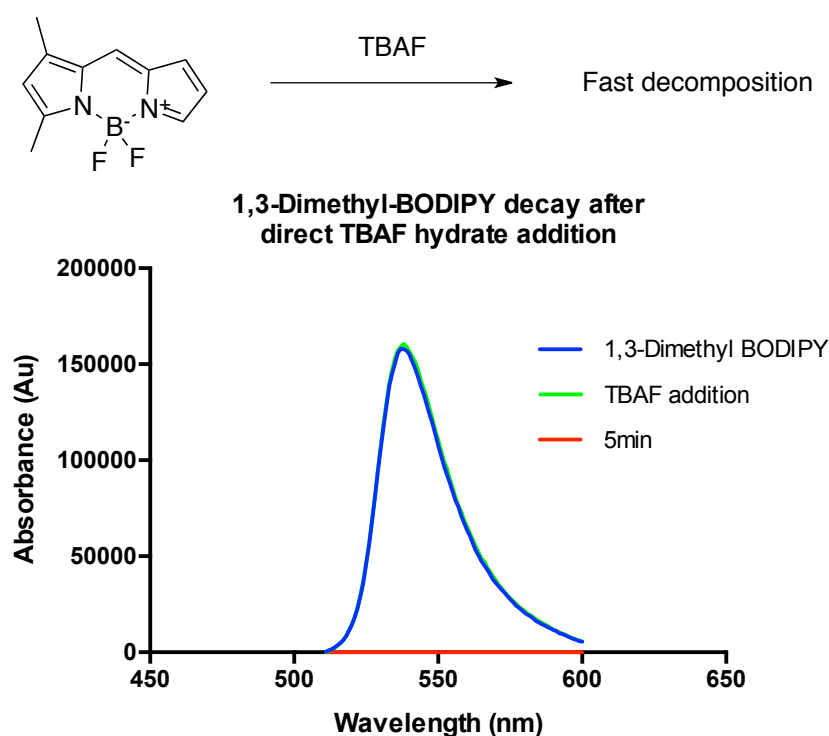


Figure 232. Direct TBAF addition to 1,3-Dimethyl BODIPY.

1,3-Dimethyl BODIPY, **3**, (5.6 mg, 25.4 μ mol) in dry ACN:DCM 2:1 (3ml)(blue line) was treated with TBAF hydrate (3.3 mg, 12.7 μ mol), shaken and directly measured (green line) with the excitation set at 480 nm (λ max 542 nm). After 5 min the absorbance was measured again (red line).

Comparing the the decay to the fully substituted 2,8-ethyl-1,3,7,9,10-pentamethyl-BODIPY, **88**, revealed a slowed decay on increased substitution (Figure 233).⁶²⁴



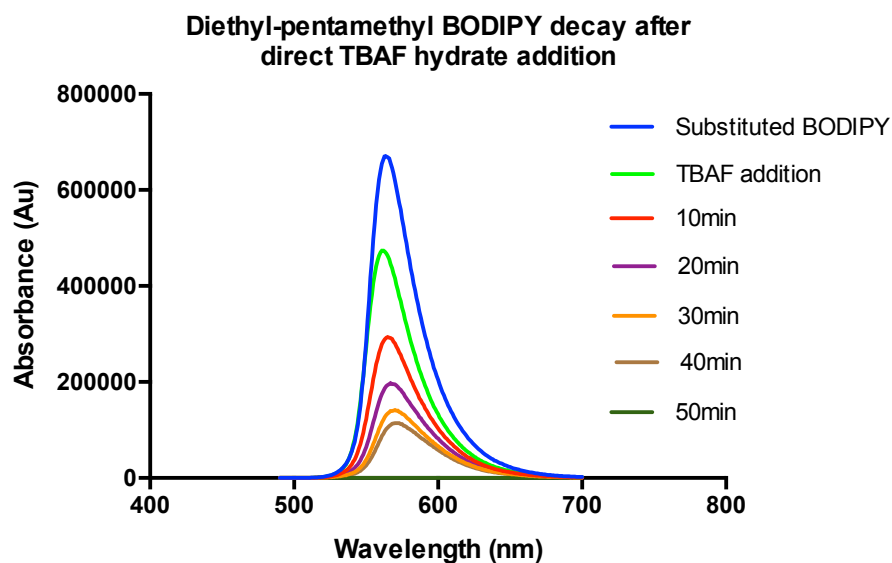
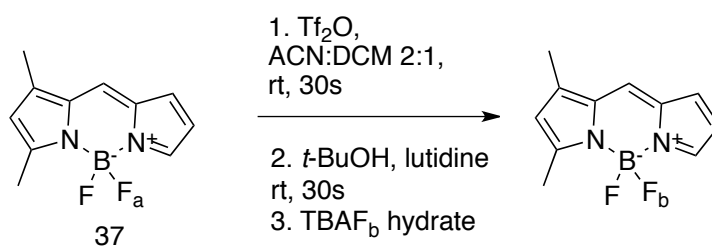


Figure 233. Direct TBAF addition to 2,8-diethyl-1,3,5,7,9-pentamethyl BODIPY.

2,8-Diethyl-1,3,5,7,9-pentamethyl BODIPY (2.8 mg, 8.8 μmol) in dry ACN:DCM 2:1 (3 ml)(blue line) was treated with TBAF hydrate (2.3 mg, 8.8 μmol), shaken and directly measured (green line) with the excitation set at 480 nm (λ max 562 nm). The absorbance was measured at 10 min intervals.

The addition of *t*-BuOH and lutidine helped to stop the decomposition.⁶²² To better monitor the conversion the reaction was conducted in a UV/Vis spectrometer. UV absorption before the reaction showed a lambda maximum at 503 nm. Addition of the TMSOTf led to a color change from green to orange, with a wavelength of 543 nm. After the addition of *t*-BuOH, lutidine, followed by TBAF hydrate turned the color back to green. A lower absorption was observed at 503 nm (Figure 234).



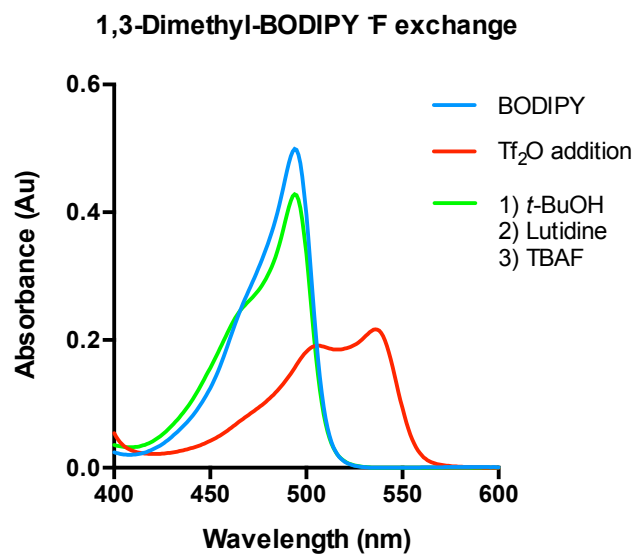


Figure 234. Fluorine exchange of 1,3-dimethyl-BODIPY, 37, followed by UV / VIS.

In a cuvette 37 ($32\ \mu\text{M}$, dry ACN:DCM 2:1) was scanned from 200-700 nm. TMSOTf (4 eq) was added to the cuvette, shaken and measured. *t*-BuOH (4 eq), Lutidine (4 eq) and TBAF hydrate (4 eq) were added, shaken and measured. $\lambda\ \text{max}$: BODIPY-F 503 nm, BODIPY-OTf 543 nm.



Figure 235. 1,3-Dimethyl-BODIPY. Left: standard reference $0.32\ \mu\text{M}$. Right cuvette: $0.32\ \mu\text{M}$. Blue line in Figure 234



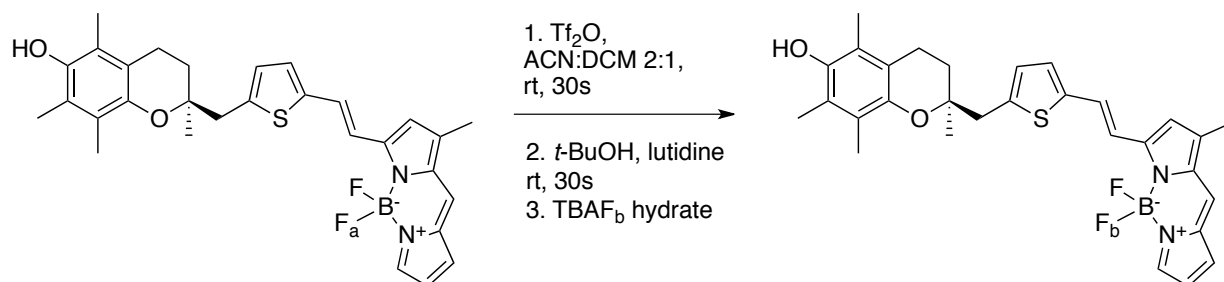
Figure 236. 1,3-Dimethyl-BODIPY. Left cuvette: standard reference 0.32 μM . Right cuvette: Tf_2O addition. Red line in Figure 234.



Figure 237. 1,3-Dimethyl-BODIPY. Left cuvette: standard reference 0.32 μM . Right cuvette: 1) *t*-BuOH
2) Lutidine 3) TBAF addition. Green line in Figure 234.

1,3-Dimethyl BODIPY successfully exchanged the boron-fluorine with a triflate and was resubstituted with fluoride. The same reaction was repeated with thienyl-ene-BODIPY, **3**. The

maximum absorption of 571 nm shifted after Tf_2O addition to 639 nm (Figure 238). A color change from pink to blue was observed when the triflate was formed.



Thienyl-ene-BODIPY F exchange

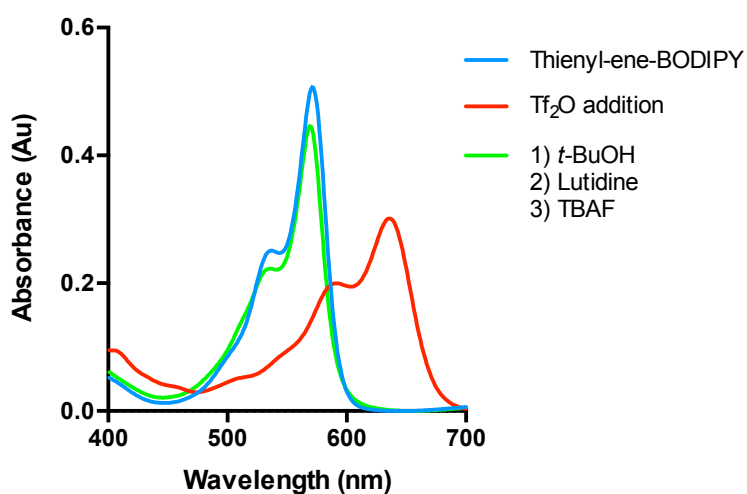


Figure 238. Fluorine exchange of thienyl-ene-BODIPY, 3, followed by UV/ Vis.

In a cuvette 3 (32 μM , dry ACN:DCM 2:1) was scanned from 200-700 nm. TMSOTf (4 eq) was added to the cuvette, shaken and measured. *t*-BuOH (4 eq), Lutidine (4 eq) and TBAF hydrate (4 eq) were added, shaken and UV/Vis absorption measured. λ max: BODIPY-F 571 nm, BODIPY-OTf 639 nm.



Figure 239. Thienyl-ene-BODIPY. Left cuvette: standard reference 0.16 μM . Right cuvette: 0.32 μM . Blue line in Figure 238.



Figure 240. Thienyl-ene-BODIPY. Left cuvette: standard reference 0.16 μM . Right cuvette: Tf_2O addition. Red line in Figure 238.

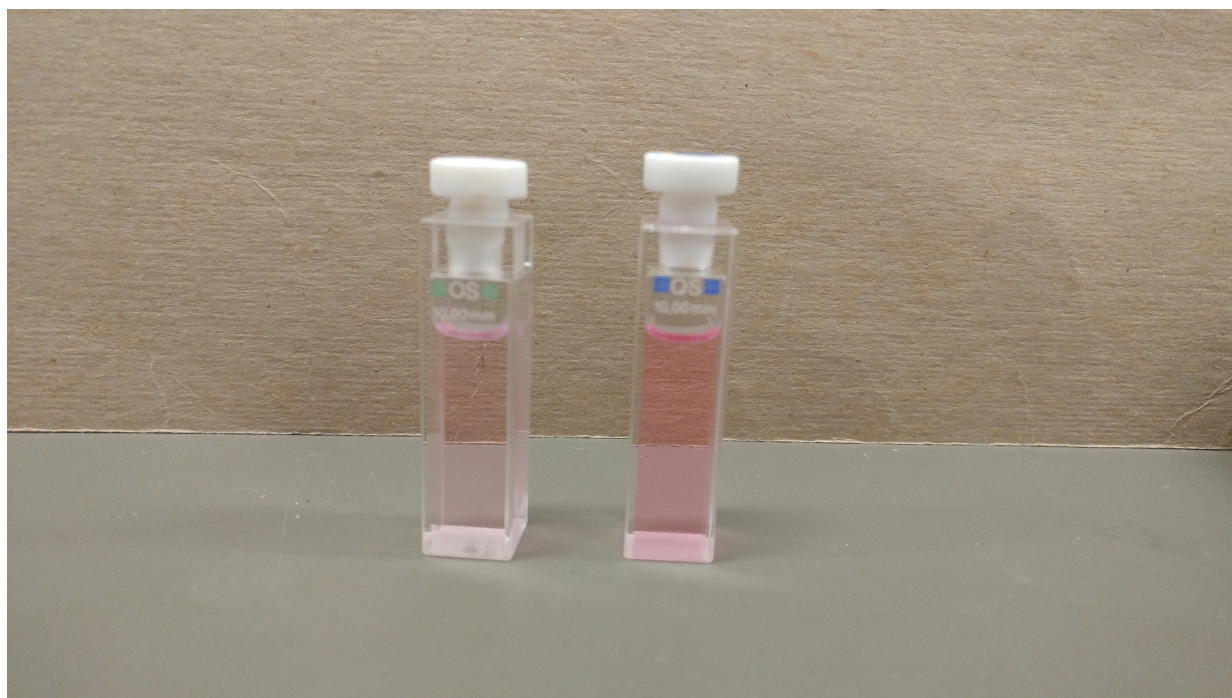


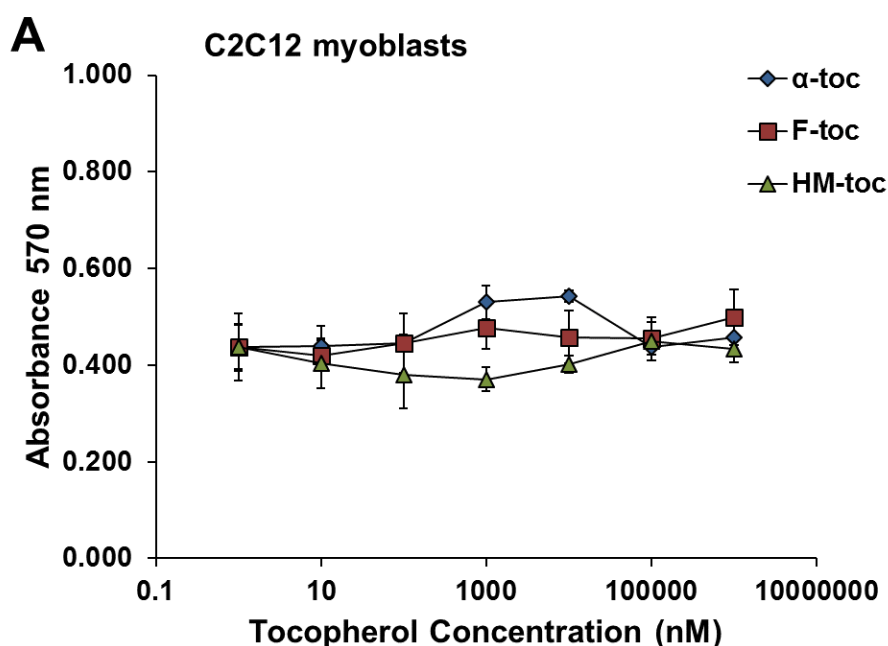
Figure 241. Thienyl-ene-BODIPY. Left cuvette: standard reference 0.16 μ M. Right cuvette: 1) *t*-BuOH 2) Lutidine 3) TBAF addition. Green line in Figure 238.

Fluorine exchange was successful with thienyl-ene-BODIPY, **3**. In conclusion, both BODIPYs, **37** and **3**, were able to undergo fluorine exchange after the boron center was exchanged with a triflate. The addition of *t*-BuOH and lutidine was helpful to stabilize the BODIPY triflate, as described by Hendricks.⁶²² The next step of the project is to exchange thienyl-ene-BODIPY, **3**, with ^{18}F -fluoride.

11.4 Cell cytotoxicity of 6-F- α -tocopherol, thienyl-ene-BODIPY and hydroxymethyl tocopherol

Before the newly created 6-F- α -tocopherol (F-Toc) and thienyl-ene-BODIPY can be tested in a living system with ^{18}F a cytotoxic analysis of the non-radioactive ^{19}F has to be performed to see if any of these compounds are toxic. Injections of ^{18}F radiolabels into patients are normally in the pico- to nanomolar (ng-mg) amounts.⁶²⁵ Everaert found that with ^{18}F -fluoroglucose good PET images were obtained when a dose of at least 8 MBq/kg (0.21 Ci/kg) bodymass was achieved, which are around 40 picomoles/kg bodymass (calculated assuming the specific activity of ^{18}F is 5,283,333 Ci/mol).⁶²⁶ Images are generally taken after 30-40 min after

injection. FDG is injected as a 0.740-7.4 GBq solution, which would mean that a maximum of 40 nanomols/kg bodymass are used.⁶²⁷ A concentration range from 1 nM to 1 mM of F-Toc was used to ensure that even at higher concentration no toxicity occurs. A methyl tetrazolium (MTT) assay was used to assess the cytotoxicity to cultured C2C12 myoblasts and mouse embryonic fibroblast cells.⁶²⁸ The assay looks at the mitochondrial metabolic activity of cells, which corresponds directly to the cell viability. MTT (3-(4,5-dimethylthiazol-2-yl)-2,5-diphenyltetrazolium bromide) is thereby converted by mitochondrial NAD(P)H-dependent reductase enzymes to formazan (*E,Z*)-5-(4,5-dimethylthiazol-2-yl)-1,3-diphenyltetrazolium bromide), which has an absorption around 570 nm. The compounds were tested in a C2C12 myoblastoma and mouse embryonic fibroblast cells, grown by our collaborator Dr. Jeff Stuart, Brock University. Cytotoxicity experiments and data processing were conducted with the help of Lucas Maddalena. α -Tocopherol was used as a non-toxic standard. Hydroxymethyl tocopherol (HM-Toc) was also tested using the same concentration range in the same cytotoxic assay. This result was used for future studies in the non-antioxidant project (see Chapter 2) (Figure 251).



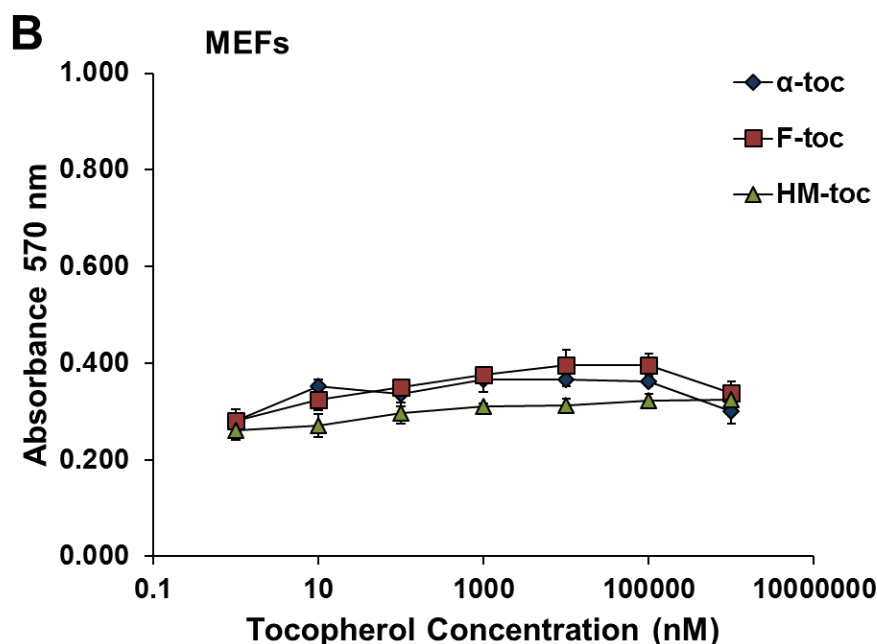


Figure 242. Viability of mouse cells cultured in the presence of α -, F-, and HM-tocopherol derivatives at concentrations ranging from 1 nM to 1 mM.

(A) C2C12 mouse myoblasts and (B) mouse embryonic fibroblasts (MEFs) were treated with α -, F-, or HM-tocopherol for 24h prior to assessing viability via spectrophotometric measurement of formazan (absorbance at 570 nm) produced from the live-cell-catalyzed reduction of MTT tetrazolium. There were no significant differences between absorbance values of all tocopherol groups compared to the corresponding vehicle control (0.1% DMSO; Tukey's post-hoc test). Data points represent means \pm SEM, with $n = 4$ for all conditions except for F-toc in MEFs ($n = 3$). *Note:* absorbance values for vehicle control groups in C2C12 cells and MEFs were 0.4343 ± 0.0299 and 0.2984 ± 0.0154 , respectively.

No increase in absorption was observed with 6-F- α -tocopherol, HM-Toc and tocopherol at all concentrations, indicating that all compounds tested are non-toxic.

The MTT assay cannot be used to assess thienyl-ene-BODIPY's toxicity, because the absorbance of formazane is at the same wavelength and has a much lower extinction coefficient than thienyl-ene-BODIPY. (formazan: 570 nm / $13,000 \text{ M}^{-1} \text{ cm}^{-1}$, thienyl-ene-BODIPY: 571 nm / $120,000 \text{ M}^{-1} \text{ cm}^{-1}$).⁶²⁹ Instead cell counting was used to determine the cell viability (Figure 252).

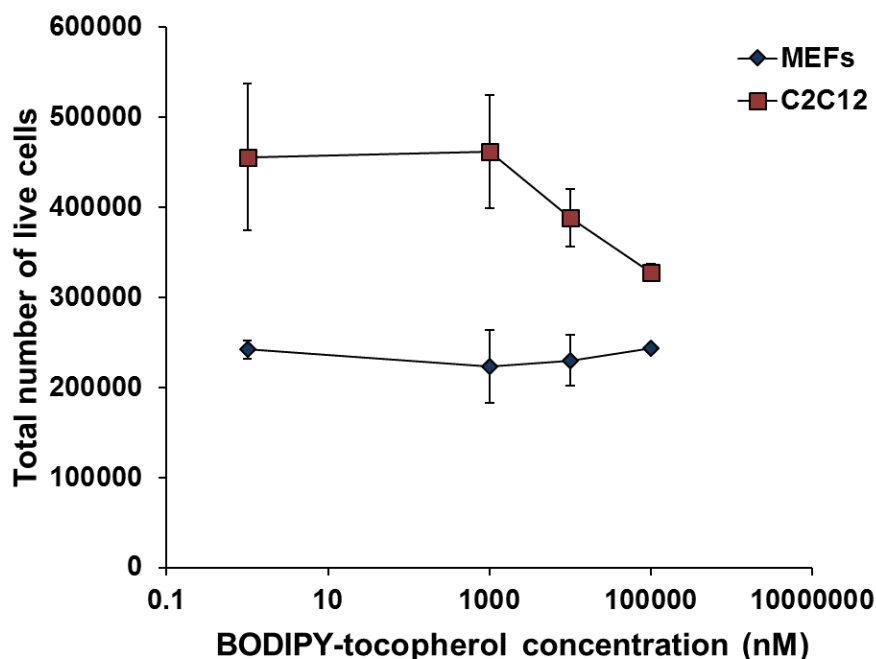


Figure 243. Viability of mouse cells cultured in the presence of BODIPY-tocopherol at concentrations ranging from 1 nM to 0.1 mM.

C2C12 mouse myoblasts and MEFs were treated with up to 0.1 mM BODIPY-tocopherol for 24h before determining the number of cells excluding Trypan blue dye. The mean number of viable cells in all BODIPY-tocopherol groups were not significantly different than that of the corresponding vehicle control (0.1% DMSO; Tukey's post-hoc test). Data points represent means \pm SEM ($n = 2$). *Note:* 0.1 mM BODIPY-toc partially precipitated out of solution when added to culture media; it completely precipitated out of solution at 1 mM and was therefore not tested at this concentration. The number of viable cells in the vehicle control groups for C2C12 cells and MEFs were $424,875 \pm 31,125$ and $249,000 \pm 3,000$.

F-Toc, HM-Toc and α -tocopherol turned out to be non-toxic up to millimolar concentrations in both, C2C12 cells and MEFs. Thienyl-ene-BODIPY showed some toxicity at higher micromolar concentrations in MEFs.

To ensure the safe use of the new F-Toc label the cytotoxicity of the starting material from the electrophilic fluorination, H-Toc (Figure 253), and byproduct from the nucleophilic fluorination, I-Toc (Figure 254), were tested in MEF and C2C12 cells.

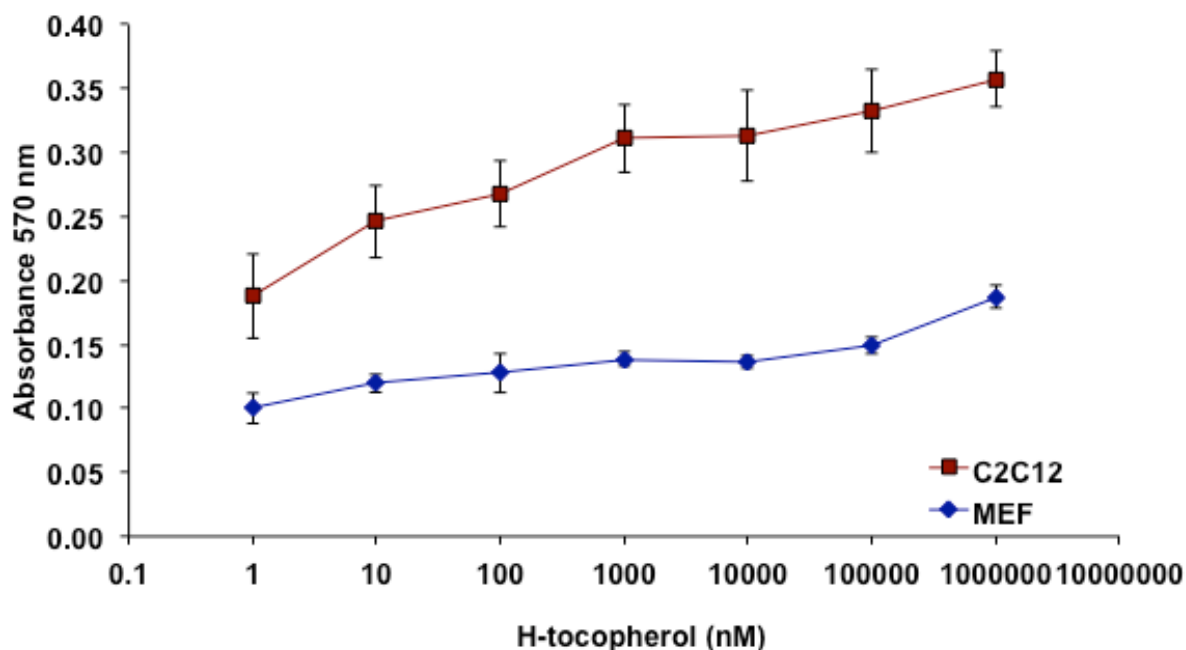


Figure 244. Viability of mouse cells cultured in the presence of H-tocopherol (H-toc) at concentrations ranging from 1 nM to 1 mM.

C2C12 mouse myoblasts (red) and mouse embryonic fibroblasts (MEFs, blue) were treated with H-tocopherol for 24h prior to assessing viability via spectrophotometric measurement of formazan (absorbance at 570 nm) produced from the live-cell-catalyzed reduction of MTT tetrazolium. There were no significant differences between absorbance values of all tocopherol groups compared to the corresponding vehicle control (0.1% DMSO; Tukey's post-hoc test). Data points represent means \pm SEM, with $n = 5$ for all conditions. *Note:* absorbance values for vehicle control groups in C2C12 cells and MEFs were 0.303 ± 0.002 and 0.151 ± 0.004 , respectively.

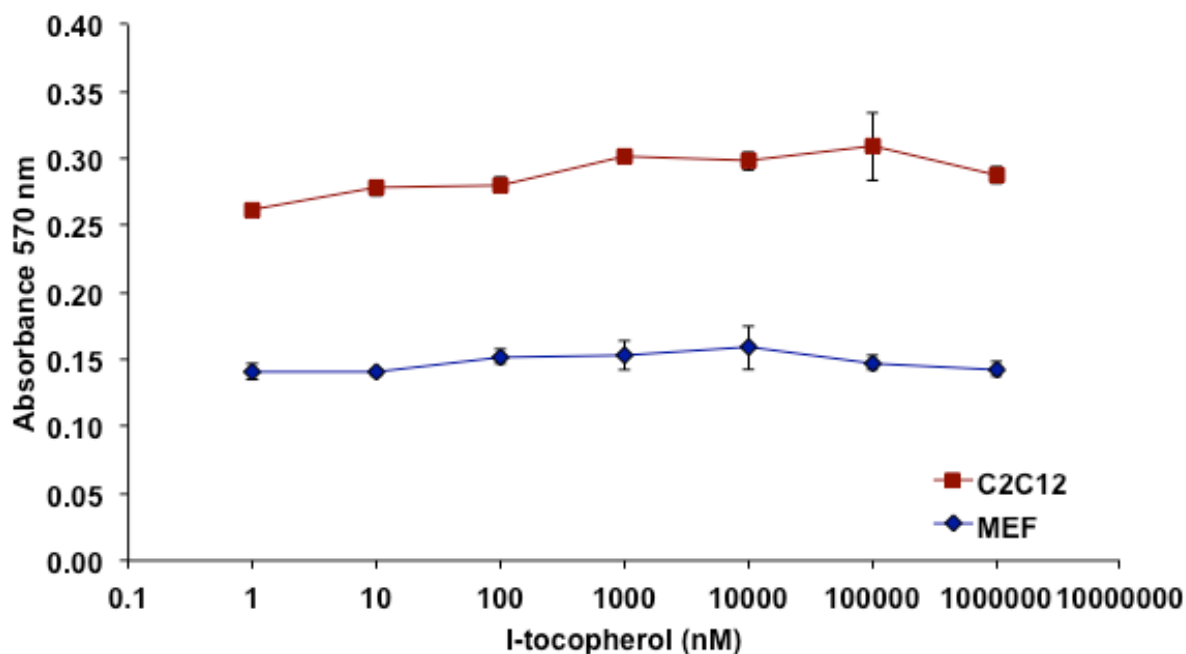


Figure 245. Viability of mouse cells cultured in the presence of I-tocopherol (I-toc) at concentrations ranging from 1 nM to 1 mM.

C2C12 mouse myoblasts (red) and mouse embryonic fibroblasts (MEFs, blue) were treated with I-tocopherol for 24h prior to assessing viability via spectrophotometric measurement of formazan (absorbance at 570 nm) produced from the live-cell-catalyzed reduction of MTT tetrazolium. There were no significant differences between absorbance values of all tocopherol groups compared to the corresponding vehicle control (0.1% DMSO; Tukey's post-hoc test). Data points represent means \pm SEM, with $n = 5$ for all conditions. *Note:* absorbance values for vehicle control groups in C2C12 cells and MEFs were 0.303 ± 0.002 and 0.151 ± 0.004 , respectively.

No toxic effect was observed in the MTT assay in both cell lines at all concentrations tested.

Unexpectedly, in C2C12 cells an increase in cell survival was seen.

Since H-Toc and I-Toc have shown no evidence of toxicity in mammalian cell culture is the injection of both materials into test animals may proceed with caution. Purification of F-Toc from these compounds is therefore not necessary, saving valuable time in the overall PET-label production process.

11.4.1 Cell cytotoxicity of the liposomal delivery 6-F- α -tocopherol

The designed PET labels, F-Toc and thienyl-ene-BODIPY, will be distributed *in vivo* with the help of a specific liposomal construct, consisting of POPC, POPG and cholesterol in a 7:3:4 ratio.⁶³⁰ Toxicity of the liposomes was tested in C2C12 (Figure 255) and MEF (Figure 256) cell lines to assure safe use in upcoming animal trials.

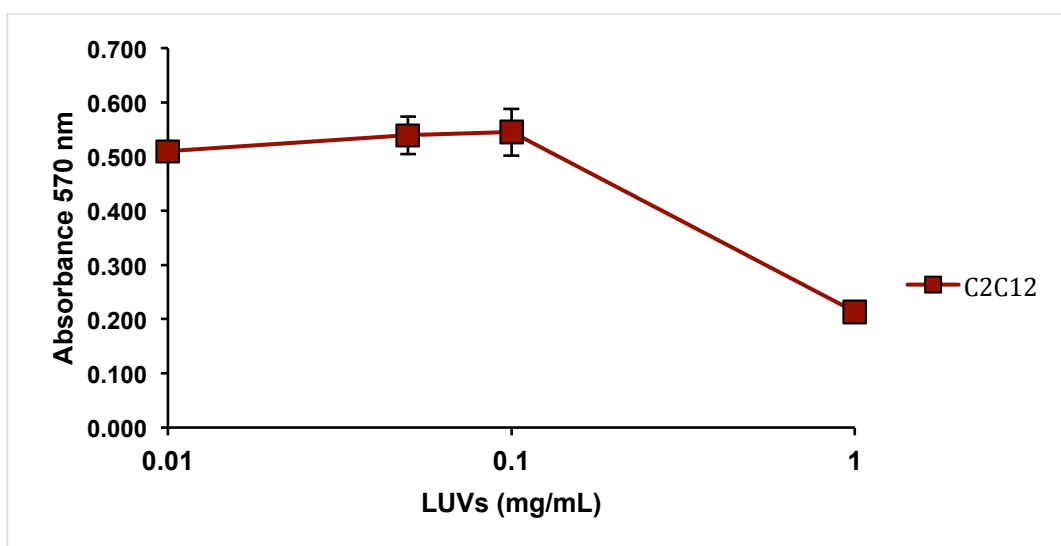


Figure 246. Viability of mouse cells cultured in the presence of varying concentrations of large unilamellar vesicles (LUVs).

C2C12 mouse myoblasts were treated with LUVs for 24h prior to assessing viability via spectrophotometric measurement of formazan (absorbance at 570 nm) produced from the live-cell-catalyzed reduction of MTT tetrazolium. Data points represent means \pm SEM (n = 8). *Note:* LUVs consisted of POPC:POPG:Cholesterol at a molar ratio of 7:3:4.

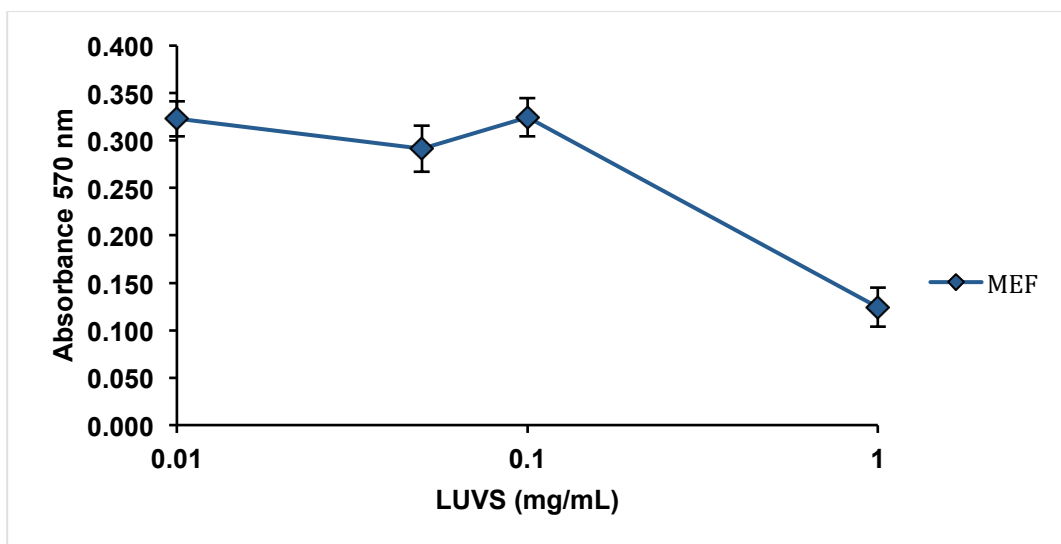


Figure 247. Viability of mouse cells cultured in the presence of varying concentrations of large unilamellar vesicles (LUVs).

Mouse embryonic fibroblasts (MEFs) were treated with LUVs for 24 h prior to assessing viability via spectrophotometric measurement of formazan (absorbance at 570 nm) produced from the live-cell-catalyzed reduction of MTT tetrazolium. Data points represent means \pm SEM (n = 8). Note: LUVs consisted of POPC:POPG:Cholesterol at a molar ratio of 7:3:4.

In both cell lines, C2C12 and MEF, the liposomes showed no toxicity until a concentration 1mg/ml was exposed to cultured cells. The reason for the toxicity at higher concentrations is the oversaturation of the cells with lipids.⁶³¹

In conclusion tested compounds showed no overt signs of cytotoxicity at concentrations used in PET imaging (5-740 mBq = pM-n) and above and can be further assessed in animal trials.⁶³²

11.5 Cellular uptake of in liposome incorporated thienyl-ene-BODIPY

Uptake of thienyl-ene-BODIPY POPC:POPG:cholesterol liposomes into cells was tested in MEF and C2C12 cells and monitored by fluorescence microscopy. The size of the prepared liposomes was 50 nm, this size being the smallest used in a patent describing this drug delivery technology.⁶³⁰ Images were reported as stacked images in fluorescent (ex. 587 nm - em. 610 nm) and brightfield mode.

The C2C12 cells were imaged, first without any label present, then 5 min, 10 min, 20 min and 30 min after addition of the fluorophore (Figure 257). After 30 min the increase in fluorescence was marginal and not included here. The effect of liposome uptake was compared to directly added thienyl-ene-BODIPY in DMSO.

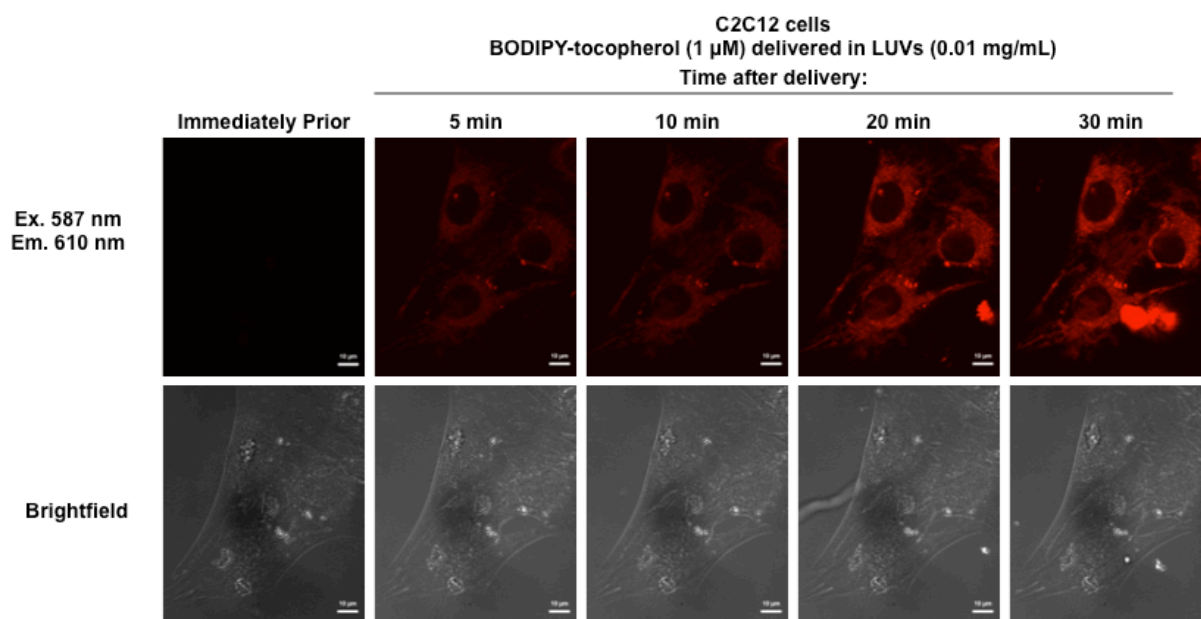


Figure 248. C2C12 cell uptake of thienyl-ene-BODIPY-tocopherol (BODIPY-tocopherol) delivered in LUVs.

Images are maximum projections of z-stacks taken at 0.32 nm intervals.

Fluorescence was observed in the cytosol of the cells. Almost no difference in fluorescence intensity was seen between 5-10 min. After 20 min, a larger increase in intensity was observed. Addition of thienyl-ene-BODIPY was compared after 30 min to the liposome delivery (Figure 258).

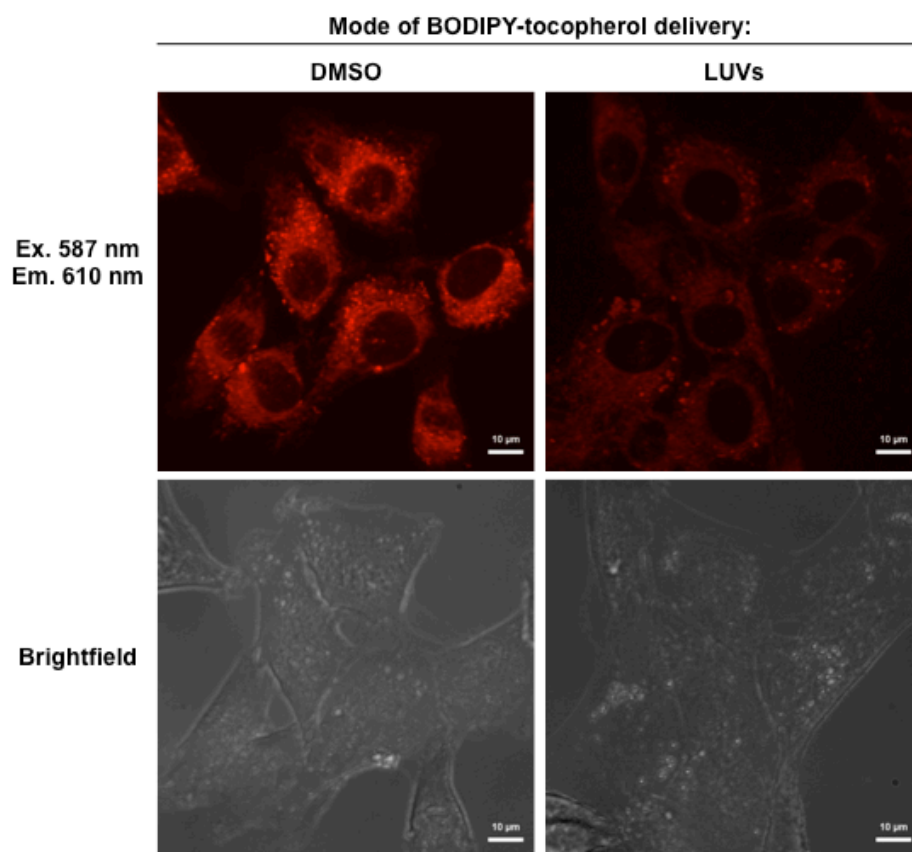


Figure 249. Uptake of thienyl-ene-BODIPY-tocopherol (BODIPY-tocopherol) in C2C12 cells at 30 min after delivery via DMSO or LUVs.

Images are maximum projections of z-stacks taken at 0.32 nm intervals.

The cells showed a higher fluorescence intensity after direct addition of the fluorophore (DMSO) than after 30 min exposure to fluorophore containing liposomes. Addition of the DMSO solution into the surrounding media offered excess thienyl-ene-BODIPY to diffuse into the cells, leading to an increased uptake compared to the liposomes, which first had to find the cells before incorporation by fusion with the cell membrane.

Tests in MEF cells were more closely monitored in terms of differences between liposomal (Figure 259) and direct delivery (Figure 260). Images were taken after 5 min, 20 min and 30 min.

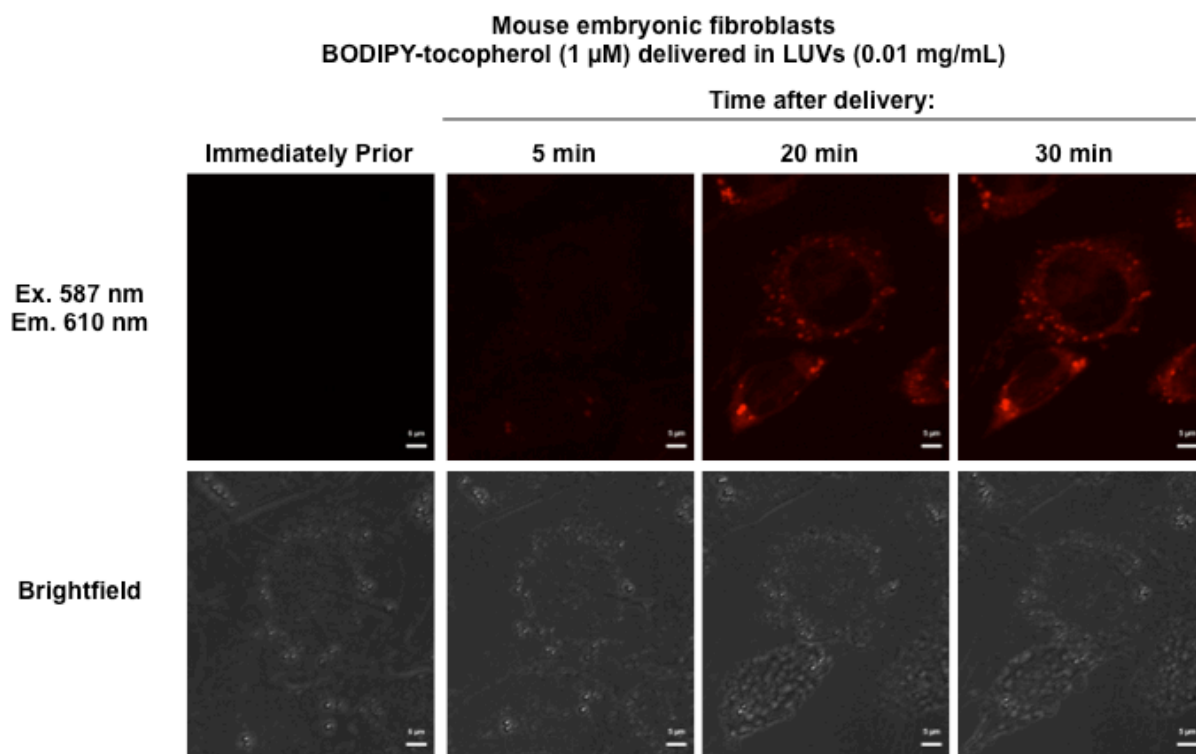


Figure 250. Mouse embryonic fibroblast uptake of thienyl-ene-BODIPY-tocopherol (BODIPY-tocopherol) delivered in LUVs.

Images are maximum projections of z-stacks taken at 0.32 nm intervals.

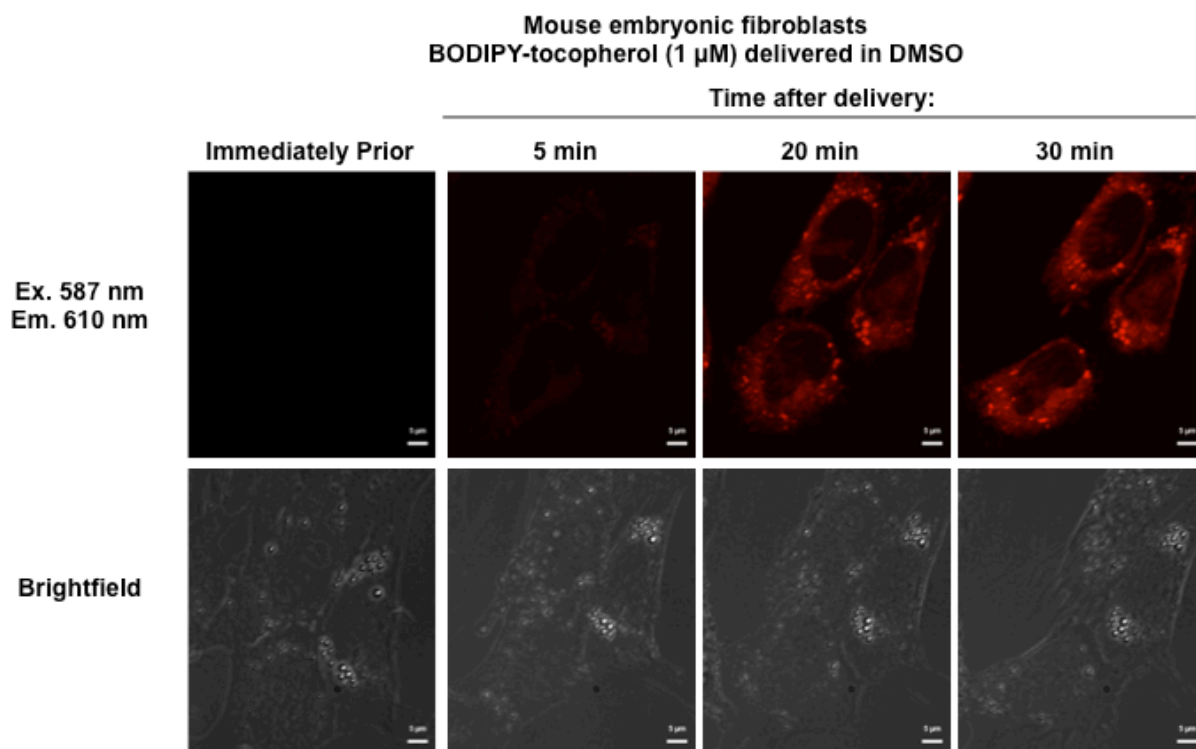


Figure 251. Mouse embryonic fibroblast uptake of BODIPY-tocopherol delivered in DMSO.

Images are maximum projections of z-stacks taken at 0.32 nm intervals.

As with MEF cells was the fluorescence intensity was higher with direct thienyl-ene-BODIPY addition in DMSO solution. However, both addition methods seem to incorporate the fluorescent label in sufficient amounts after 20-30 min. Also, MEF and C2C12 cells incorporated most of the liposomes in a 20-30 min period. PET agents have different distribution times depending on the target location. Generally PET images are taken after a maximum time of 45-90 min. This depends on the distribution of the radiolabel in the body. Cellular uptake of our liposomes may thus be sufficient in this given time frame to obtain a PET image.

12 Conclusion

The main target 6-fluoro- α -tocopherol (F-Toc) was synthesized in short reaction times by nucleophilic and electrophilic fluorinations. The synthetic process most suitable for future

studies with ^{18}F -fluoride is the electrophilic fluorination of 6-hydrogen- α -tocopherol (H-Toc) with NFSI, yielding F-Toc in a 40-45% yield. NFSI has been prepared and used successfully as an ^{18}F -reagent in literature.^{563,564} H-Toc is a stable against light, heat and oxidation and produced in high yields (> 90%) over a two-step synthesis from α -tocopherol (Figure 263).

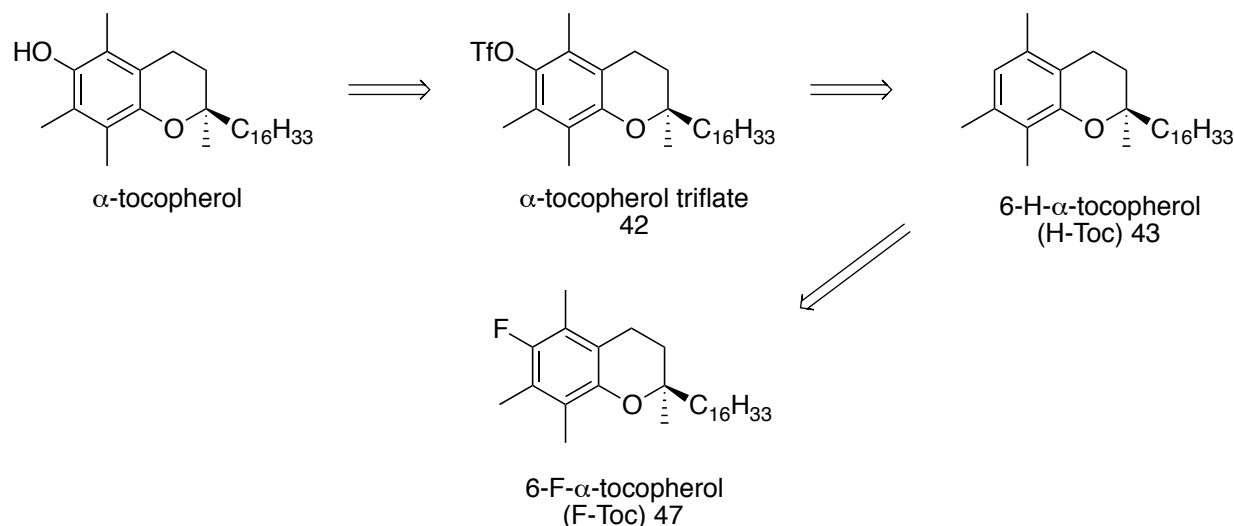


Figure 263. Synthesis of F-Toc from α -tocopherol.

In cell viability assays it was found that F-Toc and H-Toc showed no signs of overt cytotoxicity, potentially allowing the administration of F-Toc into a living organism as a crude mixture with H-Toc present. Furthermore, we showed that the liposomal construct used to deliver F-Toc displayed cytotoxicity only at very high concentrations of applied lipid.

Both compounds were found to be partially separable by HPLC chromatography with a XBD-phenyl column. However, the retention time of both compounds was past 20 min and the separation of both compounds was not well-resolved. Future effort should be made towards the development of a more rapid and cleaner separation between F-Toc and H-Toc which might be achieved by the use of a poly-fluorinated reverse phase HPLC column.

Unfortunately, all attempts to synthesize alternative tocopherol based compounds, bearing fluorine on the 5-aromatic position or the 5- or 6-benzylic position on the chroman ring were unsuccessful. Synthetic efforts towards these secondary targeted compounds will be abandoned,

as future work will focus on the main compound, 6-F-Toc, specifically on its further performance as a PET-label in animal studies.

Fluorine exchange reaction of thienyl-ene-BODIPY boron-fluorine was succesfull and can in the future be used to create a dual label for *in vivo* (^{18}F) and *in vitro* (fluorescence) applications (Figure 261). The cellular uptake of the designed PET-labels when encapsulated in specific liposome constructs was tested with thienyl-ene-BODIPY and proved to successful occupy and allow the imaging of internal cellular membranes in a short amount of time.

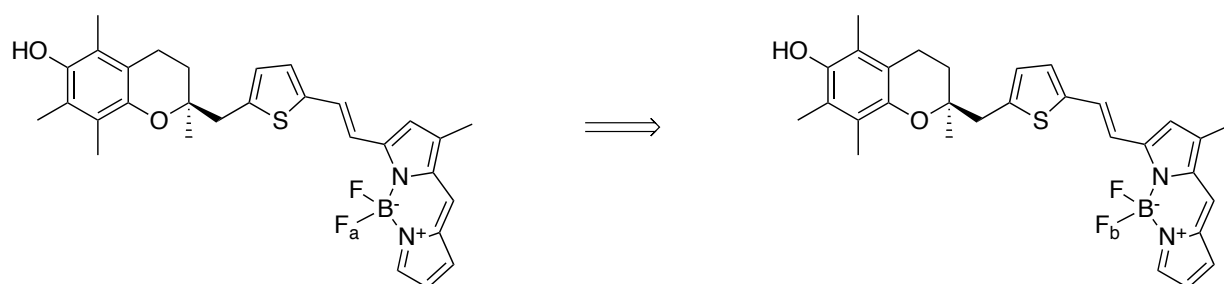


Figure 252. Fluorine exchange (F_a - F_b) on thienyl-ene-BODIPY.

Experimental

13 General procedures

13.1 Reagents

All reagents were purchased from Sigma-Aldrich Chemical Co., Oakville, Ontario. Glassware was flame dried before used. Air and moisture sensitive reactions were conducted under N₂ atmosphere. Solvents were dried according to standard procedures; THF was distilled over sodium and benzophenone; hexane and dichloromethane were refluxed for 3 h with calcium hydride and then distilled under protective atmosphere. Solvents for oxygen sensitive reactions were purged for 2 h with nitrogen. Reactions requiring hydrogenation were purged 3x with hydrogen gas (vacuum, then H₂). The Celite[®] used to filter the catalysts was washed with hexane followed by the solvent used in the reaction before use to remove any impurities. Bu₄N⁺HCO₃⁻ was synthesized by Culbert's method by bubbling CO₂ to a solution of tetrabutylammoniumhydroxide in water, till a pH of 7.4 was reached. The solution was concentrated to a colourless oil, resuspended in ACN and the suspension filtrated and evaporated.⁶³³ The 200 nm sized TiO₂ nanoparticles (rutile: EPRUI-T200, anatase: EPRUI-TA200) were purchased from EPRUI Nanoparticles & Microspheres Co. Ltd.

13.2 Ligand binding and competitive binding assays with α -TTP

Fluorescence measurements were recorded with a QuantaMaster2000 fluorometer (Photon Technologies International PTI, London, Ontario) FeliX-32, using a 150 W Hg-Xe vapor arc lamp with a LPS-220B lamp supply cooled to 5-8°C via chilled water circulation, MD-50 20 motor drive, SC-500 shutter control and a Brytebox[™]. All the data points were stored in Excel files and analyzed with GraphPad Prism 5. Slit-width was consistent for all measurements at 5

nm. OS high precision cells, 10 x 10 mm quartz glass cuvettes from Hellma Analytics were used for all assays. Human α -TTP was expressed and purified as described previously (Zhang).²⁰⁷ α -TTP stock solution concentrations were measured via Bradford assay. Fluorescence binding assays were performed essentially as previously described. (Nava²⁰¹, West²⁰⁶) The ligand **2** was added from stock solutions in EtOH, DMF or dioxane, to 3.0 mL of a 0.2-0.5 μ M solution of α -TTP in TKE buffer (50 mM Tris-HCl, 100 mM KCl, 1 mM EDTA, pH 7.4). The total amount of added organic solvent was not allowed to exceed 1% of the total volume. After each addition of ligand, fluorescence intensity was monitored for 10-15 min to assure equilibrium had been reached and a maximum signal obtained. The excitation wavelength was 564 nm (slightly less than the absorption maximum) and emission was recorded at 584 nm.

For competitive binding assays α -TTP (0.2 μ M in TKE buffer) was pre-incubated with 0.4 μ M **2** for 1 hr. To this complex was added increments of stock solutions of α -tocopherol or cholesterol, the mixture allowed to reach equilibrium for 15 minutes, and the fluorescence intensity recorded.

13.3 Cyclic voltammetry

Cyclic voltammetry experiments were conducted on a Bioanalytical System Inc. (BAS) Epsilon electrochemical workstation. Compounds were dissolved in dry DCM (2.5 mM) and purged for 5-10min with N₂. Tetrabutylammonium hexafluorophosphate (*n*-Bu₄NPF₆, 80 mM) was used as the electrolyte and a silver wire as a reference electrode. Samples were run at 200 mV/s.

13.4 AMVN lipid peroxidation

Lipid samples were prepared containing 10.7 mM soyPC, 2.53 mM AMVN, and 45.0 μ M of either α -Toc or HM-Toc. A fourth sample was prepared that contained only soyPC and was used as a blank. All necessary reagents were combined in chloroform solution then evaporated under high vacuum for one hour and re-suspended in 2.0 mL of 25 mM Tris (pH 7). Samples were vortexed for 1 min yielding cloudy suspensions of multilamellar liposomes. Reaction vials were incubated at 60°C exposed to air in a water bath. 50 μ L aliquots were taken approximately every 20 minutes, diluted with 950 μ L of acetonitrile and the absorbance measured at 234 nm.

13.5 HM-Toc stability

HM-Toc (10 mg) was dissolved in EtOH, DMSO or Dioxane (2 ml). Solid K_2CO_3 (2 mg) was used to keep the solution basic. To acidify the solution 10 drops of aqueous HCl solution (1 M) were added. The mixtures were capped and stored in the dark. After the described times the solvents were evaporated with a N_2 stream (DMSO: high vacuum at 60°C), extracted with 1 M NaOH (0.5 ml) and 2x EtOAc. The organic layers were decanted and evaporated with an N_2 stream and analyzed by 1H -NMR with $CDCl_3$ as a solvent.

13.6 Cytotoxicity study

Materials and Methods:

Materials:

C2C12 mouse myoblasts, Dulbecco's Modified Eagle Medium (DMEM; with high glucose, L-glutamine, sodium pyruvate, and sodium bicarbonate), Eagle's minimum essential medium (MEM) non-essential amino acids solution, penicillin/streptomycin solution, fetal bovine serum (FBS), and thiazolyl blue tetrazolium bromide (MTT) were purchased from Sigma-Aldrich (St. Louis, MO). Mouse embryonic fibroblasts (MEFs) were purchased from ATCC (Manassas, VA). 96-well cell culture microplates (polystyrene, clear flat-bottom) were purchased from

Greiner Bio-One (Frickenhausen, Germany). 6-well cell culture plates were purchased from Sarstedt (Newton, SC). Dimethyl sulfoxide (DMSO) was purchased from Bio-Shop (Burlington, ON, Canada). Unless otherwise indicated, all other materials were purchased from Sigma-Aldrich (St. Louis, MO, USA), BioShop (Burlington, ON, Canada), or Fisher Scientific (Mississauga, ON, Canada).

Cell culture:

C2C12 mouse myoblasts and mouse embryonic fibroblasts (MEFs) were cultured in DMEM supplemented with 10% (v/v) FBS, 4500 mg/L glucose, 4 mM L-glutamine, 1 mM sodium pyruvate, 2% (v/v) MEM nonessential amino acid solution, and penicillin (50 I.U./mL) / streptomycin (50 µg/mL) solution (complete media). Cells were cultured in a humidified 5% CO₂ atmosphere within a Thermo Forma Series II water-jacketed CO₂ incubator maintained at 37°C. Cells were transferred to fresh 96- or 6-well plates (2,000 cells/well & 60,000 cells/well, respectively) in the evening prior to commencing tocopherol treatments.

Tocopherol stock solutions and cell treatments:

Each tocopherol was dissolved in sterile 100% DMSO to yield a 1 M stock solution. Less concentrated stock solutions were subsequently prepared using ten-fold serial dilutions. All tocopherol solutions were stored at -20°C. To treat cultured cells, media was replaced with complete media containing freshly-added tocopherol; the final amount of vehicle (DMSO) for all concentrations tested was 0.1% (v/v).

MTT tetrazolium reduction assay:

Media was discarded, wells were washed once with phenol red-free complete culture media, and 100 µL/well phenol red-free complete culture media containing 0.45 mg/mL MTT was added. Two hours later, solubilization solution [40% (v/v) dimethylformamide, 2% (v/v) glacial acetic acid, 16% (w/v) sodium dodecyl sulfate, pH 4.7] was added (100 µL/well) and well contents were gently mixed by re-suspension to dissolve the formazan precipitate. Plates were

incubated at room temperature in darkness for 2 h before recording absorbance at 570 nm using a Bio-Tek PowerWave Microplate UV-Vis spectrophotometer (Winooski, VT, USA). For each plate, background signal averaged from cell-free wells containing vehicle treatments was subtracted.

Trypan blue exclusion assay:

Media was discarded, wells were washed once with phosphate-buffered saline, and cells were harvested via trypsinization. After centrifugation (240 g, 3 min), cell pellets were re-suspended in complete culture media and subsequently diluted in 0.4% (w/v) Trypan Blue solution. Three minutes later, the numbers of viable (non-stained) cells were counted using a hemocytometer (Hausser Scientific, Horsham, PA) viewed under a Hund Wetzlar Wilovert Inverted Phase-Contrast light microscope (Fisher Scientific, Mississauga, ON, Canada).

Statistical Analyses:

Data sets were analyzed in GraphPad Prism 5 using one-way ANOVA and Tukey's post-hoc test, with a p-value of less than 0.05 considered significant.

13.7 Lipid-BODIPY extrusion

| | Molar Weight (g/mol) | Molar Ratio | Weight needed (mg) | Concentration of stock lipid (mg/mL) | Volume needed (μL) |
|-------------|----------------------|-------------|--------------------|--------------------------------------|--------------------|
| POPC | 760.076 | 7 | 5.80 | 10 | 580.2 |
| POPG | 770.989 | 3 | 2.52 | 10 | 252.2 |
| Cholesterol | 386.654 | 4 | 1.69 | 1 | 1686.6 |

Table 34. Contents for 10 mg/mL of 7:3:4-POPC:POPG:Cholesterol.

| | Molar Weight (g/mol) | Molar Ratio | Weight needed (mg) | Concentration of stock lipid (mg/mL) | Volume needed (μL) |
|------------------|----------------------|-------------|--------------------|--------------------------------------|--------------------|
| POPC | 760.076 | 7 | 1.15 | 10 | 115.2 |
| POPG | 770.989 | 3 | 0.50 | 10 | 50.1 |
| Cholesterol | 386.654 | 4 | 0.33 | 1 | 334.9 |
| BODIPY, 3 | 532.2169 | 0.1 | 0.011 | 8.898×10^{-3} (16.72 μM) | 1295.2 |

Table 35. Contents for 2 mg/mL of 7:3:4:0.1-POPC:POPG:Cholesterol:BODIPY.

Contents for the desired liposomes were mixed in a glass vial in a biosafety cabinet (BSC) according to Table 34 and 35. Solvents of the lipid composition (Ethanol and Chloroform) were evaporated by blowing nitrogen in the vials near a flame. The vials were placed under vacuum for 1.5 hours. In a BSC, 1000 μ L of 1X autoclaved phosphate buffered saline (1XPBS) at pH 7.4 was added to each vial. The vials containing the lipids and 1XPBS were vortexed to resuspend the lipids. Lipids were extruded with a 50 nm sterile extruder (already sterilized with ethylene oxide) in a BSC.

Extrusion apparatus (LiposoFast 9AVestin, Ottawa, ON) was set up as follows:

- The needles were attached to their syringes. The 50nm filter along with the filter support and the scaffolds were already packaged in a plastic extrusion casing.
- A syringe was attached to one side of the extrusion casing. The other syringe was filled with approximately 0.5 mL of the lipids and then attached to the other side of the casing. The lipids in the syringe were passed through the filter to the other syringe 20 times. The lipids after extrusion were transferred to a fresh vial. The extruded lipids were stored in 4°C fridge overnight.

13.8 Imaging of cellular uptake of thienyl-ene-BODIPY liposomes

Fluorescent imaging was conducted on a Carl Zeiss Axio Observer.Z1 inverted light/epifluorescence microscope equipped with a Apotome.2 optical sectioning and a Hamamatsu Orca-Flash4.0 V2 digital camera. The excitation and emission wavelength were set for 587 / 610 nm with a X-Cite 120LED and image intensity was kept at 10%. Z-stack were taken at 0.32 μ m intervals and stacked into a 2D image using the “extended depth of focus” processing tool. A Zen 2 pro microscopy software was used.

14 Synthetic procedures and NMR & MS

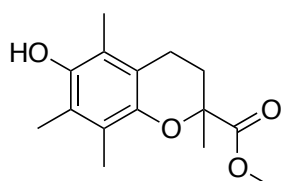
All experiments (^1H , ^{11}B , ^{13}C , ^{19}F , ^{31}P) were performed on either a Bruker Advanced DPX-300 MHz, 400 MHz or 600 MHz. Bruker TOPSPIN 3.5 PL2 (400 MHz) and Bruker TOPSPIN 2.1 PL6 software (300 MHz) were used to analysed FID data. Deuterated chloroform (CDCl_3) was used as the standard solvent if not otherwise noted. All deuterated solvents were purchased by Cambridge Isotopes Laboratories[®]. Internal standards were tetramethylsilane for ^1H -NMR and trichlorofluoromethane (CFCl_3) for ^{19}F -NMR used. Chemical shifts were reported as δ values and coupling constants as J -values and reported in Hertz (Hz). Following abbreviations were used for splitting patterns: s = singlet, d = doublet, dd = doublet of doublet, dt = doublet of triplet, t = triplet, q = quartet, p = pentet, sep = septet m = multiplet, br = broad, $enant$ = enantiotopic.

Electron impact (EI) and fast atomic bombardment (FAB) mass spectras were recorded on a ThermoFisher high resolution double focusing magnetic sector mass spectrometer system, electrospray ionization (ES) on a Bruker HCT Plus Proteineer LC-MS. High performance liquid chromatography (HPLC) analysis was conducted on an Agilent 1100 with autosampler and diode array detector, ODS-2 spherisorb column and XBD-Phenyl column were used.

Powder X-ray diffraction (pXRD) measurements of TiO_2 samples was conducted on a Rigaku SmartLab X-ray diffraction system (XRD).

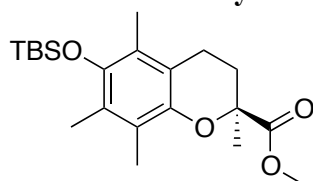
14.1 Fluorescent Tocopherol

Methyl 6-hydroxy-2,5,7,8-tetramethylchroman-2-carboxylate (4) was synthesized following Hilderling's procedure.²³⁴



| | |
|---------------------|---|
| $^1\text{H-NMR}$ | (400MHz, CDCl_3) δ 3.68 (<i>s</i> , 3H, OMe), δ 2.58 (<i>m</i> , 2H, ArCH_2CH_2), δ 2.43 (<i>m</i> , 1H (ArCH_2CH_2)) δ 2.16 (<i>s</i> , 3H, ArCH_3), δ 2.12 (<i>s</i> , 3H, ArCH_3), δ 2.03 (<i>s</i> , 3H, ArCH_3), δ 1.90-1.80 (<i>m</i> , 1H, ArCH_2CH_2), δ 1.61 (<i>s</i> , 3H, 2- <i>R</i> - CH_3) |
| $^{13}\text{C-NMR}$ | (300MHz, CDCl_3) 174.5, 145.5, 121.2, 118.4, 116.9, 52.35, 30.61, 25.42, 20.95, 20.83, 12.20, 11.81, 12.24 |
| MS [EI+] | <i>m/z</i> 264 (M^+1 , 77%), 205 (100%), 164 (75%) |

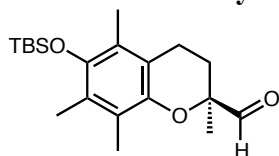
14.1.1 Synthesis of (*S*)-methyl 6-((*tert*-butyldimethylsilyl)oxy)-2,5,7,8-tetramethylchroman-2-carboxylate (**5**)



4 (3.7g, 0.014mol), *tert*-butyldimethylsilyl chloride (3.17g, 0.021mol) and imidazole (3.81g, 0.056mol) were stirred in DMF (40ml) at 85°C for 16h. The reaction was cooled to room temperature and most of the solvent evaporated. The residual mixture was resuspended in diethyl ether and washed 5x with ice-water. The organic phase was dried over Na_2SO_4 and evaporated down to dryness. Silica column chromatography (gradient Hex/ CH_2Cl_2 , 4:1 to 1:1 to CH_2Cl_2) afforded **5** (4.94g, 93.4%) as a clear oil.

| | |
|---------------------|---|
| TLC: | R_f = 0.75 (CH_2Cl_2) |
| $^1\text{H-NMR}$ | (400MHz, CDCl_3) δ 3.68 (<i>s</i> , 3H, OMe), δ 2.58 (<i>m</i> , 2H, ArCH_2CH_2), δ 2.43 (<i>m</i> , 1H (ArCH_2CH_2)) δ 2.16 (<i>s</i> , 3H, ArCH_3), δ 2.12 (<i>s</i> , 3H, ArCH_3), δ 2.03 (<i>s</i> , 3H, ArCH_3), δ 1.90-1.80 (<i>m</i> , 1H, ArCH_2CH_2), δ 1.61 (<i>s</i> , 3H, 2- <i>R</i> - CH_3), δ 1.06 (<i>s</i> , 9H, Si- <i>t</i> Bu), δ 0.137 (<i>s</i> , 6H, 2 x Si- CH_3) |
| $^{13}\text{C-NMR}$ | (400MHz, CDCl_3) 174.6, 144.0, 122.7, 124.1, 123.0, 117.9, 52.27, 30.56, 26.09, 25.38, 21.05, 18.62, 14.32, 13.86, 11.89, -3.30 |
| MS [EI+] | <i>m/z</i> 378 (M^+1 , 8.9%), 189 (25%), 147 (100%) |

14.1.2 Synthesis of (*S*)-6-((*tert*-butyldimethylsilyl)oxy)-2,5,7,8-tetramethylchroman-2-carbaldehyde (**6**)



5 (4.94g, 0.013mol) was dissolved in dry toluene (40ml) and cooled to -78°C under an N₂ atmosphere. A 1M solution of diisobutylaluminumhydride in toluene (DIBAL 1M Tol. 23.52ml, 0.0235mol) was added in 10min and stirred for 1.5h at -78°C. The reaction quenched with methanol (20ml), warmed to room temperature followed by slow addition of first water (70ml), then 2M HCl. The phases were stirred for 10min, then separated. The water phase was washed with diethyl ether 4x volume. The organic phases were dried over Na₂SO₄, combined and evaporated down to dryness. Silica column chromatography (gradient Hex/CH₂Cl₂, 1:1 to DCM) afforded **6** (3.95g, 86.8%) as a clear oil.

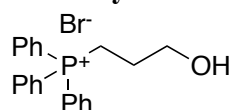
TLC: R_f = 0.53 (Hex/EtOAc, 4:1)

¹H-NMR (400MHz, CDCl₃) δ 9.65 (*s*, 1H, CHO), δ 2.56 (*m*, 2H, ArCH₂CH₂), δ 2.30 (*m*, 1H (ArCH₂CH₂) δ 2.19 (*s*, 3H, ArCH₃), δ 2.14 (*s*, 3H, ArCH₃), δ 2.04 (*s*, 3H, ArCH₃), δ 1.80-1.89 (*m*, 1H, ArCH₂CH₂), δ 1.41 (*s*, 3H, 2-*R*-CH₃), δ 1.07 (*s*, 9H, Si-*t*Bu), δ 0.137 (*s*, 6H, 2 x Si-CH₃),

¹³C-NMR (400MHz, CDCl₃) 205.2, 146.0, 145.6, 126.9, 124.3, 123.2, 118.0, 80.67, 28.34, 26.49, 22.00, 20.90, 19.01, 14.76, 13.78, 12.47, -2.92

MS [EI+] m/z 348 (100%), 319 (56%), 293 (12%), 221 (29%)

14.1.3 Synthesis of (3-hydroxypropyl)triphenylphosphonium bromide (**7**)



3-Bromopropanol (3.2g, 0.023mol) and triphenylphosphine (4.01g, 0.0153mol) were stirred in toluene (15ml) at 110°C under a nitrogen atmosphere for 16h. The reaction was cooled to room temperature and the white precipitate was filtrated and washed with cold toluene. The solid was dried, which yielded compound **7** (5.89g, 64.1%) as a white solid.

Mp: 226-228°C

TLC: R_f = 0.16 (Hex/DCM, 3:1)

¹H-NMR (300MHz, CDCl₃) δ 7.85-7.71 (*m*, 15H, P⁺-Ph), δ 4.97 (*brs*, 1H, P⁺CH₂CH₂CH₂-OH), δ 3.89 (*m*, 4H, R- P⁺CH₂CH₂CH₂OH), δ 1.86 (*dd*, 2H, P⁺CH₂CH₂CH₂-OH)

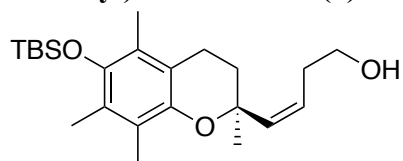
¹³C-NMR (400MHz, CDCl₃) 135.1, 133.6, 133.5, 130.6, 130.5, 60.41, 25.90, 20.56

³²P-NMR (400MHz, CDCl₃) 24.54

MS [EI+] m/z 321.2 (M⁺H, 100%), 385.1 (4%)

MS Calculated for C₂₄H₃₈O₃Si 320.259

14.1.4 Synthesis of (*S,Z*)-4-(6-((*tert*-butyldimethylsilyl)oxy)-2,5,7,8-tetramethylchroman-2-yl)but-3-en-1-ol (**8**)



To a suspension of **7** (576mg, 1.436mmol) in dry THF (30ml) was added dropwise LiHMDS 0.8M sol. in dry THF (7.58ml, 4.31mmol) at room temperature under a nitrogen atmosphere. After 1.5h, a solution of **6** (500mg, 1.436mmol) in dry THF (2ml) was added dropwise and stirred for 3h. The solvent was evaporated until only small quantities of THF were left. The residual mixture was then quenched with a 1:1 NH₄Cl : H₂O (20ml) solution and stirred with EtOAc for 5min. The phases were separated, the water phase washed 2x with EtOAc. The combined organic phases were dried over Na₂SO₄ and evaporated down to dryness. Silica column chromatography (gradient Hex/CH₂Cl₂, 4:1 to 1:1 to 2:3) afforded **8** (426mg, 76%) as a clear oil.

TLC: R_f = 0.2 (Hex/DCM, 2:3)

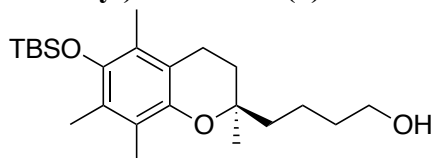
¹H-NMR (300MHz, CDCl₃) 5.63 (*d*, *J* = 15.60 Hz, 1H, -RCH=CHCH₂), 5.50 (*q*, *J* = 15.60 Hz, *J* = 6.90 Hz, 1H, -RCH=CHCH₂), 3.55 (*m*, *J* = 6.00 Hz, 2H, -RCH₂CH₂OH), δ 2.62 -2.42 (*m*, 2H, Ar-CH₂-CH₂), δ 2.50 (*q*, *J* = 6.30 Hz, 2H, RCH=CHCH₂), δ 2.14 (*s*, 3H, ArCH₃), δ 2.05 (*s*, 3H, ArCH₃), δ 2.07 (*s*, 3H, ArCH₃), δ 2.03-1.76 (*m*, 2H, ArCH₂CH₂), δ 1.40 (*s*, 3H, 2'*R*-CH₃), δ 1.06 (*s*, 9H, Si-*t*Bu), δ 0.130 (*s*, 6H, Si-CH₃)

¹³C-NMR (300MHz, CDCl₃) 137.4, 125.9, 124.8 123.6, 122.3, 117.9, 117.1, 74.79, 62.51, 61.78, 60.39, 35.63, 32.30, 27.27, 26.10, 21.19, 18.60, 14.34, 13.39, 11.99, -3.40

MS [EI+] *m/z* 390 (M⁺, 100%), 278 (60%), 221 (24%), 73 (52%)

MS Calculated for C₂₄H₃₈O₃Si 390.259

14.1.5 Synthesis of (*R*)-4-(6-((*tert*-butyldimethylsilyl)oxy)-2,5,7,8-tetramethylchroman-2-yl)butan-1-ol (**9**)



The ethyl acetate used in the reaction was dried prior to the reaction by stirring 25ml in Na₂SO₄ for 3h under an N₂ atmosphere.

To **8** (550mg, 1.409mmol) was Pd/C 10% (147mg) added and dried EtOAc (25ml). The system was purged 3x with H₂ gas and stirred overnight with an H₂ balloon. The reaction mixture was filtrated over purified celite, washed with EtOAc and evaporated down to dryness that afforded pure product **9** (530mg, 96.4%) as a clear oil.

TLC: R_f = 0.23 (DCM)

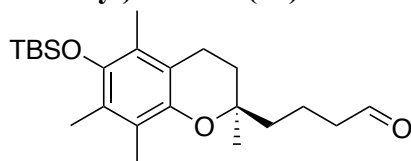
¹H-NMR (300MHz, CDCl₃) δ 2.57 (*t*, J = 6.90 Hz, 2H, ArCH₂), δ 2.11 (*s*, 3H, ArCH₃), δ 2.09 (*s*, 3H, ArCH₃), δ 2.07 (*s*, 3H, ArCH₃), δ 1.78 (*sex*, J = 6.90 Hz, 2H, ArCH₂CH₂), δ 1.69-1.52 (*m*, 8H, 2'*R*-CH₂CH₂CH₂CH₂OH), δ 1.06 (*s*, 9H, Si-*t*Bu), δ 0.145 (*s*, 3H, Si-CH₃)

¹³C-NMR (400MHz, CDCl₃) 145.8, 144.1, 125.9, 123.6, 122.1, 117.4, 74.32, 62.51, 39.33, 33.20, 31.57, 26.10, 23.73, 20.87, 19.86, 18.60, 14.32, 13.39, 11.85, -3.34

MS [EI+] m/z 392 (M⁺, 100%), 279 (43%), 73 (61%)

MS Calculated for C₂₃H₄₀O₃Si 392.275

14.1.6 Synthesis of (*R*)-4-(6-((*tert*-butyldimethylsilyl)oxy)-2,5,7,8-tetramethylchroman-2-yl)butanal (**10**)



To a suspension of Dess Martin periodinate (110.8mg, 0.2614mmol) in dry CH₂Cl₂ (1ml) was added a solution of **9** (60mg, 0.1538mol) in CH₂Cl₂ (1ml) and the solution stirred for 16h at room temperature. The reaction was diluted with CH₂Cl₂ and quenched with 1M NaOH. After extraction the water phase was washed an additional two times with CH₂Cl₂, dried over Na₂SO₄ and evaporated down to dryness. Silica column chromatography (gradient Hex/CH₂Cl₂, 3:1 to 1:1 to 1:3) afforded **10** (40mg 67.0%) as a clear oil.

TLC: R_f = 0.73 (Hex/CH₂Cl₂, 3:1)

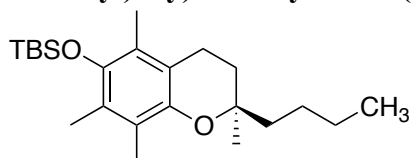
¹H-NMR (300MHz, CDCl₃) 9.79 (*t*, J = 1.80 Hz, 1H, CHO), δ 2.59 (*t*, J = 6.90 Hz, 2H, Ar-CH₂-CH₂), δ 2.59 (*tt*, J = 9.60 Hz, J = 1.50 Hz, 2H, CHO-CH₂), δ 2.12 (*s*, 3H, ArCH₃), δ 2.09 (*s*, 3H, ArCH₃), δ 2.07 (*s*, 3H, ArCH₃), δ 1.80 (*m*, 4H, ArCH₂CH₂ + CH₂CH₂CHO), δ 1.62 (*m*, 2H, CH₂CH₂CH₂CHO), δ 1.27 (*s*, 3H, 2'*R*-CH₃), δ 1.07 (*s*, 9H, Si-*t*Bu), δ 0.140 (*s*, 3H, Si-CH₃)

¹³C-NMR (300MHz, CDCl₃) 202.6, 145.6, 144.2, 126.0, 123.6, 122.7, 117.3, 74.10, 44.12, 38.96, 31.59, 26.10, 23.64, 20.79, 18.60, 16.37, 14.32, 13.40, 11.98, -3.33

MS [EI+] m/z 390 (M^+ , 100%), 279 (35%), 73 (49%)

MS Calculated for $C_{24}H_{38}O_3Si$ 390.259

14.1.7 Byproduct (*R*)-*tert*-butyl((2-butyl-2,5,7,8-tetramethylchroman-6-yl)oxy)dimethylsilane (9.2)



TLC: R_f = 0.79 (Hex/ CH_2Cl_2 , 3:1)

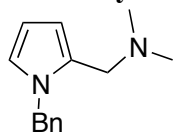
1H -NMR (300MHz, $CDCl_3$) δ 2.58 (*t*, J = 6.90 Hz, 2H, Ar- CH_2 - CH_2), δ 2.13 (*s*, 3H, Ar CH_3), δ 2.11 (*s*, 3H, Ar CH_3), δ 2.09 (*s*, 3H, Ar CH_3), δ 1.8 (*sex*, 2H, $CH_2CH_2CH_2CH_3$), δ 1.69-1.25 (*m*, 6H, Ar CH_2CH_2 + $CH_2CH_2CH_2CH_3$ + Ar- CH_2 - CH_2), δ 1.26 (*s*, 3H, 2'*R*- CH_3), δ 1.3 (*t*, J = 7.20 Hz, 2H, $CH_2CH_2CH_2CH_3$), δ 1.07 (*s*, 9H, Si-*t*Bu), δ 0.140 (*s*, 3H, Si- CH_3)

^{13}C -NMR (400MHz, $CDCl_3$) 145.9, 144.1, 125.8, 123.5, 122.7, 117.5, 74.47, 39.36, 31.54, 26.12, 25.91, 23.82, 23.27, 20.91, 18.62, 14.33, 14.15, 13.41, 11.94, -3.34

MS [ESI+] m/z 377.3 (M^+ , 100%)

MS Calculated for $C_{23}H_{40}BrO_2Si$ 376.280

14.1.8 Synthesis of 1-(1-benzyl-1*H*-pyrrol-2-yl)-*N,N*-dimethylmethanamine (11x)



To a solution of formalin 37% (0.368ml, 5.01mmol) and dimethylamine HCl (408mg, 5.01mmol) was added *N*-benzylpyrrole (788mg, 5.01mmol) dissolved in CH_2Cl_2 (2ml) and stirred for 4h at room temperature. The reaction was quenched with a NaOH solution (1g in 10ml H_2O), which was extracted 3x with ether. The combined organic phases were dried over Na_2SO_4 and evaporated down to dryness. Silica column chromatography (Hex/EE, 6:1) afforded **11x** (200mg 18.7%) as a light yellow oil.

TLC: R_f = 0.16 (Hex/EtOAc, 6:1)

1H -NMR (300MHz, $CDCl_3$) 7.42-7.32 (*m*, 3H, Bn-), 7.15-7.12 (*d*, J = 7.50 Hz, 2H, Bn-), 6.74 (*d*, J = 2.10 Hz, 1H, pyrrole-H), δ 6.20 (*t*, J = 3.0 Hz, 1H, pyrrole-H), δ 6.15

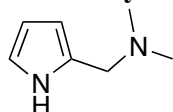
(*d*, *J* = 3.0 Hz, 1H, pyrrole-H), δ 5.32 (*s*, 2H, Bn-CH₂), δ 3.33 (*s*, 2H, Ar-pyrrole-CH₂), δ 2.27 (*s*, 6H, 2x-N-CH₃)

¹³C-NMR (300MHz, CDCl₃) 139.0, 128.7, 127.6, 127.2, 127.0, 126.7, 122.2, 121.2, 109.6, 106.8, 55.72, 50.34, 45.12

MS [ESI+] *m/z* 215.1 (M⁺, 9%), 170.1 (M+ -(CH₃)₂N, 61%)

MS Calculated for C₁₄H₁₈N₂ 214.147

14.1.9 Synthesis of *N,N*-dimethyl-1-(1*H*-pyrrol-2-yl)methanamine (10x)



A solution of formalin 37% (2.54g, 0.313mol) and dimethylamine HCl (2.54g, 0.313mol) was added over 10min. to pyrrole (2g, 0.0298mol) at room temperature. The reaction solution was stirred for 16h, quenched with 25% NaOH (10ml) and extracted 3x with ether (10ml). The organic phases were washed with brine, dried over Na₂SO₄ and evaporated down to dryness. Two fractions were collected by high vacuum distillation at 50°C as a yellow liquid, both being pure product **10x** (1.6g + 1.1g = 2.7g, 71.2%)⁶³⁴

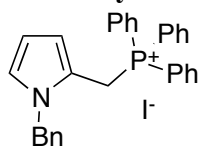
¹H-NMR (300MHz, CDCl₃) 9.08 (*brs*, 1H, pyrrole-NH), 6.74 (*q*, *J* = 3.00 Hz, *J* = 1.50 Hz, 1H, pyrrole-H), 6.12 (*q*, *J* = 3.00 Hz, 1H, pyrrole-H), 6.04 (*s*, 1H, pyrrole-H), δ 3.45 (*s*, 2H, Ar-pyrrole-CH₂), δ 2.25 (*s*, 6H, 2x-N-CH₃)

¹³C-NMR (300MHz, CDCl₃) 129.2, 117.6, 107.7, 107.4, 56.63, 45.10

MS [ESI+] *m/z* 125.1 (M⁺1, 100%), 80.2 (M+ -(CH₃)₂N, 34%)

MS Calculated for C₇H₁₂N₂ 124.100

14.1.10 Synthesis of *N,N*-dimethyl-1-(1*H*-pyrrol-2-yl)methanamine (11)



At 5°C, methyl iodide (181mg, 1.277mmol) was added to a clear solution of **11x** (111mg, 0.51mmol) in ether : methanol (8ml) at room temperature under N₂ atmosphere and stirred for 1.5h. A white solid formed and the solvent was evaporated. Triphenylphosphine (362mg, 1.38mmol) was added with benzene : methanol (6ml) and stirred at 50°C over night under N₂ atmosphere. The reaction was cooled to room temperature, ether added and sonicated. The

precipitate was filtrated and washed with ether to afford **11** (62mg, 21.7%) as a light yellow solid.

TLC: $R_f = 0.1$ (EtOAc)

$^1\text{H-NMR}$ (400MHz, CDCl_3) 7.87-7.45 (*m*, 20H, Bn-), 7.20 (*d*, $J = 1.60$ Hz, 1H, pyrrole-H), 6.97 (*d*, $J = 1.60$ Hz, 1H, pyrrole-H), δ 6.15 (*d*, $J = 3.0$ Hz, 1H, pyrrole-H), δ 4.98 (*s*, 1H, Bn- CH_2), δ 4.95 (*s*, 1H, Bn- CH_2), δ 4.77 (*s*, 2H, Ar-pyrrole- CH_2)

$^{13}\text{C-NMR}$ (400MHz, CDCl_3) 138.0, 135.5, 134.3, 134.2, 130.7, 130.5, 119.4, 119.2, 118.1, 116.1, 115.9, 110.0, 109.9, 109.3, 54.87, 50.39

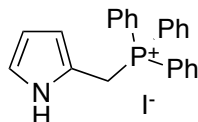
$^{31}\text{P-NMR}$ (400MHz, CDCl_3) 20.22

MS [ESI+] m/z 432.1 ($\text{M}^+ - \text{I}^-$, 100%), 170.0 (10%)

MS [ESI-] m/z 126.8 (I^- , 100%),

MS Calculated for $\text{C}_{30}\text{H}_{27}\text{IPN}$ 559.093

14.1.11 Synthesis of ((1*H*-pyrrol-2-yl)methyl)triphenylphosphonium iodide (**10**)



Methyl iodide (4.47g, 0.0315mol) and **10x** (1.6g, 0.0126mol) were stirred for 1h in ether / methanol 1:1 (25ml). A white solid instantly formed. After 1.5h, the solvents were evaporated and to the orange residue was added triphenylphosphine (4.96g, 0.0189mol) and stirred in benzene / methanol 1:1 (30ml) for 5h. The solvent was evaporated and the brownish suspension was filtered and washed with cold benzene / methanol 1:1 that afforded **10** (3.81g, 64%).

Mp: 214°C decomp.

TLC: $R_f = 0.1$ (CH_2Cl_2 :MeOH, 9:0.2)

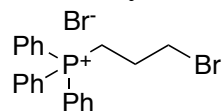
$^1\text{H-NMR}$ (300MHz, DMSO) 10.54 (*s*, 1H, pyrrole-NH), 7.94-7.89 (*t*, $J = 6.60$ Hz, $J = 1.50$ Hz, 3H, - PPh_3), 7.77-7.71 (*m*, $J = 7.50$ Hz, $J = 3.90$ Hz, $J = 1.20$ Hz, 6H, - PPh_3), 7.57-7.50 (*m*, $J = 3.90$ Hz, 6H, - PPh_3), 6.72 (*d*, $J = 1.50$ Hz, 1H, pyrrole-H), δ 6.72 (*t*, $J = 3.0$ Hz, 1H, pyrrole-H), δ 5.95 (*q*, $J = 2.7$ Hz, 1H, pyrrole-H), δ 5.52 (*s*, 1H, pyrrole-H), 3.33 (*d*, $J = 13.5$ Hz, 2H, Ar-pyrrole- CH_2),

$^{13}\text{C-NMR}$ (300MHz, DMSO) 135.5, 134.3, 134.2, 130.7, 130.5, 119.4, 119.2, 118.1, 116.1, 115.9, 110.0, 109.9, 109.3, 54.82, 50.31

MS [ESI+] m/z 342.1 ($\text{M}^+ - \text{I}^-$, 100%)

MS Calculated for $\text{C}_{23}\text{H}_{21}\text{IPN}$ 469.046

14.1.12 Synthesis of (3-bromopropyl)triphenylphosphonium bromide (**14**)



1,3-Bromopropane (5g / 2.5, 0.0248mol) and triphenylphosphine (6.5g, 0.0248mol) were stirred in toluene (12ml) at 110°C under a nitrogen atmosphere for 16h. The reaction was cooled to room temperature and the white precipitate was filtrated and washed with cold toluene. The solid was dried, and yielded compound **14** (7.61g, 66.5%) as a white solid.

Mp: 226-228°C

TLC: $R_f = 0.0$ (Hex/EtOAc, 9:1)

$^1\text{H-NMR}$ (300MHz, CDCl_3) δ 7.90-7.70 (*m*, 15H, $\text{P}^+\text{-Ph}$), δ 4.15 (*m*, 2H, $\text{P}^+\text{CH}_2\text{CH}_2\text{CH}_2\text{-OH}$), δ 3.88 (*dt*, $J = 6.40$ Hz, $J = 1.20$ Hz, 2H, R- $\text{P}^+\text{CH}_2\text{CH}_2\text{CH}_2\text{Br}$), δ 2.25 (*dq*, $J = 6.80$ Hz, $J = 1.20$ Hz, 2H, $\text{P}^+\text{CH}_2\text{CH}_2\text{CH}_2\text{-Br}$)

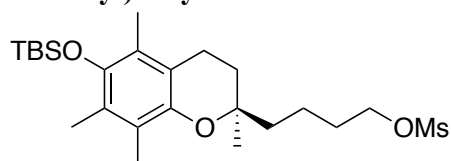
$^{13}\text{C-NMR}$ (400MHz, CDCl_3) 135.2, 135.2, 133.8, 133.7, 130.6, 130.5, 118.5, 117.6, 33.69, 33.48, 26.34, 21.90, 21.37

$^{31}\text{P-NMR}$ (400MHz, CDCl_3) 24.26

MS [EI+] m/z 383.0 (M^+H , 100%), 385.0 (98%)

MS Calculated for $\text{C}_{21}\text{H}_{21}\text{Br}_2\text{P}$ 461.975 / 383.056 (-Br)

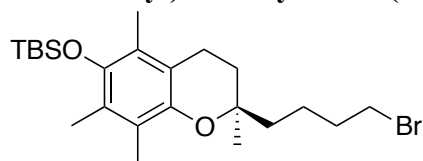
14.1.13 Synthesis of (*R*)-4-(6-((*tert*-butyldimethylsilyl)oxy)-2,5,7,8-tetramethylchroman-2-yl)butyl methanesulfonate (**9-OMs**)



Compound **9** (160mg, 0.408mmol) was dissolved in CH_2Cl_2 (2ml) and triethylamine (0.126ml, 0.901mmol) was added. The solution was cooled to 5°C and mesyl chloride (49.2 μl , 0.633mmol) was added slowly. After 1h, the reaction was quenched with ice. The layers were separated and the water phase was washed two times with CH_2Cl_2 . The organic layers were combined, dried over Na_2SO_4 and evaporated down to dryness to afford the mesylate **9-OMs** (180mg, 93.9%) as a yellow oil. The crude product was used without further purification.

TLC: $R_f = 0.78$ (CH_2Cl_2)

14.1.14 Synthesis of (*R*)-((2-(4-bromobutyl)-2,5,7,8-tetramethylchroman-6-yl)oxy)(*tert*-butyl)dimethylsilane (**16**)



9-OMs (180mg, 0.383mmol) was dissolved in THF (5ml) and lithium bromide (193mg, 2.23mmol) was added and stirred for 3h at reflux. The solvent was evaporated and the remaining was quenched with ice water. The reaction mixture was then extracted three times with CH₂Cl₂, dried over Na₂SO₄ and evaporated down to dryness. Silica column chromatography (Hex/CH₂Cl₂, 2:1) afforded **16** (100mg 57.4%) as a colourless oil.

TLC: R_f = 0.85 (Hex/CH₂Cl₂, 1:2)

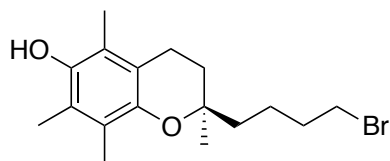
¹H-NMR (300MHz, CDCl₃) δ 3.43 (*t*, J = 6.90 Hz, 2H, CH₂Br), δ 2.58 (*t*, J = 6.90, Hz, 2H, ArCH₂CH₂), δ 2.12 (*s*, 3H, ArCH₃), δ 2.09 (*s*, 3H, ArCH₃), δ 2.07 (*s*, 3H, ArCH₃), δ 1.94-1.74 (*m(p)*, J = 6.90 Hz, 4H, ArCH₂CH₂ + CH₂CH₂Br) δ 1.65-1.56 (*m*, 4H, CH₂CH₂CH₂CH₂Br) δ 1.26 (*s*, 3H, 2'-R-CH₃), δ 1.06 (*s*, 9H, Si-*t*Bu), δ 0.136 (*s*, 6H, 2x Si-CH₃)

¹³C-NMR (300MHz, CDCl₃) 145.7, 144.2, 126.0, 123.6, 122.7, 117.4, 74.19, 38.54, 33.83, 33.13, 31.59, 26.10, 23.75, 22.65, 22.32, 20.84, 18.60, 14.32, 14.12, 13.40, 11.97, -3.34

MS [EI+] m/z 454 (M⁺, 39%), 279 (42%), 73 (100%)

MS Calculated for C₂₃H₃₉BrO₂Si 454.190

Byproduct (*R*)-2-(4-bromobutyl)-2,5,7,8-tetramethylchroman-6-ol



TLC: R_f = 0.52 (Hex/CH₂Cl₂, 1:2)

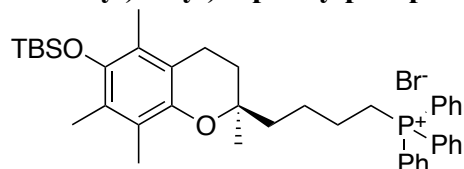
¹H-NMR (300MHz, CDCl₃) δ 4.15 (*brs*, 1H, ArOH), δ 3.44 (*t*, J = 6.90 Hz, 2H, CH₂Br), δ 2.63 (*t*, J = 6.90, Hz, 2H, ArCH₂CH₂), δ 2.18 (*s*, 3H, ArCH₃), δ 2.13 (*s*, 6H, ArCH₃), δ 1.93-1.76 (*m(p)*, J = 6.90 Hz, 4H, ArCH₂CH₂ + CH₂CH₂Br), δ 1.65-1.55 (*m*, 4H, CH₂CH₂CH₂CH₂Br), δ 1.26 (*s*, 3H, 2'-R-CH₃)

¹³C-NMR (300MHz, CDCl₃) 145.1, 144.7, 122.9, 121.3, 118.5, 117.0, 74.19, 39.01, 33.13, 31.59, 24.07, 22.65, 20.40, 14.32, 12.22, 11.80, 11.19

MS [EI+] m/z 340 (M⁺, 23%), 165 (100%)

MS Calculated for C₁₇H₂₅BrO₂ 340.104

14.1.15 Synthesis of (*R*)-(4-(6-((*tert*-butyldimethylsilyl)oxy)-2,5,7,8-tetramethylchroman-2-yl)butyl)triphenylphosphonium bromide (**18**)



Compound **16** (92mg, 0.203mmol) was dissolved with triphenylphosphine (53mg, 0.203mmol) in dry toluene (1ml). The mixture was heated for 20min at 180°C in a microwave oven. The solvent was evaporated and silica column chromatography (gradient CH₂Cl₂, 9:0.2 to CH₂Cl₂:MeOH) afforded **18** (135mg 34.4%) as a white wax.

TLC: R_f = 0.12 (CH₂Cl₂/MeOH, 9:0.2)

¹H-NMR (300MHz, CDCl₃) δ 7.90-7.67 (*m*, 15H, P⁺-Ph), δ 4.02 (*brs*, 1H, P⁺-CH₂CH₂CH₂CH₂), δ 3.81 (*brs*, 1H, P⁺-CH₂CH₂CH₂CH₂), δ 2.53 (*t*, J = 6.90, Hz, 2H, ArCH₂CH₂), δ 2.06 (*s*, 3H, ArCH₃), δ 2.05 (*s*, 3H, ArCH₃), δ 1.94 (*s*, 3H, ArCH₃), δ 1.80-1.59 (*m*, 8H, ArCH₂CH₂ + P⁺-CH₂CH₂CH₂CH₂), δ 1.22 (*s*, 3H, 2'-R-CH₃), δ 1.06 (*s*, 9H, Si-*t*Bu), δ 0.125 (*s*, 6H, 2x Si-CH₃)

¹³C-NMR (400MHz, CDCl₃) 144.1, 134.9, 133.8, 133.7, 130.5, 130.4, 125.7, 123.7, 122.4, 119.0, 118.1, 117.7, 74.43, 38.89, 31.46, 26.11, 24.61, 23.85, 23.18, 20.81, 18.60, 14.31, 13.43, 11.98, -3.30, -3.34

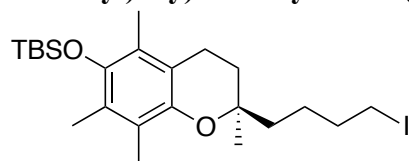
³¹P-NMR (400MHz, CDCl₃) 24.61

MS [ESI+] m/z 637.4 (M⁺, 100%), 539.3 (10%), 529.3 (M⁺, - TBS, 19%)

MS [ESI-] m/z 78.9/88.9 (Br⁻, 100%),

MS Calculated for C₄₁H₅₄BrO₂PSi 716.281

14.1.16 Synthesis of (*R*)-*tert*-butyl((2-(4-iodobutyl)-2,5,7,8-tetramethylchroman-6-yl)oxy)dimethylsilane (**17**)



Compound **9-OMs** (235mg, 0.500mmol) was dissolved in dry THF (3ml) and acetone (2ml) and potassium iodide (160mg, 1.06mmol) was added and stirred for 16h at reflux. The solvent was evaporated and silica column chromatography (gradient Hex/CH₂Cl₂, 4:1 to CH₂Cl₂) afforded **17** (135mg 53.7%) as a colourless oil.

TLC: R_f = 0.92 (CH₂Cl₂)

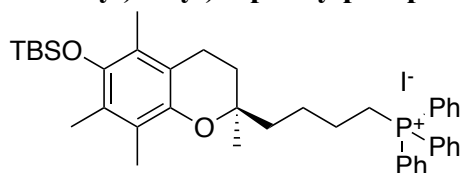
¹H-NMR (300MHz, CDCl₃) δ 3.21 (*t*, J = 7.2 Hz, 2H, CH₂I), δ 2.58 (*t*, J = 6.90, Hz, 2H, ArCH₂CH₂), δ 2.12 (*s*, 3H, ArCH₃), δ 2.09 (*s*, 3H, ArCH₃), δ 2.07 (*s*, 3H, ArCH₃), δ 1.89-1.73 (*m*(*p*), J = 6.90 Hz, 4H, ArCH₂CH₂ + CH₂CH₂I) δ 1.89-1.73 (*m*, 4H, CH₂CH₂CH₂CH₂I) δ 1.29 (*s*, 3H, 2'*R*-CH₃), δ 1.06 (*s*, 9H, Si-*t*Bu), δ 0.135 (*s*, 6H, 2x Si-CH₃)

¹³C-NMR (400MHz, CDCl₃) 145.8, 144.2, 125.9, 123.6, 122.7, 117.5, 74.34, 62.97, 39.34, 33.21, 31.58, 26.11, 23.74, 20.87, 19.88, 18.61, 14.33, 13.41, 11.97, -3.34

MS [EI⁺] m/z 502 (M⁺, 100%), 376 (M⁺ - I⁻, 72%), 362 (50%), 279 (69%), 221 (50%), 73 (100%)

MS Calculated for C₂₃H₃₉IO₂Si 502.176

14.1.17 Synthesis of (*R*)-(4-(6-((*tert*-butyldimethylsilyl)oxy)-2,5,7,8-tetramethylchroman-2-yl)butyl)triphenylphosphonium iodide (**19**)



Compound **17** (67mg, 0.133mmol) and triphenylphosphine (34.8mg, 0.133mmol) were dissolved in toluene (1ml). The mixture was reacted for 45min at 145°C in a microwave oven. The solvent was evaporated and silica column chromatography (gradient CH₂Cl₂, to CH₂Cl₂:MeOH 9:0.2) afforded **19** (135mg 43.3%) as a white oil.

TLC: R_f = 0.12 (CH₂Cl₂/MeOH, 9:0.2)

¹H-NMR (300MHz, CDCl₃) δ 7.82-7.43 (*m*, 15H, P⁺-Ph), δ 3.69-3.55 (*dm*, J = 42.6 Hz, 2H, P⁺-CH₂CH₂CH₂CH₂), δ 2.52 (*t*, J = 6.83 Hz, 2H, ArCH₂CH₂), δ 2.05 (*s*, 3H, ArCH₃), δ 2.03 (*s*, 3H, ArCH₃), δ 1.94 (*s*, 3H, ArCH₃), δ 1.80-1.62 (*m*, 6H, P⁺-CH₂CH₂CH₂CH₂ + ArCH₂CH₂), δ 1.62-1.52 (*m*, J = 7.60 Hz, 2H, P⁺-CH₂CH₂CH₂CH₂) δ 1.21 (*s*, 3H, 2'*R*-CH₃), δ 1.04 (*s*, 9H, Si-*t*Bu), δ 0.105 (*s*, 6H, 2x Si-CH₃)

¹³C-NMR (400MHz, CDCl₃) 145.7, 144.2, 133.0, 132.0, 132.0, 131.7, 131.7, 130.9, 130.8, 130.8, 130.8, 125.9, 123.6, 122.6, 117.4, 74.12, 38.98, 31.64, 30.13, 26.12, 25.10, 24.95, 23.75, 21.92, 20.82, 18.61, 14.33, 13.40, 11.97, -3.31, -3.33

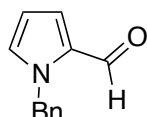
³¹P-NMR (400MHz, CDCl₃) 32.52

MS [ESI+] *m/z* 637.3 (M⁺, - I⁻, 65%), 523.3 (M⁺, -TBS 100%), 277.1 (18%)

MS [ESI-] *m/z* 126.9 (I⁻, 100%)

MS Calculated for C₄₁H₅₄IO₂PSi 764.268

Synthesis of 1-benzyl-1H-pyrrole-2-carbaldehyde⁶³⁵



To a suspension of sodium hydride 60% (1.00g, 0.01mol) in dry DMF (16ml) was added dropwise a solution of pyrrole-2-carboxaldehyde (1.00g, 0.01mol) in dry DMF (8ml) under N₂ atmosphere at 0°C. After 10min., benzyl bromide (1.5ml, 0.01mol) was added dropwise. After 30min. at room temperature. The solution was diluted with ethyl acetate and extracted four times with ice water, followed by one portion of brine. The reaction was dried over Na₂SO₄ and evaporated down to dryness. Silica column chromatography (gradient Hex/EtOAc, 9:1 to 1:1) afforded 1-benzyl-1H-pyrrole-2-carbaldehyde (0.42 g 87.4%) as a brown liquid.

TLC: *R_f* = 0.51 (Hex/EtOAc, 6:1)

¹H-NMR (400MHz, CDCl₃) 9.59 (*s*, 1H, CHO), 7.36-7.95 (*m*, 3H, Bn-), 7.18-7.16 (*m*, 2H, Bn-), δ 7.00 (*d*, *J* = 3.20 Hz, 2H, pyrrole-H), δ 6.29 (*t*, *J* = 3.20 Hz, 1H, pyrrole-H), δ 5.59 (*s*, 2H, Bn-CH₂)

¹³C-NMR (400MHz, CDCl₃) 179.5, 137.5, 131.4, 128.7, 127.7, 127.3, 124.9, 110.1, 51.97

MS [ESI+] *m/z* 186.1 (M⁺1, 100%), 208.1 (M+Na, 64%)

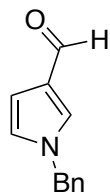
MS Calculated for C₁₂H₁₁NO 185.084

Alternative procedure⁶³⁶:

Oxalylchloride (0.6ml 6.99mol) was added under stirring at 0°C to dry DMF (0.539ml, 6.99mol) under N₂ atmosphere. A white precipitate formed and after 10min, dry CH₂Cl₂ (6ml) was added. A solution of N-benzylpyrrole (1.00g, 6.36mol) in CH₂Cl₂ (6ml) was added over 15min. The reaction was stirred for 30min. and the green solution was quenched with a NaOAc solution (2.6g in 20ml H₂O). After 30min. the green water phase was separated and washed 5x with ether. The separate organic phases (CH₂Cl₂ and ether) were each washed 3x with saturated sodium bicarbonate, followed by 3x with H₂O. The organic layers were combined and dried

over Na₂SO₄ and evaporated down to dryness. Silica column chromatography (Hex/EtOAc, 6:1) afforded 1-benzyl-1H-pyrrole-2-carbaldehyde (450mg 38.2%-45%) as a colourless oil.

Side product: 1-benzyl-1H-pyrrole-3-carbaldehyde (76mg, 6.4%)



TLC: R_f = 0.13 (Hex/EE, 6:1)

¹H-NMR (400MHz, CDCl₃) 9.76 (*s*, 1H, CHO), 7.42-7.33 (*m*, 3H, Bn-), δ 6.73 (*t*, *J* = 2.40 Hz, 1H, pyrrole-H), 7.20-7.18 (*m*, 2H, Bn-), δ 6.72 (*t*, *J* = 2.40 Hz, 1H, pyrrole-H), δ 6.68 (*dd*, *J* = 2.80 Hz, *J* = 1.60 Hz, 1H, pyrrole-H), δ 5.12 (*s*, 2H, Bn-CH₂)

¹³C-NMR (400MHz, CDCl₃) 185.4, 136.1, 129.2, 129.1, 128.4, 127.4, 126.9, 123.8, 108.7, 54.02

MS [EI⁺] *m/z* 185.02 (M, 51%), 91.01 (Bn⁺ 100%)

MS Calculated for C₁₂H₁₁NO 185.084

14.1.18 Synthesis of 4-(1-benzyl-1H-pyrrol-2-yl)but-3-en-1-ol (**20**)



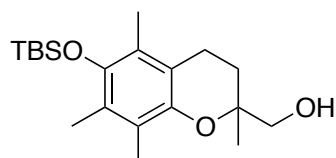
7 (583mg, 1.45mmol) was suspended in dry THF (7ml) under an nitrogen atmosphere at room temperature. A 0.8M solution of LiHMDS in THF (3.8ml, 3.8mmol) was added over 5min. The mixture was stirred for 3h at room temperature. A red solution formed, to which a solution of 1-benzyl-1H-pyrrole-2-carbaldehyde (269mg, 1.45mmol) in dry THF (3ml) was added over 5min at room temperature. The reaction solution was allowed to continue stirring for 4h. The reaction was quenched with an aqueous NH₄Cl solution (1:1), extracted with CH₂Cl₂. The organic phase was dried over Na₂SO₄ and evaporated down to dryness. Silica column chromatography (gradient, Hex:EtOAc 7:1 to 4:1 to 1:1 to EtOAc) afforded **20** (48mg 14.6%) as a colourless oil.

TLC: R_f = 0.17 (Hex/EtOAc, 3:1)

¹H-NMR (300MHz, CDCl₃) *trans* ~66% δ 7.37-7.27 (*m*, 6H, Bn- + pyrrole-H), δ 6.69 (*s*, 1H, pyrrole-H), δ 6.30 (*d*, *J* = 15.6 Hz, 1H, RCH=CHCH₂), δ 6.20 (*t*, *J* = 3.30 Hz, 1H, pyrrole-H), δ 5.95 (*dt*, *J* = 15.6 Hz, *J* = 4.20 Hz, 1H, RCH=CHCH₂), δ 5.15 (*s*, 2H, Bn-CH₂), δ 3.64 (*t*, *J* = 6.30 Hz, *J* = 5.40 Hz, 2H,

| | |
|---------------------|---|
| | RCH=CHCH ₂ CH ₂ OH), δ 2.37 (<i>dt</i> , J = 6.30 Hz, J = 5.40 Hz, 2H, RCH=CHCH ₂ CH ₂ OH) |
| | <i>cis</i> ~33% δ 7.37-7.27 (<i>m</i> , 5H, Bn-), δ 6.69 (<i>s</i> , 6H, Bn- + pyrrole-H), δ 6.40 (<i>dd</i> , J = 3.60 Hz, J = 1.20 Hz, 1H, pyrrole-H), δ 6.40 (<i>dd</i> , J = 3.60 Hz, J = 1.20 Hz, 1H, RCH=CHCH ₂), δ 6.20 (<i>t</i> , J = 3.30 Hz, 1H, pyrrole-H), δ 6.16 (<i>s</i> , J = 3.30 Hz, 1H, RCH=CHCH ₂), δ 5.35 (<i>d</i> , J = 15.90 Hz, 1H, Bn-CH ₂), δ 5.65 (<i>d</i> , J = 15.90 Hz, 1H, Bn-CH ₂), δ 3.86 (<i>m</i> , 2H, RCH=CHCH ₂ CH ₂ OH), δ 2.14 (<i>dt</i> , J = 6.90 Hz, 2H, RCH=CHCH ₂ CH ₂ OH) |
| ¹³ C-NMR | (300MHz, CDCl ₃) <i>trans</i> 138.3, 131.8, 128.7, 127.3, 126.3, 125.5, 122.0, 120.5, 108.3, 105.9, 62.43, 50.39, 36.62 <i>cis</i> 138.3, 132.0, 128.8, 127.5, 126.3, 124.6, 122.4, 121.8, 108.3, 106.2, 61.92, 50.39, 36.62 |
| MS [ESI+] | m/z 228.1 (M ⁺ 1, %), 266.1 (M+K, 33%), 244.1 (91%), 208.0 (39%), 186.1 (100%) MS Calculated for C ₁₅ H ₁₇ NO 227.131 |

Synthesis of (6-((*tert*-butyldimethylsilyl)oxy)-2,5,7,8-tetramethylchroman-2-yl)methanol, (22)⁶³⁷



To a solution of lithium aluminium hydride (124mg, 0.00326mol) in dry THF (17ml) was added a solution of **5** (1.23g, 0.00326mol) in dry THF (3ml) at 0°C under N₂ atmosphere. The reaction was stirred at room temperature for 16h, cooled back to 0°C, CH₂Cl₂ added followed by small portions of water (5x 10ml). The water phase was acidified with aqueous HCl solution, stirred for 5min followed by separation of the organic phase. The water phase was washed four times with CH₂Cl₂, the organic phases combined, dried over Na₂SO₄ and evaporated down to dryness which afforded product **22** (1.003g 87.4%) as a clear oil.

TLC: R_f = 0.25 (Hex/CH₂Cl₂ 3:1)

¹H-NMR (400MHz, CDCl₃) δ 3.64 (2x *d*, J = 19.6 Hz, 2H, CH₂OH), δ 2.63 (*t*, J = 7.6, Hz, 2H, ArCH₂), δ 2.13 (*s*, 3H, ArCH₃), δ 2.10 (*s*, 3H, ArCH₃), δ 2.09 (*s*, 3H, ArCH₃), δ 2.0 (*enant dt*, J = 5.6 Hz, 1H, ArCH₂CH₂), δ 1.74 (*enant dt*, J = 5.6

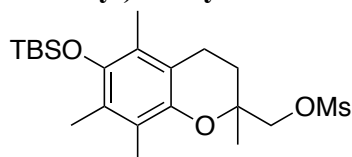
Hz, 1H, ArCH₂CH₂), δ 1.24 (*s*, 3H, 2'*R*-CH₃), δ 1.07 (*s*, 9H, Si-*t*Bu), δ 0.14 (*s*, 6H, 2x Si-CH₃)

¹³C-NMR (300MHz, CDCl₃) 145.3, 144.6, 126.1, 123.8, 122.6, 117.4, 75.05, 69.42, 29.72, 27.85, 26.20, 20.45, 20.39, 18.61, 14.33, 13.43, 12.02, -3.30, -3.35

MS [ESI+] *m/z* 353.3 (M⁺, 41%), 723.4 (2xM + Na 100%), 373.2 (M + Na 33%), 389.2 (M + K 28%)

MS Calculated for C₂₀H₃₄O₃Si 350.228

14.1.19 Synthesis of (6-((*tert*-butyldimethylsilyl)oxy)-2,5,7,8-tetramethylchroman-2-yl)methyl methanesulfonate (**22-OMs**)



To a solution of **22** (200mg, 0.571mmol) and triethylamine (159 μ l, 1.14mmol) in dry CH₂Cl₂ (2ml) was added mesyl chloride (53 μ l, 0.653mmol) at 0°C under a nitrogen atmosphere. The foggy yellow suspension was stirred for 30min., followed by extraction with water. The water phase was washed with CH₂Cl₂, the organic layers combined, dried over Na₂SO₄ and evaporated down to dryness. Silica column chromatography (Hex/CH₂Cl₂, 1:1) afforded **22-OMs** (178mg 72.8%) as a light brown powder.

TLC: R_f = 0.73 (CH₂Cl₂)

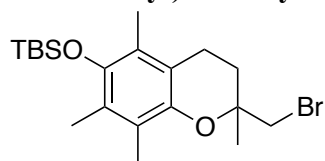
¹H-NMR (300MHz, CDCl₃) δ 4.28 (*d*, *J* = 10.2 Hz, 1H, MsCH₂) δ 4.15 (*d*, *J* = 10.2 Hz, 1H, MsCH₂), δ 3.04 (*s*, 3H, SO₂CH₃), δ 2.63 (*t*, *J* = 6.9, Hz, 2H, ArCH₂), δ 2.11 (*s*, 3H, ArCH₃), δ 2.08 (*s*, 6H, 2x ArCH₃), δ 2.02 (*dt*, *J* = 6.9 Hz, 1H, ArCH₂CH₂), δ 1.85 (*dt*, *J* = 6.9 Hz, 1H, ArCH₂CH₂), δ 1.34 (*s*, 3H, 2'*R*-CH₃), δ 1.07 (*s*, 9H, Si-*t*Bu), δ 0.14 (*s*, 6H, 2x Si-CH₃)

¹³C-NMR (300MHz, CDCl₃) 144.9, 126.5, 125.8, 125.2, 123.8, 122.7, 116.9, 73.86, 73.12, 37.40, 28.14, 26.08, 21.49, 20.12, 18.60, 14.32, 13.41, 12.01, -3.28, -3.36

MS [EI+] *m/z* 428 (M, 55%), 332 (M-OMs, 100%), 73 (55%)

MS Calculated for C₂₁H₃₆O₅SSi 428.205

14.1.20 Synthesis of ((2-(bromomethyl)-2,5,7,8-tetramethylchroman-6-yl)oxy)(*tert*-butyl)dimethylsilane (**23**)



To a solution of **22-OMs** (178mg, 0.416mmol) in DMF (2ml) was added lithium bromide (500mg, 5.76mol) and stirred at 70°C for 5 days. The reaction was cooled to room temperature, EtOAc added and extracted five times with water and once with 50% v/v sat. brine / water solution. The organic phase was dried over Na₂SO₄ and evaporated down to dryness. Silica column chromatography (Hex/EtOAc, 4:1 → 1:1) afforded **23** (98mg 72.8%) as a colourless oil.

TLC: R_f = 0.55 (CH₂Cl₂)

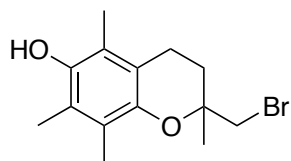
¹H-NMR (300MHz, CDCl₃) δ 3.47 (*d*, *J* = 10.5 Hz, 1H, CH₂Br), δ 3.42 (*d*, *J* = 10.5 Hz, 1H, CH₂Br), δ 2.59 (*t*, *J* = 6.6 Hz, 2H, ArCH₂), δ 2.15 (*dt*, *J* = 21.0 Hz, *J* = 7.5 Hz, 2H, Ar CH₂CH₂), δ 2.14 (*s*, 3H, ArCH₃), δ 2.10 (*s*, 3H, ArCH₃), δ 2.08 (*s*, 3H, ArCH₃), δ 1.88 (*dt*, *J* = 6.9 Hz, 1H, ArCH₂CH₂), δ 1.85 (*dt*, *J* = 21.0 Hz, *J* = 7.5 Hz, 2H, ArCH₂CH₂), δ 1.45 (*s*, 3H, 2'-R-CH₃), δ 1.06 (*s*, 9H, Si-*t*Bu), δ 0.14 (*s*, 6H, 2x Si-CH₃)

¹³C-NMR (300MHz, CDCl₃) 144.9, 126.5, 125.8, 123.8, 122.7, 116.9, 73.86, 73.12, 37.40, 28.14, 26.08, 20.12, 14.32, 13.41, 12.01, -3.28, -3.36

MS [EI⁺] *m/z* 412 (M⁺, 10%), 205 (20%), 137 (25%), 97 (39%), 57 (100%)

MS Calculated for C₂₀H₃₃BrO₂Si 412.143

Byproduct 2-(bromomethyl)-2,5,7,8-tetramethylchroman-6-ol (**24**)

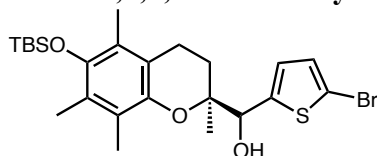


22 (410mg, 0.416mmol), tetrabromomethane (3.10g, 9.14mol), triphenylphosphine (1.50g, 5.72mol) were dissolved in toluene (15ml) and stirred at room temperature for 16h. The solvent was evaporated and extracted with EtOAc and water. The organic phase was dried over Na₂SO₄ and evaporated down to dryness. Silica column chromatography (Hex/EE, 2:1) afforded **24** (261mg 74.8%) as a colourless oil.

TLC: R_f = 0.70 (Hex/EtOAc, 2:1)

| | |
|---------------------|--|
| $^1\text{H-NMR}$ | (300MHz, CDCl_3) δ 3.44 (<i>dd</i> , $J = 10.5$ Hz, 2H, CH_2Br), δ 2.64 (<i>t</i> , $J = 3.6$ Hz, 2H, Ar $\text{CH}_2\text{CH}_2\text{CH}_2$), δ 2.18 (<i>s</i> , 3H, Ar CH_3), δ 2.14 (<i>s</i> , 6H, 2x Ar CH_3), δ 1.90 (<i>dt</i> , $J = 13.5$ Hz, $J = 7.5$ Hz, 1H, Ar CH_2CH_2), δ 1.45 (<i>s</i> , 3H, 2' <i>R</i> - CH_3) |
| $^{13}\text{C-NMR}$ | (300MHz, CDCl_3) 145.1, 144.7, 122.9, 121.3, 118.5, 117.0, 73.68, 39.01, 29.59, 24.07, 20.40, 12.22, 11.80, 11.29 |
| MS [EI+] | m/z 298 (M^+ , 100%), 165 (80%) MS Calculated for $\text{C}_{14}\text{H}_{19}\text{BrO}_5$ 298.057 |

14.1.21 Synthesis of (*R*)-(5-bromothiophen-2-yl)((*S*)-6-((*tert*-butyldimethylsilyl)oxy)-2,5,7,8-tetramethylchroman-2-yl)methanol (**25**)



2-Bromothiophene (3.09g, 0.019mol) was dissolved in dry THF (45ml) and cooled under a N_2 atmosphere to -78° . LDA (9.48ml, 2.0 M in THF) was added dropwise and stirred for 50 min. at -78°C . To the resulting red solution was added **6** (3.00g, 0.0086mol) in dry THF (10ml) slowly at the same temperature. After 1.5 h, the reaction was completed and a mixture of CH_2Cl_2 / H_2O (1:1, 100ml) was added and the mixture let warm to room temperature. The layers were separated and the aqueous layer washed with CH_2Cl_2 (3x 20 ml). The combined organic phases were dried over Na_2SO_4 and evaporated down to dryness. Silica column chromatography (Hex/ CH_2Cl_2 , 1:1) afforded **25** (3.84g 87.4%) as a light brown powder.

TLC: $R_f = 0.53$ (Hex/ CH_2Cl_2 , 1:4)

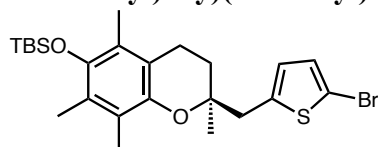
$^1\text{H-NMR}$ (300MHz, CDCl_3) diastereomers: major^a 75% / minor^b 25%; δ 6.93^b 6.92^a (*d*, $J = 3.78$ Hz, 1H, Ar-thiophene-H) δ 6.82^b 6.79^a (*d*, $J = 3.78$ Hz 1H, Ar-thiophene-H), δ 4.93^a 4.87^b (*d*, $J = 3.63$ Hz, 1H, thiophene-CH), δ 2.95^b 2.93^a (*d broad*, $J = 4.16$ Hz, 1H, OH), δ 2.59^{ab} (*m*, $J = 4.78$ Hz, 2H, Ar CH_3), δ (2.15) 2.12^{ab} (split *s*, 6H, Ar CH_3), δ 2.06^b 2.05^a (*s*, 3H, Ar CH_3), δ 1.95^{ab} δ 1.82^{ab} (*m*, 2H, Ar CH_2CH_2), δ 1.71^{ab} δ 1.65^{ab} (*m*, $J = 3.33$ Hz (^{1.71ab}), 2H, Ar CH_2CH_2), δ 1.23^a 1.19^b (*s*, 3H, (*S*)C- CH_3), δ 1.05 (*s*, 9H, Si-*t*Bu), δ 0.128 (*s*, 6H, 2x Si- CH_3),

$^{13}\text{C-NMR}$ (400MHz, CDCl_3) ^{ab} 144.9, 144.7, 144.5, 144.4, 141.4, 128.9, 126.4, 126.3, 126.2, 126.0, 123.8, 123.8, 122.8, 122.7, 117.4, 117.4, 112.1, 112.0, 77.27, 77.18, 76.50, 75.98, 34.67, 34.52, 31.59, 30.91, 27.94, 26.92, 26.19, 26.09, 25.29, 22.65, 20.71, 20.31, 20.24, 19.46, 18.60, 18.45, 14.35, 14.12, 13.42, 12.46, 12.27, -3.26, -3.34

MS [EI+] m/z 510 (M^+ , 7%), 348 (20%), 319 (100%), 73 (47%)

HRMS Calculated for $C_{24}H_{35}BrO_3SSi$ 510.1260; found: 510.1250

14.1.22 Synthesis of (*S*)-((2-((5-bromothiophen-2-yl)methyl)-2,5,7,8-tetramethylchroman-6-yl)oxy)(*tert*-butyl)dimethylsilane (**26**)



Thienyl alcohol **25** (2.37g, 0.0046mol) was dissolved in dry CH_2Cl_2 (80ml) and was cooled under an N_2 atmosphere to 0° . Triethylsilane (1.17ml, 0.0093mol) was added via syringe. $BF_3 \cdot OEt_2$ (1.17ml, 0.0093mol) was added drop wise and the solution was stirred for 1h at $0^\circ C$. The yellow solution was quenched with H_2O . The water phase was extracted three times with CH_2Cl_2 . The combined organic phases were dried over Na_2SO_4 and evaporated to dryness. SiO_2 column chromatography (Hex/ CH_2Cl_2 , 3:1) afforded **26** (1.983g 86.5%) as a light brown powder.

TLC: R_f = 0.79 (Hexane/ CH_2Cl_2 , 1:1) mp: $104^\circ C$ (after chromatography)

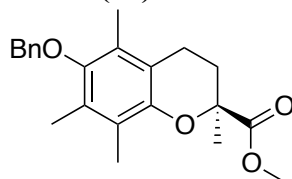
1H -NMR (300MHz, $CDCl_3$) 6.87 (*d*, J = 3.60 Hz, 1H, Ar-thiophene-H), δ 6.59 (*d*, J = 3.63 Hz, 1H, Ar-thiophene-H), δ 3.05 (*t*, J = 11.35 Hz, 2H, Ar CH_2), δ 2.60 (*t*, J = 6.83, Hz, 2H, Ar CH_2), δ 2.068 (*s*, 3H, Ar CH_3), δ 2.140 (*s*, 3H, Ar CH_3), δ 2.076 (*s*, 3H, Ar CH_3), δ 1.79 (*m*, J = 6.72 Hz, 2H, Ar CH_2CH_2), δ 1.249 (*s*, 3H, 2'*R*- CH_3), δ 1.071 (*s*, 9H, Si-*t*Bu), δ 0.144 (*s*, 6H, 2x Si- CH_3)

^{13}C -NMR (300MHz, $CDCl_3$) 145.4, 144.4, 141.1, 129.0, 127.3, 126.2, 123.5, 122.9, 116.9, 110.4, 73.97, 41.27, 30.70, 26.08, 23.52, 20.75, 18.58, 14.35, 13.39, 12.37, -3.30, -3.35

MS [EI+] m/z 494 (M^+ , 9%), 319 (100%), 147 (17%), 73 (18%)

HRMS Calculated for $C_{24}H_{35}BrO_2SSi$ 494.1310; found: 494.1315

14.1.23 Synthesis of (*S*)-methyl 6-(benzyloxy)-2,5,7,8-tetramethylchroman-2-carboxylate (**27**)



To a solution of *rac* **4** (940mg, 3.56mmol) in dry DMF (10ml) was added potassium carbonate (738mg, 5.34mmol) and the suspension stirred for 20min at $0^\circ C$. Benzyl bromide (0.5ml) was

added at 0°C and stirring continued for 16h at room temperature. The reaction was quenched with water and extracted with ethyl acetate. The organic phase was washed several time with ice water, dried with Na₂SO₄ and evaporated down to dryness. Silica column chromatography (gradient Hex/CH₂Cl₂, 2:1 to CH₂Cl₂) afforded **27** (1.26g 98.4%) as a white solid.

TLC: R_f = 0.57 (CH₂Cl₂)

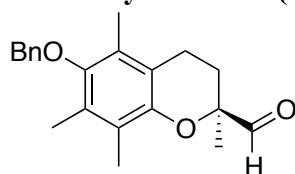
¹H-NMR (300MHz, CDCl₃) 7.53-7.36 (*m*, 5H, Bn-), δ 4.71 (*s*, 2H, Bn-CH₂), δ 3.71 (*s*, 3H, ArCH₂), δ 2.70-2.43 (*m*, 3H, ArCH₂ + ArCH₂CH₂), δ 2.25 (*s*, 3H, ArCH₃), δ 2.21 (*s*, 3H, ArCH₃), δ 2.15 (*s*, 3H, ArCH₃), δ 1.96-1.86 (*m*, 1H, ArCH₂CH₂), δ 1.64 (*s*, 3H, 2'*R*-CH₃),

¹³C-NMR (300MHz, CDCl₃) 174.4, 148.9, 147.8, 138.0, 128.5, 128.3, 127.8, 127.7, 125.7, 122.9, 117.2, 74.63, 52.35, 31.60, 30.47, 25.42, 22.66, 20.87, 14.13, 12.89, 11.97, 11.86

MS [EI+] *m/z* 354 (M⁺, 11%), 263 (100%), 231 (35%), 203 (33%), 105 (40%), 91 (61%)

MS Calculated for C₂₂H₂₆O₄ 354.183

14.1.24 Synthesis of (*S*)-6-(benzyloxy)-2,5,7,8-tetramethylchroman-2-carbaldehyde (**21**)



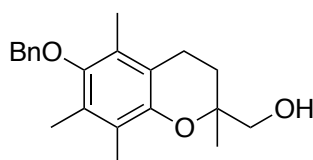
27 (1.38g, 3.89mol) was dissolved in dry toluene (10ml) and cooled to -78°C under an N₂ atmosphere. A 0.9M solution of diisobutylaluminiumhydride in toluene (DIBAL, 1M in toluene 7.8ml, 7.03mol) was added over 10min and stirred for 1.5h at -78°C. The reaction was quenched with methanol (5ml), warmed to room temperature followed by slow addition of first water (30ml), then 2M HCl. The phases were stirred for 10min, then separated. The water phase was washed with diethyl ether 4x. The organic phases were dried over Na₂SO₄, combined and evaporated down to dryness. Silica column chromatography (gradient Hex/CH₂Cl₂, 1:1 to DCM) afforded **21** (1.18g, 93.6%) as a clear oil.

TLC: R_f = 0.76 (CH₂Cl₂)

¹H-NMR (400MHz, CDCl₃) δ 9.66 (*d*, *J* = 1.20 Hz 1H, CHO), δ 7.53-7.51 (*m*, 2H, Bn-), δ 7.45-7.35 (*m*, 3H, Bn-), δ 4.71 (*s*, 2H, Bn-CH₂), δ 2.60 (*m*, 3H, ArCH₂CH₂), δ 2.30 (*m*, 1H, ArCH₂CH₂), δ 2.27 (*s*, 3H, ArCH₃), δ 2.23 (*s*, 3H, ArCH₃), δ 2.16 (*s*, 3H, ArCH₃), δ 1.85 (*m*, 1H, ArCH₂CH₂), δ 1.43 (*s*, 3H, 2'*R*-CH₃)

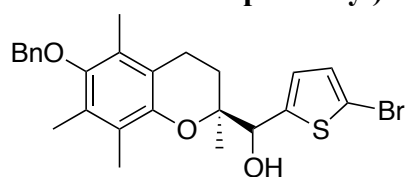
¹³C-NMR (300MHz, CDCl₃) 204.4, 149.2, 147.5, 137.8, 128.6, 128.5, 127.9, 127.7, 126.4, 123.2, 117.8, 80.46, 74.76, 27.76, 21.58, 20.30, 12.91, 11.99, 11.94,
 MS [EI+] *m/z* 325.2 (M⁺H, 41%), 379.2 (10%), 363.1 (36%), 347.2 (100%), 284.4 (7%)
 MS Calculated for C₂₁H₂₄O₃ 324.173

Byproduct (6-(benzyloxy)-2,5,7,8-tetramethylchroman-2-yl)methanol (21.2)



TLC: *R*_f = 0.3 (CH₂Cl₂)
¹H-NMR (400MHz, CDCl₃) δ 7.55-7.37 (*m*, 5H, Bn-), δ 4.73 (*s*, 2H, Bn-CH₂), δ 3.61 (*q*, *J*² = 18.6 Hz, 2H, CH₂-OH), δ 2.69 (*brt*, *J* = 8.7 Hz, 2H, ArCH₂), δ 2.26 (*s*, 3H, ArCH₃), δ 2.21 (*s*, 3H, ArCH₃), δ 2.138 (*s*, 3H, ArCH₃), δ 2.10-2.00 (*m*, 1H, ArCH₂CH₂), δ 1.81 (*m*, 1H, ArCH₂CH₂), δ 1.25 (*s*, 3H, 2'-R-CH₃)
¹³C-NMR (400MHz, CDCl₃) 148.6, 147.3, 137.9, 128.5, 128.3, 127.9, 127.7, 126.3, 122.9, 117.6, 75.37, 74.77, 69.42, 27.67, 20.54, 20.18, 12.88, 12.04, 11.92
 MS [EI+] *m/z* 326 (M⁺, 20%), 235 (100%), 205 (32%), 189 (18%), 165 (59%), 91 (52%)
 MS Calculated for C₂₁H₂₆O₃ 326.188

14.1.25 Synthesis of (*R*)-((*S*)-6-(benzyloxy)-2,5,7,8-tetramethylchroman-2-yl)(5-bromothiophen-2-yl)methanol (**28**)

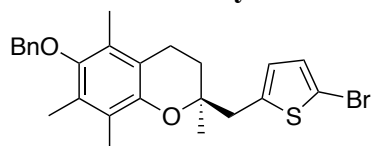


2-Bromothiophene (1.18g, 7.24mmol) was dissolved in dry THF (20ml) and was cooled under a N₂ atmosphere to -78°. LDA (3.62ml 2.0 M in THF, 7.24mmol) was added dropwise and stirred for 50 min. at -78°C. To the resulting red solution was added **21** (1.07g, 3.29mmol) in dry THF (3 ml) slowly at the same temperature. After 2.5h, the reaction was completed and a mixture of CH₂Cl₂ /H₂O (1:1, 100ml) was added and the mixture let warm to room temperature. The layers were separated and the aqueous layer washed with CH₂Cl₂ (3x 20ml). The combined organic phases were dried over Na₂SO₄ and evaporated down to dryness. Silica column chromatography (gradient Hex/CH₂Cl₂, 2:1 to CH₂Cl₂) afforded **28** (1.18g 73.8%) as a brown gum.

TLC: *R*_f = 0.54 (CH₂Cl₂)

| | |
|---------------------|---|
| ¹ H-NMR | (300MHz, CDCl ₃) diastereomers: major ^a 75% / minor ^b 25%; 7.57-7.39 (<i>m</i> , 5H, Bn-), δ 6.98 ^b 6.97 ^a (<i>d</i> , <i>J</i> = 3.90 Hz, 1H, Ar-thiophene-H) δ 6.87 ^b 6.83 ^a (<i>d</i> ^b , <i>J</i> = 3.90 Hz, <i>d</i> ^a , <i>J</i> = 3.90 Hz, 1H, Ar-thiophene-H), δ 4.97 ^a 4.92 ^b (<i>d</i> ^a , <i>J</i> = 3.90 Hz, <i>d</i> ^b , <i>J</i> = 3.90 Hz, 1H, thiophene-CH), δ 4.75 (<i>s</i> , 2H, Bn-CH ₂), δ 2.96 ^b 2.91 ^a (<i>d</i> ^b <i>J</i> = 4.20. Hz, <i>d</i> ^a <i>J</i> = 4.20. Hz, 1H, CH-OH), δ 2.69 ^{ab} (<i>m</i> , 2H, ArCH ₃), δ (2.15) 2.12 ^{ab} (split <i>s</i> , 6H, ArCH ₃), δ 2.06 ^b 2.05 ^a (<i>s</i> , 3H, ArCH ₃), δ 2.00 ^{ab} (<i>m</i> , 1H, ArCH ₂ CH ₂), δ 1.87 ^b δ 1.79 ^a (<i>m</i> , <i>J</i> = 3.33 Hz ^(1.71ab) , 1H, ArCH ₂ CH ₂), δ 1.31 ^a 1.27 ^b (<i>s</i> , 3H, (<i>S</i>)C-CH ₃) |
| ¹³ C-NMR | (400MHz, CDCl ₃) ^{ab} 148.9 ^b , 148.6 ^a , 147.4 ^a , 146.9 ^b , 144.34 ^a , 144.30 ^b , 141.0 ^a , 138.0 ^a , 137.9 ^b , 129.02 ^a , 128.99 ^b , 128.52 ^a , 128.50 ^a , 128.3 ^b , 127.9 ^b , 127.8 ^a , 127.7 ^a , 127.4 ^a , 126.33 ^b , 126.31 ^a , 126.11 ^b , 126.09 ^a , 123.2 ^a , 123.1 ^b , 117.6 ^b , 117.1 ^a , 112.3 ^b , 110.6 ^a , 74.77 ^b , 74.74 ^a , 74.31 ^a , 41.46 ^a , 30.45 ^a , 29.73 ^b , 27.79 ^b , 26.07 ^b , 23.66 ^a , 20.58 ^a , 20.06 ^b , 19.60 ^a , 18.54 ^b , 12.94 ^a , 12.39 ^b , 12.30 ^a , 12.18 ^b , 12.05 ^a |
| MS [EI+] | <i>m/z</i> 486 (M ⁺ , -%), 233 (73%), 205 (68%), 91 (100%) MS Calculated for C ₂₅ H ₂₇ BrO ₃ S 486.086 |

14.1.26 Synthesis of (*S*)-6-(benzyloxy)-2-((5-bromothiophen-2-yl)methyl)-2,5,7,8-tetramethylchroman (29)



Thienyl alcohol **28** (0.72g, 1.48mmol) was dissolved in dry CH₂Cl₂ (20ml) and was cooled under a N₂ atmosphere to 0°C. Triethylsilane (0.47ml, 2.94mmol) was added via syringe. BF₃·OEt₂ (0.37ml, 2.94mmol) was added drop wise and the solution was stirred for 1h at 0°C. The yellow solution was quenched with H₂O. The water phase was extracted three times with CH₂Cl₂. The combined organic phases were dried over Na₂SO₄ and evaporated to dryness. SiO₂ column chromatography (Hex/CH₂Cl₂, 1:1) afforded **29** (570mg 82.2%) as a light yellow oil.

TLC: *R*_f = 0.84 (CH₂Cl₂)

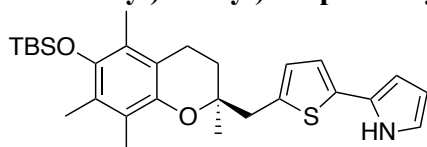
¹H-NMR (300MHz, CDCl₃) 7.58-7.34 (*m*, 5H, Bn-), 6.89 (*d*, *J* = 3.60 Hz, 1H, Ar-thiophene-H), δ 6.62 (*d*, *J* = 3.60 Hz, 1H, Ar-thiophene-H), δ 4.72 (*s*, 2H, Bn-CH₂), δ 3.09 (*s*, 2H, thiophene-CH₂), δ 2.66 (*t*, *J* = 6.83, Hz, 2H, ArCH₂), δ 2.07 (*s*, 3H, ArCH₃), δ 2.20 (*s*, 3H, ArCH₃), δ 2.19 (*s*, 3H, ArCH₃), δ 1.83 (*m*, 2H, ArCH₂CH₂), δ 1.27 (*s*, 3H, 2'-R-CH₃)

¹³C-NMR (300MHz, CDCl₃) 148.5, 141.0, 138.0, 129.0, 128.5, 128.3, 127.8, 127.7, 127.3, 126.1, 123.2, 117.1, 74.72, 74.29, 41.27, 30.43, 29.71, 23.63, 20.55, 12.91, 12.27, 12.02

MS [EI+] *m/z* 470 (M⁺, -%), 381 (6.7%), 301 (28%), 205 (100%)

MS Calculated for C₂₅H₂₇BrO₂S 470.082

14.1.27 Synthesis of (*S*)-2-(5-(((*tert*-butyldimethylsilyl)oxy)-2,5,7,8-tetramethylchroman-2-yl)methyl)thiophen-2-yl)-1*H*-pyrrole (**30**)



In a flame dried round bottom flask sodium hydride 60% in mineral oil (172mg, 4.30mmol) was washed with dry THF under N₂ atmosphere. The NaH was then suspended with dry THF (15ml) and after 5min, pyrrole (298μl, 4.30mmol) was added slowly at room temperature. After the bubbling stopped the yellow reaction was stirred for an additional 15min. Zinc chloride (586mg, 4.30mmol) was added to the light orange brown solution and after 5min palladium(II)acetate (26.8mg, 0.119mmol) followed by Johnphos[®] (35.6mg, 0.119mmol). **29** (1.18g, 2.39mmol) in dry THF (5ml) was added and stirred for 6h at 60°C under N₂. The reaction mixture was cooled to room temperature and extracted with CH₂Cl₂/ water. The water phase was washed 3x with CH₂Cl₂, the combined phases with washed with brine, dried over Na₂SO₄ and evaporated to dryness.

SiO₂ column chromatography (gradient, Hex/CH₂Cl₂ 4:1 to CH₂Cl₂) afforded a mix of **31** and some **30** (10mg 10.8%) as a light brown oil. The exact composition of **30/31** is unknown, but by NMR integration is a 50% ratio assumed.

TLC: *R*_f = 0.05-0.1 (Hex/CH₂Cl₂ 3:1)

¹H-NMR (400MHz, CDCl₃) δ 8.27 (*brs*, 1H, Ar-pyrrole-NH), δ 6.88 (*d*, *J* = 3.60 Hz, 1H, Ar-thiophene-H), δ 6.80 (*bs*, 1H, Ar-pyrrole-H), δ 6.76 (*d*, *J* = 3.60 Hz, 1H, Ar-thiophene-H), δ 6.37 (*bs*, 1H, Ar-pyrrole-H), δ 6.26 (*q*, *J* = 3.20 Hz, 1H, Ar-pyrrole-H), δ 3.10 (*dd*, *J*² = 21.60 Hz, 2H, thiophene-CH₂), δ 2.61 (*bm*, 2H, ArCH₂), δ 2.18 (*s*, 3H, ArCH₃), δ 2.14 (*s*, 3H, ArCH₃), δ 2.08 (*s*, 3H, ArCH₃), δ 1.82 (*m*, 2H, ArCH₂CH₂), δ 1.31 (*s*, 3H, 2'*R*-CH₃), δ 1.07 (*s*, 9H, Si-*t*Bu), δ 0.143 (*s*, 3H, Si-CH₃)

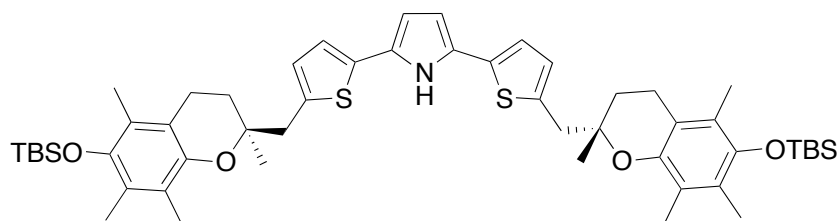
¹³C-NMR (400MHz, CDCl₃) 145.6, 144.4, 137.2, 136.9, 135.2, 127.8, 126.2, 123.6, 120.4, 118.2, 117.1, 109.9, 107.9, 106.3, 74.37, 40.73, 30.86, 26.17, 23.82, 23.79, 20.90, 19.00, 18.67, 14.44, 13.49, 12.44, -3.22, -3.27

MS [EI+] *m/z* 481 (M⁺, -%), 56 (100%)

[MALDI] (TOF, POS, RP 1000 no matrix) *m/z* 481.2 (M⁺, 12%), 319.1 (100%)

MS Calculated for C₂₈H₃₉NO₂SSi 481.247

Byproduct 2,5-bis(5-(((*S*)-6-((*tert*-butyldimethylsilyl)oxy)-2,5,7,8-tetramethylchroman-2-yl)methyl)thiophen-2-yl)-1*H*-pyrrole (31)



TLC: *R_f* = 0.05-0.1 (Hex/CH₂Cl₂ 3:1)

¹H-NMR (400MHz, CDCl₃) δ 8.19 (*brs*, 1H, Ar-pyrrole-NH), δ 6.92 (*d*, *J* = 3.20 Hz, 2H, Ar-thiophene-H), δ 6.77 (*d*, *J* = 3.20 Hz, 2H, Ar-thiophene-H), δ 6.37 (*bs*, 2H, Ar-pyrrole-H), δ 3.10 (*dd*, *J*² = 21.60 Hz, 2H, thiophene-CH₂), δ 2.61 (*bm*, 2H, ArCH₂), δ 2.18 (*s*, 3H, ArCH₃), δ 2.14 (*s*, 3H, ArCH₃), δ 2.08 (*s*, 3H, ArCH₃), δ 1.82 (*m*, 2H, ArCH₂CH₂), δ 1.31 (*s*, 3H, 2'*R*-CH₃), δ 1.07 (*s*, 9H, Si-*t*Bu), δ 0.143 (*s*, 3H, Si-CH₃)

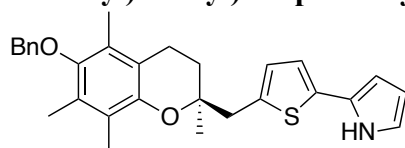
¹³C-NMR (400MHz, CDCl₃) 145.6, 144.44, 144.42, 137.2, 136.9, 135.2, 134.74, 127.75, 127.6, 127.5, 127.0, 126.19, 126.17, 123.6, 122.96, 122.94, 120.4, 120.2, 118.2, 117.1, 109.9, 107.9, 106.3, 74.37, 40.73, 30.86, 26.17, 23.82, 23.79, 20.90, 19.00, 18.67, 14.44, 13.49, 12.44, -3.22, -3.27

MS [EI+] *m/z* 481 (M⁺, -%), 56 (100%)

[MALDI] (TOF, POS, RP 1000 no matrix) *m/z* 895.2 (M⁺-H, 21%), 765.2 (M-TBSOH, 6%), 617.1 (M- H+rev. oxa-diels alder, 1%), 576.1 (M- H+chroman ring, 3%), 481.2 (M⁺ = product, 12%), 343.7 (Fragment rev. oxa-diels alder, 8%), 319.1 (Fragment TBSO-chroman+ 100%)

MS Calculated for C₅₂H₇₃NO₄S₂Si₂ 895.452

14.1.28 Synthesis of (*S*)-2-(5-((6-(benzyloxy)-2,5,7,8-tetramethylchroman-2-yl)methyl)thiophen-2-yl)-1*H*-pyrrole (**32**)



In a flame dried round bottom flask sodium hydride 60% dispersion in mineral oil (15.3mg, 0.383mmol) was washed with dry THF under N₂ atmosphere. The NaH was then suspended with dry THF (0.2ml) and after 5min, pyrrole (26.6μl, 0.383mmol) was added slowly at room temperature. After the bubbling stopped the yellow reaction was stirred for an additional 15min. Zinc chloride (52.2mg, 0.383mmol) and to the light orange-brown solution after 5min was added palladium(II)acetate (2.4mg, 0.0106mmol) followed by Johnphos[®] (3.2mg, 0.0106mmol). **26** (100mg, 0.2127) in dry THF (1ml) was added and stirred for 16h at 60°C under N₂. The reaction was cooled to r.t. and extracted with CH₂Cl₂ / water. The water phase was washed several times with CH₂Cl₂, the combined phases with washed with brine, dried over Na₂SO₄ and evaporated to dryness. SiO₂ column chromatography (gradient 1 CH₂Cl₂ increments increase, Hex/CH₂Cl₂, 4:1 to CH₂Cl₂) afforded **32** (10mg 10.3%) as a light brown oil.

TLC: R_f = 0.73 (CH₂Cl₂)

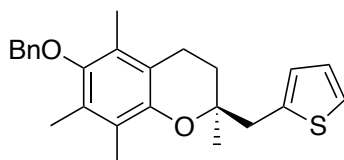
¹H-NMR (300MHz, CDCl₃) δ 8.27 (*brs*, 1H, Ar-pyrrole-NH), 7.55-7.34 (*m*, 5H, Bn-), δ 6.88 (*d*, J = 3.60 Hz, 1H, Ar-thiophene-H), δ 6.80 (*bs*, 1H, Ar-pyrrole-H), δ 6.77 (*d*, J = 3.60 Hz, 1H, Ar-thiophene-H), δ 6.38 (*bs*, 1H, Ar-pyrrole-H), δ 6.27 (*q*, J = 3.00 Hz, 1H, Ar-pyrrole-H), δ 4.73 (*s*, 2H, Bn-CH₂), δ 3.12 (*s*, 2H, thiophene-CH₂), δ 2.67 (*t*, J = 6.00 Hz, 2H, ArCH₂), δ 2.27 (*s*, 3H, ArCH₃), δ 2.22 (*s*, 3H, ArCH₃), δ 2.20 (*s*, 3H, ArCH₃), δ 1.86 (*m*, 2H, ArCH₂CH₂), δ 1.31 (*s*, 3H, 2'*R*-CH₃)

¹³C-NMR (300MHz, CDCl₃) 148.4, 147.6, 138.0, 136.8, 135.2, 128.5, 128.2, 127.8, 127.7, 127.6, 127.0, 126.1, 123.2, 120.2, 118.2, 117.2, 109.9, 106.2, 74.73, 74.63, 40.84, 30.54, 29.71, 23.84, 20.63, 12.92, 12.25, 12.03

MS [EI+] m/z 457 (M⁺, -%), 392 (6.6%), 301 (64%), 233 (49), 203 (100%), 91 (94%)

MS Calculated for C₂₉H₃₁NO₂S 457.208

Byproduct (*S*)-6-(benzyloxy)-2,5,7,8-tetramethyl-2-(thiophen-2-ylmethyl)chroman (29-H)



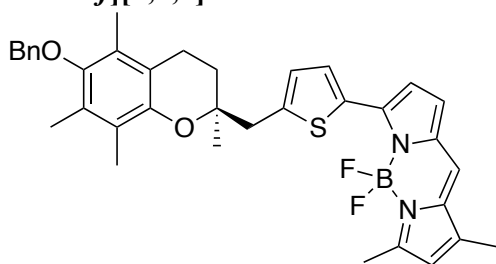
TLC: $R_f = 0.72$ (Hexane/ CH_2Cl_2 , 1:2)

$^1\text{H-NMR}$ (300MHz, CDCl_3) 7.56-7.35 (*m*, 5H, Bn-), 7.21 (*dd*, $J = 5.10$ Hz, $J = 1.2$ Hz, 1H, Ar-thiophene-H), δ 6.62 (*dd*, $J = 5.10$ Hz, $J = 3.60$ Hz, 1H, Ar-thiophene-H), δ 6.90 (*dd*, $J = 3.30$ Hz, $J = 1.2$ Hz, 1H, Ar-thiophene-H), δ 4.74 (*s*, 2H, Bn- CH_2), δ 3.18 (*s*, 2H, thiophene- CH_2), δ 2.70 (*m*, 2H, Ar CH_2), δ 2.28 (*s*, 3H, Ar CH_3), δ 2.22 (*s*, 3H, Ar CH_3), δ 2.21 (*s*, 3H, Ar CH_3), δ 1.82 (*m*, 2H, Ar CH_2CH_2), δ 1.30 (*s*, 3H, 2'-*R*- CH_3)

$^{13}\text{C-NMR}$ (400MHz, CDCl_3) 148.4, 147.6, 139.1, 138.0, 129.0, 128.5, 128.2, 127.8, 127.7, 127.1, 126.4, 126.0, 124.4, 123.2, 117.2, 74.73, 74.59, 40.61, 30.62, 23.79, 20.67, 12.92, 12.19, 12.03

MS [EI $^+$] m/z 392 (M^+ , 11%), 301 (100%), 263 (56%), 203 (35), 97 (96%)
MS Calculated for $\text{C}_{25}\text{H}_{28}\text{O}_2\text{S}$ 392.181

14.1.29 Synthesis of (*S*)-7-(5-(((6-(benzyloxy)-2,5,7,8-tetramethylchroman-2-yl)methyl)thiophen-2-yl)-5,5-difluoro-1,3-dimethyl-5*H*-dipyrrolo[1,2-*c*:2',1'-*f*][1,3,2]diazaborinin-4-ium-5-uide (33)



3,5-Dimethylpyrrole carboxaldehyde (70mg, 0.569mmol) and **32** (260mg (as a 1:1 mix with the dimer), 0.569mmol) were dissolved in dry CH_2Cl_2 (7ml) and cooled to 0°C under an nitrogen atmosphere. POCl_3 (52 μl , 0.569mmol) was added dropwise, covered in aluminum foil and stirred for 16h at room temperature, N_2 . The pink reaction mixture was cooled to 0°C and triethylamine (317 μl , 2.28mmol) was added followed by $\text{BF}_3 \cdot \text{OEt}$ (286 μl , 2.28mmol). After 16h, the reaction was cooled to 0°C , diluted with CH_2Cl_2 and quenched with water. After 5min, the water phase was washed twice with CH_2Cl_2 . The combined organic phases were dried over

Na₂SO₄ and evaporated to dryness. SiO₂ column chromatography (gradient Hex/CH₂Cl₂, 3:1 to 1:1) afforded **33** (23mg 6.6% to the mix / 13.2% to assumed pure SM) as a red oil.

TLC: R_f = 0.57 (CH₂Cl₂)

¹H-NMR (400MHz, CDCl₃) δ 8.00 (*d*, *J* = 3.6 Hz, 1H, ArH), 7.54-7.36 (*m*, 5H, Bn-), δ 7.07 (*s*, 1H, ArH), δ 6.94 (*d*, *J* = 4.0 Hz, 2H, ArH), δ 6.71 (*d*, *J* = 4.40 Hz, 1H, ArH), δ 6.14 (*s*, 1H, ArH), δ 4.73 (*s*, 2H, Bn-CH₂), δ 3.18 (*dd*, *J* = 14.88 Hz, *J* = 6.8 Hz, 2H, thiophene-CH₂), δ 2.68 (*m*, 2H, ArCH₂), δ 2.63 (*s*, 3H, ArCH₃), δ 2.28 (*s*, 3H, ArCH₃), δ 2.27 (*s*, 3H, ArCH₃), δ 2.24 (*s*, 3H, ArCH₃), δ 2.20 (*s*, 3H, ArCH₃), δ 1.84 (*m*, *J* = 6.80 Hz, 2H, ArCH₂CH₂), δ 1.28 (*s*, 3H, 2'-R-CH₃)

¹³C-NMR (400MHz, CDCl₃) 159.5, 148.5, 147.5, 142.9, 142.5, 138.0, 135.5, 133.6, 129.8, 129.4, 128.5, 128.3, 127.8, 127.7, 126.1, 123.2, 122.4, 120.4, 118.7, 117.2, 74.73, 74.64, 40.94, 31.94, 30.77, 29.71, 29.38, 23.90, 20.63, 15.05, 12.93, 12.28, 12.04, 11.31

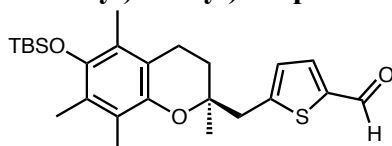
¹⁹F-NMR (400MHz, CDCl₃) δ -143.6, -143.8 (*dq*, *J* = 36.00 Hz, 2F, BF₂)

¹¹B-NMR (400MHz, CDCl₃) δ 1.30 (*t*, *J* = 104.00 Hz, 1B, BF₂)

MS [EI+] *m/z* 610 (M, -%), 149 (25%), 97 (34%), 85 (53), 71 (71), 57 (100%)

MS Calculated for C₃₆H₃₇O₂BF₂S 610.264

14.1.30 Synthesis of (*S*)-5-((6-((*tert*-butyldimethylsilyl)oxy)-2,5,7,8-tetramethylchroman-2-yl)methyl)thiophene-2-carbaldehyde (**34**)



Compound **26** (1.74 g, 0.0035 mol) was dissolved in dry THF (15 ml) and cooled under a N₂ atmosphere to -78°. *n*-BuLi (2.77 ml, 1.4 M in hexane) was added dropwise over 20 min. After 30 min at -78°C, dry DMF (0.3 ml) was added dropwise and the solution stirred for 2.5 h at the same temperature. The orange solution was then warmed to room temperature and extracted with H₂O. The water phase was extracted three times with CH₂Cl₂. The combined organic phases were dried over Na₂SO₄ and evaporated.

SiO₂ column chromatography (Hex/CH₂Cl₂, 4:1 to CH₂Cl₂) afforded **34** (1.57 g 82.9%) as a light yellow, brown powder.

TLC: R_f = 0.63 (CH₂Cl₂)

¹H-NMR (400MHz, CDCl₃) 9.852 (*s*, 1H, CHO), δ 7.65 (*d*, *J* = 3.76 Hz, 1H, Ar-thiophene-H), δ 6.99 (*d*, *J* = 3.76 Hz, 1H, Ar-thiophene-H), δ 3.19 (*dd*, *J* = 16.76

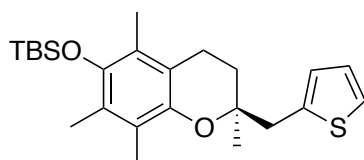
Hz, 2H, thiophene-CH₂), δ 2.64 (*t*, *J* = 6.84 Hz, 2H, ArCH₂), δ 2.14 (*s*, 3H, ArCH₃), δ 2.08 (*s*, 3H, ArCH₃), δ 2.06 (*s*, 3H, ArCH₃), δ 1.84 (*m*, *J* = 6.43 Hz, 2H, ArCH₂CH₂), δ 1.27 (*s*, 3H, 2'-R-CH₃), δ 1.07 (*s*, 9H, Si-*t*Bu), δ 0.1444 (*s*, 3H, Si-CH₃), δ 0.1441 (*s*, 3H, Si-CH₃)

¹³C-NMR (400MHz, CDCl₃) 182.8, 151.1, 145.2, 144.6, 143.0, 136.4, 128.7, 126.4, 123.6, 123.0, 116.8, 73.99, 41.27, 31.07, 26.11, 23.80, 20.76, 18.62, 14.38, 13.43, 12.40, -3.28, -3.32

MS [EI+] *m/z* 444 (M⁺, 56%), 319 (100%), 73 (23%)

HRMS Calculated for C₂₅H₃₆O₃SSi 444.2154; found: 444.2165

Byproduct (*S*)-*tert*-butyldimethyl((2,5,7,8-tetramethyl-2-(thiophen-2-ylmethyl)chroman-6-yl)oxy)silane (35)



TLC: *R_f* = 0.96 (CH₂Cl₂)

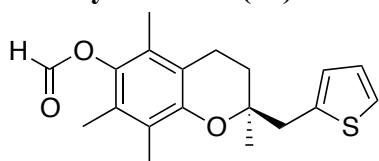
¹H-NMR (400MHz, CDCl₃) 7.19 (*dd*, *J* = 5.20 Hz, *J* = 1.20 Hz, 1H, Ar-thiophene-H), δ 6.96 (*dd*, *J* = 5.20 Hz, *J* = 3.20 Hz, 1H, Ar-thiophene-H), δ 6.87 (*t*, *J* = 3.20 Hz, *J* = 1.20 Hz, 1H, Ar-thiophene-H), δ 3.14 (2x *d*, *J* = 23.8 Hz, 2H, thiophene-CH₂), δ 2.66 (*dt*, *J* = 6.80 Hz, 2H, ArCH₂CH₂), δ 2.07 (*s*, 3H, ArCH₃), δ 2.04 (*s*, 3H, ArCH₃), δ 2.08 (*s*, 3H, ArCH₃), δ 1.81 (*m*, 2H, ArCH₂CH₂), δ 1.57 (*s*, 3H, 2'-R-CH₃), δ 1.07 (*s*, 9H, Si-*t*Bu), δ 0.141 (*s*, 3H, Si-CH₃)

¹³C-NMR (300MHz, CDCl₃) 145.6, 144.4, 139.3, 127.0, 126.3, 126.1, 124.3, 123.6, 122.9, 117.1, 74.29, 40.45, 30.90, 26.12, 23.70, 20.85, 18.62, 14.37, 13.43, 12.32, -3.28, -3.33

MS [EI+] *m/z* 416 (M⁺ 26%), 319 (M⁺ -thienyl-CH₂, 100%), 115 (30%), 58 (71%)

MS Calculated for C₂₄H₃₆O₂SSi 416.221

14.1.31 Synthesis of byproduct (*S*)-2,5,7,8-tetramethyl-2-(thiophen-2-ylmethyl)chroman-6-yl formate (36)



35 (50mg, 0.12mmol) was dissolved in dry dichloroethane (2ml) at room temperature under a N₂ atmosphere. Dry dimethylformamide (11.1μl, 0.144mmol) was added. POCl₃ (13.2μl, 0.144mmol) was added and the solution was stirred for 16h at room temperature. The yellow solution was quenched with H₂O. 1M NaOH was added until pH 8 was reached. The water phase was extracted three times with CH₂Cl₂. The combined organic phases were dried over Na₂SO₄ and evaporated to dryness. SiO₂ column chromatography (gradient Hex/CH₂Cl₂, 3:1 to CH₂Cl₂/MeOH 9:1) afforded **36** (39.6mg 38%) as a clear oil.

TLC: R_f = 0.19 (CH₂Cl₂:MeOH, 1:1)

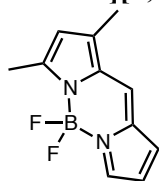
¹H-NMR (400MHz, CDCl₃) 8.34 (*s*, 1H, CHO), 7.19 (*dd*, *J* = 5.20 Hz, *J* = 1.60 Hz, 1H, Ar-thiophene-H), δ 6.97 (*dd*, *J* = 5.20 Hz, *J* = 3.20 Hz, 1H, Ar-thiophene-H), 6.90 (*t*, *J* = 3.20 Hz, *J* = 1.60 Hz, 1H, Ar-thiophene-H), 3.17 (*s*, *J* = 6.80 Hz, 2H, Ar-thiophene-CH₂), δ 2.70 (*q*, *J* = 6.80 Hz, 2H, ArCH₂CH₂), δ 2.21 (*s*, 3H, ArCH₃), δ 2.11 (*s*, 3H, ArCH₃), δ 2.05 (*s*, 3H, ArCH₃), δ 1.83 (*m*, 2H, ArCH₂CH₂), δ 1.29 (*s*, 3H, 2'*R*-CH₃)

¹³C-NMR (400MHz, CDCl₃) 160.0, 149.5, 140.0, 138.8, 127.2, 126.9, 126.4, 125.0, 124.5, 123.6, 117.3, 74.95, 40.71, 30.25, 23.78, 20.58, 13.16, 12.29, 12.22

MS [EI+] *m/z* 331.1 (M⁺ 17%), 369.1 (19%), 348.2 (100%)

MS Calculated for C₁₉H₂₂O₃S 330.129

14.1.32 Synthesis of 5,5-difluoro-7,9-dimethyl-5H-dipyrrolo[1,2-*c*:2',1'-f][1,3,2]diazaborinin-4-ium-5-uide (**37**)



Pyrrole-2-carboxaldehyde (1.0 g, 10.5 mmol) and 2,4-dimethylpyrrole (1.0 g, 10.5 mmol) were dissolved in dry CH₂Cl₂ (40 ml) at room temperature. Phosphoryl chloride (0.98 ml, 10.5 mmol) was added drop wise at 0°C under a N₂ atmosphere. The solution was stirred for 5 h at room temperature. The reaction solution was cooled to 0°C, and triethylamine was added (7.32 ml, 52.6 mmol) followed after 5 min. by BF₃•OEt₂ (6.60 ml, 52.6 mmol). Stirring was continued for 8 h. The reaction mixture was extracted 3x times with a large excess of CH₂Cl₂ (500 ml) and H₂O (500ml). The organic phase was filtered through Celite to get rid of the remaining salts. The combined organic phases were dried over anhydrous Na₂SO₄ and evaporated to dryness.

SiO₂ column chromatography (Hex/CH₂Cl₂, 1:1 to CH₂Cl₂) afforded **37** (1.8 g 78.3 %) as a shiny green-orange solid.

TLC: R_f = 0.52 (CH₂Cl₂) mp: 144°C

¹H-NMR (300MHz, CDCl₃) δ 7.65 (*s*, 1H, ArH), δ 7.19 (*s*, 1H, ArH), δ 6.92 (*d*, *J* = 3.72 Hz, 1H, ArH), δ 6.43 (*s*, 1H, ArH), δ 6.16 (*s*, 1H, ArH), δ 2.59 (*s*, 3H, Ar-CH₃), δ 2.56 (*s*, 3H, Ar-CH₃)

¹³C-NMR (400MHz, CDCl₃) 163.1, 145.9, 139.1, 136.3, 132.7, 126.5, 124.8, 121.3, 116.3, 15.15, 11.35,

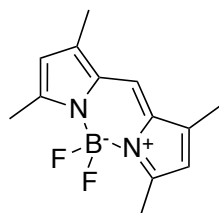
¹⁹F-NMR (400MHz, CDCl₃) δ -146.1 (*q*, *J* = 31.16 Hz, 2F, BF₂)

¹¹B-NMR (400MHz, CDCl₃) δ 0.58 (*t*, *J* = 31.10 Hz, 1B, BF₂)

MS [EI+] *m/z* 220 (M⁺, 36%), 219 (52%), 200 (56%), 86 (100%) 43 (72%),

HRMS Calculated for C₃₁H₃₃O₂BF₂S 220.0977; found: 220.0983

Side product 5,5-difluoro-1,3,7,9-tetramethyl-5*H*-dipyrrolo[1,2-*c*:2',1'-*f*][1,3,2]diazaborinin-4-ium-5-uide (**38**)



TLC: R_f = 0.50 (CH₂Cl₂)

¹H-NMR (300MHz, CDCl₃) δ 7.06 (*s*, 1H, Ar-*meso*-H), δ 6.07 (*s*, 2H, ArH), δ 2.55 (*s*, 6H, Ar-CH₃), δ 2.27 (*s*, 6H, Ar-CH₃)

¹³C-NMR (400MHz, CDCl₃) 156.8, 141.2, 133.4, 133.4, 120.1, 119.0, 14.65, 11.28

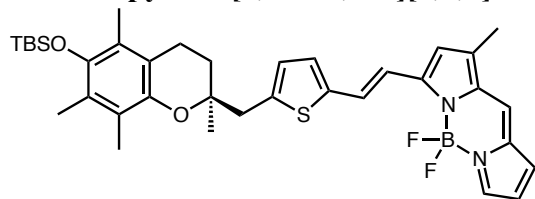
¹⁹F-NMR (400MHz, CDCl₃) δ -146.6 (*q*, *J* = 35.20 Hz, 2F, BF₂)

¹¹B-NMR (400MHz, CDCl₃) δ 0.88 (*t*, *J* = 104 Hz, 1B, BF₂)

MS [ESI+] *m/z* 249.1 (M⁺H, 23%), 431.1 (M-F, 100%) 271.1 (48%), 229.1 (M-F, 30%)

MS Calculated for C₁₃H₁₅BF₂N₂ 248.130

14.1.33 Synthesis of (*S,E*)-7-(2-(5-((6-((*tert*-butyldimethylsilyl)oxy)-2,5,7,8-tetramethylchroman-2-yl)methyl)thiophen-2-yl)vinyl)-5,5-difluoro-9-methyl-5H-dipyrrolo[1,2-*c*:2',1'-*f*][1,3,2]diazaborinin-4-ium-5-uide (39**)**



Compound **34** (155 mg, 0.35 mmol) and compound **37** (76.8 mg, 0.35 mmol) were dissolved in benzene (9 ml) at room temperature. Piperidine (0.17 ml, 1.74 mmol) was added followed by acetic acid (87 μ l, 1.40 mmol). The red solution was stirred for 11 h at 110°C. Benzene was evaporated by rotary evaporation and the oily residue was partitioned between CH₂Cl₂ and H₂O. The water phase was extracted three times with CH₂Cl₂. The combined organic phases were dried over Na₂SO₄ and evaporated to dryness.

SiO₂ column chromatography (Hex/CH₂Cl₂, 3:1 to CH₂Cl₂) afforded silyl-protected **39** (55 mg 24.5%) as shiny blue, bronze oil.

TLC: R_f = 0.87 (CH₂Cl₂)

¹H-NMR (400MHz, CDCl₃) δ 7.68 (*s*, 1H, ArH), δ 7.46 (*d*, J = 15.8 Hz, 1H, CH=CH), δ 7.36 (*d*, J = 16.29 Hz, 1H, CH=CH), δ 7.17 (*d*, J = 3.68 Hz, 1H, ArH), δ 7.15 (*s*, 1H, ArH), δ 6.92 (*d*, J = 3.76, 1H, ArH), δ 6.85 (*d*, J = 3.68 Hz, 1H, ArH), δ 6.72 (*s*, 1H, ArH), δ 6.47 (*q*, J = 1.99 Hz, 1H, ArH), δ 3.13 (*q*, J = 14.88 Hz, J = 6.8 Hz, 2H, thiophene-CH₂), δ 2.65 (*m*, 2H, ArCH₂), δ 2.33 (*s*, 3H, ArCH₃), δ 2.18 (*s*, 3H, ArCH₃), δ 2.15 (*s*, 3H, ArCH₃), δ 2.09 (*s*, 3H, ArCH₃), δ 1.87 (*m*, J = 7.20 Hz, 2H, ArCH₂CH₂), δ 1.29 (*s*, 3H, 2'*R*-CH₃), δ 1.07 (*s*, 9H, Si-*t*Bu), δ 0.148 (*s*, 6H, 2x Si-CH₃)

¹³C-NMR (400MHz, CDCl₃) 158.8, 145.5, 144.5, 144.2, 140.7, 138.4, 138.1, 133.0, 129.8, 128.7, 126.5, 126.3, 125.3, 123.6, 123.0, 122.2, 117.2, 117.0, 116.7, 116.2, 74.32, 40.87, 31.01, 26.12, 23.97, 20.85, 18.62, 14.37, 13.43, 12.32, 11.46, 11.40, -3.27, -3.31

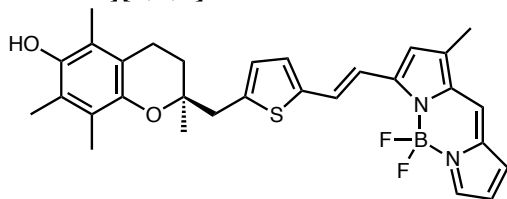
¹⁹F-NMR (400MHz, CDCl₃) δ -142.6 (*q*, J = 31.61 Hz, 2F, BF₂)

¹¹B-NMR (400MHz, CDCl₃) δ 0.74 (*q*, J = 31.06 Hz, 1B, BF₂)

MS [EI+] m/z 532 (M-TBS, 7%), 512 (10%), 309 (24%), 205 (100), 55 (66)

HRMS Calculated for C₃₆H₄₅O₂BF₂SSi 646.3032 (M-TBS) 532.2167; found: 532.2177

14.1.34 Synthesis of (S,E)-5,5-difluoro-7-(2-(5-((6-hydroxy-2,5,7,8-tetramethylchroman-2-yl)methyl)thiophen-2-yl)vinyl)-9-methyl-5H-dipyrrolo[1,2-c:2',1'-f][1,3,2]diazaborinin-4-ium-5-uide (3)



TBS-protected **39** (104 mg, 0.16 mmol) was dissolved in THF (6 ml) at room temperature. 8% HCl in MeOH (4 ml) was added and the violet-coloured solution was stirred under N₂ atmosphere for 48 h at room temperature. The solution was partitioned between with CH₂Cl₂ and H₂O. The water phase was extracted three times with CH₂Cl₂. The combined organic phases were dried over Na₂SO₄ and evaporated to dryness.

SiO₂ column chromatography (Hex/CH₂Cl₂, 3:1 to CH₂Cl₂) afforded **3** (36 mg 42%) as a shiny blue, bronze oil.

TLC: $R_f = 0.51$ (CH₂Cl₂)

¹H-NMR (400MHz, CDCl₃) δ 7.68 (*s*, 1H, ArH), δ 7.45 (*d*, $J = 15.93$ Hz, 1H, CH=CH), δ 7.35 (*d*, $J = 15.93$ Hz, 1H, CH=CH), δ 7.16 (*d*, $J = 4.0$ Hz, 1H, ArH), δ 7.15 (*s*, 1H, ArH), δ 6.92 (*d*, $J = 3.6$ Hz, 1H, ArH), δ 6.85 (*d*, $J = 3.6$ Hz, 1H, ArH), δ 6.72 (*s*, 1H, ArH), δ 6.47 (*q*, 1H, ArH), δ 4.240 (*s broad*, 1H, OH), δ 3.13 (*q*, 2H, thiophene-CH₂), δ 2.70 (*m*, 2H, ArCH₂), δ 2.33 (*s*, 3H, ArCH₃), δ 2.23 (*s*, 3H, ArCH₃), δ 2.22 (*s*, 3H, ArCH₃), δ 2.15 (*s*, 3H, ArCH₃), δ 1.86 (*m*, $J = 6.84$ Hz, 2H, ArCH₂CH₂), δ 1.30 (*s*, 3H, 2'R-CH₃)

¹³C-NMR (400MHz, CDCl₃) 158.7, 145.0, 145.0, 144.4, 144.0, 140.7, 138.3, 138.1, 133.1, 133.0, 129.8, 128.7, 125.3, 122.9, 122.2, 121.4, 118.6, 117.2, 116.9, 116.7, 116.2, 74.35, 40.85, 30.92, 23.96, 20.71, 12.27, 12.19, 11.48, 11.34

¹⁹F-NMR (400MHz, CDCl₃) δ -142.6 (*s*, $J = 31.43$ Hz, 2F, BF₂)

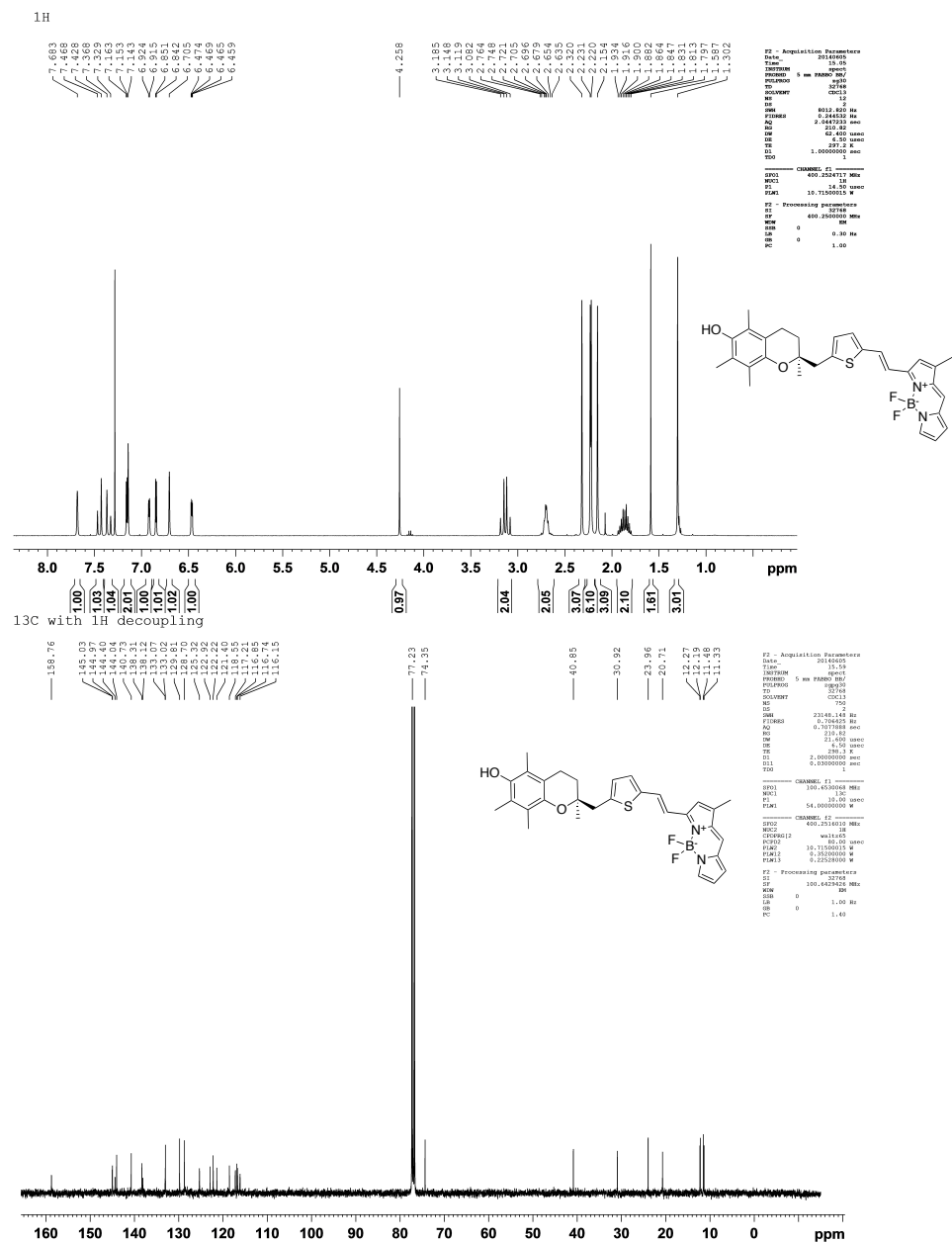
¹¹B-NMR (400MHz, CDCl₃) δ 0.82 (*t*, $J = 31.70$ Hz, 1B, BF₂)

MS [EI+] m/z 532 (M⁺, 3%), 512 (4%), 309 (11%), 205 (100), 190 (7%), 98 (7%), 84 (13) 80 (20) 43 (100)

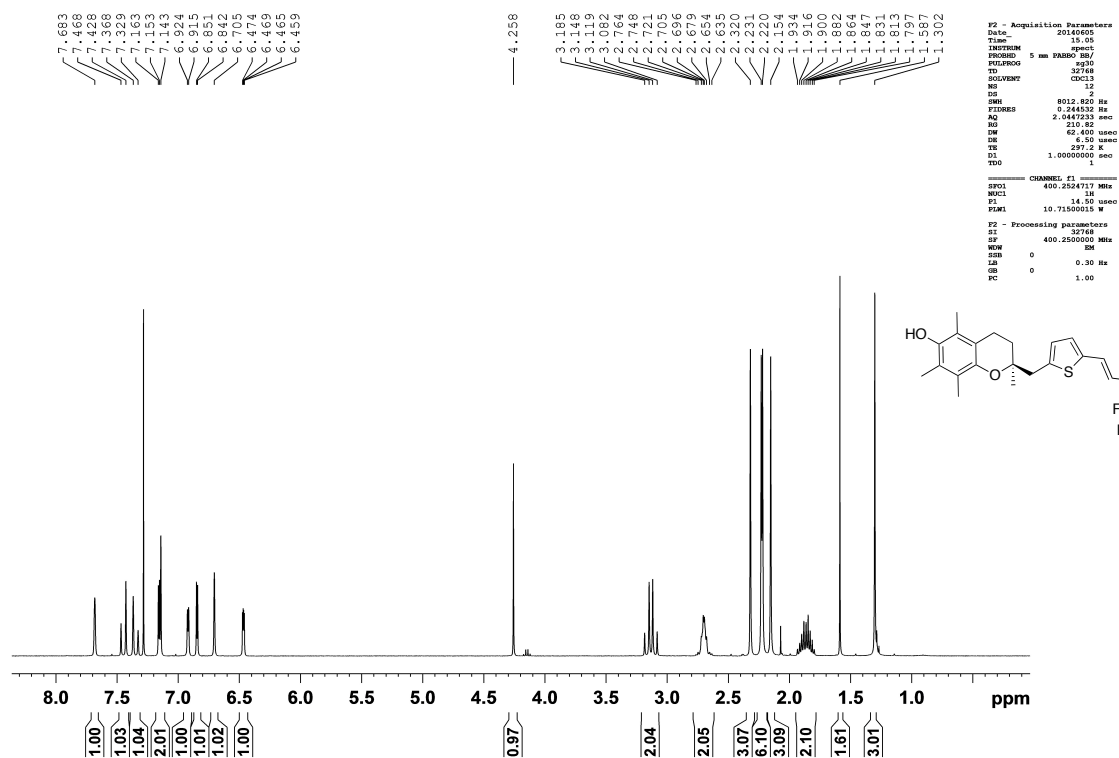
HRMS Calculated for C₃₀H₃₁O₂BF₂S 532.2167; found: 532.2169

[ES-] (%) m/z 531 (M⁺, 100%), 327 (12%),

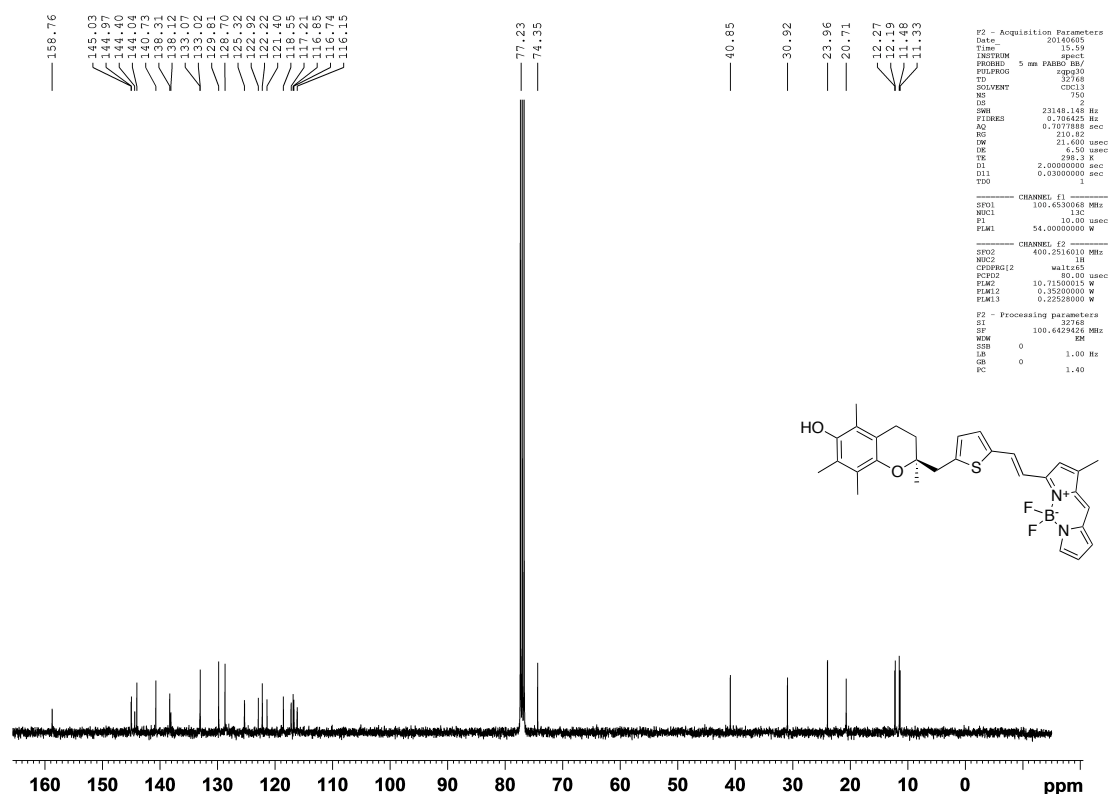
HRMS Calculated for C₃₀H₃₁O₂BF₂S 531.2095; found: 531.3



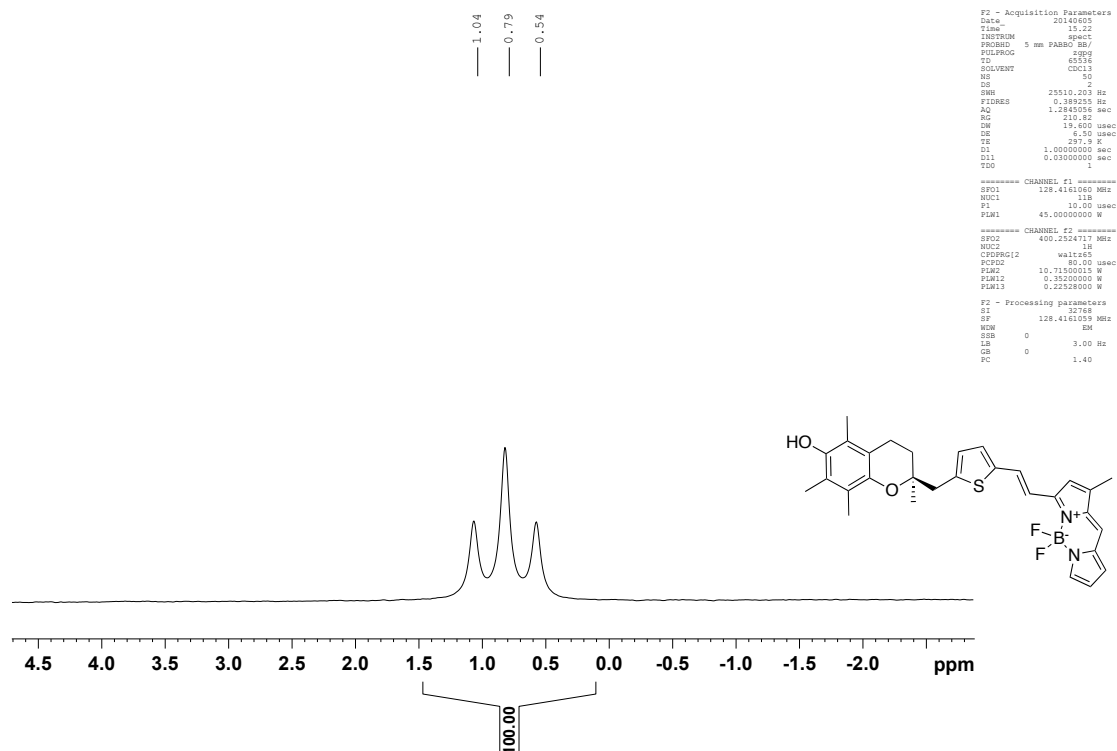
¹H



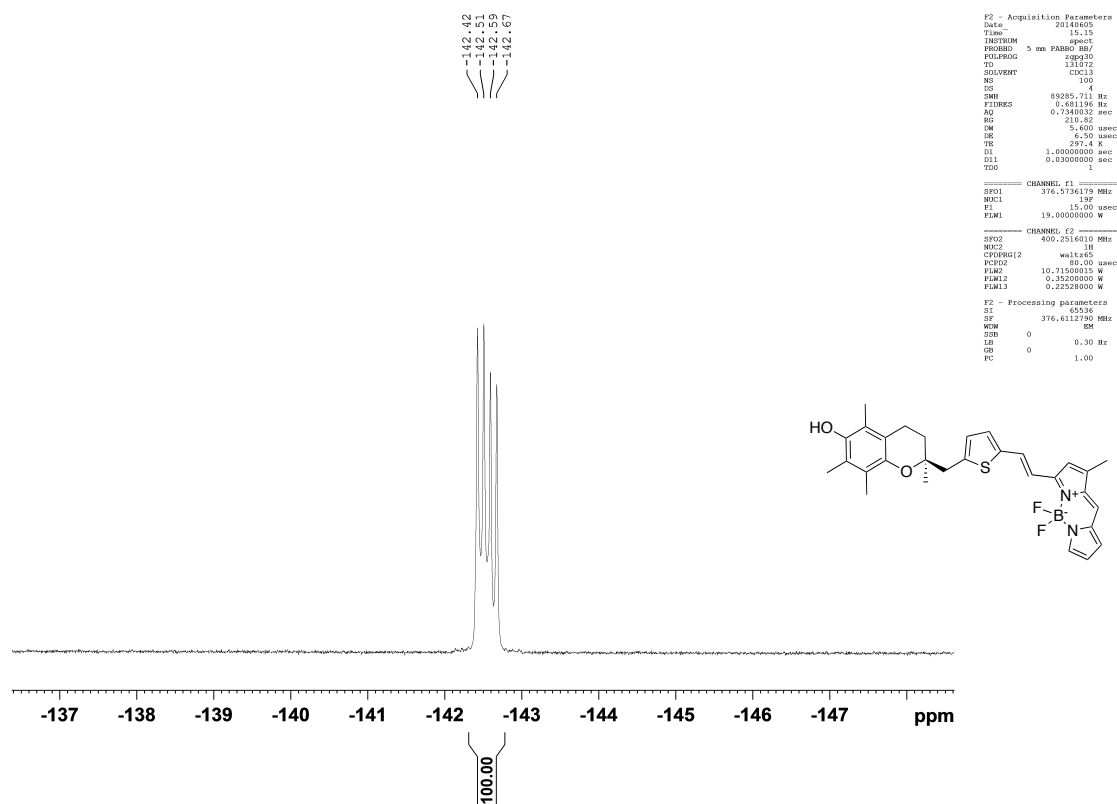
¹³C with ¹H decoupling



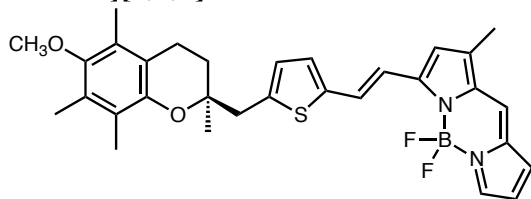
11B with 1H decoupling



F19 with 1H decoupling



14.1.35 Synthesis of (*S,E*)-5,5-difluoro-7-(2-(5-((6-methoxy-2,5,7,8-tetramethylchroman-2-yl)methyl)thiophen-2-yl)vinyl)-9-methyl-5H-dipyrrolo[1,2-*c*:2',1'-f][1,3,2]diazaborinin-4-ium-5-uide (40**)**



Compound **3** (4.6 mg, 4.72 μ mol) was dissolved in dry THF (1 ml) at room temperature.

Methyl iodide (0.74 μ l, 47.2 μ mol) and activated NaH (60% dispersion in mineral oil decanted 3x with hexane and dried) (0.2 mg, 4.72 μ mol) were added and the violet solution was stirred under N₂ atmosphere for 20 minutes at room temperature. The solvent was evaporated and the residue was purified by SiO₂ column chromatography (Hex/CH₂Cl₂, 1:1 to Hex/CH₂Cl₂ 1:4, CH₂Cl₂) which afforded **40** (0.49 mg 22.7 %) as a shiny blue, bronze oil.

TLC: R_f = 0.72 (CH₂Cl₂)

¹H-NMR (600MHz, CDCl₃) δ 7.68 (*s*, 1H, ArH), δ 7.45 (*d*, J = 15.79 Hz, 1H, CH=CH), δ 7.36 (*d*, J = 15.97 Hz, 1H, CH=CH), δ 7.16 (*d*, J = 3.66 Hz, 1H, ArH), δ 7.15 (*s*, 1H, ArH), δ 6.93 (*d*, J = 3.72 Hz, 1H, ArH), δ 6.86 (*d*, J = 3.60, 1H, ArH), δ 6.71 (*s*, 1H, ArH), δ 6.47 (*q*, J = 1.96 Hz, 1H, ArH), δ 3.66 (*s*, 3H, OCH₃), δ 3.14 (*q*, J = 13.14 Hz, J = 6.8 Hz 2H, thiophene-CH₂), δ 2.67 (*t*, J = 7.16 Hz, 2H, ArCH₂), δ 2.323 (*s*, 3H, ArCH₃), δ 2.24 (*s*, 3H, ArCH₃), δ 2.20 (*s*, 3H, ArCH₃), δ 2.18 (*s*, 3H, ArCH₃), δ 1.86 (*m*, J = 7.33 Hz, 2H, ArCH₂CH₂), δ 1.30 (*s*, 3H, 2-*R*-CH₃),

¹³C-NMR (from HMBC/HSQC) (600MHz, CDCl₃) 158.7, 149.5, 147.1, 144.2, 143.9, 140.7, 138.4, 138.0, 133.0, 128.8, 128.7, 128.0, 125.8, 125.4, 123.1, 122.3, 118.5, 117.1, 117.0, 116.7, 116.3, 74.3, 60.3, 41.2, 30.7, 23.9, 20.71, 12.33, 12.12, 11.48, 11.33

¹⁹F-NMR (400MHz, CDCl₃) δ -142.8 (*q*, J = 31.36 Hz, F, BF₂)

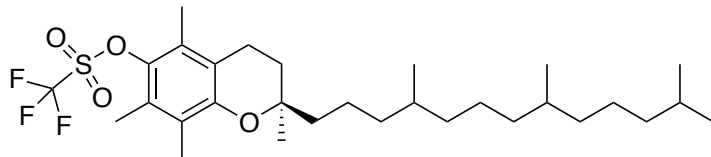
¹¹B-NMR (400MHz, CDCl₃) δ 0.82 (*t*, J = 31.55 Hz, 1B, BF₂)

MS [EI+] m/z 546 (M⁺, 13%), 219 (100%), 207 (18%), 43 (13%),

HRMS Calculated for C₃₁H₃₃O₂BF₂S 546.2324; found: 546.232

14.2 Non-antioxidant-Tocopherol

14.2.1 Synthesis of (2*R*)-2,5,7,8-tetramethyl-2-(4,8,12-trimethyltridecyl)chroman-6-yl trifluoromethanesulfonate (**41**)



To a solution of α -tocopherol (9.08g, 0.0211mol), pyridine (4.8ml) in CH_2Cl_2 (100ml) was trifluoromethanesulfonate anhydride (5.96ml) added at 0°C and stirred for 1h at rt. The reaction was quenched with aqueous NaHCO_3 and extracted. The water phase was washed with CH_2Cl_2 , the organic phases combined, dried over Na_2SO_4 and evaporation down to dryness afforded **41** (11.17g, 94.1%) as a clear oil.

TLC: $R_f = 0.62$ (Hex/ CH_2Cl_2 , 5:1)

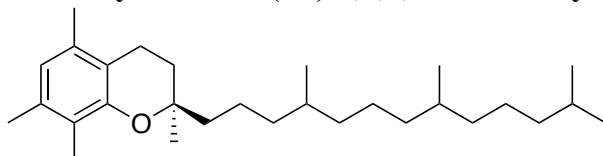
$^1\text{H-NMR}$ (400MHz, CDCl_3) δ 2.62 (*t*, $J = 6.80$, Hz, 2H, ArCH_2CH_2), δ 2.25 (*s*, 3H, ArCH_3), δ 2.22 (*s*, 3H, ArCH_3), δ 2.12 (*s*, 3H, ArCH_3), δ 1.84 (*enant dt*, $J = 6.80$ Hz, 2H, ArCH_2CH_2), δ 1.67 – 1.09 (*m*, 21H, phytyl- $\text{CH}/\text{CH}_2 + 2'R\text{-CH}_3$) δ 0.88 (*m*, 12H, phytyl- CH_3)

$^{13}\text{C-NMR}$ (400MHz, CDCl_3) 150.9, 139.7, 128.1, 126.7, 124.4, 118.5, 75.68, 39.98, 39.38, 37.29, 32.79, 32.67, 30.86, 27.99, 24.81, 24.44, 23.87, 22.72, 22.63, 21.00, 20.71, 19.75, 19.67, 19.60, 14.02, 13.22, 11.99

$^{19}\text{F-NMR}$ (400MHz, CDCl_3) -73.59

MS [HRMS] HRMS Calculated for $\text{C}_{30}\text{H}_{49}\text{O}_3\text{F}_3\text{S}$ 562.3304; found: 562.3235

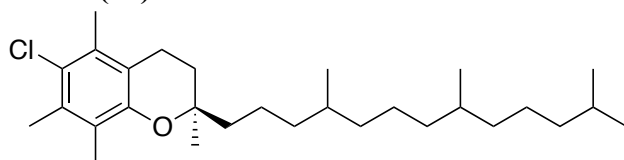
14.2.2 Synthesis of (2*R*)-2,5,7,8-tetramethyl-2-(4,8,12-trimethyltridecyl)chroman (**42**)



Compound **41** (11.18g, 0.01987), palladium on carbon 10% (5.1g) and triethylamine (12.2ml, 0.0871mol) were dissolved in MeOH/THF 2:1 (200ml) and stirred for 2 days under H_2 (15psi). The reaction mixture was filtered over purified celite, washed with EtOAc and the solvent was evaporated. The residue was extracted with CH_2Cl_2 and H_2O . The water phase was washed with CH_2Cl_2 five times, the organic phases were combined, dried over Na_2SO_4 and evaporated down to dryness. Silica column chromatography (Hex/ CH_2Cl_2 , 15:1) afforded **42** (8.12g, 98.6%) as a clear oil.

| | |
|---------------------|---|
| TLC: | $R_f = 0.45$ (Hexane/ CH_2Cl_2 , 10:1) |
| $^1\text{H-NMR}$ | (400MHz, CDCl_3) δ 6.57 (<i>s</i> , 1H, Ar-H), δ 2.60 (<i>t</i> , $J = 6.80$, Hz, 2H, ArCH_2CH_2), δ 2.22 (<i>s</i> , 3H, ArCH_3), δ 2.18 (<i>s</i> , 3H, ArCH_3), δ 2.09 (<i>s</i> , 3H, ArCH_3), δ 1.82 (<i>enant dt</i> , $J = 6.72$ Hz, 2H, ArCH_2CH_2), δ 1.63 – 1.09 (<i>m</i> , 21H, phytyl-CH/ CH_2 + 2' <i>R</i> - CH_3) δ 0.88 (<i>m</i> , 12H, phytyl- CH_3) |
| $^{13}\text{C-NMR}$ | (400MHz, CDCl_3) 151.6, 134.6, 133.3, 122.1, 122.0, 116.8, 75.09, 40.14, 40.06, 39.38, 37.56, 37.47, 37.30, 32.79, 32.70, 31.13, 31.07, 27.99, 24.82, 24.46, 24.01, 22.73, 22.64, 21.06, 20.11, 19.76, 19.70, 18.82, 11.35 |
| MS [EI+] | m/z 414 (M, 44%), 189 (13%), 149 (100%) MS Calculated for $\text{C}_{29}\text{H}_{50}\text{O}$ 414.386 |

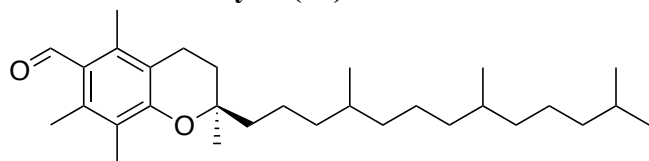
14.2.3 Synthesis of (2*R*)-6-chloro-2,5,7,8-tetramethyl-2-(4,8,12-trimethyltridecyl)chroman (43)



42 (100mg, 0.241mmol) was stirred over night with *N*-chloro succinimide (33.8mg, 0.253mmol) in dry acetonitrile (2ml) at 60°C under N_2 atmosphere in the dark (reaction flask covered with aluminum-foil) for 16h. The solvent was evaporated and remaining reaction mixture was extracted with 1M NaOH and CH_2Cl_2 . The organic phase was washed with water, brine and dried over Na_2SO_4 and evaporated down to dryness. Silica column chromatography (Hexane/ CH_2Cl_2 15:1 to 5:1) afforded **43** (61mg, 56.4%) as a light yellow oil.

| | |
|---------------------|--|
| TLC: | $R_f = 0.45$ (10:1 Hexane/ CH_2Cl_2) |
| $^1\text{H-NMR}$ | (400MHz, CDCl_3) δ 2.66 (<i>t</i> , $J = 6.80$ Hz, 2H, ArCH_2CH_2), δ 2.35 (<i>s</i> , 3H, ArCH_3), δ 2.30 (<i>s</i> , 3H, ArCH_3), δ 2.16 (<i>s</i> , 3H, ArCH_3), δ 1.82 (<i>enant. dt</i> , $J^2 = 25.36$ Hz, $J = 6.80$ Hz, 2H, ArCH_2CH_2), δ 1.66-1.04 (<i>m</i> , 21H, phytyl-CH/ CH_2 + 2' <i>R</i> - CH_3) δ 0.88 (<i>m</i> , 12H, phytyl- CH_3) |
| $^{13}\text{C-NMR}$ | (400MHz, CDCl_3) 150.0, 132.8, 131.3, 125.7, 123.7, 118.2, 75.19, 39.87, 39.78, 39.39, 37.56, 37.52, 37.47, 37.40, 37.37, 37.33, 37.30, 32.81, 32.79, 32.72, 32.69, 31.35, 31.29, 29.72, 28.00, 24.82, 24.46, 23.81, 22.74, 22.64, 21.35, 21.03, 19.76, 19.70, 19.66, 19.65, 19.60, 17.23, 16.29, 12.43 |
| MS [EI+] | m/z 448 (M^+ , 97%), 223 (15%), 183 (100%) MS Calculated for $\text{C}_{29}\text{H}_{49}\text{O}$ 448.347 |

14.2.4 Synthesis of (2*R*)-2,5,7,8-tetramethyl-2-(4,8,12-trimethyltridecyl)chroman-6-carbaldehyde (**46**)



42 (8.35g, 0.0202mol) and α,α' -dichloromethoxymethane (3.56ml, 0.0403mol) were dissolved in dry CH_2Cl_2 (85ml) under a nitrogen atmosphere. At room temperature, titanium(IV)chloride 1M in toluene (48.4ml) was added dropwise over 15min. The reaction was stirred for 1.5h, diluted with CH_2Cl_2 (30ml), then quenched slowly with water and stirred for 10 extra minutes. The phases were separated and the water phase was washed two times with CH_2Cl_2 . The organic phases were combined and dried over Na_2SO_4 and evaporated down to dryness. Silica column chromatography (Hex/ CH_2Cl_2 , 1:1) afforded **46** (6.9g 77.3%) as a clear oil.

TLC: $R_f = 0.55$ (Hex/ CH_2Cl_2 , 1:1)

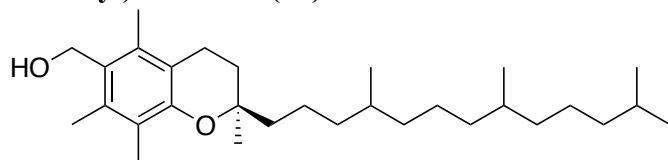
$^1\text{H-NMR}$ (400MHz, CDCl_3) δ 10.58 (s, 1H, Ar-CHO), 2.67 (t, $J = 6.80$ Hz, 1H, Ar- CH_2CH_2), δ 2.50 (s, 3H, Ar CH_3), δ 2.47 (s, 3H, Ar CH_3), δ 2.15 (s, 3H, Ar CH_3), δ 1.85 (enant dt, $J = 6.80$ Hz, 2H, Ar CH_2CH_2), δ 1.68-1.04 (m, 21H, phytyl- $\text{CH}/\text{CH}_2 + 2'R\text{-CH}_3$) δ 8.88 (m, 12H, phytyl- CH_3)

$^{13}\text{C-NMR}$ (400MHz, CDCl_3) 193.9, 155.7, 138.6, 138.2, 126.1, 123.5, 117.8, 77.23, 76.30, 40.04, 39.97, 39.38, 37.50, 37.45, 37.40, 37.36, 37.29, 32.80, 32.79, 32.67, 21.04, 30.99, 27.99, 24.82, 24.44, 23.95, 22.73, 22.64, 21.02, 20.34, 19.76, 19.69, 19.65, 19.59, 15.70, 14.88, 11.40

MS [EI+] m/z 442 (M^+ , 41%), 217 (22%), 177 (100%)

MS Calculated for $\text{C}_{30}\text{H}_{50}\text{O}_2$ 442.381

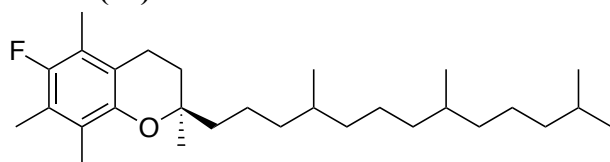
14.2.5 Synthesis of ((2*R*)-2,5,7,8-tetramethyl-2-(4,8,12-trimethyltridecyl)chroman-6-yl)methanol (**44**)



To a solution of **46** (6.9g, 0.0156mol) in dry THF (50ml), lithium aluminiumhydride (1.18g, 0.0312mol) was added in two batches at 0°C under a nitrogen atmosphere. After 3.5h, the reaction mixture was quenched slowly with water and then brought to pH 6-7 with 1M HCl. The phases were separated and the water phase was washed 5x with CH_2Cl_2 . The organic phases were combined and dried over Na_2SO_4 and dried down to dryness. Silica column chromatography (CH_2Cl_2 to $\text{CH}_2\text{Cl}_2/\text{MeOH}$ 50:1) afforded **44** (6.9g, 97.7%) as a clear oil.

14.3 PET-Tocopherol

14.3.1 Synthesis of (2*R*)-6-fluoro-2,5,7,8-tetramethyl-2-(4,8,12-trimethyltridecyl)chroman (47)



Electrophilic fluorination of H-Toc:

H-Toc **42** (50mg, 1eq) was mixed with *N*-fluorobenzenesulfonimide (38mg, 1eq) and stirred in dry acetonitrile as a 1M solution for 10-15min at 150°C in a sealed vial. The reaction was cooled to room temperature, extracted with CH₂Cl₂ and water, the organic phase dried over Na₂SO₄ and evaporated down to dryness. The crude product was filtered through a silica plug with hexane to remove polar byproducts. Silica column chromatography (gradient hexane to hexane/CH₂Cl₂ 99:1) afforded **47** (23mg, 44%) as a clear oil.

Electrophilic fluorination of I-Toc:

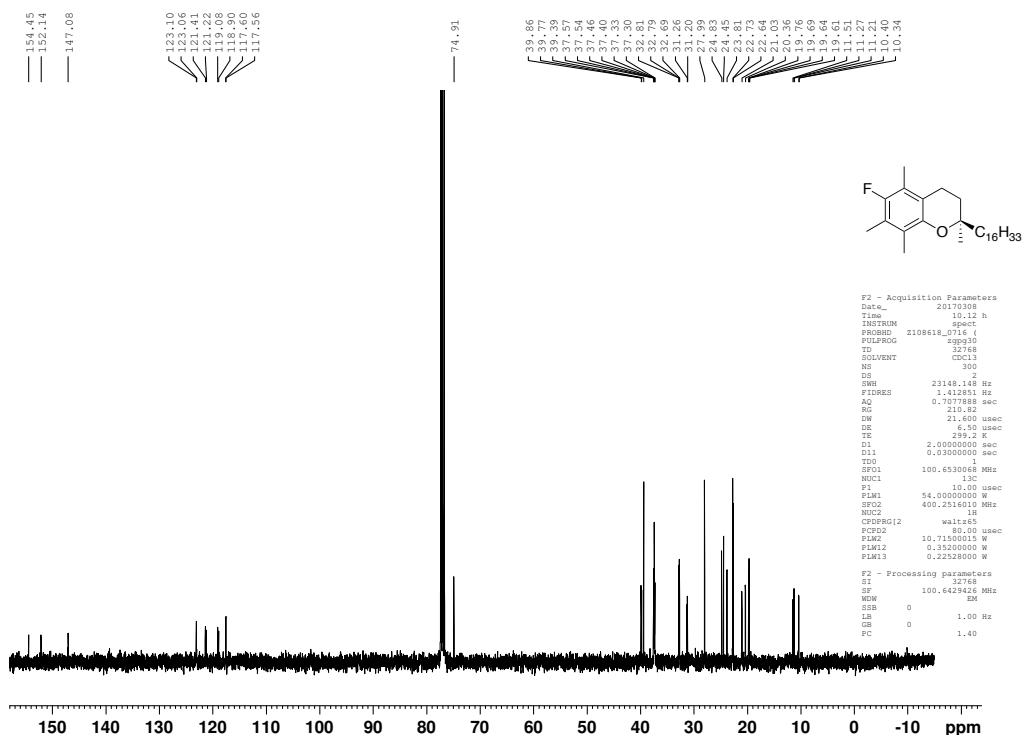
To a 0.85M solution of I-Toc **70** (100mg, 1eq) in dry THF at 0°C under an N₂ atmosphere was a 1.7M *t*-BuLi solution in pentane (0.217ml, 2eq) added and stirred for 1min. A 0.35M *N*-fluorobenzenesulfonimide (116mg, 2eq) solution in THF was slowly added and stirred for 1min at 0°C. The reaction was quenched with methanol, the solvents evaporated, extracted with CH₂Cl₂ and water, the organic phase dried over Na₂SO₄ and evaporated down to dryness. Silica column chromatography (gradient hexane to hexane/CH₂Cl₂ 99:1) afforded **47** (12mg, 15%) as a clear oil.

Nucleophilic fluorination (Phenyl)tocopherol iodonium tosylate

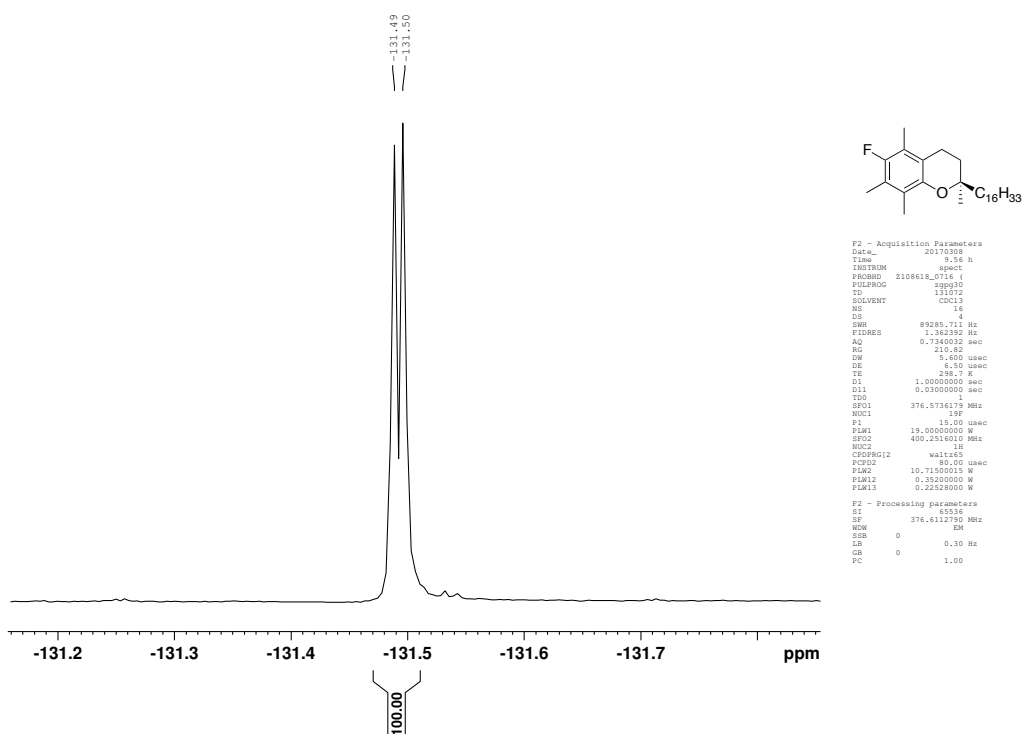
(Phenyl)tocopherol iodonium tosylate **69** (10mg, 1eq) was dissolved in DMF as a 5mM solution, 1M tetrabutylammonium fluoride in THF (1M TBAF in THF, 1eq) was added and stirred for 15min at 150°C. The solvent was evaporated and the residual mixture partitioned between with hexane and water. The organic phase was dried with Na₂SO₄, filtrated and purified over a small SiO₂ column with hexane. Silica column chromatography (gradient Hexane to Hexane/CH₂Cl₂ 99:1) afforded **47** (1.33mg, 24%) as a clear oil.

TLC: R_f = 0.27 (Hexane)

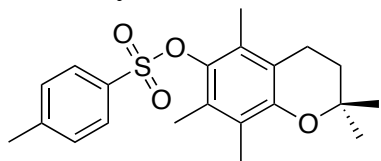
¹³C with ¹H decoupling



F19 with ¹H decoupling



14.3.2 Synthesis of 2,2,5,7,8-pentamethylchroman-6-yl 4-methylbenzenesulfonate (**52**)



Pentamethylchromanol (800mg, 3.63mmol) was dissolved in dry CH₂Cl₂ (10ml), pyridine (468μl, 5.81mmol) was added under a nitrogen atmosphere and the solution cooled to 0°C. Tosyl chloride (830mg, 4.36mmol) was added in three portions. The reaction solution was stirred for 5h, quenched with water, the phases separated and the water phase washed with CH₂Cl₂. The combined organic phases were dried over Na₂SO₄ and evaporated down to dryness. Silica column chromatography (gradient Hexane/CH₂Cl₂ 7:1 to 1:1 to CH₂Cl₂) afforded **52** (1.36g, 50.3%) as a light yellow oil.

TLC: R_f = 0.79 (CH₂Cl₂)

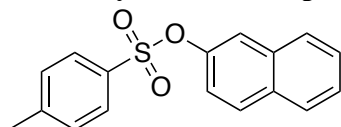
¹H-NMR (400MHz, CDCl₃) 7.84 (*d*, *J* = 8.00 Hz, 1H, Ar-Ts-H), 7.36 (*d*, *J* = 8.00 Hz, 1H, Ar-Ts-H), δ 2.58 (*t*, *J* = 6.80 Hz, 2H, ArCH₂CH₂), δ 2.49 (*s*, 3H, Ar-Ts-CH₃), δ 2.06 (*s*, 3H, ArCH₃), δ 1.99 (*s*, 3H, ArCH₃), δ 1.96 (*s*, 3H, ArCH₃), δ 1.81 (*t*, *J* = 6.80 Hz, 2H, ArCH₂CH₂), δ 1.32 (*s*, 6H, 2'*R*-CH₃)

¹³C-NMR (400MHz, CDCl₃) 150.1, 144.8, 140.2, 134.4, 129.7, 128.9, 128.3, 127.5, 123.6, 117.7, 73.25, 32.61, 26.81, 21.72, 20.96, 14.27, 13.54, 11.91

MS [ESI+] *m/z* 375.2 (M⁺H, 45%), 392.2 (M⁺NH₃, 100%), 397 (M⁺Na, 67%), 219.2 (M-Ts, 8%)

MS Calculated for C₂₁H₂₆O₄S 374.155

14.3.3 Synthesis of naphthalen-2-yl 4-methylbenzenesulfonate (**54**)

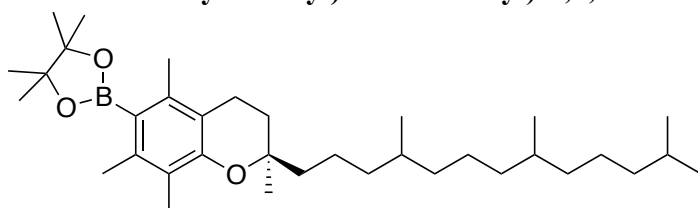


To 2-naphthol (300mg, 2.08mmol) and potassium carbonate (517mg, 3.74mmol) in water (5ml) / tetrahydrofuran (2ml) was added tosyl chloride in tetrahydrofuran (4ml) and the mixture stirred for 16h. The THF was evaporated and the residual mixture was extracted with CH₂Cl₂ 3x, the organic phases dried over Na₂SO₄ and evaporated down to dryness. Silica column chromatography (gradient Hexane/CH₂Cl₂ 6:1 to 1:1 to CH₂Cl₂) afforded **54** (620mg, 93.2%) as a light yellow oil.

TLC: R_f = 0.74 (CH₂Cl₂)

| | |
|---------------------|---|
| $^1\text{H-NMR}$ | (400MHz, CDCl_3) 7.83 (<i>s</i> , 1H, Ar-H), 7.76 (<i>s</i> , 4H, Ar-H), 7.52 (<i>s</i> , 3H, Ar-H), 7.31 (<i>s</i> , 2H, Ar-H), 7.14 (<i>s</i> , 1H, Ar-H), δ 2.45 (<i>s</i> , 3H, Ar-Ts- CH_3) |
| $^{13}\text{C-NMR}$ | (400MHz, CDCl_3) 147.2, 145.4, 133.5, 132.5, 131.9, 129.8, 129.7, 128.6, 127.9, 127.8, 126.8, 126.4, 121.2, 120.0, 21.73 |
| MS [EI+] | <i>m/z</i> 337.0 (M^+K , 32%), 321.1 (M^+Na , 32%), 316.1 (100%), MS Calculated for $\text{C}_{17}\text{H}_{14}\text{O}_3\text{S}$ 298.066 |

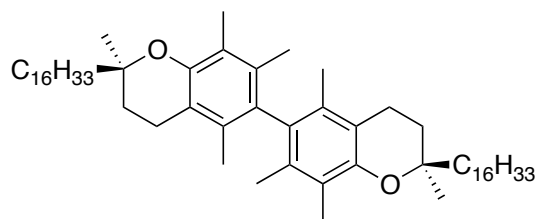
14.3.4 Synthesis of 4,4,5,5-tetramethyl-2-((2*R*)-2,5,7,8-tetramethyl-2-(4,8,12-trimethyltridecyl)chroman-6-yl)-1,3,2-dioxaborolane (**56**)



70 (42mg, 0.078mmol) in dry DMSO (0.46ml) with bis(pinacolato)diborone (43mg, 0.17mmol), $\text{PdCl}_2(\text{dppf})$ (6.3mg, 0.0078mmol) and potassium carbonate (32.2mg, 0.233mmol) was heated to 80°C and stirred for 16h. The reaction was cooled to room temperature and extracted with ether and water and the organic phase was washed an additional three times with water. The organic phase was dried over Na_2SO_4 and evaporated down to dryness. The crude product was purified by silica column chromatography (gradient Hex, to Hex/ CH_2Cl_2 1:1) afforded **56** (15mg 35.7%) as a clear oil.

| | |
|---------------------|---|
| TLC: | R_f = 0.34 (Hex/ CH_2Cl_2 , 1:1) |
| $^1\text{H-NMR}$ | (400MHz, CDCl_3) δ 2.57 (<i>t</i> , J = 6.80 Hz, 2H, ArCH_2CH_2), δ 2.28 (<i>s</i> , 6H, ArCH_3), δ 2.25 (<i>s</i> , 3H, ArCH_3), δ 2.07 (<i>s</i> , 3H, ArCH_3), δ 1.78 (enant. <i>dt</i> , J = 6.80 Hz, 2H, ArCH_2CH_2), δ 1.64-1.07 (<i>m</i> , 33H, $\text{phytyl-CH/CH}_2 + 2'\text{-R-CH}_3 + \delta$ 1.41 pinacole CH_3 4x) δ 8.88 (<i>m</i> , 12H, phytyl-CH_3) |
| $^{13}\text{C-NMR}$ | (400MHz, CDCl_3) 152.5, 138.1, 137.1, 121.9, 121.4, 116.7, 83.41, 74.95, 39.74, 39.66, 39.38, 37.58, 37.56, 37.47, 37.41, 37.38, 37.33, 37.30, 32.79, 32.74, 32.73, 31.50, 31.46, 29.71, 27.99, 25.05, 24.82, 24.46, 23.93, 22.73, 22.64, 21.05, 20.34, 19.76, 19.74, 19.70, 19.68, 19.63, 19.57, 19.51, 18.56, 11.32 |
| MS [ESI+] | <i>m/z</i> 541.5 (M^+1 , 100%), 563.4 (M^+Na , 95%) MS Calculated for $\text{C}_{35}\text{H}_{61}\text{BO}_3$ 540.471 |

Byproduct (2*R*,2'*R*)-2,2'-dihexadecyl-2,2',5,5',7,7',8,8'-octamethyl-6,6'-bichroman (**66**)



TLC: $R_f = 0.08$ (Hex/ CH_2Cl_2 , 10:1)

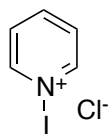
$^1\text{H-NMR}$ (400 MHz, CDCl_3) δ 2.64 (*t*, $J = 6.80$, 4H, ArCH_2CH_2), δ 2.15 (*s*, 6H, ArCH_3), δ 1.86 (*enant dt*, 4H, $J = 6.80$), δ 1.76 (*s*, 3H, ArCH_3), δ 1.75 (*s*, 3H, ArCH_3), δ 1.72 (*s*, 3H, ArCH_3), δ 1.71 (*s*, 3H, ArCH_3), δ 1.67-1.10 (*m*, 21H, $\text{phytyl-CH/CH}_2+2'R\text{-CH}_3$), δ 0.88 (*t*, $J = 6.80$, 12 H, phytyl-CH_3)

$^{13}\text{C-NMR}$ (400 MHz, CDCl_3) 149.9, 133.3, 132.7, 131.6, 121.3, 116.5, 74.67, 39.39, 37.44, 37.41, 37.31, 32.82, 32.80, 32.69, 31.62, 27.99, 24.82, 24.45, 23.80, 22.73, 22.64, 21.06, 20.89, 19.77, 19.70, 19.61, 16.64, 15.71, 11.97

MS [ESI+] m/z 827.8 (M, 100%), 585.4 (54%)

MS Calculated for $\text{C}_{58}\text{H}_{98}\text{O}_2$ 826.757

14.3.5 Synthesis of 1-iodopyridin-1-ium chloride (71)



In an Erlenmeyer flask a solution of acetic acid (45ml) and pyridine (1.49ml, 0.0185mol) was cooled to 0°C and iodochloride (0.92ml, 0.0185) was added dropwise. A yellow precipitate formed, the reaction stirred for 15min at 0°C and was then filtrated and washed with acetic acid (120ml) until most of the red colour disappeared. The yellow crystals were suspended in methanol (35ml), heated until they dissolved, filtered hot and washed with hot methanol (20ml). The red solution was cooled for 30min. The suspension was filtrated at room temperature and washed three times with methanol (3x 20ml). The yellow filamentous crystals were dried. The mother liquor was cooled in the fridge for 20min. filtrated and washed with cold methanol. The second mother liquor was kept in the fridge for 2 days and filtered.

Crystal 1: 977mg, + 2: 647mg, + 3: 844mg = 55.4% of **71**)

TLC: $R_f = 0.2$ (CH_2Cl_2)

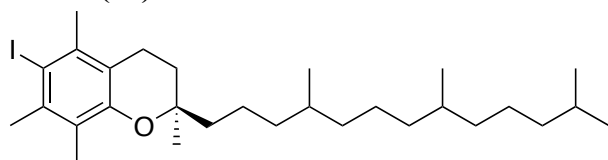
$^1\text{H-NMR}$ (400MHz, Acetone- D_6) 8.84 (*dd*, $J = 6.40$ Hz, $J = 1.60$ Hz, 2H, Ar-pyridine-H), δ 8.25 (*tt*, $J = 7.60$ Hz, $J = 1.60$ Hz, 1H, Ar-pyridine-H), 8.01 (*d*, $J = 6.40$ Hz, $J = 1.20$ Hz, 2H, Ar-pyridine-H)

^{13}C -NMR (400MHz, Acetone- D_6) 148.6, 140.5, 127.2

MS [ESI+] m/z 205.9 (M-Cl, 100%)

MS Calculated for $\text{C}_4\text{H}_4\text{NICl}$ 240.916

14.3.6 Synthesis of (2*R*)-6-iodo-2,5,7,8-tetramethyl-2-(4,8,12-trimethyltridecyl)chroman (70)



42 (126mg, 0.303mmol) and 1-iodopyridin-1-ium chloride (69mg, 0.303mmol) were stirred in methanol (3ml) for 5h at room temperature. The yellow / white emulsion was evaporated and the residue extracted with CH_2Cl_2 and water. The phases were separated and the water phase was washed 3x with CH_2Cl_2 . The organic phases were combined and dried over Na_2SO_4 and dried down to dryness. Silica column chromatography (Hex to Hex/ CH_2Cl_2 10:1) afforded **70** (131mg 78.1%) as a clear oil.

TLC: R_f = 0.48 (Hexane)

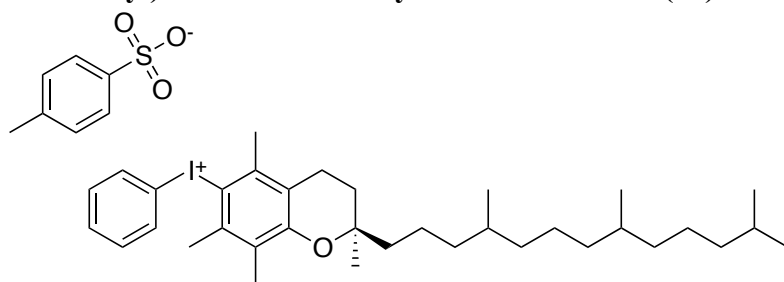
^1H -NMR (400MHz, CDCl_3) δ 2.70 (*t*, J = 6.80 Hz, 2H, ArCH_2CH_2), δ 2.50 (*s*, 3H, ArCH_3), δ 2.45 (*s*, 3H, ArCH_3), δ 2.22 (*s*, 3H, ArCH_3), δ 1.80 (enant. *dt*, J = 6.80 Hz, 2H, ArCH_2CH_2), δ 1.65-1.08 (*m*, 21H, phytyl-CH/ CH_2 + 2'*R*- CH_3) δ 8.88 (*m*, 12H, phytyl- CH_3)

^{13}C -NMR (400MHz, CDCl_3) 151.8, 137.9, 136.8, 123.5, 118.0, 99.48, 75.67, 39.91, 39.82, 39.38, 37.54, 37.46, 37.41, 37.37, 37.30, 32.81, 32.79, 32.69, 31.51, 31.45, 28.00, 26.97, 26.02, 24.83, 24.45, 23.81, 22.74, 22.64, 22.41, 21.04, 19.76, 19.70, 19.66, 19.60, 13.46

MS [EI+] m/z 540.4 (M, 100%), 414.5 (M, 16%), 275.0 (M, 68%)

HRMS Calculated for $\text{C}_{29}\text{H}_{49}\text{OI}$ 540.2828; found: 540.2823

14.3.7 Synthesis of phenyl((2*R*)-2,5,7,8-tetramethyl-2-(4,8,12-trimethyltridecyl)chroman-6-yl)iodonium 4-methylbenzenesulfonate (**69**)



To a suspension of *p*-toluenesulfonic acid monohydrate (458mg, 2.41 mmol) in acetonitrile (7ml) was added (diacetoxy)iodobenzene (776mg, 2.41mmol) added. Chloroform (70ml) was quickly added and the whole mixture directly transferred to a sealable flask with **42** (1g, 2.41mmol). The remaining mixture was washed into the reaction flask with some chloroform (10ml). The yellow reaction mixture was heated to 50°C and stirred for 16h under a N₂ atmosphere. The solvents were evaporated. No crystallisation occurred upon ether addition. The crude product was purified by silica column chromatography (CH₂Cl₂ to CH₂Cl₂/MeOH, 9:1) afforded **69** (404mg 21.4%) as a light yellow oil.

TLC: R_f = 0.2 (CH₂Cl₂/MeOH, 9:0.5)

¹H-NMR (400MHz, CDCl₃) δ 7.72 (*d*, *J* = 7.60 Hz, 2H, Ar-Ts-H), δ 7.69 (*d*, *J* = 7.60 Hz, 2H, Benzene-H), δ 7.48 (*t*, *J* = 7.60 Hz, 1H, Benzene-H), δ 7.37 (*t*, *J* = 7.60 Hz, 2H, Benzene-H) δ 7.11 (*d*, *J* = 7.60 Hz, 2H, Ar-Ts-H), δ 2.68 (*t*, *J* = 6.80 Hz, 2H, ArCH₂CH₂), δ 2.58 (*s*, 6H, ArCH₃), δ 2.34 (*s*, 3H, Ar-Ts-CH₃), δ 2.19 (*s*, 3H, ArCH₃), δ 1.83 (*enant. dt*, *J* = 6.80 Hz, 2H, ArCH₂CH₂), δ 1.64-1.07 (*m*, 21H, phytyl-CH/CH₂ + 2'*R*-CH₃) δ 8.87 (*m*, 12H, phytyl-CH₃)

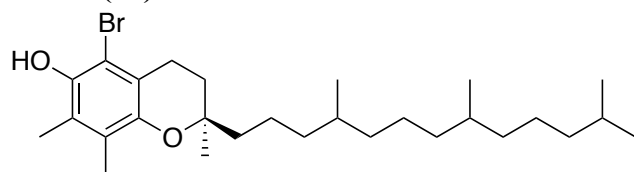
¹³C-NMR (400MHz, CDCl₃) 155.9, 142.7, 139.5, 138.9, 138.8, 132.3, 131.8, 131.0, 128.5, 126.0, 125.9, 119.8, 116.6, 114.8, 76.88, 40.18, 39.37, 37.46, 37.39, 37.29, 32.80, 32.70, 27.99, 25.05, 24.81, 24.45, 24.25, 23.86, 22.73, 22.63, 22.29, 21.33, 21.01, 20.77, 19.75, 19.69, 19.63, 19.57, 13.66

MS [EI+] *m/z* 617.3 (M⁺ - TsO 100%)

MS [EI-] *m/z* 171.0 (TsO⁻, 100%)

MS Calculated for C₄₂H₆₁O₄IS 788.334

14.3.8 Synthesis of (2*R*)-5-bromo-2,7,8-trimethyl-2-(4,8,12-trimethyltridecyl)chroman-6-ol (76)



γ -Tocopherol (273mg, 0.655mmol) was added as a solution in CH_2Cl_2 (20ml) to a stirring solution of tetrabutylammonium bromide (211mg, 0.655mmol) in CH_2Cl_2 (20ml). Bromine (33 μ l, 0.655mmol) was added and the solution stirred for 1h at room temperature. The solvent was evaporated and the crude mixture was purified by silica column chromatography (Hex/EE, 95:5) and afforded **76** (208mg 64.3%) as a light yellow oil.

TLC: R_f = 0.61 (Hex/EtOAc, 95:5)

$^1\text{H-NMR}$ (400MHz, CDCl_3) δ 5.21 (*s*, 1H, Ar-OH), δ 2.69 (*t*, 2H, J = 6.80 Hz, ArCH₂CH₂), δ 2.24 (*s*, 3H, ArCH₃), δ 2.11 (*s*, 3H, ArCH₃), δ 1.81 (*enant dt*, 1H, J = 17.6 Hz, J = 6.8 Hz, ArCH₂CH₂), δ 1.62-1.03 (*m*, 21H, phytyl CH₂), δ 0.88 (*m*, 12H, phytyl 4-CH₃)

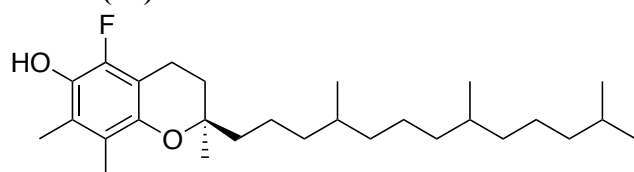
$^{13}\text{C-NMR}$ (400MHz, CDCl_3) 145.9, 143.4, 125.4, 122.4, 122.4, 117.3, 109.3, 75.42, 39.54, 39.38, 37.45, 37.41, 37.29, 32.81, 32.68, 31.05, 27.99, 24.81, 24.45, 24.08, 23.69, 22.73, 22.64, 20.99, 19.76, 19.66, 12.98, 11.85

MS [ESI+] m/z 495.3 (M-H, 100%)

MS [ESI-] m/z 493.2 (M-H, 100%)

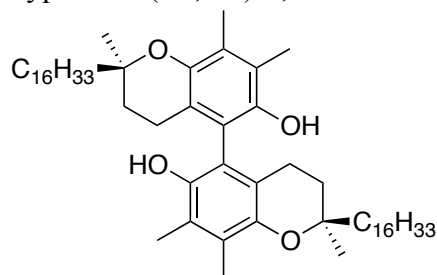
MS calculated for C₂₈H₄₇O₂Br 494.276

14.3.9 Synthesis of (2*R*)-5-fluoro-2,7,8-trimethyl-2-(4,8,12-trimethyltridecyl)chroman-6-ol (48)



γ -Tocopherol (200mg, 0.48mmol) and N-fluorobenzenesulfonimide (151mg, 0.48mmol) were stirred in dry THF (2ml) under N₂ at 0°C for 1.5h. The yellow solution was quenched by addition of 1M HCl. CH_2Cl_2 was added to the red mixture, stirred for 5min and the phases separated. The organic phase was evaporated and purified by silica column chromatography (gradient Hex/ CH_2Cl_2 2:1, CH_2Cl_2 to CH_2Cl_2 /MeOH 9:1). and afforded **74** (10mg, 2.5%) as a brown oil and **75** (78mg, 22.8%) as a brown oil. Product **48** was not produced.

Byproduct (2*R*,2'*R*)-2,2'-dihexadecyl-2,2',7,7',8,8'-hexamethyl-[5,5'-bichroman]-6,6'-diol (74)



TLC: $R_f = 0.7$ (Hex/ CH_2Cl_2 1:1)

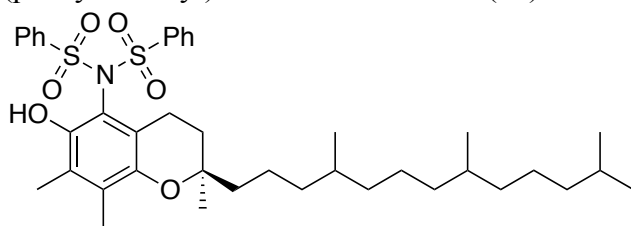
$^1\text{H-NMR}$ (400MHz, CDCl_3) δ 4.44 (*s*, 1H, Ar-OH), δ 2.20 (*enant dt*, 1H, $J = 17.6$ Hz, $J = 6.8$ Hz, ArCH_2CH_2), δ 2.22 (*s*, 3H, ArCH_3), δ 2.20 (*s*, 3H, ArCH_3), δ 2.17 (*enant dt*, 1H, $J = 17.6$ Hz, $J = 6.8$ Hz, ArCH_2CH_2), δ 1.74 (*enant dt*, 1H, $J = 6.8$ Hz, ArCH_2CH_2), δ 1.65 (*enant dt*, $J = 17.6$ Hz, $J = 6.8$ Hz, 1H, ArCH_2CH_2), δ 1.61-1.07 (*m*, 21H, phytyl CH_2), δ 0.88 (*m*, 12H, phytyl 4- CH_3)

$^{13}\text{C-NMR}$ (400MHz, CDCl_3) 145.9, 122.6, 126.9, 122.2, 117.5, 115.2, 75.16, 40.12, 39.39, 37.48, 37.44, 37.30, 32.82, 32.68, 31.37, 27.99, 24.82, 24.47, 23.76, 22.74, 22.64, 20.96, 20.62, 19.76, 19.65, 12.29, 11.99

MS [ESI-] m/z 829.8 (M^- H, 100%)

MS calculated for $\text{C}_{56}\text{H}_{94}\text{O}_4$ 830.715

Byproduct *N*-((2*R*)-6-hydroxy-2,7,8-trimethyl-2-(4,8,12-trimethyltridecyl)chroman-5-yl)-*N*-(phenylsulfonyl)benzenesulfonamide (75)



TLC: $R_f = 0.36$ (Hex/ CH_2Cl_2 1:1)

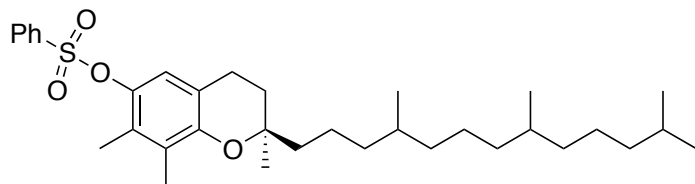
$^1\text{H-NMR}$ (400MHz, CDCl_3) δ 8.05 (*dd*, $J = 7.60$ Hz, $J = 1.60$ Hz, 4H, Ph-H), δ 8.05 (*t*, $J = 7.60$ Hz, $J = 1.60$ Hz, 2H, Ph-H), δ 7.58 (*t*, $J = 7.60$ Hz, $J = 1.60$ Hz, 4H, Ph-H), δ 5.61 (*s*, 1H, Ar-OH), δ 2.24 (*s*, 3H, ArCH_3), δ 2.20 (*t*, 2H, $J = 7.2$ Hz, ArCH_2CH_2), δ 2.15 (*s*, 3H, ArCH_3), δ 1.86 (*enant dt*, 2H, $J = 6.8$ Hz, ArCH_2CH_2), δ 1.45-1.09 (*m*, 21H, phytyl CH_2), δ 0.88 (*m*, 12H, phytyl 4- CH_3)

$^{13}\text{C-NMR}$ (400MHz, CDCl_3) 146.2, 145.8, 139.5, 139.4, 134.22, 129.8, 129.0, 125.6, 120.7, 118.4, 75.65, 40.32, 39.37, 37.47, 37.29, 32.81, 32.70, 30.81, 27.98, 24.81, 24.48, 24.09, 22.73, 22.63, 20.94, 19.75, 19.64, 19.08, 12.73, 12.54

MS [ESI+] m/z 734.4 (M^+ Na, 100%), 750.3 (M^+ Na, 46%)

MS calculated for C₄₀H₅₇NO₆S 711.363

Byproduct (2*R*)-2,7,8-trimethyl-2-(4,8,12-trimethyltridecyl)chroman-6-yl benzenesulfonate (77)



γ -Tocopherol (38mg, 91.2 μ mol) was dissolved in dry THF (2ml) under N₂ and cooled to 0°C. Sodium hydride (3.6mg, 91.2 μ mol) was added to the solution and stirred for 5min. N-fluorobenzenesulfonimide (58mg, 0.18mmol) was added. After 5min was the reaction quenched with methanol and 1M HCl, the solvents evaporated and extracted with CH₂Cl₂ and water. The organic phase was dried over Na₂SO₄ and purified by silica column chromatography (gradient Hex/CH₂Cl₂ 3:1 to Hex/CH₂Cl₂ 1:1) and afforded **cc** (28.7mg, 56.6%) as a clear oil.

TLC: R_f = 0.33 (Hex/CH₂Cl₂ 1:1)

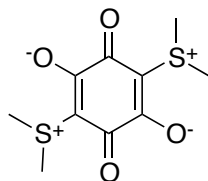
¹H-NMR (400MHz, CDCl₃) δ 7.89 (*d*, J = 6.40 Hz, 2H, SO₂ArCH), δ 7.68 (*t*, J = 6.40 Hz, 2H, SO₂ArCH), δ 7.55 (*t*, J = 6.40 Hz, 2H, SO₂ArCH), δ 6.61 (*s*, 1H, ArCH), δ 2.70 (*m*, J = 6.40 Hz, 2H, ArCH₂CH₂), 2.05 (*s* J = 1.60 Hz, 3H, ArCH₃), δ 1.90 (*s*, 3H, ArCH₃), δ 1.76 (enant. *dt*, J = 6.40 Hz, 2H, ArCH₂CH₂), δ 1.59-1.05 (*m*, 21H, phytyl-CH/CH₂ + 2'*R*-CH₃) δ 8.88 (*m*, 12H, phytyl-CH₃)

¹³C-NMR (400MHz, CDCl₃) 150.3, 140.6, 136.4, 133.9, 129.0, 128.6, 128.5, 126.2, 119.8, 118.5, 76.34, 40.20, 39.38, 37.46, 37.29, 32.81, 32.69, 30.93, 27.99, 24.81, 24.45, 24.12, 22.73, 22.64, 22.21, 20.98, 19.76, 19.66, 12.94, 11.96

MS [ESI+] m/z 579.3 (M⁺Na, 100%), m/z 574.4 (M+NH₃, 39%),

MS calculated for C₃₄H₅₂O₄S 556.36

14.3.10 Synthesis of (2,5-dihydroxy-3,6-dioxocyclohexa-1,4-diene-1,4-diyl)bis(dimethylsulfonium) acetate (*S*-Ylide)



2,5-Dihydroxy-1,4-benzoquinone (1.4g, 10mmol), dimethylsulfoxide (5ml) and acetic anhydride (20ml) were stirred at 100°C for 1h. A yellow precipitate occurred. The reaction was

cooled to room temperature and stirred for an additional 3h. The suspension was filtered, washed with ethyl acetate, and light brown crystals were obtained.

$^1\text{H-NMR}$ (300MHz, H_2O) δ 2.98 (s, 12H, S^+CH_3), δ 1.99 (s, 3H, CH_3COOH),

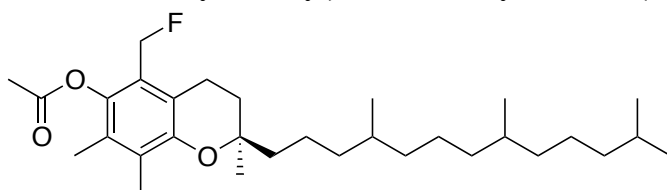
$^{13}\text{C-NMR}$ (75MHz, H_2O) 176.7, 176.2, 93.52, 24.58, 20.36

MS [EI+] m/z 261.0 (M-2H, 100%) 283.0 (M-2H + Na^+ , 18%)

MS [EI-] m/z 75.0 (100%), 59.1 (AcO^- , 4%),

MS Calculated for $\text{C}_{10}\text{H}_{14}\text{O}_4\text{S}_2$ 262.018

14.3.11 Synthesis of (2R)-5-(fluoromethyl)-2,7,8-trimethyl-2-(4,8,12-trimethyltridecyl)chroman-6-yl acetate (**78**)



(2R)-5-(Bromomethyl)-2,7,8-trimethyl-2-(4,8,12-trimethyltridecyl)chroman-6-ol (**77**) (51mg, 0.363mmol) and caesium fluoride (166mg, 1.09mmol) were stirred in *t*-butanol (2ml) at 80°C in a sealed vial under a nitrogen atmosphere for 16h. The *t*-butanol was evaporated and the reaction mixture was purified by silica column chromatography (gradient Hex/ CH_2Cl_2 4:1 to CH_2Cl_2) and afforded **78** (26.4mg 30.1%) as a clear oil.

TLC: R_f = 0.26 (Hex/ CH_2Cl_2 , 1:1)

$^1\text{H-NMR}$ (600MHz, CDCl_3) δ 5.31 (d, J = 47.2 Hz, 2H, Ar- CH_2F), δ 2.85 (t, J = 6.6 Hz, 2H, Ar CH_2), δ 2.38 (s, 3H, Ar CH_3), δ 2.16 (d, J = 3.0 Hz, 3H, Ar CH_3), δ 2.06 (s, 3H, Ac CH_3), δ 1.86 (p, J = 6.6 Hz 2H, Ar CH_2CH_2), δ 1.79 (p, J = 6.6 Hz 2H, Ar CH_2CH_2), δ 1.66-1.52 (m, 3H, R-CH), δ 1.49-1.09 (m, 21H, phytyl CH_2), δ 0.9-0.86 (m, 12H, phytyl 4- CH_3)

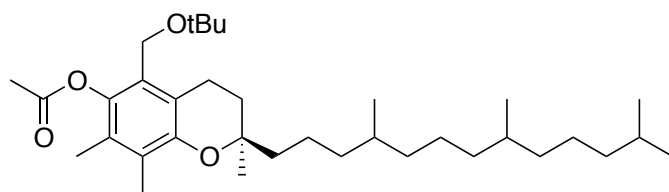
$^{13}\text{C-NMR}$ (600MHz, CDCl_3) 170.0, 169.9, 149.8, 141.3, 128.1, 127.6, 122.6, 118.7, 77.79, 75.78, 75.58, 39.40, 38.22, 37.42, 36.63, 33.18, 32.31, 28.42, 27.58, 24.84, 24.44, 23.99, 23.68, 23.17, 23.08, 22.32, 21.84, 20.98, 20.35, 20.12, 19.49, 19.26, 28.64, 14.27, 13.60, 13.43, 12.76, 12.58, 11.91, 11.74, 11.07

$^{19}\text{F-NMR}$ (600MHz, CDCl_3) 208.6 (t, J = 54 Hz, 1F, Ar- CH_2F)

MS [ESI+] m/z 508.2 (M^+NH_4 , %), 513.3 (M^+Na , %), 529.2 (M^+K , %),

MS calculated for $\text{C}_{31}\text{H}_{51}\text{O}_3\text{F}$ 490.382

Side product (2R)-5-(*tert*-butoxymethyl)-2,7,8-trimethyl-2-(4,8,12-trimethyltridecyl)chroman-6-yl acetate (**79**)



Mass amount: (12mg, 18%)

TLC: R_f = 0.06 (Hex/ CH_2Cl_2 , 1:1)

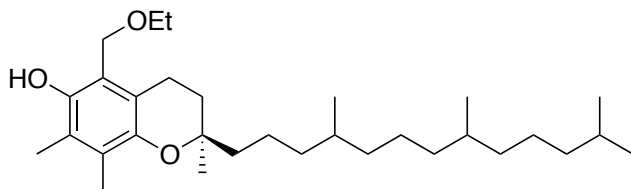
$^1\text{H-NMR}$ (400MHz, CDCl_3) δ 4.26 (*s*, 2H, Ar- CH_2OBu), δ 2.81 (*brs*, 2H, Ar CH_2), δ 2.33 (*s*, 3H, Ac CH_3), δ 2.10 (*s*, 3H, Ar CH_3), δ 2.02 (*s*, 3H, Ar CH_3), δ 1.80 (*enant dt*, J = 6.8 Hz 2H, Ar CH_2CH_2), δ 1.66-1.06 (*m*, 21H, phytyl- CH/CH_2 + 2' R-CH_3), δ 1.26 (*s*, 9H, - OCCH_3)
 δ 0.9-0.86 (*m*, 12H, phytyl 4- CH_3)

$^{13}\text{C-NMR}$ (400MHz, CDCl_3) 169.9, 149.8, 141.1, 127.6, 125.8, 125.3, 118.7, 75.25, 72.96, 55.98, 39.37, 37.39, 37.29, 32.78, 32.70, 30.93, 29.70, 27.97, 27.47, 24.80, 24.44, 22.72, 22.62, 21.02, 20.61, 19.74, 19.68, 19.58, 19.37, 14.11, 12.99, 12.07

MS [EI+] m/z 508.4 (M-*t*-Bu + Na, 45%), 471.4 (M-*t*-BuO, 100%)

MS calculated for $\text{C}_{35}\text{H}_{60}\text{O}_4$ 544.449

Side product (2*R*)-5-(ethoxymethyl)-2,7,8-trimethyl-2-(4,8,12-trimethyltridecyl)chroman-6-ol (**80**)



Mass amount: (61mg, 91%)

TLC: R_f = 0.58 (CH_2Cl_2 , 1:1)

$^1\text{H-NMR}$ (400MHz, CDCl_3) δ 7.73 (*s*, 1H, Ar-OH), δ 4.73 (*s*, 2H, Ar- CH_2), δ 3.63 (*q*, J = 6.80 Hz, 2H, O- $\text{CH}_2\text{-CH}_3$), δ 2.60 (*t*, 2H, J = 6.80 Hz, Ar CH_2), δ 2.18 (*s*, 3H, Ar CH_3), δ 2.14 (*s*, 3H, Ar CH_3), δ 1.80 (*enant dt*, J = 6.8 Hz, 2H, Ar CH_2CH_2), δ 1.65-1.08 (*m*, 24H, phytyl- CH/CH_2 + 2' R-CH_3 + O- $\text{CH}_2\text{-CH}_3$) δ 0.88 (*m*, 12H, phytyl 4- CH_3)

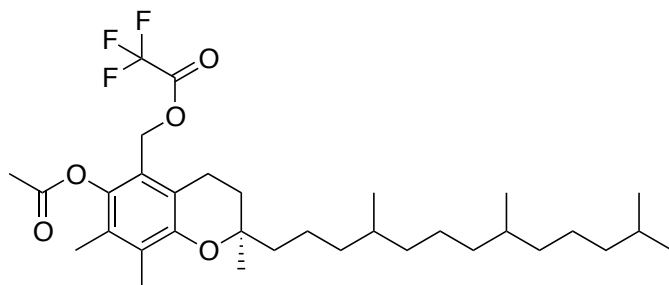
$^{13}\text{C-NMR}$ (400MHz, CDCl_3) 147.4, 144.6, 125.6, 123.1, 116.1, 115.2, 74.41, 68.03, 66.19, 39.83, 39.75, 39.37, 37.55, 37.46, 37.39, 32.78, 32.70, 31.39, 29.71, 27.98, 24.81, 24.45, 23.75, 22.75, 22.72, 22.63, 21.03, 19.94, 15.13, 14.13, 11.90, 11.70

MS [EI+] m/z 445.4 (M-Et, 60%), 391.3 (100%)

MS [ESI-] m/z 473.3 (M-H, 14%), 459.3 (M- CH_3 , 100%), 443.3 (M-Et, 39%)

MS calculated for C₃₁H₅₄O₃ 474.407

Side product ((2*R*)-6-acetoxy-2,7,8-trimethyl-2-(4,8,12-trimethyltridecyl)chroman-5-yl)methyl 2,2,2-trifluoroacetate (81)



Mass amount: (15mg, 23%)

TLC: R_f = 0.50 (CH₂Cl₂, 1:1)

¹H-NMR (400MHz, CDCl₃) δ 5.34 (*s*, 2H, Ar-CH₂OTFA), δ 2.60 (*brs*, 2H, ArCH₂CH₂), δ 2.35 (*s*, 3H, ArCH₃), δ 2.15 (*s*, 3H, ArCH₃), δ 2.05 (*s*, 3H, ArCH₃), δ 1.83 (*enant dt*, J = 6.8 Hz, 2H, ArCH₂CH₂), δ 1.65-1.08 (*m*, 21H, phytyl-CH/CH₂ + 2'*R*-CH₃) δ 0.88 (*m*, 12H, phytyl 4-CH₃)

¹³C-NMR (400MHz, CDCl₃) 169.7, (*q*, 158.1, 157.7, 157.2, 156.8), 149.9, 141.5, 128.5, 128.1, 120.3, 118.7, (*q*, 118.8, 115.9, 113.1, 110.3), 75.68, 61.94, 39.38, 37.52, 37.46, 37.41, 37.40, 37.37, 37.30, 32.79, 32.70, 32.67, 30.61, 29.72, 27.99, 24.83, 24.82, 24.45, 23.96, 22.73, 22.63, 21.00, 20.48, 19.75, 19.69, 19.64, 19.59, 13.08, 12.36

¹⁹F-NMR (400MHz, CDCl₃) -74.80 (*s*, 3F, COCF₃)

MS [ESI+] m/z 524.4 (100%)

MS calculated for C₃₃H₅₁O₅F 584.369

References

- ¹ Mattill, H. A., Conklin, R. A. The nutritive properties of milk, with special reference to reproduction in the albino rat. *J. Biol. Chem.* **44**, 137–158 (1920).
- ² Mattill, H. A., Stone, N. C. The nutritive properties of milk, with special reference to reproduction in the albino rat. II. *J. Biol. Chem.* **55**, 443–452 (1923)
- ³ Long, J. A., Evans, H. M. The oestrous cycle in the rat. *Memoirs of the California Academy of Sciences.* **6**, 1–320 (1922)
- ⁴ Evans, H. M., Bishop, K. S. On the existence of a hitherto unrecognized dietary factor essential for reproduction. *Science* **56**, 649–651 (1922)
- ⁵ Sure, B. Dietary requirement for reproduction. II. The existence of a specific vitamin for reproduction. *J. Biol. Chem.* **58**, 693–709 (1923).
- ⁶ Emerson, O. H., Emerson, G. A. The isolation from wheat germ oil of an alcohol, α -tocopherol, having the properties of vitamin E. *J. Biol. Chem.* **113**, 319–332 (1936).
- ⁷ Wolf, G. The discovery of the antioxidant function of vitamin E: the contribution of Henry A. Mattill. *J. Nutr.* **135**, 363–6 (2005).
- ⁸ Wolf, R., Wolf, D., Ruocco, V. Vitamin E: The radical protector. *J. Eur. Acad. Dermatology Venereol.* **10**, 103–117 (1998).
- ⁹ Fernholz, E. On the Constitution of α -Tocopherol. *J. Am. Chem. Soc.* **60**, 700–705 (1938).
- ¹⁰ DellaPenna, D. A decade of progress in understanding vitamin E synthesis in plants. *J. Plant Physiol.* **162**, 729–737 (2005).
- ¹¹ Traber, M. G.; Sies, H. Vitamin E in humans: Demand and Delivery. *Annu. Rev. Nutr.* **16**, 321 (1996).
- ¹² Sundram, K., Sambanthamurthi, R., Tan, Y. Palm fruit chemistry and nutrition Palm fruit chemistry and nutrition. *Asia Pacific J. Clin. Nutr.* **12**, 355–362 (2003).
- ¹³ http://www.palmoilworld.org/about_malaysian-industry.html, (2011)
- ¹⁴ Biesalski., H. K. Mikronährstoffe als Motor der Evolution. *Springer Berlin Heidelberg*, P.38 (2015).
- ¹⁵ Sundram, K., Sambanthamurthi, R., Tan, Y. Palm fruit chemistry and nutrition. **12**, 355–362 (2003).

-
- ¹⁶ Flumerfelt, R. W. Vitamins, 4. Vitamin E Tocopherols Tocotrienols. *ULLMANN's Encycl. Ind. Chem.* 390–411 (2012).
- ¹⁷ Hess JL. Vitamin E α -tocopherol. In: Alscher RG, Hess JL, editors. Antioxidants in higher plants. Boca Raton, FL: CRC p. 111–34 (1993)
- ¹⁸ Speek, A. J., Schrijver, J., Schreurs, W. H. P. Vitamin E Composition of Some Seed Oils as Determined by High-Performance Liquid Chromatography with Fluorometric Detection. *J. Food Sci.* **50**, 121–124 (1985).
- ¹⁹ Barnes, P. J., Taylor, P. W. The composition of acyl lipids and tocopherols in wheat germ oils from various sources. *J. Sci. Food Agric.* **31**, 997–1006 (1980).
- ²⁰ Taylor P, Barnes P. Analysis of vitamin E in edible oils by high performance liquid chromatography. *Chem Ind* 1981:722–6.
- ²¹ Sundl, I., Murkovic, M., Bandoniene, D., Winklhofer-Roob, B. M. Vitamin E content of foods: Comparison of results obtained from food composition tables and HPLC analysis. *Clin. Nutr.* **26**, 145–153 (2007).
- ²² Traber, M. G., Atkinson, J. Vitamin E, antioxidant and nothing more. *Free Radic. Biol. Med.* **43**, 4–15 (2007).
- ²³ COMP/E-1/37.512 Vitamine EWR: K(2001) 3695) *European commission* **6**, 01–89 (2003)
- ²⁴ DSM Naamloze Vennootschap. *DSM annual report*. P.1-214 (2015).
- ²⁵ Tsao, G. T., Ouyang, P., Chen, J. *Biotechnology in China II: Chemicals, Energy and Environment*. (Springer Berlin Heidelberg, 2010) p 16.
- ²⁶ Carril, M., Altmann, P., Drees, M., Bonrath, W., Netscher, T., Schütz, J., Kühn, F. E. Methyltrioxorhenium-catalyzed oxidation of pseudocumene for vitamin e synthesis: A study of solvent and ligand effects. *J. Catal.* **283**, 55–67 (2011).
- ²⁷ Campo, D. E. L., Javier, F., Pascual, M., Xavier, F. European patent application. EP 2 050 743 A1 **1**, 1–27 (2011).
- ²⁸ Mercier, C., Chabardes, P. Organometallic chemistry in industrial vitamin A and vitamin E synthesis. *Pure & Appl. Chem* **66**, 1509–1518 (1994).
- ²⁹ Leth, T., Sondergaard, H. Biological activity of all-rac- α -tocopherol and RRR- α -tocopherol determined by three different rat bioassays. *Int. J. Vitam. Nutr. Res.* **53**, 297–311 (1983).
- ³⁰ Muller, R. K., Schneider, H. Aminomethylation of tocopherols. (2000).
- ³¹ Paull, D. H., Dogo-isonagie, C., Lectka, T. Diastereoselective Synthesis of α -Tocopherol *Synlett* 1651–1654 (2009).

-
- ³² Odínokov, V. N., Spivak, A. Y., Emelyanova, G. A., Mallyabaeva, M. I., Nazarova, O. V., Dzhemilev, U. M. Synthesis of α -tocopherol (vitamin E), vitamin K1-chromanol, and their analogs in the presence of aluminosilicate catalysts Tseokar-10 and Pentasil. *Arkivoc* **2003**, 101–118 (2003).
- ³³ Tietze, L. F., Stecker, F., Zinngrebe, J., Sommer, K. M. Enantioselective palladium-catalyzed total synthesis of vitamin E by employing a domino Wacker-Heck reaction. *Chem. - A Eur. J.* **12**, 8770–8776 (2006).
- ³⁴ Carmen Carreño, M., Hernández-Torres, G., Ribagorda, M., Urbano, A., Andersen, K. K. Enantiopure sulfoxides: recent applications in asymmetric synthesis. *Chem. Commun.* **86**, 6129 (2009).
- ³⁵ Bienaymé, H., Ancel, J. E., Meilland, P., Simonato, J. P. Rhodium(I)-catalyzed addition of phenols to dienes. A new convergent synthesis of vitamin E. *Tetrahedron Lett.* **41**, 3339–3343 (2000).
- ³⁶ Bonrath, W., Dittel, C., Giraudi, L., Netscher, T., Pabst, T. Rare earth triflate catalysts in the synthesis of Vitamin E and its derivatives. *Catal. Today* **121**, 65–70 (2007).
- ³⁷ Bonrath, W. & Netscher, T. Catalytic processes in vitamins synthesis and production. *Appl. Catal. A Gen.* **280**, 55–73 (2005).
- ³⁸ Netscher, T., Malaisé, G., Bonrath, W., Breuninger, M. A new route to Vitamin E key-intermediates by olefin cross-metathesis. *Catal. Today* **121**, 71–75 (2007).
- ³⁹ Termath, A. O., Velder, J., Stemmler, R. T., Netscher, T. Bonrath, W., Schmalz, H-G. Total synthesis of (2R)- α -tocopherol through Ni-catalyzed 1,4-addition to a chromenone intermediate. *European J. Org. Chem.* **2014**, 3337–3340 (2014).
- ⁴⁰ Termath, A. O., Sebode, H., Schlundt, W., Stemmler, R. T., Netscher, T., Bonharth, W., Schmalz, H-G. Total synthesis of (R,R,R)- α -tocopherol through asymmetric Cu-catalyzed 1,4-addition. *Chemistry* **20**, 12051–12055 (2014).
- ⁴¹ Uria, U., Vila, C., Lin, M. Y., Rueping, M. Gold-catalyzed asymmetric allylic substitution of free alcohols: An enantioselective approach to chiral chromans with quaternary stereocenters for the synthesis of Vitamin E and analogues. *Chem. - A Eur. J.* **20**, 13913–13917 (2014).
- ⁴² Grafen, P. D., Kiefer, H. D., Jaedicke, H. D. Verfahren zur herstellung von vitamin E. *DE4208477 A1* (1993).
- ⁴³ Baak, M., Bonrath, W., Kreienbuhl, P. Process for the synthesis of vitamin E. *US6066745A* (2000).
- ⁴⁴ Cohen, N., Eichel, W. F., Lopresti, R. J., Neukom, C., Saucy, G. Synthetic studies on (2R,4'R,8'R)- α -tocopherol. An alternative synthesis of (2R,6R)-(+)-2,6,10-trimethylundecan-1-ol, a key side chain synthon. *J. Org. Chem.* **41**, 3512–3515 (1976).

-
- ⁴⁵ Barner, R. Schmid, M. Totalsynthese von natürlichem α -Tocopherol 4. Aufbau des Chromanringsystems aus Trimethylhydrochinon und einem optisch aktiven C4 bzw. C5-Synthon *Helvetica chimica acta* **62**, 2384–2399 (1979).
- ⁴⁶ Schmierer, R., Helmchen, S. A total synthesis of enantiomerically pure vitamin E side chain using a chiral propionate synthon. *Tetrahedron let.* **24**, 1235–1238 (1983).
- ⁴⁷ Heathcock, C. H., Jarvi, E. T., Acyclic stereoselection: Sequential aldol-claisen as a method for 1,S-stereoselection. Total synthesis of the vitamin E side chain. *Tetrahedron Lett.* **23**, 2825–2828 (1982).
- ⁴⁸ Matsumoto, A., Takahashi, S., Nakano, K., and Kijima, S. Identification of a New Vitamin E in a Plant Oil, *J. Jpn. Oil Chem. Soc.* **44**, 593–597 (1995).
- ⁴⁹ Mariani, C.; Bellan, G., Presence of tocopherol derivatives in vegetable oils. *Rivista Italiana delle Sostanze Grasse* **74**, 545–552 (1997)
- ⁵⁰ Mei, H. N., Yuen, M. C., Ah, N. M., Cheng, H. C., Hashim, M. A. Separation of vitamin E (tocopherol, tocotrienol, and tocomonoenol) in palm oil. *Lipids* **39**, 1031–1035 (2004).
- ⁵¹ Butinar, B., Bučar-Miklavčič, M., Mariani, C., Raspor, P. New vitamin E isomers (gamma-tocomonoenol and alpha-tocomonoenol) in seeds, roasted seeds and roasted seed oil from the Slovenian pumpkin variety ‘Slovenska golica’. *Food Chem.* **128**, 505–512 (2011).
- ⁵² Fiorentino, A., Mastellone, C., D’Abrosca, B., Pacifico, S., Scognamiglio, M., Cefarelli, G., Caputo, R., Manaco, P. δ -Tocomonoenol: A new vitamin E from kiwi (*Actinidia chinensis*) fruits. *Food Chem.* **115**, 187–192 (2009).
- ⁵³ Sroka, Z., Cisowski, W. Hydrogen peroxide scavenging, antioxidant and anti-radical activity of some phenolic acids. *Food Chem. Toxicol.* **41**, 753–758 (2003).
- ⁵⁴ Brand-Williams, W., Cuvelier, M. E., Berset, C. Use of a free radical method to evaluate antioxidant activity. *LWT - Food Sci. Technol.* **28**, 25–30 (1995).
- ⁵⁵ Dasgupta, N., De, B. Antioxidant activity of Piper betle L. leaf extract in vitro. *Food Chem.* **88**, 219–224 (2004).
- ⁵⁶ Yamamoto, Y., Fujisawa, A., Hara, A., Dunlap, W. C. An unusual vitamin E constituent (alpha-tocomonoenol) provides enhanced antioxidant protection in marine organisms adapted to cold-water environments. *Proc. Natl. Acad. Sci. U. S. A.* **98**, 13144–13148 (2001).
- ⁵⁷ MacCrehan, W. A., Schönberger, E. Determination of retinol, alpha-tocopherol, and beta-carotene in serum by liquid chromatography with absorbance and electrochemical detection. *Clin. Chem.* **33**, 1585–1592 (1987).

-
- ⁵⁸ Wu, E. S., Jacobson, K., Papahadjopoulos, D. Lateral diffusion in phospholipid multibilayers measured by fluorescence recovery after photobleaching. *Biochemistry* **16**, 3936–3941 (1977).
- ⁵⁹ Serbinova, E., Kagan, V., Han, D., Packer, L. Free radical recycling and intramembrane mobility in the antioxidant properties of alpha-tocopherol and alpha-tocotrienol *Free Radical Biol. Med.* **10**, 263–275, (1991).
- ⁶⁰ Gotoh, N., Watanabe, H., Oka, T., Mashimo, D. Noguchi, N., Hata, K. Wada, S. Dietary marine-derived tocopherol has a higher biological availability in mice relative to alpha-tocopherol. *Lipids* **44**, 133–143 (2009).
- ⁶¹ Ingold, K. U., Burton, G. W., Foster, D. O., Hughes, L., Lidsay, D. A., Webb, A. Biokinetics of and discrimination between dietary RRR and SRR- α -tocopherols in the male rat. *Lipids* **22**, 163–172, (1987)
- ⁶² Herrmann, K. M., Weaver, L. M. The shikimate pathway. *Annu Rev Plant Physiol Plant Mol Biol* **50**, 473–503 (1999).
- ⁶³ Coggins, J. R., Abell, C., Evans, L. B., Frederickson, M., Robinson, D. A., Roszak, A. W., Laphorn, A. P. Experiences with the shikimate-pathway enzymes as targets for rational drug design. *Biochem. Soc. Trans.* **31**, 548–552 (2003).
- ⁶⁴ Herrmann, K. M., Weaver, L. M. The shikimate pathway. *Annu Rev Plant Physiol Plant Mol Biol* **50**, 473–503 (1999).
- ⁶⁵ Nakayama, S., Watanabe, H. On the mechanism of the chorismate mutase reaction. *Microbiology* **188**, 3121–3125 (2006).
- ⁶⁶ Bonvin, J., Aponte, R. A., Marcantonio, M., Singh, S., Christendat, D., Turnbull, J. L. Biochemical characterization of prephenate dehydrogenase from the hyperthermophilic bacterium *Aquifex aeolicus*. *Protein Sci.* **15**, 1417–32 (2006).
- ⁶⁷ Eisenreich, W., Bacher, A., Arigoni, D., Rohdich, F. Biosynthesis of isoprenoids via the non-mevalonate pathway. *Cell. Mol. Life Sci.* **61**, 1401–1426 (2004).
- ⁶⁸ Rohmer, M., Rohmer, M. The discovery of a mevalonate-independent pathway for isoprenoid biosynthesis in bacteria, algae and higher plants. *Nat. Prod. Rep.* **16**, 565–574 (1999).
- ⁶⁹ Hofius, D., Sonnewald, U. Vitamin E biosynthesis: Biochemistry meets cell biology. *Trends Plant Sci.* **8**, 6–8 (2003).
- ⁷⁰ Mahmood Hussain, M. A proposed model for the assembly of chylomicrons. *Atherosclerosis* **148**, 1–15 (2000).
- ⁷¹ Stocker, A. Molecular mechanisms of vitamin E transport. *Ann. N. Y. Acad. Sci.* **1031**, 44–59 (2004).

-
- ⁷² Frank, J. Beyond vitamin E supplementation: An alternative strategy to improve vitamin E status. *J. Plant Physiol.* **162**, 834–843 (2005).
- ⁷³ Schmölz, L., Birringer, M., Lorkowski, S., Wallert, M. Complexity of vitamin E metabolism. *World J. Biol. Chem.* **7**, 14–43 (2016).
- ⁷⁴ Traber, M. G., Kayden, H. J. Preferential incorporation of alpha-tocopherol vs gamma-tocopherol in human lipoproteins. *Am. J. Clin. Nutr.* **49**, 517–26 (1989).
- ⁷⁵ Traber, M. G. Burton, G. W., Huges, L., Ingold, K. U., Hidaka, H., Malloy, M., Kane, J., Hyams, J., Kayden, H. J. Discrimination between forms of vitamin E by humans with and without genetic abnormalities of lipoprotein metabolism. *J. Lipid Res.* **33**, 1171–82 (1992).
- ⁷⁶ Bjorneboe, A., Bjorneboe, G. E., Bodd, E., Hagen, B. F., Kveseth, N; Drevon, C. A. Secretion of alpha-tocopherol from cultured rat hepatocytes *Biochem. Biophys. Acta.*, **3**, 310-315, (1986)
- ⁷⁷ Chung, S., Ghelfi, M., Atkinson, J., Parker, R., Qian, J., Carlin, C., Manor, D. Vitamin E and phosphoinositides regulate the intracellular localization of the hepatic α -tocopherol transfer protein. *J. Biol. Chem.* **291**, 17028–17039 (2016).
- ⁷⁸ Kono, N., Ohto, U., Hiramatsu, T., Urabe, M., Uchida, Y., Satow, Y., Arai, H. Impaired α -TTP-PIPs Interaction Underlies Familial Vitamin E Deficiency. *Science* **340**, 1106–1110 (2013).
- ⁷⁹ Goti, D., Reicher, H., Malle, E., Kostner, G. M., Panzenboeck, U., Sattler, W. High-density lipoprotein (HDL3)-associated alpha-tocopherol is taken up by HepG2 cells via the selective uptake pathway and resecreted with endogenously synthesized apo-lipoprotein B-rich lipoprotein particles. *Biochem. J.* **332**, 57–65 (1998).
- ⁸⁰ Kayden, J. Vitamin E is delivered to cells via the high affinity. *Am. J. Clin. Nutr.* **40**, 747–751 (1984).
- ⁸¹ Schultz, M., Leist, M., Petrzika, M., Gassmann, B., Brigelius-Flohé, R. Novel urinary metabolite of alpha-tocopherol, 2,5,7,8-tetramethyl-2(2'-carboxyethyl)-6-hydroxychroman, as an indicator of an adequate vitamin E supply? *Am. J. Clin. Nutr.* **62**, 1527S–1534S (1995).
- ⁸² Pope, S. A. S., Burtin, G. E., Clayton, P. T., Madge, D. J., Muller, D. P. R. Synthesis and analysis of conjugates of the major vitamin E metabolite, α -CEHC. *Free Radic. Biol. Med.* **33**, 807–817 (2002).
- ⁸³ Bardowell, S. A., Duan, F., Manor, D., Swanson, J. E., Parker, R. S. Disruption of mouse cytochrome P450 4f14 (Cyp4f14 gene) causes severe perturbations in vitamin E metabolism. *J. Biol. Chem.* **287**, 26077–26086 (2012).

-
- ⁸⁴ Zhao, Y., Lee, M.-J., Cheung, C., Ju, J.-H., Chen, Y.-K., Liu, B., Hu, L.-Q. Analysis of multiple metabolites of tocopherols and tocotrienols in mice and humans. *J. Agric. Food Chem.* **58**, 4844–4852 (2010).
- ⁸⁵ Lebold, K. M., Ang, A., Traber, M. G., Arab, L. Urinary α -carboxyethyl hydroxychroman can be used as a predictor of α -tocopherol adequacy, as demonstrated in the Energetics Study. *Am. J. Clin. Nutr.* **96**, 801–809 (2012).
- ⁸⁶ Bruno, R. S., Ramakrishnan, R., Montine, T. J., Bray, T. M., Traber, M. G. α -Tocopherol disappearance is faster in cigarette smokers and is inversely related to their ascorbic acid status. *Am. J. Clin. Nutr.* **81**, 95–103 (2005).
- ⁸⁷ Sharma, G., Muller, D. P., O’Rinda, S. M., Bryan, S., Dattani, M. T., Hindmarsh, P. C., Mills, K. Urinary conjugated α -tocopheronolactone - a biomarker of oxidative stress in children with type 1 diabetes. *Free Radic. Biol. Med.* **55**, 54–62 (2013).
- ⁸⁸ Catignani, G. L. An α -Tocopherol binding protein in rat liver cytoplasm. *Biochem. Biophys. Res. Comm.* **65**, 66–72 (1975).
- ⁸⁹ Catignani, G. L., Bieri, J. G. Rat Liver α -Tocopherol Binding Protein *Biochimica et Biophysica Acta* **497**, 349–357 (1977).
- ⁹⁰ Arita, M., Sato, Y., Miyata, A., Tanabe, T., Takahashi, E., Kayden, H. J., Arai, H., Inoue, K. Human α -tocopherol transfer protein: cDNA cloning, expression and chromosomal localization. *Biochem. J.* **306**, 437–443 (1995).
- ⁹¹ Copp, R. P., Wisniewski, T., Hentati, F., Larnaout, A., Hamida, M. B., Kayden, H. J. Localization of α -tocopherol transfer protein in the brains of patients with ataxia with vitamin E deficiency and other oxidative stress related neurodegenerative disorders. *Brain Res.* **822**, 80–7 (1999).
- ⁹² Saito, K., Tautz, L., Mustelin, T. The lipid-binding SEC14 domain. *Biochim. Biophys. Acta - Mol. Cell Biol. Lipids* **1771**, 719–726 (2007).
- ⁹³ Sato, Y., Arai, H., Miyata, A., Tokitas, S., Tanabe, T. Primary Structure of α -Tocopherol Transfer Protein from Rat Liver. *J. Biol. Chem.* **268**, 17705–17710 (1993).
- ⁹⁴ Meier, R., Tomizaki, T., Schulze-Briese, C., Baumann, U., Stocker, A. The molecular basis of vitamin E retention: Structure of human α -tocopherol transfer protein. *J. Mol. Biol.* **331**, 725–734 (2003).
- ⁹⁵ Merkulova, M., Huynh, H., Radchenko, V., Saito, K., Valery, L., Shuvaeva, T., Mustelin, T. Secretion of the mammalian Sec14p-like phosphoinositide-binding p45 protein. *FEBS J.* **272**, 5595–5605 (2005).
- ⁹⁶ Min, K. C., Kovall, R. A., Hendrickson, W. A. Crystal structure of human α -tocopherol transfer protein bound to its ligand: implications for ataxia with vitamin E deficiency. *Proc. Natl. Acad. Sci. U. S. A.* **100**, 14713–14718 (2003).

-
- ⁹⁷ Hosomi, A., Arita, M., Sato, Y., Kiyose, C., Ueda, T., Igarashi, O., Arai, H., Inoue, K. Affinity for α -tocopherol transfer protein as a determinant of the biological activities of vitamin E analogs. *FEBS Lett.* **409**, 105–108 (1997).
- ⁹⁸ Leth, T., Sondergaard, H. Biological activity of vitamin E compounds and natural materials by the resorption-gestation test, and chemical determination of the vitamin E activity in foods and feeds. *J. Nutr.* **107**, 2236–2243 (1977).
- ⁹⁹ Panagabko, C., Morley, S., Hernandez, M., Cassolato, P., Gordon, H., Parsons, R., Manor, D., Atkinson, J. Ligand specificity in the CRAL-TRIO protein family. *Biochemistry* **42**, 6467–6474 (2003).
- ¹⁰⁰ Zhang, W. X. Thakur, V., Lomize, A., Pogozheva, I., Panagabko, C., Cecchini, M., Baptist, M., Morley, S., Manor, D., Atkinson, J. The contribution of surface residues to membrane binding and Ligand transfer by the α -tocopherol transfer protein (α -TTP) *J. Mol. Biol.* **405**, 972–988 (2011).
- ¹⁰¹ Lamprakis, C., Stocker, A., Cascella, M. Mechanisms of recognition and binding of α -TTP to the plasma membrane by multi-scale molecular dynamics simulations. *Front. Mol. Biosci.* **2**, 36 (2015).
- ¹⁰² Voegelé, A. F., Jerkovic, L., Wellenzohn, B., Eller, P., Kronenberg, F., Liedl, K. R., Dieplinger, H. Characterization of the vitamin E-binding properties of human plasma afamin. *Biochemistry* **41**, 14532–14538 (2002).
- ¹⁰³ Seeber, B. E. Czech, T., Buchner, H., Rarnhart, K. T., Seger, C., Daxenbichler, G., Wildt, L., Dieplinger, H. The vitamin E-binding protein afamin is altered significantly in the peritoneal fluid of women with endometriosis. *Fertil. Steril.* **94**, 2923–2926 (2010).
- ¹⁰⁴ Manor, D. & Morley, S. in *Vitamin E* **76**, 45–65 (2007).
- ¹⁰⁵ Cavalier, L., Ouahchi, K., Kayden, H. J., Donato, S. D., Reutenauer, L., Mandel, J-L., Koenig, M. Ataxia with isolated vitamin E deficiency: heterogeneity of mutations and phenotypic variability in a large number of families. *Am. J. Hum. Genet.* **62**, 301–310 (1998).
- ¹⁰⁶ Schuelke, M., Finckh, B., Sistiernans, E. A., Hu, C. Ataxia with vitamin E deficiency : Biochemical effects of malcompliance with. 1584–1587 (2000).
- ¹⁰⁷ Mariotti, C., Gellera, C., Rimoldi, M., Mineri, R., Uziel, G., Zorzi, G., Pareyson, D., Piccolo, G., Gambi, D., Picentini, S., Squitieri, F., Capra, R., Castellotti, B., Di Donato, S. Ataxia with isolated vitamin E deficiency: neurological phenotype, clinical follow-up and novel mutations in *TTPA* gene in Italian families. *Neurol. Sci.* **25**, 130–137 (2004).
- ¹⁰⁸ Hentati, A., Deng, H-X., Hung, W-Y., Nayer, M., Ahmed, S. M., He, X., Tim, R., Stumpf, D. A., Siddique, T. Human alpha-tocopherol transfer protein: gene structure and mutations in familial vitamin E deficiency. *Ann. Neurol.* **39**, 295–300 (1996).

-
- ¹⁰⁹ Usuki, F., Maruyama, K. Ataxia caused by mutations in the alpha-tocopherol transfer protein gene. *J. Neurol. Neurosurg. Psychiatry* **69**, 254–256 (2000).
- ¹¹⁰ Urano, S., Asai, Y., Makabe, S., Matsuo, M., Izumiyama, N., Ohtsubo, K., Endo, T. Oxidative injury of synapse and alteration of antioxidative defense systems in rats, and its prevention by vitamin E. *Eur. J. Biochem.* **245**, 64–70 (1997).
- ¹¹¹ Ulatowski, L., Parker, R., Warriar, G., Sultana, R., Butterfield, D. A. Manor, D. Vitamin E is essential for Purkinje neuron integrity. *Neuroscience* **260**, 120–129 (2014).
- ¹¹² Haber, F., Weiss, J. Über die Katalyse des Hydroperoxydes. *Naturwissenschaften* **20**, 948–950 (1932).
- ¹¹³ Imlay, J. A., Linn, S. DNA damage and oxygen radical toxicity. *Science* **240**, 1302–1309 (1988).
- ¹¹⁴ Golden, N., Bagiada, N. A., Darmadipura, S. Lipid Peroxidation After Intracortical Injection of Ferric Chloride Increases the Incidence of Seizures in Young Rats. (2014).
- ¹¹⁵ Schor, N. F. Inactivation of mammalian brain glutamine synthetase by oxygen radicals. *Brain Res.* **456**, 17–21 (1988).
- ¹¹⁶ Davenport Jones, J. E., Fox, R. M., Atterwill, C. K. NMDA-induced increases in rat brain glutamine synthetase but not glial fibrillary acidic protein are mediated by free radicals. *Neurosci. Lett.* **247**, 37–40 (1998).
- ¹¹⁷ George-Hyslop, P. S. Alzheimer disease. *Neurobiol. Dis.* **7**, 546–548 (2000).
- ¹¹⁸ Zuo, L., Hemmelgarn, B. T., Chuang, C. C., Best, T. M. The Role of Oxidative Stress-Induced Epigenetic Alterations in Amyloid- β Production in Alzheimer's Disease. *Oxid. Med. Cell. Longev.* **2015**, (2015).
- ¹¹⁹ Lee, D. W., Andersen, J. K. Iron elevations in the aging Parkinsonian brain: A consequence of impaired iron homeostasis? *J. Neurochem.* **112**, 332–339 (2010).
- ¹²⁰ Lan, J., Jiang, D. H. Desferrioxamine and vitamin E protect against iron and MPTP-induced neurodegeneration in mice. *J. Neural Transm.* **104**, 469–481 (1997).
- ¹²¹ Navarro, A., Bandez, M. J., Lopez-Cepero, J. M., Gómez, C., Boveris, A. D., Cadenas, E., Boveris, A. High doses of vitamin E improve mitochondrial dysfunction in rat hippocampus and frontal cortex upon aging. *Am. J. Physiol. Regul. Integr. Comp. Physiol.* **300**, 827–834 (2011).
- ¹²² Lezoualc'h, F., Sparapani, M., Behl, C. N-acetyl-serotonin (normelatonin) and melatonin protect neurons against oxidative challenges and suppress the activity of the transcription factor NF-kB. *J. Pineal. Res.* **24**, 168–178 (1998).

-
- ¹²³ Siu, A. W., Cheung, J. P., To, C. H., Chan, E. K., Chan, J. K., Cheung, J. C. N-acetyl-serotonin reduces copper (I) ion-induced lipid peroxidation in bovine retinal homogenates. *Acta Ophthalmol. Scand.* **79**, 69–71 (2001).
- ¹²⁴ Rumbaugh, R. C., Colby, H. D., Wright, J. R., Miles, P. R. The relationship between Chemiluminescence and Lipid peroxidation in Rat hepatic microsomes. *Arch. Biochem and Biophys.* **192**, 344–351 (1979).
- ¹²⁵ Gavazza, M., Catalá, A. Relative efficacies of α -tocopherol, N-acetyl-serotonin, and melatonin in reducing non-enzymatic lipid peroxidation of rat testicular microsomes and mitochondria. *Mol. Cell. Biochem.* **321**, 37–43 (2009).
- ¹²⁶ Nakamizo, T., Urushitani, M., Inoue, R., Shinohara, A., Sawada, H., Honda, K., Kihara, T., Akaike, A., Shimohama, S. Protection of cultured spinal motor neurons by estradiol. *Neuroreport* **11**, 3493–7 (2000).
- ¹²⁷ Sawada, H., Ibi, M., Kihara, T., Urushitani, M., Akaike, A., Shimohama, S. Estradiol protects mesencephalic dopaminergic neurons from oxidative stress-induced neuronal death. *J. Neurosci. Res.* **54**, 707–719 (1998).
- ¹²⁸ Behl, C. Vitamin E protects neurons against oxidative cell death in vitro more effectively than 17-beta estradiol and induces the activity of the transcription factor NF-kappaB. *J. Neural Transm.* **107**, 393–407 (2000).
- ¹²⁹ Monroe, E. B., Jurchen, J. C., Lee, J., Rubakhin, S. S., Sweedler, J. V. Vitamin E imaging and localization in the neuronal membrane. *J. Am. Chem. Soc.* **127**, 12152–12153 (2005).
- ¹³⁰ Southam, E., Thomas, P. K., King, R. H. M., Goss-Sampson, M. A., Muller, D. P. R. Experimental Vitamin E Deficiency in Rats. *Brain* **114**, 915–936 (1991).
- ¹³¹ Bourre, J. M., Clement, M. Kinetics of rat peripheral nerve, forebrain and cerebellum alpha-tocopherol depletion: comparison with different organs. *J Nutr* **121**, 1204–7. (1991).
- ¹³² Hosomi, A., Goto, K., Kondo, H., Iwatsubo, T., Yokota, T., Ogawa, M., Arita, M., Aoki, J., Arai, H., Inoue, K. Localization of α -tocopherol transfer protein in rat brain. *Neurosci. Lett.* **256**, 159–162 (1998).
- ¹³³ Yu, C., Youmans, K. L., LaDu, M. J. Proposed mechanism for lipoprotein remodelling in the brain. *Biochim. Biophys. Acta - Mol. Cell Biol. Lipids* **1801**, 819–823 (2010).
- ¹³⁴ Vatassery, G. T., Quach, H. T., Smith, W. E., SantaCruz, K. S., Roy, S. Apolipoprotein e deficiency leads to altered brain uptake of alpha tocopherol injected into lateral cerebral ventricles. *Biochim. Biophys. Acta - Mol. Basis Dis.* **1772**, 797–803 (2007).
- ¹³⁵ Vance, J. E., Hayashi, H. Formation and function of apolipoprotein E-containing lipoproteins in the nervous system. *Biochim. Biophys. Acta - Mol. Cell Biol. Lipids* **1801**, 806–818 (2010).

-
- ¹³⁶ Alberts B, Johnson A, Lewis J, Raff, M., Roberts, K., Walter, P. Molecular Biology of the Cell. 4th edition. *New York: Garland Science*; (2002)
- ¹³⁷ Wilson, S. M., Bacic, A. Preparation of plant cells for transmission electron microscopy to optimize immunogold labeling of carbohydrate and protein epitopes. *Nat. Protoc.* **7**, 1716–1727 (2012).
- ¹³⁸ Abbe, E. Beiträge zur Theorie des Mikroskops und der mikroskopischen Wahrnehmung. *Archiv für Mikroskopische Anatomie* **9**, 413–418 (1873)
- ¹³⁹ Rayleigh, Lord. On the theory of optical images, with special reference to the microscope. *Phil. Mag.* **42**, 167–195 (1896)
- ¹⁴⁰ Punshon, T., Guerinot, M. Lou, Lanzirotti, A. Using synchrotron X-ray fluorescence microprobes in the study of metal homeostasis in plants. *Ann. Bot.* **103**, 665–672 (2009).
- ¹⁴¹ Gianoncelli, A., Vaccari, L., Kourousias, G., Cassese, D., Bedolla, D. E., Kenig, S., Storici, P., Lazzarino, M., Kiskinova, M. Soft X-Ray Microscopy Radiation Damage On Fixed Cells Investigated With Synchrotron Radiation FTIR Microscopy. *Sci. Rep.* **5**, 10250 (2015).
- ¹⁴² Siemann, D. W., Keng, P. C. Cell Cycle Specific Toxicity of the Hoechst 33342 Stain in Untreated or Irradiated Murine Tumor Cells. *Cancer Res.* **46**, 3556–3559 (1986).
- ¹⁴³ Krishna, M. Role of special stains in diagnostic liver pathology. *Clin. Liver Dis.* **2**, 8–10 (2013).
- ¹⁴⁴ Day, C. E. Histopathology: Methods and Protocols *Histopathology*. **1180**, (2014).
- ¹⁴⁵ Ettinger, A., Wittmann, T. Fluorescence Live Cell Imaging. *Methods Cell Biol.* **123**, 77–94 (2015).
- ¹⁴⁶ Nutting, P. G. Purity and intensity of MONOmonochromatic light. 439–456 (1906).
- ¹⁴⁷ Raymond, K., Sell, H. Revolution in lamps: a chronicle of 50 years of progress 2nd ed. *Fairmount press inc.* 1-275 (2001)
- ¹⁴⁸ Jonkman, J. & Brown, C. M. Any way you slice it - A comparison of confocal microscopy techniques. *J. Biomol. Tech.* **26**, 54–65 (2015).
- ¹⁴⁹ Bewersdorf, J., Egner, A., Hell, S. W. 4Pi-Confocal Microscopy Is coming of Age. *Imaging Microsc.* 24–25 (2004).
- ¹⁵⁰ Rouquette, J., Cremer, C., Cremer, T., Fakan, S. Functional nuclear architecture studied by microscopy: Present and future. *Int. Rev. Cell Mol. Bio.* **282**, 1-90 (2010).
- ¹⁵¹ Hell, S. & Stelzer, E. H. K. Properties of a 4Pi confocal fluorescence microscope. *J. Opt. Soc. Am. A* **9**, 2159 (1992).

-
- ¹⁵² Hell, S. W., Wichmann, J. Breaking the diffraction resolution limit by Stimulated-Emission-Depletion Fluorescence Microscopy. *Opt. Lett.* **19**, 780–782 (1994).
- ¹⁵³ Weljie, A. M., Vogel, H. J. Calcium-Binding Protein Protocols: Volume 2: Methods and Techniques. Steady-State Fluorescence Spectroscopy. *Methods in Molecular Biology* **173**, 75–87
- ¹⁵⁴ Lakowicz, J. R. in Principles of Fluorescence Spectroscopy *Springer US* 187–215 (1983).
- ¹⁵⁵ Mustroph, H. & Ernst, S. Das Franck-Condon-Prinzip: Wer kennt es heute noch? *Chemie Unserer Zeit* **45**, 256–269 (2011).
- ¹⁵⁶ Jabłoński, A. Über den Mechanismus der Photolumineszenz von Farbstoffphosphoren. *Zeitschrift für Phys.* **94**, 38–46 (1935).
- ¹⁵⁷ Turro, N. J., Ramamurthy, V. & Scaiano, J. C. *Principles of Molecular Photochemistry: An Introduction*. (2009).
- ¹⁵⁸ Jabłoński, A. Über den Mechanismus der Photolumineszenz von Farbstoffphosphoren. *Zeitschrift für Phys.* **94**, 38–46 (1935).
- ¹⁵⁹ Photochemistry.worldpress.com
<https://photochemistry.files.wordpress.com/2009/08/jablonski.png?w=630>
- ¹⁶⁰ Fouquet, C., Gilles, J-F., Heck, N., Dos Santos, M., Schwartzmann, R., Cannaya, V, Morel, M-P., Davidson, R. S., Trembleau, A. Bolte, S. Improving axial resolution in confocal microscopy with new high refractive index mounting media. *PLoS One* **10**, 1–17 (2015).
- ¹⁶¹ Strickler, S. J., Berg, R. A. Relationship between Absorption Intensity and Fluorescence Lifetime of Molecules. *J. Chem. Phys.* **37**, 814 (1962).
- ¹⁶² Thomas, J. V., Brimijoin, M. R., Neault, T. R., Brubaker, R. F. The fluorescent indicator pyranine is suitable for measuring stromal and cameral pH in vivo. *Exp. Eye Res.* **50**, 241–249 (1990).
- ¹⁶³ Mohammed, O. F., Dreyer, J., Magnes, B. Z., Pines, E., Nibbering, E. T. J. Solvent-dependent photoacidity state of pyranine monitored by transient mid-infrared spectroscopy. *ChemPhysChem* **6**, 625–636 (2005).
- ¹⁶⁴ Liu, L., Wang, A., Wang, G., Muniyentwari, A., Zhou, Y. Solvent-dependent fluorescence enhancement and piezochromism of a carbazole-substituted naphthopyran. *J. Lumin.* **165**, 159–166 (2015).
- ¹⁶⁵ Kalyanasundaram, K., Thomas, J. K. Solvent-dependent fluorescence of pyrene-3-carboxaldehyde and its applications in the estimation of polarity at micelle-water interfaces. *J. Phys. Chem.* **81**, 2176–2180 (1977).

-
- ¹⁶⁶ Haus, J. *Optische Mikroskopie: Funktionsweise und Kontrastierverfahren*. Wiley VCH Verlag GmbH, (2014).
- ¹⁶⁷ Watson, D., Hagen, N., Diver, J., Marchand, P., Chachisvilis, M. Elastic Light Scattering from Single Cells: Orientational Dynamics in Optical Trap. *Biophys. J.* **87**, 1298–1306 (2004).
- ¹⁶⁸ Mischenko, M., Travis, L., Lacis, A. Scattering, absorption, and emission of light by small particles. *NASA Goddard Inst. Sp. Stud.* 1–128 (2002).
- ¹⁶⁹ Horvath, H. Gustav Mie and the scattering and absorption of light by particles: Historic developments and basics. *J. Quant. Spectrosc. Radiat. Transf.* **110**, 787–799 (2009).
- ¹⁷⁰ Yushanov, B. Y. S., Crompton, J. S., Koppenhoefer, K. C., Scattering of Electromagnetic Waves by Particles. *AltaSim Technologies* 142–43 (2014).
- ¹⁷¹ Hale, G. M., Querry, M. R. Optical Constants of Water in the 200-nm to 200-microm Wavelength Region. *Appl. Opt.* **12**, 555–563 (1973).
- ¹⁷² Tyler, J. E., Smith, R. C., Wilson, W. H. J. Predicted optical properties for clear natural water. *J. Opt. Soc. Am.* **62**, 83–91 (1972).
- ¹⁷³ Clarke, G. L., James, H. R. Laboratory Analysis of the Selective Absorption of Light by Sea Water. *J. Opt. Soc. Am.* **29**, 43 (1939).
- ¹⁷⁴ Quickenden, T. I., Irvin, J. A. The ultraviolet absorption spectrum of liquid water. *J. Chem. Phys.* **72**, 4416–4428 (1980).
- ¹⁷⁵ Held, P. Quantitation of Peptides and Amino Acids with a SynergyTM HT using UV Fluorescence. *BioTek Appl. Note* 1–8 (2006).
- ¹⁷⁶ Jacques, S. L. Optical properties of biological tissues: a review. *Phys. Med. Biol.* **58**, R37–R61 (2013).
- ¹⁷⁷ Cleaver, J. E., Thomas, G. H., Burki, H. J. Biological damage from intranuclear tritium: DNA strand breaks and their repair. *Science* **177**, 996–998 (1972).
- ¹⁷⁸ Norris, K. H. *KC Smith, ed., Plenum Press*, **1977**, p. 400
- ¹⁷⁹ Chen, T. R. In situ detection of mycoplasma contamination in cell cultures by fluorescent Hoechst 33258 stain. *Exp. Cell Res.* **104**, 255–262 (1977).
- ¹⁸⁰ Tanious, F. A., Veal, J. M., Buczak, H., Ratmeyer, L. S., Wilson, W. D. DAPI (4',6-diamidino-2-phenylindole) binds differently to DNA and RNA: minor-groove binding at AT sites and intercalation at AU sites. *Biochemistry* **31**, 3103–3112 (1992).

-
- ¹⁸¹ Greenspan, P., Mayer, E. P., Fowler, S. D. Nile red: a selective fluorescent stain for intracellular lipid droplets, *J. Cell Biol.* **100** (1985) 965–973. *J. Cell Biol.* **100**, 965–973 (1985).
- ¹⁸² Duarte, F. J. Tunable Lasers Handbook ed. 1 *Optics and Photonics* (1995).
- ¹⁸³ Brackmann, U. Lambdachrom[®] Laser dyes. *Lambdachrom[®] 3th ed.* (2000).
- ¹⁸⁴ Duckett, J. G., Read, D. J. The use of the fluorescent dye, 3,3'- dihexyloxacarbocyanine iodide, for selective staining of ascomycete fungi associated with liverwort rhizoids and ericoid mycorrhizal roots. *New Phytol.* **118**, 259–272 (1991).
- ¹⁸⁵ Soltys, B. J., Gupta, R. S. Interrelationships of endoplasmic reticulum, mitochondria, intermediate filaments, and microtubules--a quadruple fluorescence labeling study. *Biochem. Cell Biol.* **70**, 1174–1186 (1992).
- ¹⁸⁶ Darzynkiewicz, Z. Simultaneous analysis of cellular RNA and DNA content. *Methods Cell Biol.* **41**, 401–20 (1994).
- ¹⁸⁷ Lecoecur, H. Nuclear apoptosis detection by flow cytometry: influence of endogenous endonucleases. *Exp. Cell Res.* **277**, 1–14 (2002).
- ¹⁸⁸ Kolmakov, K., Belov, V. N., Bierwagen, J., Ringemann, C., Müller, V., Eggeling, C., Hell, S. W. Red-emitting rhodamine dyes for fluorescence microscopy and nanoscopy. *Chem. - A Eur. J.* **16**, 158–166 (2010).
- ¹⁸⁹ Drexhage, K. H. H. Fluorescence efficiency of laser dyes. *J. Res. Natl. Bur. Stand. Sect. A Phys. Chem.* **80A**, 421 (1976).
- ¹⁹⁰ Taneja, L., Sharma, A. K., Singh, R. D. Study of photophysical properties of Coumarins: substituent and concentration dependence. *J. Lumin.* **63**, 203–214 (1995).
- ¹⁹¹ Shi, J. M., Zhang, X. P., Neckers, D. C. Xanthenes - Fluorone Derivatives. 2. *J. Org. Chem.* **57**, 4418–4421 (1992).
- ¹⁹² Levitus, M., Ranjit, S. Cyanine dyes in biophysical research: the photophysics of polymethine fluorescent dyes in biomolecular environments. *Q. Rev. Biophys.* **44**, 123–151 (2011).
- ¹⁹³ Banerjee, S., Veale, E. B., Phelan, C. M., Murphey, S. A., Tocci, G. M., Gillespie, L. J., Frimannsson, D. O., Kelly, J. M., Gunnlaugsson, T. Recent advances in the development of 1,8-naphthalimide based DNA targeting binders, anticancer and fluorescent cellular imaging agents. *Chem. Soc. Rev.* **42**, 1601–1618 (2013).
- ¹⁹⁴ Peurtz, M. F. Dye Lasers in the Ultraviolet. *Nature* **228**, 726–734 (1970).
- ¹⁹⁵ Parker, C. A., Rees, W. T. Correction of fluorescence spectra and measurement of fluorescence quantum efficiency. *Analyst* **85**, 587 (1960).

-
- ¹⁹⁶ Ghazy, R., Zim, S. A., Shaheen, M., El-Mekawey, F. Energy transfer and excited state lifetime of some anthracene laser dyes. *Opt. Laser Technol.* **36**, 463–469 (2004).
- ¹⁹⁷ Heidt, J. R. Luminescence and Laser Properties of the 10-Phenyl-9-acetoxanthracene Derivatives. *Z. Naturforsch.* **1205**, 1197–1205 (1983).
- ¹⁹⁸ Shimomura, O. The discovery of green fluorescent protein. *J. Microsc.* **217**, 3–15 (2005).
- ¹⁹⁹ Chalfie, M., Tu, Y., Euskirchen, G., Ward, W. W. & Prasher, D. C. Green fluorescent protein as a marker for gene expression. *Science* **263**, 802–805 (1994).
- ²⁰⁰ Heim, R., Tsien, R. Y. Engineering green fluorescent protein for improved brightness, longer wavelengths and fluorescence resonance energy transfer. *Curr. Biol.* **6**, 178–182 (1996).
- ²⁰¹ Nava, P., Ceccini, M., Chirico, S., Gordon, H., Morley, S., Manor, D., Atkinson, J. Preparation of fluorescent tocopherols for use in protein binding and localization with the α -tocopherol transfer protein. *Bioorganic Med. Chem.* **14**, 3721–3736 (2006).
- ²⁰² Chattopadhyay, A. Chemistry and biology of N-(7-nitrobenz-2-oxa-1,3-diazol-4-yl)-labeled lipids: fluorescent probes of biological and model membranes. *Chem. Phys. Lipids* **53**, 1–15 (1990).
- ²⁰³ Ulrich, G., Zissel, R., Harriman, A. The chemistry of fluorescent bodipy dyes: Versatility unsurpassed. *Angew. Chemie - Int. Ed.* **47**, 1184–1201 (2008).
- ²⁰⁴ Bittman, R. The 2003 ASBMB-Avanti Award in Lipids Address: Applications of novel synthetic lipids to biological problems. *Chem. Phys. Lipids* **129**, 111–131 (2004).
- ²⁰⁵ Johnson, I. D., Kang, H. C., Haugland, R. P. Fluorescent membrane probes incorporating dipyrrometheneboron difluoride fluorophores. *Anal. Biochem.* **198**, 228–237 (1991).
- ²⁰⁶ West, R., Panagabko, C., Atkinson, J. Synthesis and characterization of BODIPY- α -tocopherol: a fluorescent form of vitamin E. *J. Org. Chem.* **75**, 2883–92 (2010).
- ²⁰⁷ Zhang, W. X., Frahm, G., Morley, S., Manor, D., Atkinson, J. Effect of bilayer phospholipid composition and curvature on ligand transfer by the α -tocopherol transfer protein. *Lipids* **44**, 631–641 (2009).
- ²⁰⁸ López, G. V., Gomez, L. E., Campillo, N., Paez, J. A., Giles, K., Atkinson, J., Gonzales, M., Rubbo, H., Cerecetto, H. Interaction studies between human α -tocopherol transfer protein and nitric oxide donor tocopherol analogues with LDL-protective activity. *Bioorganic Med. Chem.* **17**, 8143–8148 (2009).
- ²⁰⁹ Morley, S., Cross, V., Ceccini, M., Nava, P., Atkinson, J., Manor, D. Utility of a fluorescent vitamin E analogue as a probe for tocopherol transfer protein activity. *Biochemistry* **45**, 1075–1081 (2006).

-
- ²¹⁰ Qian, J., Wilson, K., Nava, P., Morley, S., Atkinson, J., Manor, D. Intracellular localization of α -tocopherol transfer protein and α -tocopherol. *Ann. N. Y. Acad. Sci.* **1031**, 330–331 (2004).
- ²¹¹ Morley, S., Ceccini, M., Zhang, W., Virgulti, A., Noy, N., Atkinson, J., Manor, M. Mechanisms of ligand transfer by the hepatic tocopherol transfer protein. *J. Biol. Chem.* **283**, 17797–17804 (2008).
- ²¹² Ulatowski, L. M. Regulation of Vitamin E and the Tocopherol Transfer Protein. *Case Western Reserve University* (2012).
- ²¹³ McCary, C. A., Yoon, Y., Panagabko, C., Cho, W., Atkinson, J., Cook-Mills, J. M. Vitamin E isoforms directly bind PKC α and differentially regulate activation of PKC α . *Biochem J* **441**, 189–198 (2012).
- ²¹⁴ Churchward, M. A., Rogasevskaja, T., Brandman, D. M., Houman, K., Nava, P., Atkinson, J. K., Coorssen, J. R. Specific lipids supply critical negative spontaneous curvature - an essential component of native Ca²⁺-triggered membrane fusion. *Biophys J* **94**, 3976–3986 (2008).
- ²¹⁵ Qian, J., Atkinson, J., Manor, D. Biochemical consequences of heritable mutations in the α -tocopherol transfer protein. *Biochemistry* **45**, 8236–8242 (2006).
- ²¹⁶ Buyukcakil, O., Bozdemir, O. A., Kolen, S., Erbas, S., Akkaya, E. U. Tetraethyl-bodipy dyes: Convenient synthesis and characterization of elusive near IR fluorophores. *Org. Lett.* **11**, 4644–4647 (2009).
- ²¹⁷ Sun, Z. B., Guo, M., Zhao, C. H. Synthesis and Properties of Benzothieno[b]-Fused BODIPY Dyes. *J. Org. Chem.* **81**, 229–237 (2016).
- ²¹⁸ Ulrich, G., Goeb, S., De Nicola, A., Retailleau, P., Ziessel, R. Chemistry at boron: Synthesis and properties of red to near-IR fluorescent dyes based on boron-substituted diisindolomethene frameworks. *J. Org. Chem.* **76**, 4489–4505 (2011).
- ²¹⁹ Roy, I., Shin, J.-Y., Shetty, D., Khedkar, J. K., Park, J. H., Kim, K. E-Bodipy fluorescent chemosensor for Zn²⁺ ion. *J. Photochem. Photobiol. A Chem.* **331**, 233–239 (2016).
- ²²⁰ Davies, L. H., Harrington, R. W., Clegg, W., Higham, L. J. B R 2 BodPR 2 : highly fluorescent alternatives to PPh₃ and PhPCy₂. *Dalt. Trans.* **43**, 13485 (2014).
- ²²¹ Woodward, R. B. Structure and absorption spectra. IV. Further observations on α,β -unsaturated ketones. *J. Am. Chem. Soc.* **64**, 76–77 (1942).
- ²²² Fieser, L. F., Fieser, M., Rajagopalan, S. Absorption spectroscopy and the structures of the diosterols. *J. Org. Chem.* **13**, 800–806 (1948).

-
- ²²³ Arroyo, I. J., Hu, R., Tang, B. Z., López, F. I., Peña-Cabrera, E. 8-Alkenylborondipyrromethene dyes. General synthesis, optical properties, and preliminary study of their reactivity. *Tetrahedron* **67**, 7244–7250 (2011).
- ²²⁴ Kim, R., Lou, K., Kraft, M. L. A new long wavelength borondipyrromethene (BODIPY) sphingosine for studying sphingolipid dynamics in live cells *J. Lipid Res.* **54**, 265–275 (2013)
- ²²⁵ Rohand, T., Qin, W., Boens, N., Dehaen, W. Palladium-catalyzed coupling reactions for the functionalization of BODIPY dyes with fluorescence spanning the visible spectrum. *European J. Org. Chem.* **20**, 4658–4663 (2006).
- ²²⁶ Yoshida, Y., Shimakawa, S., Itoh, N., Niki, E. Action of DCFH and BODIPY as a probe for radical oxidation in hydrophilic and lipophilic domain. *Free Radic. Res.* **37**, 861–872 (2003).
- ²²⁷ Haugland, R. P. Handbook of Fluorescent Probes *Molecular Probes*, pp 288–289 (1996)
- ²²⁸ Rihn, S., Retailleau, P., Bugsaliewicz, N., Nicola, A. D., Ziessel, R. Versatile synthetic methods for the engineering of thiophene-substituted Bodipy dyes. *Tetrahedron Lett.* **50**, 7008–7013 (2009).
- ²²⁹ Poirel, A., Nicola, A. De, Retailleau, P., Ziessel, R. Oxidative Coupling of 1,7,8-Unsubstituted BODIPYs: Synthesis and Electrochemical and Spectroscopic Properties. *J. Org. Chem.* **77**, 7512–7525 (2012).
- ²³⁰ Pellegrini, N., Serafini, M., Colombi, B., Del Rio, D., Salvatore, S., Bianchi, M., Bighenti, F. Total antioxidant capacity of plant foods, beverages and oils consumed in Italy assessed by three different in vitro assays. *J. Nutr.* **133**, 2812–2819 (2003).
- ²³¹ Lei, H., Atkinson, J. Synthesis of Phytol- and Chroman-Derivatized Photoaffinity Labels Based on α -Tocopherol groups at either the terminus of an alkyl chain of varying length mimicking the phytol tail or on compounds display equivalent or better antioxidant. *J. Org. Chem.* **65**, 2560–2567 (2000).
- ²³² Ohnmacht, S., Nava, P., West, R., Parker, R., Atkinson, J. Inhibition of oxidative metabolism of tocopherols with ω -N-heterocyclic derivatives of vitamin E. *October* **141**, 520–529 (2008).
- ²³³ Wang, Y., Panagabko, C., Atkinson, J. Synthesis of α -tocohexaenol (α -T6) a fluorescent, oxidatively sensitive polyene analogue of α -tocopherol. *Bioorganic Med. Chem.* **18**, 777–786 (2010).
- ²³⁴ Hildering, A. The Synthesis of α -Tocopentaenol (α T5), A fluorescent Analogue of α -Tocopherol *MSC Thesis Brock University* (2016)

-
- ²³⁵ Maryanoff, B. E., Reitz, A. B., Duhl-Emswiler, B. a. Correction. stereochemistry of the Wittig reaction. Effect of nucleophilic groups in phosphonium ylide. *J. Am. Chem. Soc.* **108**, 557 (1986).
- ²³⁶ Couturier, M., Dory, Y. L., Rouillard, F., Deslongchamps, P. Studies directed towards the total synthesis of aldosterone and naturally occurring analogues. A unified approach using the transannular Diels-Alder reaction. *Tetrahedron* **54**, 1529–1562 (1998).
- ²³⁷ Page, P. C. B., Vahedi, H., Batchelor, K. J., Hindley, S. J., Edgar, M., Beswick, P. Synthesis of an Isomer of the Oxaspirobicyclic Tetronic Acid Unit of the CCK-B Receptor Antagonist Tetronothiodin. *Synlett* 1022–1024 (2003).
- ²³⁸ Sajiki, H., Ikawa, T., Hattori, K., Hirota, K. A remarkable solvent effect toward the Pd/C-catalyzed cleavage of silyl ethers. *Chem. Commun. (Camb)*. 654–655 (2003).
- ²³⁹ Tamaru, Y., Yamada, Y., Inoue, K., Yamamoto, Y., Yoshida, Z. Oxidation of primary and secondary alcohols by the catalysis of palladium. *J. Org. Chem.* **48**, 1286–1292 (1983).
- ²⁴⁰ Musolino, M. G., De Maio, P., Donato, A., Pietropaolo, R. Hydrogenation versus isomerization in α,β -unsaturated alcohols reactions over Pd/TiO₂ catalysts. *J. Mol. Catal. A Chem.* **208**, 219–224 (2004).
- ²⁴¹ Clark, H. C., Kurosawa, H. Chemistry of Metal Hydrides. XV. Mechanism of Double-Bond Migration Induced by Platinum(II)hydrides **12**, 1970–1973 (1973).
- ²⁴² Bianchini, C., Meli, A., Oberhauser, W. Isomerization of allylic alcohols to carbonyl compounds by aqueous-biphase rhodium catalysis. *New J. Chem.* **25**, 11–12 (2001).
- ²⁴³ Baudry, D., Michel, E., Felkin, H. Isomerisation of Allyl Ethers Catalysed by the Cationic Iridium Complex. *J.C.S. Chem. Comm* **370**, 694 (1978).
- ²⁴⁴ Sabitha, G., Nayak, S., Bhikshapathi, M. & Yadav, J. S. Palladium hydroxide catalyzed isomerization of primary allylic alcohols to aldehydes: Application to the formal synthesis of (-)-brevisamide. *Org. Lett.* **13**, 382–385 (2011).
- ²⁴⁵ Griffin, K., Johnston, P., Bennett, S., Kalik, S. Use of Platinum Group Metal Catalysts for the Selective Oxidation of Alcohols to Carbonyls in the Liquid Phase. *Chem. Ind. York-Marcel Dekker*- 169–178 (2003).
- ²⁴⁶ John, A. H., Skelton, C. A kinetic resolution route to the (S)-chromanmethanol intermediate for synthesis of the natural tocots *Tetrahedron Asym.* **8**, 523–526 (1997).
- ²⁴⁷ Flitsch, W., Kneip, H. 2,5-Bis(piperidinomethyl)pyrrol und (2,5-Pyrroldiyl)dimethylen) bis(triphenylphosphoniumiodid): Synthesen und Umsetzungen zu [2.2](2,5)Pyrrolophanen und 2,5- bisvinylsubstituierten Pyrrolen. *European J. Org. Chem.* 1895–1903 (1985).

-
- ²⁴⁸ Martyn, D. C., Vernall, A. J., Clark, B. M., Abell, A. D. Ring-deactivated hydroxyalkylpyrrole-based inhibitors of alpha-chymotrypsin: synthesis and mechanism of action. *Org. Biomol. Chem.* **1**, 2103–2110 (2003).
- ²⁴⁹ Soares, M. I. L., Lopes, S. M. M., Cruz, P. F., Brito, R. M. M., Pinho e Melo, T. M. V. D. Flash vacuum pyrolysis of 2,2-dioxo-1H,3H-pyrrolo[1,2-c]thiazoles and 2-vinyl-1H-pyrroles. *Tetrahedron* **64**, 9745–9753 (2008).
- ²⁵⁰ Dobbs, A. P., Venturelli, A., Butler, L. A., Parker, R. J. First total synthesis of the irciniasulfonic acids. *Synlett* 652–654 (2005).
- ²⁵¹ Vogel, J. C., Butler, R., Procter, D. J. An asymmetric, SmI₂-mediated approach to γ -butyrolactones using a new, fluorous-tagged auxiliary. *Tetrahedron* **64**, 11876–11883 (2008).
- ²⁵² Li, S., Luo, Y., Wu, J. An efficient approach to fused indolines via a copper(I)-catalyzed reaction of sulfonyl azide with 2-ethynylaryl methylenecyclopropane. *Org. Lett.* **13**, 3190–3193 (2011).
- ²⁵³ Mubarak, M. S., Jennermann, T. B., Ischay, M. A., Peters, D. G. Catalytic reduction of phenyl-conjugated acetylenic halides by nickel(I) salen: Cyclization versus coupling. *European J. Org. Chem.* 5346–5352 (2007).
- ²⁵⁴ Peng, S., Okeley, N. M., Tsai, A-L., Wu, G., Kulmacz, van der Donk, W. A. Synthesis of isotopically labeled arachidonic acids to probe the reaction mechanism of prostaglandin H synthase. *J. Am. Chem. Soc.* **124**, 10785–10796 (2002).
- ²⁵⁵ Kiddle, J. J. Microwave irradiation in organophosphorus chemistry. Part 2: Synthesis of phosphonium salts. *Tetrahedron Lett.* **41**, 1339–1341 (2000).
- ²⁵⁶ Mahboobi, S. 2-Substituierte Indole als Zwischenprodukte von Pyrrolino [3,4-c]carbazolen. *Arch. Pharm. (Weinheim)* **328**, 45–52 (1995).
- ²⁵⁷ Russell, R. K., Press, J. B. Chapter 5.1 Five-membered ring systems: Thiophenes & Se, Te analogs. *Prog. Heterocycl. Chem.* **7**, 82–105 (1995).
- ²⁵⁸ Ghosh, S., Miller, S., Davis, R., Moos, W. Mitochondria protecting agents for treating mitochondria associated diseases. *US2002/10195 A1* (2002).
- ²⁵⁹ Baughman, T. W., Sworen, J. C., Wagener, K. B. The facile preparation of alkenyl metathesis synthons. *Tetrahedron* **60**, 10943–10948 (2004).
- ²⁶⁰ Hoye, T., North, J., Yao, L. A Total Synthesis of (+)-Xestospongine A/(+)-Araguspongine D. *J. Am. Chem.* **116**, 2617–2618 (1994).
- ²⁶¹ Arsenyan, P., Paegle, E., Belyakov, S. A novel method for the bromination of thiophenes. *Tetrahedron Lett.* **51**, 205–208 (2010).

-
- ²⁶² Peyron, C., Navarre, J. M., Van Craynest, N., Benhida, R. First example of base-promoted tandem alkylation-bromination of 2-bromothiophene via halogen dance process: A remarkable temperature effect. *Tetrahedron Lett.* **46**, 3315–3318 (2005).
- ²⁶³ Bárta, J., Pohl, R., Klepetárová, B., Ernsting, N. P., Hocek, M. Modular synthesis of 5-substituted thiophen-2-yl C-2'-deoxyribonucleosides. *J. Org. Chem.* **73**, 3798–3806 (2008).
- ²⁶⁴ Banno, Y., Hara, R., Tokunoh, R. Heterocyclic compound. *EP2210876 A1* (2010).
- ²⁶⁵ Moulin, C., Duflos, M., Braut, G. L., Grimaud, N., Renard, P., Caignard, D-H. Synthesis and anti-inflammatory activity of N-(aza)arylcarboxamides derived from Trolox®. *Eur. J. Med. Chem.* **33**, 321–329 (1998).
- ²⁶⁶ Chenevert, R., Courchesne, G., Pelchat, N. Chemoenzymatic synthesis of both enantiomers of α -tocotrienol. *Bioorg. Med. Chem.* **14**, 5389–5396 (2006).
- ²⁶⁷ Burk, R., Holoboski, M., Posner, M. Omega-cycloalkyl 17-heteroaryl prostaglandin E2 analogs as EP2-receptor agonists. *US20030130239 A1* (2003).
- ²⁶⁸ Holder, R. W., Matturro, M. G. Lithium triethylborohydride reduction of alkyl methanesulfonate esters *J. Org. Chem.* **42**(12), 2166–2168 (1977).
- ²⁶⁹ Barbosa, H. J., Collins, E. A., Hamdouchi, C., Hembre, E. J., Hipkind, P. A., Johnston, R. D., Lu, J., Rupp, M. J., Takakuwa, T., Thompson, R. C. Imidazopyridazine compounds. *WO2006102194 A1* (2006).
- ²⁷⁰ Facchetti, A., Chen, Z., Usta, H., Newman, C. Yan, H. Semiconducting Compounds and Related Compositions and Devices. *WO2012030662* (2013).
- ²⁷¹ Shoji, H. Kobatake, S. Thermal bleaching reactions of photochromic diarylethenes with thiophene-S,S-dioxide for a light-starting irreversible thermosensor. *Chem. Commun.* **49**, 2362 (2013).
- ²⁷² Rossi, R., Salvadori, P. A. Synthesis of Both Enantiomers of 6-Methyl-3-octanone, a Component of the Alarm Pheromone of Ants in the Genus *Crematogaster*. *Synthesis* **3**, 209-210 (1979)
- ²⁷³ Fronza, G., Fuganti, C., Grasselli, P., Marinoni, G. Synthesis of N-benzoyl L- and D-2,3,6-trideoxy-3-aminoxyl-hexose from non-carbohydrate precursors. *Tetrahedron Lett.* **20**, 3883–3886 (1979).
- ²⁷⁴ Gevorgyan, V., Rubin, M., Liu, J. X., Yamamoto, Y. A direct reduction of aliphatic aldehyde, acyl chloride, ester, and carboxylic functions into a methyl group. *J. Org. Chem.* **66**, 1672–1675 (2001).

-
- ²⁷⁵ Rieth, R. D., Mankad, N. P., Calimano, E., Sadighi, J. P. Palladium-catalyzed cross-coupling of pyrrole anions with aryl chlorides, bromides, and iodides. *Org. Lett.* **6**, 3981–3983 (2004).
- ²⁷⁶ Boukou-Poba, J. P., Farnier, M., Guillard, R. A general method for the synthesis of 2-arylpyrroles *Tetrahedron Lett.* **19**, 1717–1720, (1979).
- ²⁷⁷ Lankhorst, P. P., Netscher, T., Duchateau, A. L. L. A Simple ¹³C NMR Method for the Discrimination of Complex Mixtures of Stereoisomers: All Eight Stereoisomers of α -Tocopherol Resolved. *Chirality* **27**, 850–855 (2015).
- ²⁷⁸ Mandal, P. K., McMurray, J. S. Pd–C-Induced Catalytic Transfer Hydrogenation with Triethylsilane. *J. Org. Chem.* **72**, 6599–6601 (2007).
- ²⁷⁹ Wuts, P. G. M., Greene, T. W. Greene's protective groups in organic synthesis -4th ed. Wiley p. 396-402 (2007)
- ²⁸⁰ Quai, M., Repetto, C., Barbaglia, W., Cereda, E. Fast deprotection of phenoxy benzyl ethers in transfer hydrogenation assisted by microwave. *Tetrahedron Lett.* **48**, 1241–1245 (2007).
- ²⁸¹ Rajakumar, P., Murali, V. TiCl₄, Dioxane - A Facile and Efficient System for De-O-Benzylation, De-O-Allylation, and De-O-Xylylation of Phenolic Ethers. *Synth. Commun.* **33**, 3891–3896 (2003).
- ²⁸² Ward, D. E., Gai, Y. & Kaller, B. F. [3 + 3] 1 Annulation Based on 6-Endo-Trig Radical Cyclization: Regioselectivity and Diastereoselectivity. 7830–7836 (1995).
- ²⁸³ Lundrigan, T. & Thompson, A. Conversion of F-BODIPYs to Cl-BODIPYs: enhancing the reactivity of F-BODIPYs. *J. Org. Chem.* **78**, 757–61 (2013).
- ²⁸⁴ Barden, C. J., Henneberry, A. L., Byers, D. M., McMaseter, C. R., Weaver, D. Wu, F. Therapeutic pro-antibiotic agents and methods of use thereof WO2008128321 A1 (2008).
- ²⁸⁵ Wong, K-T., Chien, Y-Y., Liao, Y-L., Lin, C-C-. Chou, M-Y., Leung, M-K. Efficient and convenient nonaqueous workup procedure for the preparation of arylboronic esters. *J. Org. Chem.* **67**, 1041–1044 (2002).
- ²⁸⁶ Billingsley, K., Buchwald, S. L. Highly efficient monophosphine-based catalyst for the palladium-catalyzed Suzuki-Miyaura reaction of heteroaryl halides and heteroaryl boronic acids and esters. *J. Am. Chem. Soc.* **129**, 3358–3366 (2007).
- ²⁸⁷ Gilow, H. M., Burton, D. E. Bromination and chlorination of pyrrole and some reactive 1-substituted pyrroles. *J. Org. Chem.* **46**, 2221–2225 (1981).
- ²⁸⁸ Nagaki, A., Moriwaki, Y., Yoshida, J. Flow synthesis of arylboronic esters bearing electrophilic functional groups and space integration with Suzuki–Miyaura coupling without intentionally added base. *Chem. Commun.* **48**, 11211 (2012).

-
- ²⁸⁹ Leen, V., Leemans, T., Boens, N., Dehaen, W. 2- and 3-monohalogenated BODIPY dyes and their functionalized analogues: Synthesis and spectroscopy. *European J. Org. Chem.* 4386–4396 (2011).
- ²⁹⁰ Bura, T., Leclerc, N., Fall, S., Leveque, P., Heiser, T., Retailleau, P., Rhin, S., Mirloup, A., Ziessel, R. High-performance solution-processed solar cells and ambipolar behavior in organic field-effect transistors with thienyl-BODIPY scaffoldings. *J. Am. Chem. Soc.* **134**, 17404–17407 (2012).
- ²⁹¹ Hartough, H. D., Hochgesang, F. P., Blicke, F. F. Chemistry of Heterocyclic Compounds: Thiophene and its Derivatives, Volume 3. (2008).
- ²⁹² Vielsmeier, A., Haack, A. Über die Einwirkung von Halogenphosphor auf Alkyl-formanilide. Eine neue Methode zur Darstellung sekundärer und tertiärer *p*-Alkylamino-benzaldehyde. *Chem. Lab. Univ. Erlangen* **2**, 119-122 (2012).
- ²⁹³ Schultz, A. G., Wang, A., York, N. First Asymmetric Synthesis of a Hasubanan Alkaloid . Total Synthesis of (+) -Cepharamine hasubanan alkaloids are of pharmacological interest because of their structural resemblance to the morphine alkaloids. *Tetrahedron* **7863**, 8259–8260 (1998).
- ²⁹⁴ Ochiai, M., Yoshimura, A., Miyamoto, K., Hayashi, S. & Nakanishi, W. Hypervalent π - π -bromane strategy for Baeyer-Villiger oxidation: Selective transformation of primary aliphatic and aromatic aldehydes to formates, which is missing in the classical Baeyer-Villiger oxidation. *J. Am. Chem. Soc.* **132**, 9236–9239 (2010).
- ²⁹⁵ Jiang, L.-B., Li, R., Zhou, C., Qi, X., Peng, J.-B., Wu, X.-F. A general and practical Lewis acids-catalyzed aryl formates synthesis. *Mol. Catal.* **433**, 8–11 (2017).
- ²⁹⁶ Lee, J.-S., Kim, H. K., Feng, S., Vendrell, M., Chang, Y.-T. Accelerating fluorescent sensor discovery: unbiased screening of a diversity-oriented BODIPY library. *Chem. Commun. (Camb)*. **47**, 2339–41 (2011).
- ²⁹⁷ Zatsikha, Y. V., Yakubovskiy, V. P., Shandura, M. P., Kovtun, Y. P. Boradipyrromethenecyanines on the base of a BODIPY nucleus annelated with a pyridone ring: a new approach to long-wavelength dual fluorescent probe design. *RSC Adv.* **3**, 24193 (2013).
- ²⁹⁸ Shivran, N., Mula, S., Ghanty, T. K., Chattopadhyay, S. Steric strain release-directed regioselective functionalization of meso-methyl bodipy dyes. *Org. Lett.* **13**, 5870–5873 (2011).
- ²⁹⁹ Williams, A. T. R., Winfield, S. A., Miller, J. N. Relative fluorescence quantum yields using a computer-controlled luminescence spectrometer. *Analyst* **108**, 1067 (1983).
- ³⁰⁰ Yang, Z.-C., Wang, M., Yong, A. M., Wong, S. Y., Zhang, X.-H., Tan, H., Chang, A. Y., Li, X., Wang, J. Intrinsically fluorescent carbon dots with tunable emission derived from

-
- hydrothermal treatment of glucose in the presence of monopotassium phosphate. *Chem. Commun.* **47**, 11615 (2011).
- ³⁰¹ Chu, K.-Y., Thompson, A. R. Densities and Refractive Indices of Alcohol-Water Solutions of n-Propyl, Isopropyl, and Methyl Alcohols. *J. Chem. Eng. Data* **7**, 358–360 (1962).
- ³⁰² Li, X., Wang, G., Chen, D., Lu, Y. Binding of ascorbic acid and α -tocopherol to bovine serum albumin: a comparative study. *Mol. Biosyst.* **10**, 326–337 (2014).
- ³⁰³ Pawlak, K., Skrzypczak, A., Bialek-byłka, G. E. Inner Filter Effect in the Fluorescence Emission Spectra of Room Temperature Ionic Liquids. **1**, 401–420 (2007).
- ³⁰⁴ Liepinsh, E., Otting, G. Organic solvents identify specific ligand binding sites on protein surfaces. *Nat. Biotechnol.* **15**, 264–268 (1997).
- ³⁰⁵ Wong, P. S. L., Yan, D., Guittard, G. V. Compositions and dosage forms for enhanced absorption of metformin. (2005).
- ³⁰⁶ Gupte, A. A., Landis, M. E., Marler, D. O. Zusatz eines co-Lösungsmittels zu Furfural zur Extraktion von Aromaten. (1998).
- ³⁰⁷ Melavanki, R. M., Patil, N. R., Sanningannavar, F. M., Kusanur, R. A., Nagaraja, D., Patil, H. D., Kadadevarmath, J. S. Solvent effect on fluorescence quenching of biologically active 6-methoxy-4-azidomethyl coumarin by aniline in different solvents. *Indian J. Pure Appl. Phys.* **51**, 499–505 (2013).
- ³⁰⁸ Bharate, S. S., Vishwakarma, R. A. Thermodynamic equilibrium solubility measurements in simulated fluids by 96-well plate method in early drug discovery. *Bioorg. Med. Chem. Lett.* **25**, 1561–1567 (2015).
- ³⁰⁹ Qian, J., Morley, S., Wilson, K., Nava, P., Atkinson, J., Manor, D. Intracellular trafficking of vitamin E in hepatocytes: the role of tocopherol transfer protein. *J. Lipid Res.* **46**, 2072–2082 (2005).
- ³¹⁰ Ulatowski, L., Parker, R., Davison, C., Yanjanin, N., Kelley, T. J., Corey, D., Atkinson, J., Porter, F., Arai, H., Walkley, S. U., Manor, D. Altered vitamin E status in Niemann-Pick type C disease. *J. Lipid Res.* **52**, 1400–1410 (2011).
- ³¹¹ Ghelfi, M., Ulatowski, L., Manor, D., Atkinson, J. Synthesis and characterization of a fluorescent probe for α -tocopherol suitable for fluorescence microscopy. *Bioorganic Med. Chem.* **24**, 2754–2761 (2016).
- ³¹² Das, A. T., Tenenbaum, L., Berkhout, B. Tet-On systems for doxycycline-inducible gene expression. *Curr. Gene Ther.* **16**, 156–167 (2016).

-
- ³¹³ Ueno, I., Hoshino, M., Miura, T., Shinriki, N. Ozone exposure generates free radicals in the blood samples in vitro. Detection by the ESR spin-trapping technique. *Free Radic. Res.* **29**, 127–135 (1998).
- ³¹⁴ Schneider, C. Update on products and mechanisms of lipid peroxidation. *Mol. Nutr. Food Res.* **53**, 315–321 (2010).
- ³¹⁵ Storey, K. B. Functional metabolism: Regulation and adaptation *Ed. Wiley* p. 594, (2004)
- ³¹⁶ Winterbourn, C. C. Reconciling the chemistry and biology of reactive oxygen species. *Nat Chem Biol* **4**, 278–286 (2008).
- ³¹⁷ Brash, A. R. Autoxidation of methyl linoleate: Identification of the bis-allylic 11-hydroperoxide. *Lipids* **35**, 947–952 (2000).
- ³¹⁸ Pratt, D. A., Mills, J. H., Porter, N. A. Theoretical calculations of carbon-oxygen bond dissociation enthalpies of peroxy radicals formed in the autoxidation of lipids. *J. Am. Chem. Soc.* **125**, 5801–5810 (2003).
- ³¹⁹ Buettner, G. R. The Pecking Order of Free Radicals and Antioxidants: Lipid Peroxidation, α -Tocopherol, and Ascorbate. *Archives of Biochemistry and Biophysics* **300**, 535–543 (1993).
- ³²⁰ Wang, W., Yang, H., Johnson, D., Gensler, C., Decker, E., Zhang, G., Chemistry and biology of ω -3 PUFA peroxidation-derived compounds. *Prostaglandins Other Lipid Mediat.* In press (2016)
- ³²¹ Maillard, B., Ingold, K. U., Scaiano, J. C. Rate constants for the reactions of free radicals with oxygen in solution. *J. Am. Chem. Soc.* **105**, 5095–5099 (1983).
- ³²² Peers, K. E., Coxon, D. T., Chan, H. W. S. Autoxidation of methyl linolenate and methyl linoleate: The effect of α -tocopherol. *J. Sci. Food Agric.* **32**, 898–904 (1981).
- ³²³ Kamal-Eldin, A., Appelqvist, L. Å. The chemistry and antioxidant properties of tocopherols and tocotrienols. *Lipids* **31**, 671–701 (1996).
- ³²⁴ Burton, G. W., Doba, T., Gabe, E. J., Hughes, G. L., Lee, F. L., Prasad, L., Ingold, K. U. Autoxidation of Biological Molecules . 4 . Maximizing the Antioxidant Activity of Phenols. *J. Am. Chem. Soc.* **107**, 7053–7065 (1985).
- ³²⁵ Yanez, J., Sevilla, C. L., Becker, D., Sevilla, M. D. Low-Temperature Autoxidation in Unsaturated Lipids: An Electron Spin Resonance Study. *J. Phys. Chem.* **91**, 487–491 (1987).
- ³²⁶ Situnayake, R. D., Crump, B. J., Zezulka, A. V., Davis, M., McConkey, B., Thurnham, D. I. Measurement of conjugated diene lipids by derivative spectroscopy in heptane extracts of plasma. *Ann Clin Biochem* **27** (Pt 3), 258–266 (1990).

-
- ³²⁷ Gardner, H. W., Eskins, K., Grams, G. W., Inglett, G. E. Radical addition of linoleic hydroperoxides to α -tocopherol or the analogous hydroxychroman. *Lipids* **7**, 324–334 (1972).
- ³²⁸ Yamauchi, R., Kato, K., Ueno, Y. Free-Radical Scavenging Reactions of α -Tocopherol during the Autoxidation of Methyl Linoleate in Bulk Phase. *J. Agric. Food Chem.* **43**, 1455–1461 (1995).
- ³²⁹ Niki, E., Saito, T., Kawakami, A., Kamiya, Y. Inhibition of oxidation of methyl linoleate in solution by vitamin E and vitamin C. *J. Biol. Chem.* **259**, 4177–4182 (1984).
- ³³⁰ Burton, G. W., Ingold, K. V. Autooxidation of biological molecules: The antioxidant activity of vitamin E and related chain breaking phenolic antioxidants in vitro. *J. Am. Chem. Soc.* **103**, 6472–6477. (1981).
- ³³¹ Kontush, A., Finckh, B., Karten, B., Kohlschütter, A., Beisiegel, U. Antioxidant and prooxidant activity of α -tocopherol in human plasma and low density lipoprotein. *J. Lipid Res.* **37**, 1436–1448 (1996).
- ³³² Mukai, K., Yasuhiro, K., Ishizu, K. Kinetic study of the reaction between vitamin E radical and alkyl hydroperoxides in solution. *Biochem. Biophys. Res. Commun.* **155**, 1046–1050 (1988).
- ³³³ Mukai, K., Sawada, K., Kohno, Y., Terao, J. Kinetic study of the prooxidant effect of tocopherol. Hydrogen abstraction from lipid hydroperoxides by tocopheroxyls in solution. *Lipids* **28**, 747–752 (1993).
- ³³⁴ Okauchi, Y. Kinetic Study of the Reaction Between Tocopheroxyl Radical and Unsaturated Fatty Acid Esters in Benzene. **24**, 936–939 (1989).
- ³³⁵ Burton, G. W., Cheeseman, K. H., Doba, T., Ingold, K. U., Slater, T. F. Vitamin E as an antioxidant in vitro and in vivo. *Ciba Found.Symp.* **101**, 4–18 (1983).
- ³³⁶ Mahoney, L. R., DaRooge, M. A. Kinetic behavior and thermochemical properties of phenoxy radicals. *J. Am. Chem. Soc.* **97**, 4722–4731 (1975).
- ³³⁷ Burton, G. W., Ingold, K. U. Vitamin E: application of the principles of physical organic chemistry to the exploration of its structure and function. *Acc. Chem. Res.* **19**, 194–201 (1986).
- ³³⁸ Traber, M. G., Atkinson, J. Vitamin E, antioxidant and nothing more. *Free Radic. Biol. Med.* **43**, 4–15 (2007).
- ³³⁹ Wacks, W. Elektrometrische Redoxmessungen an Natürlichen Fett-Antioxydantien, *Biochem. Z.* **319**, 561–570. (1949)

-
- ³⁴⁰ Fuzukawa, K., Gebicki, J. M. Oxidation of α -Tocopherol the Hydroxyl, Perhydroxyl, in Micelles and Liposomes by and Superoxide Free Radicals. *Arch. Biochem. Biophys.* **226**, 242–251 (1983).
- ³⁴¹ Mccay, P. B. Vitamin E : Interactions With Free Radicals and Ascorbate. *Ann Rev Nutr* **5**, 323–340 (1985).
- ³⁴² Packer, J. E., Slater, T. F., Willson, R. L. Direct observation of a free radical interaction between vitamin E and vitamin C. *Nature* **278**, 737–738 (1979).
- ³⁴³ Tsuchihashi, H., Kigoshi, M., Iwatsuki, M., Niki, E. Action of β -Carotene as an Antioxidant against Lipid Peroxidation. *Arch. Biochem. Biophys.* **323**, 137–147 (1995).
- ³⁴⁴ Foote, C. S. in: Pryor W. A. (Ed.) Free Radicals in Biology. Vol. 2. *Elsevier Academic Press, New York*; 85–133 (1976).
- ³⁴⁵ Schultz, J., Kaminker, K. Myeloperoxidase of the leucocyte of normal human blood. I. Content and localization. *Arch. Biochem. Biophys.* **96**, 465–467 (1962).
- ³⁴⁶ Kellogg, E. W. Friedovich, I. Superoxide, hydrogen peroxide, and singlet oxygen in lipid peroxidation by a xanthine oxidase system. *J. Biol. Chem.* 8812–8817 (1975).
- ³⁴⁷ Anderson, S. M., Krinsky, N. I. Protective Action of Carotenoid Pigments Against Photodynamic Damage To Liposomes*. *Photochem. Photobiol.* **18**, 403–408 (1973).
- ³⁴⁸ Junji, T., Minami, Y., Bando, N., “Singlet Molecular Oxygen-Quenching Activity of Carotenoids: Relevance to Protection of the Skin from Photoaging.” *Journal of Clinical Biochemistry and Nutrition* **48**, 57–62 (2011).
- ³⁴⁹ Burton, G. W., Ingold, K. U. beta-Carotene: an unusual type of lipid antioxidant. *Science* **224**, 569–73 (1984).
- ³⁵⁰ Cranea, F. L., Navas, P. The Diversity of Coenzyme Coenzyme Q in Mitochondria Coenzyme Q in the Plasma Membrane. *Science* **18**, 1-6(1997).
- ³⁵¹ Navas, P., Villalba, J. M., de Cabo, R. The importance of plasma membrane coenzyme Q in aging and stress responses. *Mitochondrion* **7**, 34–40 (2007).
- ³⁵² Petillo, D., Hultin, H. O. Ubiquinone-10 as an antioxidant. *J. Food Biochem.* **32**, 173–181 (2008).
- ³⁵³ Constantinescu, A., Maguire, J. J., Packer, L. Interactions between ubiquinones and vitamins in membranes and cells. *Mol. Aspects Med.* **15**, (1994).
- ³⁵⁴ Gómez-Díaz, C., Rodriguez-Aguilera, J. C., Barroso, M. P., Villalba, J. M., Navarro, F., Crane, F. L., Navas, P. Antioxidant ascorbate is stabilized by NADH-Coenzyme Q10 reductase in the plasma membrane. *J. Bioenerg. Biomembr.* **29**, 251–257 (1997).

-
- ³⁵⁵ Buttriss, J. L., Diplock, A. T. The relationship between α -tocopherol and phospholipid fatty acids in rat liver subcellular membrane fractions. *Biochim. Biophys. Acta - Lipids Lipid Metab.* **962**, 81–90 (1988).
- ³⁵⁶ Wang, X., Quinn, P. J. Vitamin E and its functions in membranes. *Prog. Lipid Res.* **38**, 309–336 (1999).
- ³⁵⁷ Schultz, J., Kaminker, K. Myeloperoxidase of the leucocyte of normal human blood. I. Content and localization. *Arch. Biochem. Biophys.* **96**, 465–467 (1962).
- ³⁵⁸ Incardona, J. P., Eaton, S. Cholesterol in signal transduction. *Curr. Opin. Cell Biol.* **12**, 193–203 (2000).
- ³⁵⁹ Sheng, R., Chen, Y., Gee, H. Y., Stec, E., Melowic, H. R., Blatner, N. R., Tun, M. P., Kim, Y., Källberg, M., Fujiwara, T. K., Hong, J. H., Kim, K. P., Lu, H., Kusumi, A., Lee, M. G., Cho, W. Cholesterol Modulates Cell Signaling and Protein Networking by Specifically Interacting with PDZ Domain-Containing Scaffold Proteins *Nature comm.* **3**, (2013).
- ³⁶⁰ Cooper, R. A. Influence of increased membrane cholesterol on membrane fluidity and cell function in human red blood cells. *J. Supramol. Struct.* **8**, 413–430 (1978).
- ³⁶¹ Sonnen, A. F. P., Bakirci, H., Netscher, T., Nau, W. M. Effect of temperature, cholesterol content, and antioxidant structure on the mobility of vitamin E constituents in biomembrane models studied by laterally diffusion-controlled fluorescence quenching. *J. Am. Chem. Soc.* **127**, 15575–15584 (2005).
- ³⁶² Gramlich, G., Zhang, J., Nau, W. M. Diffusion of α -Tocopherol in Membrane Models: Probing the Kinetics of Vitamin E Antioxidant Action by Fluorescence in Real Time. *J. Am. Chem. Soc.* **126**, 5482–5492 (2004).
- ³⁶³ Takahashi, M., Tsuchiya, J., Niki, E. Scavenging of Radicals by Vitamin E in the Membranes As Studied by Spin Labeling. *J. Am. Chem. Soc.* 6350–6353 (1989).
- ³⁶⁴ Marquardt, D., Williams, J. A., Kucerka, N., Atkinson, J., Wassal, S. R., Katsaras, J., Harron, T. A. Tocopherol activity correlates with its location in a membrane: A New Perspective on the Antioxidant Vitamin E. *J. Am. Chem. Soc.* **135**, 7523–7533 (2013).
- ³⁶⁵ Atkinson, J., Epand, R. F., Epand, R. M. Tocopherols and tocotrienols in membranes: A critical review. *Free Radic. Biol. Med.* **44**, 739–764 (2008).
- ³⁶⁶ Zimmerberg, J., McLaughlin, S. Membrane curvature: How BAR domains bend bilayers. *Curr. Biol.* **14**, 250–252 (2004).
- ³⁶⁷ Giroud, C. Transversal distribution of phospholipids in prothylakoid and thylakoid membranes from oat. **201**, 215–220 (2000).

-
- ³⁶⁸ Popescu, D., Victor, G. The transversal diffusion coefficient of phospholipid molecules through black lipid membranes. *J. Electroanal. Chem.* **320**, 105–108 (1991).
- ³⁶⁹ Gummadi, S. N., Kumar, K. S. The mystery of phospholipid flip-flop in biogenic membranes. *Cell. Mol. Biol. Lett.* **10**, 101–121 (2005).
- ³⁷⁰ Devaux, P. F. Phospholipid flippases. *FEBS Lett.* **234**, 8–12 (1988).
- ³⁷¹ Howard, A. C., McNeil, A. K., McNeil, P. L. Promotion of plasma membrane repair by vitamin E. *Nat. Commun.* **2**, 597 (2011).
- ³⁷² Boonnoy, P., Karttunen, M., Wong-ekkabut, J. Alpha-tocopherol inhibits pore formation in oxidized bilayers. *Phys. Chem. Chem. Phys.* **19**, 5699–5704 (2017).
- ³⁷³ Moscat, J., Diaz-meco, M. T., Rennert, P. NF- κ B activation by protein kinase C isoforms and B-cell function. *EMBO Rep.* 1–6 (2003).
- ³⁷⁴ Boscoboinik, D., Szewczyk, A., Henseys, C., Ami, A. Inhibition of Cell Proliferation by α -Tocopherol. *J. Biol. Chem.* **266**, 6188–6194 (1991).
- ³⁷⁵ Ricciarelli, R., Tasinato, A., Clement, S., Özer, N. K., Boscoboinik, D., Azzi, A. α -Tocopherol specifically inactivates cellular protein kinase C α by changing its phosphorylation state. *Biochem. J.* **334**, 243–249 (1998).
- ³⁷⁶ Devaraj, S., Li, D., Jialal, I. The effects of α tocopherol supplementation on monocyte function: Decreased lipid oxidation, interleukin 1 β secretion, and monocyte adhesion to endothelium. *J. Clin. Invest.* **98**, 756–763 (1996).
- ³⁷⁷ Hehenberger, K., Hansson, A. High Glucose-Induced Growth Factor Resistance in Human Fibroblasts Can be Reversed by Antioxidants and Protein Kinase C-Inhibitors. *Cell Biochem. Funct.* **15**, 197–201 (1997).
- ³⁷⁸ Kanno, T., Utsumi, T., Takehara, Y., Ide, A., Akiyama, J., Yoshioka, T., Horton, A. A. Utsumi, K. Inhibition of Neutrophil-Superoxide Generation by α -tocopherol and Coenzyme Q. *Free Radic. Res.* **24**, 281–289 (1996).
- ³⁷⁹ Studer, R. K., Craven, P. A., DeRubertis, F. R. Antioxidant inhibition of protein kinase C-signaled increases in transforming growth factor-beta in mesangial cells. *Metabolism.* **46**, 918–925 (1997).
- ³⁸⁰ Tada, H., Company, S., Culture, C. Protective Effect of 1)-oz-Tocopherol on the Function of Human Mesangial Cells Exposed to High Glucose Concentrations. **46**, 779–784 (1997).
- ³⁸¹ Chandra, V., Jasti, J., Kaur, P., Betzel, Ch., Srinivasan, A., Singh, T. P. First structural evidence of a specific inhibition of phospholipase A2 by α -tocopherol (Vitamin E) and its implications in inflammation: Crystal structure of the complex formed between phospholipase A2 and α -tocopherol at 1.8 Å resolution. *J. Mol. Biol.* **320**, 215–222 (2002).

-
- ³⁸² Steinberg, D. Oxidation and Its Pathobiological Significance. *jbmc* **272**, 20963-20966, (1997).
- ³⁸³ Esterbauer, H., Dieber-Rotheneder, M., Striegl, G., Waeg, G. Role of vitamin E in preventing the oxidation of low-density lipoprotein. *Am. J. Clin. Nutr.*, **53**, 314-321, (1991).
- ³⁸⁴ Østerud, B. & Bjørklid, E. Role of Monocytes in Atherogenesis. *Physiol Rev* **83**, 1069–1112 (2003).
- ³⁸⁵ Abdala-Valencia, H., Berdnikovs, S., Cook-Mills, J. M. Vitamin E isoforms differentially regulate intercellular adhesion molecule-1 activation of PKC α in human microvascular endothelial cells. *PLoS One* **7**, 1–10 (2012).
- ³⁸⁶ Williams, J. C., Forster, L. A., Tull, S. P., Wong, M., Bevan, R. J., Ferns, G. A. A. Dietary vitamin E supplementation inhibits thrombin-induced platelet aggregation, but not monocyte adhesiveness, in patients with hypercholesterolaemia. *Int. J. Exp. Pathol.* **78**, 259–266 (1997).
- ³⁸⁷ Meydani, M., Freedman, J. E., Keaney, J. F. Vitamin E Inhibition of Platelet Aggregation Is Independent of Antioxidant Activity 1, 2. *J. Nutr. Biochem.* **131**, 374–377 (2001).
- ³⁸⁸ Wu, D., Meydani, M., Beharka, A. A., Serafini, M., Martin, K. R., Meradani, S. N. In vitro supplementation with different tocopherol homologues can affect the function of immune cells in old mice. *Free Radic. Biol. Med.* **28**, 643–651 (2000).
- ³⁸⁹ Teupser, D., Thiery, J., Seidel, D. Alpha-tocopherol down-regulates scavenger receptor activity in macrophages. *Atherosclerosis* **144**, 109–115 (1999).
- ³⁹⁰ Ricciarelli, R., Zingg, J. M., Azzi, A. Vitamin E 80th anniversary: a double life, not only fighting radicals. *IUBMB Life* **52**, 71–76 (2001).
- ³⁹¹ Zingg, J.-M. Vitamin E: A Role in Signal Transduction. *Annu. Rev. Nutr.* **35**, 135–73 (2015).
- ³⁹² Zingg, J.-M., Azzi, A. Non-Antioxidant Activities of Vitamin E. *Curr. Med. Chem.* **11**, 1113–1133 (2004).
- ³⁹³ Azzi, A., Ricciarelli, R., Zingg, J. M. Non-antioxidant molecular functions of α -tocopherol (vitamin E). *FEBS Lett.* **519**, 8–10 (2002).
- ³⁹⁴ Prasad, K. N., Kumar, B., Yan, X.-D., Hanson, A. J., Cole, W. C. α -Tocopheryl Succinate, the Most Effective Form of Vitamin E for Adjuvant Cancer Treatment: A Review. *J. Am. Coll. Nutr.* **22**, 108–117 (2003).
- ³⁹⁵ Hahn, T., Szabo, L., Gold, M., Ramanathapuram, L., Hurley, L. H., Akporiaye, E. T. Dietary administration of the proapoptotic vitamin E analogue α -tocopheryloxyacetic acid inhibits metastatic murine breast cancer. *Cancer Res.* **66**, 9374–9378 (2006).

-
- ³⁹⁶ Chang, E., Ni, J., Yin, Y., Lin, C. C., Chang, P., James, N. S., Chamler, S. R., Yeh, S. Alpha-vitamin E derivative, RRR-alpha-tocopheryloxybutyric acid inhibits the proliferation of prostate cancer cells. *Asian J. Androl.* **9**, 31–39 (2007).
- ³⁹⁷ Nishikawa, K., Satoh, H., Hirai, A., Suzuzki, K., Asano, R., Kumadaki, I., Hagiwara, K., Yano, T. α -Tocopheryloxybutyric acid enhances necrotic cell death in breast cancer cells treated with chemotherapy agent. *Cancer Lett.* **201**, 51–56 (2003).
- ³⁹⁸ Gohil, K., Godzdnker, R., O’Roark, E., Schock, B. C., Kaini, R. R., Packer, L., Cross, C. E., Traber M. G. α -Tocopherol Transfer Protein Deficiency in Mice Causes Multi-Organ Deregulation of Gene Networks and Behavioral Deficits With Age. *Ann. N. Y. Acad. Sci.* **1031**, 109–126 (2004).
- ³⁹⁹ Desiraju, G., Steiner, T. The Weak Hydrogen Bond: In Structural Chemistry and Biology. *Oxford Sci. Pub.* (2001).
- ⁴⁰⁰ Murray, J. S., Riley, A. K. E., Politzer, B. P., C, T. C. Directional Weak Intermolecular Interactions : σ -Hole Bonding. **1**, 1598–1607 (2010).
- ⁴⁰¹ Riley, K. E., Murray, J. S., Politzer, P., Concha, M. C., Hobza, P. Br \cdots O complexes as probes of factors affecting halogen bonding: Interactions of bromobenzenes and bromopyrimidines with acetone. *J. Chem. Theory Comput.* **5**, 155–163 (2009).
- ⁴⁰² Auffinger, P., Hays, F. A., Westhof, E., Ho, P. S. Halogen bonds in biological molecules. *Proc. Natl. Acad. Sci. U. S. A.* **101**, 16789–94 (2004).
- ⁴⁰³ Cavallo, G., Metrangolo, P., Milani, R., Pilati, T., Priimagi, A., Resnati, G., Terraneo, G. The halogen bond. *Chem. Rev.* **116**, 2478–2601 (2016).
- ⁴⁰⁴ Scholfield, M. R., Vander Zanden, C. M., Carter, M., Ho, P. S. Halogen bonding (X-bonding): A biological perspective. *Protein Sci.* **22**, 139–152 (2013).
- ⁴⁰⁵ Liantonio, R., Metrangolo, P., Pilati, T., Resnati, G., Stevenazzi, A. Perfluorocarbon-hydrocarbon self-assembly: First crystalline halogen-bonded complex involving bromoperfluoroalkanes. *Cryst. Growth Des.* **3**, 799–803 (2003).
- ⁴⁰⁶ Harman, C. A., Turman, M. V., Kozak, K. R., Marnett, L. J., Smith, W. L., Garavito, M. R. Structural basis of enantioselective inhibition of cyclooxygenase-1 by S- α -substituted indomethacin ethanolamides. *J. Biol. Chem.* **282**, 28096–28105 (2007).
- ⁴⁰⁷ Guengerich, F. P. Oxidation of halogenated compounds by cytochrome P-450, peroxidases, and model metalloporphyrins. *J. Biol. Chem.* **264**, 17198–17205 (1989).
- ⁴⁰⁸ Hanzlik, R. P., Hogberg, K., Judson, C. M. Microsomal hydroxylation of specifically deuterated monosubstituted benzenes. Evidence for direct aromatic hydroxylation. *Biochemistry* **23**, 3048 (1984).

-
- ⁴⁰⁹ Korzekwa, K. R., Swinney, D. C., Trager, W. F. Isotopically Labeled Chlorobenzenes as Probes for the Mechanism of Cytochrome P-450 Catalyzed Aromatic Hydroxylation. *Biochemistry* **28**, 9019–9027 (1989).
- ⁴¹⁰ Lucarini, M., Pedulli, G. F., Cipollone, M. Bond Dissociation Enthalpy of α -Tocopherol and Other Phenolic Antioxidants. *J. Org. Chem.* **59**, 5063–5070 (1994).
- ⁴¹¹ Foti, M. C., Daquino, C., Mackie, I. D., DiLabio, G. A., Ingold, K. U. Reaction of phenols with the 2,2-diphenyl-1-picrylhydrazyl radical. Kinetics and DFT calculations applied to determine ArO-H bond dissociation enthalpies and reaction mechanism. *J. Org. Chem.* **73**, 9270–9282 (2008).
- ⁴¹² Kapur, S., Shusterman, A., Verma, R. P., Hansch, C., Selassie, C. D. Toxicology of benzyl alcohols: A QSAR analysis. *Chemosphere* **41**, 1643–1649 (2000).
- ⁴¹³ Helbling, R. E., Aeschimann, W., Simona, F., Stocker, A., Cascella, M. Engineering Tocopherol Selectivity in α -TTP: A Combined In Vitro/In Silico Study. *PLoS One* **7**, 1–11 (2012).
- ⁴¹⁴ Fridén-Saxin, M., Seifert, T., Landergen, M. R., Suuronen, T., Lahtela-Kakkonen, M., Jarho, E. M., Luthman, K. Synthesis and evaluation of substituted chroman-4-one and chromone derivatives as sirtuin 2-selective inhibitors. *J. Med. Chem.* **55**, 7104–7113 (2012).
- ⁴¹⁵ Nguyen, V. C., Kim, Y., Yu, Y., Kang, H. Synthesis of Chromane Derivatives by Palladium-Catalyzed Intramolecular Allylation of Aldehydes with Allylic Acetates or Chlorides Using Indium and Indium (III) Chloride. **26**, 711–712 (2005).
- ⁴¹⁶ Hartshorn, S. R. Non-conventional electrophilic aromatic substitutions and related reactions. *Chem. Soc. Rev.* **3**, 167 (1974).
- ⁴¹⁷ Leckie, S. M., Harkness, G. J., Clarke, M. L. Catalytic constructive deoxygenation of lignin-derived phenols: new C–C bond formation processes from imidazole-sulfonates and ether cleavage reactions. *Chem. Commun.* **50**, 11511–11513 (2014).
- ⁴¹⁸ Bay, E., Bak, D. A., Timony, P. E., Leone-Bay, A. Preparation of aryl chlorides from phenols. *J. Org. Chem.* **55**, 3415–3417 (1990).
- ⁴¹⁹ Bestmann, H. J., Schnabel, K. H. Über die Reaktion von Chlorameisensäureestern mit Triphenylphosphin. *Ann. der Chemie* **698**, 106–108 (1966).
- ⁴²⁰ Beller, M., Cartney, D. M., Guiry, P. J. Palladium-catalyzed carbonylative coupling reactions between Ar–X and carbon nucleophiles. *Chem. Soc. Rev.* **40**, 4877–5208 (2011).
- ⁴²¹ Cacchi, S., Ciattini, P. G., Morera, E., Ortari, G. Palladium-catalyzed carbonylation of aryl triflates. Synthesis of arenecarboxylic acid derivatives from phenols. *Tetrahedron Lett.* **27**, 3931–3934 (1986).

-
- ⁴²² Galabov, B., Nalbantova, D., Schleyer, P. V. R., Schaefer, H. F. Electrophilic Aromatic Substitution: New Insights into an Old Class of Reactions. *Acc. Chem. Res.* **49**, 1191–1199 (2016).
- ⁴²³ Mulik, S., Sotiriou-leventis, C., Leventis, N. Time-Efficient Acid-Catalyzed Synthesis of Resorcinol - Formaldehyde Aerogels. *Chem. Mater.* **19**, 6138–6144 (2007).
- ⁴²⁴ Mahdavian, E., Sangsura, S., Landry, G., Eytina, J., Salvatore, B. A. A novel synthesis of tocopheryl amines and amides. *Tetrahedron Lett.* **50**, 19–21 (2009).
- ⁴²⁵ Wang, X-Y., Leng, J., Wang, S-M., Asiri, A. M., Marwani, H. M., Qin, H-L. A facile and mild Pd-catalyzed one-pot process for direct hydrodeoxygenation (HDO) phenols to arenes through a ArOSO₂F intermediates transformation. *Tetrahedron Lett.* **58**, 2340–2343 (2017)
- ⁴²⁶ Sajiki, H., Mori, A., Mizusaki, T., Ikawa, T., Maegawa, T., Hirota, K. Pd/C-catalyzed deoxygenation of phenol derivatives using mg metal and MeOH in the presence of NH₄OAc. *Org. Lett.* **8**, 987–990 (2006).
- ⁴²⁷ Mori, A., Mizusaki, T., Ikawa, T., Maegawa, T., Monguchi, Y., Jajiki, H. Palladium on carbon-diethylamine-mediated hydrodeoxygenation of phenol derivatives under mild conditions. *Tetrahedron* **63**, 1270–1280 (2007).
- ⁴²⁸ Benedikt, F. W. K., Friedrich, H. B. G., Prillinger, F. Zur Kenntnis der Carboxylierung von Phenolen. *Monatshefte für Chemie* **98**, 1071–1091 (1950).
- ⁴²⁹ Rieche, A., Gross, H., Höft, E. über α -Halogenäther, IV: Synthesen aromatischer Aldehyde mit Dichlormethyl-alkyläthern *Chemische Berichte* **93**, 88–94 (1960).
- ⁴³⁰ Prakash, G. K. S., Mathew, T., Hoole, D., Esteves, P. M., Wang, Q., Rasul, G., Olah, G. A. N-Halosuccinimide/BF₃-H₂O, Efficient Electrophilic Halogenating Systems for Aromatics. *J. Am. Chem. Soc.* **126**, 15770–15776 (2004).
- ⁴³¹ Güngör, T., Chen, Y., Golla, R., Ma, Z., Corte, J. R., Northrop, J. p., Bin, B., Dickson, J. K., Stouch, T., Zhou, R., Johnson, S. E., Seethala, R., Feyen, J. H. M. Synthesis and characterization of 3-arylquinazolinone and 3-arylquinazolinethione derivatives as selective estrogen receptor beta modulators. *J. Med. Chem.* **49**, 2440–2455 (2006).
- ⁴³² Schudel P, Mayer H, Isler O. Tocopherols, II. Chemistry. In: The Vitamins. Chemistry, Physiology, Pathology and Methods. 2nd edition, eds. Sebrell WH Jr & Harris RS. *Academic Press, New York*, pp 168–218 (1972).
- ⁴³³ Kontush, A, Finckh, B., Karten, B., Kohlschütter, A., Beisiegel, U. Antioxidant and prooxidant activity of alpha-tocopherol in human plasma and low density lipoprotein. *J. Lipid Res.* **37**, 1436–1448 (1996).

-
- ⁴³⁴ Gal, S., Pinchuk, I., Lichtenberg, D. Peroxidation of liposomal palmitoyllinoleoylphosphatidylcholine (PLPC), effects of surface charge on the oxidizability and on the potency of antioxidants. *Chem. Phys. Lipids* **126**, 95–110 (2003).
- ⁴³⁵ Liu, P. H., Aoi, W., Takami, M., Terajima, H., Tanimura, Y., Naito, Y., Itoh, Y., Yoshikawa, T. The astaxanthin-induced improvement in lipid metabolism during exercise is mediated by PGC-1 α increase in skeletal muscle. *J. Clin. Biochem. Nutr* **54**, 86–89 (2014).
- ⁴³⁶ Webster, R. D. New insights into the oxidative electrochemistry of vitamin E. *Acc. Chem. Res.* **40**, 251–257 (2007).
- ⁴³⁷ Eckart, W. U. ‘Der König der Krankheiten’ - Wie entstand die besondere Aufmerksamkeit für Krebskranke? Ein Essay. *Z. Evid. Fortbild. Qual. Gesundheitswes.* **107**, 105–115 (2013).
- ⁴³⁸ Chakraborty, S., Rahman, T. The difficulties in cancer treatment. *Ecancermedicalsecience* **6**, ed16 (2012).
- ⁴³⁹ Liao, J. B. Viruses and human cancer. *Yale J. Biology Med.* **79**, 115–122 (2006).
- ⁴⁴⁰ Jemal, A., Ward, E. M., Johnson, C. J., Cronin, K. A., Ma, J., Ryerson, B. A., Mariotto, A., Lake, A. J., Wison, R., Sherman, R. L., Anderson, R. N., Henley, S. J., Kohler, B. A., Penberthy, L., Feuer, E. J., Weir, H. K. Annual Report to the Nation on the Status of Cancer, 1975-2014, Featuring Survival. *J. Natl. Cancer Inst.* **109**, 1–22 (2017).
- ⁴⁴¹ Lodish, H., Berk, A., Zipursky, S. L., Matsudaira, P., Baltimore, D., Darnell, J. Molecular Cell Biology. Section 24.1, Tumor Cells and the Onset of Cancer 4th edition. *New York: W. H. Freeman;* (2000)
- ⁴⁴² Palmer, B. V, Walsh, G. A, McKinna, J. A, Greening, W. P. Adjuvant chemotherapy for breast cancer: side effects and quality of life. *Br. Med. J.* **281**, 1594–1597 (1980).
- ⁴⁴³ Haffty, B. G., Yang, Q., Reiss, M., Kearney, T., Higgins, S. A., Weidhaas, J., Harris, L., Hait, W., Toppmeyer, D. Locoregional relapse and distant metastasis in conservatively managed triple negative early-stage breast cancer. *J. Clin. Oncol.* **24**, 5652–5657 (2006).
- ⁴⁴⁴ Cheok, C. F. Protecting normal cells from the cytotoxicity of chemotherapy. *Cell Cycle* **11**, 2227-2227 (2012)
- ⁴⁴⁵ Mettler, F. A., Milton, J. G. Essentials of Nuclear Medicine Imaging. 6th ed *Elsevier* (2012)
- ⁴⁴⁶ Allisy-Roberts, P. J. Radiation quantities and units: understanding the sievert. *J. Radiol. Prot.* **25**, 97–100 (2005).
- ⁴⁴⁷ Saha, G. B. Basics of PET Imaging: Physics, Chemistry, and Regulations. *Springer New York* (2010).

-
- ⁴⁴⁸ United Nations Scientific Committee on the Effects of Atomic Radiation. Sources and Effects of Ionizing Radiation: United Nations Scientific Committee on the Effects of Atomic Radiation; *UNSCEAR Regulation* **10**, part 20 (2017)
- ⁴⁴⁹ Kaushik, A., Estimation of patient dose in (18)F-FDG and (18)F-FDOPA PET/CT examinations. *J. Cancer Res. Ther.* **9**, 477–83 (2013).
- ⁴⁵⁰ Sebastià, C., Luna, A., Paredes, P., Nicolau, C. Functional imaging of renal cell carcinoma. *Funct. Imaging Oncol. Clin. Appl. - Vol. 2* **7**, 1143–1171 (2014).
- ⁴⁵¹ Ansell, S. M., Armitage, J. O. Positron emission tomographic scans in lymphoma: Convention and controversy. *Mayo Clin. Proc.* **87**, 571–580 (2012).
- ⁴⁵² Kaasinen, V., Nurmi, E., Brück, A., Eskola, O., Bergman, J., Solin, O., Rinne, J. O. Increased frontal [(18)F]fluorodopa uptake in early Parkinson's disease: sex differences in the prefrontal cortex. *Brain* **124**, 1125–1130 (2001).
- ⁴⁵³ Risk, C., Law, M. W. Whole-Body PET / CT Scanning : Purpose : Methods : Results : Conclusion : **251**, (2009).
- ⁴⁵⁴ Miki, T., Shimada, H., Kin, J-S., Yamamoto, Y., Sugino, Masakazu, S., Kowa, H., Heurling, K., Zanette, M., Sherwin, P. F., Senda, M. Brain uptake and safety of Flutemetamol F 18 injection in Japanese subjects with probable Alzheimer's disease, subjects with amnesic mild cognitive impairment and healthy volunteers. *Ann. Nucl. Med.* **31**, 260–272 (2017).
- ⁴⁵⁵ Galldiks, N., Stoffels, G., Filss, C., Rapp, M., Blau, T., Tscherpel, C., Ceccon, G., Dunkl, V., Weinzierl, M., Stoffel, M., Sabel, M., Fink, G. R., Shah, N. J., Langen, K-J. The use of dynamic O-(2-18F-fluoroethyl)-l-tyrosine PET in the diagnosis of patients with progressive and recurrent glioma. *Neuro. Oncol.* **17**, 1293–1300 (2015).
- ⁴⁵⁶ Yang, L., Rieves, D., Ganley, C. Brain Amyloid Imaging - FDA Approval of Florbetapir F18 Injection. *N. Engl. J. Med* **367**, 885–887 (2010).
- ⁴⁵⁷ Nanni, C., Schiavina, R., Brunocilla, E., Boschi, S., Borghesi, M., Zanoni, L., Pettinato, C., Marorana, G., Fanti, S. 18F-Fluciclovine PET/CT for the Detection of Prostate Cancer Relapse: A Comparison to 11C-Choline PET/CT. *Clin. Nucl. Med.* **40**, 386–91 (2015).
- ⁴⁵⁸ Sohlberg, A., Watabe, H., Shidahara, M., Iida, H. Body-contour versus circular orbit acquisition in cardiac SPECT: assessment of defect detectability with channelized Hotelling observer. *Nucl. Med. Commun.* **28**, 937–42 (2007).
- ⁴⁵⁹ Houghton, M. *The American Heritage® Science Dictionary* (2002)
- ⁴⁶⁰ Chiste, V., Kuzmenko, N. K., Be, M. M. Fluorine-18. *Lab. Natl. Henri Becquerel* **9**, 1–5 (2014).

-
- ⁴⁶¹ Tilbury, R. S., Robert Dahl, J., Mamacos, J. P., Laughlin, J. S. Fluorine-18 production for medical use by helium-3 bombardment of water. *Int. J. Appl. Radiat. Isot.* **21**, 277–280 (1970).
- ⁴⁶² DeJesus, O. T., Martin, J. A., Yasillo, N. J., Gatley, S. J., Cooper, M. D. [18F]Fluoride from a small cyclotron for the routine synthesis of [18F]2-Fluoro-2-deoxy-d-glucose. *Int. J. Radiat. Appl. Instrumentation. Part* **37**, 397–401 (1986).
- ⁴⁶³ Policroniades, R., Moreno, E., Varela, A., Murillo, G. F-18 production by means of $^{20}\text{Ne}(\text{d},4\text{He})$ reaction at ININ. *Rev. Mex. Fis.* **54**, 46–49 (2008).
- ⁴⁶⁴ Nickles, R. J., Daube, M. E., Ruth, T. J. An $^{18}\text{O}_2$ target for the production of [18F]F₂. *Int. J. Appl. Radiat. Isot.* **35**, 117–122 (1984).
- ⁴⁶⁵ Levin, C. Basic Physics of Radionuclide Imaging. *Emiss. Tomogr.* 53–88 (2004).
- ⁴⁶⁶ Clark, J. H. Fluoride ion as a base in organic synthesis *Chem. Rev.* **80**, 429–452 (1980).
- ⁴⁶⁷ Lange, N. Handbook of Chemistry. *Soil Science* table 4.11 (2005).
- ⁴⁶⁸ Finch, A., Hall, F. M. Standard Enthalpies of Formation and Lattice Energies of Alkylammonium Halides .1. Propylamine Hydrochlorides. *J. Chem. Soc. Trans.* 915–916 (1982).
- ⁴⁶⁹ Reed, C. D., Launay, G. G., Carroll, M. A. Evaluation of tetraethylammonium bicarbonate as a phase-transfer agent in the formation of [18F]fluoroarenes. *J. Fluor. Chem.* **143**, 231–237 (2012).
- ⁴⁷⁰ Pressman, B. C. Biological applications of ionophores. *Annu. Rev. Biochem.* **45**, 501–530 (1976).
- ⁴⁷¹ Wynn, D. A., Roth, M. M., Pollard, B. D. The solubility of alkali-metal fluorides in non-aqueous solvents with and without crown ethers, as determined by flame emission spectrometry. *Talanta* **31**, 1036–1040 (1984).
- ⁴⁷² Lehn, J. M. Sauvage, J. P. Cryptates. XVI. [2]-Cryptates. Stability and Selectivity of Alkali and Alkaline- Earth Macrobicyclic Complexes. *J. Am. Chem. Soc.* **97**, 6700–6707 (1975).
- ⁴⁷³ Tso, W. W., Fung, W. P., Tso, M. Y. W. Variability of crown ether toxicity. *J. Inorg. Biochem.* **14**, 237–244 (1981).
- ⁴⁷⁴ Loiseau, A., Hill, M., René-Corail, L., Castaing, M. Transport of competing Na and K ions by (222) C10-cryptand, an ionizable mobile carrier: effects of pH and temperature. *Biochimica et Biophysica Acta* **1238**, 107–117 (1995).
- ⁴⁷⁵ Meisenheimer, J. Über Reactionen aromatischer Nitrokörper. *Justus Liebigs Ann. Chem.* **323**, 205–246 (1902).

-
- ⁴⁷⁶ Guo, N., Alagille, D., Tamagnan, G., Price, R. R., Baldwin, R. M. Microwave-induced nucleophilic [¹⁸F]fluorination on aromatic rings: Synthesis and effect of halogen on [¹⁸F]fluoride substitution of meta-halo (F, Cl, Br, I)-benzonitrile derivatives. *Appl. Radiat. Isot.* **66**, 1396–1402 (2008).
- ⁴⁷⁷ Khan, N. U. H., Lee, B. C., Lee, S.-Y., Choe, Y. S., Jun, C.-H., Chi, D. Y. Hydroacylation of 4-[¹⁸F]fluorobenzaldehyde: A novel method for the preparation of 4'-[¹⁸F]phenylketones. *J. Label. Compd. Radiopharm.* **45**, 1045–1053 (2002).
- ⁴⁷⁸ Lemaire, C., Damhaut, P., Plenevaux, A., Cantineau, R., Christiaens, L., Guillaume, M. Synthesis of fluorine-18 substituted aromatic aldehydes and benzylbromides, new intermediates for n.c.a. [¹⁸F]fluorination *Appl. Radiat. Isot.* **43**, 485–494 (1992).
- ⁴⁷⁹ Worrell, B. T., Hein, J. E., Fokin, V. V. Halogen exchange (Halex) reaction of 5-iodo-1,2,3-triazoles: Synthesis and applications of 5-fluorotriazoles. *Angew. Chemie - Int. Ed.* **51**, 11791–11794 (2012).
- ⁴⁸⁰ Sun, H., DiMagno, S. G. Fluoride relay: a new concept for the rapid preparation of anhydrous nucleophilic fluoride salts from KF. *Chem. Commun. (Camb)*. 528–9 (2007).
- ⁴⁸¹ Engell, T. & Grigg, J. ¹⁸F-labelled aldehyde compositions for radiofluorination. *WO2014082958 A1* (2014).
- ⁴⁸² Poethko, T., Schottelius, M., Thumshirn, G., Hersel, U., Herz, M., Henricksen, G., Kessler, H., Schwaiger, M., Wester, H.-J. Two-step methodology for high-yield routine radiohalogenation of peptides: (¹⁸F)-labeled RGD and octreotide analogs. *J Nucl Med* **45**, 892–902 (2004).
- ⁴⁸³ Balz, G., Schiemann, G. Über aromatische Fluorverbindungen, I. : Ein neues Verfahren zu ihrer Darstellung *Chemische Berichte* **60**, 1186–1190 (1927).
- ⁴⁸⁴ Argentini, M., Wiese, C., Weinreich, R. Syntheses of 5-fluoro-D/L-dopa and [¹⁸F]5-fluoro-D/L-dopa. *J. Fluor. Chem.* **68**, 141–144 (1994).
- ⁴⁸⁵ Kook, C. S., Reed, M. F., Digenis, G. A. Preparation of [¹⁸F]Haloperidol *Integr. Med.* **18**, 533–535 (1975).
- ⁴⁸⁶ Atkins, H. L., Christman, D. R., Fowler, J. S., Hauser, W., Hoyte, R. M., Klopper, S. F., Lin, S. S., Wolf, A. P. Organic radiopharmaceuticals labeled with isotopes of short half-life. V. ¹⁸F-Labeled 5- and 6-Fluorotryptophan. *J. Nucl. Med.* **13**, 713–719 (1972).
- ⁴⁸⁷ Tewson, T. J., Welch, M. J. Preparation of Fluorine-18 Aryl Fluorides: Piperidyl Triazenes as a Source of Diazonium Salts. *J Chem Soc, Chem Commun* 1149–1150 (1979).
- ⁴⁸⁸ Sander, K., Gendron, T., Yiannaki, E., Cybulska, K., Kalber, T. L., Lythgoe, M. F., Årstad, E. Sulfonium Salts as Leaving Groups for Aromatic Labelling of Drug-like Small Molecules with Fluorine-18. *Sci. Rep.* **5**, 9941 (2015).

-
- ⁴⁸⁹ Yusubov, M. S., Svitich, D. Y., Larkina, M. S., Zhdankin, V. V. Applications of iodonium salts and iodonium ylides as precursors for nucleophilic fluorination in positron emission tomography. *Arkivoc* **2013**, 364–395 (2013).
- ⁴⁹⁰ Moon, B. S., Kil, H. S., Park, J. H., Kim, J. S., Park, J., Chi, D. Y., Lee, B. C., Kim, S. E. Facile aromatic radiofluorination of [¹⁸F]flumazenil from diaryliodonium salts with evaluation of their stability and selectivity. *Org. Biomol. Chem.* **9**, 8346 (2011).
- ⁴⁹¹ Lee, H. G., Milner, P. J., Buchwald, S. L. Pd-catalyzed nucleophilic fluorination of aryl bromides. *J. Am. Chem. Soc.* **136**, 3792–3795 (2014).
- ⁴⁹² Konovalov, A. I., Gorbacheva, E. O., Miloserdov, F. M., Grushin, V. V. Ruthenium-catalyzed nucleophilic fluorination of halobenzenes. *Chem. Commun.* **51**, 13527–13530 (2015).
- ⁴⁹³ Hollingworth, C., Gouverneur, V. Transition metal catalysis and nucleophilic fluorination. *Chem. Commun.* **48**, 2929 (2012).
- ⁴⁹⁴ Kamlet, A. S., Neumann, C. N., Lee, E., Carlin, S. M., Mosley, C. K., Stephenson, N., Hooker, J. M., Ritter, T. Application of Palladium-Mediated 18F-Fluorination to PET Radiotracer Development: Overcoming Hurdles to Translation. *PLoS One* **8**, 1–10 (2013).
- ⁴⁹⁵ Lee, E., Hooker, J. M., Ritter, T. Nickel-mediated oxidative fluorination for PET with aqueous [¹⁸F] fluoride. *J. Am. Chem. Soc.* **134**, 17456–17458 (2012).
- ⁴⁹⁶ Mossine, A. V., Brooks, A. F., Makaravage, K. J., Miler, J. M., Ichiishi, N., Sanford, M. S., Scott, P. J. H. Synthesis of [¹⁸F]Arenes via the Copper-Mediated [¹⁸F]Fluorination of Boronic Acids. *Org. Lett.* **17**, 5780–5783 (2015).
- ⁴⁹⁷ Watson, D. A., Su, M., Teverovskiy, G., Zhang, Y., Garcia-Fortanet, J., Kinzel, T., Buchwald, S. L. Formation of ArF from LPdAr(F): catalytic conversion of aryl triflates to aryl fluorides. *Science* **325**, 1661–4 (2009).
- ⁴⁹⁸ Cardinale, J., Ermert, J., Kügler, F., Helfer, A., Brandt, M. R., Coenen, H. H. Carrier-effect on palladium-catalyzed, nucleophilic 18F- fluorination of aryl triflates. *J. Label. Compd. Radiopharm.* **55**, 450–453 (2012).
- ⁴⁹⁹ Tang, P., Wang, W., Ritter, T. Deoxyfluorination of phenols. *J. Am. Chem. Soc.* **133**, 11482–11484 (2011).
- ⁵⁰⁰ Murakami, M., Takahashi, K., Kondo, Y., Mitzusawa, S., Nakamichi, H., Sasaki, H., Hagami, E., Iida, H., Kanno, I., Kanno, I., Miura, S., Uemura. The comparative synthesis of 18F by electrophilic substitution with 18F-F₂ and 18F-AcOF -F₂ *J. Label. Compd. Radiopharm.* **5**, 573-578 (1987)
- ⁵⁰¹ Tius, M. A. Xenon difluoride in synthesis. *Tetrahedron* **51**, 6605–6634 (1995).

-
- ⁵⁰² Zhang, Y., Yamamoto, H. Lewis acid catalyzed halogenation of activated carbon atoms. *EP1928559A2* (2008).
- ⁵⁰³ Bergman, J., Solin, O. Fluorine-18-labeled fluorine gas for synthesis of tracer molecules. *Nucl. Med. Biol.* **24**, 677–683 (1997).
- ⁵⁰⁴ Forsback, S., Marjamäki, P., Eskola, O., Bergman, J., Rokka, J., Grönroos, T., Haaparanta, M., Solin, O. [18F]CFT synthesis and binding to monoamine transporters in rats. *EJNMMI Res.* **2**, 3 (2012).
- ⁵⁰⁵ Kachur, A. V., Arroyo, A. D., Popov, A. V., Saylor, S. J., Delikatny, E. J. Synthesis of F-18 labeled resazurin by direct electrophilic fluorination. *J. Fluor. Chem.* **178**, 136–141 (2015).
- ⁵⁰⁶ Borodkin, G. I., Zaikin, P. A., Shubin, V. G. Electrophilic fluorination of aromatic compounds with NF type reagents: Kinetic isotope effects and mechanism. *Tetrahedron Lett.* **47**, 2639–2642 (2006).
- ⁵⁰⁷ Lou, S.-J., Xu, D. Q., Xia, A. B., Wang, Y. F., Liu, Y. K., Du, X. H., Xu, Z. Y. Pd(OAc)₂-catalyzed regioselective aromatic C-H bond fluorination. *Chem. Commun. (Camb)*. **49**, 6218–20 (2013).
- ⁵⁰⁸ Furuya, T., Strom, A. E., Ritter, T. Silver-mediated fluorination of functionalized aryl stannaries. *J. Am. Chem. Soc.* **131**, 1662–1663 (2009).
- ⁵⁰⁹ Furuya, T., Rios, D. Fluorination of Boronic Acids Mediated by Silver (I) Triflate. *Org. Lett.* 5993–5996 (2009).
- ⁵¹⁰ Perrin, J. C. Hodgkin's lymphoma, PET scan C001/7581 *ISM / Science photolibrary*
- ⁵¹¹ Zarogoulidis, P., Cheva, A., Zarampouka, K., Huang, H., Li, C., Huang, Z., Katsikogiannis, N., Zarogoulidis, K. Tocopherols and tocotrienols as anticancer treatment for lung cancer: Future nutrition. *J. Thorac. Dis.* **5**, 349–352 (2013).
- ⁵¹² Yang, C. S., Suh, N., Kong, A. T. Does vitamin E prevent or promote cancer? *Cancer Prev. Res.* **5**, 701–705 (2013).
- ⁵¹³ Keliher, E. J., Klubnick, J. A., Reiner, T., Mazitschek, R., Weissleder, R. Efficient Acid-catalyzed ¹⁸F/¹⁹F Fluoride Exchange of BODIPY Dyes *ChemMedChe* **9**, 1368–1373 (2014).
- ⁵¹⁴ Azhdarinia, A., Ghosh, P., Ghosh, S., Wilganowski, N., Sevick-Muraca, E. M. Dual-labeling strategies for nuclear and fluorescence molecular imaging: A review and analysis. *Mol. Imaging Biol.* **14**, 261–276 (2012).

-
- ⁵¹⁵ Van der Born, D., Pees, A., Poot, A. J., Orru, R. V. A., Windhorst, A. D., Vugts, D. J. Fluorine-18 labelled building blocks for PET tracer synthesis. *Chem. Soc. Rev.* **46**, 4709–4773 (2017).
- ⁵¹⁶ Jacobson, O., Kiesewetter, D. O., Chen, X. Fluorine-18 Radiochemistry, Labeling Strategies and Synthetic Routes. *Bioconjugate chem.* **26**, 1-18 (2015).
- ⁵¹⁷ Tang, P., Wang, W., Ritter, T. Deoxyfluorination of phenols. *J. Am. Chem. Soc.* **133**, 11482–11484 (2011).
- ⁵¹⁸ Neumann, C. N., Hooker, J. M., Ritter, T. Corrigendum: Concerted nucleophilic aromatic substitution with $^{19}\text{F}^-$ and $^{18}\text{F}^-$. *Nature* **538**, 274–274 (2016).
- ⁵¹⁹ Sergeev, M. E., Morgia, F., Lazari, M., Wang, C., van Dam, R. M. Titania-Catalyzed Radiofluorination of Tosylated Precursors in Highly Aqueous Media. *J. Am. Chem. Soc.* **137**, 5686-5694 (2015).
- ⁵²⁰ Nagaki, A., Uesugi, Y., Kim, H., Yoshida, J. I. Synthesis of functionalized aryl fluorides using organolithium reagents in flow microreactors. *Chem. - An Asian J.* **8**, 705–708 (2013).
- ⁵²¹ Tredwell, M., Preshlock, S. M., Taylor, N. J., Gruber, S., Huiban, M., Passchier, J., Mercier, J., Génicot, C., Gouverneur, V. A general copper-mediated nucleophilic ^{18}F fluorination of arenes. *Angew. Chemie - Int. Ed.* **53**, 7751–7755 (2014).
- ⁵²² Ohtani, B., Prieto-Mahaney, O. O., Li, D., Abe, R. What is Degussa (Evonic) P25? Crystalline composition analysis, reconstruction from isolated pure particles and photocatalytic activity test. *J. Photochem. Photobiol. A Chem.* **216**, 179–182 (2010).
- ⁵²³ Xiong, Z. G., Wu, H., Zhang, L. H., Gu, Y., Zhao, X. S. Synthesis of TiO_2 with controllable ratio of anatase to rutile. *J. Mater. Chem. A* **2**, 9291–9297 (2014).
- ⁵²⁴ Preliminary data received April 27 2015 from Dr. Bourikas via Dr. Stamatatos.
- ⁵²⁵ Kordouli, E., Dracopoulos, V., Vaimakis, T., Bourikas, K., Lycourghiotis, A., Kordulis, C. Comparative study of phase transition and textural changes upon calcination of two commercial titania samples: A pure anatase and a mixed anatase-rutile. *J. Solid State Chem.* **232**, 42–49 (2015).
- ⁵²⁶ Lei, X., Jalla, A., Abou Shama, M., Stafford, J., Cao, B. Chromatography-Free and Eco-Friendly Synthesis of Aryl Tosylates and Mesylates. *Synthesis (Stuttg.)* **47**, 2578–2585 (2015).
- ⁵²⁷ Coenen, H. H., Moerlein, S. M. Regiospecific aromatic fluorodemetalation of group IVb metalloarenes using elemental fluorine or acetyl hypofluoride *J. Fluo. Chem.* **36**, 63–75 (1987).

-
- ⁵²⁸ Hess, E., Sichler, S., Kluge, A., Coenen, H. H. Synthesis of 2-[18F]fluoro-l-tyrosine via regioselective fluoro-de-stannylation. *Appl. Radiat. Isot.* **57**, 185–191 (2002).
- ⁵²⁹ Miller, D. K. Facile conversion of chromane-6-triflate to chromane-6-alanines under palladium conditions. *Tetrahedron Lett.* **54**, 811–813 (2013).
- ⁵³⁰ Mazzini, F., Netscher, T., Salvadori, P. Efficient synthesis of vitamin E amines. *European J. Org. Chem.* 2063–2068 (2009).
- ⁵³¹ Thompson, A. L. S., Kabalka, G. W., Akula, M. R., Huffman, J. W. The conversion of phenols to the corresponding aryl halides under mild conditions. *Synthesis (Stuttg.)*. 547–550 (2005).
- ⁵³² Diemer, V., Chaumeil, H., Defoin, A., Carré, C. Syntheses of extreme sterically hindered 4-methoxyboronic acids. *Tetrahedron* **66**, 918–929 (2010).
- ⁵³³ Schmidt-Leithoff, J., Pichlmair, S., Bello, C. Process for the borylation of organohalides. *US20130023689 A1* (2013).
- ⁵³⁴ Preshlock, S., Calderwood, S., Verhoog, S., Tredwell, M., Huiban, M., Hienzsch, A., Gruber, S., Wilson, T. C., Taylor, N. J., Cailly, T., Schedler, M., Collier, T. L., Passchier, J., Smits, R., Mollitor, J., Hoepping, A., Mueller, M., Chhristophe, G., Mercier, G., Gouverneur, V. Enhanced copper-mediated 18F-fluorination of aryl boronic esters provides eight radiotracers for PET applications. *Chem. Commun.* **52**, 8361–8364 (2016).
- ⁵³⁵ Fujimoto, T., Becker, F., Ritter, T. PhenoFluor: Practical Synthesis, New Formulation, and Deoxy fluorination of Heteroaromatics. 10–13 (2014).
- ⁵³⁶ Chand, S., Banwell, M. G. Biomimetic preparation of the racemic modifications of the stilbenolignan aiphanol and three congeners. *Aust. J. Chem.* **60**, 243–250 (2007).
- ⁵³⁷ Cohen, N., Saucy, G. Synthesis of Optically Active Vitamin E *US4208332* (1980).
- ⁵³⁸ Beyzavi, M. H., Mandal, D., Strebl, M. G., Neumann, C. N., D’Amato, E. M., Chen, J., Hooker, J. M., Ritter, T. F-Deoxyfluorination of Phenols via Ru π -Complexes. Aug. 3 (2017).
- ⁵³⁹ Ross, T. L., Ermert, J., Hocke, C., Coenen, H. H. Nucleophilic 18F-fluorination of heteroaromatic iodonium salts with no-carrier-added [18F]fluoride. *J. Am. Chem. Soc.* **129**, 8018–8025 (2007).
- ⁵⁴⁰ Chun, J. H., Lu, S., Lee, Y. S., Pike, V. W. Fast and high-yield microreactor syntheses of ortho-substituted [18F]Fluoroarenes from reactions of [18F]Fluoride ion with diaryliodonium salts. *J. Org. Chem.* **75**, 3332–3338 (2010).
- ⁵⁴¹ Chun, J.-H., Pike, V. W. Single-step syntheses of no-carrier-added functionalized [18F]fluoroarenes as labeling synthons from diaryliodonium salts. *Org. Biomol. Chem.* **11**, 6300–6 (2013).

-
- ⁵⁴² Bielawski, M., Aili, D., Olofsson, B. Regiospecific one-pot synthesis of diaryliodonium tetrafluoroborates from arylboronic acids and aryl iodides. *J. Org. Chem.* **73**, 4602–4607 (2008).
- ⁵⁴³ Cardinale, J., Ermert, J., Humpert, S., Coenen, H. H. Iodonium ylides for one-step, no-carrier-added radiofluorination of electron rich arenes, exemplified with 4-([¹⁸F]fluorophenoxy)-phenylmethyl)piperidine NET and SERT ligands. *RSC Adv.* **4**, 17293–17299 (2014).
- ⁵⁴⁴ Satyamurthy, N., Barrio, J. R. No-carrier-added nucleophilic [F-18] fluorination of aromatic compounds. *WO2010117435A2* (2010).
- ⁵⁴⁵ Bielawski, M., Olofsson, B. High-yielding one-pot synthesis of diaryliodonium triflates from arenes and iodine or aryl iodides. *Chem. Commun. (Camb)*. **2**, 2521–2523 (2007).
- ⁵⁴⁶ Wu, Y., Izquierdo, S., Vidossich, P., Lledos, A., Shafir, A. NH-Heterocyclic Aryliodonium Salts and their Selective Conversion into N1-Aryl-5-iodoimidazoles. *Angew. Chemie - Int. Ed.* **55**, 7152–7156 (2016).
- ⁵⁴⁷ Chun, J-H., Pike, V. W. Regiospecific syntheses of functionalized diaryliodonium tosylates via [hydroxy(tosyloxy)iodo]arenes generated in situ from (diacetoxyiodo)arenes. *J. Org. Chem.* **17**, 1931–1938 (2012).
- ⁵⁴⁸ Heider, U., Schmidt, M., Sartori, P., Ignatyev, N., Kucherina, A., Ludmila, Z. Verfahren zur herstellung von bis (trifluormethyl)imido-salzen. *WO2002064542 A2* (2002).
- ⁵⁴⁹ Chun, J-H., Telu, S., Lu, S., Pike, V. W. Radiofluorination of diaryliodonium tosylates under aqueous-organic and cryptand-free conditions *Org. Biomol. Chem.* **11**, 5094–5099 (2013).
- ⁵⁵⁰ Brömme, T., Oprych, D., Horst, J., Pinto, P. S. & Strehmel, B. New iodonium salts in NIR sensitized radical photopolymerization of multifunctional monomers. *RSC Adv.* **5**, 69915–69924 (2015).
- ⁵⁵¹ Hamnett, D. J., Moran, W. J. Improving alkynyl(aryl)iodonium salts: 2-anisyl as a superior aryl group. *Org. Biomol. Chem.* **12**, 4156 (2014).
- ⁵⁵² Carroll, M. A., Jones, C., Tang, S. L. Fluoridation of 2-thienyliodonium salts. *J. Label. Compd. Radiopharm.* **50**, 450–451 (2007).
- ⁵⁵³ Carroll, M. A., Nairne, J., Smith, G., Widdowson, D. A. Radical scavengers: A practical solution to the reproducibility issue in the fluoridation of diaryliodonium salts. *J. Fluor. Chem.* **128**, 127–132 (2007).
- ⁵⁵⁴ Bachmann, B., Carlson, C. L., Robinson, M. Monomers and polymers. VII. Synthesis with the aid of metallostyrenes. *Purdue University* **73**, 1964–1965 (1951).

-
- ⁵⁵⁵ Al-Qahtani, M. H., Pike, V. W. Rapid mild synthesis of [¹¹C] benzophenones by Pd(0)-catalysed [¹¹C]-carbonylative coupling of iodoarenes with phenyltributylstannane in DME-water. *J. Labelled. Cpd. Radiopharm.* **43**, 825-835 (2000).
- ⁵⁵⁶ Chen, K., Zhang, S., He, P., Li, P. Efficient metal-free photochemical borylation of aryl halides under batch and continuous-flow conditions. *Chem. Sci.* **7**, 3676–3680 (2016).
- ⁵⁵⁷ Rotstein, B. H., Stephenson, N. A, Vasdev, N., Liang, S. H. Spirocyclic hypervalent iodine(III)-mediated radiofluorination of non-activated and hindered aromatics. *Nat. Commun.* **5**, 4365 (2014).
- ⁵⁵⁸ Robbins, D. W., Hartwig, J. F. Sterically Controlled Alkylation of Arenes through Iridium-Catalyzed C-H Borylation. *Angew. Chem. Int. Ed.* **52**, 933–937 (2013).
- ⁵⁵⁹ Mukaiyama, T., Kitagawa, H., Matsuo, J. Aromatic iodination with iodine monochloride by using a catalytic amount of ferrocenium tetrakis(3,5-bis(trifluoromethyl)phenyl)borate. *Tetrahedron Lett.* **41**, 9383–9386 (2000).
- ⁵⁶⁰ Mulholland, G. K., Zheng, Q. A. Direct Iodination Method With Iodine and Silver Triflate for the Synthesis of Spect and Pet Imaging Agent Precursors. *Synth. Commun.* **30**, 3059–3068 (2001).
- ⁵⁶¹ Khansole, S. V., Junne, S. B., Sayyed, M. A., Vibhute, Y. B. Convenient and Efficient Method for the Iodination of Aromatic Amines by Pyridinium Iodochloride. *Synth. Commun.* **38**, 1792–1798 (2008).
- ⁵⁶² Barnette, W. E. N-Fluoro-N-alkylsulfonamides: Useful Reagents for the Fluorination of Carbanions. *J. Am. Chem. Soc.* **106**, 452–454 (1984).
- ⁵⁶³ Satyamurthy, N., Bida, G. T., Phelps, M. E., Barrio, J. R. N-[¹⁸F]fluoro-N-alkylsulfonamides: Novel reagents for mild and regioselective radiofluorination. *Int. J. Radiat. Appl. Instrumentation. Part* **41**, 733–738 (1990).
- ⁵⁶⁴ Teare, H., Robins, E. G., Årstad, E., Luthra, S. K., Gouverneur, V. Synthesis and reactivity of [¹⁸F]-N-fluorobenzenesulfonimide. *Chem. Commun.* **23**, 2330–2332 (2007).
- ⁵⁶⁵ Ziegler, K., Crössmann, F., Kleiner, H., Schäfer, O. Untersuchungen über alkali-organische Verbindungen. I. Reaktionen zwischen ungesättigten Kohlenwasserstoffen und Alkalimetall-alkylen Justus *Liebigs Ann. Chemie* **473**. 1-33, (1929).
- ⁵⁶⁶ Neumann, H., Seebach, D. Stereospecific preparation of terminal vinyl lithium derivatives by Br/Li-exchange with t-butyllithium. *Tetrahedron Lett.* **17**, 4839–4842 (1976).
- ⁵⁶⁷ Yu, S. Review of ¹⁸F-FDG synthesis and quality control. *Biomed. Imaging Interv. J.* **2**, (2006).

-
- ⁵⁶⁸ Shamma, T., Buchholz, H., Prakash, G. K. S., Olah, G. A. Electrophilic fluorination of aromatics with selectfluor[®] and trifluoromethanesulfonic acid 1. *Isr. J. Chem.* **39**, 207–210 (1999).
- ⁵⁶⁹ Andreev, R. V., Borodkin, G. I., Shubin, V. G. Fluorination of aromatic compounds with N-fluorobenzenesulfonimide under solvent-free conditions. *Russ. J. Org. Chem.* **45**, 1468–1473 (2009).
- ⁵⁷⁰ Vincent, S. P., Burkart, M. D., Tsai, C.-Y., Zhang, Z., Wong, C.-H. Electrophilic fluorination-nucleophilic addition reaction mediated by SELECTFLUOR: Mechanistic studies and new applications. *J. Org. Chem.* **64**, 5264–5279 (1999).
- ⁵⁷¹ Xia, X. F., Zhu, S. L., Liu, J. B., Wang, D., Liang, Y. M. Copper-Catalyzed Radical-Promoted Aminocyclization of Acrylamides with N-Fluorobenzenesulfonimide. *J. Org. Chem.* **81**, 12482–12488 (2016).
- ⁵⁷² Sazepin, C. C., Leung, J. C. T., Okbinoğlu, T. Fluorine Transfer to Alkyl Radicals. *J. Am. Chem. Soc.* **134**, 1–31 (2012).
- ⁵⁷³ Füchtner, F., Angelberger, P., Kvaternik, H., Hammerschmidt, F., Simovc, B. P., Steinbach, J. Aspects of 6-[18F]fluoro-L-DOPA preparation: Precursor synthesis, preparative HPLC purification and determination of radiochemical purity. *Nucl. Med. Biol.* **29**, 477–481 (2002).
- ⁵⁷⁴ Nells, H., Deleenheer, A. Isocratic non-aqueous reversed-phase liquid-chromatography of carotenoids. *Anal. Chem.* **55**, 270–275 (1983).
- ⁵⁷⁵ Long, W., Mack, A. Comparison of selectivity differences among different Agilent ZORBAX Phenyl columns using acetonitrile or methanol. *Agil. Technol. Publ.* 12 (2009).
- ⁵⁷⁶ Zhang, W. Fluorocarbon stationary phases for liquid chromatography applications. *J. Fluor. Chem.* **129**, 910–919 (2008).
- ⁵⁷⁷ Jereb, M., Zupan, M., Stavber, S. Regioselectivity and kinetics of fluorination of alkyl substituted. *Arkivoc* **2003**, 187–197 (2003).
- ⁵⁷⁸ Poon, J. fei, Yan, J., Singh, V. P., Gates, P. J., Engman, L. Regenerable Radical-Trapping Tellurobistocopherol Antioxidants. *J. Org. Chem.* **81**, 12540–12544 (2016).
- ⁵⁷⁹ Chirakal, R., Brown, K. L., Frinau, G., Garnett, E. S. Synthesis of 2- and 3-fluorotyrosine with dilute fluorine gas. *J. Fluo. Chem.* **37**, 267–278 (1987).
- ⁵⁸⁰ Kachur, A.V., Popov, A. V., Karp, J. S., Delikatny, E. J. Direct fluorination of phenolsulfonphthalein: a method for synthesis of positron-emitting indicators for in vivo pH measurement. *Cell Biochem. Biophys* **66**, 1–5 (2013).

- ⁵⁸¹ Coenen, H. H., Franken, K., Kling, P., Stöcklin, G. Direct electrophilic radiofluorination of phenylalanine, tyrosine and dopa. *Int. J. Radiat. Appl. Instrumentation. Part* **39**, 1243–1250 (1988).
- ⁵⁸² DeJesus, O. T., Nickles, R. J., Murali, D. Synthesis of radiofluorinated O-tyrosine and preliminary evaluation as possible aromatic amino acid decarboxylase tracer. *J. Labelled Cpd. Radiopharma.* **42**, 781-788 (1999)
- ⁵⁸³ Lerman, O., Tor, Y., Hebel, D., Rozen, S. A novel electrophilic fluorination of activated aromatic rings using acetyl hypofluorite, suitable also for introducing fluorine-18 into benzene nuclei. *J. Org. Chem.* **49**, 806–813 (1984).
- ⁵⁸⁴ Lal, G. S., Pez, G. P., Syvret, R. G. Electrophilic NF Fluorinating Agents. *Chem. Rev.* **96**, 1737–1756 (1996).
- ⁵⁸⁵ Buckingham, F., Gouverneur, V. Asymmetric ¹⁸F-fluorination for applications in positron emission tomography. *Chem. Sci.* **7**, 1645–1652 (2016).
- ⁵⁸⁶ Kiselyov, A. S. Chemistry of N-fluoropyridinium salts. *Chem. Soc. Rev.* **34**, 1031 (2005).
- ⁵⁸⁷ Umemoto, T., Tomita, K., Kawada, K., Tomizawa, G. N-fluoropyridinium salt and process for preparing same. *EP0204535* (1986).
- ⁵⁸⁸ Bluck, G. W., Carter, N. B., Smith, S. C., Turnbull, M. D. Microwave fluorination: A novel, rapid approach to fluorination with Selectfluor® *J. Fluor. Chem.* **125**, 1873–1877 (2004).
- ⁵⁸⁹ Rosenau, T., Habicher, W. D. Novel tocopherol compounds I. Bromination of α -tocopherol - reaction mechanism and synthetic applications. *Tetrahedron* **51**, 7919–7926 (1995).
- ⁵⁹⁰ Patel, A., Mazzini, F., Netscher, T., Rosenau, T. A Novel Dimer of α -Tocopherol. *Res. Lett. Org. Chem.* **2008**, 1–4 (2008).
- ⁵⁹¹ Patel, A., Netscher, T., Rosenau, T. Stabilization of ortho-quinone methides by a bis(sulfonium ylide) derived from 2,5-dihydroxy-[1,4]benzoquinone. *Tetrahedron Lett.* **49**, 2442–2445 (2008).
- ⁵⁹² Huang, X., Liu, W., Ren, H., Groves, J. T. Late stage benzylic C-H fluorination with [¹⁸F]fluoride for PET imaging. *J. Am. Chem. Soc.* **136**, 6842–5 (2014).
- ⁵⁹³ Yuan, G., Wang, F., Stephanson, N. A., Wang, L., Rotstein, B. H., Vasdev, N., Tang, P., Liang, S. H. Metal-free ¹⁸F-labeling of aryl-CF₂H via nucleophilic radiofluorination and oxidative C–H activation. *Chem. Commun.* **53**, 126–129 (2017).
- ⁵⁹⁴ Lien, V. T., Riss, P. J. Radiosynthesis of [18F]trifluoroalkyl groups: Scope and limitations. *Biomed Res. Int.* **2014**, 1-10 (2014).
- ⁵⁹⁵ Kuboyama, T., Nakahara, M., Yoshino, M., Cui, Y., Sako, T., Wada, Y., Imanishi, T., Obika, S., Watanabe, Y., Suzuki, M., Doi, H. Stoichiometry-focused ¹⁸F-labeling of

-
- alkyne-substituted oligodeoxynucleotides using azido([18F]fluoromethyl)benzenes by Cu-catalyzed Huisgen reaction. *Bioorganic Med. Chem.* **19**, 249–255 (2011).
- ⁵⁹⁶ Adelwöhrer, C., Rosenau, T., Binder, W. H. & Kosma, P. Novel tocopheryl compounds. Part 15: One-pot formation of furotocopheryl derivatives. *Tetrahedron* **59**, 3231–3235 (2003).
- ⁵⁹⁷ Rosenau, T., Habicher, W. D., Chen, C. L. Preparation of protected amines or alkylated amino acids. *US5684132* (1997).
- ⁵⁹⁸ Dong, W. K., Hwan, J. S., Tae, L. S., Myung, H., Katzenellenbogen, J. A., Dae, Y. C. Facile nucleophilic fluorination reactions using tert-alcohols as a reaction medium: Significantly enhanced reactivity of alkali metal fluorides and improved selectivity. *J. Org. Chem.* **73**, 957–962 (2008).
- ⁵⁹⁹ 1. Pratt, D. A., Wright, J. S., Ingold, K. U. Theoretical study of carbon-halogen bond dissociation enthalpies of substituted benzyl halides. How important are polar effects? *J. Am. Chem. Soc.* **121**, 4877–4882 (1999).
2. Benson, S. W. III – Bond energies *J. Chem. Educ.* **42**, 502–518 (1965)
- ⁶⁰⁰ Patel, A., Mazzini, F., Netscher, T., Rosenau, T. A Novel Dimer of -Tocopherol. *Res. Lett. Org. Chem.* **2008**, 1–4 (2008).
- ⁶⁰¹ Rosenau, T., Potthast, A., Elder, T., Kosma, P. Stabilization and first direct spectroscopic evidence of the o-quinone methide derived from vitamin E. *Org. Lett.* **4**, 4285–4288 (2002).
- ⁶⁰² Patel, A., Netscher, T., Rosenau, T. Stabilization of ortho-quinone methides by a bis(sulfonium ylide) derived from 2,5-dihydroxy-[1,4]benzoquinone. *Tetrahedron Lett.* **49**, 2442–2445 (2008).
- ⁶⁰³ Lheureux, A., Beaulieu, F., Bennet, C., Bill, D. R., Clayton, S., LaFlamme, F., Mirmehrabi, M., Tadayon, S., Tovell, D., Couturier, M. Aminodifluorosulfonium salts: Selective fluorination reagents with enhanced thermal stability and ease of handling. *J. Org. Chem.* **75**, 3401–3411 (2010).
- ⁶⁰⁴ Kochi, J. K., Hammond, G. S. Benzyl Tosylates. I. Preparation and Properties. *Iowa State College* **75**, 3443–3444 (1953).
- ⁶⁰⁵ Makino, K., Yoshioka, H. Selective fluorination of substituted methanols with methanesulfonyl fluoride and cesium fluoride as modified with crown ethers. *J. Fluor. Chem.* **35**, 677–683 (1987).
- ⁶⁰⁶ Choe, Y. S., Song, D. H., Lee, K.-J., Kim, S. E., Choi, Y., Lee, K. H., Kim, B.-T., OH, S. Y., Chi, D. Y. [18F]fluoromethylbenzylsulfonate ester: A rapid and efficient synthetic method for the N[18F]fluoromethylbenzylation of amides and amines. *Appl Radiat Isot* **49**, 73–77 (1998).

-
- ⁶⁰⁷ Magata, Y., Lang, L., Kieseewetter, D. O., Jagoda, E. M., Channing, M. A., Eckelman, W. C. Biologically stable [¹⁸F]-labeled benzylfluoride derivatives. *Nucl. Med. Biol.* **27**, 163–168 (2000).
- ⁶⁰⁸ L'heureux, A., Beaulieu, F., Bennetti, C., Bill, D. R., Claytoni, S., LaFlamme, F., Mirmehrabi, M., Tadayon, S., Tovell, D., Couturier, M. Aminodifluorosulfonium salts: Selective fluorination reagents with enhanced thermal stability and ease of handling. *J. Org. Chem.* **75**, 3401–3411 (2010).
- ⁶⁰⁹ Middleton, W. J. New fluorinating reagents. Dialkylaminosulfur fluorides *J. Org. Chem.* **40**, 574–578 (1975).
- ⁶¹⁰ Straatmannand, M., Welch, M. Fluorine-18-Labeled Diethylaminosulfur Fluorinating Trifluoride (DAST): An F-for OH fluorinating agent *J. Nucl. Med.* **11**, 151–158 (1976).
- ⁶¹¹ Crossland, R. K., Servis, K. L. A facile synthesis of methanesulfonate esters *J. Org. Chem.* **36**, 3195–3196 (1970).
- ⁶¹² Boisnard, S., Carbonnelle, A. C., Zhu, J. Studies on the Total Synthesis of RP 66453: Synthesis of Fully Functionalized 15-Membered Biaryl-Containing Macrocyclic. *Org. Lett.* **3**, 2061–2064 (2001).
- ⁶¹³ Hajipour, A. R., Falahati, A. R., Ruoho, A. E. Iodination of alcohols using triphenylphosphine/iodine under solvent-free conditions using microwave irradiation. *Tetrahedron Lett.* **47**, 4191–4196 (2006).
- ⁶¹⁴ Iranpoor, N., Firouzabadi, H., Jamalian, A., Kazemi, F. Silicaphosphine (Silphos): A filterable reagent for the conversion of alcohols and thiols to alkyl bromides and iodides. *Tetrahedron* **61**, 5699–5704 (2005).
- ⁶¹⁵ Ellwood, A. R., Porter, M. J. Selective conversion of alcohols into alkyl iodides using a thioiminium salt. *J. Org. Chem.* **74**, 7982–7985 (2009).
- ⁶¹⁶ Hajipour, A. R., Rafiee, F., Ruoho, A. Efficient and Selective Iodination of Benzylic Alcohols Using NaI/Brønsted Ionic Liquid System at Room Temperature. *Synth. Commun.* **41**, 603–611 (2011).
- ⁶¹⁷ Andrus, M., Meredith, E. Synthesis of resveratrol. *WO2001060774 A1* (2001).
- ⁶¹⁸ Luca, L. De, Giacomelli, G., Porcheddu, A. An Efficient Route to Alkyl Halides from Alcohols Using the Complex TCT/DMF. *Org. Lett.* **75**, 127–128 (2002).
- ⁶¹⁹ Osakada, F., Hashino, A., Kume, T., Katsuki, H., Kaneko, S., Akaike, A. α -Tocotrienol provides the most potent neuroprotection among vitamin E analogs on cultured striatal neurons. *Neuropharmacology* **47**, 904–915 (2004).
- ⁶²⁰ Mazzini, F., Betti, M., Netscher, T., Galli, F., Salvadori, P. Configuration of the vitamin E analogue garcinoic acid extracted from garinia kola seeds. *Chirality* **21**, 519–524 (2009).

-
- ⁶²¹ Garcinoic acid:
<http://www.sigmaaldrich.com/catalog/product/sigma/smb00141?lang=en®ion=CA>
 (2017). α -Tocotrienol:
http://www.sigmaaldrich.com/catalog/product/sial/07205?lang=en®ion=CA&cm_sp=Insite-_-prodRecCold_xviews-_-prodRecCold10-2
- ⁶²² Hendricks, J. A., Keliher, E. J., Wan, D., Hildebrand, S. A., Weissleder, R., Mazitschek, R. Synthesis of [¹⁸F]BODIPY: Bifunctional reporter for hybrid optical/positron emission tomography imaging. *Angew. Chemie - Int. Ed.* **51**, 4603–4606 (2012).
- ⁶²³ Liu, S., Lin T-P., Li, D., Leamer, L., Shan, H., Li, Z., Gabbai, F. P., Conti, P. S. Lewis acid-assisted isotopic ¹⁸F-¹⁹F exchange in BODIPY dyes: Facile generation of positron emission tomography/fluorescence dual modality agents for tumor imaging. *Theranostics* **3**, 181–189 (2013).
- ⁶²⁴ Yang, L., Yalagala, R. S., Hutton, S., Lough, A., Yan, H. Reactions of BODIPY fluorophore with cupric nitrate. *Synlett* **25**, 2661–2664 (2014).
- ⁶²⁵ Khalil, M. M. Basic Science of PET Imaging. *Springer Int. Publ.* 1-619 (2017)
- ⁶²⁶ Everaert, H., Vanhove, C., Lahoutte, T., Muylle, K., Caveliers, V., Bossuyt, A., Franken, P. R. Optimal dose of ¹⁸F-FDG required for whole-body PET using an LSO PET camera. *Eur. J. Nucl. Med. Mol. Imaging* **30**, 1615–1619 (2003).
- ⁶²⁷ NDA 21-870: Fludeoxyglucose F 18 Injection. *North Shore / LIJ Research Institute* 4–17
- ⁶²⁸ Mosmann, T. Rapid colorimetric assay for cellular growth and survival: Application to proliferation and cytotoxicity assays. *J. Immunol. Methods* **65**, 55–63 (1983).
- ⁶²⁹ Bergmeyer, H.U. Ed. Methods of Enzymatic Analysis, 3rd Ed., Vol. I, *Verlag Chemie GmbH New York* 210-220 (1983).
- ⁶³⁰ Barenholz, Y., Israel, J., Gabizon, A. Liposome/Doxorubicin composition and method *US* 4898735 (1990).
- ⁶³¹ Yao, H. R., Liu, J., Plumeri, D., Cao, Y-B., He, T., Lin, L., Li, Y., Jiang, Y-Y., Li, J., Shang, J. Lipotoxicity in HepG2 cells triggered by free fatty acids. *Am. J. Transl. Res.* **3**, 284–291 (2011).
- ⁶³² Delbeke, D., R. Coleman, E., Guiberteau, M. J., Brown, M. L., Royal, H. D., Siegel, B. A., Townsend, D. W., Berland, L. L., Parker, J. A., Hubner, K., Stabin, M. G., Zubal, G., Kachelriess, M., Cronin, V., Holbrook, S. Procedure guideline for tumor imaging with ¹⁸F-FDG PET/CT 1.0. *J. Nucl. Med.* **47**, 885–895 (2006).
- ⁶³³ Mall, W., Columbia, B., Op-, T. Automated Synthesis of [¹⁸F]FDG using Tetrabutylammonium Bicarbonate. *Appl. Radiat. Isot.* **46**, 887–891 (1995).

-
- ⁶³⁴ Gossauer, A. Die Chemie der Pyrrole, *Springer Verlag, Berlin 1974*; R. A. Jones und G. P. Brun, The Chemistry of Pyrroles, Series Organic Chemistry, Bd. 34, *Academic Press, London, 1977*; Kutritzky, A. R., Rees, C. W. Comprehensive Heterocyclic Chemistry, Bd. 4, Teil 3, Five-membered rings with one oxygen, sulfur or nitrogen atom. *Pergamon Press, Oxford* (1984)
- ⁶³⁵ Yanabe, H., Okuyama, M., Nakao, A., Ooizumu, M., Saito, K-I. *US 2003/212094 A1*, (2003)
- ⁶³⁶ Mikhaleva, A. I., Ivanov, A. V., Skital'tseva, E. V., Ushakov, I. A. Vasil'tsov, A. M., Trovimov, A. E. An efficient route to 1-vinylpyrrole-2-carbaldehydes. *Synthesis (Stuttg)*. **4**, 587–590 (2009).
- ⁶³⁷ Hyatt, J. A., Skelton, C. A kinetic resolution route to the (S)-chromanmethanol intermediate for synthesis of the natural tocols. *Tetrahedron: Asymmetry* **8**, 523-526 (1997)